ISBN : 978 – 602 – 70050 – 4 – 4

Integrated Sci-Tech

The Interdisciplinary Research Approach

VOLUME 3

IC-STAR 2017

The 3rd International Conference on Science, Technology, and Interdisciplinary Research 2017

Bandar Lampung, 18 - 20 September 2017

Integrated Sci-Tech : Interdisciplinary Research Approach

Volume 3

Publisher :

Research Institute and Community Services
University of Lampung

Integrated Sci-Tech : Interdisciplinary Research Approach
Volume 3

ISBN :
978 – 602 – 70050 – 4 – 4

Editorial Board :

Cover and layout :
IC-STAR Team

Publisher :
Research Institute and Community Services
University of Lampung

Preface

The 3rd Volume of Integrated Sci-Tech: Interdisciplinary Research Approach book is published by the Research Institute and Community Services, University of Lampung. It integrates engineering, life sciences and biomedical engineering, and agriculture engineering and food sciences. The aim was to provide a cross section roadmap from basic research, technological and developments, processes development, and their applications and integrity in the real-world usage. The motivation for this Volume-3 book was to provide a suitable reference text for those who interested in the interdisciplinary studies and research. The book was also planned to provide advanced orientation and understanding for related industries and governments to looking across industrial partnerships, business strategic, and policy and regulations, with expected for a wider range of readers.

This book consists of several chapters divided into four sections i.e., Engineering and Technology, Life and Applied Sciences, Medical Sciences and Biomedical Engineering and alsoAgricultural Engineering and Food Science. Each chapter is a completely self-directed contribution in chained discussion which aims to bring academia, researcher, practitioners and students rise to speed with the novel developments within the particular area. In order to enhance the reader experience, each book chapter contains its own abstract, instruction, main body, as well as conclusion sections. Moreover, bibliography resources are available at the end of each chapter.

We are pleased and thankful for all distinguish authors and reviewers for their contribution that have made this book possible. We do hope that you will enjoy this book and find it as a useful guide and reference.

Editorial board:
Irza Sukmana (Dept. of Mechanical, University of Lampung)
Ardian Ulvan (Dept. of Electrical Engineering, University of Lampung)

Reviewer Acknowledgement

Joni Agustian – *University of Lampung, Indonesia*
Anna Antonyova – *University of Presov, Slovakia*
Naseem Ahmed – *Indian Institute of Technology Roorkee, India*
Fitri Arnia – *Syiah Kuala University, Indonesia*
Edwin Azwar - *University of Lampung, Indonesia*
Yanuar Burhanuddin – *University of Lampung, Indonesia*
R.Y. Ferry Burhan – *10 November Institute of Technology, Indonesia*
Homero Toral-Cruz – *University of Quintana Roo, Quintana Roo, Mexico*
Joy Rizky Pangestu Djuansjah – *Universiti Teknologi Malaysia, Malaysia*
Taha Abd. El-Rahman – *University of Sherbrooke, QC, Canada*
Ainul Ghurri – *Udayana University, Indonesia*
Cipta Ginting – *University of Lampung, Indonesia*
Lukmanul Hakim – *University of Lampung, Indonesia*
Agus Haryanto – *University of Lampung, Indonesia*
Khomaini Hasan – *Biosciences and Biotechnology Research Centre, ITB, Indonesia*
Udin Hasanudin – *University of Lampung, Indonesia*
Basem Abu Izneid – *Effate University, Saudi Arabia*
Ismail Tasib Karas – *Karabuk University, Turkey*
Naoya Kasai – *Yokohama National University*
Mamoru Kikumoto – *Yokohama National University*
Irdika Mansur – *Bogor Institute of Agriculture, Indonesia*
Antonin Mazalek – *University of Defence, Brno, Czech Republic*
Agung Mataram – *Sriwijaya University, Indonesia*
Christia Meidiana – *Brawijaya University, Indonesia*
Lee Meyer – *University of Kentucky, USA*
Khairul Munadi – *Syiah Kuala University, Indonesia*
Noor Danish Mundari – *LPU, India*
Kaneko Nabuhiro -*Yokohama National University, Japan*
Maksum Pinem – *University of Sumatera Utara, Indonesia*
RR. Poppy Puspitasari – *Universitas Negeri Malang, Indonesia*
Chithra Reghuvaran – *National Institute of Technology, Rourkela, Odisha, India*
Uceu Fuad Hassan R.S. – *GKSS, Germany*
Emerson Pascawira Sinulingga – *University of Sumatera Utara, Indonesia*
Suherman – *University of Sumatera Utara, Indonesia*
Ahmad Saudi Samosir – *University of Lampung, Indonesia*
Shirley Savetlana – *University of Lampung, Indonesia*
Diding Suhandy – *University of Lampung, Indonesia*

Table of Contens

Section 2 Life and Applied Sciences

Section 3 Medical Sciences and Biomedical Engineering

Section 4 Agricultural Engineering and Food Science

Keynote and Invited Speaker

Integrated Sci-Tech :
Interdisciplinary Research Approach
Volume 3

Indonesia Supergrid : Enabler for 100% Renewable Energy

Pekik Argo Dahono[1,a]

[1] Institute Technology of Bandung, Indonesia
[a]dwi.gustiono@bppt.go.id

Abstract. *Moving toward renewable energy is a must rather an option. Indonesia has abundant renewable energy resources that enough to fulfill our demand on energy. Unfortunately, renewable energy resources are distributed unevenly and sometimes faraway from the load centers. In order to solve the problem, a concept of Indonesia supergrid is proposed. By using this supergrid, all renewable energy resources can be utilized effectively. By using supergrid, economic development can be distributed more evenly. The supergrid can be implemented by using AC or DC grids, or combination of the two. A simple concept of how to fund the construction of Indonesia Supergrid is proposed.*

Keywords: *supergrid, renewable energy*

Chemical Engineering Approach for the Design and Evaluation of Sound Material Cycle Network

Koichi Fujie[1,a]

[1] Institute of Advanced Sciences, Yokohama National University, Japan
[a]fujie@ynu.ac.jp

Abstract. *Chemical engineering concept and methodology were applied for the minimization of environmental load from industrial and agricultural processes, and our daily activities in the regional area. The results of material flow analysis on those processes and regional area are conveniently used to evaluate the materials input and the consumption, and thus the resource productivity as well as the environment loading. The results of material flow analysis and their evaluation were essential for the design and evaluation of sound material flow/recycle network. In this presentation, design and evaluation of biomass residue recycle system in the plantation and that of wastes recycle system in a regional material area will be illustratively shown based on material flow analysis. Through the presentation, it will be emphasized the importance of material and energy flow analyses to achieve the sustainable development goals with less consumption of resources and less environment loading while providing sufficient services to our daily life*

Keywords: *material cycle, waste management*

Sustainable Land Use Management for Mitigating Greenhouse Gas Emission

Muhajir Utomo[1,a]

[1] Faculty of Agricultural, University of Lampung, Indonesa
[a] mutomo2011@gmail.com

Abstract. *Food shortage and climate change due to greenhouse gas (GHG) emissions are currently receiving considerable attention worldwide. While most of the increase of global warming is due to CO2 from fossil fuel, in fact, land uses and agriculture globally account for around 30% of global warming. Difference compared to fossil fuel sectors, how ever, land uses including agriculture and forest have opportunity to mitigate GHG emission. The strategies are by implementing sustainable land use management practices such as (1) sustainable soil management, (2) carbon rich farming, (3) perennial/agroforest farming, (4) sustainable grassland management, and (5) sustainable forest management. The objectives of this paper are to revieuw the influence of some sustainable land use managements on CO2 emission, C stock and C sequestration. From long-term no-tillage (NT) research (29 years of cropping), it revealed that cumulative CO2 emission of conventional tillage (CT) was 2.0 ton CO2-C/ha/season, minimum tillage (MT) was 1.5 ton CO2-C/ha/season and NT was 1.0 ton CO2-C/ha/season. Soil C stock under NT corn at 0-20 cm depth was 34,03 ton C/ha, or 11.1% higher than CT. Soil C sequestration rate by NT was the highest, that was 118.4 kg C/ha/yr; while in contrast, soil C sequestration under CT was the lowest (-20.7 kg C ha-1yr-1). In soil profile, C stock under NT corn in upper horizon was higher than CT, but decreased with depth. In 5 years of sugarcane research, it turned out that after 5 years of treatment applications, NT had significantly stored 39.82 ton C/ha, or 23.7% higher than CT. While mulching with 150 ton bagasse/ha had stored 38.91 ton C/ha, or 17.6% higher than without mulching. Soil C sequestration rate under NT sugarcane was 2.40 Mg C/ha/year, while in CT was only 0.81 Mg C/ha/year. Mean while, bagasse mulch with 150 ton/ha contributed 2.07 ton C/ha/year, and treatment with no mulch contributed 1.15 tonC/ha /year. In peatland, emission of CO2 average of three years of measurements (2011-2013) from Acacia (Ac) was the highest among land uses (59 ton CO2/ha/yr); while CO2 emissions from mixed forest (Mf), and tall forest (Tf) were 28, and 27 ton CO2/ha/yr, respectively. Compared to business as usual value, the CO2 emission from Ac was 44% lower, but still 5% higher than that of bare peatland. The carbon sequestration of Ac biomass was equal to 97 ton CO2/ha/yr. As a green campus, University of Lampung also sequestered above ground C as much as 35.5 ton C/ha or 2000 ton C/total area.*

Keywords*: Carbon stock and sequestration, sustainable land use management*

Development of Porous Hydroxyapatite Biomaterials for Bone-Graft Substitute

Dwi Gustiono[1,a], Agus Hadi Santosa Wargadipura[1], Mochammad Dachyar Effendi[1], Seto Roseno[1], Nendar Herdianto[1] , Ferdiansyah Mahyudin[2]

[1] Centre for Materials Technology, Agency for Assessment and Application of Technology, Gedung 224 Puspitek Tangerang Selatan, Banten, Indonesia
[2] Biomaterials Centre and Tissue Bank, Dr Soetomo Hospital, Airlangga University, Surabaya, Indonesia
[a]dwi.gustiono@bppt.go.id

Abstract. *Hydroxyapatite is the main constituent material of bone and teeth. In this paper, a hydroxyapatite powder material was made from local limestone with a simple chemical method. The porous hydroxyapatite material is prepared by replica techniques using polymer sponges. The characterization of this hydroxyapatite material is carried out by chemical, physical and biological methods. The results of analysis using FTIR and XRD equipment showed that the hydroxyapatite characteristics are similar to natural ones. The result of measurement with TEM equipment shows that the invisible particles of this hydroxyapatite powder have a rod-like shape and are about 30 - 60 nm in size. The porous hydroxyapatite materials made with replica techniques revealed a pore size of about 200-500 µm and had good interconnections as determinate by SEM measurements. Biological test results in rabbit animals show that the implantation of this hydroxyapatite material can stimulate bone growth faster than if it is allowed to grow alone (control). Bone ingrowth was significantly increasing over the time between 3 and 6 weeks.*

Keywords: *porous hydroxyapatite, bone graft, polymer sponges, limestone.*

Biomechanical Tuning of Biomaterials, Extracellular Matrix, and Culture Model to Engineer the Angiogenesis and Microvascular Development

Irza Sukmana[1,a]
[1]Department of Mechanical Engineering, Faculty of Engineering, University of Lampung, Gedung H, Lt. 2;
*[a] irza.sukmana@eng.unila.ac.id

Abstract. *The guidance of human endothelial cell (HEC) organization into a newly capillary-like network from the pre-existing ones (i.e., angiogenesis) has been a long standing challenge in the development of thick engineering tissue and artificial organ. Some efforts have been made to develop biomaterial, extracellular matrix environment and specific culture model for the promotion of capillary-like structure inside the engineering scaffold and artificial tissue constructs. Capillary-like structure and micro-vascular networks would mimic blood vessel function that can be used to subsequently facilitate oxygen and nutrient transport as well as biological waste removal inside the artificial tissue and organ system. Vascularization of engineering tissue is one of the most favorable strategies to overpass nutrient and oxygen supply limitation, which is often the major hurdle in developing a complete artificial organ. This paper aims to highlight the mechanical and biophysical properties of biomaterial, extracellular matrix and cell culture model for the purpose of angiogenesis and micro-vascular development studies. The recent in vitro investigation of Human Endothelial Cells (HECs) in a three-dimensional (3D) culture system for the guidance of HUVEC's angiogenesis development is also presented..*

Keywords: *biomechanical tuning, angiogenesis development, three-dimensional culture, endothelial cells.*

Synthesis and Characterization of Hydroxyapatitematerial Performed from Indonesian Limestone by Precipitation Method

Sudirman Habibie[1,a], Nendar Herdianto[1],Muslim E. Harahap,Diah Ayu Fitriani[1], Lukmana[1], Stephen Clarke[2]
[1]Center of Technology forMaterial, Agency for the Assessment and Application of Technology,
[2]24th Building, Puspiptek Area, Serpong, South Tangerang – Banten 15314, Indonesia
[2]AdvancedMaterial Solutions, Australia
[a]sudirmanhabibie@yahoo.com

Abstract. *Limestone which is one of the raw materials for the manufacture of materials and medical devices obtained scattered in almost all provinces in Indonesia. In this paper, synthesis of hydroxyapatite using limestone as the raw material was studied. Synthesis of hydroxyapatite was done using precipitation method. The main material of forming a hydroxyapatite in this study is diammonium hydrogen phosphate and calcination of limestone at 9000C for 4 hours that produce calcium oxide (CaO). The pure calcium oxide was observed in order to know the effect of calcium solution addition rate and calcium precursor size. The calcium oxide precursor was prepared wit h high energy milling (HEM). HEM usage is intended to produce a precursor size of calcium in nano size. Furthermore, the characterization of second phase precursors using x-ray diffraction (XRD), analysis of morphology and element content using scanning electron microscopy-energy dispersive X-ray (SEM-EDX) and analyzes the size and distribution of particles of calcium resulted from milling using a particle size analyzer (PSA).*

Keywords: *Limestone, hydroxyapatite, precipitation method, x-ray diffraction, SEM-EDX, particle size analyzer.*

Section I

Engineering and Technology

Integrated Sci-Tech :
Interdisciplinary Research Approach
Volume 3

A Conceptual Model on Integrating Supply Chain Operation Reference (SCOR) into Disaster Response Service Supply Chain FMEA (#588)

Agung Sutrisno[1,a], Benny L Maluegha[1], J. Soukotta[1], Santa L.Nusa Putri[1]
Department of Mechanical Engineering, Sam Ratulangi University, Manado, 95115, INDONESIA
[a]agungsutrisno@ unsrat.ac.id,

Abstract. *Becoming country prone to the occurrence of natural disasters, determination on risk variables affecting successful operation of disaster response service supply chain using supply chain FMEA (Failure Mode and Effect Analysis) is undeniably important to support successfulness of humanitarian operation. However, scientific studies concerning on integrating SCOR into Risk evaluation of disaster response supply chain is rarely found in references. To response such gap, this paper presents a conceptual model on integrating disaster response supply chain FMEA with Supply Chain Operational Reference (SCOR) to determine a conceptual risk-based performance evaluation model in disaster response supply chain. A framework on integrating Service Supply Chain FMEA with SCOR is presented coupled with a decision support model for evaluating criticality of risk-based performance index and followed with discussions and new opportunity for further investigations.*

Keywords: *Service Supply Chain, FMEA, SCOR, Disaster Response, Risk.*

I. Introduction

During the last two decades, the world is witnessing the increasing number of global disastrous events. In the era of 1980s, the yearly average number of disastrous events was 180, however, in 2010 the number is increasing to 384, indicating three times increase [1]. The impact of that disaster is very huge, as for the year of 2011 alone as the example, total economic losses are reaching US $ 109.3 Billion Dollars. In terms of the disasters' victim, during the past three decades, the number of reported disasters have increased fourfold, and around 6.1 billion people have been affected by disasters with an estimated damage of almost 2.3 Trillion dollars [2]. Among countries suffered from the natural –made global disastrous events, Indonesia, together with US, India, China, and The Philippines was among the five most frequent disaster sufferers. Considering large amount of its potential number of disaster's victim and unbearable economic impact, advancement of tools and methodology/techniques to improve quality of response in disaster relief operations is obviously very important for sustaining development of a country. According to [3], research intended to prevent failure in disaster relief operation is still becoming top priority in disaster prevention discipline and very rare references discussing developing a framework on embedding SCOR into disaster response risk assessment method within supply chain framework. Motivated by this discrepancy, the goal of this study in concerning on proposing a conceptual model on integrating a conceptual model on integrating SCOR (Supply chain Operation Reference) model into disaster response supply chain to guide failure prevention in operation of disaster response services. The structure of the paper is in followings. In

Manuscript received July 8, 2017. This work was supported by the Research Grant of Sam Ratulangi University under research Grant Penelitian Unggulan Universitas Sam Ratulangi 2017.

section II, an overview of SCOR and Supply Chain FMEA is introduced and followed with a conceptual model on embedding SCOR concept into disaster response service supply chain FMEA in section III. Section V related to a risk-based decision support model for evaluating risk variables in disaster response Supply chain FMEA. Conclusions and new inquiries for further investigation are provided in section VI.

II. SCOR and Service Supply Chain FMEA-AN OVERVIEW

a. Supply Chain Operational Reference (SCOR)

Developed by the supply chain council, the SCOR model is a kind of reference model in operationalizing a typical supply chain. As the reference model, the major of supply chain process within SCOR framework are consisting of plan, make, source, deliver and return [4]. The use of the SCOR model enables decision makers to drive supply chain operation to reach the intended performance of the disaster response supply chain.

Figure 1. Schematic model of SCOR

b. Service Supply Chain Failure Mode and Effect Analysis

Service supply chain FMEA, as its name implies is a kind of failure mode and effect analysis model applied into supply chain level. Different from design and manufacturing type FMEA, the scope of service supply chain FMEA is exceeding companywide level with coverage on information, material and financial flow among suppliers, distributors and end customers. Becoming the risk appraisal tool in supply chain, service supply chain FMEA utilizes the risk priority number as product of adverse event probability occurrence level and estimated severity of its consequences in evaluating criticality of risky events. An exemplar on appraising the risk within supply chain can be referred into [5]. By implementing FMEA in service operation, decision makers enable to take any preventative measures to prevent the re-occurrence of adverse events derail operability of disaster response supply chain.

III. A Framework on Integrating SCOR into Disaster response Service Supply Chain FMEA

Integrating Risk Assessment method into SCOR enabling decision makers to prevent any preventative measures against the occurrence of any factors affecting disruptions in the operation of disaster response supply chain. A representation of framework in integrating Service Supply Chain FMEA into SCOR is presented in Figure 1.

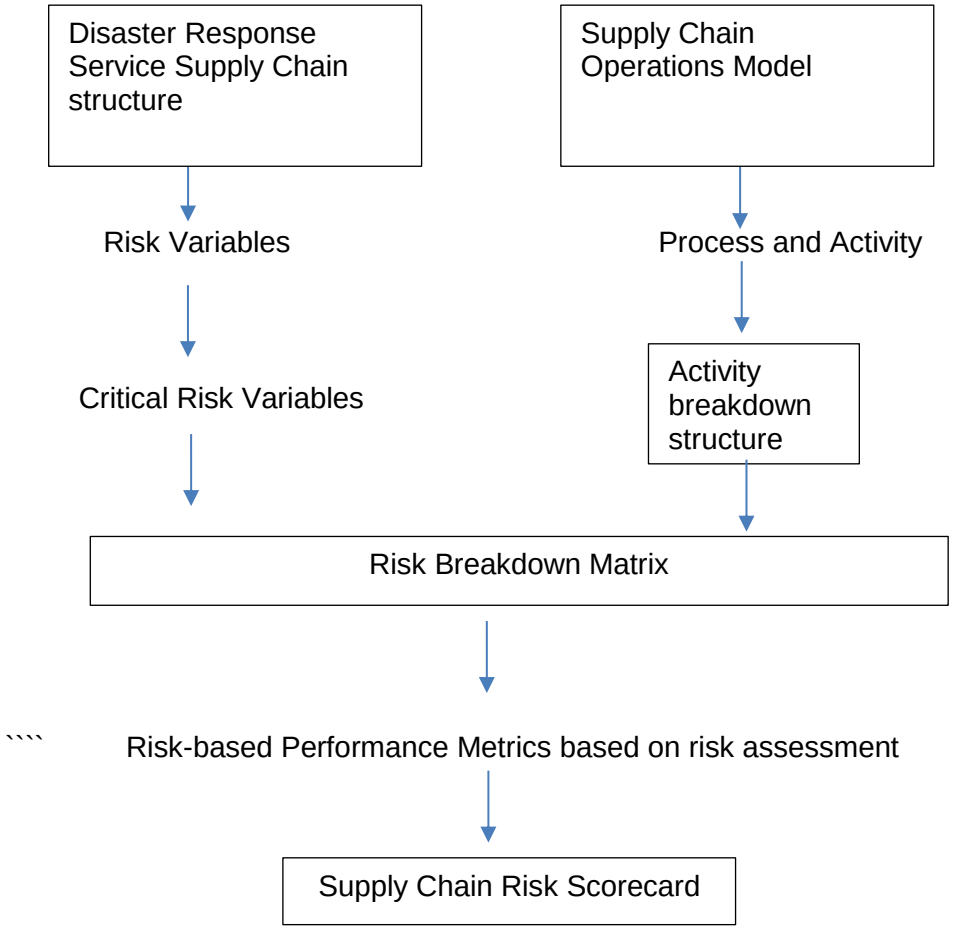

Figure 1. Integrating SCOR into Disaster Response Service FMEA

In Figure 1, disaster response service supply chain structures are used to map potential risk modes of disaster response supply chain. The result of this approach is the critical risk variables. At the other side, the SCOR model is used to determine related activity of disaster response supply chain. The outcome of mapping disaster response supply chain is the structure of relevant activity responding to disaster effect. Linking critical risk variables and activity structure will enable to determine the score of the supply chain risk variables in the form of Supply Chain Risk Score.

Properly linking SCOR into disaster response supply chain, it is necessary to identify relevant the SCOR elements and their corresponding risk indicators and affected supply chain performance dimensions. Using scientific study of [6], [7] and [8] as references, the linkage of the SCOR element with its risk variables and their affected Supply Chain performance in a typical disaster response supply chain is presented into the Table 1.

Table 1. Linking SCOR Elements into SC Risk Variables and Affected Performance Dimensions

First Layer Factors	Second Layer Factors	Exemplar of Potential Risk Variables	Affected Performance Dimension
Plan	Strategy	Inconsistent Strategic Objectives	Reliability
	Culture	Weak risk awareness	Flexibility
	Demand	Uncertain demand	Agility
Source	Purchasing	Low quality of purchased goods	Reliability
	Supply	Unreliable suppliers	Reliability
Make	Environment	Politics, economics and social Risk	Reliability
	Production	Technical production problems	Reliability
	Control	Inappropriate service control	Reliability
Deliver	Relation	Distrusted partners Increasing commodity prices	Reliability Cost
	Transportation	Inappropriate distribution method	Reliability
	Origination	Improper delegation of supply chain authority	Responsiveness
Return	Return Way	Lack of consensus with customers	Responsiveness
	Return Procedure	Imperfect return process and rules	Responsiveness

Linking the SCOR elements of disaster response supply chain with their performance dimensions will enable decision makers to identify which SCOR elements correspond to the performance dimensions of disaster response supply chain. In Table 1, relationship among SCOR, risk variables and performance dimensions of supply chain is presented. Among other dimensions of supply chain, reliability is becoming the prime variables related to performability of disaster relief supply chain. Figure 2 represented the map of impact of a certain risk to an activity in a typical risk breakdown matrix

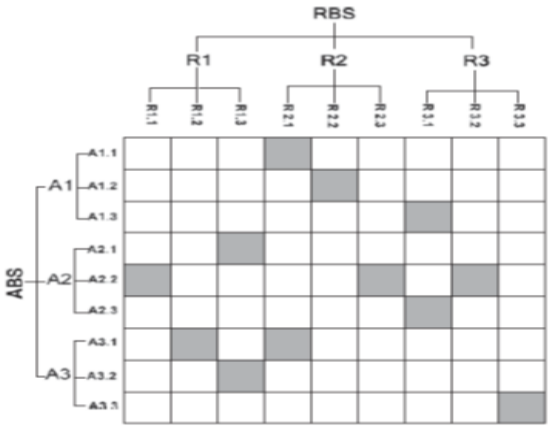

Figure 2. Chart depicting relationship between a risk variable and an activity [9]

IV. Quantifying Risk-Based Performance Index

Intended becoming tool to manage performability of disaster response supply chain, determination of an index as basis to estimate criticality of risk variables due to failure in reaping response operation is imperative. In this regard, the basis determination of such index is based on derivation of risk as product of likelihood of the risk variables occurrence and their severity scale. Considering that not all SCOR elements are having equal importance, weightage of SCOR using decision making technique such the AHP (Analytic Hierarchy Process) should be accomplished. Denote RPI_k as risk-based performance index k,OR_k as occurrence scale of risk variables k, WS_k represents the weight of a certain SCOR attribute and L_k as the estimated loss score because of occurrence risk variables k, then the score of the risk-based performance index of a certain supply chain performance variables is given in equation (1).

$$RPI_k = WS_k OR_k L_k \quad (1)$$

The score of L_k can be estimated using Taguchi Loss Functions. By identifying the threshold of critical risk, decision makers enable to determine appropriate corrective and preventative measures to prevent re-occurrence of critical risk variables.

In this paper, a model depicting integration of SCOR into disaster response supply chain is presented. Using the model enable decision makers to determine relationship among source of risk variables affecting supply chain performance dimensions. Ability to determine critical risk variables affecting performability of disaster response supply chain will become basis to take any measures preventing derailment of humanitarian service operation.

V. Conclusion

Driven by the frequent occurrences of natural disaster in Indonesia, endeavor to improve quality of risk assessment in disaster response supply chain is undeniably important to sustain country's development. In this paper, a conceptual model on integrating SCOR into disaster response risk assessment using FMEA framework is presented and followed with derivation on SCOR elements and their corresponding risk variables. Using this framework enables decision makers to anticipate any unintended outcomes of their response's operation thus will improve success operations of disaster alleviation. Opportunities for further investigations are viable in several ways, for example by undertaking empirical observation in testing appropriateness of the model and developing risk metrics of disaster response supply chain using vast array of multi attributes decision making techniques and linked it with performance evaluation techniques.

References

[1] D.C. Whybark, “Co-Creation of Improved Quality in Disaster Response and Recovery,” *International Journal of Quality Innovation*, Vol.1, pp.1-10, 2016.
[2] S. Kumar and T. Havey, “Before and After Disaster Strike: A relief Supply Chain Decision Framework,” *International Journal of Production Economics,* Vol.145, pp.613-625, 2013.
[3] S. Gupta, M.K. Starr, R.Janjiari and N.Matinrad, “ Disaster Management from Production and Operations Management Perspective: Mapping a New Domain,” *Production and Operation Management*, Vol.25, pp.1611-1637, 2016.
[4] S. Chabcoub and W.Hachica, “ Associating Risk Management with a Performance Measurement System: Case of Academic Libraries,” *Proc. Int. Conf. in Advanced Logistics and Transport*, Hammamet, 2014,pp.383-388.
[5] D.Nakandala, H.Lau and L.Zhao, “ Development of a Hybrid Fresh Food Supply Chain Risk Assessment Model,” *International Journal of Production Research*, Vol.55,pp.4180 – 4195, 2016.
[6] T.C. Weng and F.K. Chan, “AnalyzeQ and Predict the Co-movement Effect of Risks in the Supply Chain Management,” *Research in Electronic Commerce Frontiers*, Vol.2, pp. 6- 15, 2014.
[7] J. Liu, F. Liu, H. Zhou and Y. Kong, “An Integrated Method of Supply Chains Vulnerability Assessment,” *Scientific Programming*, Vol.2016, pp. 1-10, 2016.
[8] Q. Lu, M. Goh and R.D.Souza, “ A SCOR Framework to measure logistics performance of Humanitarian Organizations,” *Int. J. Humanitarian Logistics and Supply Chain Management*, Vol.6, pp. 222-239, 2016.
[9] A.C. Cagliano, A.D. Marco, S.Grimaldi, and C. Rafele, “ An Integrated Approach to Supply Chain Risk Analysis,” *Journal of Risk Research*, Vol.15, pp.817-890, 2012.

Monitoring Temperature and Humidity Wireless Realtime-Based LabVIEW (#591)

Asep Andang[1,a], Nurul Hiron[1,b]
[1]Electrical Engineering Departement, Universitas Siliwangi
[a]andhangs@unsil.ac.id, [b]hiron@unsil.ac.id

Abstract. *In this study, the temperature monitoring system used was the MyRIO with LabVIEW-based programming. LabVIEW-based programming is known for its versatility and ease of access to the hardware and internet technology. The instrument used was the DHT11 sensor to communicate with MyRIO, whereas to bridge the communication between MyRIO and CPU wireless communication was used. Then, the captured results were displayed on the CPU by using IEEE 802.11 Protocols. Based on the tests conducted on 10 experimental conditions, it was known that the DHT11 temperature sensor resulted in a 1.99% error rate. This value indicated the acceptable accuracy that is below 5% while the error rates of the humidity measurement varied, i.e. in the 5th to the 10th test conditions in which the acquired error rates enlarged up to 13.5%. This meant that humidity sensor accuracy had good accuracy in the 1st to the 4th testing conditions.*

Keywords **:** *DHT 11, LabVIEW, MyRIO, temperature, humidity*

I. Introduction

The observation system or remote monitoring currently has undergone very rapid developments, one of which is in measuring the monitoring system of new and renewable energy parameters. Various systems have been proposed with various methods, both in processing and in the process of data transmission, as well as data communication systems which are experiencing rapid development. With the standard protocol IEEE 802.11, communications between processor sensor to the collector become easier, one of which by using the zigbee protocol combined with an arduino with real-time monitoring system [1] which generates data in accordance with the data in the field, while the data transmission system with batching methods [2] generate compressed data per day which are sent and collected in the memory of the arduino sent per day as well. The use of zigbee protocols in a standalone process also used in monitoring the weather [3] at the lab scale by using LM 35 as well as DHT 11.

The combination of Zigbee Protocol and data transmission communications from sensors to hosts or to servers is performed by incorporating GSM technology [4], by using a GSM Modem and TCP/IP protocol the data is sent, generating considerable distance in accordance with GSM modem capabilities. Another system used in weather monitoring is a radio frequency (RF)[5] using the module 1020U-Kyl as a delivery medium.

The research conducted using this platform either incorporated the arduino or Zigbee and LabVIEW interface generated output in the form of MS Excel[6] using the sensor SHT 11 with communications systems that were quite different from others in order to connect to an arduino. Other studies using LIFA facilities (LABVIEW Interface For the Arduino)[7] although the sensor used was still LM35. In another study [8] the integration was performed on software ie Labview as the interface and KEIL software by using LM35 as the temperature sensor.

The integration of the above-mentioned systems was performed in order to use a sensor that has a communication pattern with other systems. LM35 temperature sensor output has an analog output with the increase rate of the current of 100mV/°C, the sensor can be directly accessed by LABVIEW, unlike SHT 11 or DHT 11 which uses single wire interface that needs a bit different handling.
DHT11 sensor, which had the sufficient capability, was used in the system that was being built. The form of DHT11 can be seen in Figure 1 below

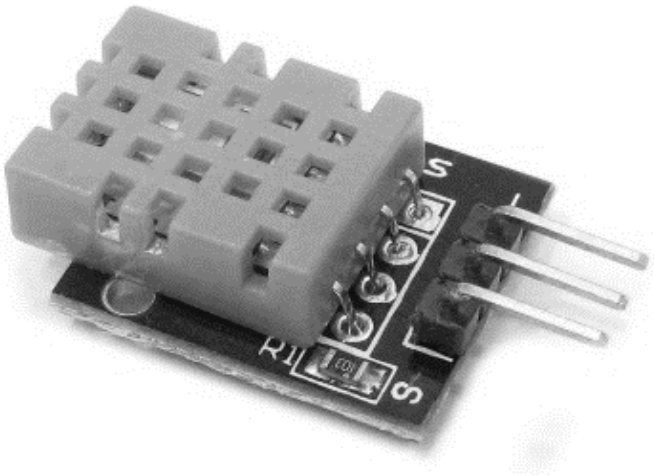

Figure 1. DHT11 Temperature and Humidity sensor

This DHT sensor has a quite unique communication with the transmitted data of 40 bits with the accuracy of ± 4% RH and resolution temperature of 1°C. Make this sensor is quite sought after and used in various temperature and humidity metering systems.

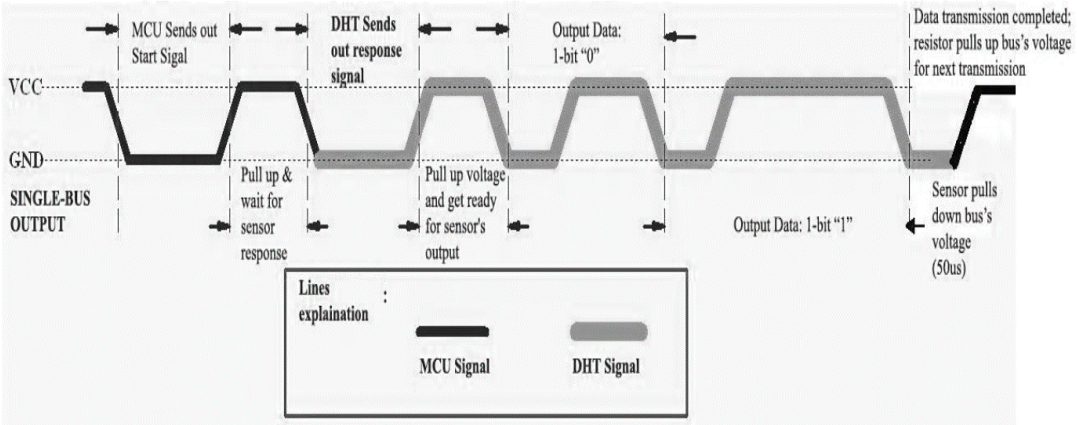

Figure 2. DHT11 Communication Process

Figure 2 shows the DHT11 working process which depends on the MCU signal. When the signal goes into the sensor, the DHT will be turned into running-mode, and then send a 40 bits signal including the humidity and temperature data. In the absence of signals from the MCU, DHT11 will not give the input signal [9].

As for the MCU, MyRIO, which is the product of National Instrument, was used. It has Z-7010 Xilinx processors with a speed of 667 MHz and has a non-volatile memory of 256 MB and 512 MB DDR memory. While for communication, MyRIO has wireless connection IEEE 802.11 b, g, n with 2.4 GHz frequency band with 20 MHz channel depth, MyRIO is equipped with Digital I/O and Analog I/O with 12-bit resolution.

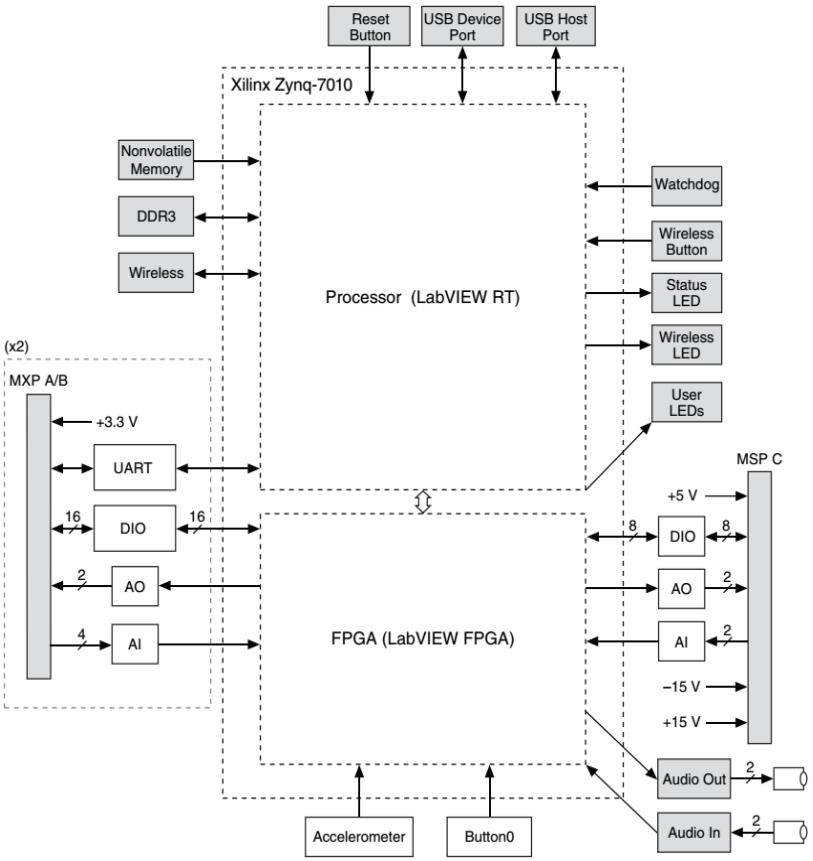

Figure 3. MyRIO 1900 Diagram Block

II. Procedure

A. System Plan

The developed system consisted of 2 parts namely, system sensor and MCU consisting of temperature and humidity sensor as well as the MCU in the form of MyRIO 1900, and also a recipient that is CPU. The communication between MyRIO 1900 and the CPU was performed by using IEEE 802.11b network with 2.4 GHz working frequency. In this developed system, the access point used in MyRIO presents on the system itself without external reinforcement.

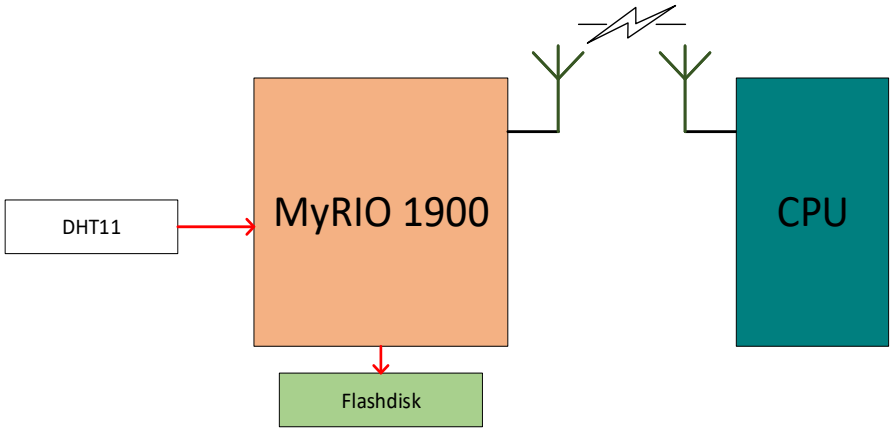

Figure 4. Block Diagram of Temperature and Humidity Monitoring Hardware

The mechanism of the block diagram can be seen in the flowchart below, the first process was the initialization program that would prepare the necessary things for processing temperature and humidity data. Figure 5 is a flow diagram of the system.

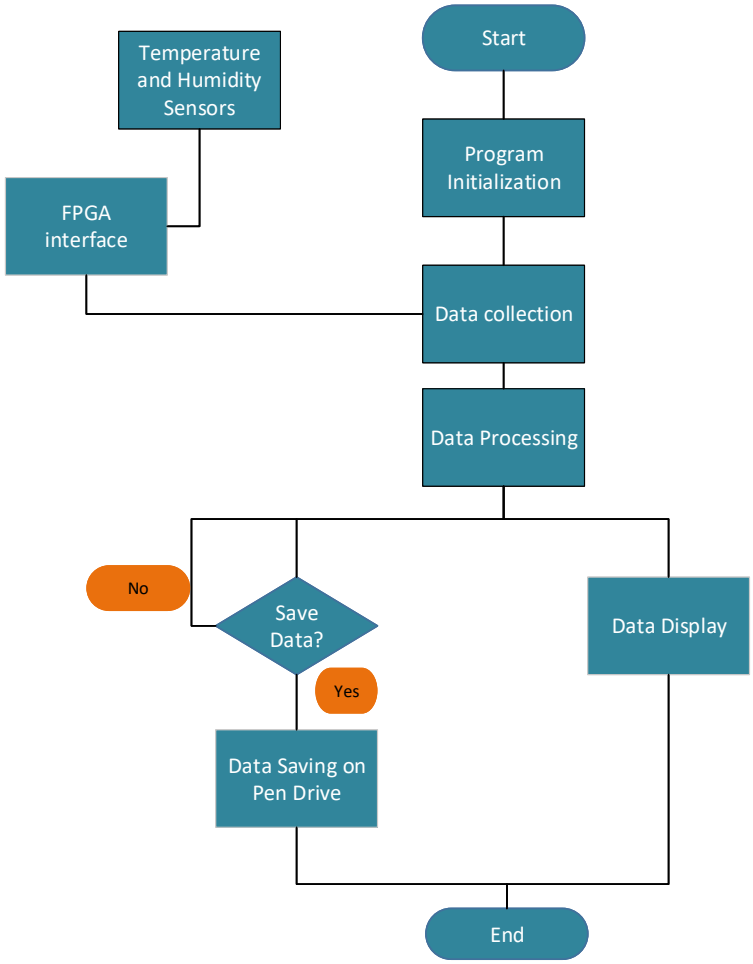

Figure 5. Flowchart

This data was then processed to be displayed in graphical form in real time and stored in the form of excel. As for storage media, a Pendrive, which was connected with MyRIO, was used. However, this data still could be accessed from the CPU.

The following figure shows what was displayed in the settings panel which was the front panel of the LabVIEW system. This view was accessed from the CPU using wireless 2.4 GHz consisted of a graphics display, storage options, and other settings.

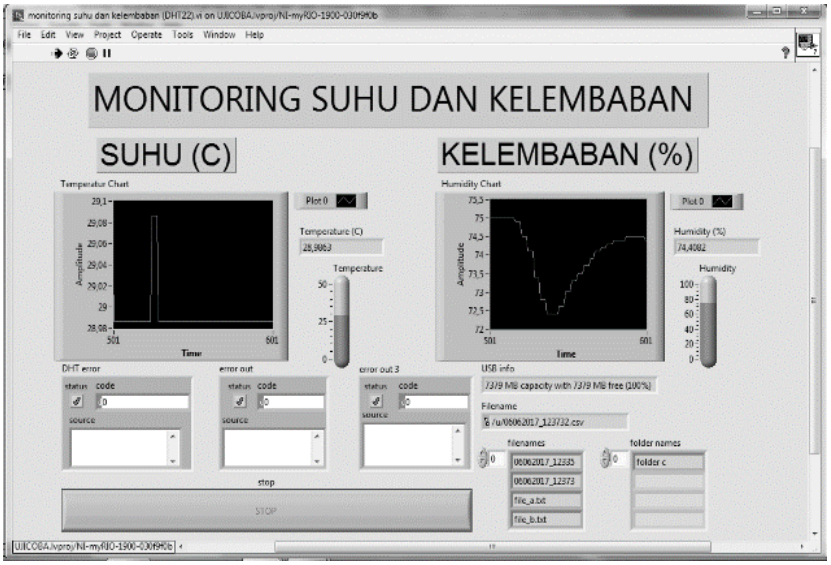

Figure 6. LabVIEW Front Panel

B. Result

In order to get the results, then a series of tests was performed by comparing the DHT11 sensor with a measuring instrument so that two data that could be displayed in graphical form. The series of tests performed is shown in the picture below.

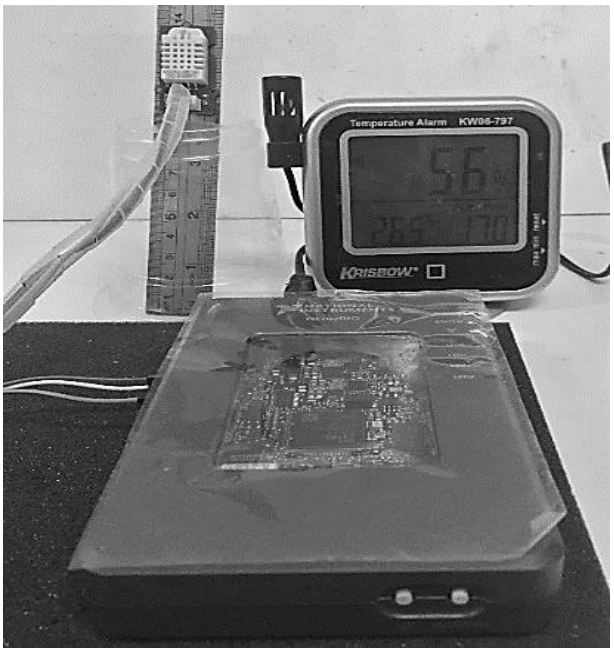

Figure 7. System Testing

With a series like the one above, the test was performed with varying temperature and humidity resulting in the graph which is a comparison of the measuring instrument.

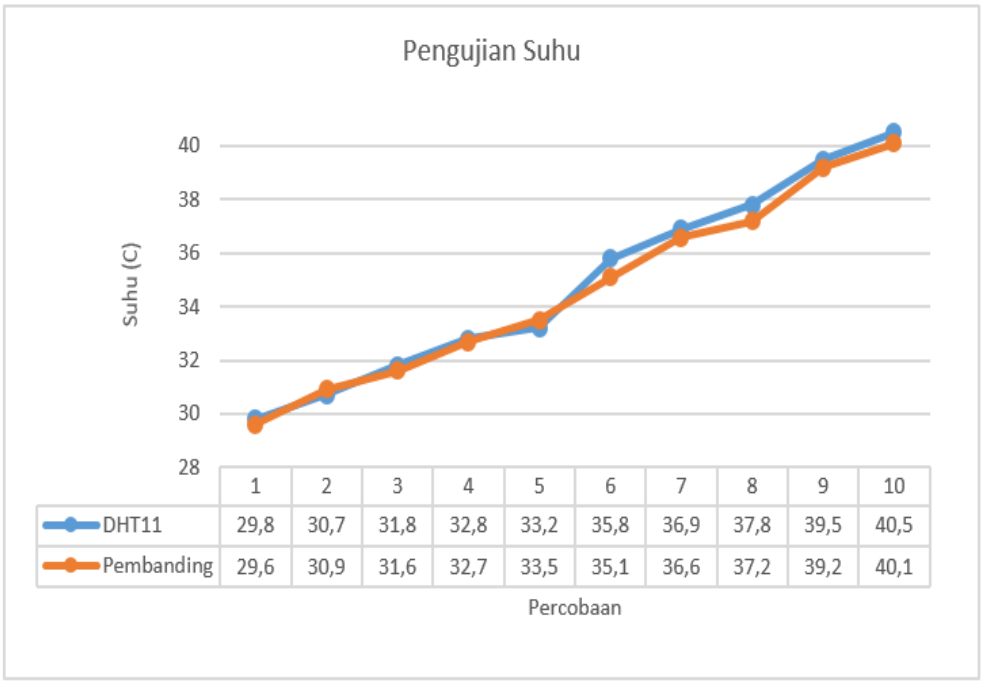

	1	2	3	4	5	6	7	8	9	10
DHT11	29,8	30,7	31,8	32,8	33,2	35,8	36,9	37,8	39,5	40,5
Pembanding	29,6	30,9	31,6	32,7	33,5	35,1	36,6	37,2	39,2	40,1

Fig 8. Temperatur Testing

The test was carried out at the lowest temperature of 29.6°C and the highest one was 40.1°C. As can be seen the temperature rate was rising. Based on the calculation, the smallest error difference was 0.31% and the largest difference error was 1.99% so there was an error range of ± 1.5%.

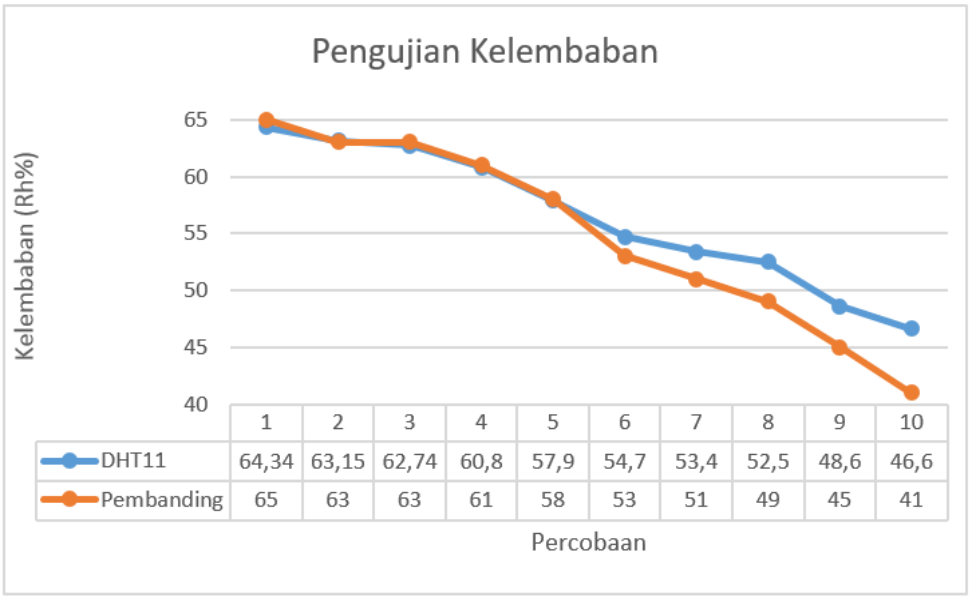

	1	2	3	4	5	6	7	8	9	10
DHT11	64,34	63,15	62,74	60,8	57,9	54,7	53,4	52,5	48,6	46,6
Pembanding	65	63	63	61	58	53	51	49	45	41

Figure 9. Humidity Testing

Meanwhile, in humidity testing, there were differences of error as the shown in the graph below. The test was carried out in humidity range 65% to 41%, the minimum error was 0.17% and maximum error was 13.66%, so the range of error was about ± 13, 50%.

The use of LabVIEW with MyRIO Hardware simplified the tools configuration used for the connection both between MyRIO and the sensor and between MyRio and the computer to display measurement results and data storage. The use of wireless communication with the IEEE 802.11 protocol b, g, n facilitated communication link.

The test results could be accessed by using the webpage as shown below

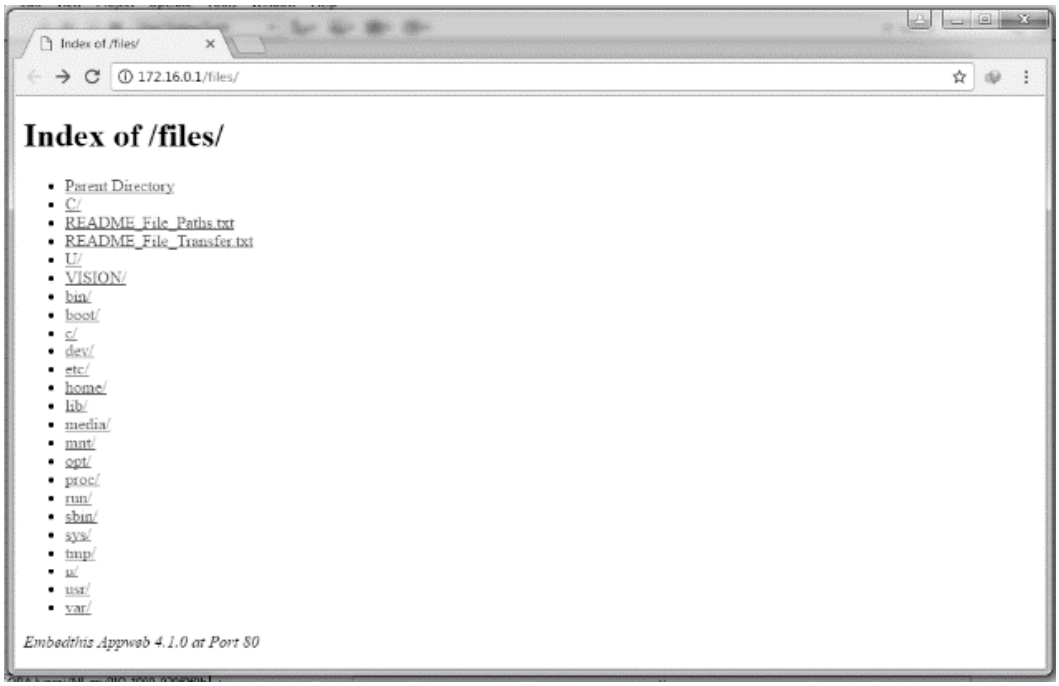

Figure 10. Data acces using MyRIO wifi

which will generate the CSV data in accordance with the desired sampling time.

III. Conclusions

Temperature and humidity monitoring systems using LabVIEW and MCU MyRIO and DHT11 sensor managed to sense temperature and humidity even though DHT11 used/equipped with (dilengkapi) a rare-use single-wire interface. This could be overcome by using the FPGA interface so that the data communications could be stored and displayed with adjustable sampling rates.

The results obtained from the humidity and temperature test which was performed by using DHT 22 sensor resulted in test error rate under 5% that is, at the smallest rates, 0.31% and 1.99%. Whereas, for the humidity, there was the biggest error i.e. 13.5%. One of the things which led to the existence of a fairly large error was the construction of DHT which had a hollow. It could cause humidity, especially because water still clung to the hollow.

The test resulted in a comparison between the DHT11 sensor with other test equipment. Although the measurement range was not so wide but still able to know the performance of the system created, this can be seen based on the number of experiments. Meanwhile, the error in the temperature test was fairly good.

References

[1] V. S. Kale and R. D. Kulkarni, “Real Time Remote Temperature & Humidity Monitoring Using Arduino and Xbee S2,” *Int. J. Innov. Res. Electr. Electron. Instrum. Control Eng.*, vol. 4, no. 6, pp. 175–179, 2016.

[2] N. Hiron and A. Andang, “Wireless Communication with Batching Method Based on Xbee-PRO S2B Module for Sensing of Wind Speed,” *2nd Int. Conf. Sci. Inf. Technol. Wirel.*, pp. 250–253, 2016.

[3] N. Gahlot, V. Gundkal, S. Kothimbire, and A. Thite, “Zigbee based weather monitoring system,” *Int. J. Eng. Sci.*, vol. 4, no. 4, pp. 2319–1813, 2015.

[4] A. Pusatkar and V. Gulhane, “Survey of Implementation of Wireless Sensor Network for Real Time Monitoring of Agriculture,” *Int. Res. J. Eng. Technol.*, vol. 3, no. 2, pp. 997–1003, 2016.

[5] Iswanto and M. Helman, “WEATHER MONITORING STATION WITH REMOTE RADIO FREQUENCY WIRELESS COMMUNICATIONS,” *Int. J. Embed. Syst. Appl.*, vol. 2, no. 3, pp. 1009–1016, 2012.

[6] N. Sabharwal, R. Kumar, A. Thakur, and S. Jitender, “A LOW COST ZIGBEE BASED AUTOMATIC WIRELESS WEATHER STATION WITH GUI AND WEB,” *ICRTEDC-2014*, vol. 1, no. 2, pp. 258–263, 2014.

[7] K. P. J. Pradeep, K. S. P. Reddy, D. H. Kumar, K. N. Raju, and C. Nagaraja, “Monitoring of Temperature and Humidity Using LIFA,” *Int. J. IT, Eng. Appl. Sci. Res.*, vol. 3, no. 6, pp. 1–3, 2014.

[8] P. Susmitha and G. Sowmyabala, “Design and Implementation of Weather Monitoring and Controlling System,” *Int. J. Comput. Appl.*, vol. 97, no. 3, pp. 975–8887, 2014.

[9] D. Uk, “Temperature Sensor DHT 11 Humidity & Temperature Sensor,” *DHT11 Datasheet*, p. 9, 2010.

Microstructures and Mechanical Properties of Duplex Low Carbon Steel (#599)

Alfirano[1,a], Eben Urip Santoso[1,b] , Maulud Hidayat[2,c]
[1]Department of Metallurgical Engineering, Faculty of Engineering, University of Sultan Ageng Tirtayasa, Cilegon, Indonesia
[2]Iron Making Division, PT. Krakatau Steel, 42435, Indonesia
[a]alfirano@untirta.ac.id, [b]eben.santoso@gmail.com, [c]maulud.hidayat@krakatausteel.com

Abstract—*The microstructures behavior of duplex cold-rolled low carbon steel for use as machine body parts and vehicle panels has been investigated. A representative composition of low carbon steel was utilized to produce ferrite–martensite dual phase of varied proportions by intercritical annealing treatment. The specimens were heated at inter-critical annealing temperature of 775^{o}C - 825^{o}C, for heating time up to 20 minutes, followed by water quenching in order to get a dual phase ferrite and martensite. The hardness of specimens was studied. The optical microscopy was used to analyze the microstructures. After quenching, it was obtained the optimal annealing conditions (martensite volume fraction approaching 20%) at 775^{o}C with a holding periods of 10 minutes. The highest hardness value was obtained in cold-rolled specimens of 41% in size reduction for intercritical annealing temperature of 825^{o}C. In this condition, the hardness value was 373 HVN. The relationship between temperature and time of intercritical annealing with martensite volume fraction showed that a equation as f□/fe = 1 - exp(-Kt^{n}) can be used to give the variation of martensite volume fraction with heating temperature and time. Also it is found that K coefficient changes exponentially with annealing temperature. In addition, the value of K (grain growth rate constant) and n (Avrami's exponent) were 0.15 and 0.461, respectively, with activation energy (Q) of 267 kJ/mol.*

Keywords—*Duplex steel, ferrite, martensite, hardness, activation energy.*

I. Introduction

The high demand for materials of automotive industry with improved mechanical properties has led to the development of wide variety of dual phase steels. The structure of dual phase steel consists of ferritic matrix and islands of martensite. Martensite contribute to strength of base material and ferritic provide good ductility [1]. Dual phase steel is appropriate material for automotive industry because this material has good combination of high strength, good ductility and reasonable yield strength [2]. The interest originates from the demand for lighter, more fuel efficient vehicles and the fact that the dual phase steels combine superior ductility, with good tensile strength, and in this regard their properties are very similar to plain carbon steels [3]. The ferrite matrix provides the ductility while the high strength particles provide strength. Low yield strength, continuous yielding behavior, and highly uniform total elongation are also beneficial properties of dual phase steel [4]. The mechanical properties of dual phase steels are affected by the volume fraction, the morphology of hard phase [5], and the ferrite grain size [6]. Alaneme [7] noted that treatment variables can help provide duplex microstructures of ferrite and martensite of the right volume proportion that will yield a good combination of tensile and strength and ductility. Intercritical heat treatment is an effective way to transform low carbon steels to dual phase steels with superior strength. Increasing in heating time at low temperature decreases the microstructural strapping in cold-rolled dual phase steel [8], while in the intercritical range, the formation of ferrite was observed more by quenching [9]. The present work examines the microstructural changesin cold-rolled low carbon steel during intercritical annealing with a focus on the formation of dual phase structure.

II. Experimental Procedure

The material for the investigation is a low carbon steel as-supplied as hot-rolled plates with 100x75x3.40 mm in dimension. The chemical composition (in wt%) is as follows: C (0.155); Si (0.18); Mn (1.05); P (0.056); S (0.0065); Cr (0.011); Ni (0.008); Mo (0.0025); V (0.0036); Nb (0.0019); Ti (0.0012); W (0.0041).The plates were initially subjected to intercritical annealing and quenching. Cold rolling of the plates to approximately 41% of the original diameter (3.40 mm) was carried out after intercritical treatment which performed by first determining the lower critical temperature (A_1) and the upper critical temperature (A_3) for the test material following empirical relations in accordance with Andrews [10]. The plates were then treated at intercritical temperatures of 775^{o}C, 800^{o}C, and 825^{o}C; and were held for 10, 15, 20 minutes, followed by water quenching. Control samples were prepared by tempering a set of the cold-rolled samples at 200^{o}C for 20 minutes and then air cooling. For hardness test used micro Vickers hardness. The microstructures of samples were studied by optical microscopy. Martensite volume fraction was measured based on ASTM E562-83 standard.

III. Result and Discussion

The microstructure of specimens before and after quenching is shown in Figure.1. The specimens before quenching were consisted of ferrite and pearlite phases (Figure.1 (a)). Volume fraction of the phase was obtained by using point counting calculations. Volume fraction of ferrite and pearlite were 79.7% and 20.3%, respectively. Microstructures formed after the quenching were formed ferrite, pearlite and martensite phase, which can be seen in Figure.1(b-d). Martensite volume fractions for heating time of 10, 15 and 20 minutes were 26.5%, 29.2% and 31.8%, respectively.

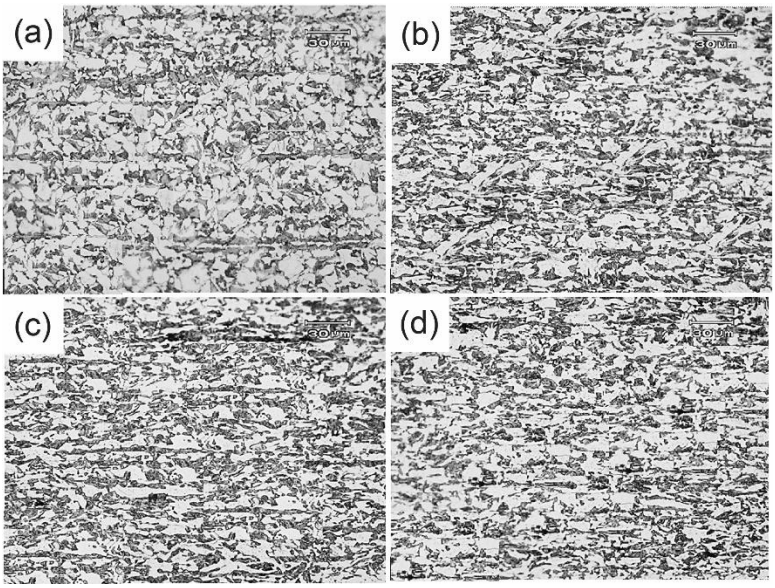

Figure.1. Microstructure of specimens (a) before heat treatment and after heat treatment at 775 ^{o}C for (b) 10, (c) 15 and (d) 20 minutes, water-quenched, 41% cold-rolled.

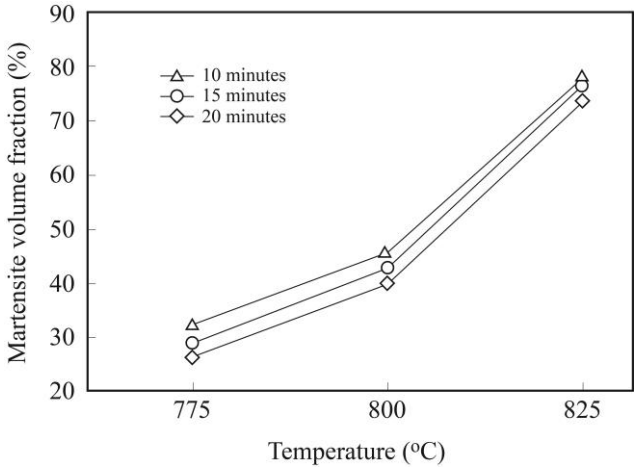

Figure.2. Effect of temperature on martensite volume fraction of specimens heated at various holding time.

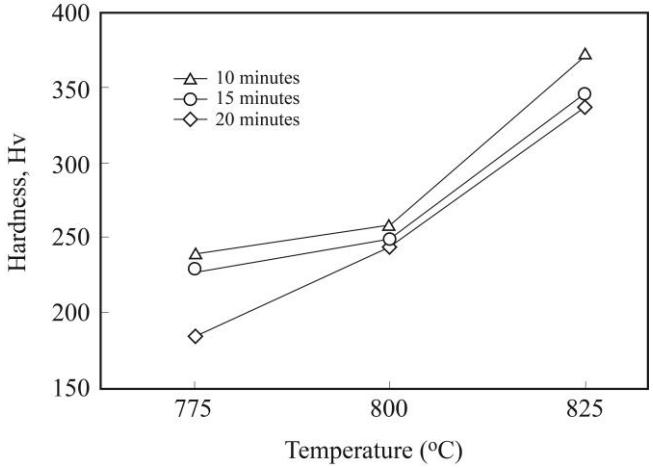

Figure.3. Effect of temperatures on hardness at various heating time.

The effect of intercritical temperature on martensite volume fraction at various heating time are shown in Figure.2. Intercritical temperature has significant effect on increasing the hardenability compared to that of heating time. Martensite volume fraction will significantly increases with increasing temperature. When the specimens were heated at intercritical annealing point, austenite start to nucleate and grow [11]. Austenite is unstable phase and it will be transformed during cooling. In the A_1 temperature austenite began to transform by eutectoid reaction into ferrite, cementite and pearlite.

When the temperature is raised above the A_1, the austenite ability to dissolve carbon will be increased, so that the carbon that had been located on the ferrite gradually dissolves into austenite. [8]. Therefore, increasing heating temperature will increase the volume fraction of austenite under rapid cooling. Increasing in holding time will promote the formation of austenite. The heating time affected to the phase formation, because the holding time provides an opportunity for atoms to diffuse thus homogenize the austenite [7]. Austenite is an unstable phase and when the cooling process can be transformed into another phase in accordance with the cooling rate.

When the temperature is raised above the A_1, carbon atom easily dissolved into austenite [12]. Therefore, increasing heating temperature increase the volume fraction of austenite after rapid cooling. Increasing in holding time will promote the formation of austenite. The

heating time affected to the phase formation, because the holding time provides an opportunity for atoms to diffuse thus homogeneously into austenite [11]. Austenite is an unstable phase and it can be transformed easily into another phase during cooling process.

The hardness value of specimens can be seen on Figure.3. The hardness value of the specimen before heat treatment was 135.6 HVN. Heating was performed on the ferrite and austenite region. Increased in hardness occurs caused by increase in the volume fraction of martensite. The difference of cooling rate between specimens before and after heat treatment can cause the difference in phase formations; ferrite-pearlite and ferrite-martensite, respectively. In low carbon steel, ferrite and pearlite were formed and its hardness is determined by the carbon content, therefore the hardness of low carbon steel will be affected by ferrite and pearlite content. While the specimens were quenched, it produces the final structure of ferrite and martensite, where the carbon content in the martensite was saturated. The formation of martensite can cause on increasing in hardness value. Increasing heating temperature will increase the cooling rate so that martensite easily formed. Increase in martensite volume led to the increasing of hardness value [13]. The main factor of strengthening mechanism of dual-phase steel is caused by martensite microstructure as a strong and able to load carrying constituent in the soft ferrite matrix. Dual phase steel also has a high rate of work hardening due to dislocation density resulting in high tensile strength. The presence of high density of dislocation can be obstacle for the movement of the other dislocations.

TABLE I
N AND K VALUE AT 775OC, 800OC AND 825OC

Temp. (^oC)	Equilibrium Austenite volume fraction (f_e)	Avrami's exponent (n)	Rate constant (K)
775	0,2808	0,461	0,15
800	0,4265	0,598	0,41
825	0,7692	0,281	0,52

Formation kinetics of austenite-martensite transformation during the heat treatment point of view intercritical annealing has long been examined. The formation kinetics of austenite formation in dual phase steel is controlled by diffusion growth. Johnson-Mehl-Avrami equation (JMA) with Kolomogrov (JMAK) can be used to determine for transformation of austenite during intercritical annealing [14].

By modifying the JMA equation, the grain growth rate constant (K) and the Avrami exponent (n) can be determined. It is obtained from the slope and intercept which is resulted from linear equation relationship between ln [ln (1/(1-f□/fe)] versus ln t, as can be shown in Figure.4. From Figure.4, the n and K can be obtained, as listed in Table 1.

Rate constant (K) is a parameter that depends on the temperature and velocity associated with grain growth, nucleation frequency. The higher the heating temperature intercritical annealing point it will increase the value of K [15]. While the Avrami exponent (n) depends on the nucleation and growth processes and the grain nucleation rate has a significant effect on the value of n [14].

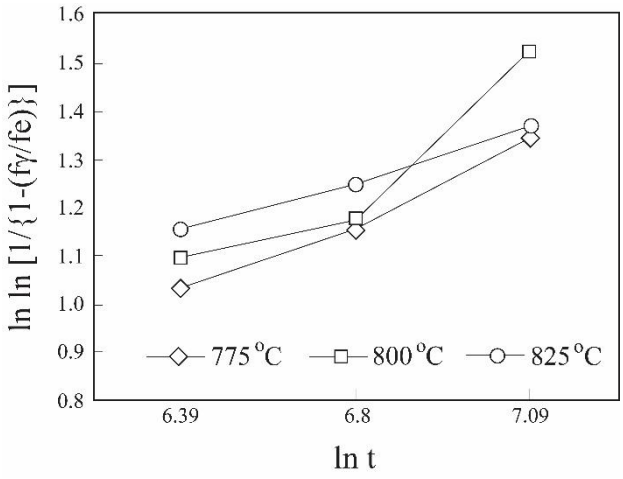

Figure.4. Relationship between austenite volume fraction and heating time from experiment.

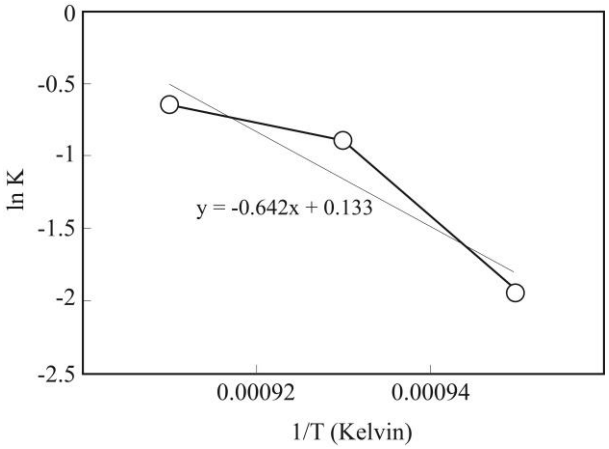

Figure.5. Relationship between K and temperatures based on JMAK equation.

From the data of grain growth rate constant (K), the value of activation energy (Q) and constant (A) can be determined [15]. The value of activation energy (Q) and constant (A) were obtained from the slope and intercept resulting from linear equation between ln K and 1/T, as show in Figure.5. From this relationship, activation energy (Q) and constant (A) will be 267kJ/mol and 2.97 x 1012, respectively.

IV. Conclusion

After the The chemical composition of the investigated steel enables to manufacture the products with the ferritic–martensitic structure by under hardening from the austenite and ferrite area. Dual phase steel shows an excellent combination between strength and ductility due to the coexistence of harder (martensite) and softer (ferrite) phase in their microstructure. The promising hardness was obtained when treatment was performed at 825ºC in comparison to 800ºC and 777ºC. The optimum value was 373 HVN with 78% of martensite. At the optimum point (at volume fraction of martensite approaching 20%), the value of hardness was 184 HVN. Rate constant will increase with increasing heating temperature. In this work, activation energy (Q) of specimen was 267 kJ/mol.

References

[1] K. Buriková, G. Rosenberg. Quantification of microstructural parameter ferritic martensite dual phase steel by image analysis, Metal. 5 (2009) 19-21.

[2] J. Lis, Lis A.K, C. Kolan. Processing and properties of C-Mn steel with dual phase structure, Journal of Mater. Process. Tech. 162-163 (2005) 350-354.

[3] S. Tavares, P.D. Pedroza, J.R. Teodosio. Mechanical properties of a quenched and tempered dual phase steels, Script. Mater. 40 (1999), 887-892.

[4] Ahmad E., Manzoor T., Ali K. L., Akhter J. I., Effect of microvoid formation on the tensile properties of dual-phase steel, Journal of Materials Engineering and Performance, 2000, 9(3), p. 306-310.

[5] M. Erdogan, R. Priestner. Effect of martensite content, its dispersion, and epitaxial ferrite content on Bauschinger behavior of dual phase steel, Journal of Mater. Sci. Tech. 18 (2002) 369-376.

[6] S. Sun, M. Pugh. , Properties of thermo mechanically processed dual phase steel containing fibrous martensite, Mater. Sci. Eng. A, 335 (2002) 298-308.

[7] K.K. Alaneme. Phase transformation studies of a low alloy steel in the (α-γ) phase region, Mater. Res. 13(1) (2010) 113-117.

[8] G.C. Francisca, G.J. Andrea, C. Carlos, G.A. Carlos. Evolution of microstructural banding during the manufacturing process of dual phase steel, Mater. Trans. 47(9) (2006) 2269-2276.

[9] A.K Panda, P.K. Ray, R.I Ganguly. Effect of thermomechanical treatment parameters on mechanical properties of duplex ferrite-martensite structure in dual phase steel, Mater. Sci. and Tech. 16 (2000) 648-656.

[10] K.W. Andrews. Empirical formulae for the calculation of some transformation temperatures, J. of the Iron and Steel Institute. 203 (1965) 721-727.

[11] M. Calcagnotto, D. Ponge, D. Raabe. On the effect of manganese on grain size stability and hardenability in ultrafine grained ferrite/martensite dual-phase steels, Metall, Mater. Trans. A, 43 (2012) 37-46.

[12] S. Sawitree, U. Vitoon. High strength dual phase steels and flow curve modeling approach, The Second TSME International Conference on Mechanical Engineering (2011) AMM34.

[13] G.R. Speech, R.L. Miller. Mechanical properties of ferrite–martensite steels, New Orleans, LA, USA, 1979.

[14] T. Waterschoot, K. Verbeken, B. C. De Cooman. Tempering kinetics of the martensitic phase in DP steel, ISIJ Inter. 46 (2006), 138-146.

[15] Alfirano, W. Samdan, H. Maulud. Effect of intercritical annealing temperature and holding time on microstructure and mechanical properties of dual phase low carbon steel, App. Mech. Mater. 493 (2014) 721-726.

Analysis Growth of Model Von Bertalanffy and Mortality from Fish Kurau (*Polynemustaenitatus*) of The Catch Fisherman in Waters Bunyu (#601)

Gazali Salim[1,a], Pius Bae Kelen[1]
[1]Department Management Resources of Waters
FPIK University of Borneo Tarakan (UBT) Kampus Pantai Amal Gedung E,
Jl. Amal Lama No.1,Po. Box. 170 Tarakan KAL-TARA.
[a] axza_oke@yahoo.com

Abstract.*The aim of the research are analyzing the growth model using Von Bertalanffy and mortality in Polynemus taeniatus. Research methods a descriptive kuantitatif by using the case study. Determining the location of sampling are purposive sampling, by following fishing boats Drift Gill Net. Sampling funded every two weeks once upon a huge tide. Data collection techniques using survey. Data retrieval in the form of total length and total weight. The samples from 4 (times) for 3 months. Each sample taking having vulnerable time between 2-5 day in bunyu waters. Research results use the model von bertalanffy obtained maximum length fish kurau (p.taeniatus) is 156,794 cm in 349 days. Value K of 0.0364 cm. Value To of -1,2819 cm. The results of data processing of fish catch kurau (P.taeniatus) obtained by mortalitas natural 0,435; mortalitas total of 1.121; mortalitas arrest of 0,6859; the exploitation of fish kurau 0,61.*

Keywords *: Growth ; Model Von Bertalanffy; Mortality ; Polynemustaeniatus ; Bunyu Waters*

I. Introductions

Indonesia has one of the having biological resources the sea abounding, because indonesia has tropical climate with the temperature the sea who warm enough for daily necessities and habitat of ecosystem for biota waters.Waters has a temperature of warm so as to cause habitats ecosystem be used as the ecological preference for species of of especially kurau that is in the waters bunyu. This is in accordance with the results of the study of Salim and Kelen (2017) **(1)** explained that based on identification of the fish use drift gill net obtained as many as 12 species yangada in the waters bunyu which is a otek, stingrays, fish selangi, fish machete, snapper white, fish mackerel, fish white sand sharks, fish gulamah, fish arut-arut, fish manyung, red fishes and fish kurau.

Many species of fish on the areas of waters Bunyu, made waters who was in the area a meeting between the pacific ocean and sea sulawesi as waters in accordance with their condition decent for life and many the fishermen catch fish over the areas of waters bunyu island, especially fishermen drift gill net that is the catch thing is fish kurau (P. taenitatus).

Based on the results of the research from Salim and Kelen (2017) **(2)** look at of composition of the fish fishermen used a get drift gill net the main catch of fish kurau (P.taeniatus) as much as 56,04 % with weight about 281,2 kg ; results fish catch a side (HTS) as much as 29,57 % with weight about 148,4 kg and the catch discard of 14,39 % with weigh as much as 72,2 kg.

In addition also according to Salim and Kelen (2017) **(3)** explained that fish p.taeniatus having economic value look at from the price of a high there are two composition the composition of meat is approximately rp.150,000, - / kg and composition ose (bubbles its belly) around rp.5.200.000, -- per kilogram. The growth of fish p.taeniatus have been over do by Salim and Kelen (2017) **(4)** where growth allometri good male and female is allometri negative, where the form of the body a male fish the average thin and bodily form a female the average fat. Research has been done on the P.taenitus is research on study the population with growth allometri and codition index fish of kurau (Polynemus taenitus) acquired in bunyu island waters, north borneo (Salim and Kelen,2017) **(5)** ; Analysis identification the composition catch used a get jarring gills drift (drift gill nett) around island bunyu, kalimantan the north (Salim and Kelen, 2017) **(6)** ; Analysis Growth and Age Structure Fish of Nomei (*Harpodon nehereus*) In Sea Jauta Waters Tarakan City Firdaus (2013) **(7)**.

However research on growth von analysis model bertalanffy and mortalitas of fish kurau (P.taeniatus) of fish catch in waters bunyu, has rarely been implemented.Research purposes and analyze growth use the model von bertalanffy and analyze mortalitas fish kurau (P. taeniatus) of fish catch derived from bunyu waters.

II. Procedure for Paper Formatting

Time and place

Study was conducted for approximately two months, December 2016 until January 2017, begun when collecting first sampling to finish the sampling held in waters off bulungan bunyu district, Province of Borneo North.

Tools and materials

Instrument in use the research is fishing vessels used a catch gill nets drifting (drift gill net), gps, digital camera, the meter and weight.Material used the research is sample kurau fish (p.taeniatus); table tides ; book of idenfication taxonomy fish.

The methodology

The methodology use the methodology descriptive in kuantatif by using the method case study.

The determination of procedure research Locations the sample

Techniques and methods of the using “purposive sampling” , based on the fishing vessels used a catch drift gill net.The sample kurau fish in every two weeks for based on the tide large.The data on the ground in doing some 4 times looping (2 months).

A design study

Methods and engineering in data collection research using design survey.Fish catch kurau (P.taeniatus) derived from catch fishermen using jarring gills drifting (drift gill net) in waters ofbunyu, district bulunganBorneo Northern Province.The samples from 4 (times) for 3 months.

The sample collection done by following fishermen jarring gills drift (drift gill net who made island bunyu for areas of the fish (fishing ground). Each sample taking having

susceptible time between 2 to 5 days in waters bunyu, KabupatenBulungan, North Borneo. Fish at gunpoint by by jarring gills drift (drift gill net), in measuring long total and a total weight.The data in extract of the total length and a total weight.

III. Equations

Growth absolute (absolute)

Model von bertalanffy parameter growth using formulas according to Von Bertalanfy (Sparre & Venema, 1999) with equation as follows :

$$\mathbf{L_t = L_\infty (1-e^{-k(t-t0)})} \qquad \mathbf{(8)}$$

Description :

Lt = long fish nomei at age t (unit time)
L∞ = maximum length fish Kurau theoretically (Lenght asimtotik)
K = the fish growth kurau (per unit time)
t_0 = age teortis fish kurau at length equal to zero

Structure age

To analyze structure, used method of shifting class mode of with a model Von Bertalanffy in Sparre,*et al* (1999) namely:

$$\mathbf{(\Delta L/\Delta t) = (L_2 - L_1) / (t_2 - t_1)} \qquad \mathbf{(9)}$$

$$\mathbf{L_{(t)} = (L_2 + L_1)} \qquad \mathbf{(10)}$$

Description :

ΔL/Δt = Growth relative
ΔL = Length fish
Δt = Interval time
$L_{(t)}$ = Length average modus

Value $L_{(t)}$ dan (ΔL/Δt) obtained a regression linear:

$$\mathbf{Y = a + bx} \qquad \mathbf{(11)}$$

Description :

a = $((\sum y/n) - (b(\sum x/n)))$
b = $(n\sum(xy) - (\sum x)(\sum y)) / ((n\sum x^2 - (\sum x)^2)$

The average value length of a mode of length of this method to count lenght asimtotik (L∞) is a / b , while the coefficients growth (k) is -b.

Age theoretical a fish on when long equal to zero might be expected separately use equation empirical (Pauly in Sparre and Venema, 1999);

$$\mathbf{Log (-t_0) = 0,3922- 0,275(Log L_\infty 1,038 (Log K} \qquad \mathbf{(12)}$$

Description :

L∞ =Length asymptote fish kurau (cm)
K =The coefficients growth rate fish kurau
T =Age theoretical fish kurau at the time long equal to zero (in years)

Mortality

Mortality natural (M) due to allegedly with using formulas empirical Pauly (1984) :

$$\mathbf{Log\ M = -0,0066-0,279 \log L_\infty +0,6543 \log K+0,4634 \log T} \qquad \mathbf{(13)}$$

Mortalitas total (Z) due to allegedly with using formulas Beverton &Holt (Sparre &Venema, 1999) as follows:

$$Z = K \cdot \left[\frac{L_{\infty} - \bar{L}}{\bar{L} - L'} \right] \qquad (14)$$

Mortality Catching (F) as follows :

$$F = Z - M \qquad (15)$$

Rate of The exploitation (E) allegedly using formula Baranov (Sparre & Venema, 1999) as follows:

$$E = \frac{F}{Z} \qquad (16)$$

IV. Figures and Tables

4.1. Structure age

Structure age at fish P.taeniatus having to scatter class as many as 10 classes in processing von bertalanffy model.The results to scatter class was the number of species fish kurau found during 4 times the sample collection.To scatter class the most found on the size the average length of about 79,4 cm and 116 cm with 4 sample. The smallest size of fishes kurau by one sample with size of 59,8 centimeters and of the largest size of fishes kurau as much as two sample with size of 140,2 cm.The following is to scatter class of a structure age based on of the atch the number ocies fish kurau (P. taeniatus).

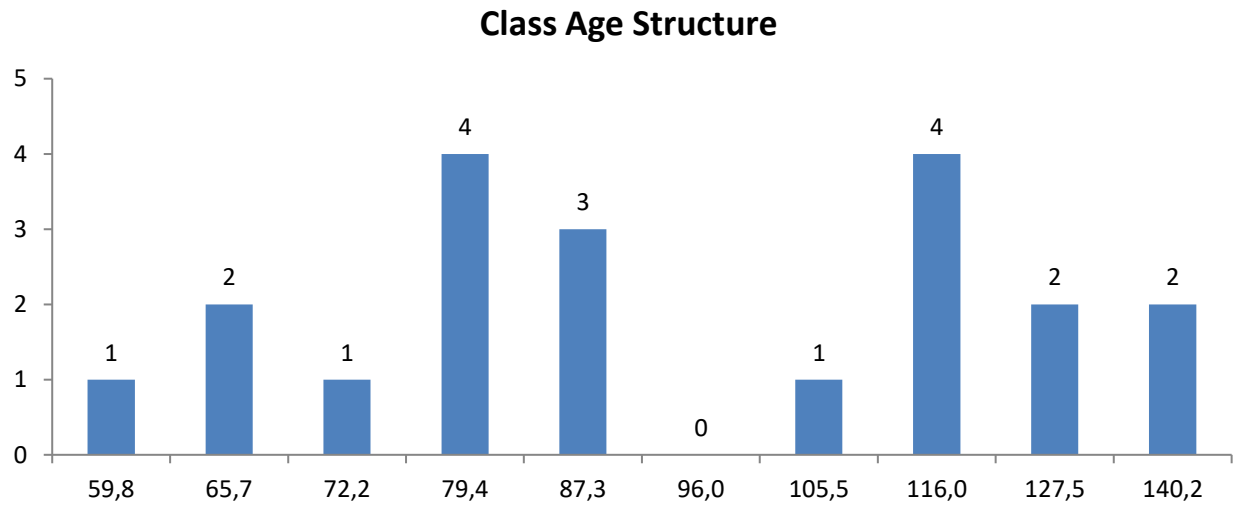

Figure 1. To scatter classes in structure age based on fish catch kurau

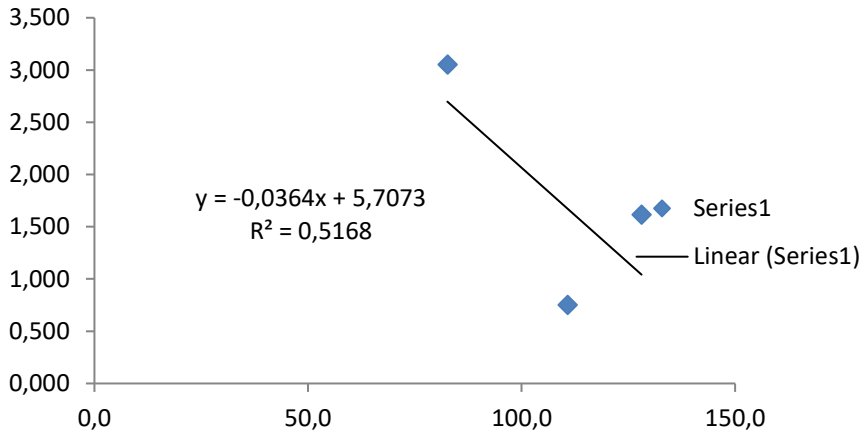

Figure 2 .Age structure fish kurau (P. taeniatus)

In figure 2 elaborate about age structure fish P.taeniatus there were graphs the regression equation is linear.The regression equation is linear in the picture to explain that the regression line is linear when exposed to the axis X, hence the regression line was figures stating that lenght fish from P.taeniatus already have speed zero (see axis Y) by having maximum length of fish worth p.taeniatus 156,794 cm.Charts the regression equation is linear explain that the increasingly increasing fish age hence the speed of growth of fish will decrease so causing long growth of fish will suffer constant. The speed of growth if fish reached the point of zero (constant) then fish has not experienced growth lenght (lenght maximum). This is consistent with the value of the strong correlation worth 0,718. Correlation value this explains that when increase old the fish so rapidity of growth will be more low, and when rapidity of growth fish reach a point zero then growth fish is not experienced growth again (lenght maximum).

4.2. Model Von Bertalanffy

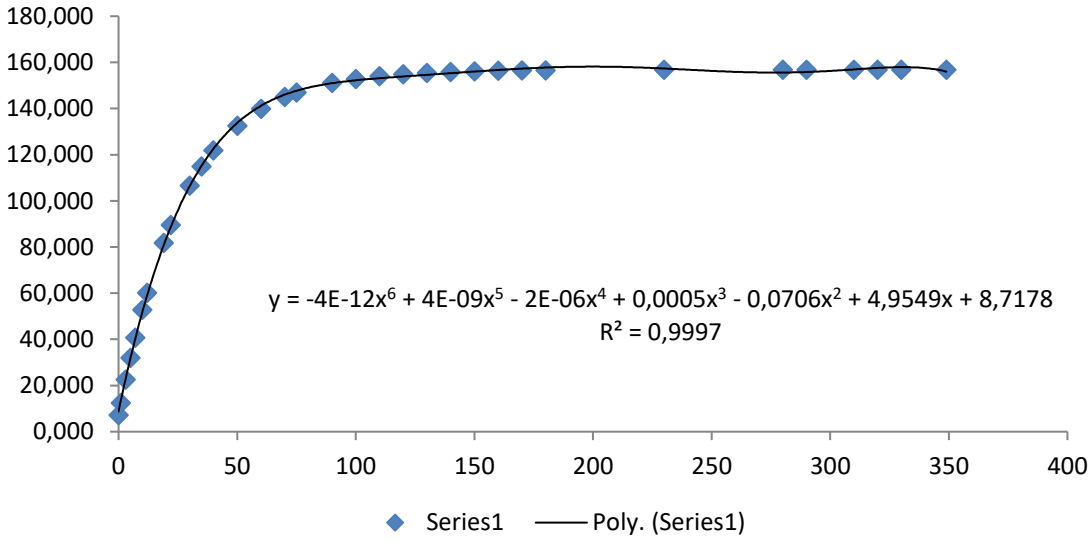

Figure 3.Model von bertalanffy fish kurau (P.Taeniatus)

In figure 3 of what the models von bertalanffy fish kurau (p . Taeniatus) explained that, on the x axis is old the fish kurau and the y axis is long total of fish kurau.The picture describing on equation polynomial orthogonal type 6 in get as follows: y = -4e-12x6 + 4e-

09x5-2e-06x4 + 0.000x3 - 0.07x2 + 4.954x + 8.717 with the r2 = 0.999 and correlation value of 0.999.

A picture model von bertalanffy explained that growth early since fish P.taeniatus entered the stage larvae already has growth by use the model von bertalanffy is as much as 7.148 cm.Growth fish kurau including growth fast enough where growth in when larvae to juvenile growth fast enough to age 90 days to the growth of long as 151,140 cm.

In addition the growth of fish kurau growth slowdown at the age of 100 days to the size of a 152,865 cm to reach growth maximum (L∞) on the size 156,794 cm to the days of about 349 days.The average speed of the growth of fish P.taeniatus 0.0364 cm per day.

4.3 .Mortalitas fish kurau (P. taeniatus)

Mortality on fish kurau there are three parts those are mortalitytotal , mortality the cathcing and mortality natural.The influence of mortalitas an impact on the rate of exploitation.In figure 4 explain who mortality value and the exploitation of fish P.taeniatus.

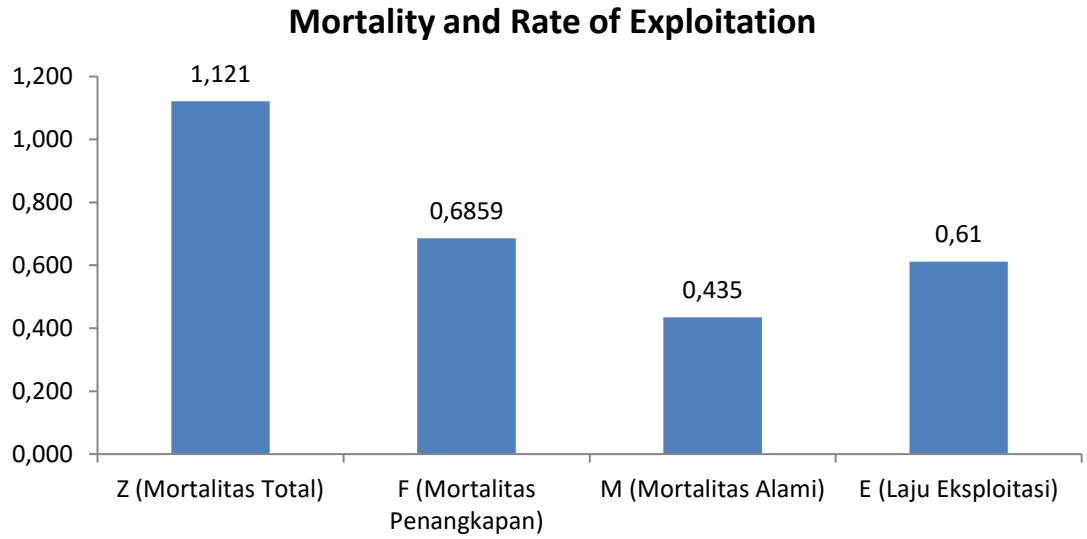

Figure 4. Mortality and Rate of Exploitation fish of Kurau (*P. taeniatus*)

In figure 4 describing on the results of data processing based on fish catch p.taeniatus obtained mortality natural of 0,435 / year; mortality total of p.taeniatus of 1.121 /year and mortalitas because the results of the fish catch fish kurau obtained mortalitas arrest of 0,6859 / year.In addition also berdarakan on the results of data processing derived of the catch fishermen fish kurau obtained the rate of exploitation fish kurau of 0.61 / year.

V. Conclusion

Growth use the model von bertalanffy obtained long maximum is (L∞) as much as 156,794 cm with advanced about 349 day.An average speed growth p.taeniatus of 0,364 cm per day.Growth at the age of zero years reached 7,148 cm. Mortality total (z) = 1,121 per year, mortality natural (M) = 0,435 per year and mortality cathing (F) = 0,6859 per year.The rate of exploitation (E) = 0.61 per year.

References

[1] Firdaus, M ; Salim G ; Ermawaty ; Maya I. A ; Syahrun. 2013. Analisis Pertumbuhan dan Struktur Umur Ikan Nomei (*Harpodon nehereus*) Yang Terdapat Di Perairan Juata Laut Kota Tarakan. (Jurnal Akuatika, Volume 4 Nomer 2 Bulan Oktober Tahun 2013).

[2] Pauly, D. 1984. Fish Population Dynamics In Tropical Waters : a manual for use with programmable calculators. ICLARM.Studies and reviewes) Paperback-1984.

[3] Pauly, D. 1980. A Selection of Simple Method for the Assesment Tropical Fish Stock. FAO. Fish Tech. New York.

[4] Salim G dan Kelen P. B. 2017. Study Population With Growth Allometri And Codition Index Fish Of Kurau (*Polynemustaeniatus*) Acquired In Bunyu Island Waters, North Borneo. ISBN : 978.602.60736-5-5. Procceding10th ADRI 2017 International Multidiciplinary Conference and Call For Paper. Batam, March3-4, 2017.

[5] Salim G dan Kelen P B. 2017. Analsis Identifikasi Hasil Komposisi Tangkapan Menggunakan Alat Tangkap Jaring Insang Hanyut (*Drift Gill Nett*) Di Sekitar Pulau Bunyu Kalimantan Utara. Jurnal Harpodon Borneo Volume 10 No 1 Bulan April 2017. ISSN.2087-121X. Website :http://jurnal. borneo.ac.id/ index.php/harpodon/index

[6] Sparre, P., Siebren C dan Venema. 1999. Introduksi Pengkajian stok Ikan Tropis. Pusat Penelitian dan Pengambangan Perikanan. Badan Penelitian dan Pengembangan Pertanian, Jakarta, 438 hlm.

[7] Sparre, P.E., Ursin and S.C. Venema. 1989. Introduction to tropical Fish Stock Assessment. Part I Manual. FAO Fisheries Technical Paper 306/1.

[8] Sparre, P.E., Ursin and S.C. Venema. 1999. Introduksi Pengkajian Stok Ikan Tropis. Buku Manual I. FAO.

Magnetic and Microstructural Properties of Cobalt Samarium Thin Films Deposited on Niobium Underlayer for Higher Density Magnetic Recording Media (#605)

Erwin Amiruddin[1,a], Salomo, Krisman, Maksi Ginting , Sugianto
[1]Physics Department Faculty of Mathematics and Natural Sciences Riau University
Pekanbaru - Indonesia 28293
[a]erwin251271@gmail.com

Abstract- *The effect of niobium underlayer thicknesses on magnetic and microstructural properties of $Co_{80}Sm_{20}$ thin films deposited on silicon (100) substrates have been studied. These films were fabricated using dc magnetron sputtering technique. Scanning electron microscope (SEM) was used to study the microstructure of the films. The SEM study shows that the grain size and the grain morphology of film becomes more uniform for the films deposited on the thicker niobium underlayers. It was found that the coercivity of the films increases monotonically with increasing niobium thickness up to 100 nm. Further increase of the Nb thickness leads to a decrease of coercivity. The decrease of coercivity value for films deposited on 120 nm thick underlayers could be indicative that the grain size of the niobium underlayer is past the optimum value. Thus the increase and decreases of the coercivity of the films with increasing niobium thickness is discussed.*

Keywords— *magnetic, microstructural properties, exchange interaction, and magnetic thin films.*

I. Introduction

Over the last decades, interest in Co_5Sm alloys in the form of thin films has increased very significantly. This is due to high value of magnetocrystalline anisotropy constant of 1.1 x 10^8 erg/cm^3 that possessed by these alloys [1]. Fundamental research studying various microstructure with corresponding magnetic properties have utilized thin films of cobalt samarium alloys for various applications namely high density magnetic recording media[2], electromagnetic microactuators[3] and microwave devices[4]. According to *Murdock et al.* [5] thin films for high-density magnetic recording media require a material consisting of small and magnetically isolated grains of about 10 nm or below. Several methods[6,7,8] have been reported for fabrication of thin films for high density magnetic recording media. However, thin films with controlled geometry and surface smoothness as well as composition can be prepared by the magnetron sputtering method.[9] . One of the advantages of the sputtering technique compared to other techniques is that it is capable of producing thin films with uniform thickness and composition over large areas.

The magnetic properties of cobalt samarium thin films are determined by their microstructure. However, controlling the microstructure is quite difficult. Deposition of cobalt samarium films at room temperature or lower results in an alloy with an amorphous structure

which has low magnetic anisotropy.[10] There has been a number of significant attempts to improve the magnetic properties of cobalt samarium films. These have included the use of appropriate underlayer materials, that is the layer between the substrate and magnetic layer,[11] as well as depositing the film at high substrate temperature.[12,13] Recently, several underlayer materials such as bcc alloys of Cr, including CrCo, [14] and CrMo, CrTi and CrV[15] have been used between the substrate and magnetic layer in order to control the Co alloy grain size and epitaxy. In this work, we investigated the effects of niobium underlayer thicknesses on the magnetic and microstructural properties of the cobalt samarium thin films.

II. Experimental Procedures

Thin films of cobalt samarium on niobium underlayer were deposited on silicon (100) substrate at room temperature using dc magnetron sputtering technique. The composition of cobalt samarium alloy thin films was obtained by adjusting the power of magnetrons. In order to obtain an atomic ratio of 5:1, then the magnetron power of cobalt and samarium was kept constant at 100 watt and 25 watt respectively. The pressure of sputtering chamber prior to deposition process was 5 x 10^{-8} mbar, while argon gas during the film fabrication was 8x10^{-3} mbar. The thicknesses of niobium underlayer was varied from 20 to 120 nm. The films were protected using gold overlayer.

Magnetic properties were studied using alternating gradient force magnetometer (AGFM) in the applied magnetic field up to 3000 Oe. The structural properties of the films were analyzed using X ray diffraction (XRD) technique. The film composition was determined using energy dispersive x-ray spectroscopy (EDX). The microstructural properties of the films were examined using scanning electron microscope SEM.

III. Results and Discussions

X-ray diffraction analysis of the films deposited on niobium underlayer performed using a Siemens D500 XRD with CuK_α radiation of wavelength λ = 0.15405 nm are shown in Fig. 1. It is clear that the diffraction pattern exhibits two clear maxima that are from an samarium oxide (Sm_2O_3) peak and the (110) plane of the body centered cubic (b.c.c) niobium underlayer. The *d*-spacing value for this line is 0.235 nm. No crystalline diffraction peaks can be observed from any of the cobalt samarium films, suggesting that the crystal size of the films is too small to show well defined peaks. This result is agree well with the results of previous researchers [16,17,18] From these results, it is probable that the grain size of the niobium films was comparatively small with the presence of some oxide. The orientation texture of the niobium films is as expected.

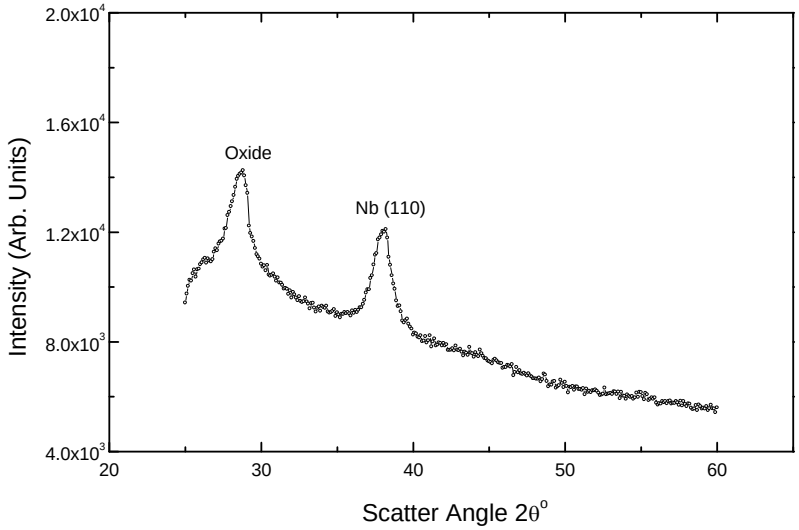

Figure 1. X-ray diffraction pattern of cobalt samarium film deposited on niobium underlayer

The composition of the cobalt samarium film examined by EDX in SEM is $Co_{80}Sm_{20}$ which is close to the composition of Co_5Sm. The magnetic properties especially coercivity of the films are affected significantly by the presence of the underlayer materials. The coercivity of the films increases monotonically with increasing niobium thickness up to 100 nm. Further increase of the niobium thickness leads to an apparent decrease of coercivity. The decrease of coercivity value for films deposited on 120 nm thick underlayers could be indicative that the grain size of the niobium underlayer is past the optimum.[19] In general, the enhancement of the coercivity of the films deposited on this underlayer material could be due to enhanced topography-induced isolation and increased size of the magnetic grains.

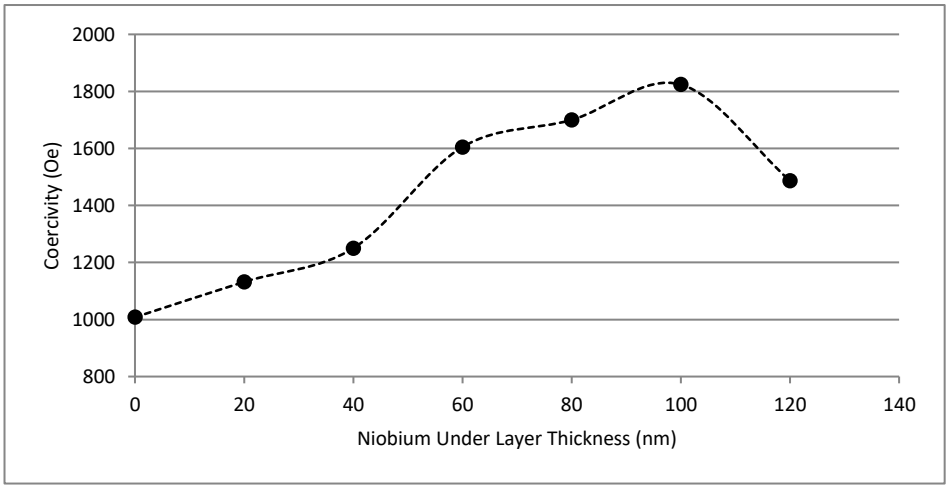

Figure 2. Dependence of coercivity of cobalt samarium thin films on the niobium underlayer thicknesses.

Figures 3 shows hysteresis loops for $Co_{80}Sm_{20}$ thin films without niobium underlayer and with niobium underlayer. It is clear that the coercivity increases and the remanence or loop squareness (M_r/M_s) of these films decreases from 0.95 to 0.90 as the underlayer thickness increases from 40 nm to 100 nm. The reason for the increase of the coercivity of $Co_{80}Sm_{20}$ films deposited on thicker niobium underlayers could be due to more separation

between grains, as shown in SEM micrographs (Fig. 6). The increase of the coercivity value is also indicated by a reduction of the exchange interaction between the grains, as indicated in Fig. 5. The hysteresis loops for films deposited on niobium underlayer exhibit a small kink in both field directions i.e., near zero field as shown in Fig. 4 (b) and (c) , indicating the presence of either a second soft phase or low field nucleation phenomena that initiates magnetization reversal.[20] Notice also the diamagnetic contribution to the loops from the substrate at higher applied field. Moreover, The hysteresis loop squareness of films deposited on niobium decreases as underlayer thickness is increased. A similar result in hysteresis loop squareness is observed in ternary alloys, such as Co-Ni-Pt thin films deposited on NiP/Al substrates and on Cr underlayers[21] and attributed to a reduction of grain separation.[22]

It also can be noticed that the coercivity values of the films deposited on niobium underlayer with the thickness of 100 nm, the coercivity of the films was more than 1.5 times larger than those without underlayers. This enhancement in coercivity values could be due to the microstructure of the $Co_{80}Sm_{20}$ films, which is different for different underlayers thicknesses.

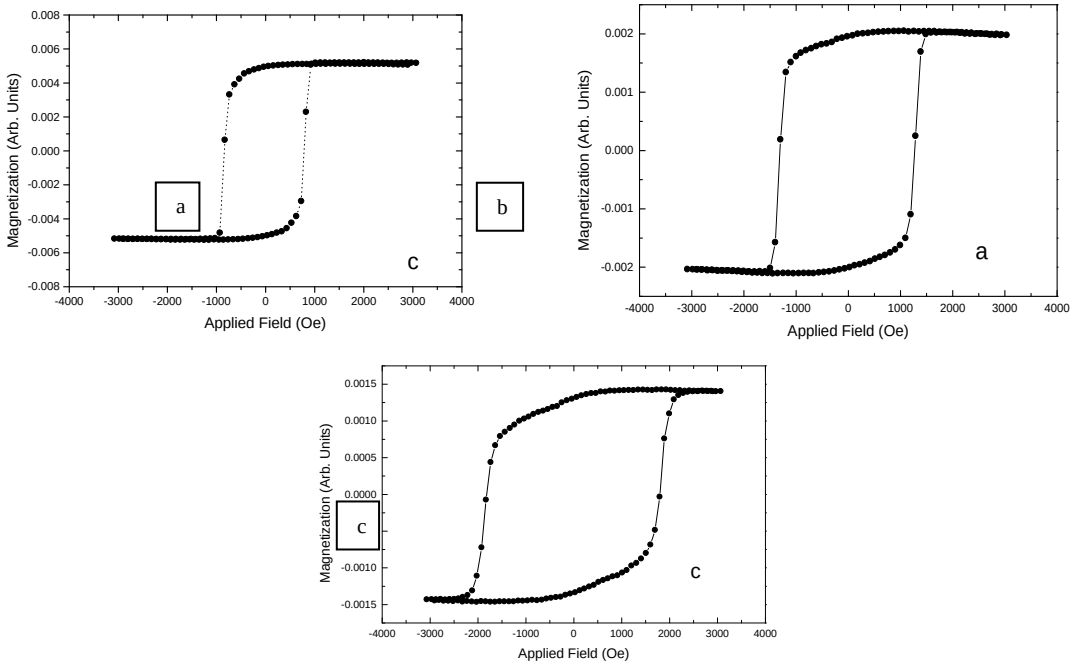

Figure 3 Hysteresis loops of $Co_{80}Sm_{20}$ thin films (a) without niobium underlayer (b) deposited on 40 nm niobium underlayer and (c) deposited on 100 nm niobium underlayer

Figure 4 shows the intergranular exchange interaction plots of $Co_{80}Sm_{20}$ films deposited without niobium underlayer and with niobium underlayer for two different thicknesses. The intergranular exchange interaction can be qualitatively estimated by the δM method.[23] The thickness of niobium underlayer is found to influence the intergranular exchange interaction intensity. It is clear that with increasing niobium underlayer thickness the positive maximum interaction value decreases, indicating reduction of intergranular exchange interaction and also suggests that intergranular exchange coupling is much larger than any magnetostatic interaction between the grains of the films. The increase of the average grain separation of $Co_{80}Sm_{20}$ thin films, as shown in Fig. 5, causes the decreases of

intergranular exchange coupling. The decrease of intergranular exchange coupling could be one of the reasons for any increase of observed coercivity.

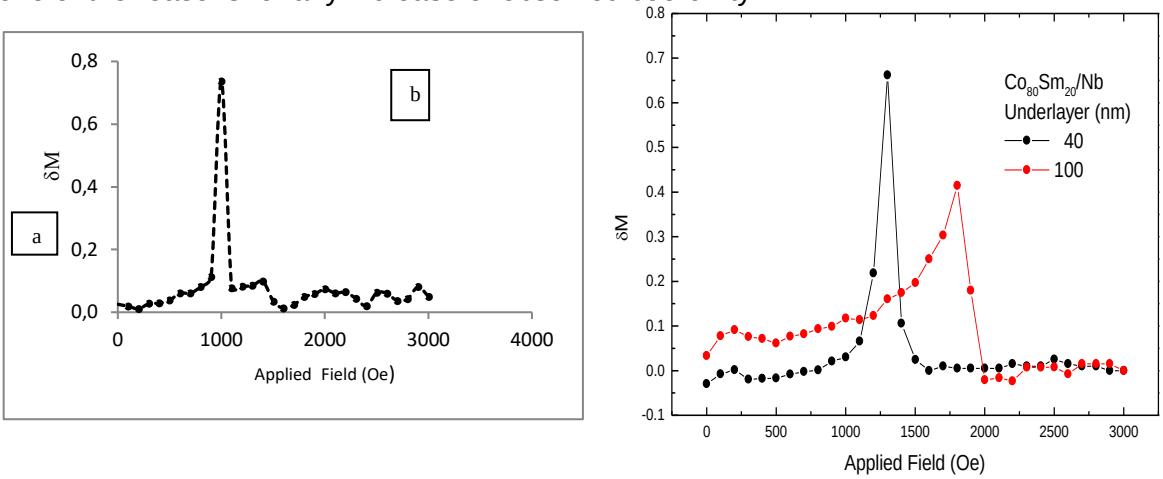

Figure 4. Intergranular exchange interaction of $Co_{80}Sm_{20}$ films for (a) without niobium underlayer, (b) with 40 nm and 100 nm thick niobium underlayer

Thin films of $Co_{80}Sm_{20}$ deposited on niobium underlayer materials of different thickness was investigated by observing the grain morphology using scanning electron microscopy (SEM). The plan view SEM micrographs shown in Fig 5 display an important effect of this underlayer material on the grain morphology of $Co_{80}Sm_{20}$ thin films.

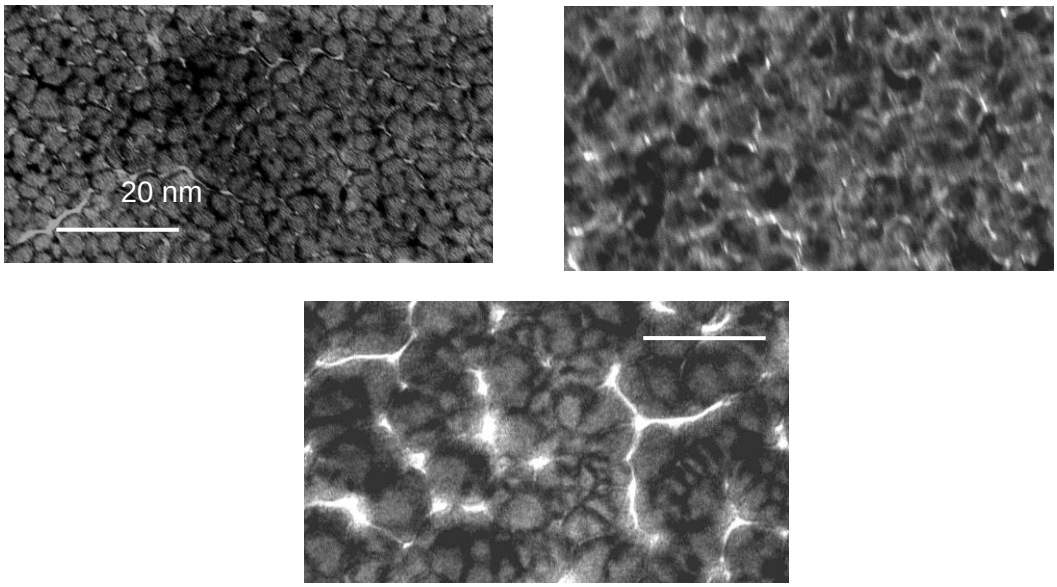

Figure 5. Microstructure of $Co_{80}Sm_{20}$ thin film deposited on (a) without underlayer and with different niobium underlayer thicknesses (b) 40 nm and (c) 100 nm

Films deposited on a 40 nm thick niobium underlayer show irregularly shaped grains with narrow voided boundaries. The coercivity of 1290 Oe was obtained with high loop squareness (*S*) of 0.95 and the high intergranular exchange interaction shown in Fig. 4. Depositing films on a 40 nm thick niobium underlayer leads to an increase in the grain size and the grain morphology of film becomes more uniform than that deposited on the thinner niobium underlayers. It can also be seen that the grains are separated from neighbouring grains by wider void boundaries compared to those in Fig. 5(a). The increase of the

coercivity is possibly associated with this effect. However, films grown on a 100 nm thick niobium underlayer, Fig. 5(c), showed a remarkably different grain morphology from the film grown on the thinner niobium underlayers. The grain morphology becomes even more uniform with sub-grains having a diameter of 2 nm to 5 nm. These fine sub-grains inside the large grains are very obvious.

IV. Conclusion

The results of this research are The coercivity value of 1820 Oe are obtained in cobalt samarium thin films deposited on a 100 nm thick niobium underlayer, that is more than 1.5 times larger than that without underlayers. The SEM observation for plane view of cobalt samarium thin films has revealed different grain morphology from the film deposited without niobium underlayers. The grain morphology becomes even more uniform for cobalt samarium deposited on thicker niobium underlayer namely 100 nm thick. The XRD profile shows no crystalline diffraction peaks that can be observed from any of the cobalt samarium films, implying that the crystal size in the films is too small to show well defined peaks. The decrease in intergranular exchange interaction in the film implies that the niobium underlayer plays a very important role in decoupling the grain in the cobalt samarium thin films.

Acknowledgments

The authors would like to acknowledge P.J. Grundy at Salford University England for helping fabrication of the thin films and also for his valuable discussions of the manuscript. We are also thankful to C.A Faunce for his technical advice and SEM analysis. Thank also goes to Mr. Brian for showing the authors how to prepare SEM Samples.

References

[1] K. J. Strnat, “Rare earth-cobalt permanent magnets,” in *Ferromagnetic Materials*, E. P. Wohlfarth and K. H. J. Buschow, Eds. Amsterdam,The Netherlands: North-Holland, 1988, vol. 4, pp. 131–209

[2] D. Weller, A. Moser, L. Folks, M. E. Best, W. Lee, M. F. Toney, M. Schwickert, J.-U.Thiele, and M. F. Doerner, “High K Materials Approach to 100 Gb/in ,” *IEEE Trans. Magn.*, vol. 36, no. 1, pp. 10–15, Jan. 2000.

[3] T. Budde and H. H. Gatzen, “Thin film SmCo magnets for use in electromagnetic microactuators”, *J. Appl. Phys*., vol. 99, pp.08N304-1-3, Apr 2006.

[4] B. K. Kuanr et al., “Increasing operational frequency in microwave devices by using [SmCo/NiFe] multilayered structures”, *IEEE Trans. Magn*, vol. 43, no. 6, pp. 2648-2650, Jun 2007.

[5] E. S. Murdock, R. Simon & R. Davidson. Intermag ’92, St. Louis, Missouri USA, 1992.

[6] H.C. Theuerer, E.A. Nesbitt, and D.D. Bacon, *J.* ***Appl.*** *Phys.,* vol. **40,** pp. 2994-2996, 1969.

[7] M**.** Gronau, H.Goeke, D. Schuffler, and S. Sprenger, *IEEE Trans. Magn.,* vol. **19,** pp. 1653-1655, September 1983.

[8] K. Kumar, D. Das, and E. Wettstein, *J. Appl. Phys.,* vol. **49,** pp. 2052- 2054, March 1978

[9] P. Robert, '*Thin Film Process II*', Edited by J.L. Vossen and W. Kern, Academic Press, Inc, pp 177, 1991.
[10] F.J. Cadieu, T.D. Cheng, L. Wickramasekara N. Kamprath, H. Hedge andN.C. Liu, J. Appl. Phys., **62**, 3866, 1987.
[11] Y. Okumura, H. Fujimori, O. Suzuki, N. Hosoya, X.B. Yang and H. Morita, IEEE Trans. Magn., **30**, 4038, 1994.
[12] H.C. Theurrer, E.A. Nesbitt, D.D. Bacon, J. Appl. Phys., **40**, 2994, 1969.
[13] F.J. Cadieu, T.D. Cheung, and L. Wickramasekera, J. Appl. Phys., **57**, 4161, 1985.
[14] J.K. Howard, R. Ahlert, and G. Lim, J. Appl. Phys., **61**, 3438, 1987.
[15] M.A. Parker, J.K. Howard, R. Ahlert, and K.R. Coffey, J. Appl. Phys., **73**, 5560, 1993.
[16] Y. Liu, D.J. Sellmyer, B.W. Robertson, Z.S. Shan, and S.H. Liou, IEEE Trans. Magn., **31**, 2740, 1995.
[17] Y. Liu, B.W. Robertson, Z.S. Shan, S.H. Liou, and D.J. Sellmyer, J. Appl. Phys., **77**, 3831, 1995.
[18] Y. Okumura, H. Fujimori, O. Suzuki, N. Hosoya, X.B. Yang and H. Morita, IEEE Trans. Magn., **30**, 4038, 1994.
[19] Q.Peng, H.N. Bertram, N. Fussing, M. F. Doerner, M. Mizamaani, D.Margulies, R. Sinclair, and S. Lambert. IEEE Tran. Magn., **31**, 2821, 1995.
[20] M.L. Yan, Z.S. Shan, Y. Liu and D. J. Sellmyer, IEEE Trans. Magn., **33**, 3706, 1997.
[21] M. Nahvan, A.M. Zeltser, D.N. Lambeth, D.E. Laughlin and M.H. Kryder, IEEE Trans. Magn., **26**, 2277, 1990.
[22] S. Miura, T. Yamashita, G. Ching and T. Chen, IEEE Trans. Magn., **24**, 2718, 1988.
[23] P.E. Kelly, K. O'Grady, P.I. Mayo, R.W. Chantrell, IEEE Trans. Magn., **25**, 3881, 1989.

Interaction Effectiveness Measurement on Traditional Game for Children using Relative Manipulation Time Method (#614)

Maharani Asri Rahayu[1], Mira Kania Sabariah[2,a], Veronikha Effendy[3]
[1]Telkom University, Bandung, Indonesia
[a]mirakania@telkomuniversity.ac.id

Abstract. *Game application has lacked in training children's cognitive and motoric skills. However, a number of reviews stated that game application is able to help children in training children's motoric skill especially in the period of children's motoric development. Based on that, a study related to measuring the use of interaction tool to determine the extent of the game application in helping motoric development was conducted. In this study, several pairs of children were involved by playing the "congklak" game based on mouse, touch screen and using traditional equipment as value benchmark. Evaluation was conducted by identifying the variable value in calculating interaction which has been determined. The result showed that interaction based on touch screen has higher value in training children's motoric and cognitive skills compared to interaction based on mouse. The score was better compared to traditional equipment at several variables.*

Keywords **:** *Game Application*, *Interaction*, *indirect physical manipulation,* 'congklak', *user experience, touch screen, mouse,* traditional.

I. Introduction

Nowdays, technology has developed rapidly and been able to create things related to chidren's daily activities, especially in the form of digital games. Some reports also stated that children are increasingly using computer technology[7]. Children are using computers to perform tasks related to their occupation as a school student, to support their hobbies and leisure interests[8]. This kind of game enables us to carry out an act in indirect physical interaction and provides a user experience which can resemble the real thing.

A number of assumptions are around in which by helping users carry out something using digital equipment, it willthen be more beneficial. What is meant by beneficial here is it is more efficient and effective [1]. However, this is in contrast to the statement that all kinds of human cognitive activities will weaken if the use of hands are obstructed. [1]. From the assumptions, they indirectly state that indirect physical manipulation is not preferable in training cognitive and motoric skills. Especially in this context, it is on children. This is important to be learned because especially for children, the role of hands is essential in children's growth and development in terms of cognitive skill [6].

Referring to the above assumptions, in this study, interaction value calculation based on certain variables will be conducted and its effectivity will be analysed, in which it is closely related to supporting child's growth and development. The study will use the game of 'congklak'. It was chosen because according to child's psychologist, the game of 'congklak' is able to train child's cognitive and motoric skills.

II. Literature Review

‘Congklak’ Traditional Game

‘Congklak’ is a game consisting of two equipments. The equipment is a long board usually made of wood. The board has hollows/holes on the right and left sides and a larger hole at both ends. This game is played using seeds or rocks. The seeds can be from ‘sawo’, candle-nut, corn, etc. It even can be played using rocks or shells [2]. Figure 1 is ‘congklak’ traditional game equipment.

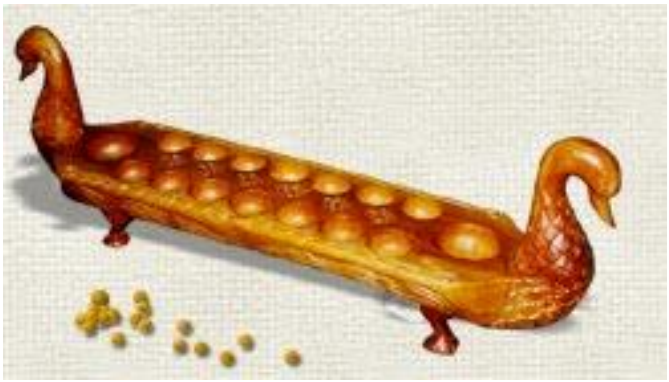

Figure 1. ‘congklak’ traditional game equipment

Each side of the board consists of 5-9 holes depending on the origin of the board. For boards which have seven holes on each sides, the total number of seeds is therefore 98 ‘congklak’ seeds.The following is how ‘congklak’ is played in general [3]:

1) Make sure that there are seven seeds in each own’s hole and opponent’s hole. Keep the end home hole (located at the very ends) empty.
2) Determine the first player. (Can be done by tossing/making a deal)
3) The first player will take the seeds from his/her side and will place a seed in each hole clockwise, but will skip the opponent’s home.
4) When the last hole is given a seed and there are seeds already inside, continue playing like the beginning.
5) When the last hole filled with seeds is the player’s own hole, continue playing as the beginning.
6) When the last hole filled with seeds is actually empty, the turn therefore ends.
7) When the last hole filled with seeds is actually empty and the hole is the player’s own, check the opponent’s hole. If there are seeds then the seeds can be taken and put into the player’s own home hole.

8) The game ends when the players run out of seeds in each of the holes on his/her side.

9) The winner is the one with the most seeds in the home hole.

With the development of time, there are more technological *games* which can create a *user interface* and *experience* resembling the original games. There are many forms of interactions that can be used, one of which is interaction using *touch screen* and *mouse.*

In figure2, it is an example of 'congklak' game which can be downloaded in *playstore*. In the beginning of the game, players will touch the hole to select which seeds to be distributed. The distribution of seeds will move automatically. Besides movement automation, score can also be shown by the system. Similar to the *mouse* based. The only difference is on the use of a*mouse* to manipulate the game.

Figure 2. Sample of touch screen based 'congklak' Child (*Late Childhood*)

Childhood period basically begins from the age of 2 years up to 12 or 13 years. This period is divided into two namely Early childhood at the age of 2 – 6/7 years and Late Childhood at the age of 6/7 – 12/13 years [6]. The term children is usually elementary school age children. Besides that at the period of growth children have the characteristics of the period when they learn to adapt, likes to be in groups, there is an urge to achieve, fight/argue, etc. Some research reported that by the time children grow up, their skill at tapping and dragging items on digital skill are getting better[10]. These are factors that must be considered in child growth:

1) Increasing physical and motoric ability. Fine motoric for example are writing and drawing. Gross motoric are for example games and sports.

2) Building a healthy attitude about themselves.

3) Developing basic skills of reading, writing and counting.

4) Developing concepts on the surrounding/the environment.

5) Developing moral behaviour.

6) Learning to cooperate with peers.

7) Learning to play a role according to gender.

8) Developing an attitude towards social groups.

9) Learning to become an individual who can be independent.

B. Cognitive and Motoric

Motoric development is one in the element of body movement control through the coordinated activities of the central nervous system, neurons and muscles. Motoric development consists of two kinds: gross and soft motoric. Gross motoric is activities carried out by the large muscle such as running, standing up, walking, etc. Soft motoric is activities conducted by small muscles namely writing, reaching for things, etc[6].

Child's cognitive development at the age of 6-12 years is put into the 3rd period. In this period, a child develops his/her brain for thinking systematically but limited to objects or behaviour which is concrete. Surely they are now able to carry out variety of mental operations. For example, they are able to communicate, clarify, do mathematical operations, and connect series of facts [6]. For the children itself, different kind of interaction style can trigger different kind of communication[9]. Based on Piaget's theory, there are four stages of cognitive development [11]:

1. **Sensorimotor stage**: In this stage child begin to develop new intellectual abilities. They start to recognize some symbol.
2. **Pre-operational stage** (Toddler and Early Childhood): In this stage, children understand the use of symbols and language use matures. Memory and imagination are developed, but thinking is done in a nonlogical, nonreversable manner.
3. **Concrete operational stage** (Elementary and early adolescence): They start to understand logical and systematic manipulation of symbols related to concrete objects. Operational thinking develops (mental actions that are reversible).
4. **Formal operational stage** (Adolescence and adulthood): In this stage, they start to understand about abstract concepts.

C. Interaction Style

Interaction *style* is all kinds of ways that can be done to communicate or interact between computer and *users*[4]. The selection of an interaction also can affect the dialog process being conducted. There are several kinds of *interaction styles* which are generally used [5], namely Command Line *Interface,* menu, natural language, query dialog, form-fills, WIMP, point-and-click, three-dimensional *interfaces.*

D. Interaction Testing Variable

In order to explore interaction value based on *mouse* and *touch screen*, testing using method by considering several variables which have been determined is conducted. These

variables will be tested using the formula of *Relative Manipulation Time* (RMT). The following is the explanation of variables which will be used for this case [1].

1. *Time to First Completion*

   The entire time needed from starting the *task* to the end of *task* is for the first time. In this case, children are allowed to play more than once. However, what is to be used as test material is the session in which the children play for the first time.

2. *Time Spent Manipulating Pieces*

   This variable will calculate time which the *users* spend to manipulate object in the *task* in the first time game. There are three *tasks* which will be considered by this variable, namely:

   - *Relative manipulation time* (RMT) : When *users* starts touching the object to manipulate up to releasing the object.
   - *On task but non-touch* (ONT): When *users* should deal with a *task*, but is not doing it or is not touching the object.
   - *Off task (OffT)*: Time when *users* is actually not at the time of doing *task*.

3. *Direct Placement*

   Condition when a *user* is doing object manipulation quickly and without a doubt. In this case, the *user* will directly take a specific object without a doubt and hand follows eye direction. For example, when children decide to take seeds from a hole without thinking further.

4. *Indirect Placement*

   The condition when *users* need time to decide what to be done with the object by manipulating or thinking. In this case, cognitive plays a big role in physical action to be carried out. For example, when children take a moment of silence and observe seeds in the hole before taking one of them.

E. Relative Manipulation Time

Relative Manipulation Time (RMT) is a formula to calculate proportion of relative time spent by *users* to carry out *task* done according to the form of interaction [1]. In the calculation of interaction testing, a formula which can be used to calculate RMT, RONT, and RoffT was developed. From “Hands on What? Comparing Children’s Mouse-based and Tangible-based Interaction” paper by Antle, the following is example of formula used to calculate RMT.

$$RMT_{CT1} = \frac{[MT_{CT1} \text{ subject a} + MT_{CT1} \text{ subject b}]}{[2*CT_1]} \quad (1)$$

The above formula is used to calculate variables in *time spent manipulating pieces*. Here, MT (*manipulation time*) on subject is time used by *users* at condition of RMT, ONT, or OffT. CT (*completion time*) is game time from the beginning to the end. In general, RMT_{CT1} is the total MTs from each *user* divided by n multiplied by CT_1 (where n is the total number of *users*). In this case n is 2 because each session is played by a pair of kids. For example, $T_{CT1} = 0.75$ means 75% of time is used to manipulate objects to accomplish the game.

III. Methodology

a. Application Display

User interface(UI)that has been made will be used for both types of interaction based on *mouse* in PC device and based on *touch screen* in tab device. UI made is made based on several things prepared beforehand. These are :

1)Data collecting and observation on 'congklak' game and users.

2)Modelling user experience including within it analysing user's persona. After obtaining persona from each user, the user's persona will be grouped based on high persona user, middle persona user, and low persona user. The classification is based on their ability in manipulating technology and playing 'congklak'. For middle persona user with a relatively lower ability in playing, a special training is provided so that their ability is the same as high persona user.

3)Creating conceptual model which will become the base of application prototype.

4)The application prototype is tested on users using Heuristic Evaluation testing.

b. Interaction Variable Testing

After the *game* application is made based on data collected and going through *heuristic evaluation* testing phase, the application is ready to be used for interaction variable testing. Each of the three types of s interaction will be measured its interaction value and the interaction using traditional equipment will become a benchmark.

Figure 3 is the *sample pattern interaction play* carried out by a child in one game period. In one game period, a child conduct activities of RMT (orange), RoffT (blue), DP (red), and IP (green).

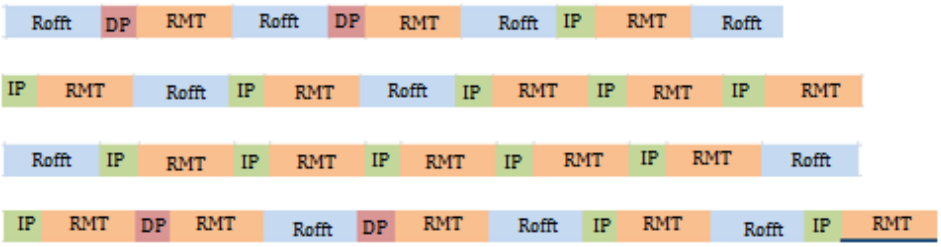

Figure 3. Sample of pattern formed in one game period Time to First Completion

In this variable, the average time spent by each pair in order to complete a game in an interaction was observed. Within 10 minutes, children are free to play. However, just as the definition given in the previous chapter, time here means the entire time used from starting the *task* to the end of the *task* for the first time. This means that time observed is time when first playing.

The following is the result of *time to first completion* calculation as shown in table 2.

Table 2: Table of time to first completion testing result

***Time to first completion* Testing**				
Type of Interaction	**Pair I**	**Pair II**	**Pair III**	***mean***
Traditional	324 s	438 s	600 s	454 s
Mouse-based	509 s	401 s	418 s	442 s
Touch screen-based	355 s	298 s	300 s	317 s

It can seen from the above data that the average longest time to play is found in traditional type interaction and the quickest is found in the *touch screen* based. This data show that the hypothesis on game will be faster completed using *touch screen* based interaction type is proven.

Seeing from the child's behavior in playing 'congklak', one of the factors why *mouse* based interaction is slower is because the child must keep holding the *mouse* and shifting the *mouse* to distribute 'congklak' seeds/beads. The shifts quite increase duration of playing time.

Besides that, the size and weight of mouse also give impact as the shape of children's hands which is on average keementara at *touch screen* based interaction does not require tools and only by touching the screen. This direct hand movement is easier to be carried out than having to shift the *mouse.* Besides the effect of time of hand movement or object manipulation, time spent on thinking or other activities when playing also influence the duration of game. These aspects will be explained in the following variable.

c. Time Spent Manipulating Pieces

As explained, this variable will study in depth how long on average children spend in carrying out several types of object manipulation at each interaction. In this variable, the types of manipulation to be observed are as follows:

1) *Relative manipulation time* (RMT) : When *user* start touching the object to manipulate up to releasing the object.

2) *On task but non-touch* (ONT): When *user* should carry out a *task*, but fail to do so or does not touch the object.

3) *Off task (OffT)*: When *user* actually is not at the time for doing the *task*.

In the case of 'congklak' game used, RMT is when children actively manipulate object or in this case seeds/beads, for example, when it is time for the child to take the 'congklak' seeds/beads one by one. ONT is when it is time for a child to manipulate an object (turn to play) but does not do so, for example, thinking for a while to work out a strategy. OffT is when a child is not playing or in this case waiting for his/her turn to play.

Seeing from the below data of *touch screen* interaction type, it can be seen that the majority of players spent their time in manipulating object effectively (RMT), considering from the previous data on average the games finish faster in *touch screen* interaction, which means that the RMT carried out in this interaction is faster and more effective than other interactions. This has proven the second hypothesis which is the *touch screen* interaction type, spend more time in conducting object manipulation effectively.

The following is the average result of *time spent manipulating pieces* calculation as shown in table 3.

Table 3: Table of time spent manipulating pieces testing result

***Time spent manipulating pieces* Testing**			
JenisInteraksi	**RMT**	**RONT**	**ROffT**
Tradisional	40.7 %	8 %	49.8 %
Mouse	36.1 %	14.2 %	49.4 %
Touch screen	40.5 %	12.4 %	47.2 %

In the data, it can be seen that children spend their time in RONT more on *mouse* interaction than on *touch screen* interaction. More complete explanation can be seen in the following variable.

d. Indirect and Direct Placement

In this variable there are two things that are analyzed namely *direct placement* and *indirect placement.* In the *direct placement* variable, it is a situation in which children manipulate an object directly without the presence of thinking or cognitive activity. *Indirect placement* is a condition where a child carry out a thinking or cognitive activity before conducting object manipulation. Both variables are found in ONT condition. Besides DP and IP, there is Non DP-IP condition in which children do not carry out DP or IP at ONT but carry out activities such as talking/chatting, joking, eating, day-dreaming, etc. The following is the result of *time spent manipulating pieces* calculation average as shown in table 4.

Table 4: Table of DP & IP testing result

DP & IP Testing			
Type of Interaction	**DP**	**IP**	**Non DP-IP**
Traditional	23 %	52.1 %	25.1 %
Mouse	25.3 %	60.1 %	13.8 %
Touch screen	23.1 %	64.1 %	12.7 %

From the above data, it can be seen that IP figure in*mouse* interaction is far higher than DP. This data prove that the hypothesis on pairs will spend more time to conduct *direct placement* in *mouse* based interaction is proven wrong. However, for the hypothesis that pairs will spend time more on conducting *indirect placement* in *touch screen* based interaction is proven right.

Seen from both IP values in both interactions, it can be seen that both figures are higher than traditional. This is influenced by UI factor in *game* application which makes it easy for children to count the seeds/beads.

IV. Discussion

Based on the opinion of an expert in child psychology, a good and effective game of 'congklak' is when children can manipulate quickly and accurately. This is related to the child's motoric growth and development. Besides that, ideally children build strategy first by thinking or counting before they start to take the seeds.

a. Data Analysis Result

From the data obtained and based on opinion of expert, analysis obtained is as follows.

1) In *Time to First Completion* variable, it can be seen that the quickest playing time is found in *touch screen* based interaction and the slowest is found in *mouse*. This is because in interaction using *mouse* tool, it affects the child's movement. Shifts, *mouse,* weight and mouse size compared to a child's hand which is smaller become the main factor why a child's movement is slower. While *touch screen* interaction without using tools frees the players to move thus freer and faster.

2) In *Time Spent Manipulating Pieces* variable, it is proven that children spend time more on manipulating seeds effectively (RMT) found in *touch screen* based interaction.

3) In *direct & indirect placement* variable, seen from the IP figure which is higher than DP, children spend their time more on thinking at both interactions. The factor affecting this is figures at UI which show total number of seeds in the hole or in the hand. This can help a child in thinking and this convenience is able to attract the child's interest in thinking.

4) Both interactions basically can train a child's motoric and cognitive skills. However, from the motoric side, *touch screen* interaction has the fastest playing time and a high RMT value, which shows that *touch screen* interaction trains motoric better than *mouse.*

From the cognitive side, *indirect placement* value from both interactions are both higher than *direct* placement. However, IP figure in *touch screen* interaction is still higher than *mouse.* This shows that children spend their time more on thinking in this interaction. This can be influenced by the position of the child playing, which is horizontal which is similar to the original thus making it easier for children to conduct cognitive activity. For example, a child easily see the total number of seeds in game area and count. However, both interactions are still quite satisfactory in training a child's cognitive skill.

Seeing from the data analysis explained, we can see that there are several things that can be improved to increase interaction value. They are as follows:

1) Playing time in *mouse* based interaction still takes longer than the game of 'congklak'.

2) Ideally in playing, children must think about the strategy first before taking action. Seen from IP and DP figures, both interactions have fulfilled this. However, IP value from *mouse* interaction is still lower than *touch screen.*

Seeing from both aspects that should be improved, it can be concluded that interaction using *mouse* should be improved more. This proves that hypothesis on average variables in *touch screen* interaction testing will show higher effectivity figure is proven.

b. Recommendation for Value Increase

The following are recommendations that can be done in trying to increase such value:

1) By using *game* application with the same UX, *touch screen* based interaction has faster time than *mouse*. Therefore, improvement is focused more on *hardware* used. Use *mouse* in medium size and not too heavy so that children can shift the *mouse* well. Better yet, use good quality *mouse*pads.

2) To increase IP more, it means similar to children who have to do more cognitive activities such as thinking. This depends on the individuals whether each person's thinking ability is already satisfactory or not, whether they wish to think or not. It is the most possible thing to conduct in increasing children's intention to think. This can be done by giving number help using attractive colors. Besides that, at the change of turns, 'congklak's' UI can swivel 180 degrees. Thus, each child is facing the appropriate side.

V. Conclusion

From the result of data and analysis of interaction variables in 'congklak' *game* application which has been processed. Result of variable measurement is a duration of game time in *mouse* interaction is slower than *touch screen* based interaction. The affecting factor is *interaction device* in the form of *mouse* which hampers a child's hand movements. In *time spent manipulating pieces*, the highest RMT time is found in *touch screen*. interaction. This shows that children spend time more on manipulating seeds of 'congklak' effectively (RMT) in *touch screen* interaction. The value of *Indirect placement* cis quite high in both interactions namely *touch screen* and *mouse.* However, these variable figures are influenced by several aspects namely the value of repetition iteration in the testing of HE and *persona user.* In general, evaluation of *touch screen*lbasedintraction is more effective in training chilld's cognitive and motoric than *mouse* based interaction. Factors that can be recommended to optimize interaction value is by considering the*interaction* device used and UI which attracts children's attention to trigger their willingness to thin.

References

[1]. A. Antle, M. Droumeva and D. Ha, "Hands on What? Comparing Children's Mouse-Based and Tangible-Based Interaction", *IDC*, 2009.
[2]. "Congklak, A Traditional Game of Indonesia", *Expat.or.id*, 2016. [Online]. Available: http://www.expat.or.id/info/congklak.html. [Accessed: 12- Apr- 2016].
[3]. "Congklak Instructions - How the game is played in Indonesia", *Expat.or.id*, 2016. [Online]. Available: http://www.expat.or.id/info/congklakinstructions.html. [Accessed: 17- Apr- 2016].
[4]. "Interaction Styles: The Glossary of Human Computer Interaction", *The Interaction Design Foundation*, 2016. [Online]. Available: https://www.interaction-design.org/literature/book/the-glossary-of-human-computer-interaction/interaction-styles. [Accessed: 17- Apr- 2016].
[5]. A. Dix, J. Finlay, G. Abowd and R. Beale, *Human-computer interaction. Third edition*, 3rd ed. Harlow: [Prentice Hall], 2004.
[6]. Santrock, *Life-span development*. Madison, Wis.: WCB Brown & Benchmark Publishers, 1995.
[7]. J. Hourcade, "Interaction Design and Children", *Foundations and Trends® in Human-Computer Interaction*, vol. 1, no. 4, pp. 277-392, 2007.

[8]. L. Straker and C. Pollock, "Optimizing the interaction of children with information and communication technologies", *Ergonomics*, vol. 48, no. 5, pp. 506-521, 2005.
[9]. I. Jamil, K. O'Hara, A. Karnik and S. Subramanian, "The Effects of Interaction Techniques on Talk Patterns in Collaborative Peer Learning around Interactive Tables", *CHI*, 2011.
[10]. R. Vatavu, G. Cramariuc and D. Schipor, "Touch interaction for children aged 3 to 6 years: Experimental findings and relationship to motor skills", *International Journal of Human-Computer Studies*, vol. 74, pp. 54-76, 2015.
[11]. Huitt, W., & Hummel, J. (2003). Piaget's theory of cognitive development. *Educational Psychology Interactive*. Valdosta, GA: Valdosta State University. Available: http://www.edpsycinteractive.org/topics/cognition/piaget.html[Accessed: 5-Mei-2016]

The Feasibility of Desorption on Zeolite-Water Pair Using Dry Gas (#616)

Erfina Oktariani[1,a], Kazuya Nakashima[2], Atsushi Noda[2], Bing Xue [2], Keisuke Tahara[2], Koichi Nakaso[2], and Jun Fukai[2,b]

[1]Department of Polymeric Chemical Engineering, Polytechnic of STMI Jakarta, Ministry of Industry, Jakarta, Indonesia

[2]Department of Chemical Engineering, Faculty of Engineering, Kyushu University, Fukuoka 819-0395, Japan

[a]erfina@kemenperin.go.id, [b] jfukai@chem-eng.kyushu-u.ac.jp

Abstract— *The increase in temperature, reduction in partial pressure, reduction in concentration, purging with an inert fluid, and displacement with a more strongly adsorbing species are the basic things that occur in the practical method of desorption. In this study, dry gas at constant temperature and pressure was employed as the aid to reduce the partial pressure in the water desorption on the zeolite 13X. The objective of this study is to confirm the feasibility of desorption using dry gas experimentally and numerically. The implication of heat and mass transfers were numerically investigated to find the most influential. The results of numerical simulation agree with the experimental ones for the distribution of local temperature and average water adsorbed in the packed bed.*

Keywords— *desorption, zeolite-water pair, dry gas, numerical simulation, heat transfer.*

I. Introduction

ADSORPTION heat pump systems using zeolite-water pairs have been developed since long time ago [1]. Direct contact system between water as working fluid and zeolite as adsorbent has been proposed to develop the adsorption heat pump system for steam generation [2]. The reason for proposing this direct contact system was described in the previous study [2,3]. The possibility for steam generation using this system has been confirmed experimentally although it still could not reach the prediction/ theoretical value. Steam generation is on the adsorption stage. For regeneration of saturated zeolite after adsorption process, inert gas is chosen to strip/release the water content which is believed in vapor/gas phase in the zeolite. From the experimental study before [1], inert gas such as dry nitrogen and dry air can regenerate zeolite for almost 80-90%. But there is problem in desorption study such as long time needed to release/remove water in the zeolite particle in the packed bed which means impractical to be applied in the industries. Long time needed for desorption accomplish means reaction rate occurs slowly.

Study about the solution to increase desorption rate was found in some report used microwave to shorten the time and also could decrease the energy level needed to remove water content in the zeolite [4,5]. Methods for regeneration of saturated zeolite have been investigated in various types [6,7]. General problem in desorption /regeneration process of zeolite is low reaction rate that may be because of high energy required to desorb water

vapor from zeolite. Practical methods of desorption and regeneration including one, or more usually a combination, of the following such as increase in temperature, reduction in partial pressure, reduction in concentration, purging with an inert fluid, displacement with a more strongly adsorbing species, and change of chemical condition such as pH. As a variable for changing thermodynamic potential, a change in temperature is much more effective than a change in pressure. However, the final choice of regeneration method(s) depends upon technical and economic considerations. The most common methods are changes in temperature (thermal swing adsorption) and changes in pressure (pressure swing adsorption). The general advantages and disadvantages of each method together with some process examples.

The main objective of whole study is to regenerate steam from waste water in the industries such as petrochemical industries using the dry inert gas in medium/low level energy (noticed by the temperature degree). Because in the plant, there are plenty amount of gas at around 150 °C exhausted from the cracking furnace. It is wiser to use this gas for the regeneration of saturated zeolite after it producing the steam. In terms of the type of zeolite 13X is hydrophilic adsorbent, thermal swing is better method for desorption [7]. The purpose of this study is to find the best condition of desorption process of zeolite 13X to release the water vapor using dry gas stripping. Therefore the gas condition as the stripper was investigated experimentally and numerically.

II. Research Methods

A. Experiment

Similar with the previous study [2], zeolite 13X was investigated in this study. Two different particle shape of 13X were examined. Initially, zeolite was calcined in furnace at 350 °C for 4.5 hours. Then the dry zeolite were put in a box at high humidity 98% until reached equilibrium condition to get saturated zeolite with water vapor. The mass fraction of water adsorbed in 13X at 25°C under atmospheric pressure is 0.271 kg-water/kg-dry zeolite as theoretical value. In the experiment, the amount of water adsorbed was also around 0.27 kg-water/kg-dry zeolite.

Figure 1 shows the schematic diagram of experimental apparatus. Saturated zeolite was packed in the reactor and kept at constant temperature. Water content in the zeolite particles at 110 °C at initial condition was 0.27 kg water/kg dry zeolite without free water. Free water was obtained from the difference between water concentration in the zeolite after experiment subtracted by the the maximum value of water can be adsorbed in the zeolite (for 13X was 0.27 kg water/kg dry zeolite). Dry N_2 gas at temperature 80 and 140 °C with various flow rates at 10, 30 and 50 L/min were then introduced to the reactor. The mass of water released was obtained by measuring the mass of water vapor in the air at outlet of the reactor.

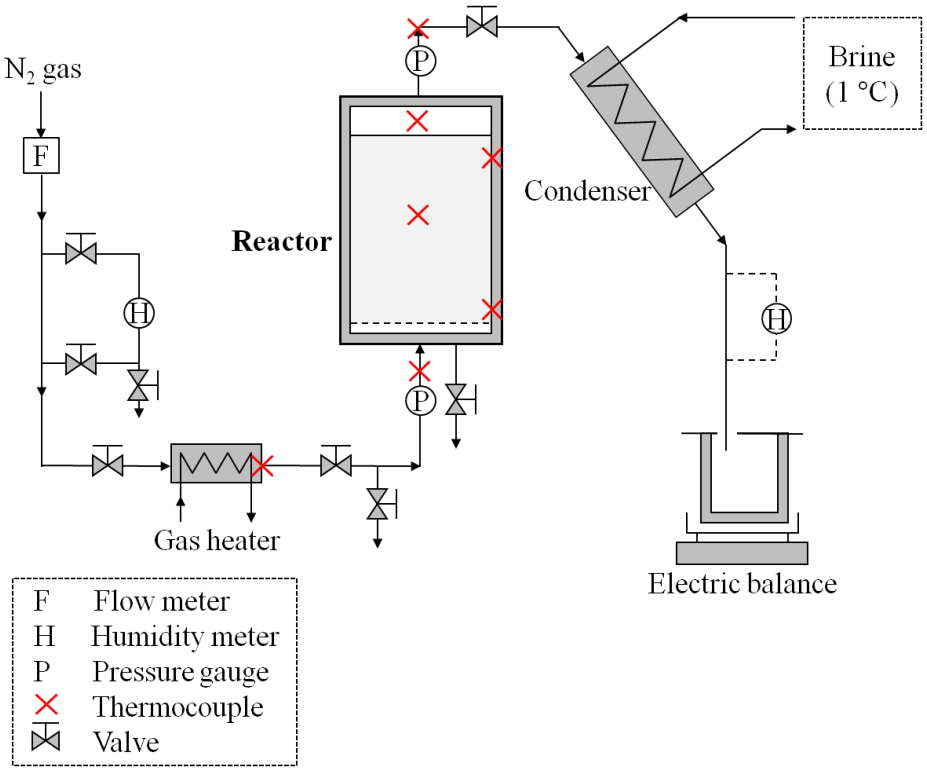

Figure 1. Schematic diagram of experimental apparatus

B. Mathematical Model

Phenomenon during desorption using N_2 gas in packed bed was studied using a two-dimensional cylindrical model (r-z axes). Fig.2 shows scheme of module of the packed bed from the experiment that would be numerically calculated.

The main assumptions in the modeling are:

(a) All the zeolite particles have uniform properties such as geometry and size
(b) The gas velocity (including vapor) in the packed bed is determined using Darcy's equation
(c) The gaseous phase behaves as an ideal gas
(d) The particle is covered by laminar film, bounding the particle from the gas fluid.
(e) Macropores conducts the transportation of gas molecule from inside to the surface of particle.
(f) Molecules of water vapor are only adsorbed on the surface of zeolite crystal, therefore effect of micropores diffusion is not considered.

The governing equations of the studied system consist of energy balance of solid and gas (water vapor and N_2 gas) and mass balance in the solid related to the gas in the pores. Model equations of energy balance, mass balance, momentum, and kinetic model are shown in the following and the computational domain including initial and boundary conditions is shown in Figure 3. The temperature of gas and solid is solved separately.

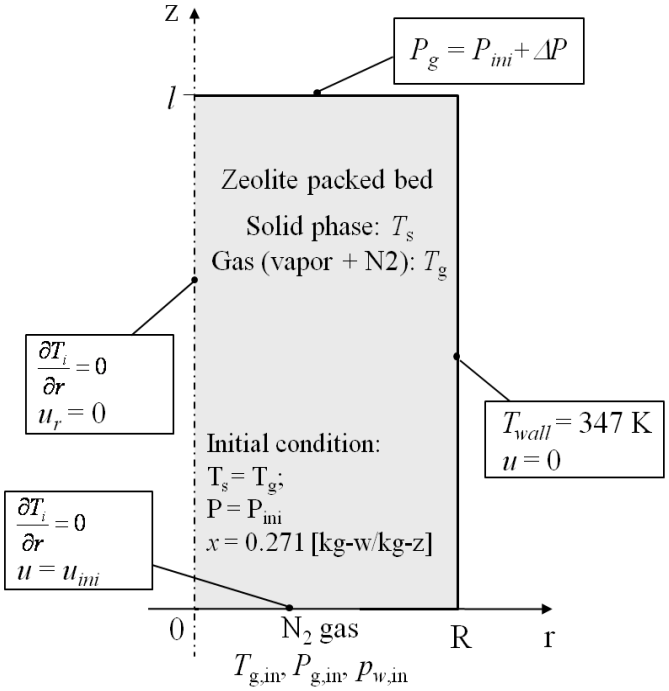

Figure 2. Computational domain, initial and boundary condition of calculation

- Energy balance for solid phase (the zeolite):

$$(1-\varepsilon_t)\rho_s C_{ps}\frac{\partial T_s}{\partial t} = (1-\varepsilon_t)\nabla\cdot k_s\nabla T + (1-\varepsilon_t)Q_0\frac{dv}{dt} + S_{sg}h_{sg}(T_s - T_g) \quad (1)$$

- Energy balance for gas phase (N_2 and vapor):

$$\varepsilon_t\rho_g C_{pg}\frac{\partial T_g}{\partial t} + \rho_g C_{pg}u_g\nabla T = \varepsilon_t\nabla\cdot k_g\nabla T + S_{sg}h_{sg}(T_s - T_g) \quad (2)$$

- Mass balance for the zeolite:

$$(1-\varepsilon_t)\frac{\partial}{\partial t}\rho_s = m \quad (3)$$

- Mass balance for gas phase:

$$\frac{\partial}{\partial t}\varepsilon_t\rho_g + \nabla\cdot(\rho_g u) = -m \quad (4)$$

where m is the desorption rate of water desorbed from zeolite which is defined as the following:

$$m = (1-\varepsilon_t)\Delta\rho_s\frac{\partial v}{\partial t} \quad (5)$$

Gas diffusive velocity *u* is calculated using Darcy's equation as the momentum equation:

$$u = -\frac{K}{\mu}\nabla P \quad (6)$$

with K as the permeability calculating using Kozeny-Carman's:

$$K = \frac{1}{5}\frac{\varepsilon_t^{\,3}}{(1-\varepsilon_t)^2}\frac{1}{S_p^{\,2}} \quad (7)$$

The specific surface area Sp depends on the particle shape is determined by $6/d_p$ and $4/d_p$, for spherical and cylindrical particles, respectively.

Reaction rate model is expressed as below:

$$\frac{\partial v}{\partial t} = k\left(v_{eq} - v\right) \quad (8)$$

where v is the reacted fraction defined from the water content in the zeolite based on thermal analysis (TG/DTA) measurement. Reacted fraction is obtained from:

$$v = \frac{x_0 - x}{x_0 - x_f} \quad (9)$$

Reaction rate controller *k* is defined using Linear Driving Force (LDF) model because diffusion on the surface (external film) of particle and macropores influence the desorption rate.

$$k = k_{LDF} \quad (10)$$

$$\frac{1}{k_{LDF}} = \frac{\wedge r_p}{3(1-\varepsilon_b)k_f} + \frac{\wedge r_p^{\,2}}{15(1-\varepsilon_b)\varepsilon_p D_p} \quad (11)$$

Therefore, the rate controller consists of effect of external film and macropores region, respectively. $\wedge$ is partition ration that represent the fraction of water vapor as adsorbate that is exactly adsorbed in the zeolite particle, expressed as follow:

$$\wedge = \frac{\rho_b x}{\rho_g} \quad (12)$$

k_f as the mass transfer coefficient on the external film is defined using Wakao equation as:

$$k_f = \left(2.0 + 1.1\mathrm{Sc}^{1/3}\,\mathrm{Re}^{0.6}\right)\frac{D_{AB}}{r_p} \quad (13)$$

The gas diffusivity is calculated assuming both Knudsen and molecular diffusion:

$$\frac{1}{D_p} = \tau_p\left(\frac{1}{D_K} + \frac{1}{D_{AB}}\right) \quad (14)$$

with

$$D_{AB} = 1.8583\times10^{-3}\,\frac{\sqrt{T^3/MM_g}}{p\sigma^2\Omega_D} \quad (15)$$

and

$$D_K = 4.85 d_{pore}\sqrt{\frac{T}{MM_g}} \quad (16)$$

where τ_p as the particle tortuosity is determined as the inverse of particle pore ($1/\varepsilon_p$) based on Wakao while the molar mass of gas (nitrogen and vapor) MM_g, defined as:

$$\frac{1}{MM_g} = \left(\frac{1}{MM_{N_2}} + \frac{1}{MM_{H_2O}}\right) \quad (17)$$

Enthalpy of desorption (ΔH), heat capacity (C_{ps}) obtained from DSC measurement and such as frequency factor (A) and activation energy (E_a) obtained from TG/DTA measurement. Kunii and Smith's equation is used to get λ_{eff}. The total number of mesh points in the computational domain are 80×15 with the time step is 10^{-3} s.

The governing equations above are numerically solved using finite element method (FEM). The followings are the discretization of the governing equations which are solved for mass and heat balances separately.

III. Results and discussions

Good agreements of temperature variations with time were obtained for desorption using spherical particles which the flow-rate of Nitrogen gas varies at 10, 30 and 50 L/min at temperatures 80 and 140°C (Figure 3). According to the temperature variations in the center of the bed, flow-rate of Nitrogen gas has big influence in desorption. This is confirmed from the peak of temperature distribution becomes narrower when flow-rate of inlet gas increased. Higher flow-rate will influence the distribution because it can reduce the pressure drop in the bed (Eq. 6) and increase the heat transfer coefficient (Eqs. (1) and (2)).

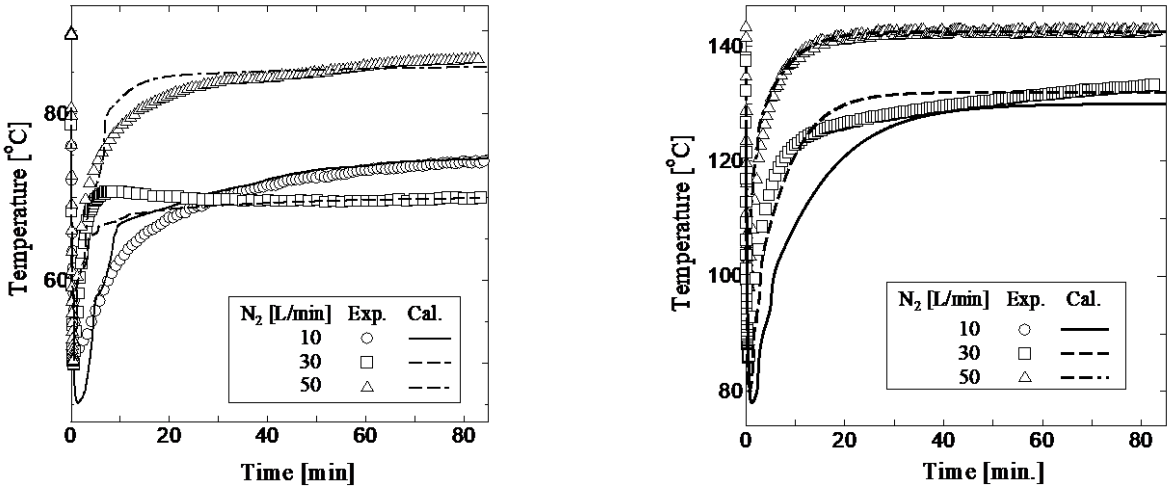

a. Inlet temperature of N_2 at 80°C b. Inlet temperature of N_2 at 140°C

Figure 3. Comparison between experimental and calculation results for spherical particles ϕ2.1 mm: local bed temperatures

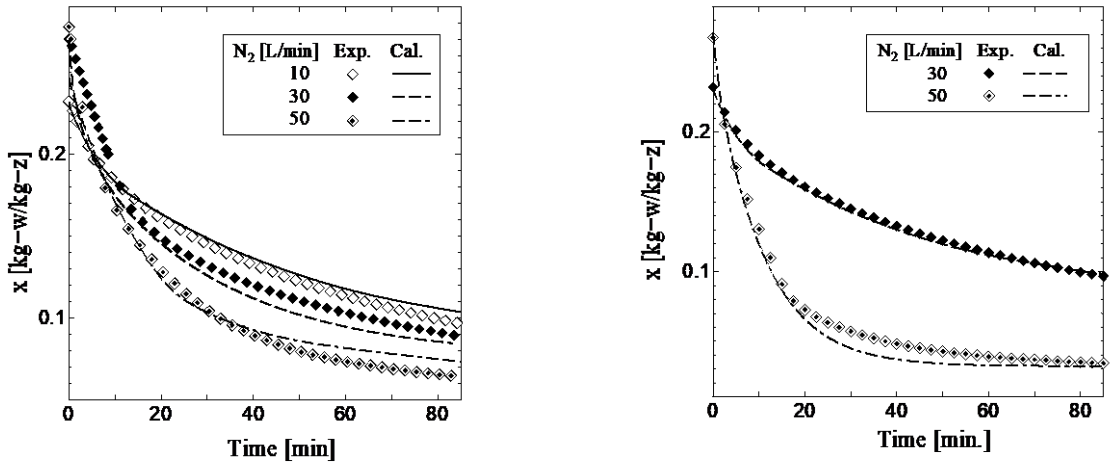

a. Inlet temperature of N_2 at 80°C b. Inlet temperature of N_2 at 140°C

Figure 4. Comparison between experimental and calculation results for spherical particles ϕ2.1 mm: average water adsorbed in the zeolite [kg-water/kg-dry zeolite]

Figure 4 shows water adsorbed variations with time between experiment and calculation confirmed good agreement for various flow-rate and temperature of Nitrogen gas. Initial value of water adsorbed in the zeolite is not uniform for each desorption condition due to difficulty to get uniform temperature in the preparation of saturated zeolite. The amount of water released from zeolite depends on the flow-rate and temperature of Nitrogen gas.

Higher flow rate and temperature, more water can be desorbed. Furthermore, time required to release 80% of water adsorbed in zeolite can be shortened if the flow rate increased. Temperature of inlet gas also has effect in the shortening desorption time. This implies desorption rate can be increased if temperature and flow-rate of inlet gas increased.

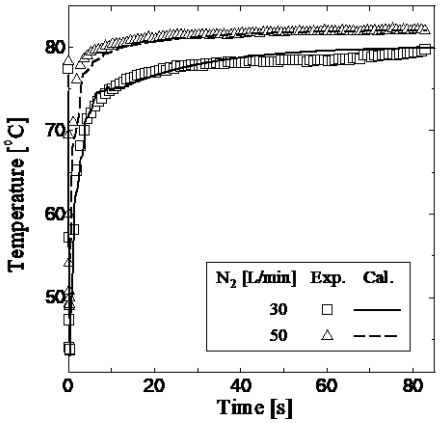

a. Local bed temperature in the center

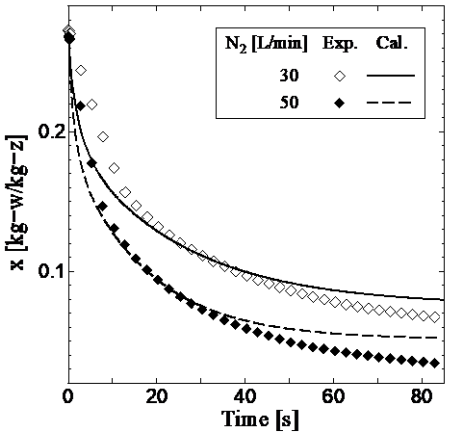

b. Average water adsorbed

Figure 5. Comparison between experimental and calculation results for cylindrical particles ϕ1.6 mm, temperature of inlet gas at 80°C

Desorption on cylindrical particles of zeolite 13X was investigated using Nitrogen gas at 80°C with flow-rate 30 and 50 L/min. Figure 5 shows a good agreement of temperature variations with time can be obtained for desorption using spherical particles which the flow-rate of Nitrogen gas varies at 30 and 50 L/min at 80°C. The temperature distribution becomes narrower when flow-rate of inlet gas increased similar tendency with using spherical particles. More amount of water adsorbed can be released if higher flow rate used to desorb zeolite. This is confirmed experimentally and numerically through Figure 5-8. However, theoretical calculation predicted the amount of water released from zeolite is 0.015 [kg-w/kg-z] higher than experimental one.

IV. Conclusion

This study could confirm the feasibility of desorption using dry gas where the results were According to the overall heat balance of desorption, the drying time is theoretically calculated. From the comparison of drying time between experiments and calculations, the relative errors were within 9%. The relative errors show that heat transfer was dominant in desorption. The results of numerical simulation agree with the experimental ones for the distribution of local temperature and average water adsorbed in the packed bed. From the calculations, there was limitation in the operating condition of desorption. There was almost no different when the gas flow rate was more than 50 L/min and the gas temperature was more than 100 °C.

Acknowledgment

This work was supported in part by.Global Center of Excellence in Novel Carbon Resource Sciences, Kyushu University and JSPS Grant in aids for young scientist

References

[1] Demir, H., M. Mobedi, S. Ulku. A review on adsorption heat pump: Problems and solutions. Sustain Energy Rev.; 2007.

[2] Oktariani, E., A. Noda, K. Nakashima, K. Tahara, B. Xue, K. Nakaso, and J. Fukai. Potential of a Direct Contact Adsorption Heat Pump System for Generating Steam from Waste Water. International Journal of Energy Research (DOI: 10.1002/er.1855).

[3] Oktariani, E., A. Noda, K. Nakashima, K. Tahara, B. Xue, A.T. Wijayanta, K. Nakaso, and J. Fukai. Experimental Investigation on The Adsorption Process for Steam Generation Using A Zeolite-Water System. Journal of Chemical Engineering of Japan; (Submitted 17 June 2011).

[4] Watanabe F., K. Sumitani, T. Kashiwagi,H. Huang, M. Hasatani and N. Kobayashi. Influence of Microwave Irradiation on Water-Vapor Desorption from Zeolites. Kagaku Kogaku Ronbunshu; 2009; 35(5): 431-435.

[5] Saitake M., M. Kubota, F. Watanabe, H. Matsuda. Enhancement of Water Desorption from Zeolite by Microwave Irradiation. Kagaku Kogaku Ronbunshu; 2007; 33(1):53-58.

[6] Kärger, J., D. M. Ruthven. Diffusion in zeolites and other microporous solids. Wiley. 1992.

[7] Thomas, W. J., B. D. Crittenden. Adsorption and technology design. Butterworth-Heinemann. 1998.

Nickel Recovery from Hydrocracking Spent Catalyst using Acetic Acid: Leaching Performance and Kinetics Study (#620)

Himawan Tri Bayu Murti Petrus[1,a], Andreas Diga Pratama Putera[1], Arini Muthiah Rosmaya Putri[1], Yosua Pangihutan Sihotang[1], Wiratni1, Widi Astuti[2], Yusuf iskandar[3], Danu Bratakusuma[3]

[1]Center of Advanced Material and Sustainable Mineral Processing, Department of Chemical Engineering, Universitas Gadjah Mada, Jl. Grafika 2, Yogyakarta 55281, Indonesia.
[2]Research and Development Division for Mineral Technology – Indonesian Institute of Sciences, Jl. Ir. Sutami Km. 15 Tanjung Bintang, Lampung Selatan, Lampung, Indonesia.
[3] Pertamina balongan, Unit Operation VI, Balongan, Sukareja, Indramayu, Kabupaten Indramayu, Jawa Barat 45217, Indonesia
[a] bayupetrus@ugm.ac.id

Abstract. *Hydroprocessing technology has been used widely and its capacity is increasing nowadays. Metal catalysts, namely nickel (Ni), are used intensively in Indonesia. Often, the spent catalysts are treated in landfill method which is not economically beneficial and requires large processing area. Moreover, the heavy metal, particularly Ni, is proven to be harmful to the soil environment and so, spent catalyst recycling process is necessary. In this work, hydrometallurgy process was used and the hydrocracking spent catalyst was leached in acetic acid solution. The effect of time, acetic acid concentration, and temperature, on the results are observed. The spent catalyst was roasted in a muffle furnace at 200°C for 30 minutes and 525°C for 120 minutes to remove its carbon content. The roasted spent catalyst is analyzed by Energi-dispersive X-ray Spectroscopy (EDX) to find out its constituents. After roasting process, the spent catalyst was sieved to get the desired size of -60 and +200 mesh. The leaching process was conducted in a shaker water bath at three different acid concentration and temperature, that are 0.1, 1.0, 4.0 N, and 30, 60, and 90°C. The observed time of leaching in this work is in 5, 15, 30, 60, and 120 minutes. In each measured time, suspensions were taken and stored. The samples are then centrifuged at 1,000 rpm for 10 minutes and the solutions are analyzed using AAS (Atomic Absorption Spectroscopy). The results show that the temperature affects the rate of the leaching process. After 5 minutes, the samples which are leached in the temperature of 60°C and 90°C show a sloping trend of nickel leached in the solution, showing that the equilibrium was reached. On the contrary, the sample that is treated at 30°C shows a steady inclining trend of leached nickel in the overall process, in the absence of a sloping trend. In addition, acid concentration significantly determines the maximum leached nickel in the sample. Higher acid concentration yields more leached nickel.*

Keywords: *Environment; Spent Catalyst; Hydrometallurgy; Acetic Acid; Nickel Recovery*

I. Introduction

Catalytic hydrotreating processes are used extensively in the petroleum refining industry for the production of clean fuels from petroleum distillates and residues. Hydrotreating catalysts usually consist of molybdenum (Mo) supported on an alumina carrier with promoters

such as cobalt (Co) or nickel (Ni). Hydrotreating catalysts enhance the removal of undesirable impurities such as sulfur, nitrogen, and metals (V and Ni) present in the feed by promoting hydrodesulfurization (HDS), hydrodenitrogenation (HDN) and hydrodemetallization (HDM) reactions during the hydrotreating operations (Marafi and Stanislaus, 2008).

These operations generate large quantities of spent catalysts as solid wastes every year. The total quantity of spent hydroprocessing catalyst generated currently worldwide is estimated to be in the range of 150,000–170,000 t/year and it will continue to increase as new hydrotreating units are built (Marafi and Stanislaus, 2008). The storage, transportation, treatment and disposal of these spent catalysts require compliance with stringent environmental regulations because of their hazardous nature. The most important hazardous characteristic of spent hydroprocessing catalysts is their toxic property. Chemicals such as V, Ni, Mo, and Co present in the catalyst can be leached by water after disposal and pollute the environment (Marafi and Stanislaus, 2003). The contamination was sufficient to create toxic conditions for plants, to allow accumulation to high levels in the tissues of various organisms, and to disrupt the normal functioning of the ecosystem. (McIlveen and Negusanti, 1994)

Disposal by landfilling is the oldest and was the most widely used method years ago. Due to increased environmental consciousness and regulations, landfilling is, fortunately, less and less used. The issue is that liability still belongs to the waste producer as long as this waste has not been destroyed, and thus lasts on long term (Dufresne, 2007). A few companies are active in the field of spent hydrotreatment catalysts recycling. They use two types of reclamation processes, hydrometallurgy, and pyrometallurgy. The hydrometallurgical route starts with a roasting to at least partially removing coke. Then a leaching with either sulfuric acid or soda is used to dissolve totally or partially the substrate. Finally, the metals have to be recovered from the solution and further purified (Dufresne, 2007).

There are still limited works that had been done to study the possibility of using organic acid to recover nickel content in the spent catalysts and other resources. Moreover there are contradictory mechanism in the nickel recovery using organic acid in which Ni^{2+} can not form complexes (Chaudhary *et al.*, 1993) so that the nickel present in the leachate is only found in ionic form while on the other hand Ni^{2+} can form complexes (Hedwig et al., 1980; Wanta et al, 2016). Recently in 2014, Yan et al. studied leaching properties of Pb, Cd, Zn, Cu at pH of 2-6 using different inorganic acids (hydrochloric acid, sulfuric acid, nitric acid) and organic acids (acetic acids, citric acid, malic acid, succinic acid). Mulak,2015 studied kinetics of leaching from spent catalyst in sulphuric acid. This leaching mechanism is controlled by a solid state diffusion process with maximum recovery of about 75%. On the other side,(Parhi, Park and Senanayake, 2013) studied the recovery of nickel from Ni-Al_2O_3 spent catalyst using hydrochloric acid leaching and the nickel recovery with the optimum condition is 99.9%.

In this work, the hydrocracking spent catalyst was leached in acetic acid solution with varied temperatures and acid concentrations.

II. Experimental

2.1. Materials

Hydrocracking spent catalyst from PT. Pertamina (Persero) Refinery Unit VI, Balongan, Indonesia was used in this work. The leaching agent in this work is an organic acid (acetic acid) with certain concentrations.

The spent catalyst was roasted in temperature of 200°C for 30 minutes and 550°C for 5 hours to remove its carbon content, with a heating rate of 10°C/ minutes. The roasted spent catalyst was then sieved to get the desired size (-60 +200 mesh). To determine its elemental composition, the roasted spent catalyst was analyzed using XRF (X-ray fluorescence).

2.2. Instruments

There are several instruments used in this study. Water bath which was used to adjust temperature of nickel leaching in this experiment is Memmert Waterbath WNB 14. The shaking speed scale was adjusted for 3.5 out of 5. In order to analyze the sample as well as results of the leaching process Energy-dispersive X-ray spectroscopy (EDX), Shimadzu Energy Dispersive X-ray Fluorescence Spectrometer EDX-7000/EDX-8000 is used in this experiment with a 10mm collimator and Atomic absorption spectroscopy (AAS). The Ni content of the leachates was observed using AAS in LPPT, Laboratorium Penelitian dan Pengujian Terpadu, Universitas Gadjah Mada, Yogyakarta, Indonesia. While the roasted *spent catalyst* is analyzed by XRD in LIPI (Lembaga Ilmu Pengetahuan Indonesia) to assess its crystal form.

2.3. Leaching process

As much as 20 grams of spent catalyst was leached in 200 mL acetic acid solution. The observed molarity of the acids were 0.1, 1.0, and 4.0 M and the leaching temperatures were 30, 60, and 90°C. The sampling was taken in 5, 15, 30, 60, and 120 minutes of the leaching process.

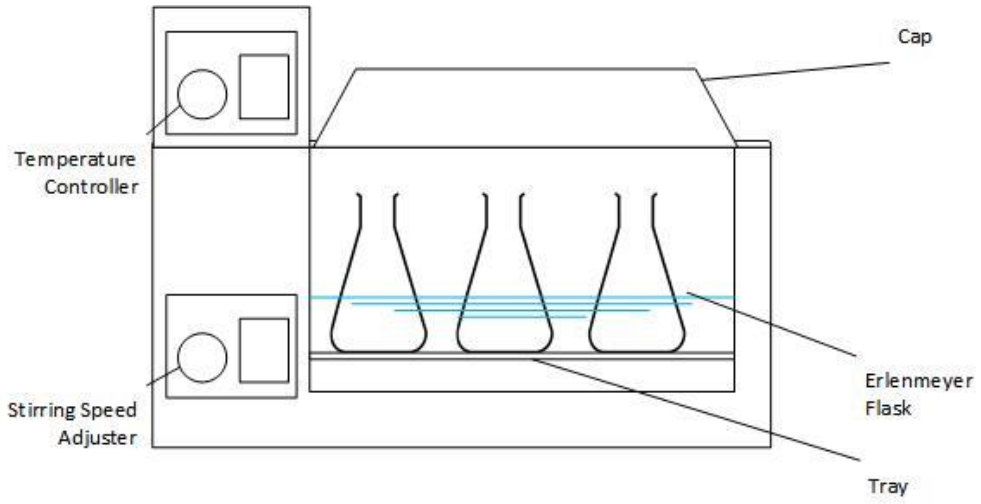

Figure 1. Laboratory water bath leaching reactor.

The sampling took 5 mL in each observed time of reaction and the samples were diluted as much as twice its initial volume using aquadest. The diluted samples contained solid spent catalyst in a small portion so that it need to be separated from the solution. A centrifuge with 1000 rpm was used for 10 minutes for each sample to do so. Finally, the Ni content in the solution was observed using atomic absorption spectroscopy (AAS). Overall, the process can be seen in figure 2.

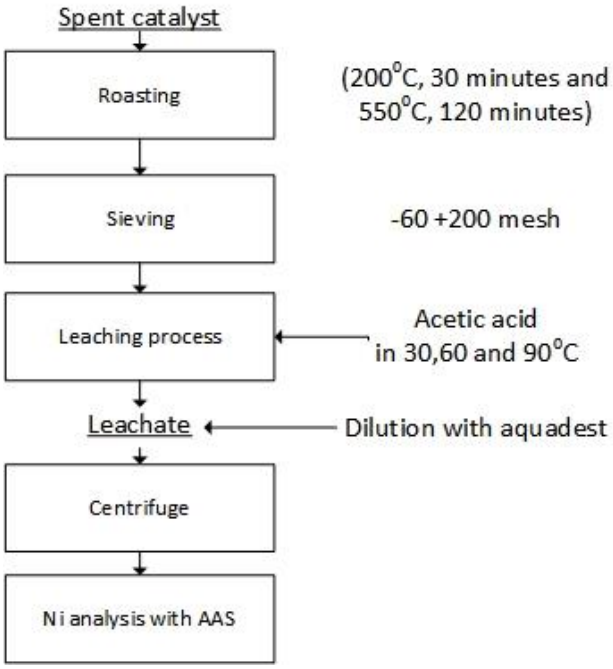

Figure 2. Flow sheet for the spent catalyst leaching.

All of the presented data is the average value of 3 measurements of each data point.

III. Results and Discussion

3.1. XRD Result

The XRD result of raw spent catalyst can be seen from Figure 3. From Figure 3, it can be seen that the nickel in the spent catalyst is associated with the aluminosilicate crystaline. This initial characteristic can affect the leaching mechanism of nickel at which aluminosilicate has low leachability in organic acids (Marafi and Stanislaus, 2008; Yan et al., 2014). In this study nickel could not be effectively leached using acetic acid.

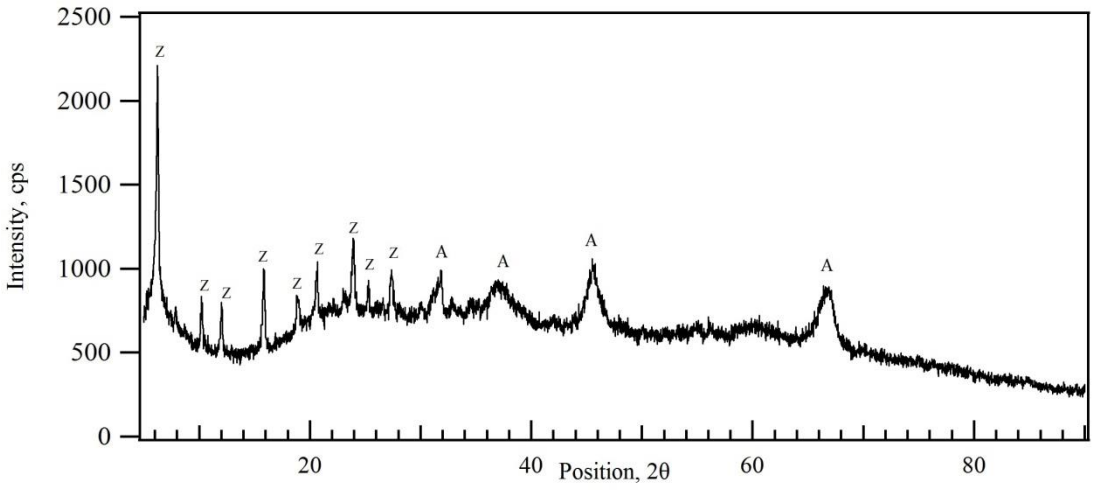

Figure 3. Roasted spent catalyst XRD pattern.

3.2. Spent catalyst EDX result

As it can be seen in table 1, Aluminium, Lanthanum, Silica, Nickel, and Iron are found in the sample. The spent catalyst is abundance with silica and alumina in the form of aluminosolocate as confirmed in the XRD result (Figure 3), while nickel as the active surface is about 2.72 % w/t. In this paper the leaching study is concentrated on nickel as one of the valuable metals with non renewable sources. The EDX was conducted with area measurement method in order to be able to measure the bulk concentration of the sample.

Table 1. EDX result of hydrocracking spent catalyst

Constituents	Al	Si	La	Ni	Fe
%mass	51.88	41.13	3.65	2.72	0.62

3.3. Recovery of Nickel

The maximum mass recovery of the nickel in each sample can be deducted from point 2.3 and 3.1, as it can be seen in equation (1)

$$m_{0,Ni} = \%massNi\ x\ m_{sample} \quad (1)$$

Where,

$m_{0,Ni}$: maximum mass recovery of nickel, grams
$\%massNi$: nickel mass percentage in the sample, 2.72%
m_{sample} : spent catalyst used in each erlenmeyer flask, 20 grams

Moreover, the recovery percentage of nickel leached in the sample is measured by equation (2) below.

$$\%R = \frac{m_{extracted}}{m_{0,Ni}} x100\% \quad (2)$$

Where,

%R : nickel recovery percentage
$m_{extracted}$: nickel mass leached from each sample, grams

3.4. Leaching results

The leaching behavior of the nickel in acetic acid is greatly affected by the temperature. While the samples with 30°C leaching temperature show a constant and slow inclining nickel concentration trend each time, samples with 60 and 90°C leaching temperature tend to be stagnant from the first 5 minutes. In this case, the process is considered to be at equilibrium.

In terms of maximum recovery, acid concentration and temperature are the most two affecting variables. Higher temperature always yields higher nickel recovery, especially between 30°C and 60°C. On the other side, in all leaching temperatures, the highest nickel recovery is always obtained in the order by the highest acid concentration, that is 4.0 M, 1.0 M, and 0.1 M. Moreover, the highest nickel recovery (nearly 4%) was obtained by 90°C leaching temperature with 4.0 M acid concentration. This result is in the same idea with point 3.1. that hypothesize small nickel recovery.

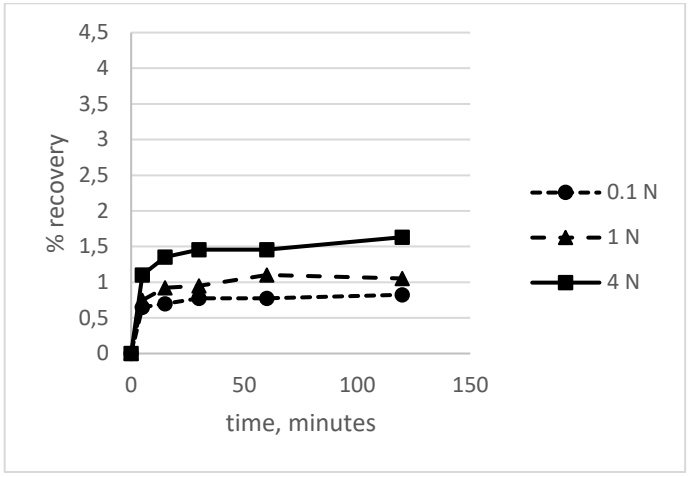

Figure 4. Nickel recovery percentage in 30°C leaching temperature.

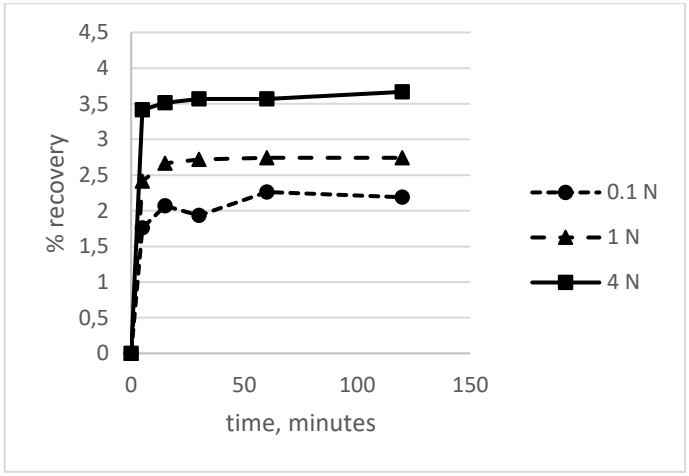

Figure 5. Nickel recovery percentage in 60°C leaching temperature.

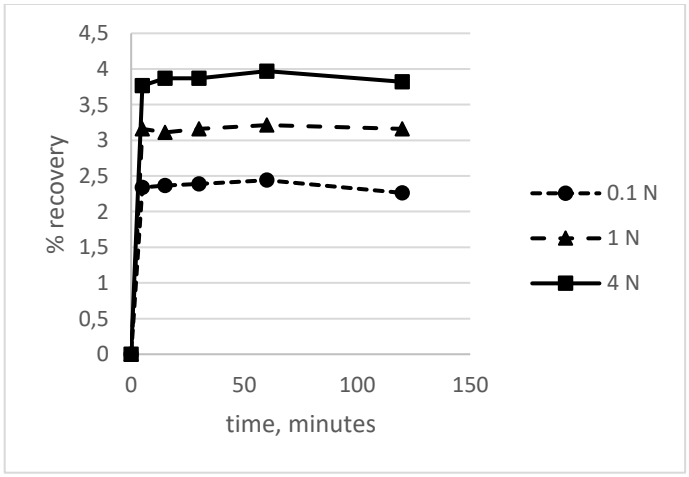

Figure 6. Nickel recovery percentage in 90°C leaching temperature.

The low recovery of nickel in this study is caused by the association of nickel in the spent catalyst matrix as it can be seen in the XRD result (Figure 3). The previous study using citric acid as well as organic acid showing a similar pattern (Hedwig et al, 1980; Marafi and Stanislaus, 2008). Somehow, the effect of temperature is quite significant up to the temperature of 60^{o}C at which the amplification is about twice from the lower temperature

(30°C). At the temperature level of 90°C, the increase of nickel recovery has reached its maximum level of about 4%.

3.5. Leaching kinetics

Recently, nickel leaching behavior in strong acid (H_2SO_4) has been studied (Mulak, Miazga and Szymczycha, 2005) and the results show that the process can be fitted with a diffusion model of Ginstling and Brounhstein. However, it is nearly impossible to fit the data with the model because the maximum percentage of nickel leached are very far from 100%. Another study on metal leaching, particularly Fe and Al in CFA (coal fly ash) using the same acid, revealed that the process involves a rate controlling step of mass transfer with an existing inhibiting mechanism. It is stated that, in the leaching process, with respect to the formation of the unreacted core that is encapsulated by a leached, porous, layer, particles follow the shrinking core model. The model is then described as shown below(Seidel and Zimmels, 1998).

$$C_2 = a.\ln(t) + b \quad (3)$$

Where C_2 is the concentration of the metal leached (also can be deducted from *%R*), and *t* is the elapsed leaching time. the value of *a* and *b,* however, verifies the correlation of the initial ash content. Furthermore, the value of *a* and *b* are not used to assess the relationship between the ash and the leaching process, but only to predict the leaching percentage in a certain elapsed time. The values of *a* and *b* are presented in table 2 and the data fitting is shown in figure 7-9.

Table 2. Kinetic parameter of the leaching process

Leaching temperature	Acetic acid concentration	*a*	*b*
30°C	0.1 M	5.6962e-05	0.0055
	1.0 M	10.2342e-05	0.0059
	4.0 M	16.0261e-05	0.0085
60°C	0.1 M	17.2519e-04	0.014
	1.0 M	11.3712e-04	0.0224
	4.0 M	7.3941e-04	0.0329
90°C	0.1 M	14.3933e-04	0.0225
	1.0 M	7.2854e-04	0.0292
	4.0 M	8.1313e-04	0.0362

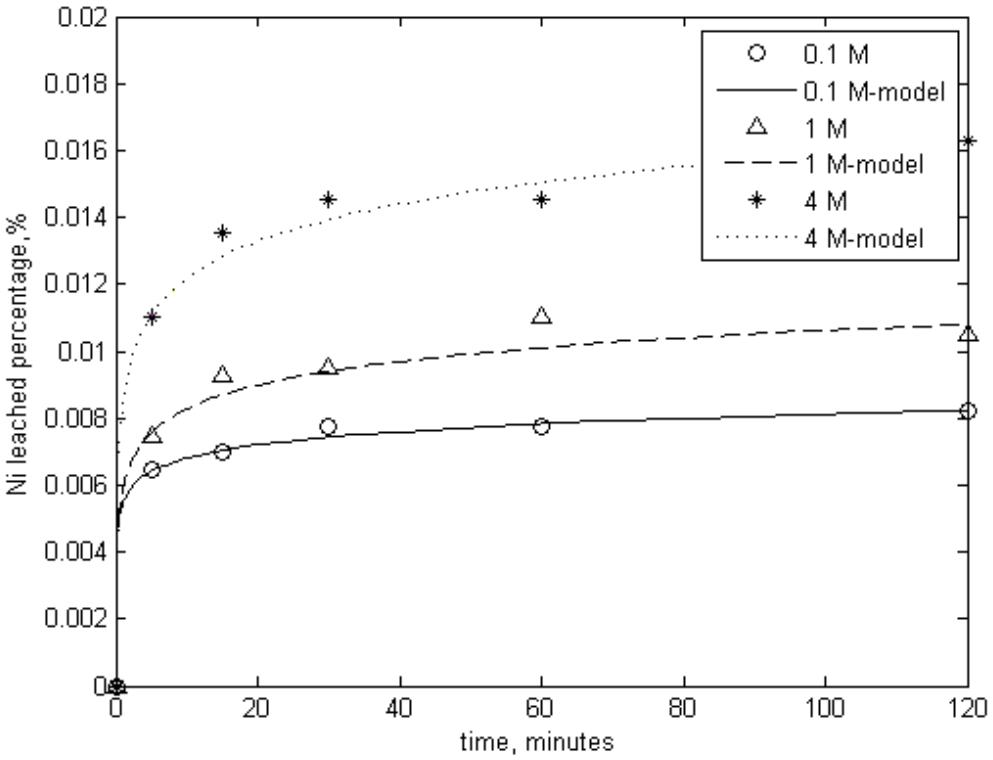

Figure 7. Ni leached percentage vs. time data fitting of leaching process in 30°C

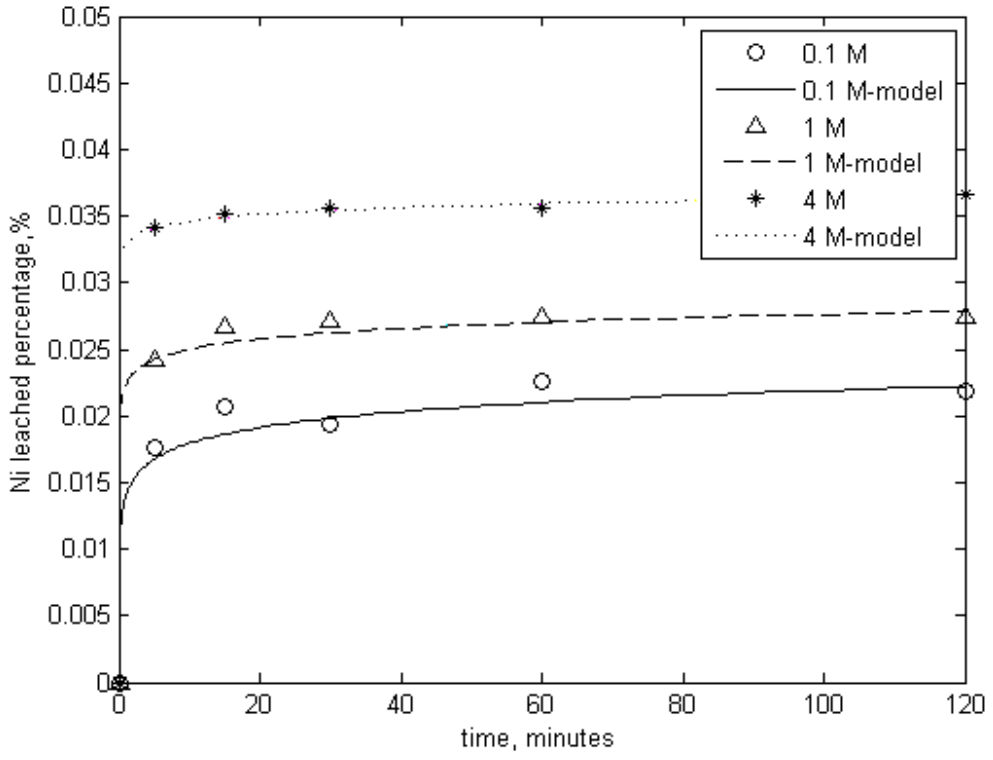

Figure 8. Ni leached percentage vs. time data fitting of leaching process in 60°C

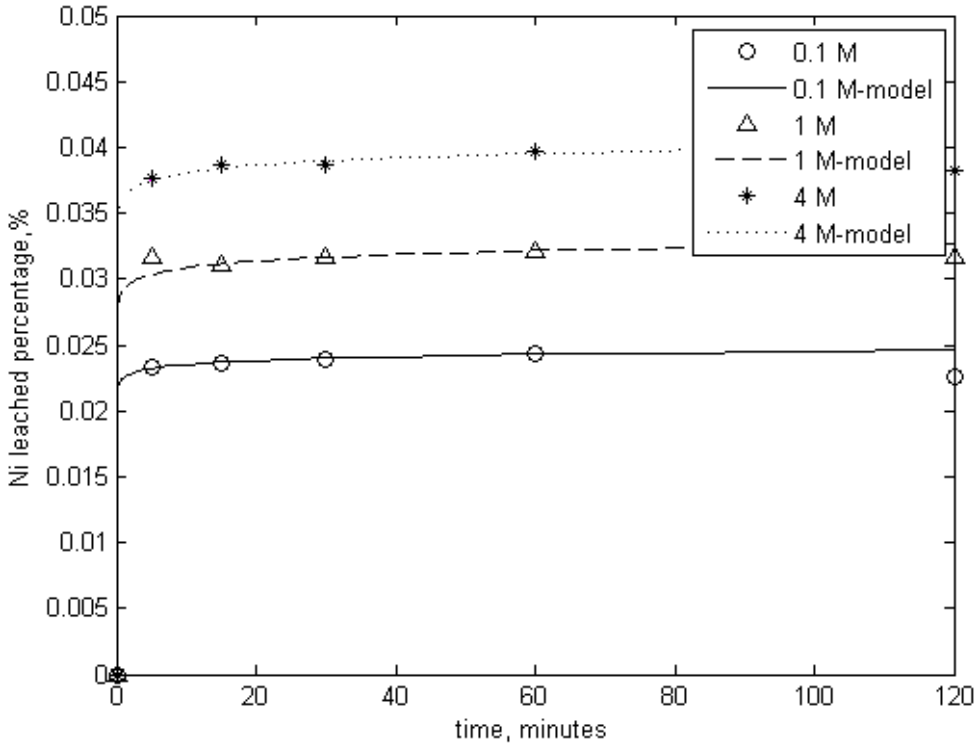

Figure 9. Ni leached percentage vs. time data fitting of leaching process in 90°C

The *a* and *b* constant represent the bulk caracteristic of the unreacted core (ash layer) at which the mineralogy of nickel included into these constant. *b* is the value at which maximum recovery can be reach meaning that the intrinsic value of nickel in the spent catalyst is included, while *a* showing the rate constant at which optimum condition can be reached. As it can be seen from Table 2, the a constant is getting higher with temperature showing that the mechanism of leaching is dominated by the reaction regime, while concentration of acetic acid affects the b constant representing the optimum nickel recovery that can be achieved. Higher concentrationof acid will surely possess higher energy to break up the associated nickel mineral resulting higher maximum nickel recovery.

IV. Conclusion

From the results above, the conclussion is higher acid concentration and higher temperature yield higher nickel recovery. In this work, the highest nickel recovery was obtained by 90°C leaching treatment in 4.0 M acetic acid solution. Temperature affects the leaching rate of nickel in the solution. The sample that is treated in 30°C leaching temperature shows a slow inclining nickel recovery trend while the sample with 60 and 90°C leaching temperature reached equilibrium suddenly in the first 5 minutes. The maximum recovery of the nickel leaching using acetic acid is considered to be very low (only nearly 4%). The logarithmic correlation kinetic model by Seidel fit the data satisfactorily.

ACKNOWLEDGEMENT

The financial support from Directorate of Human Resources of the Directorate General of Higher Education (DGHE or DIKTI) through Kerjasama Luar Negeri (KLN) programme is gratefully acknowledged.

REFERENCES

[1]. Chaudhary, A. J., Donaldson, J. D., Boddington, S. C. and Grimes, S. M. (1993) 'Heavy metals in the environment. Part II: a hydrochloric acid leaching process for the recovery of nickel value from a spent catalyst', *Hydrometallurgy*, 34(2), pp. 137–150. doi: 10.1016/0304-386X(93)90031-8.

[2]. Dufresne, P. (2007) 'Hydroprocessing catalysts regeneration and recycling', 322, pp. 67–75. doi: 10.1016/j.apcata.2007.01.013.

[3]. Hedwig, G.R., Liddle, J.R., and Reeves, R.D. (1980) 'Complex Formation of Nickel(II) Ions with Citric Acid in Aqueous Solution: a Potentiometric ans Spectroscopic Study', Australian Journal of Chemistry, 33, pp. 1685-1693.

[4]. Marafi, M. and Stanislaus, A. (2003) 'Studies on rejuvenation of spent residue hydroprocessing catalysts by leaching of metal foulants', 202, pp. 117–125. doi: 10.1016/S1381-1169(03)00184-5.

[5]. Marafi, M. and Stanislaus, A. (2008) 'Resources , Conservation and Recycling Spent catalyst waste management : A review Part I — Developments in hydroprocessing catalyst waste reduction and use', 52, pp. 859–873. doi: 10.1016/j.resconrec.2008.02.004.

[6]. McIlveen, W. D. and Negusanti, J. J. (1994) 'Nickel in the terrestrial environment', *the Science of the Total Environment*, 148, pp. 109–138.

[7]. Mulak, W., Miazga, B. and Szymczycha, A. (2005) 'Kinetics of nickel leaching from spent catalyst in sulphuric acid solution', *International Journal of Mineral Processing*, 77(4), pp. 231–235. doi: 10.1016/j.minpro.2005.06.005.

[8]. Parhi, P. K., Park, K. H. and Senanayake, G. (2013) 'A kinetic study on hydrochloric acid leaching of nickel from Ni-Al2O3 spent catalyst', *Journal of Industrial and Engineering Chemistry*. The Korean Society of Industrial and Engineering Chemistry, 19(2), pp. 589–594. doi: 10.1016/j.jiec.2012.09.028.

[9]. Seidel, A. and Zimmels, Y. (1998) 'Mechanism and kinetics of aluminum and iron leaching from coal fly ash by sulfuric acid', 53(22), pp. 3835–3852.

[10]. Wanta, K.C., Perdana, I., and Petrus, H. T. B. M. (2016) ' Evaluation of shrinking core model in leaching process of Pomalaa nickel laterite using citric acid as leachant at atmospheric conditions', Materials Science and Engineering 162 (1), 012018.

[11]. Yan, Y., Gao, J., Wu, J. and Li, B. (2014) 'Effects of Inorganic and Organic Acids on Heavy Metals Leaching in Contaminated Sediment', 10, pp. 406–410.

Integrated Reservoir Study to Optimize Gas Production of Water Drive Gas Reservoir Case Study: Lower Menggala Gas Field (#649)

Panca Suci Widiantoro[1,a], Astra Agus Pramana[2,b], Putu Suarsana, Anis N. Utami[2,c]
[1]Sr Reservoir Engineer in Energi Mega Persada and Master of Petroleum engineering Trisakti University, Jakarta, Indonesia;
[2]Petroleum engineering Department, Pertamina University, Jakarta, Indonesia;
[a]pancasuciwidiantoro@gmail.com, [b]agus.prama@gmail.com, [c]ips3150@yahoo.com

Abstract. *Production optimization in mature field water drive gas reservoir is not easy especially when water already breakthrough in producing wells. An integrated reservoir study is needed to get reliable strategy to optimize production of water drive gas reservoir.*

This research presents the integrated reservoir study of Lower Menggala (LM) Gas Field which is located Central Sumatera Basin, Riau Province. LM had been produced since 1997, current RF are 55%, which is quite high for water drive gas reservoir. The current gas rate production is about 1.97 MMscfd with high water production around 4250 BWPD, consequently some of wells suffered liquid loading problem.

This research comprises of well performance analysis, estimate OGIP , aquifer strength of the reservoir by using conventional material balance method and modern production analysis method then conduct dynamic reservoir simulation to identify the best strategy to optimize gas production. Economic analysis also be performed to guide in making decision which scenario will be selected.

DST analysis on DC-01 well defined reservoir parameter, boundary and deliverability which are P= 2520 psia, k= 229 mD, Total skin= 8, detected sealing fault with distance 175 m, and AOF 45 MMscfd. Conventional material balance method gave OGIP 22.7 BScf, aquifer strength 34 B/D/Psi, whereas modern production analysis estimated OGIP 22.35 BScf, aquifer strength 34 B/D/psi. Those two method shows good consistency with OGIP volumetric calculation with discrepancy OGIP value +/- 1%. Six (6) scenario of production optimization has been analyzed, the result shows that work over in two wells and drilling of 1 infill well (case 6) achieve gas recovery factor up to 75.2%, minimal water production and attractive economic result.*

Keywords: *Aquifer Strengths, Economic, OGIP, Recovery Factor (RF), Water Drive Gas Reservoir*

I. Introduction

Production optimization in water drive gas reservoir is not easy especially when water already breakthrough in producing wells. An integrated production analysis is needed to get reliable strategy to optimize production of water drive gas reservoir.

Lower Menggala Gas Field is one of two gas field of EMP Malacca Straits SA located in Padang Island, Bengkalis Regency Riau Province. The location map shown in Figure 1. Lower menggala had been produced since 1997, when this study conducted the RF are 55%, which is quite high for water drive gas reservoir. The current gas rate production is about 1.97 MMscfd with high water production around 4250 BWPD, consequently some of wells suffered liquid loading problem. The existing perforation in a bottom part mostly already below gas water contact. To optimize the production and increase RF of this reservoir need to conduct integrated production analysis which cover several analysis such as: well modeling analysis, modern production analysis, reservoir simulation and economic analysis.

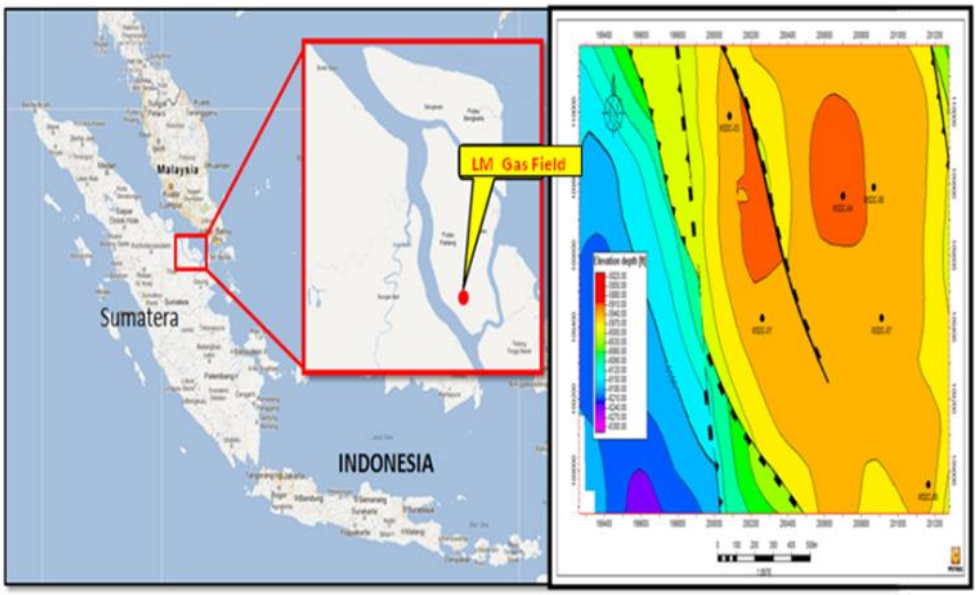

Figure 1. Lower Menggala Gas Field Location Map

This research presents the integrated Reservoir study and optimization of Lower Menggala (LM) Gas Field. The objectives of this research are:

1. To understanding performance of each well by conduct well testing interpretation and well performance analysis.
2. To estimate OGIP and aquifer strength of the reservoir by using conventional material balance method and modern production analysis method.
3. To construct dynamic reservoir model on latest production data and conduct history matching to tested the model whether it represent field behavior.
4. To predict future field performance to find out an optimal development plan to optimize gas production of the field.
5. To identify the best strategy to optimize gas production of this field which consider operational aspect, technical aspect and also economic wise.

II. Methodology

Several task work will be performed during this research as listed below:

1. Data acquisition and selection

Collect well testing and or DST data, daily wellhead pressure and gas rate data from the beginning of production, as well as static data like initial reservoir pressure and temperature, rock properties, gas properties, open-hole logs ,well completion diagram and economic input data.

2. Data validation

Make sure all the dynamic data is valid. For example, if wellhead pressure increases, the gas rate should decrease. This step often takes the longest time, and involves much detective work to chase down the reason for step-changes and other anomalies. It is critical because "rubbish in equals rubbish out".

3. Well Modeling

First of all conduct well testing analysis to get reservoir pressure initial, reservoir parameter of tested well such as permeability, skin and possible reservoir boundary. The result then use as input for gas deliverability analysis to get IPR curve and AOF.

4. Material Balance Analysis

In this step, the production data and limited static reservoir pressure data will be analyzed using material balance analysis to get OGIP and aquifer strength parameter of the reservoir. The material balance is expressed in reservoir volume of production, expansion and water influx as [1]

$$GB_g + W_p B_w = G(B_g - B_{gi}) + GB_{gi} \frac{(c_w S_{wc} + c_f)}{1 - S_{wc}} \Delta P + W_p B_w \quad \text{.... (1)}$$

Production = Gas Expansion + Water Expansion and or pore compaction + Water influx

$$F = G(E_g + E_{fw}) + W_e B_w \quad \text{.....(2)}$$

In most practical cases Efw << Eg and may be omitted but not before checking that this is a valid neglect of the term across the entire range of pressure depletion. The material balance then become (Craft, et. al., 1991);

$$F = GE_g + W_e B_w \text{ or } \frac{F}{E_g} = G + \frac{W_e B_w}{E_g} \quad \text{.....(3)}$$

Schilthuis (1963) proposed that for an aquifer that is flowing under the steady-state flow regime, the flow behavior could be describe by Darcy's equation. The rate of water influx ew can be determined by applying Darcy's equation [1]:

$$\frac{dW_e}{dt} = e_w = \left[\frac{0.00708kh}{\mu_w \ln\left(\frac{r_a}{r_e}\right)}\right](p_i - p) \quad \text{.....(4)}$$

The above relationship can be more conveniently expressed as:

$$\frac{dW_e}{dt} = e_w = C(p_i - p) \quad \text{.....(5)}$$

5. Modern Production Analysis using Type curve matching (Blasingame)

Modern Production Data Analysis is a method to evaluate the reservoir using combined rate and pressure data without the need to shut in wells. This analysis is able to estimate hydrocarbon in place, aquifer strength, with flowing material balance and other modern techniques. Reservoir characteristics, such as permeability and skin factor can also be determined by using type curves. Figure 2 shows the integration of knowledge of Modern Production Analysis.

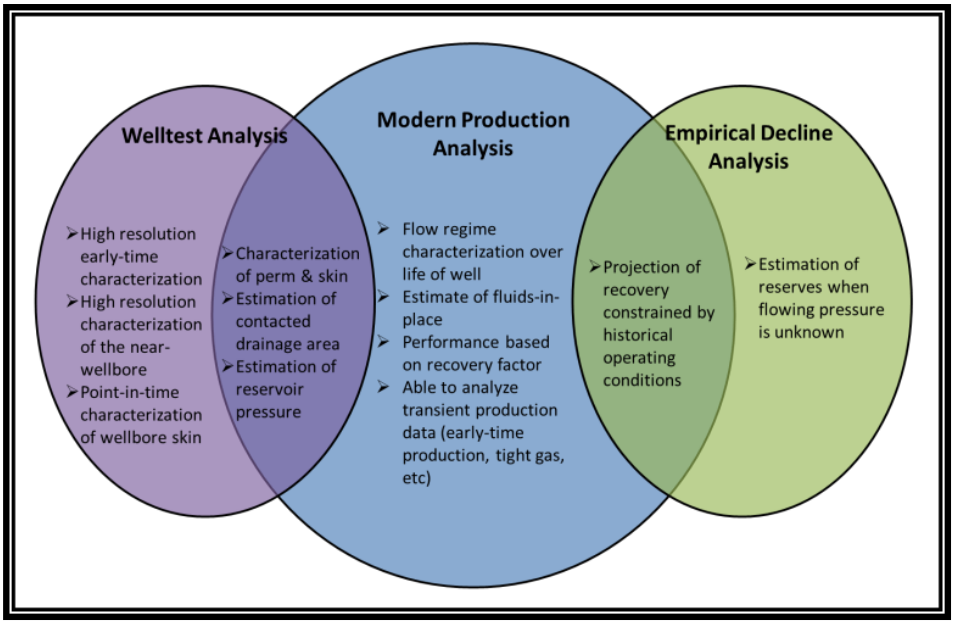

Figure 2. Integration of Knowledge of Modern Production Analysis [8].

Figure 3 shows the Type curve matching (Blasingame) which able to analysis reservoir performance.

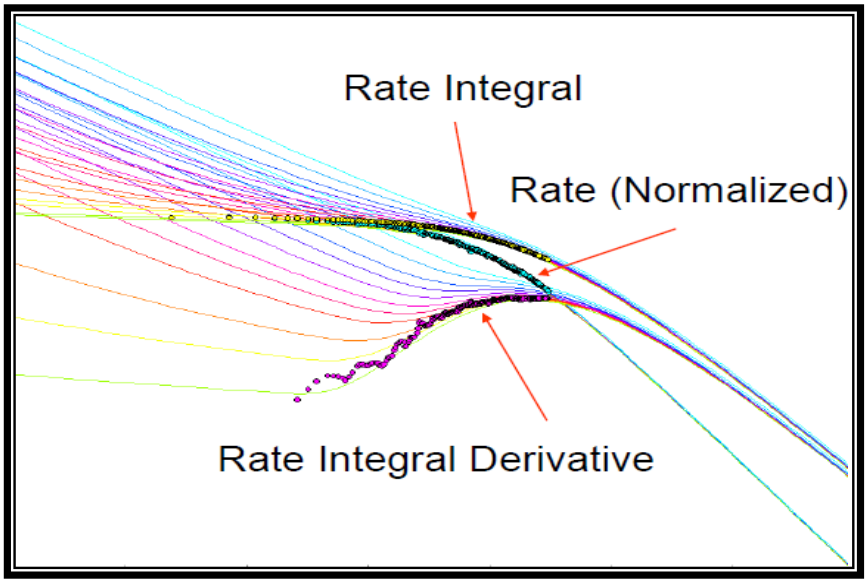

Figure3. Rate Integral and Rate Integral Derivative [8]

In this step, the production data will be matched with the type curve. As well as an OGIP and aquifer strength estimate, type curves also confirm whether the reservoir is in transient or boundary-dominated flow. This is a useful quality-control, because all these techniques only work with boundary-dominated flow. Those two analysis (in step 4 and 5) are useful to validate OGIP static model. The OGIP value of those two analysis then compare with OGIP from reservoir static model. The OGIP value should be in a good agreement with difference <5%.

6. Dynamic reservoir model/ Reservoir simulation

Reservoir simulation is a commonly used tool in the gas and oil field development. It helps engineers to simulate their recovery techniques before implementing them on the original field. It is multi-disciplinary and incorporates effort from geophysics, petrophysics, reservoir, production and facilities engineering.

Reservoir simulation comprise of several step: up scaling, initialization, history matching and prediction/forecasting. Reservoir simulation will generate several forecast scenario and a development plan will be prepared to ensure gas deliverability.

7. Economic evaluation

Economic evaluation will be run for each scenario then rank based on economic indicator result, the best economic result will selected as recommendation. This step guide in making decision which scenario will be selected.

III. Result

A. Well Modeling

The type of well testing which conducted in this well was DST. In Log-log plot (figure 4) clearly identified three time region: early, middle and late. In early time region data were very limited due to DST in this well were using subsurface valve to close and open the well, hence wellbore storage effect were minimal. After early time appear hump on the plot, it is indicated skin factor on this well. In Middle time region was appear radial flow, in this period several reservoir

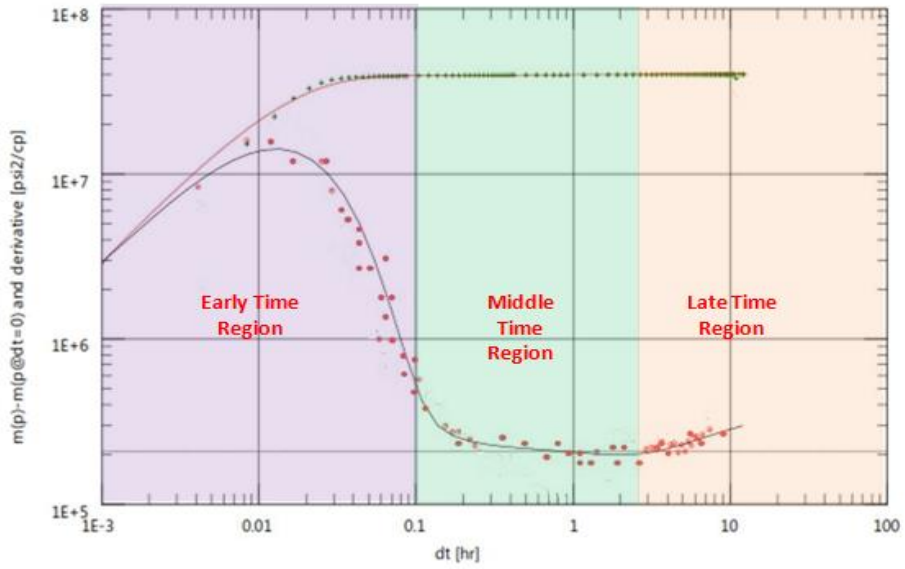

Figure4. Well test Interpretation of DC-01 well

parameter were interpreted such as: P* (P initial reservoir) 2520 psia, Permeability 229 mD, and total skin factor 8 (mechanical skin 3, whereas geometrical skin 5). In term of skin factor there were 2 value mechanical and geometrical. Geometrical skin happened due to this well perforated partially 60 ft of 117 ft, hence the analysis were using vertical-limited entry model. After radial flow period finished then follow by increasing derivative curve, it is strong indicated transient pressure response already achieve boundary. In other hand late time region already detected in this MSDC-01 DST. A sealing one fault model was selected as a best match to the raw data of MSDC-01 DST. Based on match model detected distance to boundary (sealing fault) was 175 m.

B. Material Balance Analysis

As there were limited static reservoir data available in LM gas reservoir. However, in this study material balance analysis also conducted. Driving mechanism in LM gas field is believed as strong water drive, its proved by plot of p/z against the cumulative produced gas in figure 6. The Material Balance p/z plot shows deflection from straight line (see red dashed line), it's clearly indicated presence of aquifer support during gas depletion (see blue line), hence this method not applicable to estimate OGIP. The prediction would definitely be too optimistic if the OGIP is determined solely by extrapolating the p/z data.

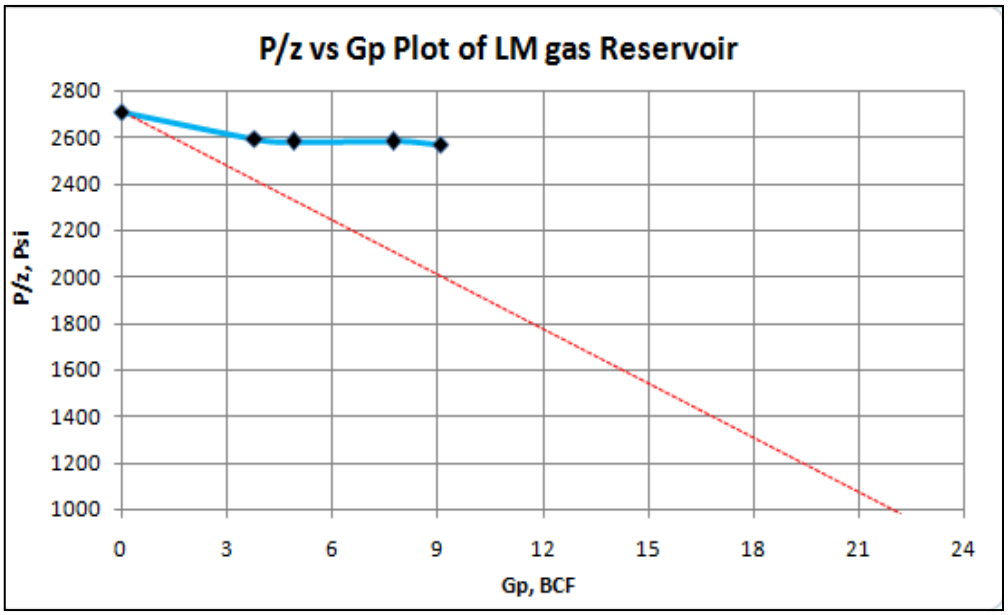

Figure 5.The Material Balance p/z Methods Indicated Aquifer Support

As previously described in methodology, when p/z method not working, Havlena-Odeh is the best method to estimate OGIP incorporated with water influx of water drive gas reservoir. In this study M-BAL software are used for the analysis. Figure 6 shows the result Havlena-Odeh plot with Schilthuis aquifer model.

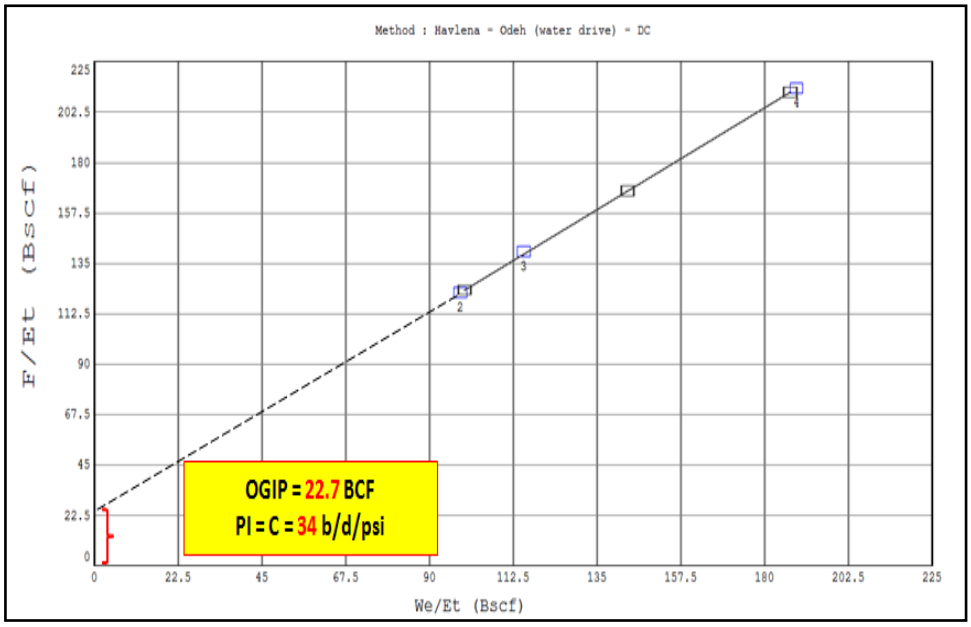

Figure 6. The Material Balance Havlena-Odeh estimates OGIP 22.7 BCF and Aquifer strength 34 B/D/Psi

C. Modern Production Analysis

Modern Production Data Analysis is a method to evaluate the reservoir using combined rate and pressure data without the need to shut in wells. Since the LM gas field has good monitoring production data, so in this study also conducted Modern Production Analysis using Type curve matching (Blasingame). This analysis aimed to increase the confidence level of OGIP and Aquifer strength estimation. The plot of production monitoring data on Blasingame type curve presented in Figure 7. As we can see in figure 7, production monitoring data perfectly matched with Blasingame Type curve. The data dominantly laid on boundary dominated flow, hence OGIP value can be estimated confidently. Based on the above Blasingame type curve matching OGIP and Aquifer strength are 22.35 BCF and 34 B/D/Psi respectively.

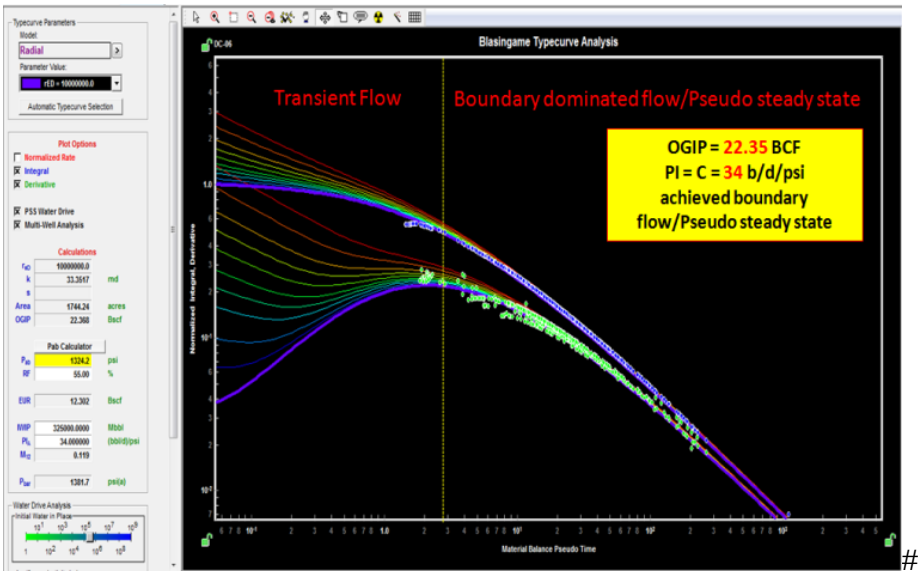

Figure 7. The Blasingame Type curve matching estimates OGIP 22.35 BCF and Aquifer strength 34 B/D/Psi

Table 1 presented OGIP and aquifer strength comparison several method which already discussed in previous section. Based on the comparison on the table below, OGIP value all those methods shows good agreement with discrepancy only 1 % respect to volumetric OGIP of static model. In other hand OGIP value from previous Integrated reservoir study 2009 are still valid, hence static model can be used for dynamic reservoir simulation. In term of aquifer strength, Material balance Havlena-Odeh and Blasingame Type Curve matching shows good consistency.

Table 1 OGIP and Aquifer Strength Comparison

Parameter	Volumetric (Static model)	Material Balance (Havlena -Odeh)	Modern Production Analysis
OGIP (BCF)	22.5	22.7	22.35
Aquifer strength (B/D/Psi)	-	34	34
Different OGIP respect to volumetric (%)	-	+1%	-1%

D. Dynamic Reservoir Model/Reservoir Simulation

Data input to Petrel RE or Eclipse was taken from all the analysis conducted and explained in the previous section. Dynamic reservoir model/ simulation grid was created with dimension 71 x 57 x 80 or 323,760 cells, grid size 50 x 50 m, and 80 layers. Reservoir simulation comprise of three section; initialization, history matching and prediction.

- Initialization

The gas saturation distribution in 3D model view and the cross section of LM reservoir at the initial condition is shown in Figure 8

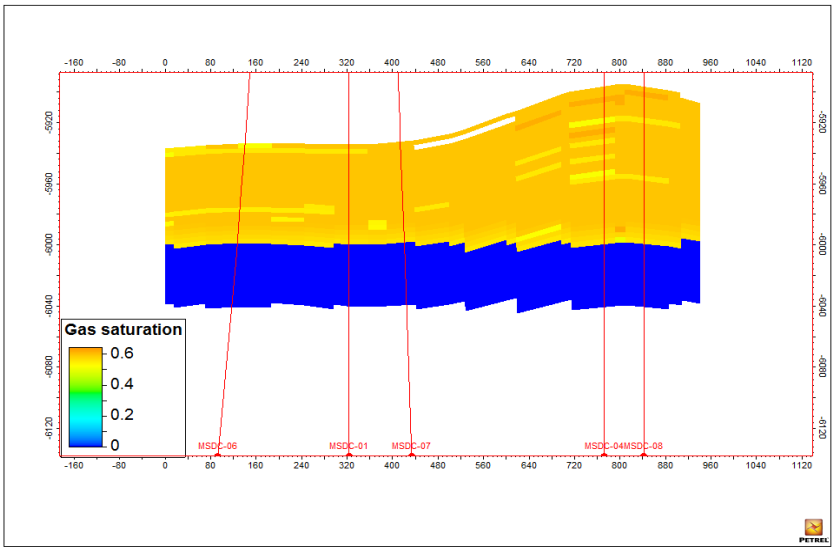

Figure 8. The Gas Saturation Distribution At Initial Condition (x-section view North- South direction)

- History matching

This section showed the history matching of the simulation model with the aims of confirming the initial reservoir conditions and obtaining an acceptable match of the observed reservoir behavior. History matching analyses are performed to check the reliability of model in dynamic condition. To achieve the accurate history matching results, the simulation model was run based on the available data (Up to December 2015). It was observed that the field gas production rate match was excellent. Field water production rate match was moderate good. Reservoir pressure measurements were very few and showed pretty good match. The set of graphs comparing the simulation model (presented as line) results with measured data (presented as point/dot) were presented in figure 9 and gas saturation distribution in 3D model at end of history matching (December 2015) as presented in figure 10.

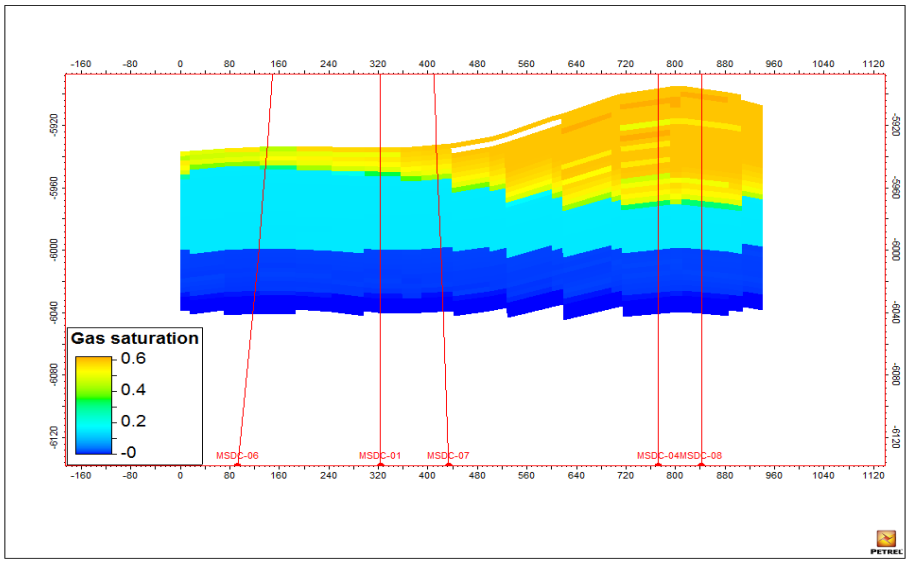

Figure 9. The Gas Saturation Distribution at End of History Matching (x-section view North-South Direction)

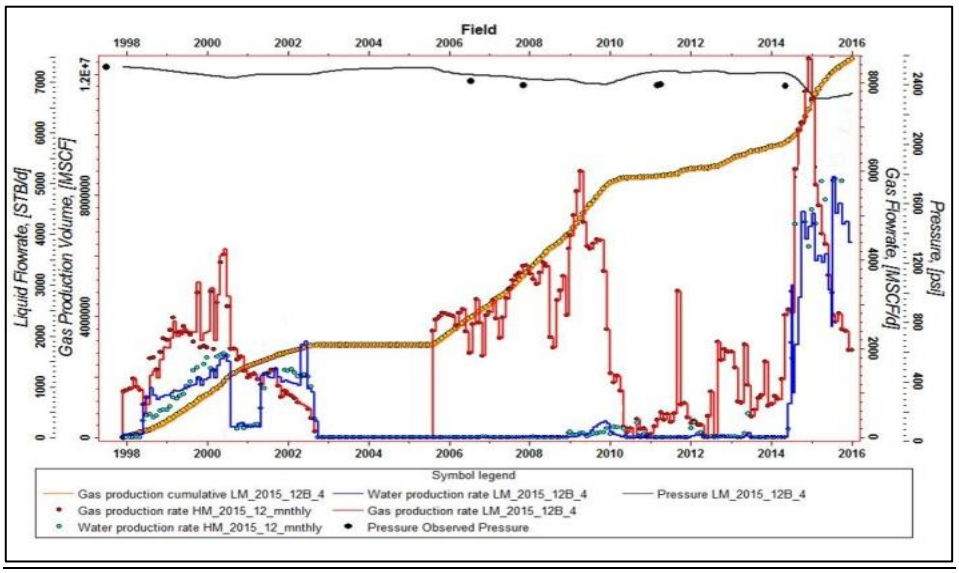

Figure 10. Field Gas rate, Gas Cum,Water rate, And Reservoir Pressure History Match.

- Prediction

This section focused the prediction of the future field/reservoir performance. To obtain the perfect scenario to optimize production of the field, a total number of 6 (six) different forecast cases were run up to December 2024. The forecast cases considered were as follows:

Case 1: Base Case or No Further Action (NFA)

Case 2 : Install low pressure compressor

Case 3 : Work over 2 wells

Case 4 : Add 1 infill drilling well

Case 5 : Combination Scenario 2 and 3

Case 6 : Combination of Scenario 3 and 4

Figure 11 and 12 presented the result of case 1 (Base Case) and 6 respectively.

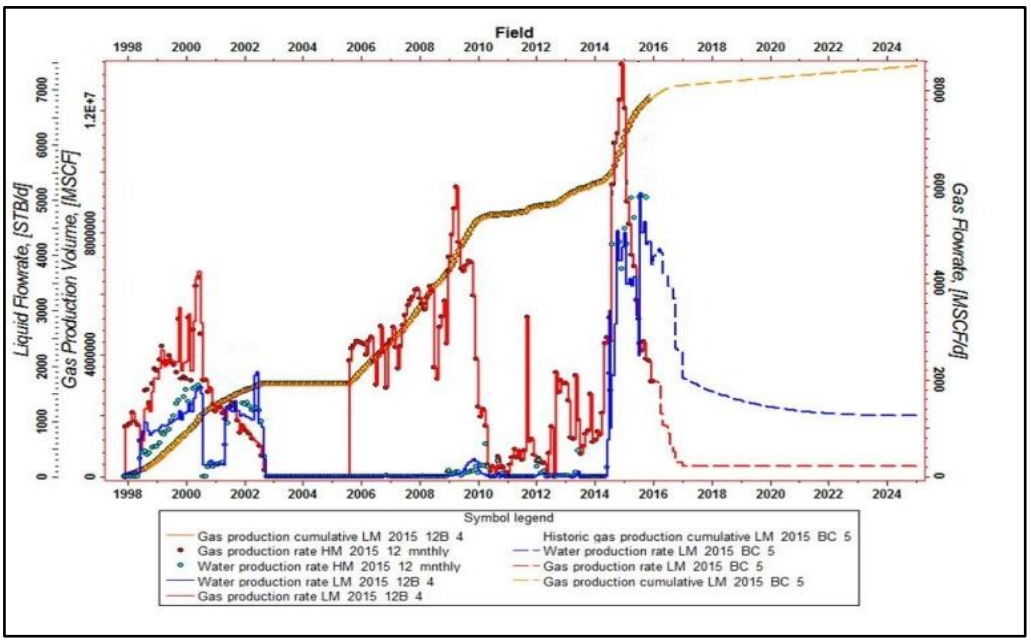

Figure 11. Performance Prediction of Case 1: No Further Action (NFA)

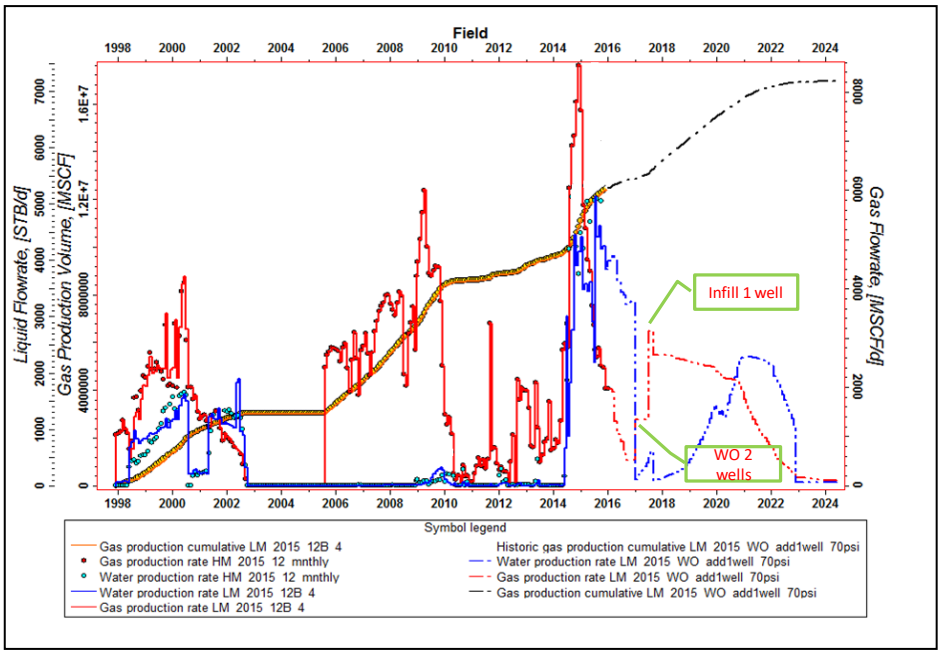

Figure 12. Performance Prediction of Case 6 : Combination of Case 3 and Case 4

Table 2 listed the result of Case 1-6.

Predictive Case	Definition	OGIP (BScf)	Peak gas prod (MMScfD)	Peak water prod (STB/D)	cum gas production (BScf)	RF
Case 1	No Further Action (NFA)	22.5	0.3	1566	13.47	59.87%
Case 2	Install low pressure compressor		1.2	3234	14.85	66.0%
Case 3	Workover 2 wells		1.35	478	15.13	67.2%
Case 4	Drilling 1 infill well		2	2561	16.75	74.4%
Case 5	Combination of Scenario 2 and 3		2	1128	15.94	70.8%
Case 6	Combination of Scenario 3 and 4		2.89	2100	16.93	75.2%

Based on RF comparison above case 6 is the best case. To select the best scenario economic evaluation of each scenario will be consider.

E. Economic Evaluation

In determining the economic feasibility of each oil development cases, net present value (NPV), with 10 % interest rate will be used as the main indicator. The following cost and condition assumption will be used to conduct the economic analysis :

Drilling Cost/well	=	4.5	MMUS$
Workover cost/well	=	353	kUS$
Opex / year	=	531	kUS$
Gas price	=	8.74	$/MMBTU
Compressor	=	1231	kUS$
Maint. Comp	=	49	kUS$

To generate economic calculation the PSC rule for gas project is applied for split calculation between government and PSC. The following term and condition is applied:

Contractor share after tax	35%
Government share after tax	65%
Contractor tax	44%
First Tranche Petroleum (FTP)	20%

Economic analysis run was made for the performance prediction cases explained in the previous section. Table 3 presented economic comparison of each case. According to above table, case 6 showing best result.

Table 3 Economic Comparison of Several Case Run

Summary Result							
Parameter	Cae 1	Case 2	Case 3	Case 4	Case 5	Case 6	Unit
	Base Case	Compressor	WO	Drilling	Comb. case 2&3	Comb. case 3&4	
General Input							
Initial Gas Rate	0.2	1.1	1.1	1.0	1.7	1.8	MMSCFD
Gas Cum	640	1,996	2,262	3,917	3,061	4,085	MMSCF
Gas price (esc. 2% p.a)	8.74	8.74	8.74	8.74	8.74	8.74	US$/MMBTU
CAPEX - Drilling Cost	-	-	-	4500	-	4500	kUS$
CAPEX - Facilities Cost	-	1,231	-	0	1,231	0	kUS$
OPEX - Workover Cost	-	-	706	-	706	706	kUS$
OPEX Cost	531	580	531	531	580	531	kUS$/year
Gross Rev.	7312	22,289	25,586	43,919	34,147	44,891	kUS$
Cost Recovery	1415	5,870	4,951	10,089	6,576	10,503	kUS$
Government share							
- Gov. income	4128	10,672	13,413	22,863	17,921	23,093	kUS$
- NPV @ 10% disc. rate	2709	7,734	9,091	15,652	12,847	16,988	kUS$
Unrecovered Cost	-	-	-	-	-	-	kUS$
Contractor Share							
- Cont. income	3184	11,617	12,173	21,056	16,226	21,798	kUS$
- IRR	>100%	>100%	>100%	>100%	>100%	>100%	
- POT	-	-	-	0.6	-	0.03	Year
- NCF - Net Cashflow	1769	5,747	7,222	12,311	9,650	12,347	kUS$
- NPV @ 10% disc. rate	1161	3,892	4,895	8,146	6,645	8,936	kUS$

IV. Conclusion

LM gas field is water drive gas reservoir with current RF about 55%, an integrated production analysis and optimization had been conducted with conclusions as listed below:

1) DST analysis on DC-01 well defined reservoir parameter, boundary and deliverability which are P*= 2520 psia, k= 229 mD, Total skin= 8, detected sealing fault in north east with distance 175 m, and AOF 45 MMscfd.
2) Conventional material balance method gave OGIP 22.7 BScf, aquifer strength 34 B/D/psi, whereas modern production analysis estimated OGIP 22.35 BScf, aquifer strength 34 B/D/psi. Those two method shows good consistency with OGIP volumetric calculation of previous static reservoir model 22.50 BScf with discrepancy OGIP value +/- 1%.
3) Dynamic reservoir model able to describe reservoir performance, by conducted history matching it was observed that the field gas production rate, water production rate, and reservoir pressure measurement was almost accurately matched.
4) The production optimization of LM gas field was achieved by using the dynamic reservoir simulation method . In this thesis work, 6 (six) different prediction cases were run up to December 2024 to optimize production. Case 6 is the best result with highest RF 75.2% and minimal water production.

5) Economic analysis was run for six (6) cases to guide in selecting the best case. Economic result suggested case 6 is the best result with highest value of contractor NPV 8.93 MMUS$ and fastest POT 0.03 year.

References

[1] Ahmed, Tarek H., Reservoir Engineering Handbook, 3th Edition, Texas : Gulf Publishing Company, 2006.
[2] Arcaro, D. P., Bassiouni, Z.: “The Technical and Economic Feasibility of Enhanced Gas Recovery in the Eugene Island Field by Use of the Coproduction Technique,” JPT, May, 1987, pp. 585-590.
[3] Dake, L., The Practice of Reservoir Engineering. Amsterdam: Elsevier Publishing Company, 1994.
[4] El-Ahmadi, et all, "Overestimation of Original Gas in Place in Water-Drive Gas Reservoirs Due to a Misleading Linear p/z plot", presented at Canadian International Petroleum Conference, Canada, 2001.
[5] EMP Malacca Straits S.A Team, "Lower Menggala Integrated Reservoir Study Report", Jakarta, 2009.
[6] Gomaa, Ezzat, “Reliability & Consistency of Core Analysis PVT Data”, In-House Training Course, Jakarta, 2009.
[7] Mattax, Calvin C., Reservoir Simulation, USA : Society of Petroleum Engineer Inc., 1990.
[8] Widiantoro, Panca S., and Hakim, Arif R., "Production Data Analysis: Estimating OGIP and Forecasting Gas Production Profile From Rough Data of Over-Pressured Gas Reservoir", presented at APOGCE, Bali, 2015.
[9] Wang, Sharon and Tunjar, Cesar, "Quickly Identifying Well Problem by Modern Production Analysis for a Better Stimulation Plan", SPE Production and Operation Symposium, Oklahoma, 2009, p.1-3.

Surface Deformation Monitoring of Sinabung Volcano using Multi Temporal InSAR Method and GIS Analysis for Prone Area Assessment(#651)

Arif Aditiya[1,a], **Yosuke Aoki**[2,b] , **Ranie Dwi Anugrah**[3,c]
[1] Civil Engineering Department, The University of Tokyo, Tokyo 151-0063, Japan
[2] Earthquake Research Institute, The University of Tokyo, Tokyo 151-0063, Japan
[3] Urban Engineering Department, The University of Tokyo, Tokyo 151-0063, Japan
[3] Geospatial Information Agency of Indonesia, Jl. Raya Jakarta-Bogor Km. 46, Cibinong, Indonesia
[a]arif@iis.u-tokyo.ac.jp, [b]yaoki@eri.u-tokyo.ac.jp, [c]ranie@env.t.u-tokyo.ac.jp

Abstract. *Sinabung Volcano located in northern part of Sumatera island is part of a hundred active volcano in Indonesia. Surface deformation is detected over Sinabung Volcano and surrounded area since the first eruption in 2010. We present Interferometric Synthetic Aperture Radar (InSAR) time-series method of ALOS-2 L-band SAR data acquired from December 2014 to July 2017 to reveal surface deformation with high spatial resolution. The method includes focusing the SAR data, generating interferogram and phase unwrapping using SNAPHU tools. The result reveal significant deformation over Sinabung Volcano areas at rates up to 10 cm during observation period and the highest deformation occurs in western part which is trajectory of lava. We concluded the observed deformation primarily caused by volcanic activity respectively after long period of rest. In addition, Geographic Information System (GIS) analysis produces disaster affected areas from Sinabung eruption. GIS is reliable technology used to estimate the impact of the hazard scenario to the exposure data and develop scenarios of disaster impacts to inform their contingency and emergency response plan. The GIS results include the estimated affected area divided into 3 zones based on pyroclastic lava flow, pyroclastic fall (incandescent rock and ash), such as disaster prone area I, disaster prone area II, and disaster prone area III. The highest damage occurred in zone II due to many settlements are scattered in this zone. This information will be support stakeholders to take emergency preparation for disaster reduction. The continuation of this high rate of decline tends to endanger the population in next periods.*

Keywords: *Surface deformation, Sinabung, InSAR, Time Series, ALOS-2*

I. Introduction

Sinabung volcano which located in northern part of Sumatera island is part of a hundred active volcano in Indonesia called by ring of fire (figure 1). Therefore some of disasters caused by tectonic and volcanic activities are frequently occurred in surround area. As the active volcano, Sinabung has potential impact of disaster such as eruption, lanslide and earthquake caused by volcanic activity. Reported by the Center for Volcanology and Geological Hazard Mitigation (CVGHM) of Indonesia,

Sinabung volcano since early August 2017 showed its activity until recent days. It has been observed thin white smoke reaches a height of 50-1000 m from the mount. Visually and through the seismograph has been observed 1 eruption with the ash column height reaching 2000 m above the mount, leaning to the east. Observed lava falling as far as 500-1000 m to

the southeast and east.

In the context of volcano monitoring, microwave remote sensing technique has reliable tool to observe suface deformation due to volcanic activity [1]. Interferometric Synthetic Aperture Radar (InSAR) has demonstrated its high performance in measuring surface displacements in different conditions and scenarios [2]. In particular, the advanced InSAR time series processing method referred to as Small BAseline Subset (SBAS) [3], that allows studying both the spatial and temporal variability of the surface displacements, has proven to be particularly suitable in volcanoes, earthquakes and landslides and human-induced deformation such as subsidence due to aquifer exploitation, gas and mining activities, and building of large infrastructures.

We will show surface deformations due to activities of Sinabung eruption are detectable with InSAR approach and estimate disaster prone area by using GIS technique. The main objective this research is to obtain rates of deformation and to assess disaster prone area to reduce risk of disaster in the term of towards civilian resilience.

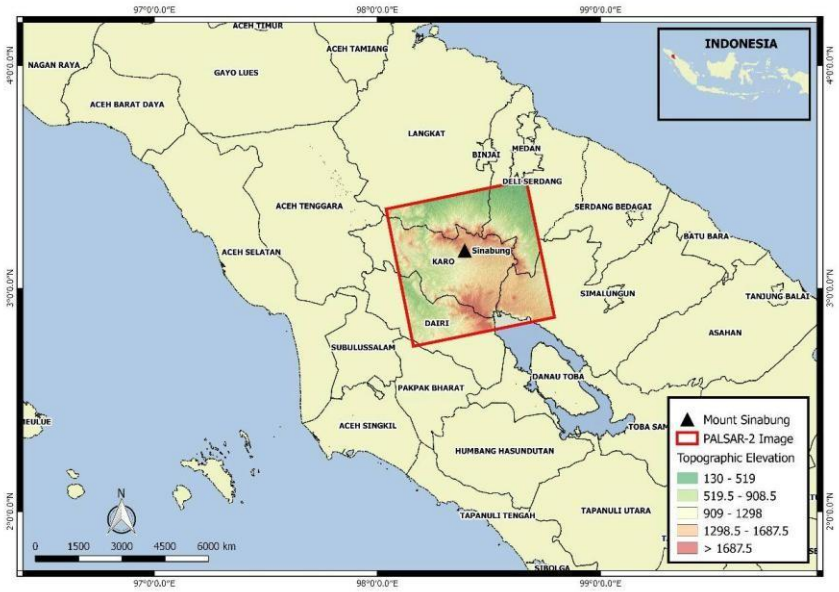

Figure 1. Geographic location of Mt. Sinabung, North Sumatera of Indonesia and red rectangle of PALSAR-2 image

II. Methodology

1.1. Data

The data used in this study is the PALSAR-2 (Phased Array Type L-band Synthetic Aperture Radar) sensor onboard of the Advanced Land Observing Satellite (ALOS-2) images and acquired period from December 2014 to July 2017. Table 1 shows the cover ranges of the PALSAR-2 data used in this study. These data sets were acquired in the ascending orbit with an off-nadir angle 28.2°. Observation parameters for all the images were as mode Strip Map and right looking direction. All baseseline of pairs images less than 300 m, but one pairs had a baseline of 318 m. The coherence was good performs at volcano summit and its surround, meanwhile less coherence in vegetation area.

Table 1. List of ALOS-2/PALSAR-2 data

Satellite	Orbit	B_{PERP}	Track	Nadir	Acquisition	Look
ALOS-2	Asc.	0 (M)	152	28.2°	20141202	Right
ALOS-2	Asc.	-125.1	152	28.2°	20150922	Right
ALOS-2	Asc.	-318.9	152	28.2°	20151201	Right
ALOS-2	Asc.	-123.1	152	28.2°	20160531	Right
ALOS-2	Asc.	0	152	28.2°	20160712	Right
ALOS-2	Asc.	-4.4	152	28.2°	20160920	Right
ALOS-2	Asc.	-34.6	152	28.2°	20170207	Right
ALOS-2	Asc.	-258.2	152	28.2°	20170711	Right

These data were used to generate interferogram and to obtain rates of surface deformation. A Shuttle Radar Topography Mission (SRTM) version 4.1 was used to eliminate the topographic phase.

1.2. InSAR Technique

Interferometric Synthetic Aperture Radar (InSAR) is a reliable microwave remote sensing technique using at least two or more SAR images acquired at different times to generate displacement maps to detect surface changes over a specific area. In the interferometric SAR data processing, the interferograms are generated by combining two complex SAR images **[3]**.

$$\phi_{int} = \phi_{topo} + \phi_{defo} + \phi_{orb} + \phi_{atm} + \phi_{scat} + \phi_{noise}$$

where ϕ_{int} is interferometric phase, ϕ_{topo} is topographic phase, ϕ_{defo} is deformation phase due to the deformation in the radar line of slight, ϕ_{orb} is deterministic flat earth phase and the residual phase signal due to orbit in determination, ϕ_{atm} is atmospheric phase, ϕ_{scat} is phase due to a temporal and spatial change in the scatter characteristics of the earth surface between the two observation times, and ϕ_{noise} is phase degradation factors, caused by e.g., thermal noise, coregistration noise and interpolation noise. Furthermore InSAR approach, two SAR images from slightly different orbit configurations and at different times are combined to exploit the phase difference of the signals LOS (line of sight). By assuming that the scattering phase is the same in both images, the interferometric phase ϕ is a very sensitive measure of the range difference R_2 - R_1 i.e:

$$\varphi = \varphi 1 - \varphi 2 = 4\pi/\lambda\ (R2 - R1)$$

(Here, ϕ_1 and ϕ_2 are the phases of the first and second SAR images, respectively; R_1 is the distance from the SAR to the scatterer by the first acquisition; R_2 is the distance by the second acquisition; and , λ is the wavelength, as for L-band ALOS-2 data λ is 23.6 cm.

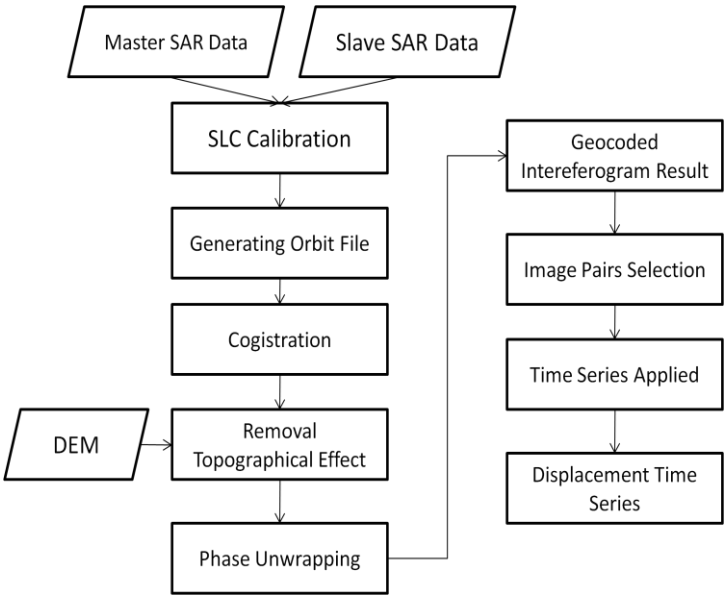

Figure 2. Methodology of InSAR Diagram

InSAR measures the change in path length in the satellite line-of-sight (LOS) between observations. Many factors contribute to changes in path length, but with appropriate removal of topographic effects, and if atmospheric and ionospheric effects are small and/or can be isolated, path length changes correspond to deformation of the Earth's surface.

1.3. GIS Technique

Geographic Information System (GIS) technique has applied to assess disaster prone area whereas many population living in Sinabung volcano. Disaster prone assessment aim to reduce the impact of disasters by prepared to respond when a disaster occurs. In order disaster mitigation, contingency planning activities can be undertaken prior to a disaster based on a realistic disaster scenario. This study has been used InaSAFE plugin tool of Quantum GIS to assess disaster impact and obtain affected people and building. InaSAFE package that produces natural hazard impact scenarios for better planning, preparedness, and response activities [4]. The population data should be in a raster format and it can be obtained from national demographic agency or WorldPop. WorlPop is open population data set for almost all of Africa, Asia and America with high resolution data, approximately 100 m cell size.

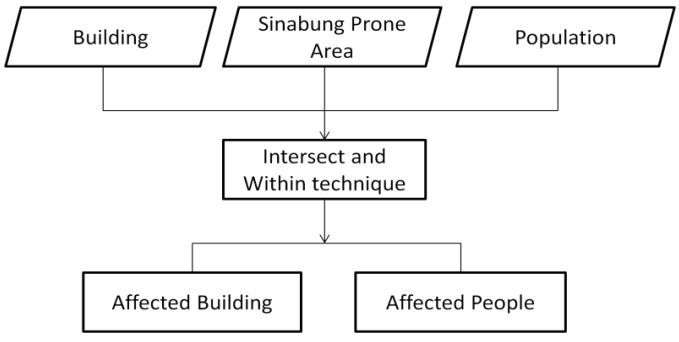

Figure 3. Diagram of GIS technique for Affected Disaster Estimation

This method will be directly related to the geographical conditions, social and economic communities living around the volcano. By adopted the result obtained from this method can be mitigate disaster impact.

III. Result and Discussion

We generated 28 interferograms and processed time series data for a region of Sinabung volcano by using GIAnT program [5]. For the SBAS approach, we computed all interferograms and the wrapped phase was corrected for spatially-uncorrelated look angle error and noise associated with the master image. We have applied Small Baseline Subset (SBAS) technique [2] to reduce spatial decorrelation. Atmospheric artifacts are reduced through spatial-temporal filtering after the mean deformation is obtained. Iterative processing can further improve the time-series deformation estimates. By using this algorithm each deformation according to time period is able to calculate more precisely by minimizing all error components.

Figure 5 shows point A and B were located in western part of Sinabung summit have been surface deformation during image obervation period. Its deformation reach up to ~ -6-7 cm/ year. Meanwhile point C which is located in northern of Sinabung summit has deformation ~ -1.9 cm/ year and point D~ -0.8 cm/ year. Point G has significant deformed up to ~ -16 cm during obsevation period and followed by point F ~ -9 cm which near Sinabung summit.

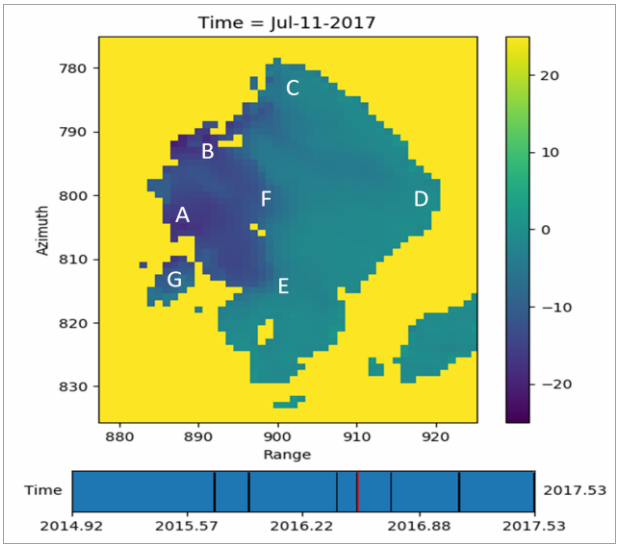

Figure 4. Observation Point at Sinabung Volcano

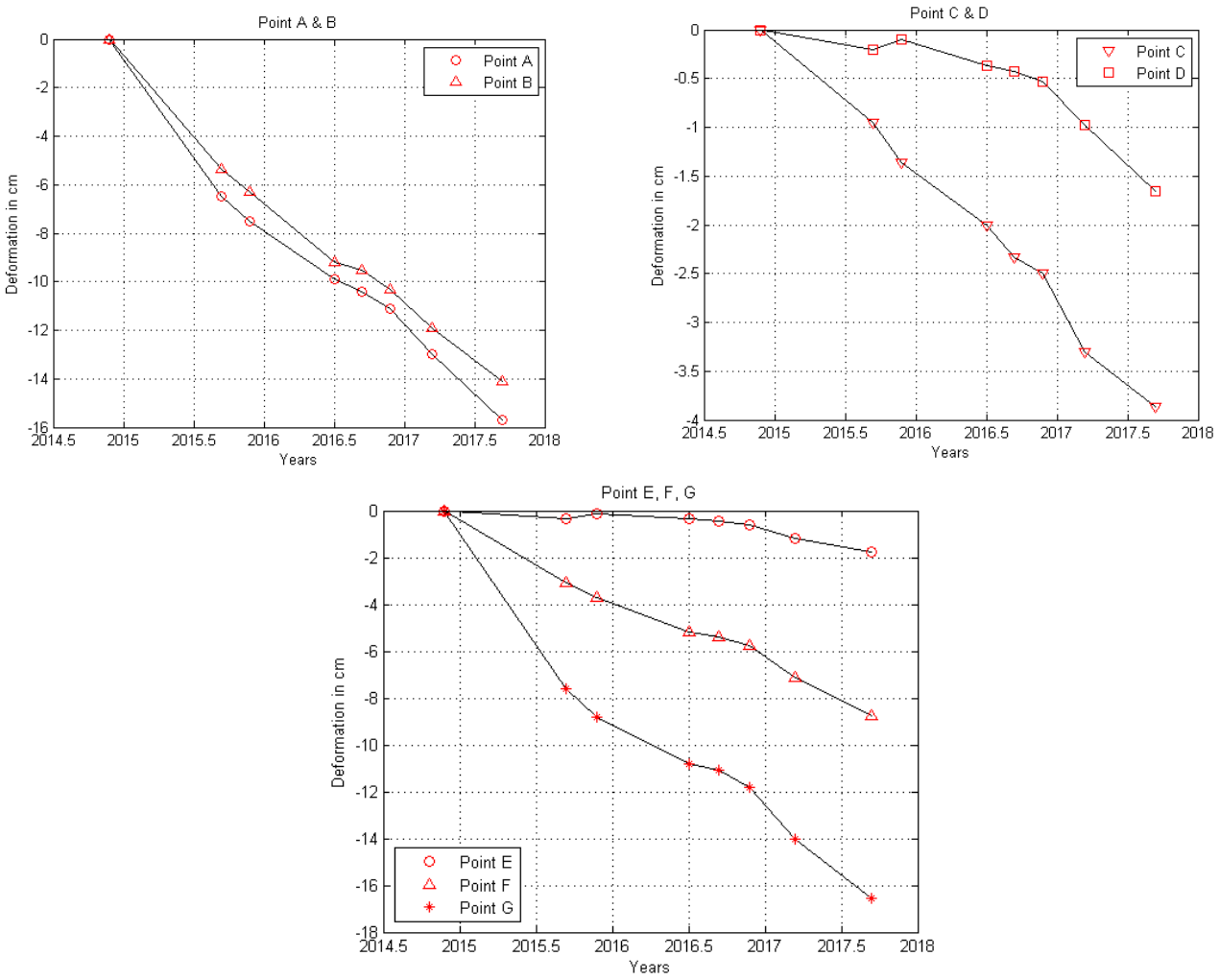

Figure 5. Time Series InSAR

The deformation was likely due to the deflation of magma from a deep source to the shallow reservoir. This phenomenon may have been caused by the deppressurization of the magma chamber due to periodic volcanic degassing at the Sinabung summit.

The GIS data were used to estimate the number of affected buildings and residents are data of hazard and exposure. Data hazard is a eruption data of Sinabung eruption obtained from Sinabung summit meanwhile exposure data consist of building data which obtained from OpenStreetMap and population data obtained from World Pop. Furthermore hazard and exposure data was processed using InaSAFE. The outputs generated by InaSAFE are estimates of the number of affected buildings and estimates of the number of affected people based on disaster prone areas of Sinabung eruption.

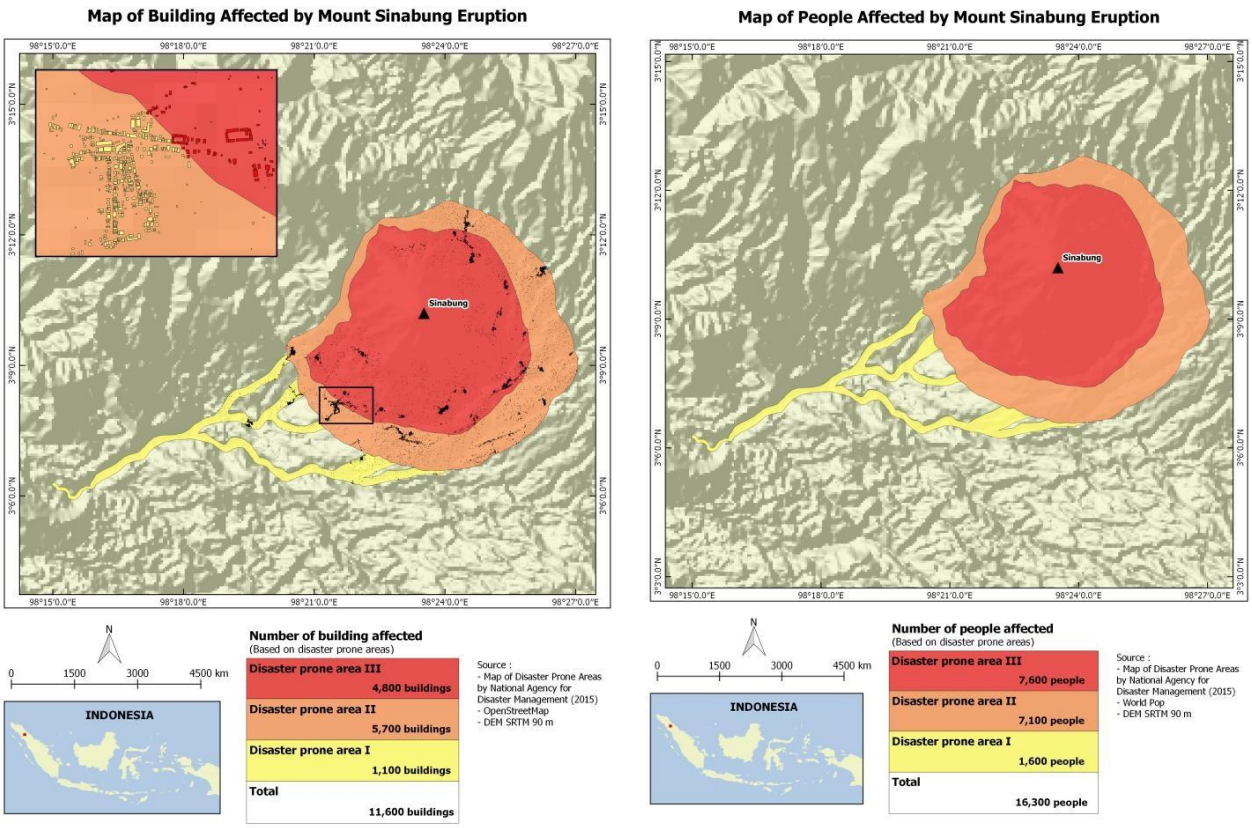

Figure 6. GIS Result of Building (left) and People Affected (right)

Figure 6 shows the results of GIS techniques to determine the number of buildings and people affected by eruptions. Criteria of affected areas refers to the National Disaster Management Agency (Badan Nasional Penanggulangan Bencana). Table 2 shows the number of buildings and affected persons in prone areas 1, 2 and 3. The disaster-prone area 2 has potential to suffer huge losses due to the large number of residents who live and the number of building affected by eruption.

Table 2. The Estimation Results of Buildings and Populations affected by the eruption of Sinabung

	Building affected	People affected
Disaster prone area 3	4800	7600
Disaster prone area 2	5700	7100
Disaster prone area 1	1100	1500
Total	**11,600**	**16,200**

IV. Conclusion

This work has presented an analysis of the surface deformation phenomena in Sinabung volcano. The advanced multi-temporal InSAR technique has applied to this site by using 8 PALSAR-2 images acquired from December 2014 to July 2017. We identified a few locations have deformed rates up to

15 cm during observation period. The average subsidence velocity map has been retrieved by Small Baseline technique processing to reduce spatial decorrelation characteristics among image itself. A rapid period of surface defromation occured during the 2,5 years of the post-eruption period. The greatest surface deformation was measured to be ~6-7 cm/ year at the western part of Sinabung summit. We concluded the observed deformation primarily caused by volcanic activity respectively after long period of rest. The surface deformation at Sinabung volcano was correlated greater locally. there could also be possible existence of other causes due to geological factors in almost all deformation areas such as tectonic processes in Sumatra island. Future investigation can improve the findings of this study by utilizing GPS technique.

In addition the results of GIS analysis show that disaster-prone area 2 has potential to suffer huge losses than disaster prone area 1 due to the large number of residents who live and the number of building affected by eruption. This information can be used by local government to mitigate disaster impact and evacuation people needed.

Acknowledgement

We thank to Indonesia Endowment Fund for Education (LPDP) for financial support during study period. These data were made available by the PALSAR Interferometry Consortium to Study our Evolving Land surface (PIXEL) under a cooperative research contract with the Earthquake Research Institute (ERI) of the University of Tokyo.

References

[1] E. Chaussard, F. Amelung, and Y. Aoki, "Characterization of open and closed volcanic systems in
Indonesia and Mexico using InSAR time series," *J. Geophys. Res. Solid Earth*, vol. 118, pp. 3957– 3969, 2013.

[2] Yan Zhan and Patricia M. Gregg, "Data Assimilation Strategies for Volcano Geodesy," *J. Volcanol. Geotherm. Res.*, 2017.

[3] Paolo Berardino, Gianfranco Fornaro, Riccardo Lanari, and Eugenio Sansosti, "A New Algorithm for Surface Deformation Monitoring Based on Small Baseline Differential SAR Interferograms," *IEEE Transactions on Geoscience and Remote Sensing*, pp. 2375-2382, 2002.

[4] R F Hanssen, *Radar Interferometry : Data Interpretation and Error Analysis*. Dordrecht: Kluwer Academic, 2001.

[5] I. R. Pranantyo, M. Fadmastuti, and F. Chandra, "InaSAFE Applications in Disaster Preparedness," in *4th International Symposium on Earthquake and Disaster Mitigation 2014 (ISEDM 2014)*, Bandung, 2015.

[6] P. S. Agram et al., "New Radar Interferometric Time Series Analysis Toolbox Released," *Eos Trans. AGU*, vol. 97, no. 7, pp. 69-70, February 2013.

Geo-mechanics Data Analysis Applied to Hydraulic Fracturing Design in Lower Pematang Formation, Malacca Strait PSC (#656)

Sri Rahayu[1,a], Astra Agus Pramana[1,b], Trijana Kartoadmodjo[1,c]
[1]Petroleum engineering Department, Trisakti University, Jakarta, Indonesia
[a]srahayu.effendi@yahoo.com, [b]agus.prama@gmail.com, [c]trijana@trisakti.ac.id

Abstract—*Oil and gas industry has huge impact to Indonesia economic growth. As major of oil producer, development of technology to improve the production should be as a priority. The Lower Pematang Formation is a high-temperature sandstone reservoir up to 350 F in the Central Sumatra Basin in Indonesia. It is a low-permeability reservoir around 0.5 to 3 mD, and so oil flow rates are often sub-commercial, despite high initial reservoir pressure and gas-lift. The obvious method to improve oil rates and recoveries in this reservoir is hydraulic fracturing. During simulating the hydraulic fracturing design, there some uncertainty parameter which effect to the geometry and fracturing propagation. Geo-mechanic data is one of most important data to be inputted in hydraulic fracturing design. The data source generate from core lab test, open-hole log, sonic log, formation leak of test or drilling report. Little is known about this formation and drilled cores are rare. Proposes of studying geo-mechanic are to analyze wellbore stability, elastic rock properties, in-situ stress distribution, to estimate pore pressure, to determine the prospect of hydraulic fracturing potential. Geo-mechanical calculation is one of main focused on this study in order to improve the Hydraulic fracturing design.*

Keywords—*Elastic Rock Properties, Geo-Mechanics, Hydraulic Fracturing, In-situ Stress, Pore Pressure*

I. Introduction

THE technological one-two punch of horizontal drilling and hydraulic fracturing has created a remarkable energy boom and created hundreds of thousands of jobs in the U.S. The possibility of continuously low natural gas prices is turning the United States into a prime destination for chemical companies and other businesses that rely on abundant amounts of natural gas. That is one of the reasons of this research. Hydraulic fracturing makes a significant contribution to the worldwide oil and gas production. It has proved to be capable of increasing both well production and the ultimate recovery achievable from a particular well and/or field. Geo-mechanical modeling is one of the important parameter while hydraulic fracturing designs.

This study applied in Srikandi field well design which has undergone three development phases. The third development phase is hydraulic fracturing which started from 2008 until 2014. Hydraulic fracturing summary and oil production history can be seen in Figure 1.

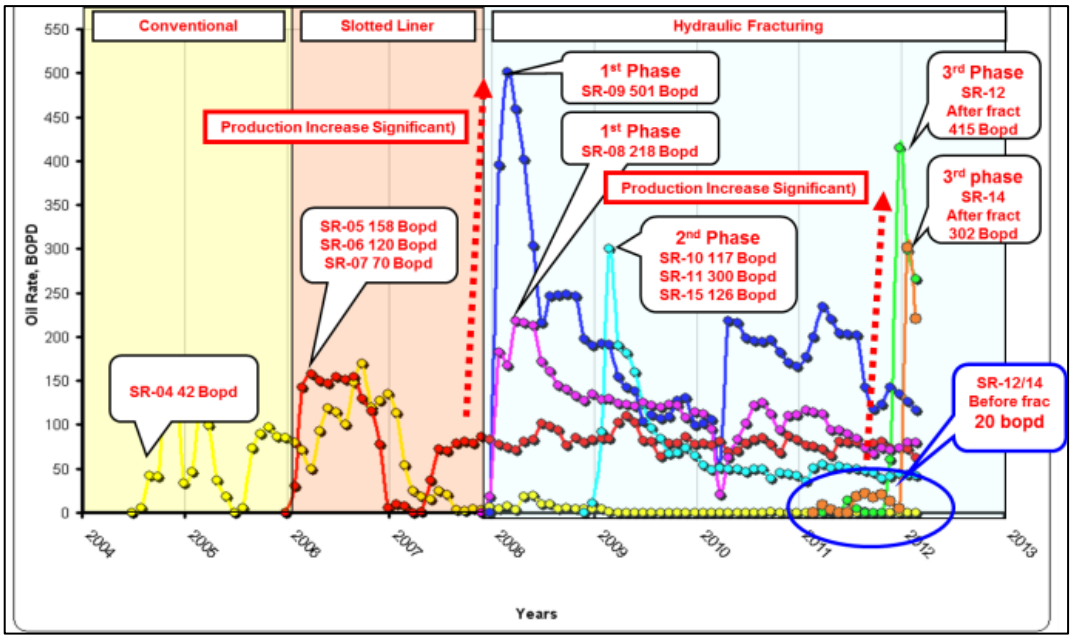

Figure 1. Srikandi field Production comparison [1]

Based on the history above, almost all wells was performed hydraulic fracturing in Lower Pematang CD so for the further hydraulic fracturing project will conduct in Lower Pematang AB which refer to success job in SR-12. The history of hydraulic fracturing in this field proves that the obvious method to improve oil rates and recoveries in this reservoir is hydraulic fracturing.

This study is chosen with several objectives as follow; Integrate and analyze the relevant logs, pressure survey and other data, to evaluate pore pressure and generate geo-mechanical modeling describing stress magnitude, stress orientation and rock mechanical properties then re-arrange the geo-mechanical modeling based on previous hydraulic fracturing result and current pressure data to improve hydraulic fracturing design and increase oil recovery and verify effect of geo-mechanical parameter to current hydraulic fracturing design compare with previous design.

II. Methodology

Geo-Mechanical Modeling is a description of formation geo-mechanic parameters which includes; a description of rock fabric; Rock elastic parameters, including young modulus and Poisson's ratio; Rock strength parameters - unconfined compressive strength, tensile strength and internal friction angle; and Stress model - vertical stress, minimum and maximum horizontal stress magnitudes and orientation and pore pressure

Rock mechanics is the study of the mechanical properties of a rock, especially those properties which are of significance to Engineers. It includes the determination and effects of physical properties such as bending strength, crushing strength, shear strength, moduli of elasticity, porosity, permeability and density, and their interrelationships.

The fundamental theory for pore pressure prediction is based on Terzaghi's and Biot's effective stress law (Terzaghi et al., 1996; Biot, 1941). This theory indicates that pore pressure in the formation is a function of total stress or overburden stress and effective stress. The overburden stress, effective vertical stress and pore pressure can be expressed in the following form:

$$P_p = \frac{\sigma_v - \sigma_e}{\alpha} \qquad (1)$$

Where, Pp is the pore pressure, σ_v is the overburden stress; σ_e is the vertical effective stress; α is the Biot's effective stress coefficient. It is conventionally assumed α = 1 in geo-pressure community

Rock Elastic Properties - The only tool that responds to the elastic properties of the formation is the sonic. When a pressure pulse is created in a wellbore filled with fluid, the complex phenomena that occur at the boundary between the wellbore and the formation result in the propagation of several types of waves into the formation [8].

Dynamic elastic properties can be calculated based on compressional and shear slowness data from sonic scanner. Together with bulk density logs data, dynamic elastic properties data for isotropic can be calculated by using equation from fjaer et al [7]. Dynamic shear modulus can be calculated by using equation below:

$$G_{dyn} = 13474.45 \left[\frac{\rho_b}{(\Delta t_s)^2}\right] \quad (2)$$

By substitution of equation 2 above, dynamic bulk modulus can be calculated by using equation below:

$$K_{dyn} = 13474.45\rho_b \left[\frac{1}{(\Delta t_s)^2}\right] - \frac{4}{3}G_{dyn} \quad (3)$$

Based on shear and compressional slowness data from sonic, dynamic poisson's ratio can be calculate by using equation below:

$$v_{dyn} = \frac{\frac{1}{2}(\Delta t_s/\Delta t_c)^2 - 1}{(\Delta t_s/\Delta t_c)^2 - 1} \quad (4)$$

Rearrange the equation 3 and 4, so dynamic young modulus can be obtained by equation below:

$$E_{dyn} = 2G(1 + v) \quad (5)$$

The dynamic elastic properties are different from their static properties measurement. For hydraulic fracturing design need static elastic properties as input. To calibrate the parameter, Eissa's correlation can be used [4].

In-situ Stress - Vertical stress was computed by integrating formation bulk density from surface to total depth (TD). The overburden is the weight of the column of sediments.

Although it is not measured directly, it can be easily computed as the integral over depth of the bulk density:

$$\sigma_v = \int_0^z \rho_{b(z)} . g . dz \quad (6)$$

However, ρb is rarely measured up to the surface more than once in the lifetime of a field (i.e., for seismic profiling). Research may be necessary to obtain an estimate of ρb between the top of the log and the surface. Furthermore, for deep-water projects, the significant effect of the water column on σv must be included.

A continuous profile of σh is obtained by using the following equation with the Biot constant α as an ad hoc potentially lithology-dependent calibration parameter:

$$\sigma_h = \frac{v}{1-v}(\sigma_v - \alpha p) + \alpha p \quad (7)$$

Use of this model is reasonable for low-porosity, low-permeability sandstones, shale and carbonates

A. Geomechanical modeling Procedures

The Geo-Mechanical Modeling is built by mathematical calculation and calibrate by core and current data. The calculation procedure as below:

1. Prepare well survey to determine true vertical depth as basic calculation.
2. Prepare raw logs data such as Gama ray, porosity log, bulk density log, neutron log, water saturation, and volume clay from composite log
3. Select the target zone based on petro-physical and reservoir evaluation.
4. Prepare raw sonic logs consists of compressional, shear slowness and dynamic poison's ratio
5. Dynamic elastic properties can be calculated based on compressional and shear slowness data from sonic scanner. Together with bulk density logs data, dynamic elastic properties data for isotropic can be calculated by using equation 2 until 5. As input to hydraulic fracturing design, need static values so the calibration of that parameters can be calculate by using Eissa's correlation [4] as follow:

$$E_S = 10^{[-0.11+0.77\ Log(\rho_b . E_{dyn})]} \quad (8)$$

This equation applies for medium porosity around 15 - 20%.

6. Calculate the overburden gradient by using the equation below from Matthews, 1967:

$$\sigma_{ovg} = 0.433\left[(1-\varphi)\rho_{ma} + (\varphi.\rho_f)\right] \quad (9)$$

7. Calculate Pore pressure gradient by using Eaton's equation for sonic logs data as follow:

$$\sigma_p = \sigma_{ovg} - (\sigma_{ovg} - P_{ng})\left(\frac{Vi}{Vn}\right)^x \quad (10)$$

Calculate Pore pressure Pp by using the equation below:

$$P_p = \sigma_p . z \quad (11)$$

8. Calculate overburden pressure and define as vertical stress. The equation as follow:

$$P_{ovg} = \sigma_{ovg} . z \quad (12)$$

9. Calculate minimum horizontal stress σh by using equation 7 with Biot's constant α as an ad hoc potentially lithology-dependent calibration parameter [6].Calibrate the biot's constant α based on current history of hydraulic fracturing.
10. Determine maximum horizontal stress σH value by using tectonic value in this area by using Formation Micro imager log.

B. Hydraulic fracturing simulation

Prepare input data based on research well available data. The data will categorize as follow:

1. Well data input consists of well completion, tubular, and perforation
2. Zone, describe the type of zone, geo mechanical parameters and Petro-physical properties
3. Reservoir Fluid, describe PVT and fluid properties
4. Fluid frac, information about compatible frac which will use on design complete with fluid frac properties
5. Type of proppant and properties choice which will used on design
6. Schedule, to input schedule treatment as simulation type choice.
7. Execute, Simulation execution

III. Result

A. Geo-mechanical model data

Formation Micro Imager log - In this study, Bore-hole image data (FMI) are available for SR-08 well which is vertical and it allowed to determination of in-situ stress direction and stress contras.

Base on analysis of the formation micro imager, the maximum regional stress direction approximately N50°E and the minimum stress azimuth of N140°E. Resistive fractures show one preferred orientation as seen as Figure 2

Rock Mechanical Tri-axial Core testing result from Lower Pematang formation of SR-15 - The testing program consisted of single and multi-stage tri-axial compression tests on supplied plug samples at room temperature for obtaining Mohr-Coulomb failure envelope delineation, Young's modulus and Poisson's ratio. The summary of tri-axial compression testing was shown in Figure 3 for multi stage respectively.

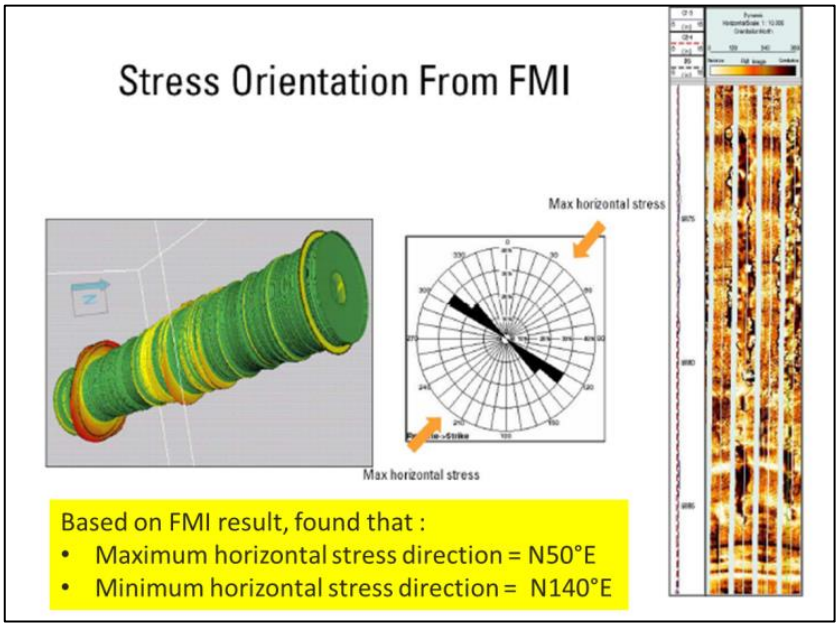

Figure 2. Formation Micro Imager result

sample ID	depth (ft)	orientation	Lithology	As-tested bulk density (gr/cm3)	Effective confining pressure (psi)	effective compressive strength (psi)	effective residual compressive strength (psi)	loading quasi-static young's modulus (psi)	loading quasi-static poisson's ratio
MS-3	6926.5	Vertical	sandstone	2427	415	8415		2.16E+06	0.31
					1245	14760		3.13E+06	0.28
					2283	19928		3.50E+06	0.28
					4105	26660		4.01E+06	0.25
					6226	38300	21450	4.32E+06	0.25
MS-2	6938.4	Vertical	shale	2436	882	13378		2.21E+06	0.23
					2425	20267		2.98E+06	0.29
					4410	29540	18480	3.15E+06	0.30

Figure 3. Summary of Multi-stage Triaxial Compression Tests

B. Geo-mechanical Calculation and Modeling

The geo-mechanical study was conducted in well SR-08 and SR-14 in Srikandi field. The study involved the integration and incorporation of a variety of logs, and field data to generate geo- mechanics model by using manual calculation based on several equation. Those two wells were chosen to compare between isotropic and anisotropic model, but SR-

14 not shown significant different trend compare with SR-08 due to formation type is mostly clean sand. Anisotropy effect only can be seen in layering shale formation type such as unconventional formation. This phenomenon should be studied in future.

a) Rock Elastic Properties

Rock elastic properties represent the elastic deformation behavior of the rock. For isotropic, the stress-strain behavior can be describe in two parameters, typically young modulus and Poisson's ratio.

Dynamic elastic properties can be calculated based on compressional and shear slowness data from sonic scanner. Together with bulk density logs data, dynamic elastic properties data for isotropic can be calculated by using equation from fjaer et al., 1992.

The dynamic rock elastic parameters are different with their static parameters. As input to hydraulic fracturing design, need static values so the calibration of that parameters can be calculate by using Eissa's [4].

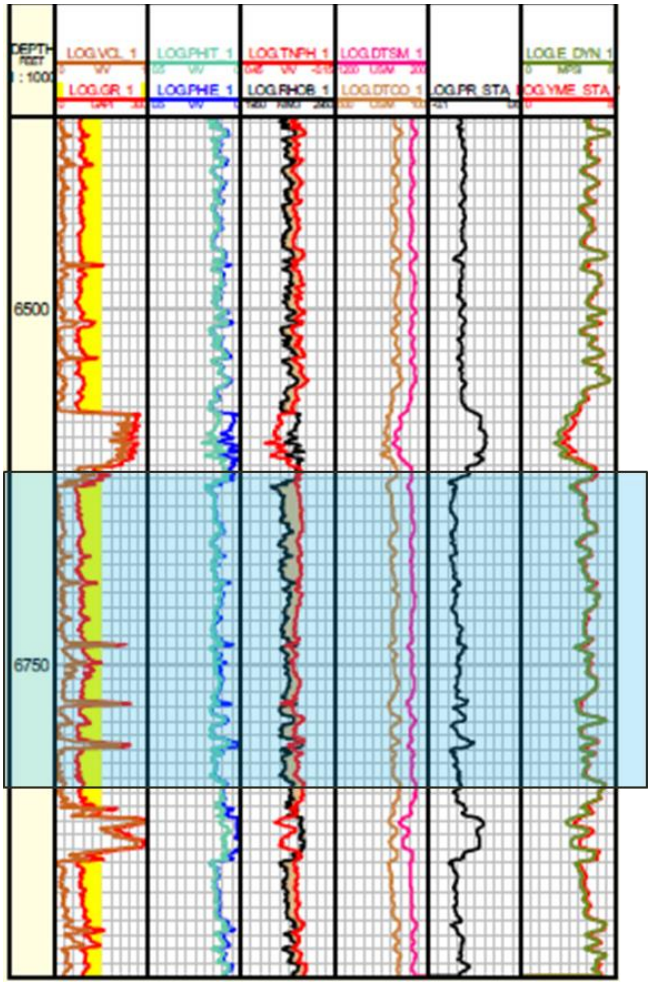

Figure 4. Rock elastic properties profile in SR-08

After calibration, the result of static rock elastic properties had shown in Figure 4. and 5. Track five and six describe the rock elastic properties such as poisson's ratio and young modulus as input of the calculation. The data was converted to static parameter and calibrated by using tri-axial core test data.

During the study of calibration dynamic to static poison's ratio, there is no direct relation between dynamic and static Poisson' ratio. Calibration of local data seems possible, but there is no universal correction factor.

Target zone in SR-08 is Lower Pematang AB in depth 6622 – 6737 ft.MD and perforated zone in 6630 – 6650 ft.MD. Based on isotropic calculation and calibrate with Eissa's correlation and core data, average value of sandstone young modulus in target zone is

around 4.26 E+06 psi and Poisson's ratio is around 0.25. The value of rock elastic properties in sandstone and shale is similar due to the sandstone in this formation typically tight formation with small permeability.

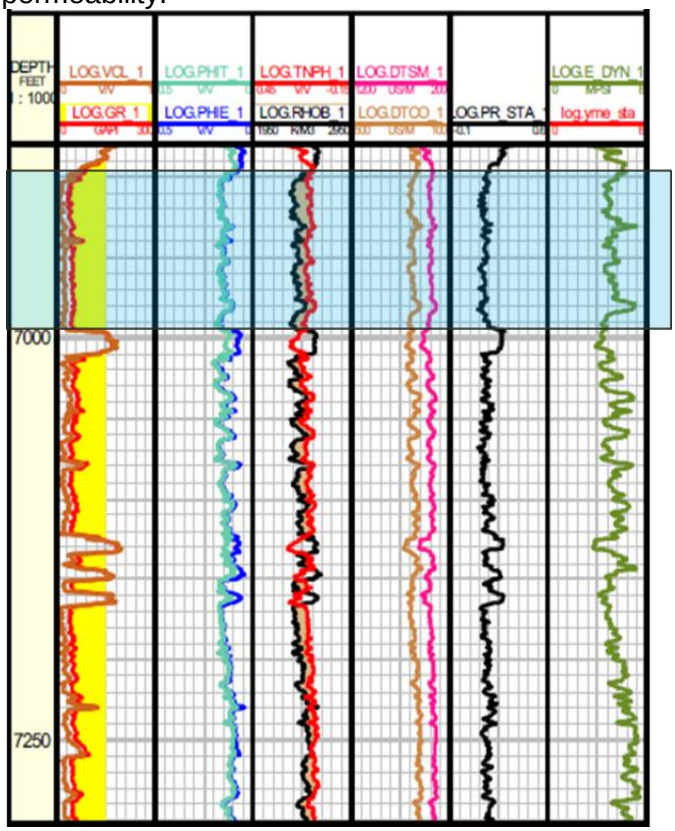

Figure 5. Rock elastic properties profile in SR-14

Figure 4. and 5. Has shown the calculation result of rock elastic properties in SR-14. Target zone in this well as same as SR-08 in Lower Pematang AB at depth 6890 feet until 7010 feet. The average Young's modulus is around 4.51E+06 psi and Poisson's ratio around 0.22.

b) Pore Pressure Estimation

The pressure data had taken from the analog well which has same layer. Before the data used for calibration, it should be interpolated into the datum survey. Pore pressure in this formation verified by the pressure data. Pore pressure is calculated by delta time shear compressional which convert to velocity as shown in Figure 6 and 7.

The delta time shear compressional pick to find the normal compaction trend. There are two kind of normal compaction trend that is normal compaction trend in shale and sand. Based on the velocity and normal compaction trend, pore pressure can be calculated by using Eaton's equation.

The track five described the result of hydrostatic pressure in black line and pore pressure in green line. The hydrostatic pressure is calculated by fluid gradient and true vertical depth. Eaton's equation shown in equation 10 has "x" as Eaton's constant variable. This parameter is modified based on current pore pressure data to adjust the pore pressure value from calculation to pore pressure measurement. The modified was done by shift the green line into the black dot by changing the Eaton's constant variable until got matching line.

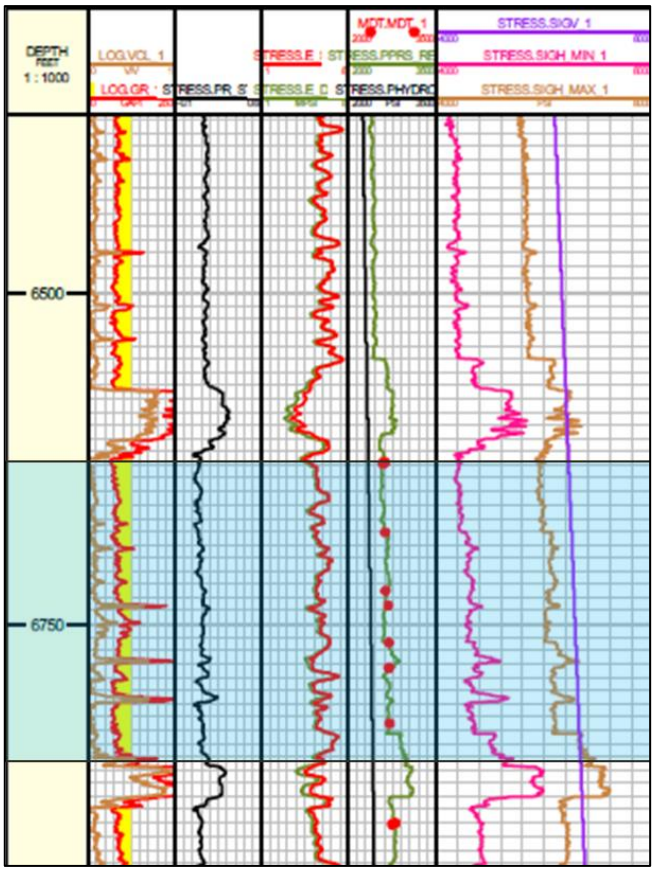

Figure 6. Stress profile in SR-08 after calibrated with current pressure data

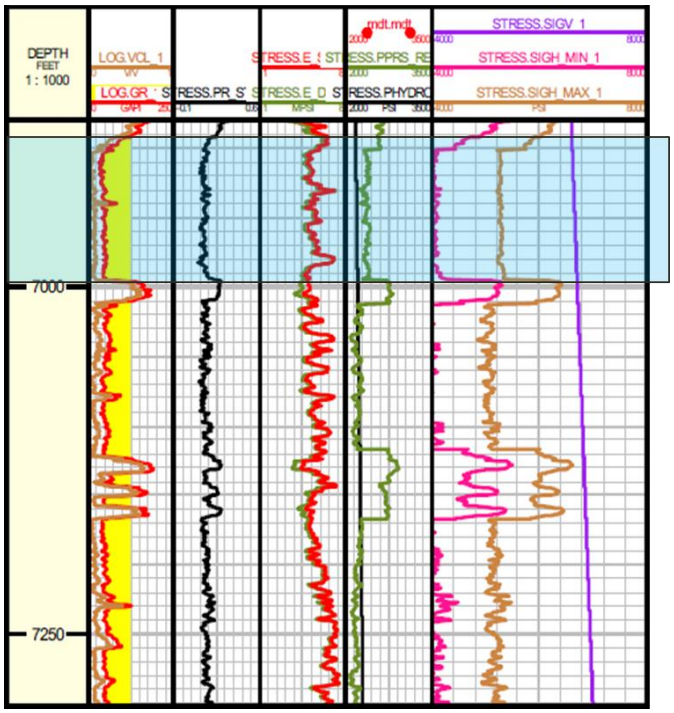

Figure 7. Stress profile in SR-14 after calibrated with current pressure data

c) Stress Profile Determination

The stress profile for both of wells is shown in Figure 6 and 7 specify in last track. Minimum horizontal stresses expressed the value of closure pressure in hydraulic fracturing design. This value calculated by using equation (Biot and Willis, 1957) with Biot's constant α as an ad hoc potentially lithology-dependent calibration parameter (Economides, 2000).

C. Hydraulic Fracturing Design Optimation

The hydraulic fracturing design in this study is built by using fracturing simulation software.

a) Fluid fract

The fluid used in this simulation called as ThermaFract which compatible with high temperature type of well around 305 Fahrenheit

b) Proppant selection

The type of proppant and properties choice which will be used on design is carboHSP mesh 16/30. Carbo-ceramics proppant also have good roundness and sphericity. The major considerations of proppant type and size selection are optimizing conductivity versus beneficial.

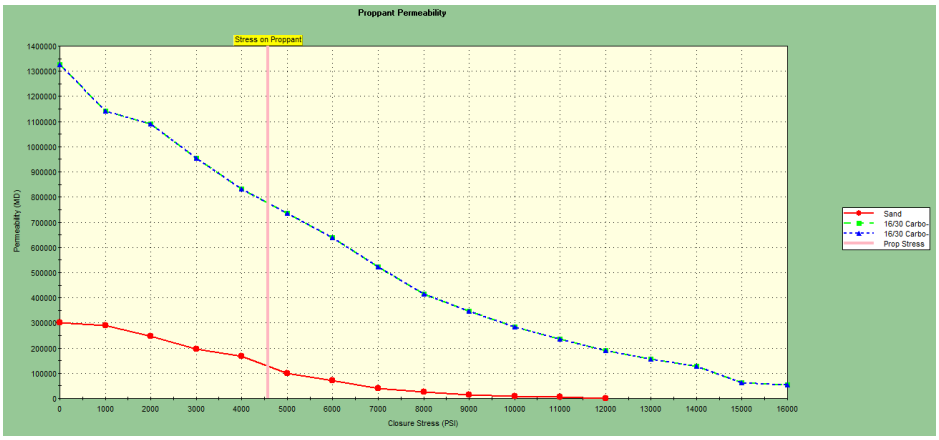

Figure 8. Proppant permeability vs closure stress

c) Execution

Simulation execution is final part of the simulation to generate the fracturing geometry result. Figure 9 is shown the result of hydraulic fracturing SR-08, which geo-mechanical parameters calculated by using isotropic concept. The result not showed good FCD compare with SR-14 in Figure 10. Those both of design will apply in Lower Pematang AB.

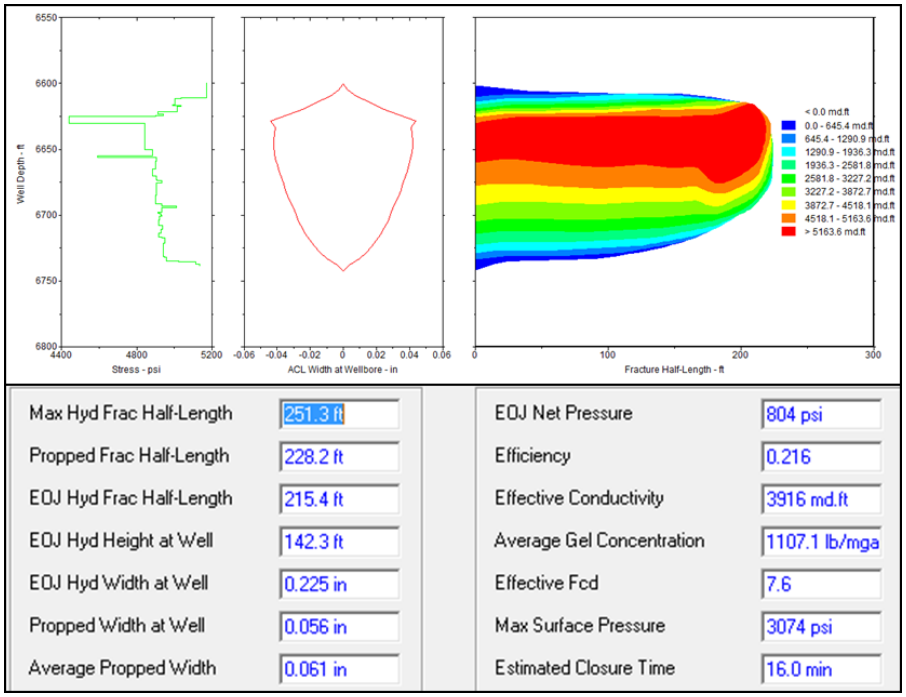

Figure 9. SR-08 Fracturing Geometry Result

Figure.11. is shown the result of SR-12 hydraulic fracturing design in previous campaign. This design has given good result which initial rate after hydraulic fracturing execution around 415 BOPD. So for both of two further propose of hydraulic fracturing which is SR-08 and SR-14 expect will give same result.

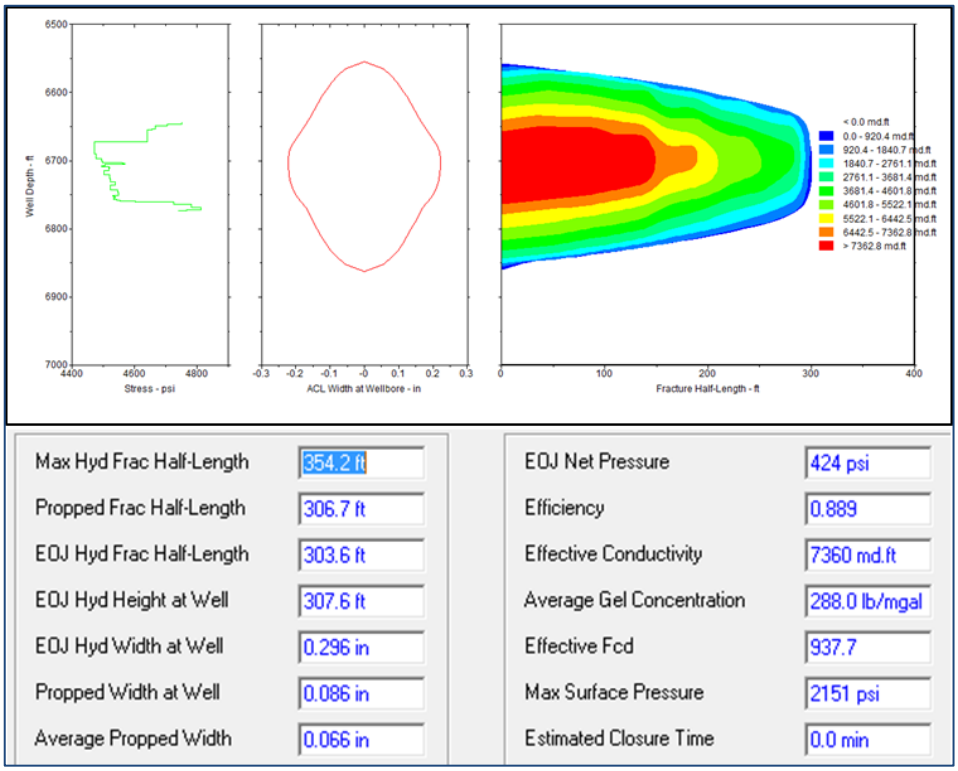

Figure 10. SR-14 Fracturing Geometry Result

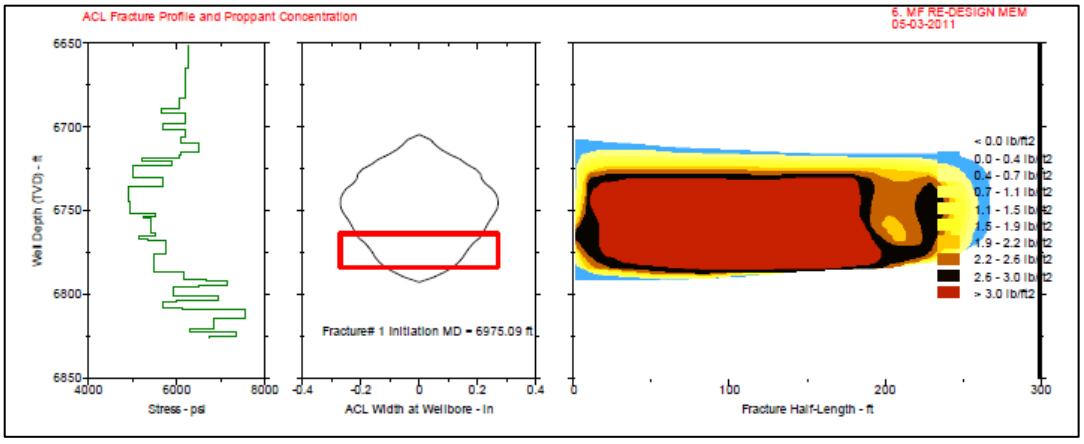

Figure 11. SR-12 Fracturing Geometry Result in Lower Pematang AB

IV. Conclusion

SR-14 previously studied for identify anisotropy effect into stress determination, but the formation target has clean sand so the anisotropy effect do not shown the significant different between isotropic but shown optimistic calculation. The main parameters calculate in geo mechanical modeling in Lower Pematang AB formation are rock elastic properties such as Young's modulus and Poisson's ratio, pore pressure, and stress profile. All those parameters are calibrated with current data. Treatment schedule was done by sensitivity to create the best fracture geometry design. SR-08 design by 90000 lb proppant with 29256 gal fluid and SR-14 design by 118600 lb proppant and 36561 gal

fluid. Based on the schedule treatment, fracturing job executed. The result of the design for SR-08 less than SR-14 due to SR-08 geo-mechanical calculation over estimated then SR-14 due to the geo mechanic parameter was generated by using anisotropy concept. SR-08 fracture geometry created in 228 ft half of length, 0.06 inch of width, and 3916 mD.ft of conductivity and SR-14 fracture geometry created in 306 ft half of length, 0.06 inch of width, and 7360 mD.ft of conductivity.

References

[1] Anonymous, “Well File Kondur Petroleum S.A”, Jakarta, 2010
[2] Anonymous, “Fracbook Design Aid and Data Manual”, Halliburton Company, Duncan, Oklahoma, 1971.
[3] Anonymous, ”Stimulation Book; A Course on Formation Damage, Acidizing and Hydraulic Fracturing”, BJ Company, Jakarta, 2006.
[4] Crain et al.,”Crain’s Petro physical Handbook”, website online.
[5] Economides, M.J., A Daniel Hill & Economides Christine E., “Petroleum Production System”, Prentice Hall, Englewoods Cliffs, New Jersey, 07632
[6] Economides, M.J., and Nolte, K.G., “Reservoir Stimulation”, Prentice Hall, Englewoods Cliffs, New Jersey
[7] Howard, G.C. and Fast, C.R., “Hydraulic Fracturing”, Monograph Volume of Henry L. Doherty Series, Society of Petroleum Engineers of AIME, New York, 1970
[8] Jaeger, J.C. and Cook, N.G.W., “Fundamentals of Rock Mechanics”, Chapman and Hall Ltd, Great Britain, 1971
[9] [9] Kermit E. Brown. “The Technology Of Artificial Lift Methods”, Tulsa, Oklahoma, 1984
[10] Tjondro. B., Kamiso, D. Rich &Suryaman., “Acidizing and Hydraulic Fracturing Intermediate”, Jakarta, 1997.
[11] Zhang, et al., “Pore Pressure Prediction from Well Logs: Methods, Modifications, and New Approaches”, Texas, 2011.
[12] Zoback. Mark D., “Reservoir Geomechanics”, New york, 2007

Balinese Cultural Values in Partnership (659)

I Kadek Budi Sandika[1,a]
[1]STMIK STIKOM Indonesia
[a]ikbsandika@stiki-indonesia.ac.id

Abstract. *An organization could establish a partnership with other organization to reach a particular purpose. Partnership between two or more organizations does not only transpire on intuition that works on the same sector, but also in different sectors (intersectoral). Furthermore, partnership could also be agreed between multinational companies, or multinational company and local company. Therefore, the stakeholders in partnership must be committed in maintaining and respecting the principles and values, which are commonly regulated as well as the local values in an operational area. The general principles that underline partnership are justice, trust, faith/ loyalty, wholeness/integrity, honesty, equality, human dignity, service, excellence/high quality, and growth. The value aspects needed in establishing partnership are leadership, customer satisfaction, mutual prosperity, friendship, innovation, security/ health/environment, teamwork, quality, and continuous improvement. Some cultural values of Balinese society that can support the partnership are the values of associating oneself to community (menyama braya), unity in joy and sorrow while respecting each other's point of view (sagilik-saguluk salunglung sabayantaka paras paros sarpanaya), reminding and caring as well as helping each other (saling asah saling asih saling asuh), and volunteerism/work as worship and worship in work (ngayah)*
Keywords: *Balinese, local culture, partnerships, principles, values*

I. Introduction

Many stakeholders realize that establishing a partnership is more profitable than competing to optimize the gained result. Partnership is a continuous form of strategic alliance/fellowship among various actors (multi-organizational and multi-sector) with an agreed purpose, both formally (written agreement) and informally (oral agreement), which is based on trust, equality and understanding towards rights and obligations, along with involving the exchange or sharing of resources, risks, and responsibilities [1] [2] [3] [4]. Some important elements related to partnership are its cross-border organizations nature, involving the sharing of resources and management (asset or competence, decision-making, supervision in complex structure), having mutually-agreed purposes (an agreement between partners towards particular purposes/*win-win solution*), being interdependence as a team, which involves commitment, trust and equality, and occuring in dynamic process[2].

The terminology, which is used to describe partnerships, varies over time. In the 1970s-1980s, the term "*network*" was frequently used, then, in the early 1990s the used term was a consortium, and the term "*partnership*" began to be widely used in the early 2000s [2]. Nowadays, the term collaboration is widely used as a more flexible and more inclusive form of cooperation. However, there is no standard procedure or rule that binds the form of cooperation which must be applied in a partnership [5]. The most important thing to understand is that the collaborative process in partnership involves the process of the change of bussiness patterns from the usual. The different types of appliedpartnerships will

involve different levels of collaboration as well, depending on the expected goals and readiness of partners to change their business patterns.

Challenges in managing the complexity, due to the differences in economic, social and cultural circumstances, and types of stakeholders,which sometimes have conflicting interests and priorities, resultsin the inability to conform certain form ofcoordination mechanisms between two or more organizations/companies[6][7][8]. In addition, the chosensupervision model in partnership will have a significant effect towards the long-term relationship sustainability [9]. Thus, each partner needs to pay attention to the main reason as a trigger/stimulant of partnership, set the long-term goals, choose a supervision model of partnership, which is appropriate with the characteristics of the organization, and consider the success factors at each stage of the partnership.

Therefore, to support the success of a partnership, the stakeholdersought to have the same understanding and perception, which are supported by the suitability of personal values and organizational culture owned by every actor involved. The existing values could be the values/ norms which are applied in the community, either within the scope of local, national, regional, or international. This is necessary to avoid misunderstanding of an attitude or action that may occur due to different values of partners.

II. Principles and Values as a Success Factor in Partnership

A partnership could be realized and maintained if the principles and values could be held by each partner [10]. Some underlyingprinciples of partnership are justice, trust, faith/loyalty, integrity, honesty, equality, human dignity, service, excellence/ high quality and growth. The value aspects needed in partnership are leadership, customer satisfaction, stakeholder wealth, friendship, cooperation/ collaboration, innovation, technology, security/ health/environment, teamwork, quality, continuous improvement and a competitive world.

When we review the stages in the collaboration process (preparation, implementation, outcome), each requires a certain success factor [11]. In the initial/preparation phase, the factors that need attention are communication, formulation of benefits obtained by each partner institution, political/social climate, trust/reward, the level of goal achievement, human resources involved, and the cross-section members. For the stages in which the partnership process has taken place, it is necessary to maintain the communication, trust/mutual respect supported by roles and responsibilities, and decision making. Meanwhile, the factors that still need to be considered after the visible achievement of the partnership results are communication, institutional benefits, goals achievement with expectations, and assessment of the impact of partnerships. Other things to consider in establishing cooperation/ partnership are (1) responsiveness and reciprocity, (2) inclusivity, (3) fairness and objectivity, (4) openness, transparence and credibility, as well as mutual respect [12].

Factors that influence the process of collaboration could be categorized according to its scale, such as factors in macro, meso and micro scale [13]. Macro-scale factor comprises of social, cultural, educational and professional systems. Meso-scale factor is a factor which arises due to conditions that occur within the organization (organizational factors), such as organizational structure and philosophy, resource support and management/ administrative, and coordination/communication mechanism within the company. Meanwhile, micro-scale factor depends on interpersonal relationships that exist between partner members (interactional factors), including willingness to collaborate, level of trust, communication and mutual respect.

These three factors could also be referred to as partnership drivers, which are grouped according to their origin [14]. The first is the external driving factor, the unity of political situation, socio-economic and cultural situation, and the rules within the area of partnership operations. The second is the organizational-level driving factor (unity of vision, mission and skills that are specifically involved for the partnership process). And thirdly, individual level driving factor is in the form of people who are directly involved in forming and implementing partnerships. When associated with the theory of organizational effectiveness, these factors are identical with the three essential elements of the organization, such as environment, process and person [10]. Therefore, the factors that influence the success of the partnership program are environmental factors (macro scale/external organization), process factor (meso scale/internal organization) and person factor (micro/individual scale).

The key issues to consider when designing cooperation processes between educational institutions and small and micro enterprises are: (1) cooperation is always related to people, (2) the school needs to understand the daily work of the company, (3) it is needed to set clear goals for cooperation, (4) it is necessary to make a mutual profitable situation *(win-win)*, (5) to attract company interests, school managers need to demonstrate the most practical benefits in relatively short time after the partnership takes place, (6) it is needed to make a good planning, while maintaining flexibility, (7) it is necessary to make sure that there are prominent people who are mutually recognized in thecooperation process, (8) it is necessary to not underestimate the role of foremost people, (9) it is needed to prepare enough time for communication and connection, (10) all of those are all related to attitude[15].

III. The Value of Bali's Local Wisdom related with Partnership

Besidesthe generally accepted principles and values as elaborated above, we also need to consider local socio-cultural contexts in a region. Bali, known for its cultural peculiarities that still retains the Balinese Hindu tradition, also has some local wisdom values related to the cooperative activities or partnerships. The forms of the values implementation are evident in the traditional social organization activities in Bali, among others, *tempekan* (neighborhood association), *banjar* (citizen organization) and *subak* (organization in agriculture). These organizations are formed on the basis of deliberation with the members (*krama*) in a meeting (*sangkep*) as outlined in the collective agreement (*pararem*) codified into statutes and bylaws (*awig-awig*). Those could also be applied in theestablishmentof an association (*sekaa*).

Sekaa is an institution or social group or a group of several people who gather themselves based on the same interest as its purpose [16]. *Sekaa* in Bali could be classified into several types according to the aspects of its members' social life. *Sekaa*, which engages in arts, for example *sekaa gong* (groups which play gamelan gong musical instruments) and *sekaa kecak* (groups of people who dance Kecak). *Sekaa* that operates on the economic life aspect, for example, *sekaa nenggala* and *sekaa manyi* in the field of agriculture, *sekaa jukung* (group of boat owners) in the field of fishing, *sekaa pengetengan* (group of traders who jointly entrust one of the members to save daily dues for the amount which has been agreed) in the field of trade, and so on. In the social life aspect, there are *sekaa patus* (neighboring group which helps each other in case of death), *sekaa tempek* (neighboring group in certain areas in *banjar* environment that help each other ifevery occasion, both joy and sorrow), and *sekaa sambang* (groups which visit each member when there is

anoccasion) and *sekaa teruna*. There is also a classification of *sekaa* in customary and religious life aspect, such as *sekaa pemaksan* in a temple (a group of people who associated in *sekaa* to organize and to liven up the ceremony in the same ancestor/clan altogether), *sekaa pesantian* (groups for studying and deepening the religion), *sekaa kidung* (group of ceremony accompanists with the singing of sacred songs and worship songs), and so on.

An association/*sekaa* operates in accordance with its rules (*awig-awig*) which has been agreed upon by each member (*krama*). *Awig-awig sekaa* contains all matters related to the *sekaa* organization management, including the rights and obligations of the members and sanctions for members who violate the rules. If it is equated in a partnership between two or more agencies, *awig-awig* is a memorandum of understanding (MoU) that will bind each member during the cooperation process.

In its operations, every *sekaa* and other Balinese social groups possess/hold the values which constitute local wisdom that has been entrenched and based on religious philosophy. In the teachings of Hinduism, the ultimate goal of the adherent is releasing themselves from secular bond in the form of the real happiness in the world and hereafter. To achieve it, every people must hold on the *tri hita karana* concept, the three harmonious relationships in human life, namely the harmonious relationship with God (*parhyangan*), the harmonious relationship with other people (*pawongan*), and harmonious relationship with nature (*palemahan*). Activity in social groups, including *sekaa*, is a form of human interaction with other human beings, thus referring to the *pawongan* concept. In maintaining the harmony of this relationship among human beings, there are several values that have been rooted in Balinese culture, such as *menyama braya*, *sagilik-saguluk salunglung sabayantaka paras paros sarpanaya*, *saling asah saling asih saling asuh*, and *ngayah*.

The first value, the *manyama braya*, is a noble value that binds members of society by assuming that each person is supposed to be their own brother (*nyama* = brother, *braya* = people around/society). Thus, in order to achieve the harmony in social or other organizational relationships, this principle or value system emphasizes the sense of brotherhood as the basis for relationships. By assuming others like our own brothers, it will increase the sense of family in the organization so that there will be an intimacy and solidarity in performing tasks. *Paras paros sarpanaya* value means the willingness to accept differences in decision making. Every individual has a sense of mutual respect for each other opinions, and willing to *berembug*/ deliberate to find the word "*mufakat"* (consensus/ win-win solution). This value is very important in establishing a partnership, where each partner should be able to recognize the strengths of each partner and respect each other's differences and be willing to coordinate with each other in their bonds/relationship (from planning, implementation, monitoring and evaluation, as well as the determination of follow-up program).

After reaching a mutual agreement, each partner should always hold on to the value of slogan *sagilik-saguluk salunglung sabayantaka* which has the meaning of togetherness, the willingness to work hand in hand through the life challenges, both in the state of joy and sorrow (one sense, one soul, being in the same fate and holding the same matters). In the organizational context, this value demonstrates the determination of each element to endure various situations in order to achieve the same goals. Each member/element in management mutually supports and synergizes in carrying out every planned program altogeher. In addition, each element/member needs to have a sense of mutual care, *asah-asih-asuh* (reminding each other, caring, and helping). Therefore, a sense of togetherness and solidarity will strengthen the foundation of cooperation, and ensure to achive the goals optimally and sustainably.

In spite of being based on a sense of togetherness, every individual in the organization must also has the spirit to work hard in carrying out every task and responsibility covered. This is related to the spirit of *ngayah*, which means dedication/loyalty to the responsibilities held. The concept of *ngayah* is the essence of the philosophical value of religion, which is "work as worship" and "worship in the work". In the teachings of Hinduism, there are four ways that can be taken in implementing religious teachings, such as through devotion and worship (*bhakti marga*), action/work sincerely (*karma marga*), the practice of science and experience possessed (*jnana marga*), and meditation (*rajamarga*). Thus, the spirit of *ngayah* is a form of religious teachings through work (*karma marga*). This is shown by the eagerness of doing the job/obligation sincerely. The term *ngayah* also figuratively means working together. Thus, the aforementioned local wisdom values are also linked to this concept of *ngayah*.

Therefore, the values contained in the slogan of *menyama braya*, *sagilik-saguluk salunglung sabayantaka paras paros sarpanaya*, *saling asah saling asih saling asuh*, and *ngayah* are interconnected in an effort to create a harmonious situation in relationship among human beings. It is also very supportive in strengthening the foundation in establishing a cooperation or partnership, because the awareness has been rooted in the culture of the surrounding society. Thus, the local wisdom values need to be considered in building and running a partnership in Bali. With the values of local wisdom held as guidance/operational basis of partnership, it is expected that the partnership process becomes more entrenched and sustainable.

IV. Conclusion

Partnerships could be well-established and sustainable if the partners have the same understanding and perception which is supported by the suitability of personal values and organizational culture owned by every actor involved. The main actor in the partnership is the people, who have certain principles and values. Besides holding principles and values which are generally accepted, they are also influenced by the local values within the society in which the partnership takes place. In Bali, the values which could support the success of the partnership are *menyama braya*, *sagilik-saguluk salunglung sabayantaka paras paros sarpanaya*, *saling asah saling asih saling asuh*, and *ngayah*. Those values have connection to each other in supporting the harmony in relationships among human beings.

References

[1] T.A. Piyasiri, B.H.S. Suraweera, and M.L.N.S. Edirisooriya, "*Identify benefits and analyze issues related to partnership programs between public TVET institutions and private sector enterprises",* Sri Lanka: National Education Commision, 2008, pp. 9-29

[2] D. Horton, G. Prain, and G. Thiele, "*Perspectives on partnership: A literature review* (Working paper style)*",* Lima: International Potato Center (CIP), 2009, pp. 77-100

[3] M. Latham, (2009, March), Public-private partnerships in education (Online source style), *EdInvest,* [Online], pp. 2-10, Retrieved December 5, 2013, from EdInvest: http://www.ifc.org/wps/wcm/connect/71d778804adbe66e9f79bfb94e6f4d75/PPPs%2B_Edinvest_FINAL_SR_03.30.09_option.pdf?MOD=AJPERES&attachment=true&id=1334655234964

[4] S. Buckup, "*Building successful partnersip, a production theory of global multi-stakeholder collaboration* (Book style)", Geneva: Springer Gabler, 2012

[5] G. W. Torres, and F. S. Margolin, *The collaboration primer: Proven strategies, considerations, and tools to get you started.* Chicago: Health Research and Educational Trust, 2003, pp. 3-14

[6] R. Hall and G. McMillan, *Industry engagement models-matching expectations of industry and RTOs* (Online source style), 2011, (Online) Retrieved February 28, 2014, from http://vital.new.voced.edu.au/vital/access/services/Download/ngv:47281/SOURCE201

[7] F. Bunning and A. Schnarr, Forging strategic partnerships between stakeholders in TVET - Implications for the Vietnamese vocational education and training system (Book style with paper title and editor), In C. Kasipar, M. Van Tien, S.-Y. LIM, P. Le Phuong, P. Quang Huy, A. Schnarr, et al., *Linking vocational training with the enterprises - Asian perspectives*, Bonn: Internationale Weiterbildung und Entwicklung gGmbH, 2009, pp. 11-18

[8] A. G. Mitchell, *Strategic training partnerships between the state and enterprises* (Working paper style), Geneva: International Labour Office, 1998, pp. 10-48

[9] Regional Breakthroughs. (2009, April). *Framework for an effective industry/education engagement model* (Online source style), 2009, (Online), Retrieved April 22, 2014, from http://www.regionalbreakthroughs.com.au/LiteratureRetrieve.aspx?ID=33753

[10] N. R. Wirapradja, "*Strategic partnering for educational management: Model manajemen pendidikan berbasis kemitraan* (Book style)", Bandung: Alfabeta, 2006

[11] J. M. Czajkowski, *Leading successful interinstitutional collaborations using the collaboration success measurement model* (Online source style), 2007, (Online), Retrieved April 5, 2014, from http://www.chairacademy.com/conference/2007/papers/leading_successful_interinstitutional_collaborations.pdf

[12] Department of Education and Early Childhood Development, *Stakeholder engagement framework* (Working paper style), Melbourne: State of Victoria (Department of Education and Early Childhood Development), 2011

[13] D. D'Amour, M.-D. Beaulieu, L. S. M. Rodriguez, and M. Ferrada-Videla, Key element of collaborative practice & frameworks: Conceptual basis for interdisciplinary practice (Book style with paper title and editor), In I. Oandasan, D. D'Amour, M. Zwarenstein, K. Barker, M. Purden, M.-D. Beaulieu, et al., *Interdisciplinary education for collaborative, patient-centred practice: Research and finding report*. Toronto: Health Canada, 2004, pp. 64-102

[14] K. Caplan, and J. Gomme, J. Mugabi, and L. Stott, *Assessing partnership performance: Understanding the drivers for success* (Working paper style), London: Building Partnerships for Development in Water and Sanitation, 2007

[15] C. Rosaleen, E. Roger, J. Kaj, M. Anne, N. Thomas, S. Lea, and T. Stefano, (n.d.). *European handbook for vocational education and training (VET) and small business co-operation: It can be done!* (Online source style), (Online), Retrieved August 8, 2015, from Suomen luontoyrittajyysverkosto ry: http://www.luontoyrittaja.fi/438.html

[16] A. Sanjaya, (2010, October 2), *THE SCARLET_ Seka dalam Kehidupan Sosial Masyarakat Bali* (Online source style), 2010, (Online), Retrieved July 12, 2016, from The Scarlet: http://adisanjaya24.blogspot.co.id/2010/10/seka-dalam-kehidupan-sosial-masyarakat.html

The Machined Surface of Magnesium AZ31 After Rotary Turning at Air Cooling Condition (#662)

Gusri Akhyar [1], Bagus Purnomo[1,a], Arinal Hamni [1], Suryadiwansa Harun [1], Yanuar Burhanuddin[1]
[1]Department of Mechanical Engineering, Faculty of Engineering, University of Lampung
Jln. Prof.Sumantri Brojonegoro No.1 Gedung H FT Lt.2 Bandar Lampung
[a]baguspurnomo22@gmail.com

Abstract *— Magnesium is a lightweight metal that is widely used as an alternative to iron and steel. Magnesium has been applied in the automotive industry to reduce the weight of a component, but the machining process has the disadvantage that magnesium is highly flammable because it has a low flash point. High temperature can cause the cutting tool wear and contributes to the quality of the surface roughness. The purpose of this study is to obtain the value of surface roughness and implement methods of rotary cutting tool and air cooling output vortex tube cooler to minimize the surface roughness values. Machining parameters that is turning using rotary cutting tool at speed the workpiece of (Vw) 50, 120, 160 m/min, cutting speed of rotary tool of (Vt) 25, 50, 75 m/min, feed rate of (f) 0.1, 0.15, 0.2 mm/rev, and depth of cut of 0.3 mm. Type of tool used is a carbide tool diameter of 16 mm and air cooling pressure of 6 bar. The results show the average value of the lowest surface roughness on the speed the workpiece of 80 m/min, cutting speed of rotary tool of 50 m/min, feed rate of 0.2 mm/rev, and depth of cut of 0.3 mm. While the average value of the highest surface roughness on the speed the workpiece of 160 m/min, cutting speed of rotary tool of 50 m/min, feed rate of 0.2 mm/rev, and depth of cut of 0.3 mm. The influence of machining parameters concluded the higher the speed of the workpiece the surface roughness value higher. Otherwise the higher cutting speed of rotary tool then the lower the surface roughness value. The observation on the surface of the rotary tool, it was found that no uniform tool wear which causes non-uniform surface roughness. The use of rotary cutting tool contributing to lower surface roughness values generated.*

Keywords *— Magnesium AZ31, machining, rotary tool, air cooling, surface roughness.*

I. Introduction

Magnesium is a lightweight metal and has characteristics similar to aluminum. Magnesium can be used as an alternative to iron and steel because magnesium is abundant elements and elements that make up the eighth most 2 % of the earth's crust, and is the third most element dissolved in seawater [1].

On development, magnesium or its alloys has been widely applied in the automotive industry among others to lose weight because of a component is a metal that is light [2]. Magnesium machining process is known to have excellent cutting characteristics because it has a low specific cutting force, furious chips are short, relatively low tool wear, high surface quality and can be cut at cutting speeds and feeds are high [3].

Although magnesium has many advantages, but has the disadvantage that magnesium is highly flammable because it has a low flash point. At such a low flash point will be burning furiously, where the cutting temperature exceeds the melting point of the material, namely (400° C - 600° C) [4].

In addressing these issues, numerous studies have been conducted to find an effective method to reduce the cutting temperature. As stated by previous researchers that a high cutting temperatures will produce a high surface roughness values [5]. Because the machining process with high temperature will cause occurrence of wear on the cutting tool so that it can degrade the quality of the workpiece surface roughness [6].

In the machining process, generally the method that is widely used to lower the temperature of cutting is to use liquid. But in its development began to minimized use this liquid because it is very dangerous for health and the environment [3].

In the study conducted by Doni [7] which aims to analyze the surface roughness value by lowering the temperature of the cutting. The chosen method is to use a rotating cutting tool on a lathe machining processes without coolant and use a rotary tool tilt angle of 0° with respect to the workpiece. Rotary tool method used successfully obtain minimum surface roughness value of 0.62 μm and a maximum surface roughness values of 2.86 μm. In his research, Doni [7] recommends using low feed rate , because the higher of feed rate will generate greater roughness values.

Research on machining magnesium is also done by Andriyansyah [8] which aims to determine the effect of cutting parameters on surface roughness values of magnesium using air cooling of vortex tube cooler with a temperature of 15° C. Machining process used is a milling machining. Research results show that the value of the minimum surface roughness of 0.35 μm and maximum roughness value of 1.50 μm.

Results of the research that has been described above concludes that the value of the surface roughness of magnesium in addition influenced by cutting parameters, including feed rate and the cutting speed, also influenced by the temperature of the cutting. Therefore in this study will be analyzed on a surface roughness values lathe machining process using a rotary cutting tool with a tilt angle of 10 °. In a previous study of this corner enabled to reduce power by 30% of the total power use and reduce the amount of cutting force [9] [10].

The cutting process will be given air cooling output of vortex tube cooler constant. By using cold air is expected to reduce the temperature of the cutting so as to reduce the rate of tool wear and improve tool life [11] [12]. So this method is expected to produce a better roughness values and can be used as a substitute for innovation in the machining process fluid. The purpose of this study is to obtain the value of surface roughness and implement methods of cutting tool rotary tool and air cooling output of vortex tube cooler to minimize the surface roughness values.

II. Research Methodology

The study was conducted at the Laboratory of Manufacturing, Mechanical Engineering, Lampung University. Materials used in the study are magnesium alloy AZ31 (Al of 3% and Zinc of 1%). Here is an AZ31 magnesium physical table property.

Table 1. Physical properties of magnesium AZ31

Physical Properties	Magnesium Alloys
Liquid point, K	922 K
Boiling point, K	1380 K
Ionization energy 1	738 kJ/mol
The ionization energy is 11	1450 kJ/mol
Mass density (ρ)	1,74 g/cm^3
Atomic radius	1,60 A
The heat capacity	1,02 J/gK
Potential ionization	7,646 Volt
Conductivity of heat	156 W/mK
Evaporation enthalpy	127,6 kJ/mol
The enthalpy of formation	8,95 kJ/mol

The machining is done on conventional lathes brands PINACHO type S-90/200. By using a rotary cutting tool system as shown in Figure 1. The material of tool used is a carbide, diameter of 16 mm and the air cooling pressure of 6 bar. Here are the figure and specifications of the tool cutting system spins and *vortex tube* :

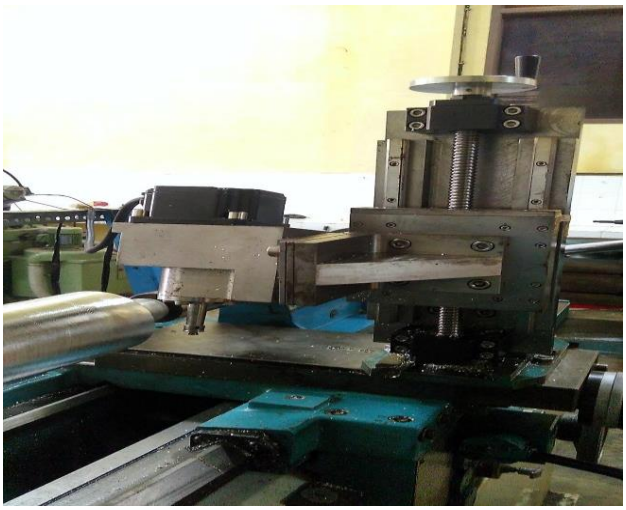

Figure 1. Rotary cutting tool system

Table 2. Specifications of rotary tool

Brand	AXUM590-A
Type of tool	*Insert-Propeller*
Speed of rotary cuuting tool	0-2000 rpm
Spin direction	CW/CCW
Diameter	16 mm

Figure 2. Vortex tube used to produce air coolling.

Machining parameters that is turning using rotary cutting tool at speed the workpiece of (Vw), cutting speed of rotary tool of (Vt), feed rate (f), depth of cut (d). Can be seen in Table 3.

Table 3. Cutting parameters selected in turning process.

Speed of Workpiece (Vc) m/min	80, 120, 160
Feed Rate (f) nmm/rev	0.10, 0.15, 0.20
Dept of Cut (d) mm	0.3
Cutting speed of Rotary Tool (Vt) m/min	25, 50, 75
Temperature Air Cooling	0° C. 6 Bar

Data collection roughness on every parameter done four times. This is done to get the maximum results. Measurement values using a surface roughness tester with an accuracy of 0.01 µm and surface profile of picture a using USB camera with a magnification of 600 x.

III. Results and Discussion

Experimental trials of AZ31 magnesium alloys using conventional turning and rotary cutting tool system with air cooling. To determine the value of the surface roughness material magnesium alloy AZ31 has been carried out with a variety of machining parameters that is turning using rotary cutting tool at speed the workpiece of (Vw) 50, 120, 160 m/min, cutting speed of rotary tool of (Vt) 25, 50, 75 m/min, feed rate of (f) 0.1, 0.15, 0.2 mm/rev, and depth of cut of 0.3 mm. Here are the data obtained from the machining process with a variety of conditions, produces a variety of data as shown in Table 4-7:

Table 4. Measurement data value of roughness on speed the workpiece of 120 m/min, depth of cut of 0.3 mm, and cutting speed of rotary tool of 25 m/min.

Number	Speed of Workpiece (Vw) (m/min)	Feed Rate (f) (mm/rev)	Dept of Cut (d) (mm)	Cutting Speed of Rotary Tool (Vt) (m/min)	Average (µm)	Times (t) (Minute)
1	120	0.1	0.3	25	**1,27**	05:28
2					**1,26**	10:53
3					**1,19**	16:20
4					**1,09**	21:47
1	120	0.2	0.3	25	**0,94**	02:43
2					**1,00**	05:27
3					**1,27**	05:28
4					**1,26**	10:53

Table 5. Measurement data value of roughness on speed the workpiece of 160 m/min, depth of cut of 0.3 mm, and cutting speed rotary tool of 50 m/min.

Number	Speed of Workpiece (Vw)	Feed Rate (f) (mm/rev)	Dept of Cut (d) (mm)	Cutting Speed of Rotary Tool (Vt) (m/min)	Average (µm)	Times (t) (Minute)
1	160	0.1	0.3	50	**1,41**	04:20
2					**1,50**	08:40
3					**1,63**	13:01
4					**1,56**	17:22
1	160	0.2	0.3	50	**1,97**	02:10
2					**2,30**	04:20
3					**2,27**	06:31
4					**1,82**	08:43

Table 6. Measurement data value of roughness on speed the workpiece of 80 m/min, feed rate of 0.15 mm/rev, and depth of cut 0.3 mm.

Number	Speed of Workpiece (Vw)	Feed Rate (f) (mm/rev)	Dept of Cut (d) (mm)	Cutting Speed of Rotary Tool (Vt) (m/min)	Average (µm)	Times (t) (Minute)
1	80	0.15	0.3	25	**0,89**	06:37
2					**0,98**	13:15
3					**0,72**	19:53
4					**0,91**	26:29
1	80	0.15	0.3	75	**0,80**	06:38
2					**0,82**	13:15
3					**0,77**	19:54
4					**0,82**	26:30

Table 7. Measurement data value raughness on the feed rate 0.15 mm/rev, depth of cut 0.3 mm, and cutting speed of rotary tool of 25 m/min

Number	Speed of Workpiece (Vw)	Feed Rate (f) (mm/rev)	Dept of Cut (d) (mm)	Cutting Speed of Rotary Tool (Vt) (m/min)	Average (µm)	Times (t) (Minute)
1	80	0.15	0.3	25	**0,89**	06:37
2					**0,98**	13:15
3					**0,82**	19:53
4					**0,91**	26:29
1	160	0.15	0.3	25	**1,37**	02:53
2					**1,58**	04:46
3					**1,63**	07:39
4					**1,49**	10:32

Feed rate and surface roughness value

The following is a graph showing the comparison surface roughness values between feed rate 0.1 mm/rev and 0.2 mm/rev at the depth of cut (d) 0.3 mm.

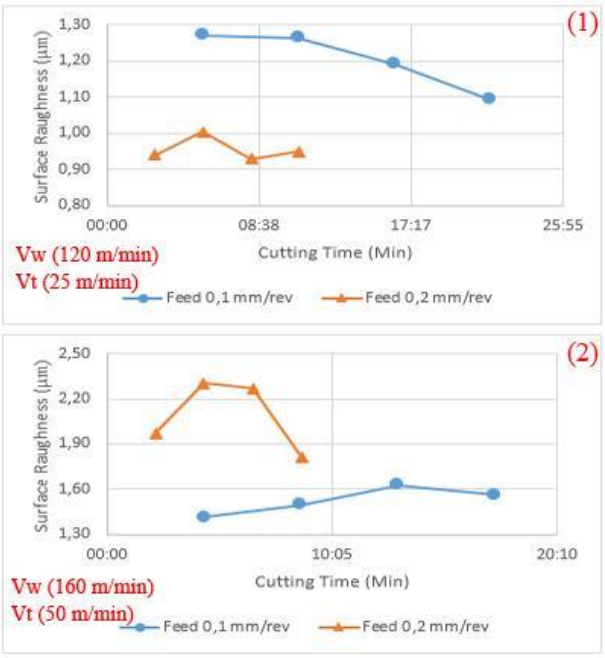

Figure 3. Comparison of surface roughness between feed rate 0.1 and 0.2 mm/rev.

Figure 3 is a comparison of the effect of feed rate on the value of surface roughness. Where in graph 1 surface roughness value was lower than in the feed rate of 0.2 mm/rev. It is inversely proportional to the statement earlier researchers [7]. Which states that the chip of feed is very influential on the surface roughness, where the greater the price of feed. the greater the level of coarseness. But in general, the value of the surface roughness is influenced by a variety of many factors. These factors include other parameters of the machining process, the condition of the tool, the workpiece and the cutting phenomenon [13]

[14]. From the statement of course in this case the value of the feed is not completely affect the value of the resulting roughness.

Whereas in Figure 2 the surface roughness value was lowest in the feed rate 0.1 mm/rev. In both cases carried out observations of the surface profile, wherein the surface profile measurements to feed mark the resulting on cutting scars. Here is a comparison of the measured surface profile of the workpiece :

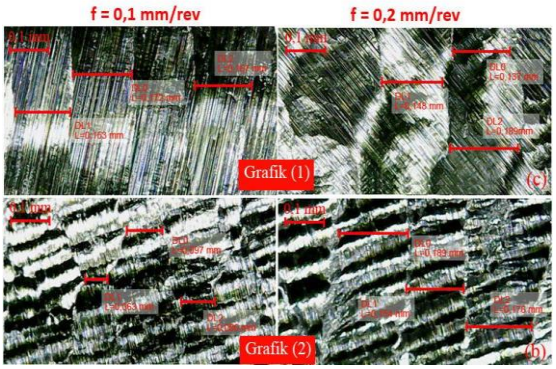

Figure 4. Comparison between profiles of feed rate (f) 0.1 and 0.2 mm/rev.

In Figure 4 obtained value feed mark on the first surface profile of feed rate 0.1 mm/rev of 0.164 mm and feed rate 0.2 mm/rev of 0.158 mm. While the second profile feed rate 0.1 mm/rev produce value feed mark of 0.082 mm and feed rate 0.2 mm/rev of 0.173 mm.

Cutting speed Rotary and surface roughness value

The following is a graph showing the comparison between the surface roughness value of the cutting speed of rotary tool of 25 m/min and 75 m/min with the depth of cut (d) 0.3 mm :

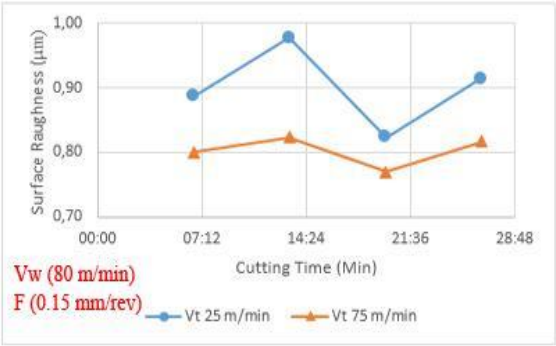

Figure 5 . Graph comparison of cutting speed of rotary tool (Vt) of the surface roughness values.

Figure 5 is a comparison of the effect of cutting speed rotary tool against the surface roughness values. Where is concluded that the value of the surface roughness was lowest in the cutting speed of rotary tool (Vt) 75 m/min and the surface roughness values were highest in cutting speed of rotary tool (Vt) 25 m/min. As already stated by Doni [7], the greater the cutting speed of the rotary cutting tool resulting roughness value would be lower. For a comparison of the surface profile can be seen in Figure 6.

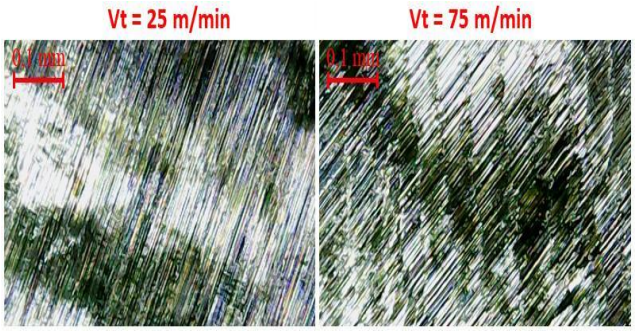

Figure 6. Comparison between the profile cutting speed of rotary tool 25 and 75 m/min.

Workpiece speed and surface roughness value

The following is a graph showing the comparison between the value of the surface roughness of the speed the workpiece of 80 m/min and 160 m/min with the depth of cut (d) 0.3 mm:

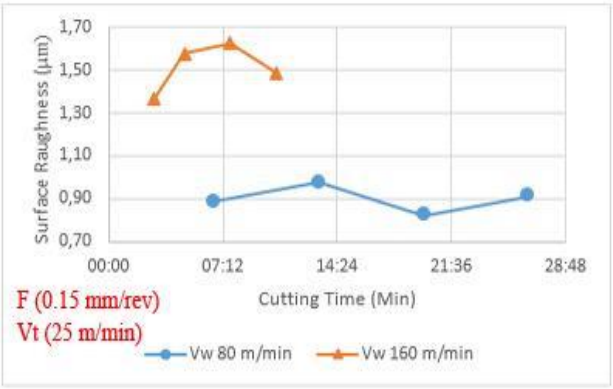

Figure 7. Graph speed the workpiece (Vw) of the surface roughness values.

Figure 7 is a comparison of the effect of speed of workpiece on the value of surface roughness. Where is concluded that the value of surface roughness was lowest in the speed of workpiece of 80 m/min and the highest surface roughness values occur at the speed of workpiece 160 m/min. As stated by Fariza [15] in his study, the greater the speed of workpiece then the resulting roughness value will be higher. For a comparison of the surface profile can be seen in Figure 8.

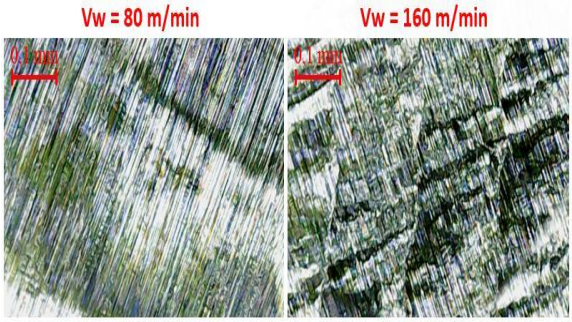

Figure 8. Comparison between the velocity profile speed of workpiece 80 and 160 m/min.

IV. Conclusion

The average value of the lowest surface roughness obtained on the speed of the workpiece (VW) to 80 m/min, cutting speed of rotary tool (Vt) of 50 m/min with feed rate 0.2 mm/rev and depth of cut 0.3 mm. While the average value of the highest surface roughness obtained on the speed of the workpiece (Vw) of 160 mm/min, the cutting speed of rotary tool (Vt) of 50 m/min with feed rate 0.2 mm/rev and depth of cut 0.3 mm. Values of surface roughness is not uniform throughout the machining process, this is due to tool wear is not uniform along the edge of the rotary cutting tool. Values of surface roughness parameters are more influenced by the speed of the workpiece (Vw) and the cutting speed of rotary tool (Vt). Higher speed of the workpiece (Vw) then the surface roughness of the resulting higher. Instead higher cutting speed of rotary tool (Vt) then the value of the resulting surface roughness is lower. Turning process using a rotary tool and air cooling can be implemented in a lathe machining process AZ31 magnesium material for producing a lower roughness values compared to using a silent tool.

References

[1] Ibrahim, G.A. 2014. Analisa Kekasaran Permukaan pada Pemesinan Paduan Magnesium. Jurusan Teknik Mesin. Universitas Lampung. Bandar Lampung.

[2] Blawert, C., Hort, N., dan Kainer, K.U. 2004. Automotive Applications Of Magnesium And Its Alloys. Trans. Indian Inst. Met. Vol.57, No. 4, pp. 397- 408.

[3] Harun, Suryadiwansa. 2012. Peningkatan Produktifitas dan Pengendalian Suhu Pengapian Pemesinan Magnesium Dengan Sistem Pahat Putar (Rotary Tool System) dan Pendingin Udara (Air Cooling). Universitas Lampung. Bandar Lampung.

[4] Mahrudi, Haris dan Burhanuddin, Yanuar. 2013. Rancang Bangun Aplikasi Thermovision Untuk Pemetaan Distribusi Suhu Dan Permulaan Penyalaan Magnesium Pada Pembubutan Kecepatan Tinggi. Jurusan Teknik Mesin. Universitas Lampung. Bandar Lampung.

[5] Bruni, C., Forcellese, A., Gabrielli, F., dan Simoncini, M. 2004. Effect Of Temperature, Strain Rate And Fibre Orientation On The Plastic Flow Behaviour And Formability Of AZ31 Magnesium Alloy. Department of Mechanics, Università Politecnica delle Marche, Via Brecce Bianche, Ancona 60131. Italy.

[6] Su, Y., He, H., Li, L., Iqbal, A., Xiao, M.H., Xu, S., Qiu, B.G., 2007. Refrigerated Cooling Air Cutting Of Difficult-To-Cut Materials. International Journal of Machine Tools & Manufacture 47, 927 – 933.

[7] Doni, A.R. 2015. Analisa Nilai Kekasaran Permukaan Paduan Magnesium AZ31 Yang Dibubut Menggunakan Pahat Potong Berputar. Tugas Akhir. Universitas Lampung.

[8] Andriyansyah. 2014. Pengaruh Parameter Pemotongan Terhadap Kekasaran permukaan Dalam Pengefreisan Magnesium Tersuplai Udara Dingin. Tugas Akhir. Universitas Lampung.

[9] Pulungan, Akhmad Isnain, Ibrahim, Gusri Akhyar, dan Burhanuddin, Yanuar. 2013. Unjuk Kerja Vortex Tube Cooler Pada Pemesinan Baja St41. Jurnal FEMA. Universitas Lampung

[10] Paryanto, Rusnaldy, dan Tony S. Utomo. 2012. Effect Of Air Jet Cooling On Surface Roughness And Tool Wear. Jurnal Teknosains. Universitas Diponegoro.

[11] Stejernstoft, T. (2004). Machining of Some Difficult-to-Cut Materials with Rotary Cutting Tools. Stockholm: The Royal Institute of Technology, KTH.

[12] Novriadi, Dwi. 2016. Rancang Bangun Sistem Pahat Putar Modular (Modular Rotary Tool System) Untuk Pemesinan Alat Kesehatan Ortopedi. Universitas Lampung. Bandar Lampung.

[13] Benardos, P.G., dan Vosniakos, G.C. 2003. “Predicting surface roughness in machining : a review, International Journal of Machine Tools & Manufacture 43, 833 – 844.

[14] Salgado, D.R., Alonso, F.J., Cambero, I., dan Marcelo, A. 2009. In-process surface roughness prediction system using cutting vibrations in turning. International Journal of Advance Manufacturing Technology 43, 40 – 51.
[15] Fariza, Feri. 2016. Evaluasi Dan Analisa Kinerja Sistem Pahat Putar Modular Untuk Pemesinan Peralatan Kesehatan Ortopedi Berbasis Material Titanium 6al-4v Eli. Tugas Akhir. Universitas Lampung.

Design of PID Controlling for Optimization of Fuel Usage in Solid Oxide Fuel Cell Applications (#673)

Darjat[1,2,a], Sulistyo[2], Aris Triwiyatno[1], Edwin Julian[1]
[1]Department of Electrical Engineering, Diponegoro University, Semarang, 50275, Indonesia
[2]Department of Mechanical Engineering, Diponegoro University, Semarang, 50275,Indonesia
[a]dr.darjat@gmail.com

Abstract*-Solid Oxide Fuel Cell (SOFC) is an electrochemical cell that converts chemical energy into electrical energy by oxidizing the fuel. Solid oxide fuel cell operates at a temperature of 600^{o}C-1000^{o}C and has high efficiency that can reach 65%, and combustion residue which is clean be in form of water (H_2O) without pollutants. Solid oxide fuel cells have been present as promising technology in the future by eco friendly electricity generation method. However, interesting challenge is to control the output voltage toward the desired value. The biggest difficulty comes from the constraints on fuel utilization in a particular response. This paper is presented to develop engineering friendly control structures for a wide range of purposes by utilizing PID control. The design of solid oxide fuel cell system consists of designing SOFC plant stack and PID controller block. The plant input or variable will be manipulated is the fuel rate (q_f). The output of the plant is the voltage (V_{DC}) and` the disturbance comes from the external load current (I). Analysis and comparison of test results are done on plant without controller and PID controller. Testing is done by giving setpoint on plant with step signal 333 volt and external load current 300 A.*
Keywords: *SOFC, PID, setpoint, plant*

I

I. Introduction

Solid Oxide Fuel Cell (SOFC) is an electrochemical cell that converts chemical energy becomes electrical energy by oxidizing the fuel [1]. The solid oxide fuel cell operates in temperature of 600^{o}C-1000^{o}C and has high efficiency that can reach 65%, and clean burning residue is water (H2O) without pollutants [2]. The research is about solid oxide fuel cells that are attractive especially in the design of precise controller because of the nonlinear system with slow dynamic response and can adapt when disturbance occurs.

J.Padulles designed a dynamic Solid Oxide Fuel Cell plant that can operate safely [3]. Sun Li and his team conducted research to regulate the SOFC output voltage by designing controllers that are PI feedback control and feedforward control and designing compensation block to overcome constraint function of fuel utilization [4]. Li, Choi, and Raja karuna did research by designing conventional PI controller [5], Knya zakin designed the optimal controller H_∞ [6]. Yiguo Li did the research by designing MPC controller (Model Predictive Controller) to overcome the constraint function on fuel usage [7]. The result of the research is known that control method can not give sufficient performance during interference and the function of constraints on fuel usage.

Based on the background, the researcher designs PID controllers on Solid Oxide Fuel Cell system toovercome non-linear system with slow dynamic response and can adapt when disturbance occurs.

II. Designing and Modeling

II.1 Solid Oxide Fuel Cell

Solid Oxide Fuel Cell (SOFC) works based on the electro-chemical reaction between hydrogen and oxygen that occurs in the anode and the cathode. They are separated by the electrolyte in the middle. The transfer of electron is from the anode to the external circuit until return again to the cathode that generates an electrical motive force (EMF).

The chemical reactions that occur are as follows:
At anode : $O_2 + 4e^- = 2O^-$ (1)
At Cathode : $2H_2 + 2O^{2-} = 2H_2O + 4e^-$ (2)
Overall cell reaction : $H_2 + 0{,}5\ O_2 = H_2O$ (3)

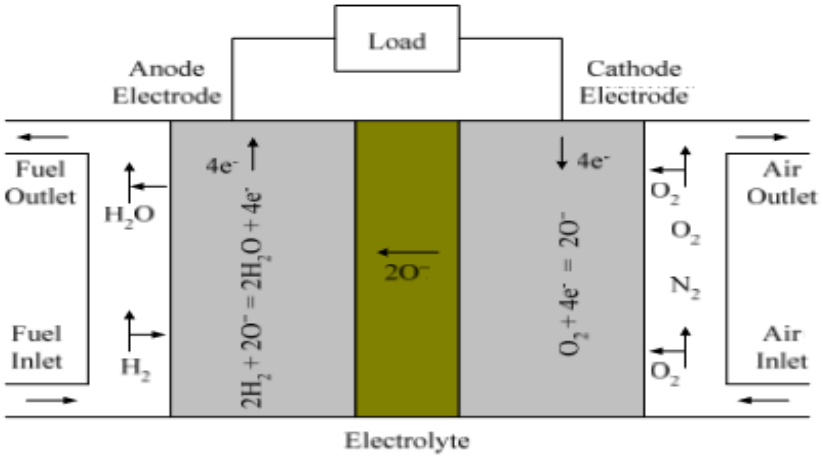

Figure 1. SOFC Schematic Diagram

This study uses a dynamic model from J.Padulles [3]. The variable that will be controlled is the plant output voltage. It is expressed with V_{DC} while the manipulated variable is the fuel flow rate (q_f). The flow rate of hydrogen gas and incoming gases is expressed qH_2 and qO_2. The partial pressure of hydrogen gas, oxygen gas and water is expressed by pH_2, pO_2, and pH_2O. The disturbance comes from the external load current (I).

- Partial pressure

The solid oxide fuel cell uses the reaction from oxygen and hydrogen gases and water as the product. Each gas is used which has a partial pressure. The mathematical equations of partial pressures for each gas are as follows:

$$p_{H_2} = \frac{{}^{1}/_{K_{H_2}}}{1+\tau_{H_2}s}\left(\frac{1}{1+\tau_f s} q_f^{in} - 2K_r I\right) \quad (4)$$

$$p_{O_2} = \frac{{}^{1}/_{K_{O_2}}}{1+\tau_{O_2}s}\left(\frac{1}{r_{H-O}}\frac{1}{1+\tau_f s} q_f^{in} - K_r I\right) \quad (5)$$

$$p_{H_2O} = \frac{{}^{1}/_{K_{H_2O}}}{1+\tau_{H_2O}s} K_r I \quad (6)$$

- Output Voltage of SOFC

By applying the Nernst voltage and calculating the voltage loss so it can be calculated SOFC output voltage is:

$$V_{DC} = N_c\left(E_o + \frac{RT}{nF}\, ln\, \frac{p_{H_2}\, p_{O_2}{}^{-\frac{1}{2}}}{p_{H_2O}}\right) - V_{loss} \quad (7)$$

$$V_{loss} = I\,r + (\alpha + \beta \ln I) + (\frac{-RT}{2F} ln \frac{I}{I_L}) \qquad (8)$$

II.2 Plant Design

The calculation of SOFC mathematical model is simulated as shown in Figure 2. The calculation parameter uses the parameter in Sun Li's research [4].

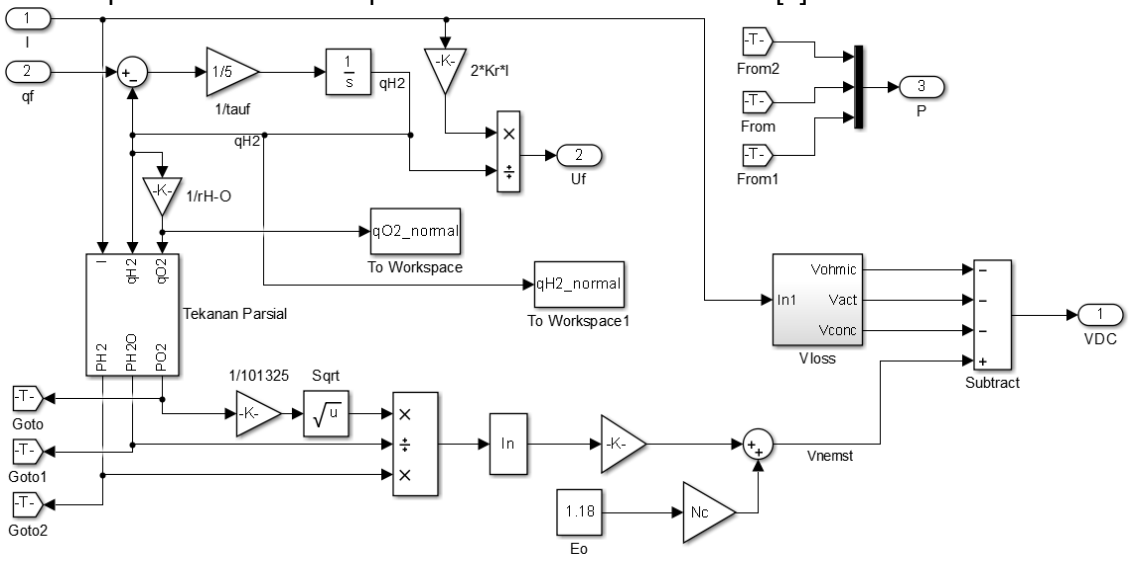

Figure 2. The Block of SOFC simulink stack

TABEL I SOFC PARAMETERS

Parameter	Nilai	Satuan
T	1273	K
F	96487	C/mol
R	C	J/(kmol K)
E_0	1,18	Volt
N_c	384	-
K_r	0,996×10^{-6}	-
K_{H_2}	8,43×10^{-4}	kmol/(second atm)
K_{H_2O}	2,81×10^{-4}	kmol/(second atm)
K_{O_2}	2,52×10^{-3}	kmol/(second atm)
τ_{H_2}	26,1	Second
τ_{H_2O}	78,3	Second
τ_{O_2}	2.91	Second
r_{H-O}	1,145	-
r	0,126	Ohm
τ_f	5	Second
α	0,05	-
β	0.11	-
I_L	800	A

II.3 Design of PID Controller

The design of the PID controller has purpose in order to output plant can reach the setpoint by faster transient response and small IAE value. The PID controller structure is shown in Figure 3.

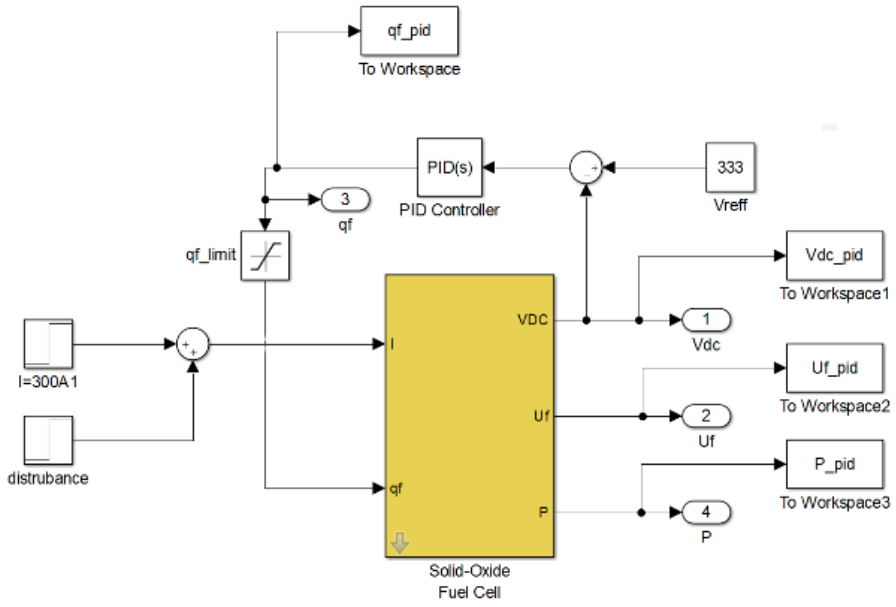

Figure 3. The block diagram of the PID controller

At first, the value of the system is given a proportional value (P) until the system oscillates. The addition of integral value (I) is used to accelerate the characteristics of system response. The derivative value (D) is given to reduce the oscillation of the system.

III. Results and Analysis

The comparison of test results conducted on the plant with PID and without controller. Testing is done by giving step signal equal to 333 volts as shown in Figure 4.

.

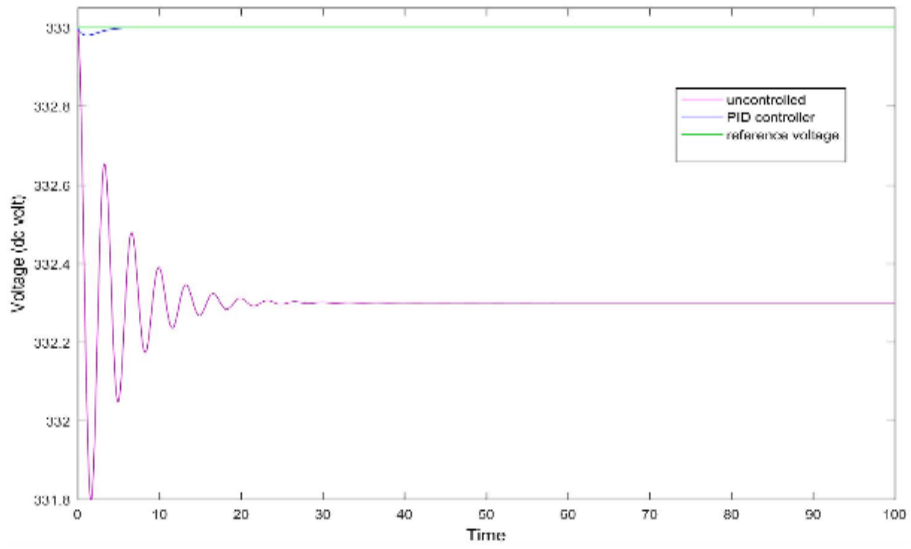

Figure 4. Graph of system output response

TABLE II Comparison of The Response Out of The System

Controll	*Rise Time* (s)	*Settling Time* (s)	*Overshoot* (%)	IAE
Uncontrolled	0,3	10,7	0.09	6,92
PID Controller	3,39	7,12	0,01	0,06

The fuel rate of SOFC plant without controller has lower fuel rate because it can not reach the setpoint and the value is constant at 0.7 mol.

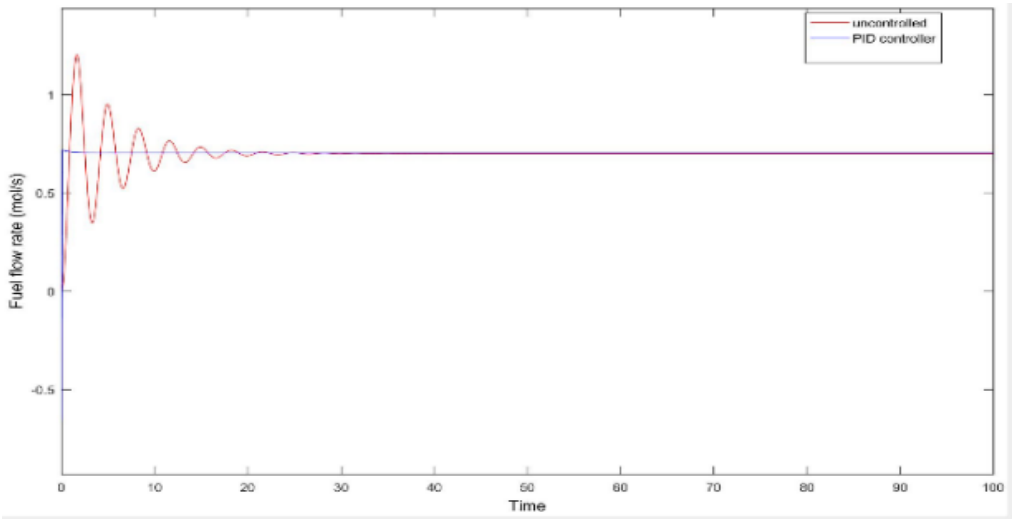

Figure 5. The comparison graph of fuel flow rate

The fuel usage test succeeded in keeping its value within safe limits between 0.7 until 0.9 with the same fuel usage 0.85, as shown in Figure 6.

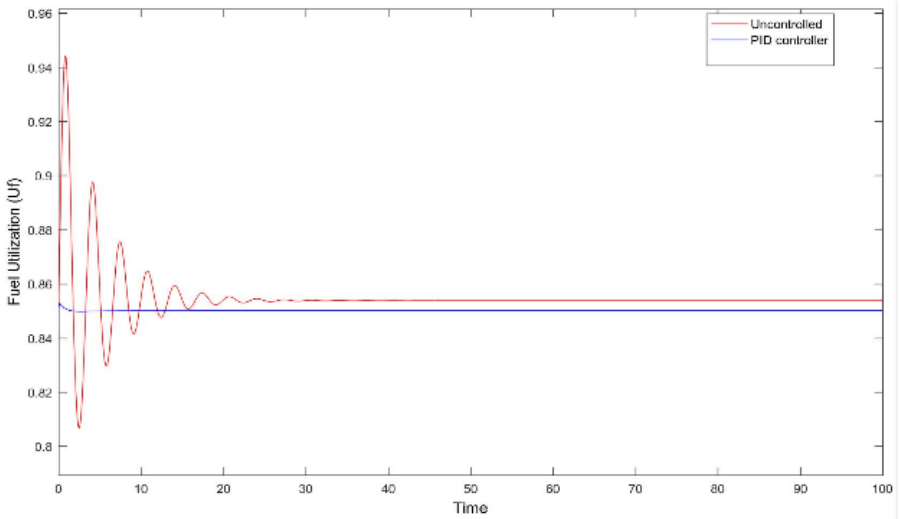

Figure 6. The comparison graph of fuel usage factor

TABEL III The Comparison of Fuel Flow Rate, Hydrogen Gas Flow Rate, and Oxygen Gas Flow Rate

Control	q_f (mol/s)	q_{H_2} (mol/s)	q_{O_2} (mol/s)
Uncontrolled	0,700	0,700	0,611
PID Controller	0,703	0,703	0,614

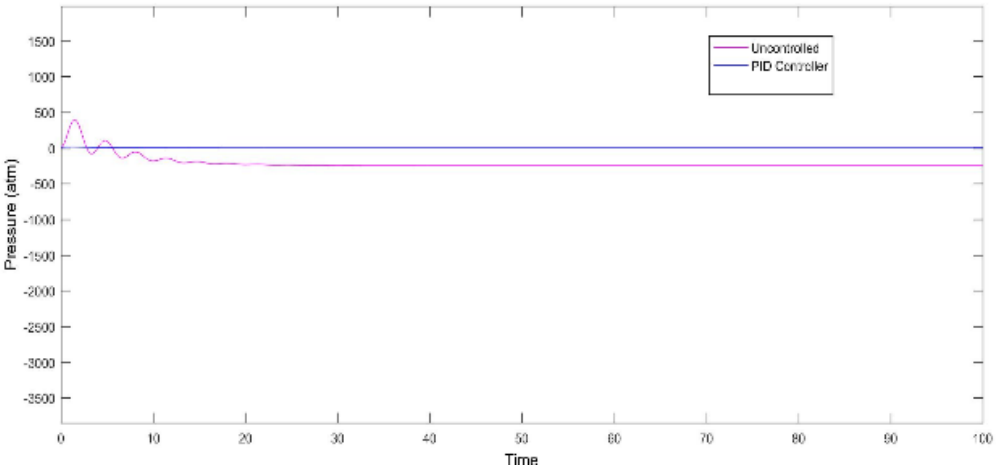

Figure 7. The difference graph of hydrogen-oxygen pressure

IV. Conclusion

The simulation result obtained PID controller able to reach setpoint with rise time (tr) 1,98s. The conventional PID controller has a fuel flow rate 0.702 mol/s. PID controllers can maintain fuel usage by 0.85 and hydrogen-oxygen pressure differences within safe limits.

Reference

[1]. Lindahl, P. A,. Simulation Design and Validation of a Solid Oxide Fuel Cell Powered Propulsion System for an Unmanned Aerial Vehicle. Thesis. Bonzeman, Montana State University; 2009.
[2]. Nguyen D, Fujita G. Modelling a SOFC Power Unit Using Natural Gas Fed Directly. INTECH.*2012: 20*
[3]. Padulles J, Ault G W, Mac Donad J R, An Integrated SOFC Plant Dynamic Model of Power Simulation System. *Journal of Power Sources*.2000, 86 (1-2) 495-500
[4]. Sun Li, Dongha Li, etc. A Practical Compound Controller Design for Solid Oxide Fuel Cells, International Federation of Automatic Control.2015, (48-30) 445-449
[5]. Li, Y. H., Choi, S. S., and Rajakurna, S. Ab Analysis of the Control and Operation of a Solid Oxide Fuel-Cell Power Plant in an Isolated System. IEEE Transaction on Energy Conversion. 2005, 20(2), 381-387
[6]. Knyazakin, V., Soder, L., and Canizare, C. Control Challenges of fuel cell-driven distributed generation. Paper presented at the *Power Tech Conference Proceedings*, 2003 IEEE Bologna
[7]. Li, Y., Shen, J,, and Lu, J. Constrained model predictive control of a solid oxide fuel cell based on genetic optimization. Journal of Power Sources, 196(14), 58

Simulation of Missile-Aircraft Separation (#691)

Hisar M. Pasaribu[1,a], Christian Reyner[1], Albert Meigo[1], Khairul Ummah[1], Rianto A. Sasongko[1]

[1] Department of Aeronautics and Astronautics,
Faculty of Mechanical and Aerospace Engineering, Institut Teknologi Bandung, Indonesia,
Institut Teknologi Bandung (ITB),
Ganesha 10, Bandung 40132, Indonesia
[a]hmpasaribu@ae.itb.ac.id

Abstract. *A comprehensive understanding of the separation process of the armament from the aircraft is fundamental to advancement in defense and military technology, since it is very crucial for safety of the aircraft and pilot himself. In order to achieve some understanding, numerical method by using Computational Fluid Dynamic is selected as a main tool to simulate interaction between a missile and aircraft. This simulation is able to generate the 6 DOF motions and forces of the missile during release phase until "thrust on" phase, in order to understand every detail step. The result indicates that the method for solving the moving body quasy-steady flow-field is accurate and feasible, concluding that the method is proven for application in real case study and further implementation on armament development and study.*

Keywords: *Missile separation, CFD simulation, Unstructured mesh.*

I. Introduction

Modern high performance fighter aircraft is increasingly dependent on external stores, including missiles, bombs and auxiliary tanks. Development of armament and payload is becoming faster and even more important than the aircraft itself. However, the lack of ability to predict behavior of armament-aircraft interaction is one of the most challenging problems in armament testing and development. Inability to fully understand their behavior will lead to serious problems, including backfiring which threatens aircraft and pilot life.

Nowadays, improvement and development are being focused by doing simulation through Computational Fluid Dynamics (CFD). CFD as a research tool for aircraft separation characteristics has been developed for many years [1, 2], because CFD could produce results with less expensive and save more time, compared to conventional method by doing experiments or flight tests. Many possible scenarios can be investigated based on combinations of stores and aircraft at various flight conditions and release parameters [3, 4]. In order to achieve such accurate and reliable result, numerical method must be done correctly and able to be compared to some data to validate the result, such as wind tunnel data which later will be used as comparison [5].

Simulations are done through discretization method by using combination of several meshing method, robust structured mesh, unstructured Cartesian cutter mesh, and unstructured optimum mesh [6, 7]. Governing equations of steady and quasi steady flow-field are based on simplified Navier-Stokes equations.

The missile separation is analyzed as a rigid body by coupling six degree of freedom kinematics and dynamics analysis and CFD simulation results to simulate every detail step of missile displacement and attitude through separation process to “thrust-on” phase.

II. Method

The starting point of any numerical method is the governing equations. Governing equations of quasy-steady flow-field is Navier-Stokes with RANS (Reynolds Average Navier-Stokes) approximation. Based on the unstructured mesh, RANS are in the integral forms of equations as follow

$$\frac{d}{dt}\iiint_V \bar{Q}\,.dv + \iint_{\partial V} \bar{F}\cdot\bar{n}\,.ds = 0 \qquad (1)$$

$$\bar{Q} == [\rho, \rho u, \rho v, \rho w, e]T$$

$k-e$ turbulent model was used for viscous term and modeling the turbulence.

RANS equations are three-dimensional, quasy-steady, nonlinear and compressible. The finite volume method is adopted to discretize flow-field domain and governing equations. Quasy-steady flow-field time advancement method is a dual-time (pseudo time and physical time) method.

Initially, the aircraft doesn’t separate from the parent aircraft, steady flow-field is computed. At 0 sec, quasy-steady flow-field is initialized by the steady flow-field result. At each time step, quasy-steady flow-field is integrated to give the aerodynamic forces and moments of the separating stores. External forces including gravity and other external forces, the aerodynamic forces and moments are passed to six-degree-of-freedom motion of separation stores model.

Through this model, the new positions and attitudes are computed for the next time step. Relying on the information, the unstructured mesh model updates the grid of the quasy-steady flow-field. The next time step quasy-steady flow-field is solved. As this sequence, iterative time advancement is executed. The flow chart of coupling solve is given in Figure. 1.

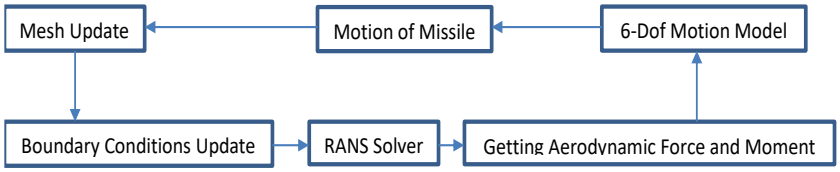

Figure. 1. Coupling Solver Flow Chart

III. Results and Discussion

To validate the model in the present research, similar missile configuration to that in [5] is used, in which multi-store separation of the aircraft missile is simulated using transient time-step. They determined the position of the missile attached to the aircraft using interfaces

before separation. Conclusively, they found that all of the missiles which are separated could be released without stores collision in all its time-step in Mach 2.0. The sequence of store separation in the present research as shown in Figure. 2b follows closely to that in Figure. 2a. Based on this reference, the store separation simulation could be done. In these store separation simulations, only one missile that is located at the tip of the left wing is released.

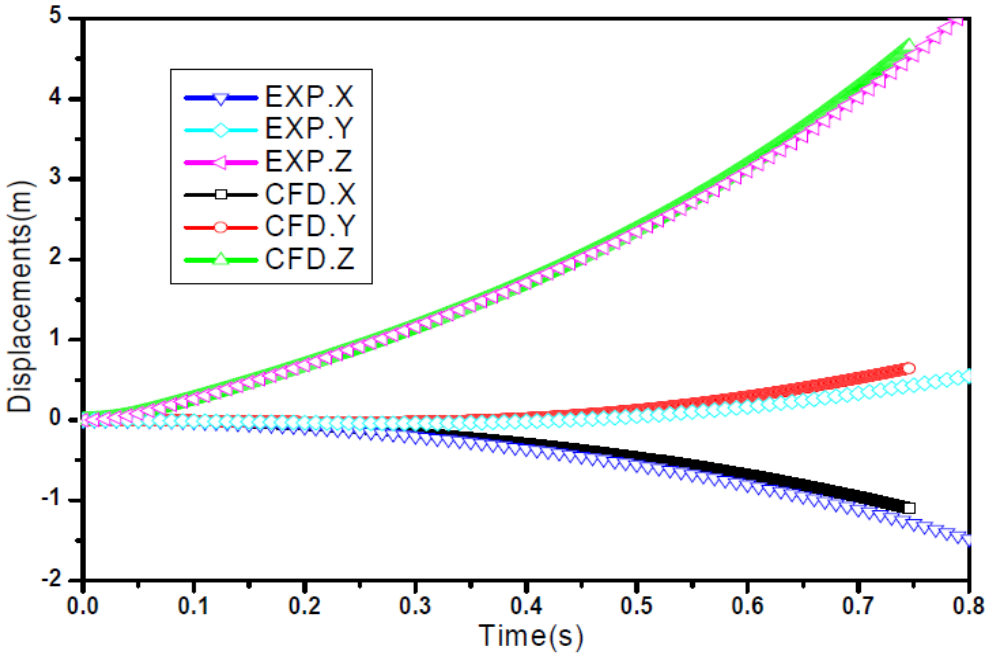

a. Based on Gong, et.al [5]

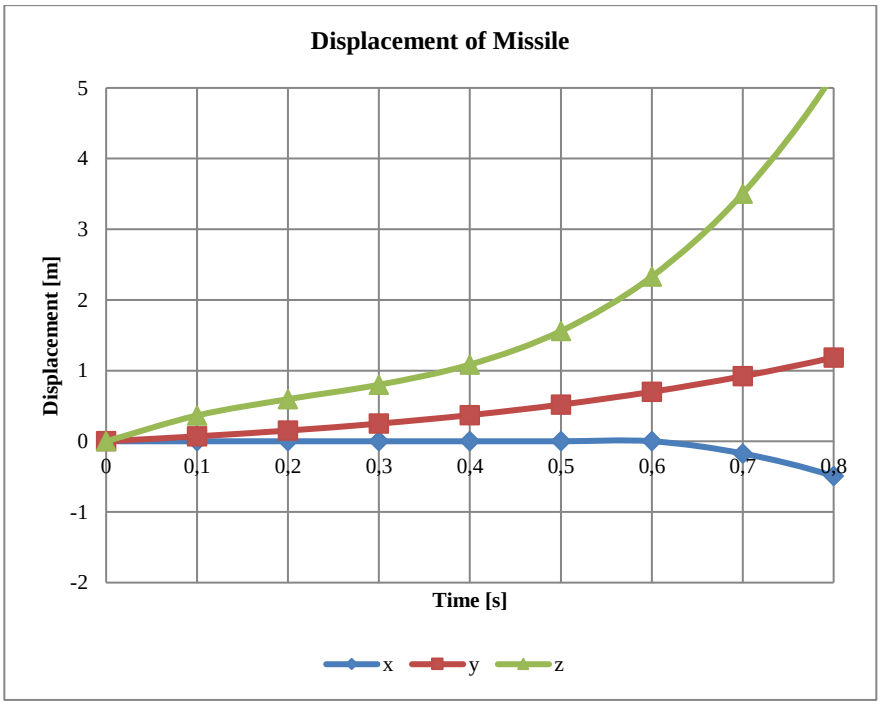

b. Current's Result

Figure 2. Linear Displacement of Missile.

Simulations of linear displacements are also in very good agreement with experimental data in short time range. Having confirmed the valid results, simulation can be carried on to the other configuration. In this paper, the configuration of R-27 missile was selected. Mach number of the flow-field was 0.6 at the height of 36.000 feet. Angle of attack of the aircraft was 0 degree. The quantity of the volume mesh is about 1 million as shown in Figure. 3. The quasy-steady time step is taken as 0.1 second.

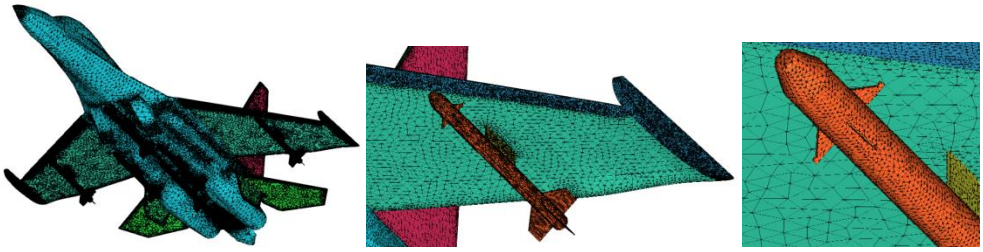

Figure 3. Unstructured Mesh of the Simulated Model.

The missile was dropped first and after 1 second, thrust was turned on. The mass of missile was 253 kg with 22 kN thrust. It had an inertia of 125.29 kgm^2 in spanwise direction of the fin and 0.94 kgm^2 at symmetry axis. Before 1 second, the displacement in x direction was influenced by drag and afterwards it was controlled by thrust and drag. The displacement in y direction was influenced the side forces. It can be seen that the side force valued very small because the missile was symmetry. The displacement, as shown in Figure. 4, in z direction was weighted by the lift force and mass of the missile. The angular displacement was controlled by rate moment of the missile and inertia in x, y, z direction, as shown in Figure. 5.

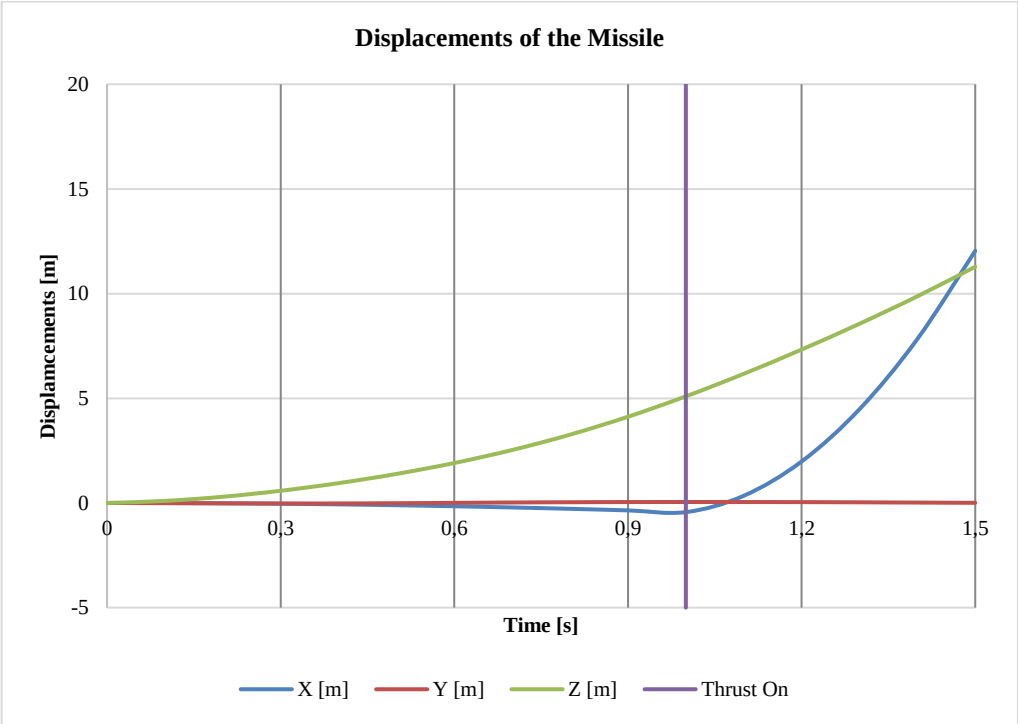

Figure 4. Linear Displacement of Missile.

Based on the Figure. 5, it can be observed that pitch and yaw angular displacement had the sinusoidal trend with small amplitude. It was proved that missile had a good stability in theta and psi rate. For the roll angular displacement, it can be viewed that the angle was increased linearly in the rise of time. It was confirmed that in order to maintain stability of the symmetry object, spin movement in flight direction was needed. Thus from the simulation of displacement and angular displacement of the missile collision, it could be concluded that the assumption was safe to be used [3].

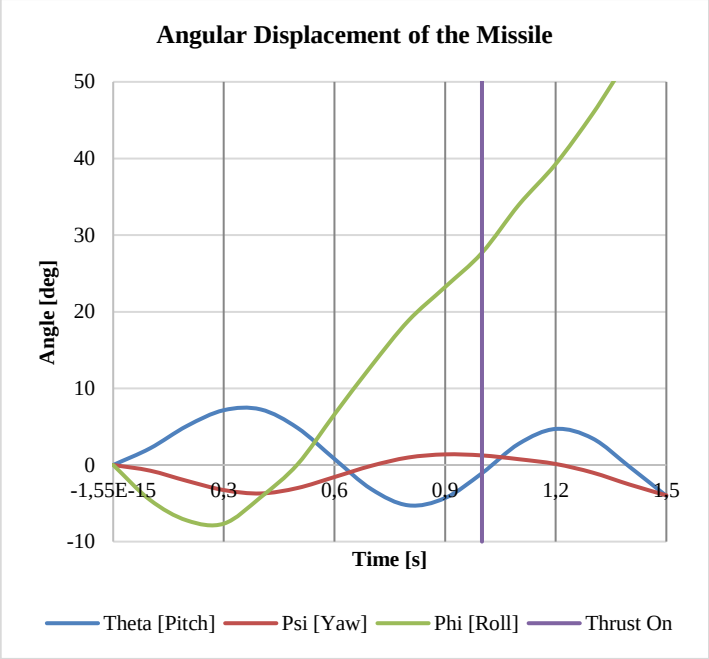

Figure 5. Angular Displacement of Missile.

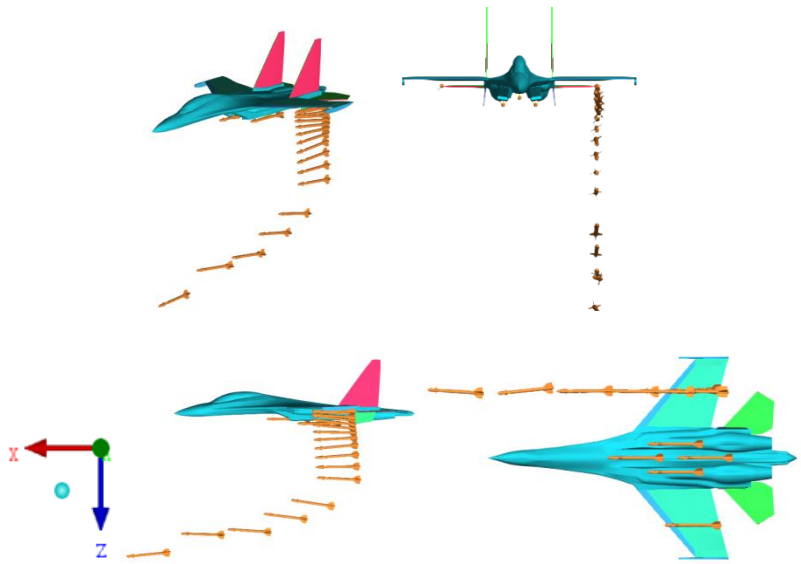

Figure 6. Separation of Missile.

The trajectory of the missile while it separates from the aircraft is displayed in Figure. 6. It could be seen that the displacements in y direction, in yaw and pitch are relatively small. This

shows that the missile can maintain the forward facing direction before thrust activates. The pitch amplitude reduces once thrust in on. The missile is well separated from the aircraft before it gains speed, thereby preventing it from hitting its own aircraft.

IV. Conclusion

This paper established CFD method to simulate store separating from aircraft. The linear and angular displacement result indicates that the method to solve the moving body quasy-steady flow-field is accurate and feasible. Simulation of active missile could be done, thus allowing us to predict behavior on armament development and modification.

References

[1] Y.E. Sunay, E. Gulay, A. Akgul “Numerical Simulations of Store Separation Trajectories Using the EGLIN Test.” Scientific Technical Review, 2013, Vol 63, No. 1, pp. 10-16.
[2] D O. Snyder, E. K. Koutsavdis, J. S. R. Anttonen, “Transonic Store Separation Using Unstructured CFD with Dynamic Meshing”, AIAA 2003-3919, June 2003.
[3] H. O. Demir, “Trajectory Calculation of a Store Released from a Fighter Aircraft” AIAA Paper 2005-847.
[4] P. S. Murthy, “Separation studies of generic store released from aircraft wing pylon configuration”, International Aerospace CFD Conference, Paris, June 2007.
[5] J. Gong, Z. Zhou, B. Liu, “Using the unstructured dynamic Mesh to simulate multi-store separating from aircraft”. Elsevier 1877-7058, 2010.
[6] N.D. Domel, S.L. Karman, “Splitflow: Progress in 3D CFD with Cartesian Omni-tree grids for complex geometries,” AIAA Paper 2000-1006.
[7] S. J. Zhang, J. Liu, Y. S. Chen, “Numerical simulation of stage separation with an unstructured Chimera grid method”, AIAA- 2004-4723.

Method for Air Combat Simulation Outcome Determination (#695)

Prasetyo Ardi P.S[1,a]. , Rianto A. Sasongko[1,b]
[1]Department of Aeronautics and Astronautics Institut Teknologi Bandung, Indonesia
[a]prasetyo303@students.itb.ac.id, [b]sasongko@ae.itb.ac.id

Abstract*—This paper discuss about the development of the calculation scheme for the probability of kill in an air combat followed by the simulation of fighter aircraft condition after taking damage. After a fighter taking a hit from its enemy, there will be two possibilities for its condition. One is a total destruction, and the other is the fighter survive but it suffer some kind of damage. The type of damage as well as the consequences can be vary depends on where the damage took place. Some of possible consequences are an alteration in flight dynamic, instability, performance degradation, reduced fighter lifetime or combination of the aforementioned consequences. Through this research the fighter behavior when damaged is simulated so the input to keep the fighter at level flight (if possible) can be estimated. The air combat simulation is done using software MATLAB and visualized using software XPlane.*

Keywords: *Air combat, Probability of Kill, flight dynamic, Monte Carlo, damage.*

I. Introduction

Air combat simulation is a vast topic in research. An interesting method to assess the fighter maneuver and the position is called Probability of Kill. This method is heavily explored in [1] and [2]. Here the PK model is developed further in 3 different scheme.

Nowadays the simulation method about air combat is well developed even though many parties especially in military field is reluctant to share this sensitive issue. Current analysis normally based on the evaluation of the combat situation [3], threats determination [4], the target assignment [5], and the aircraft approaching path and strategy [6]. However this simulation mainly only consider two condition for the fighter, namely normal condition and destroyed. In reality it is very possible although the fighter can't behave normally due to damage but it's not destroyed yet and even still could fly for a certain time.

When a fighter survive a missile, if the missile can be totally avoided, the explosion may damage some structure which in turn disturb the fighter's normal behavior. The part which take damage can be vary as well as the consequence that it holds. For example a fighter which take damage in the wing part may experience lift drop in the corresponding wing side, on the other hand a damage on the vertical tail plane may reduce the yaw maneuver performance. This uncertainty fighter condition with unknown probability can be properly modelled by montecarlo method.

Linearized Aircraft Flight Dynamic

In general, aircraft performance can be described as a point of mass centered in its center of gravity (cg). On the other hand flight qualities can't be described as simple as that, but by analytical description of aircraft and airframe movement relative to its cg [7]. Those movement is caused by aerodynamic force, thrust and other force and moments. Moreover the aircraft must be considered as 3 dimensional body not a point of mass. In this research, the aircraft movement equation is simplified into linear differential equation.

II. Air Combat Effectiveness

Probability ok Kill (PK) is a method to quantify the effectivity of an aircraft maneuver relative to its opponent. This method is heavily analyzed in [1] and [2]. It is formulated as in (1) – (3).

The P_r and P_a represents the PK by range and PK by angle value respectively. R_b is the target (bandit) distance. R_{min} and R_{max} are the minimum and the maximum distance of the missile, R_{Kmin} and R_{Kmax}, is the minimum and the maximum effective distance of the missile. φ_W is the missile boresight angle. The symbols ω, ε and γ represents the azimuth, elevation and the pitch angle respectively.

The PK calculation in air combat can be done in three different approaches as illustrated in Figure 1, which are:

a) PK calculated during missile launch with frozen target.
b) Dynamic PK with moving target relative to a frozen launching platform.
c) Dynamic PK with moving target relative to a moving missile.

$$PK = P_r \cdot P_a \quad (1)$$

$$P_r = \begin{cases} 0 & , R_b < R_{min} \\ 1 - \frac{R_{Kmin} - R_b}{R_{Kmin} - R_{min}} & , R_{min} \leq R_b < R_{Kmin} \\ 1 & , R_{Kmin} \leq R_b \leq R_{Kmax} \\ 1 - \frac{R_b - R_{Kmax}}{R_{max} - R_{Kmax}} & , R_{Kmax} < R_b \leq R_{max} \\ 0 & , R_b > R_{max} \end{cases} \quad (2)$$

$$P_a = \begin{cases} 1 - \frac{\lambda}{\varphi_W \cos\left(\frac{\pi(\sin^{-1}(\frac{\Delta h}{d}) - \gamma)}{\varphi_W}\right)} & , \lambda_f \leq \varphi_W \\ 0 & , \lambda_f > \varphi_W \end{cases} \quad (3)$$

The simplest model is the first approach which also called as 'Missile Launch Envelope Model' in [8]. This model consider Probability of kill based on the distance and the LOS between the fighter and the bandit when the attack (shoot) is done. This technique doesn't consider any evasive maneuver to maximize the missile off distance done by the bandit. The problem arise within this method when the simplified function used in PK calculation cannot rewards the bandit by increasing its survivability eventhough its correctly evading the missile.

The second approach is to calculated PK value dynamically. When the missile is launched, the fighter is seen as unmoving object (freeze) but the PK calculation will keep changing along with the bandit movement using the fighter frozen missile envelope. The advantage in this method is now the PK will gives rewards or punishment to the bandit based on its maneuver. This method however still have a drawback because the missile itself is not modelled.

The third approach use PK calculation using both the missile and the bandit position in a certain time. Here the missile is considered as a moving object faster than the bandit. The PK value is calculated using missile envelope which steadily get smaller as the missile move. Ideally the missile have a smaller rate of turn than the bandit due to the high speed and the maximum G-load. Thus the missile have a chance to overshoot the bandit flight path. When this happen, the shooting will be declared as a miss.

III. Outcome Scheme

Based on the severity level, the damage done to an aircraft can be separated into 3 categories: Attrition kill, Mission abort kill, and forced landing kill. The attrition kill can be divided further into 4 subcategories which are:

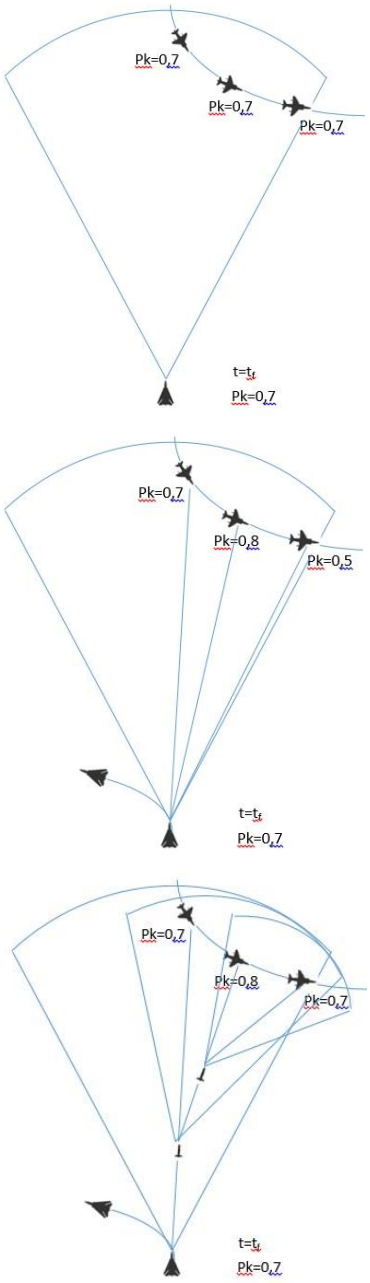

Figure 1. Different approach to calculate PK

- KK Kill, also known as catastrophic kil, is a total destruction after being hit.
- K Kill, is aircraft damage which cause the aircraft down but still can be controlled up to 30 seconds.
- A Kill, is aircraft damage which cause the aircraft down but still can be controlled up to 5 minutes.
- B Kill, is aircraft damage which cause the aircraft down but still can be controlled up to 30 minutes.
-

This paper is specifically simulate the fighter in A and B kill criteria in which after taking a hit the fighter still can be controlled by the pilot to continue the mission in a temporary period.

A. Damage Area Distribution

In this research the damage done to the aircraft are categorized into 4 area, which are: a) Fuselage

b) Wing
c) Horizontal Tail Plane
d) Vertical Tail Plane

The probability value of a certain part damaged are depend on the aircraft position relative to the incoming missile, therefore it can be seen as a function of impact angle (see table I). 0^o impact angle is defined as the tail side direction and 180^o impact angle is in the nose direction. An incoming missile from the right side of the aircraft direction is called as 'right impact with positive angle, conversely the incoming missile from the left side of the aircraft direction will be called 'left impact with negative angle value (see fig 2).

Considering the fighter aircraft geometry in general, the fuselage part is most likely vulnerable to be attacked from the front side, wing is more vulnerable to be attacked from the side, while the horizontal tail plane and vertical tail plane is vulnerable to be attacked from the rear side. Table I shows the damage probability allocation of the aircraft:

B. Monte Carlo Procedure

To find out which part of the aircraft will take the damage, each time an aircraft has been hit a random integer with value ranged from 1 to 100 is generated. The generated number will determine which part of the aircraft is damaged. For example with impact angle = 0^o then the value 1-10 means the either wing is damaged, the value 11-50 means the vertical tail plane is damaged, 51-95 means the horizontal tail plane is damaged and lastly 96-100 means the fuselage.is damaged.

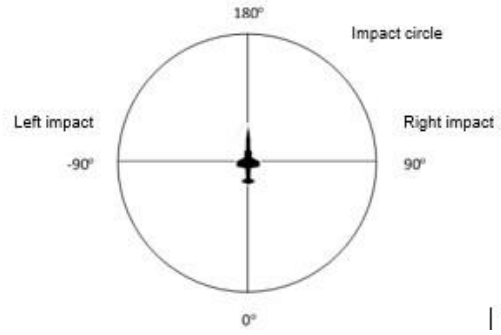

Figure 2. Impact angle

TABLE I. Damage Probability

Impact Angle (deg)	**Wing (%)**	**VT (%)**	**HT (%)**	**Fus (%)**
± 0 – 45	10	40	45	5
± 45 – 90	20	35	30	15
± 90 – 180	50	5	0	45

C. Damage Consequences

The damage consequences are vary depend on the aircraft part which take damage. The damage on the fuselage is considered as fatal and counted as immediate kill. This is chosen by consideration that the pilot position inside the fuselage make it dangerous when this part is damaged. Meanwhile the damage on the vertical tail plane will only affect the aircraft lateral – directional flight dynamic model. The effect on the longitudinal dimension is considered small enough to be neglected. On the other hand the damage on the horizontal tail plane will only affect the aircraft longitudinal flight dynamic model. The effect on the lateral – directional dimension is considered small enough to be neglected. Lastly the damage on the wing will affect both longitudinal and lateral – directional flight dynamic model. Table II describe the consequences which arise when the aircraft take a damage in the corresponding part.

To observe the aircraft response after being hit, a simulation using aircraft mathematical model is conducted. The idea is to reduce the input signal of the control surface which in turn will degrade the aircraft performance in accordance to the corresponding damage suffered by the aircraft. This idea is chosen by considering the fact that the broken part of the control surface may work ineffectively compared to the normal condition. The input signal drop is chosen as 50% of the original input. For example if the aircraft experience a damage on the horizontal tail plane then the elevator deflection of 20 degrees will produce a same aircraft response with 10 degrees deflection in a normal condition. In the future this value maybe replaced with a more reliable value based on real statistic data. When the aircraft take a damage, it also receive an additional penalty. The aircraft flight dynamic model will be replaced with new model which is more suitable to its damaged condition.

TABLE II. Damage Consequences

Part	**Wing**	**VT**	**HT**	**Fus**
Effect	inc x_u dec z_u dec m_α dec yδa dec lδa dec nδa	dec l_β dec n_β dec yδr dec lδr dec nδr	inc x_u dec z_u dec xδe dec zδe dec mδe	Instant Kill

Where inc is increase in magnitude and dec is decrease in magnitude.

IV. Simulation

To test the model, a simulation is conducted to calculate the PK value using three calculation scheme mentioned before. The simulation flow to determine the outcome of air combat is given in Figure 3. The results for this simulation can be seen in Figure 4. After the fighter assumed being hit, the new aircraft behavior will also be simulated. There are many possibilities for the type of damage suffered by the aircraft. However this paper only gives an examples where the aircraft experience a damage on the wing.

The aircraft is assumed taking a hit from the opponent and the new aircraft behavior will be simulated. Aircraft wing is damaged at simulation time, t = 17 seconds, pilot react on t = 30 and attempted to restore the aircraft to initial attitude and direction (bank angle = 0^o) using the aileron and rudder. The simulation is conducted in 50 seconds. The aircraft impact angle throughout the battle is displayed in Figure 5.

At t = 17 s, the aircraft impact angle is 106^o. The monte-carlo procedure gives damage probability value 41 which means from this time the right wing is damaged. The control surface input given to stabilize the aircraft is given at Figure 6. The output for the simulation is given in Figure 7.

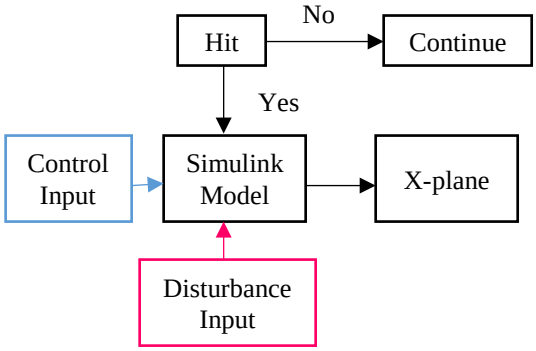

Figure 3. Simulation flow to determine air combat outcome

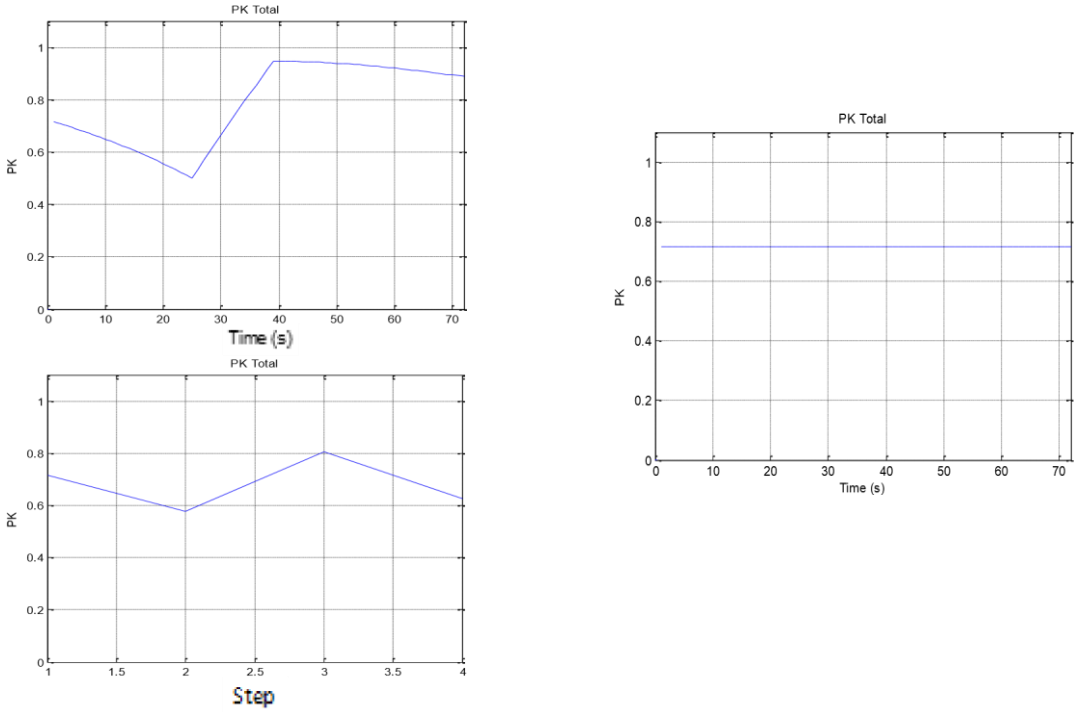

Figure 4. PK value in 3 different approach: First approach (top), second approach (middle), third approach (bottom).

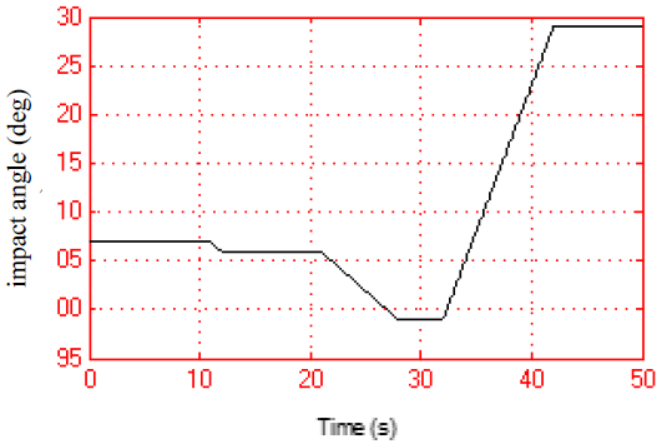

Figure 5. Aircraft impact angle (deg)

It can be seen in Figure 7 that the aircraft experience an instability caused by damaged right-side wing after being hit. This damage cause a lift drop and increases of drag on the right wing which further cause positive roll moment as well as positive yaw moment. This moment caused the heading changed positively (clockwise) and negative side slip is also comes up. In the simulation it's appear that the roll moment due to damage can still be neutralized by utilizing the aileron and rudder. The flight direction and the attitude can also be returned to normal eventhough stability can be hard to obtain manually.

The output data from the simulation are visualized using X-plane software. The visual data in the X-plane are recorded again and compared to the Simulink data. The visual data obtained from the X-Plane are shown in Figure 8.

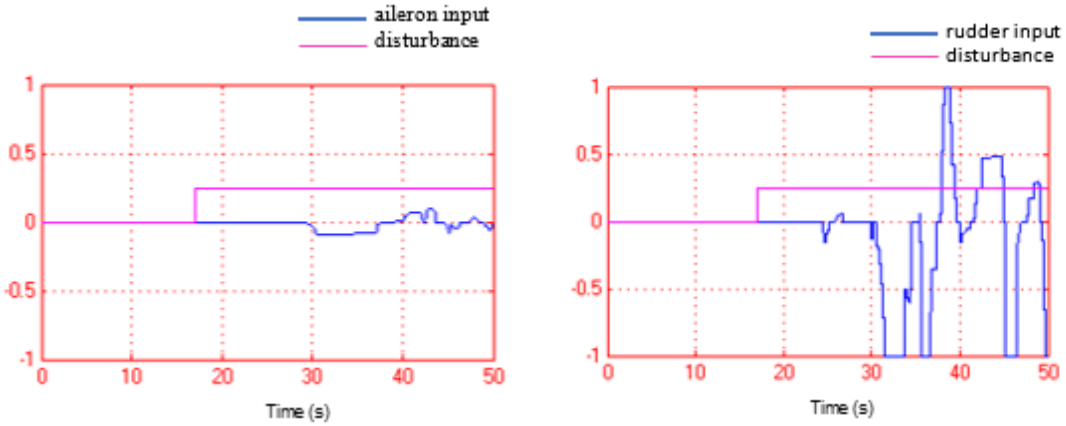

Figure 6. Aileron input (left) and rudder input (right)

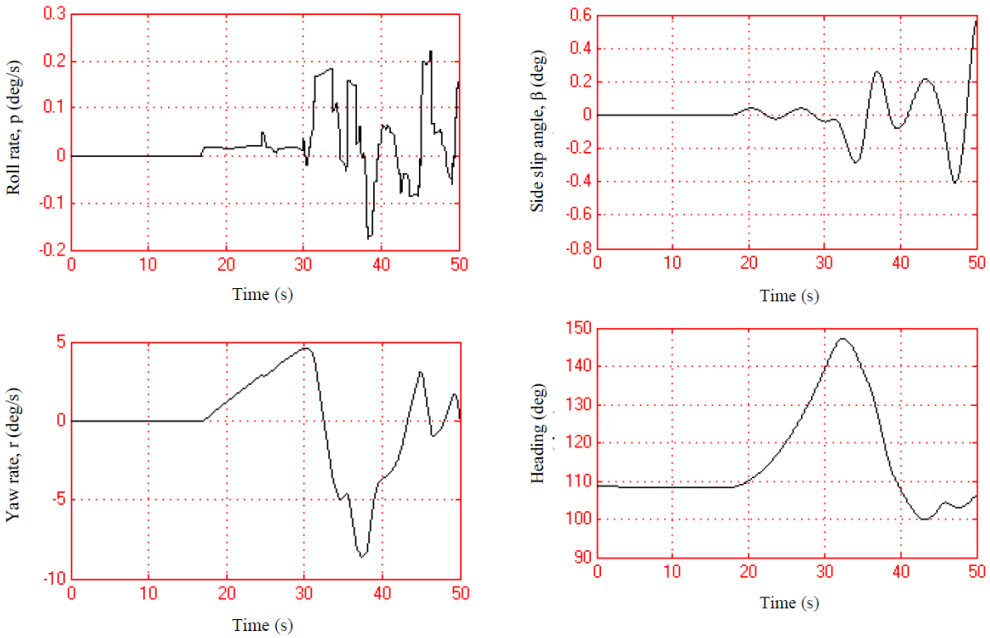

Figure 7. Dynamic variables Simulink output in scenario 1

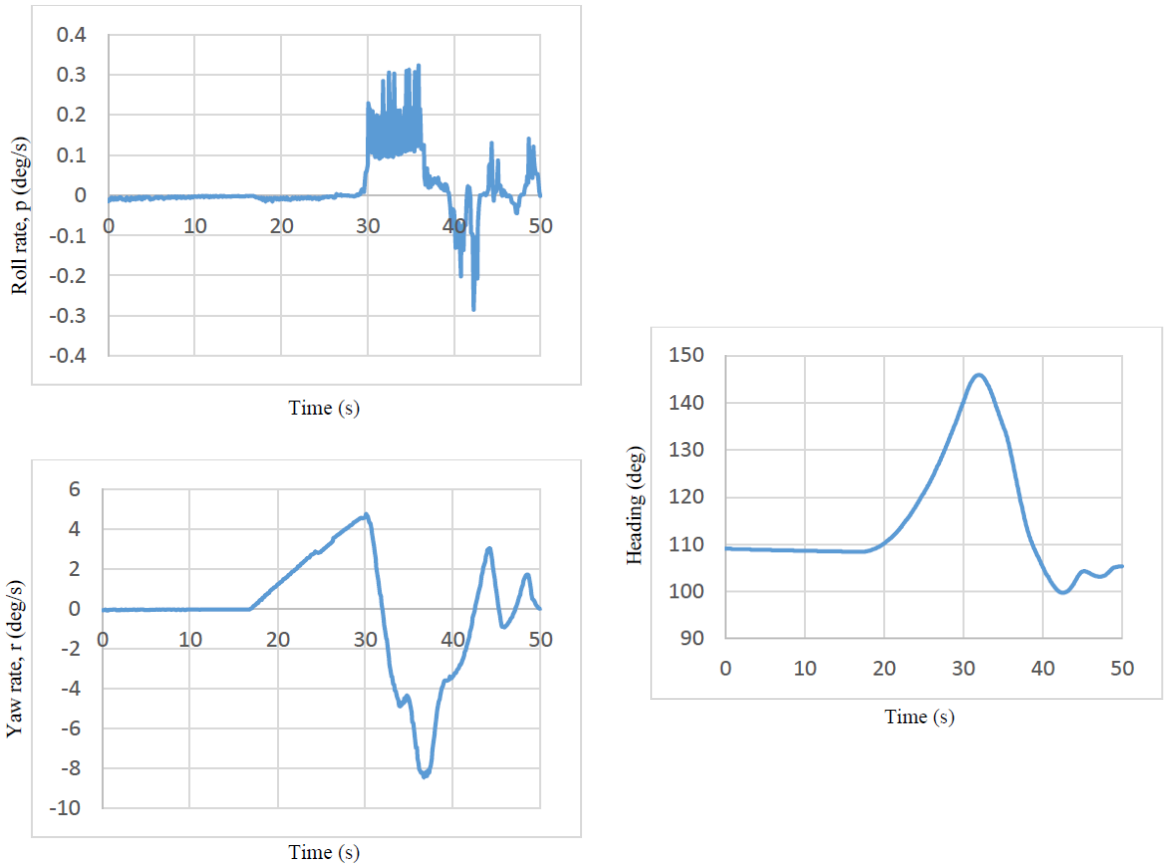

Figure 8. Dynamic variables X-Plane output in scenario 1

There are some differences between the pretransferred data and the visualized data in the XPlane. But, an observation to both data suggest that both data follow a same trendline, therefore it's relatively consistent. It should be noted that the XPlane software do a calculation to side slip angle using a difference aircraft model from the one used in the simulation. This resulting in a whole difference side slip value and can't be compared with the side slip output from the Simulink software.

V. Conclusion and Remarks

From the simulation results, it can be concluded that the model and the simulation that has been conducted able to represent the aircraft condition when taking damage with A and B kill criteria. The probability of the aircraft component taking damage is dynamically changing depends the aircraft impact angle when taking the hit. The damage to the aircraft can induce either an instability, maneuver performance degradation, or alteration to aircraft dynamic model in accordance to the damage suffered by the aircraft. The simulation also reveal that X-Plane software conduct a self-calculation to any variables that's not provided by the user when the data are transferred from the Simulink into the X-Plane.

For the future work it's important to make a better assessment of the performance degradation level when the fighter taking damage. The aircraft behavior when taking damage can also be modelled more realistically by including the degradation effect of engine performance. Furthermore it will be interesting to simulate the fighter behavior with multiple site damage condition.

Acknowledgment

This research is founded by ministry of research and higher education of republic Indonesia through INSINAS research program

References

[1] Prasetyo A.P.S. "Development of Air Combat Effectiveness Simulation and Analysis Scheme for Beyond Visual Range (BVR) Case". 2015. Applied Mechanics and Materials. Vol 842. pp 329-336.
[2] M. Sugiyanto. "Pengembangan Perangkat Lunak Analisis Probability of Kill (Pk) dan Supremacy pada Air to Air Combat Pesawat Tempur". 2014. Bandung. Institut Teknologi Bandung.
[3] Hague D S. "Multiple-Tactical Aircraft Combat Performance Evaluation System". AIAA-80-0189: 513520.
[4] QU Changwen, HE You. "A method of threat assessment using multiple attribute decision making" ICSP'02 proceedings, 2002:1091-1095.
[5] GengYanluo, JiangChangsheng, LiWeihao. "Multi-fighter coordinated multi-target attack system". Transactions of Nanjing University of Aeronautics & Astronautics, 2004, 21 (1): 18-23.
[6] Nguyen D, Fisher D C, Ryan L, "Agraph-based approach to situation assessment". Pro. of the AIAA Infotech Aerospace, 2010:1-6.
[7] Volume II "Flying Qualities Phase" Ch. 4 "Equation of Motion". 1988. USAF Test Pilot School.
[8] Kaplan, Joseph A. dkk. "The Analysis of a Generic Air-toAir Missile Simulation Model". Blacksburg. Department of Computer Science Virginia Polytechnic Institute and State University.

Electric Power Optimizing Of Solar Panel SystemThrough Solar Tracking Implementation; A Case Study in Pekanbaru (#696)

Adhy Prayitno[1,a] , Muhammad Irvan, Sigit Nurharsanto, Wahyu Fajar Yanto
[1]Mechanical Engineering Departements, Faculty of Engineering University of Riau.
[a]adhyprayitno_hadi@eng.unri.ac.id

Abstract *-- Observations and measurements have been conducted towards a solar panel electric power output that is utilized by a solar tracking system. The electrical power output depends on the position of the sun and time and the direction of the panel surface against the angle of the incident light. For power optimization, the solar panel surface should always be directed perpendicular to the direction of the sunlight falling to the surface of the panel. The application of the solar tracking system controlled by a micro controller gives the expected results. The electrical power output of a static solar panel mounted on a fixed position becomes the benchmark of the output electric power value in this study. The measurement results of the electric power output of the solar panel with sun tracking system shows a significant increase in sunny weather conditions. The average increase of that is about 57.3%.*

Key words*: LDR, micro controller, optimal power output, performance improvment, sun tracking,*

I. Introduction

Demand of electric power is increasing so high in Indoneia. Meanwhile electric power production is growing slowly. Since that the use of photo voltaic or solar panel to produce electricity grows rapidly during last few years. It is and alternative electricity source [1] particularly at remote areas which there is no near by power plant. In addition, solar energy is environmental friendly as compared with other energy sources. Although it has being widely used for supplying electricity, solar panels however are mostly fix installed. The application of that is usually mounted on static structure. It means that incident sun rays will not be able alway to perpendicular to the panel surface. So that the angle of coming sun rays to panel surface vary ith sun position. The optimum power output will be achieved only if sun position exactly perpendicular to panel surface. Regarding that manner, it is nesessary to apply sun tracking method to solar panel system. Sun tracker detect the sun position and control the panel [1, 2]. Sun-tracker drives the solar panel and keeps the panel surface remains perpendicular to the sun position. It will be able to gain desired optimum power output of the solar panel.

II. Methodology

A. Experimental mechanism

This study implements an experiment and measurement based upon build and design methodology. The structure of the system is composed based on two degree of freedom movements. The panel is able to move toward – backward, left – right in 180^{o} range. So the panel surface can be kept always in perpendicular against to the the sun rays. Light dependent resistor (LDR) and a micro controller are utilized the solar panel through motor drives system.

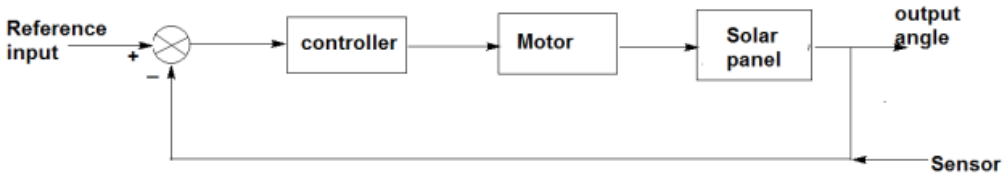

Figure 1. Sun tracker control diagram

The observation and measurement to the system take place at 8.00 a.m. – 5.00 p.m.
A set of LDR is sensing element responsible for working system of the sun tracking. The position of the LDRs are critical here and the set of LDR which corresponds to this vertical plane movement is so positioned that it senses the sun light accurately and tries to keep the panel perpendicular to the sun rays by moving the motor in the appropriate direction through a definite number of stepped rotations. The LDR sensing is actually accurately received and interpreted by a microcontroler.

B. MEASUREMENT AND DATA COLLECTION

Two solar panels from same type are prepared. One panels is supported by a sun tracker. So that this panel is dynamic or mobile system. The another one is not supported by a sun tracker so it is immobile or static. Measurement procedure is described on the following flowchard (Figure 2).

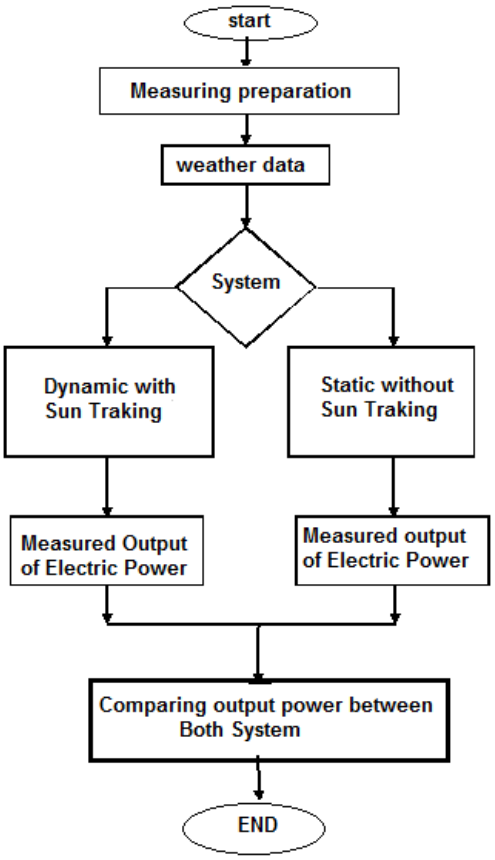

Figure 2. Flow chart of measurement procedure of electric power output for two sytems, dynamic and static system.

Data of daily weather condition are crecorded which include temperature, humidity and sky clearness before measuring electric power output of both system. Their electric current output are simultaneously measured. The measurement of those are run based upon 15 minute interval start from 8.00 a.m. to 5.00 p.m. By setting up constant voltage , the electric power output is obtained.
The associate power output is computed by utilizing the following equation;

$$P = I \times V \qquad \text{in Watt.} \qquad (1)$$

Where P is produced electric power, I is output current and V is voltage.

Performance improvement can be computed using the following formula,

$$\eta = \frac{P_D}{P_D + P_S} \times 100\% \qquad (2)$$

The following chart presents output current of the panels either with sun tracker or without sun tracker.

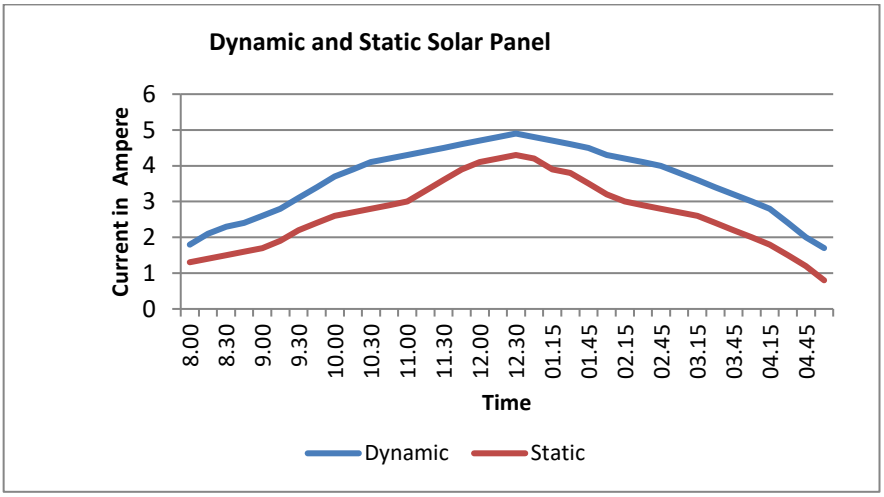

Figure 3. The output current generation comparison of applied tracking system and fixed angle system.

III. Result and Discussion

Output power of both systems, dynamic and static system are computed based on average current.

Using equation (1) in previous section under 12 Volt electricity voltage, it gives the following result; Average Power for dynamic solar panel is equal to 43 Watt and the average power for static of that is equal to 32.03 Watt. Implementation of sun tracking to solar panel system instalation by using equation (2) has improved the output power equals to 57,3 %. The improvement of solar panel generator through sun tracking implementation give advantages not only for electricity sources development erspective but also for environment perspective.

IV. Conclusion

The implementation of sun tracking system makes the system capable of adjusting panels surface always to be perpendicular against sun position. As a result optimum output power is obtained. Performance improvment equals to 57.3 % is a great value . Sun tracking system is considered so powerful to gathering solar energy and give promisse for future energy supply development.

Aknowledgement

Special thank to management of Bank BNI Pekanbaru for supporting us in doing our research and experimental through green energy program. So that we are able to join the IC-Star 2017 in Bandar Lampung. Thank you very much to friends and students who help this research work.

Reference

[1] Koh Kiong Chai, Kai Meng Tay* & Mohammad Omar Abdullah, " Development of solar photo voltaic system equiped with a sun tracker system : A case study in Kuching Sarawak" **IJRRAS** 7 (4) . June 2011.

[2] Y. J. Huang, *Member, IAENG*, T. C. Kuo, *Member, IAENG* , C. Y. Chen, C. H. Chang, P. C. Wu, and T. H. Wu, "The Design and Implementation of a Solar Tracking Generating Power System" Engineering Letters, 17:4, EL_17_4_06

[3] Salihu O. Aliyu, Michael Okwori and Elizabeth N. Onwuka, "A Prototype Automatic Solar Panel Controller (ASPC) with Night-time Hibernation". *I.J. Intelligent Systems and Applications,* 2016, 8, 18-25

Risk Assessment Approach in Airport Security (#697)

Mahardi Sadono[1,a], Saphira Alifa Harahap[1], Dani Yulianto Putra[1], Randhy[1], Muhamad Luthfi Imam Nurhakim[1]
[1] Faculty of Mechanical and Aerospace Engineering, Institut Teknologi Bandung, Indonesia
[a]mahar65@yahoo.com

Abstract. *Naturally, the threat to flight is generated from all activities at the airport by passenger or freight. With the growth of air transport, the level of threat to flight activity will also increase. Due to ensure the security of passengers, staff, and all elements of the airport, the airport as a place of flight operations need a reliable protection system. The purpose of this study is to develop a methodology for assessing the risk level at the airport in order to improve the level of protection at the airport. The level of threats that could jeopardize airport security is categorized into several levels, then analyzed to what extent the risk level can be tolerated as a reference to the formulation of standard protection systems at the airport. The results of this study can be used to deal with threats that occur in the airport through preventive action by setting up a reliable protection system. The risk assessment approach also able to evaluate the airport's existing protection system whether it is tolerable to deal with threats or not, so action can be taken to improve the protection system if the failure rate is still high and have massive consequences to the all airport elements..*

Keywords: *airport security, failure rate, protection system, risk assessment, tolerable risk level..*

I. Introduction

1.1 Airport Security

In this era, requirement of air transportation which can saving more time than other transportation type is increasing. This can be seen from growth rate of airplane movement and increased number of passengers in Indonesia[1]. This is related to airport security. Airport security is a system of methods and technology that used to protect all elements in the airport from the threats. On several occasions in Indonesian airport encounter threats that can ruin airport facility, and also threatening safety of passengers and staffs. Last case occurred in Sam Ratulangi Airport when the society break through the airport and causing the glass of arrival gate broken. It shows the importance of airport security to ensure the safety of the passengers, staff, and all elements of the airport.

1.2 *Previous Research Results*

Security issues always has been a problem for aviation industry and organization, and it always increase over years. Researched has been conducted to give recommendations to solve problems that occurred in aviation history and to prevent potential problems that might happened in the future. Previous research conducted shows that sets of scenario towards specific target can be investigated through examination of its vulnerability and its criticality[2]. Every potential scenario can be studied in order to have an estimation of the current risk level. Quantitative analysis is possible to do to investigate vulnerabilities and criticality of the airport components.

The optimized design of the airport security, its ability to innovate, and to modify itself in consequence of the results of risk assessment is the best indicator of the ability to answer new threats and to assure an acceptable security risk level. The approach shows in the Figure 1 below.

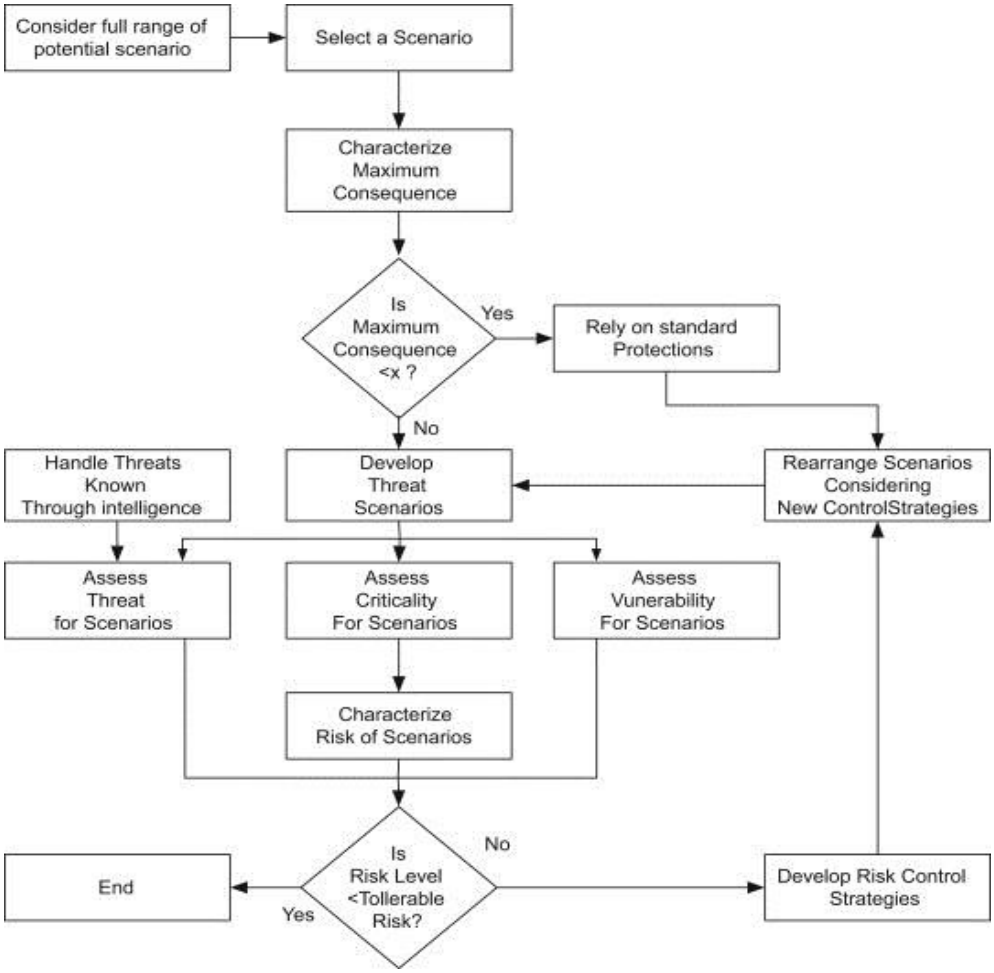

Figure 1. Risk assessment approach[2]

In order to categorizing risk level, another previous research was conducted specifically for Indonesian Airports cases has been categorizing risk level into 4 risk levels[3]. This study use six parameters to categorize the risk level: airport location, VIP flight, apron capacity, number of runway exist, international routes, and air traffic. Each parameters will give a score (range: 1-5) and the total score of these parameters will be used to categorize the risk level. The 1st level is the airport with the highest risk with score greater than 36, and the lowest risk will be the 4th level that have score less than 17. With this method, this paper analyzed 172 airports in Indonesia and categorized them into 4 level of risk based on airports parameters.

A research program[4] which conducted by Airport Cooperation Research Program (ACRP) sponsored by FAA released a guidebook for safety management for Airports in 2015 to help airports organization to prevent any security violation that might harming passengers or causing financial losses and as a guidance for airport operators, local agencies, the FAA, and other interested parties, and industry associations may arrange for workshops, training aids, field visits, and other activities. This research project is assigned to an expert panel, appointed by the Transportation Research Board (TRB). Panels include experienced practitioners and research specialists; heavy emphasis is placed on including airport professionals, the intended

users of the research products. On this research the panels prepare project statements (requests for proposals), select contractors, and provide technical guidance and counsel throughout the life of the project. The process for developing research problem statements and selecting research agencies has been used by TRB in managing cooperative research programs since 1962. As in other TRB activities, ACRP project panels serve voluntarily without compensation. This research provide guidance on conducting the Safety Risk Management (SRM) process, one of the four components of a Safety Management System (SMS).

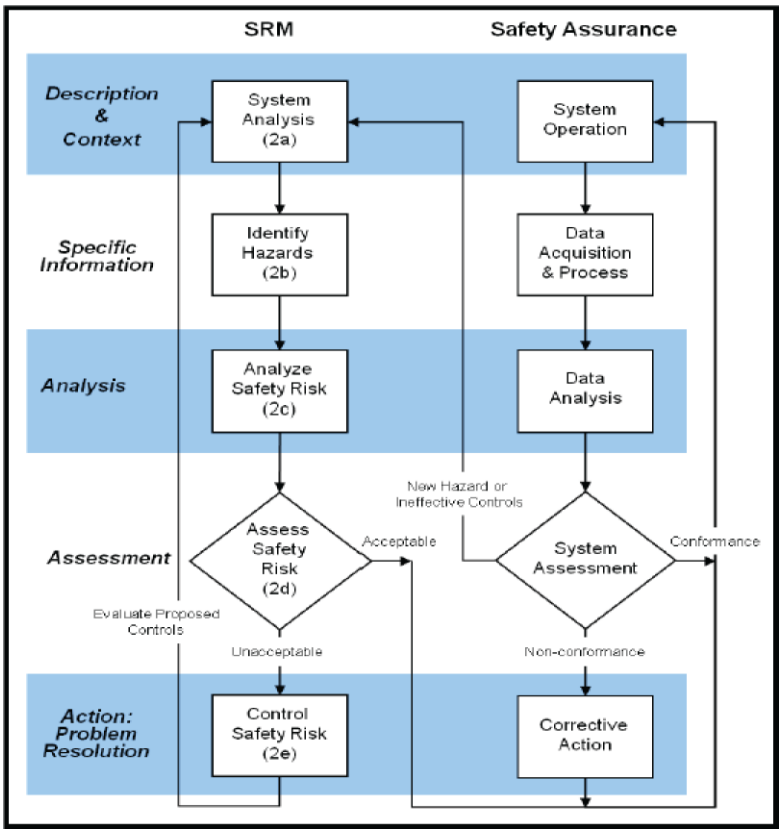

Figure 2. SRM and safety assurance processes (FAA Order 8040.4A, 2012)

1.3 Regulation of Airport Security

There are some regulations that regulate about Airport Security. Locally, Indonesia has PM 31 year 2013[5]: National Aviation Security Program (*Program Keamanan Penerbangan Nasional*) that contain regulations and have some objectives to protect security, safety, regularity, and efficiency of Indonesia's Aviation. PM 31 year 2013 also regulate about Standard and Procedure that has to be complied by passengers, aviation crew, aviation security crews, and also citizen to prevent acts of unlawful interference. For international regulations, there are ICAO Doc 8973/8 about Aviation Security Manual[6]. ICAO Doc 8973/8 has an objective to advise States on the prevention of and where necessary response to act of unlawful interference, through the application of an aviation security system comprised of four main elements: legal framework and security oversight; airport design, infrastructure and equipment; human resources recruitment, selection, training and certification; and procedures and the implementation of security measures.

II. Methodology

This research has an objective to make a risk assessment approach which will more efficient than previous research held. There are three questions that need to be explained to reach the objective:

- How to make Risk Assessment Approach?
- How to categorize the threats of Airport Security? and,
- How to determine a tolerable risks level?

To occupy these questions, this research will continues from previous research in 2013 titled "*Study of Indonesian Airports Risk Level Categories"*. Based on that research we adopt the level risk method to categorize threats level that will be faced. This research also refers to "Risk Assessment Techniques for Civil Aviation Security" from Porto Institutional Repository and "A guidebook for Safety Risk Management for Airports" from ACRP report 131 to be another consideration to compile the method in this research. The research process can be seen in the Figure 3 below.

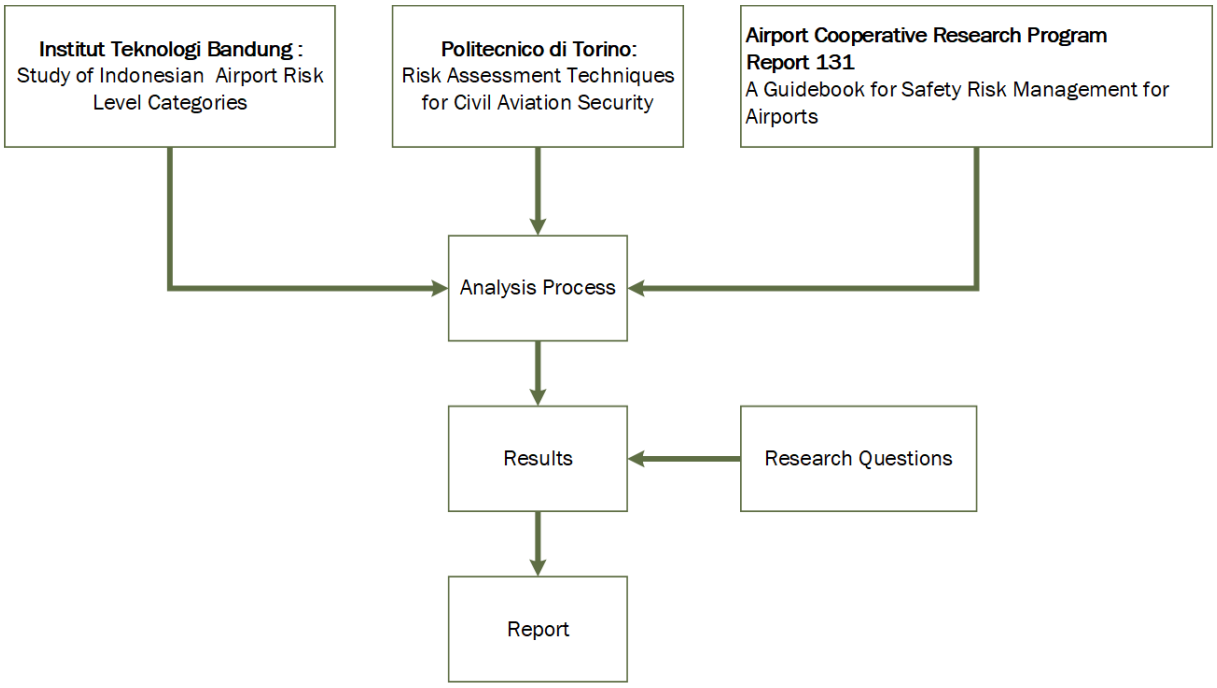

Figure 3. Research Process

According to Business Dictionary, risk is a probability or threat of damage, injury, liability, loss, or any other negative occurrence that is caused by external or internal vulnerabilities, and that may be avoided through preemptive action. While threat is negative event that can cause a risk to become a loss, expressed as an aggregate of risk, consequences of risk, and the likelihood of the occurrence of the event. Threats can also come from the many processes that support an airport and the passengers and aircraft it serves: catering, maintenance, cleaning, ticketing, baggage handling, air traffic control, retail, food services, parking, car rental and others.

There are many risk tool management that can be used to assess problems. Fault Tree analysis was chosen as risk tool management to analyze risks in this research. Fault Tree analysis is a top down, deductive failure analysis to understand of how an undesired events

can happen. This method identifies the best ways to reduce risk or to determine of how many times of a safety accident or particular system fails. Fault Tree Analysis helps to identify the potential cause of a problem before it actually occur. Fault Tree Analysis can also be used to evaluate the probability of a system failure using analytical or statistical method.

III. Analysis

III.1. Risk Assessment Approach

In previous research held by ITB[3], the research only focus on the threat analysis without adding protection system on its risk assessment approach. On the other research conducted by Politecnica di Torino [2], their risk assessment approach already considering the scenario that may happen and also considering the scenario's likelihood and consequences. However, it hasn't divide the risk level on three levels (low, med, and high), it only has two risk level (low and high). Risk Assessment Approach will be started with threat which possible to happened in the Airport. With this condition, there will be need to list down the scenario that may happen that will lead to threat for airport security. There are some act be avowed as Acts of Unlawful Interference (PM 31 year 2013):

1. Take over airplane's control,
2. Destroy airplane in land,
3. Holding hostage in airplane or airport,
4. Forced entry to airplane, airport or aeronautics place,
5. Bring weapon or dangerous goods,
6. Using airplane outside the procedure,
7. Give the wrong information, and
8. Bomb threats

These acts of unlawful interference will lead to some scenario that might happen and will threaten the airport security. The scenarios then will be analyzed to get the result whether the scenario has low risk or high risk on airport security. If the risk is low, so the scenario will be ignored. But if the risk is high, the airport management should have prepared protection standard against the threat so the scenario will not happen. If the airport has no protection standard to prevent the scenario, the airport needs to develop protection system to protect its security.

If the airport already had protection standard, the next step is to analyze the probability of the protection system failure. If the result from the analyzation process is categorized as low rate failure, the airport security already has adequate airport security system. This result is the ideal condition for the airport security system, because it means that the probability of the threat to happen is low. If the failure rate is categorized as medium, then they will need to make small improvement in the protection system. The improvement could be applied on the software, hardware, or the liveware of security system. After the improvement applied, the system failures need to be checked again, is it already have low failure rate or not. If not, so there will be need more improvements until the failure rate is low. Last, if the failure rate is high, then the airport needs to develop protection system. It will have same steps as the airport's condition

when the airport doesn't have any protection standard. New or developed protection system needs to be analyzed whether the system decreases the failure rate to acceptable amount. If the failure rate hasn't reach the acceptable amount, then the airport needs make new protection system or develop existing protection to decrease the failure rate.

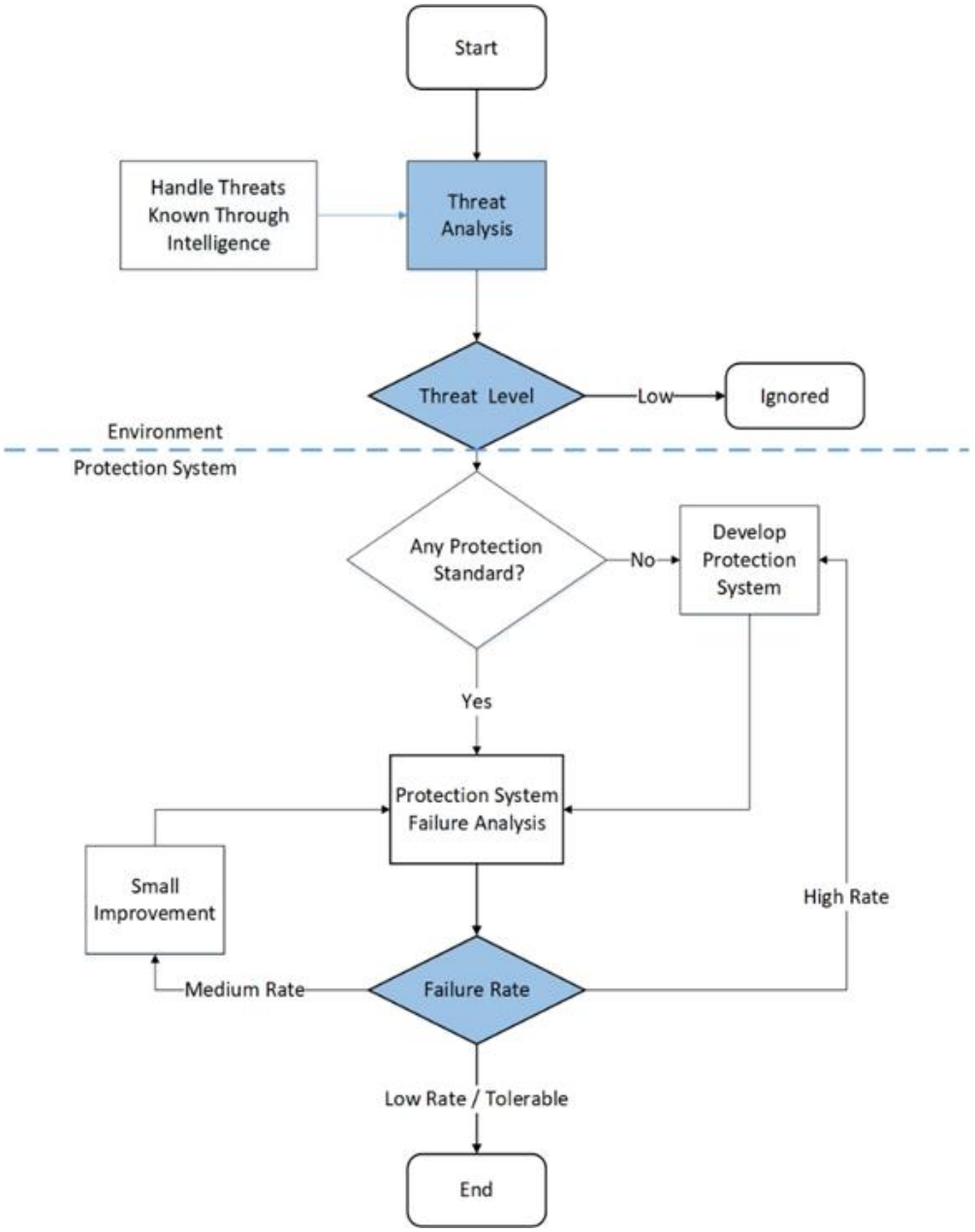

Figure 4. Airport Risk Assessment Approach Flow Process

3.2 Threat Category on Airport Security

If we break down the list of scenarios that might happen and cause threats to Airport Security, there will be many. The question is, is it necessary to make protection to every threats ahead? To answer that question in ideal condition is yes. But, that will need much works, times, and of course money. So, there will be needed to categorize which threats' scenario that need security protection.

The threat could be categorized by it likelihoods and consequences the threat will happen in the airport. There are needs to select the scenario that might happen that will make acts of unlawful interferences[2]. The scenarios selected are the threats that needed the protection system. If the threats have high likelihood or high consequences, so the threat categorized as threats that will make acts of unlawful interference, so that needed protection system. If the threats has low consequences and low likelihood, there will be no need to make protection standard.

Table 1. Threat Category on Airport Security Matrix

	Low Likelihood (LL)	High Likelihood (HL)
Low Consequences (LC)	(a)	(b)
High Consequences (HC)	(c)	(d)

Explanation:

(a): Low Consequences and Low Likelihood, so it safe

(b): Low Consequences and High Likelihood, because there are High Likelihood in this condition so it would be proceeded to the next procedure

(c): High Consequences and Low Likelihood, because there are High Consequent in this condition so it would be proceeded to the next procedure

(d): High Consequences and High Likelihood, because both are in high condition so it would be proceeded to the next procedure

3.3 Tolerable Risk Level

Tolerable risk level is the value that could be passed as good protection standard for airport security, so there'll be no need to make improvement on protection standard exist. In aviation safety, there are safety risk level that categorize the probability of failure happened in aviation as seen in Figure 5. This safety risk levels will be used as reference on deciding tolerable risk level on airport security. Variable used on deciding the level risk is the failure rate of the protection system. There are three levels of tolerable risks level:

- Low failure rate, where system's failure rate less than 10^{-5}
- Medium failure rate, where system's failure rate between 10^{-3} and 10^{-5}
- High failure rate, where system's failure rate bigger than 10^{-3}

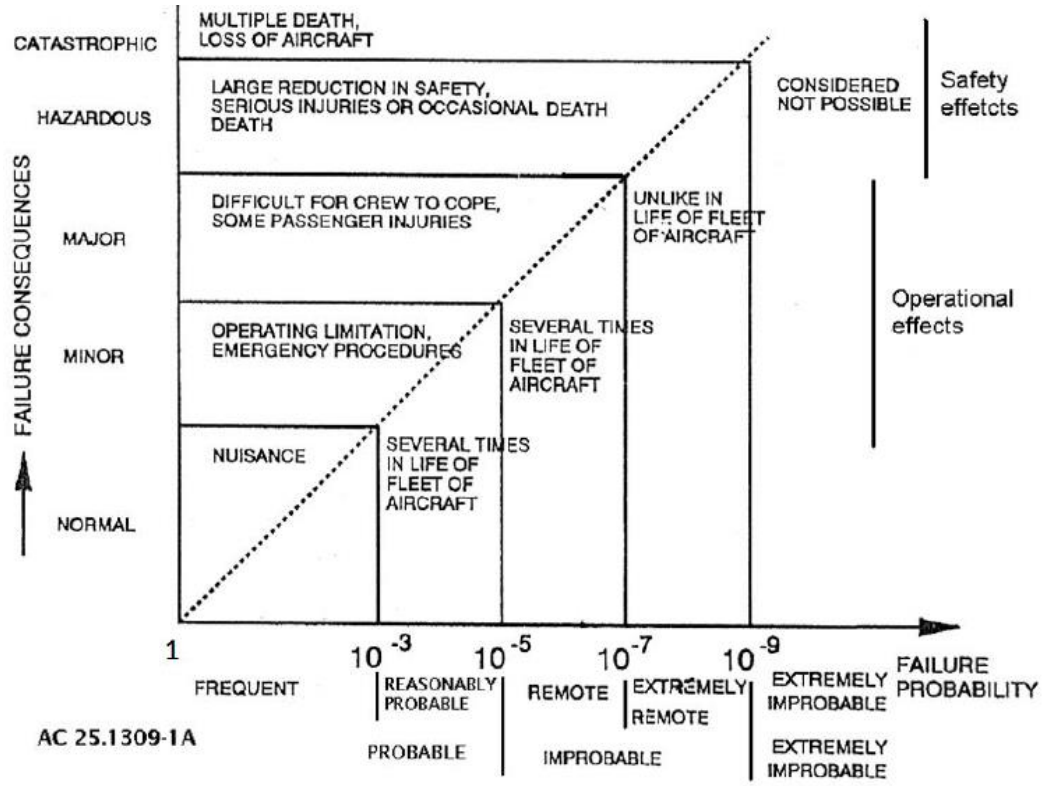

Figure 5. Aviation Safety Risks Level

The system's failure rate could be obtained by using Fault Tree Analysis Methods. This method will give value of system's failure rate. After the value obtained, the acts further that will be applied on the system can be decide. If the failure rate is low, so there no need acts applied on the protection system. If the failure rate is medium, so there will be need some improvement on protection system, whether its software, hardware, or liveware. And if the failure rate is high, there will be need to the airport to develop its protection system.

IV. Result

The airport risk assessment approach resulting from this research is the process that starting from threats analysis by using the likelihood and consequences of the scenario that could make a threat to airport security. If the result has a high likelihood or high consequences, so the next step of the process is analyze the airport's protection system. But if the result is the scenario will have a low likelihood chances and low consequences, so the scenario could be ignored.

If the airport has no protection standard, so there will be needed to develop protection system on the airport. But if the airport already has protection standard, the next thing to do is analyze the protection system failure rate. The tools will be used on this analysis is fault tree analysis methods. The result of fault tree analysis will be standard to decide on its failure rate level. Is it high rate level, medium rate level, or low rate level? The good protection system is the system with low failure rate. So, if the system's failure rate is medium there will be need small improvement of protection system. If the failure rate is high, so there will be need to redevelop protection system.

This research completed the late research [2,3] on having a process to select threats exist that need protection system or not using threat category on airport security matrix. Besides that, this research also give a method recommendation on failure rate analysis of the protection system, which is Fault Tree Analysis. The risk level also given by the reference of aviation safety risk level.

References

[1] Statistical Handbook of Indonesia. Biro Pusat Statistik, 2016.
[2] Tamasi G., Demichela M. Risk Assessment Techniques for Civil Aviation Security. 2011.
[3] Nurhakim, M.L.I.N., Sadono, M., and Chandra, D. Study of Indonesian Airports Risk Level Categories*. 5th Regional Conference on Mechanical and Aerospace Technology, Bangkok, February 2013*.
[4] Airport Cooperative Research Program. *Federal Aviation Administration, 2015*.
[5] Program Keamanan Penerbangan Nasional (National Aviation Security Program). *PM 31 Tahun 2013, Indonesia, 2013*.
[6] Aviation Security Manual. *ICAO Doc 8973/8*

The Effect Catalyst Natural Zeolite of Lampung on The Synthesis of α-Terpineol from Turpentine (#699)

Herti Utami[1,a], Simparmin Br. Ginting[1,b], Dwi Derti Sulistiowati [1,c], Ria Putri Hermiyati[1,d]
[1]Chemical Engineering Departement, Universitas Lampung, 35145 Lampung, Indonesia
[a]hertie19@ hotmail.com , [b]simparmin@ ymail.com
[c]dwiderty7@ gmail.com, [d]riaputrihermia@ gmail.com,

Abstract. *The major component of turpentine is α-pinene. Alpha pinene can be hydrated using an acid catalyst to produce α-terpineol. It can be used as a perfume, anti-insect, and disinfectants. The using of heterogeneous catalysts as natural zeolite can be a new alternative to replace homogeneous catalysts. The purpose of this study was to determine the effect of zeolite catalysts and the reaction time which resulting the highest conversion on hydration reactions of turpentine to α-terpineol. Parameters were the effect of catalyst concentration of (5%, 10% and 15%) and the reaction waktu (60 minutes, 120 minutes and 180 minutes). The turpentine, aquadest and isopropyl alcohol were reacted in the three neck flask at the temperature of 70°C. The result of this study showed that the best condition the hydration of turpentine α-terpineol was achieced at 15% catalyst concentration and the reaction time of 180 minutes. The convertion was obtained to be 4,875%.*

Keywords*: Turpentine, Hydration, Alpha terpineol, Catalys, Natural Zeolite.*

I. Introduction

Turpentine from Indonesia contains 65-85% α-pinene, 1% camphene, 1-3% β-pinene, 10-18% 3-carene and 1-3% limonene. The major component turpentine is α-pinene. Alpha pinene can be hydrated using an acid catalyst to α-terpineol. Alpha terpineol can be used as perfume, anti-insect, anti-fungal, and disinfectant. The reaction between α-pinene and water to be α-terpineol is as follows

$$C_{10}H_{16} + H_2O \longrightarrow C_{10}H_{18}O$$

The synthesis α-terpineol from α-pinene with the catalyst has been studied by several researchers. Arias et al. (2000) studied the hydration of turpentine to α-terpineol using a dealumination faujasite as catalyst. The product of α-terpineol with the highest selectivity was 44% at 70% conversion. Nuritasari (2013) has conducted α-pinene hydration to α-terpineol production by using natural zeolite catalysts. The TCA-ZA catalyst which has been used was washed with aquadest and reused with 15.36% reaction result. Amilia et al (2013) has done the research the effect of temperature on the hydration reaction of α-pinene to α-terpineol with natural zeolite catalyst and the best result was obtained at the temperature of 70°C and the conversion was 68,53%.

The catalysts used in the α-pinene hydration reaction during this homogeneous catalyst were chloroacetic acid, oxalic acid and trichloroacetic acid (TCA). Utami (2010) studied the hydration of α-terpineol from turpentine using chloroacetic acid as catalyst. The best α-terpineol conversion was 54.13% at the temperature of 80°C and the reaction time was 240 minutes. Daryono (2015) who has done α-pinene synthesis to α-terpineol by using sulfuric acid catalyst obtained the highest α-terpineol conversion of 57,05 % and the yield of 67,79 % at temperature

of 70°C. In fact, the use of the homogeneous catalyst is corrosive and this is not environmental friendly, so it is necessary to use a more environmental friendly catalyst.

One alternative catalyst that can be used is a heterogeneous catalyst such as natural zeolite. That is more economical, easy to obtain, and environmental friendly. This research was conducted for the synthesis of α-terpineol from turpentine oil by using heterogeneous solid catalyst, natural zeolite, especially natural zeolite of Lampung.

II. Materials and Methods

A. Chemical

Turpentine obtained from Perhutani Semarang. Isopropyl, dichloromethane, HCl, Na_2CO_3, and Na_2SO_4

B. Catalyst

The catalyst used was natural zeolite of Lampung which has been activated. The natural zeolite of Lampung obtained by CV. Minatama.

C. Procedure

Procedure of this research includes the initial treatment of natural zeolite. That was activated with physical and chemical treatment. In the preparation step, the natural zeolite of Lampung was sieved with a size of 100 mesh, then washed with aquadest that aim to dissolve the dirt on the zeolite surface. Then the zeolite was dried in an oven with the temperature of 200°C for 2 hours. After the zeolite preparation completed, the natural zeolite of Lampung as many of 300 grams was soaked with HCl 4 M solution of 1 L. Then the natural zeolite of Lampung after dissolved with HCl was washed with aquadest to remove Cl- ions until the pH becomes neutral. After that the zeolite was dried in an oven with the temperature of 110°C for 3 hours. Then natural zeolite of Lampung calcined in a furnace with the temperature of 400°C for 3 hours. Zeolite can already be used as a catalyst. The natural zeolite of Lampung before activation, after activation and after reaction was analyzed with Branaeur Emmet Telle (BET), Fourier Transform Infrared (FTIR) and X-ray Flourenscence (XRF) to know the content of Si/Al, surface area and the acid sites at Lampung natural zeolite.

The hydration reaction was carried out in a three-neck flask that filled 20 mL of turpentine, 109 mL of aquadest, and 80 mL of isopropyl alcohol. The three-neck flask was equipped with a thermometer and a magnetic stirrer. The mixture was warmed up to the temperature of 70°C. After the temperature was reached, the natural zeolite of Lampung was loaded into the flask. The mixture was stirred and the reaction time was started to be calculated. A sample was taken at every reaction time of 60 minutes, 120 minutes and 180 minutes at each concentration of natural zeolite of Lampung 5%, 10% and 15%. The product of the turpentine hydration reaction was introduced into the centrifuge for 15 minutes at a rotation speed of 350 rpm. The sample of centrifuge results was filtered and the natural zeolite of Lampung was not included in the product. The neutral step, the product was poured into a separating funnel to separate the top layer (product) and the bottom layer (reactants). The product has been separated, then washed with aquadest in a separation funnel. The washed product was added 10% Na_2CO_3

solution until the pH becomes neutral. Furthermore, the product was added 1 drop of dichloromethane solution in separating funnel. The latter process was added anhydrous Na_2SO_4 to bind the residual water and the product was filtered to separate the precipitate. The results of hydration α-terpineol synthesis were analyzed by Gas Chromatografy (GC) and the best result was analyzed by Gas Chromatografy Mass Spectrometry (GC-MS).

III. Analysis of Results

Zeolite may be used as a catalyst or as a catalyst support if it has a high Si/Al content, contains acid (H^+) and absence of impurities in the pores of the zeolite that the surface area of the pore was large. To know the content of Si/Al, the surface area and the acid sites in natural zeolite of Lampung can be analyzed with Branaeur Emmet Telle (BET), Fourier Transform Infrared (FTIR) and X-ray Flourenscence (XRF). The natural zeolite of Lampung has been activated by chemical and physical treatment then It was analyzed by using BET. The surface area was 35,2564 m^2/g.

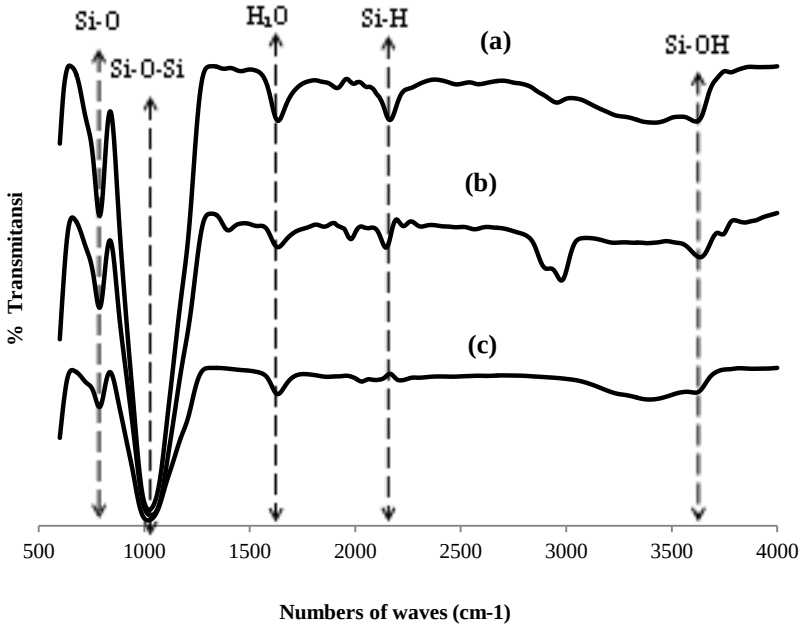

Figure 1. The results analysis FT-IR ZAL 2.

In the Figure 1. shows the characterization results of the natural zeolite of Lampung before activation (a) and after activation (b) and after being used as a catalyst in the turpentine hydration reaction to α-terpineol (c). The wavelength indicates several peaks indicating the presence of some functional groups in the natural zeolite. Based on Figure 1. we can see the absorption of waves in zeolite (a) 787,78 cm^{-1}, (b) 788,08 cm^{-1} and (c) 788,79 cm^{-1} which it shows the interpretation of bond absorption on the main structural unit of zeolite in the form Si-O. And then comes the absorption band of Si-O-Si vibration that is (a) 1018 cm^{-1}, (b) 1031 cm^{-1} and (c) 1023 cm^{-1}. In Fig. 1. the wave numbers (a) 3615 cm^{-1}, (b) 3635.68 cm^{-1} and (c) 3618 cm^{-1} show the vibration of the Si-OH group (hydroxyl group). Furthermore the absorption bands at wave numbers (a) 1632,93cm^{-1}, (b) 1634,01cm^{-1} and (c) 1644,00 cm^{-1} indicate the presence of H-O-H groups. Then the formation occurs in zeolites (b) and (c) 2146 cm-1, where absorption at 2100-2400 cm-1 shows the uptake of Si-H (Socrates, 1994). The Si-H absorption band appears due to the activation of the zeolite with the addition of acid and Si appears to bind H.

The natural zeolite of Lampung was characterized by using XRF to analyze the elements in the mineral or rock presented in Table 1.

Table 1. The result XRF natural zeolite of Lampung

Component	Concentration (%)	
	before activation	After activation
Al	13,636	13,033
Si	75,598	79,746

Based on the results of XRF analysis shown in Table 1, it can be seen that there was an increase of Si content in zeolite after activation, where before the activation of Si content in natural zeolite of Lampung was 75,598% and after activation at zeolite become 79,746%. In addition to the increase in Si content, in zeolites also decreases Al levels in zeolites from 13.636% before activation to 13.033% after activation. This indicates that the activation process at natural zeolite of Lampung using HCl with 4M concentration was successful. Activation of zeolite with HCl addition aims for dealumination (release of Al from zeolite), and the dealumination can increase the Si/Al ratio in zeolite. This is evidenced from the results of XRF in Table 1, where the ratio of Si/Al in natural zeolite after activation is higher than natural zeolite that has not been activated. In the unactivated natural zeolite has a Si/Al value of 5.544, while the Si/Al value in the activated zeolite is 6.11. The higher the Si/Al value, the higher the acidity or the more acid sites in the zeolite. The increase of acid sites it will increase the activity of zeolite (Nuryono et al, 2002). According to Triantafillidis (2000) the more Al content in zeolites (Si/ Al ratio decreases) will cause the strength or total of zeolite acid sites to decrease.

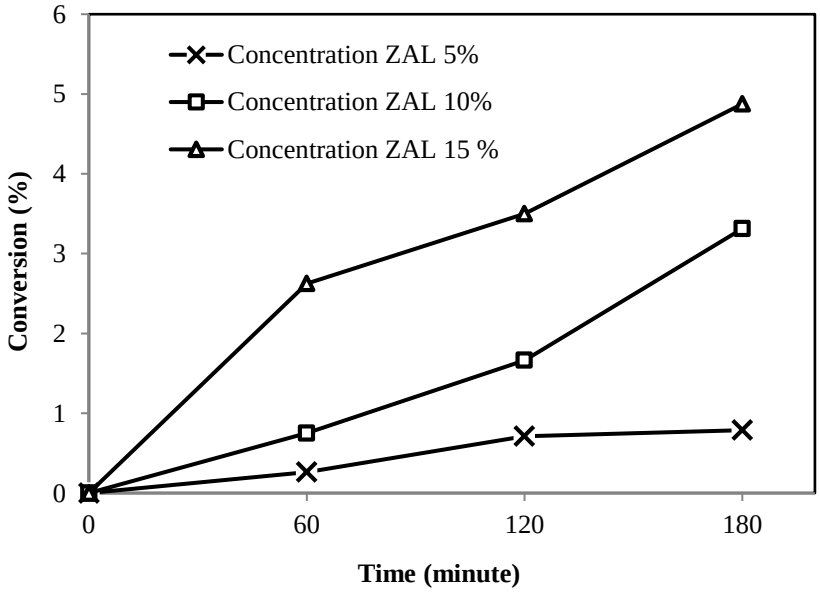

Figure 2. Effect of concentration of catalys on conversion α-pinene to α-terpineol

In Figure 2 it can be seen that at a zeolite concentration of 5% there was an insignificant increase of α-terpineol conversion from 60 min to 180 min, obtained by conversion of α-pinene to the highest α-terpineol 0.7875% at reaction time of 180 min. At the 10% zeolite concentration increased conversion from 60 minutes to 180 minutes, where the highest conversion obtained at 180 minutes and the conversion was 3.3125%. While at the concentration of 15% there was also a significant conversion increase from 60 minutes to 180 minutes with the highest conversion obtained at 180 minutes and the conversion was 4.875%.

Based on the results of conversion, the concentration of catalyst natural zeolite of Lampung influences the conversion α-pinene to α-terpineol. As the number of catalysts or concentrations of zeolite catalysts used for turpentine hydration, the higher α-terpineol conversion was obtained. The large number of catalysts affects the surface area of the catalyst during reaction. The more catalysts used, the more active sites will be utilized during the turpentine hydration reaction. The more active sites on the zeolite then the resulting product will increase. Although in this study there is an increase in conversions, the minor conversion was obtained. This is because the natural zeolite catalyst used has a Si/Al value that is not too different from before activation so that the catalyst performance is less than optimal.

To get the optimum reaction time, then experiment again with addition of reaction time is 240 minutes at 15% catalyst concentration, as follows :

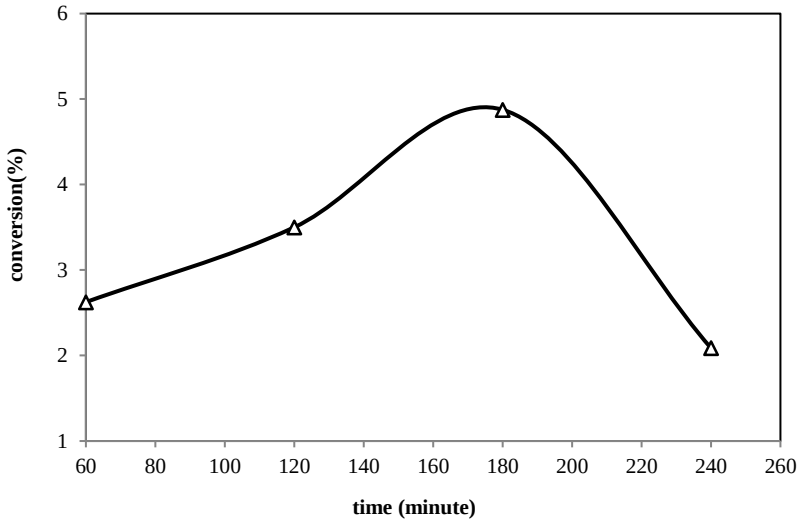

Figure 3. Effect of the reaction time on conversion α-pinene to α-terpineol

Based on the Figure 3 can be seen there is the possibility of the conversion of α-terpineol at 240 minutes reaction time. Where in 60 minutes up to 180 minutes there was an increase of 4.872%, but at 240 minutes the α-terpineol conversion decreased to 2.08%. Thus, it can be concluded at zeolite concentration of 15% the optimal reaction time occurred at 180 min.

Analysis with mass spectrum (MS) is aimed to know the compound of hydration of α-pinene for α-terpineol production. The GC-MS spectrum results are presented in Figure 4.

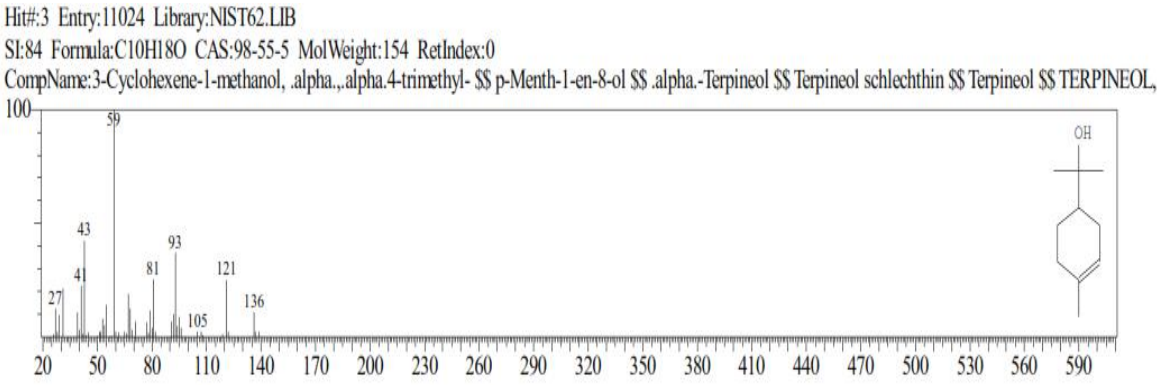

Figure 4. The result analysis of GC-MS

Based on the mass spectrum from peak 28 proves that the compound formed is α-terpineol with a molecular weight of 154 and the molecular formula $C_{10}H_{18}O$.

IV. Conclusion

Based on the result of the research, it can be concluded that the natural zeolite of Lampung that has been activated has Si/Al value of 6.11 and the surface area of 35.2564 m^2/g. The synthesis of α-terpineol from turpentine using natural zeolite catalysts, it suggested that the best result was achieved at the catalyst concentration of 15% and the optimum reaction time of 180 min. The conversion of α-pinene to α-terpineol was obtained to be 4.875%.

References

[1] Amilia, N., Siadi, Kusoro, dan Latifah.2013. *Pengaruh Temperatur pada Reaksi Hidrasi* a-*pinena menjadi* α-*terpineol terkatalis Zeolit Alam Teraktivasi.* Skripsi Jurusan Kimia Fakultas Matematika dan Ilmu Pengetahuan Alam Universitas Negeri Semarang.

[2] Arias D, Guillen Y, Carmen M, Lopez & Francisco JM. 2000.*Turpentine oil hydration using dealuminated faujasite as catalysts*. *React Kinet Catal*.

[3] Daryono, Elvianto Dwi.2015. *Sintesis α-pinene menjadi α-terpineol dengan menggunkan katalis asam sulfat dengan variasi suhu reaksi dan volume etanao*. Jurnal Teknik Kimia USU. Vol.4 No.2

[4] Utami, Herti dkk. 2010. Synthesis of α-Terpineol from Turpentine by Hydration in a Batch Reactor.

[5] Nuritasari, Afriani Laela. 2013. *Pengaruh Katalis Zeolit Alam Teraktivasi dan TCA-Zeolit Alam Dalam Reaksi Hidrasi* α-*Pinena Menjadi* α-*Terpineol*. Skripsi,Jurusan Kimia Fakultas Matematika dan Ilmu Pengetahuan Alam Universitas Negeri Semarang.

[6] Nuryono, Suyanta, dan Narsito, 2002, *Jurnal MIPA*, 25, 40-49. Jurusan Kimia UGM

[7] Socrates, G. 1994. *Infrared Spectroscopy*. Chicester: John Willey & Sons Ltd.

[8] Triantafillidis, C., Vlessidis, A., and Evmiridis, N. 2000. *Dealuminated H-Y Zeolite: Influence of The Degree and The Type of Dealumination Method on Structural and Acidic Characteristics of H-Y Zeolite*. Ind. Eng. Chem Vol. 39, No. 2, 307-3019.

Development of Numerical Platform for Aircraft Systems Simulation (#716)

Rianto A.Sasongko [1,a], Yorgi A. Ndaomanu [1], Yazdi I. Jenie [1], M. Luthfi I. Nurhakin [1], M. Rafi Hadytama [1], Yusuf K. Asalani [1]

[1] Faculty of Mechanical and Aerospace Engineering, Institut Teknologi Bandung
Jl. Ganesha 10, Bandung 40132, Indonesia
[a] asasongko@ae.itb.ac.id

Abstract. *This paper discusses the development of a numerical simulation platform that can be used for representing the principal works of aircraft systems. The platform consistes of some parts each of which is intended to replicate the operation of a system implemented in a modern aircraft, such as hydraulic line, electrical system, landing gear system, control system, etc. The platform is intended to be a tool for modeling and analyzing the operation and performance of certain systems configuration. To some extend the platform can be viewed as a virtual Iron Bird System. Iron Bird is a term representing a platform for simulating the works of aircraft systems using real components, which is very important for aircraft system development. At this stage, the numerical platform will only involve some sub-systems, namely main hydraulic line, control surface actuation, landing gear, and control system. These sub-systems are chosen to be the basis for further development where other sub-systems will be added and integrated to the platform.*

Keywords: *Aircraft System, Numerical Simulation, System Analysis*

I. Introduction

Modern aircraft comprises of many subsystems that form the whole aircraft system supporting the operation of aircraft. As the aircraft technology develops, many new devices and equipments are applied for various reasons, such as those related to aircraft operation, performance, safety, etc. The implementation of these systems introduces complexity in design of aircraft and its systems. To anticipate the complexity and difficulty in aircraft system development phases, many devices are built that can be utilized as design tools, for example an iron bird system. Iron bird is a term referenced to a set of aircraft systems/equipments which are used as simulation platform, where the works and operation of systems on real aircraft can be replicated. Usually, an Iron Bird simulator consists of real system which are implemented on the corresponding aircraft. Hence, using this platform those system can be simulated and tweaked or reconfigured, such that the desired system characteristics and performance can be achieved.

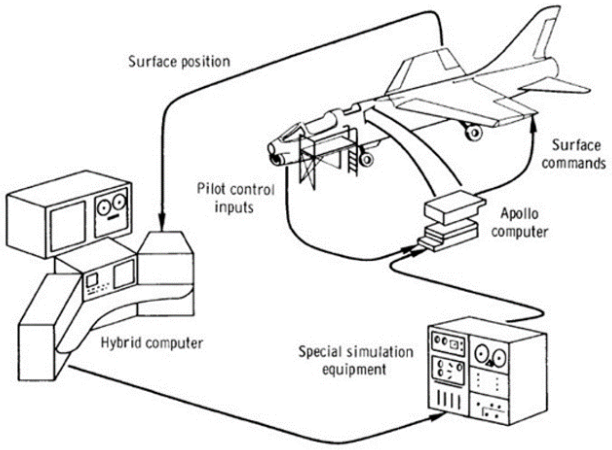

Figure 1. F-8C Iron Bird Simulator

Iron bird simulator has become a key element in aircraft design process, especially in designing the system configuration of the aircraft.

An Iron Bird simulator can be consists of all the system implemented on particular aircraft, namely the control system, hydraulic system, pneumatic system, landing gear, fuel system, etc. Since it uses real components that are applied on the aircraft, an Iron bird simulator is a very expensive equipments.

In this research, a simulator platform is developed based on numerical computation, which can simulates some systems applied on an aircraft. To some extend, this platform is intended to emulate the function of an iron bird system, but in a down-scaled capacity and complexity. This virtual platform is intended as a preliminary tool that can be used for studying, evaluating, and designing aircraft system configuration in earlier stage of aircraft development or studies.

At this stage, a numerical platform is developed which consists of only some simplified subsystems on an aircraft, namely the hydraulic line, control system, control surface actuation, and landing gear systems. Further, it is aimed to develop a more complete and complex virtual system based on this platform. Some results related to the development of this platform will be presented in this paper.

This paper will be presented in the following outline. The second section will discuss the main architecture of the developed platform, while in the second section some subsystem that are included in the platform will be described. The current stage of development of each subsystem will be presented in the third section, followed by some simulation results of the developed subsystem which are discussed in Section Four. Some conclusions and remarks regarding the development and results of the activities will be presented in the fifth section.

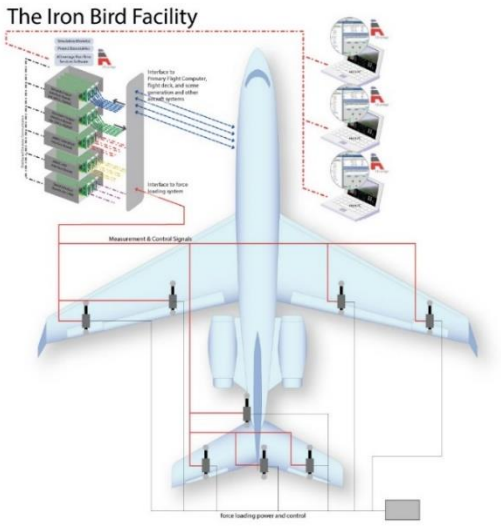

Figure 2. Iron Bird Simulator Example

II. Virtual Subsystems

As explained previously, at this stage it is aimed to first build a basis for more complete and complex virtual simulator, hence only some subsystems are developed, namely the hydraulic line, control system, control actuation, and landing gear subsystems.

A. Hydraulic Line

A virtual aircraft hydraulic line is developed as basis for building more realistic aircraft hydraulic lines and systems in the next stage of this work. The basis configuration is adopted form a generic or simple hydraulic line of a particular aircraft.

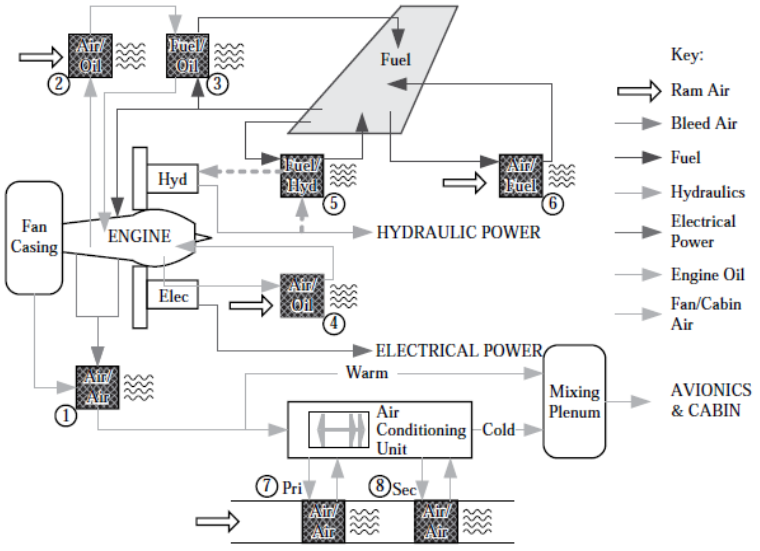

Figure 3. Hydraulic Line model

It is intended to first simulate the principle work/operation of hydraulic lines, which further will be developed to be the main basis of various model of hydraulic based device on an aircraft.

B. Landing Gear System

Landing gear system is the next subsystem to be included on the developed platform. As known, a landing gear system involves multi-domain subsystems, such as hydraulic actuator, electrical system, and mechanical linkage. The modelling of this system includes the formation of mechanical kinematics and dynamics model , and in the next step will also include the hydraulic actuation model, which will be linked to the hydraulic line model.

C. Control Device Actuation

Similar to landing gear system, control device actuation systems, such as aileron, rudder, elevator, flap, consist of multi-domain subsystems, namely the mechanical linkage, hydraulic actuators, and electrical sensors. Hence the modeling of these systems will involve aspects related the work principles and characteristic of hydraulic, mechanical, and electrical systems. Further these system will also be linked to the hydraulic line model.

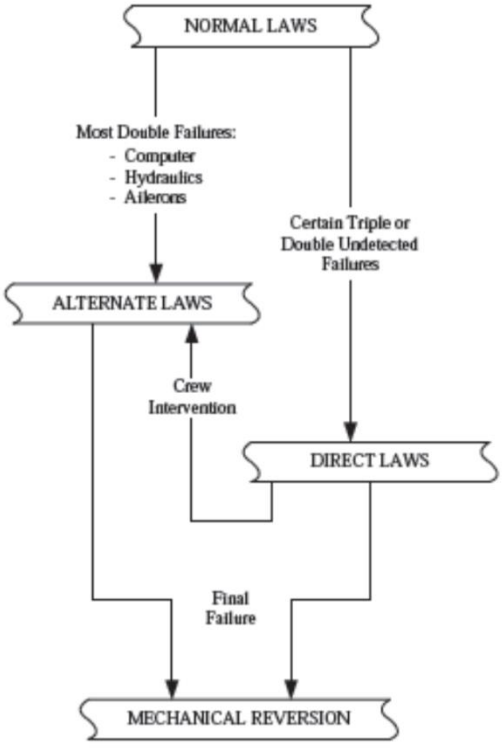

Figure 4. Flight Mode Example

D. Control System

The fourth system that will be included in the developed platform is the control system. Here, it is focused on the modeling of the implementation of flight control using fly by wire platform. The principle of flight control mode, flight control redundancy will be modeled. It is aimed to

be able to simulate the change of flight mode, some redundancy and back-up procedures implemented in fly by wire system under some scenarioed flight condition.

III. Platform Development

At this stage, some systems described previously have been developed, either their virtual representation or their basic operation formulation.

A. Hydraulic Line Model

A simple hydraulic model line is constructed as a basis for further model development. The hydraulic line of ATR 72-600 aircraft is adopted and simplified for developing the model. The model will include some components such as reservoir, hydraulic pumps, and valves. At this stage, the hydraulic system quantitative representations (mathematical models) are not used yet, but rather they are represented as a combination of rules and logics constructing the principle works of the system.

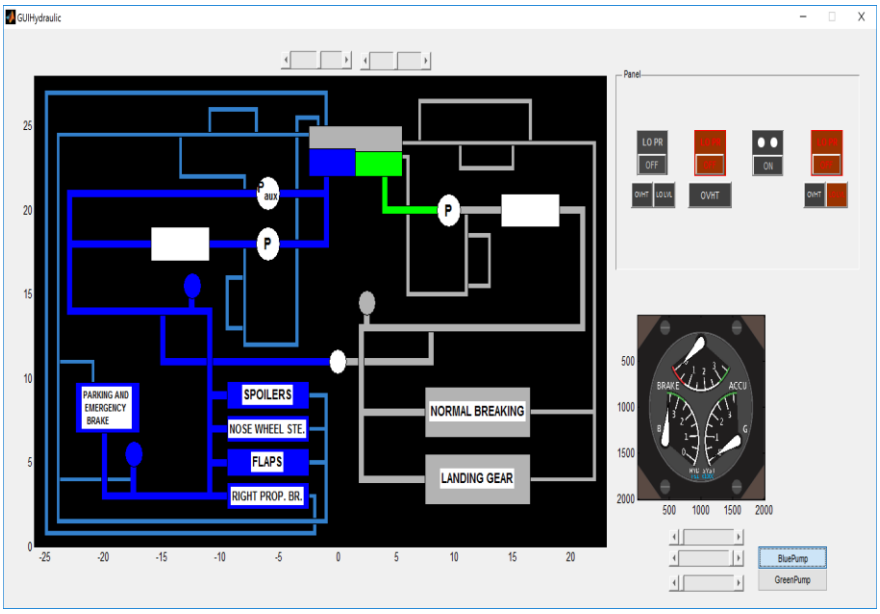

Figure 5. example of developed interface of hydraulic line model

B. Landing gear

The kinematic model of a simple landing gear mechanism is already developed. The model is formed by considering a 3 linkage kinematic formulation, which is then is also modeled using Sim-Mechanics application. The visualization of the mechanism is already developed and linked to the Sim-Mechanics model.

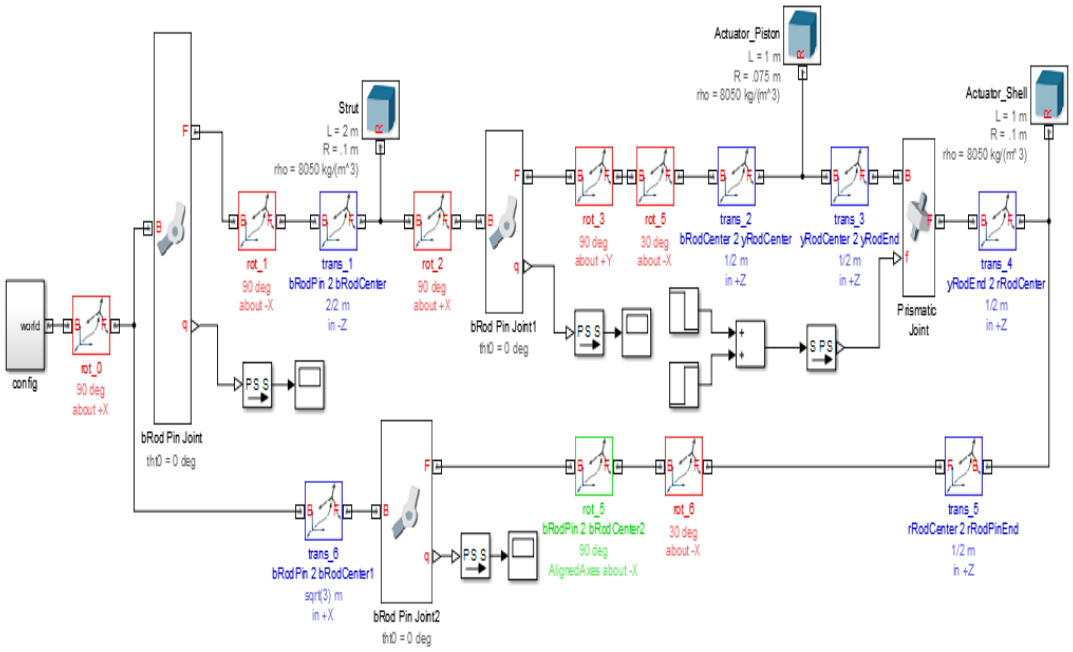

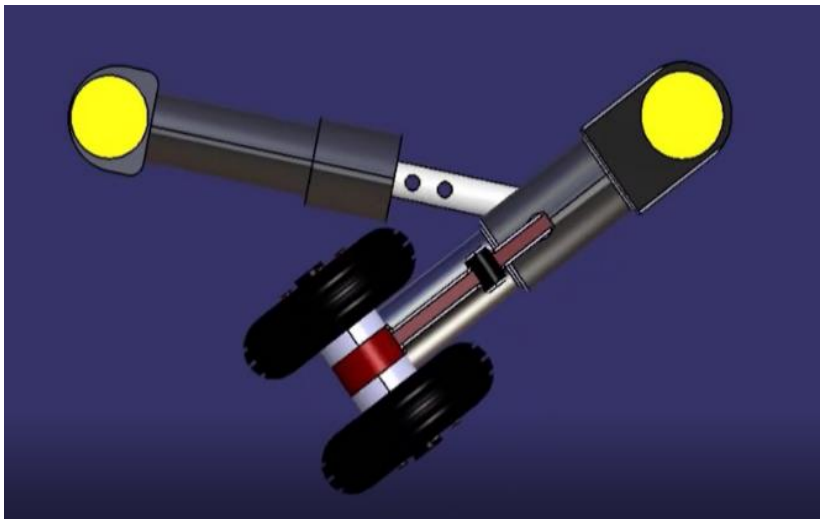

Figure 6. Landing Gear Kinematic model (above) and visualization (below)

C. Control System

A model of a rule/logic implemented in an element of a fly by wire system is already constructed. The model represents the principle of work of a link from control reference input (from pilot manipulators), control signal generator, actuator reference generator, and the actuator. The model can simulate some condition when predefined failures occur on the system, and how the back-up components handle the situations.

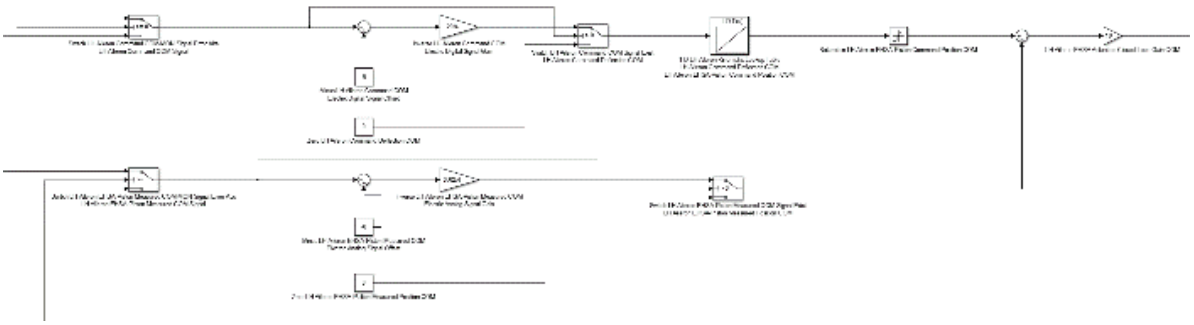

Figure 7. Control System Component Model

IV. Simulation results

Some models of the developed subsystems have been simulated for some predefined scenarios. Some results are presented here. One of the simulations that has been carried out is the one related to the landing gear kinematic model. The mathematical model of the kinematic system is implemented SIMULINK and simulated. The SIMULINK model is depicted in the figure below.

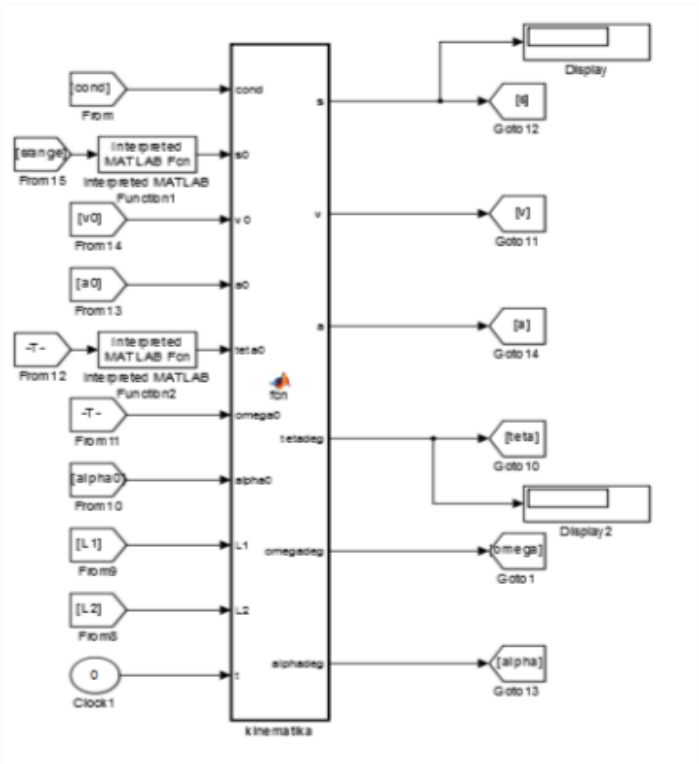

Figure 8. SIMULINK model of the landing gear kinematic

The parameter setting of the simulation is listed in the following table.

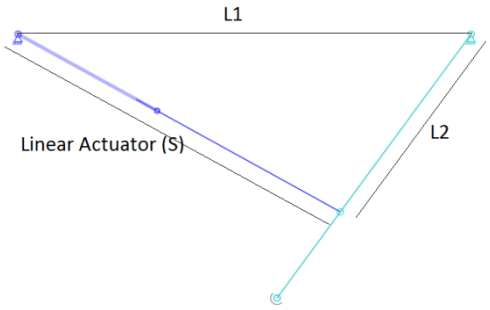

Figure 9. Simulated Linkage Mechanism

Table 1. Simulation Parameters

Parameters	Value	Unit
Kondisi	1 – constant a 2 – constant α*	-
[s_0; s_max]	[1; 5]	m
v_0	0,5	m/s
a	0	m/s^2
[θ_0; θ_max]	[0; 90]	deg
ω_0	2*	deg/s
α	0*	deg/s^2
L1	4	m
L2	3	m

The results of the simulation show the response of the variables of the model representing the motion of the landing gear mechanism. The results are showed in figures below.

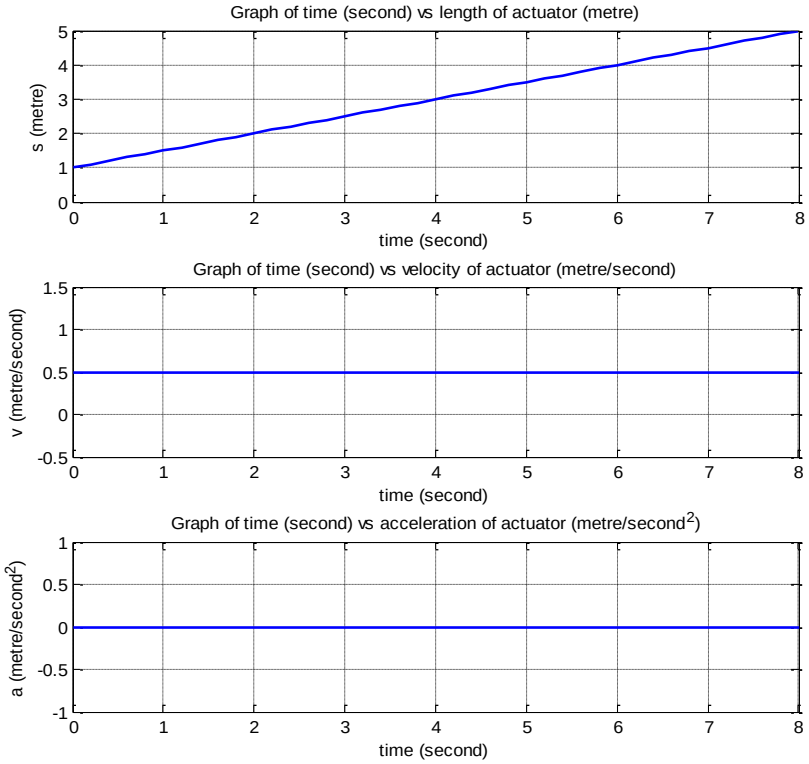

Figure 10. Linkage Translation Variable response

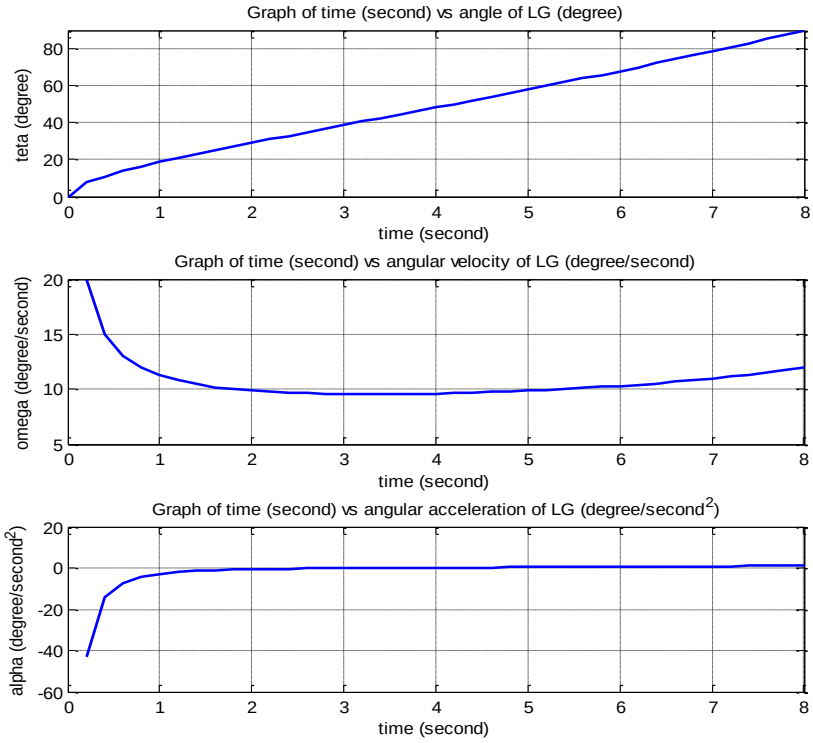

Figure 11. Linkage Angular Variable response

It can be seen that for the modeled mechanism, the quantitative kinematic representation (mathematical model) can produce the response of system variable representing realistic motions of the landing gear. This model will be improved in further development.

V. Conclusions and Remarks

The initial stage development of a numerical platform for simulating some aircraft systems has been carried out. Several models of hydraulic line, landing gear kinematics, and control system rule/logic are already constructed. Simulation of the landing gear model produces quite good results, representing a realistic motion of the landing gear system. Further improvement on the model needs to be carried out, as well as the development of other sub-systems models.

More realistic model, involving more accurate quantitative representation (mathematical model) of each subsystems of the platform may improve the quality and performance of the developed platform.

References

[1] Ian Moir, Allan Seabridge, Aircraft Systems: Mechanical, electrical, and avionics subsystems integration, John Wiley & Sons, England, 2007
[2] R.F. Stengel, Flight Dynamics, Princeton University Press, New Jersey, 2004
[3] M.V. Cook , Flight Dynamics Principles, Elsevier, Oxford, USA, 2007
[4] Peter H. Zipfel , Modeling and Simulation of Aerospace Vehicle Dynamics, AIAA Education Series, Virginia, 2007
[5] http://en.wikipedia.org/wiki/Flight_simulator
[6] David Allerton, Principles of Flight Simulation, John Wiley & Sons, United Kingdom, 2009
[7] http://www.cae.com/
[8] http://www.sim-industries.com/
[9] Harry Saktian Nugraha and Rianto Adhy Sasongko, The Development of a Computer Simulation Platform for Evaluating Mission Performance of a Low-cost UAV, Regional Conference on Mechanical and Aerospace Technology, Bali, February 9 – 10, 2010
[10] R.A. Sasongko, J. Sembiring, and H. Muhammad, Design and Development of Unmanned Aerial Vehicle Mission Simulator for Pre-Implementation Performance Test of the Autonomous Control System, 3rd Regional Conference on Mechanical and Aerospace Technology, Manila, Philippines, March 4-5, 2011
[11] MATLAB/Simulink User Manual, Mathworks Inc.

Design of Inward-Turning External Compression Supersonic Inlet for Supersonic Transport Aircraft (#717)

Muhammad Adnan Hutomo[1,a], Romie Oktovianus Bura [1,b]

[1] Faculty of Mechanical and Aerospace Engineering, Institut Teknologi Bandung (ITB), Ganesha 10, Bandung 40132, Indonesia

[a] adnanhutomo@alumni.itb.ac.id, [b] romiebura@ae.itb.ac.id

Abstract. *Inward-turning external compression intake is one of the hybrid intakes that employs both external and internal compression intakes principle. This intake is commonly developed for hypersonic flight due to its efficiency and utilizing fewer shockwaves that generate heat. Since this intake employ less shockwaves, this design can be applied for low supersonic (Mach 1.4 - 2.5) intakes to reduce noise generated from the shockwaves while maintaining the efficiency. Other than developing the design method, a tool is written in MATLAB language to generate the intake shape automatically based on the desired design requirement. To investigate the intake design tool code and the performance of the generated intake shape, some CFD simulation were performed. The intake design tool code can be validated by comparing the shockwave location and the air properties in every intake's stations. The performance parameters that being observed are the intake efficiency, flow distortion level at the engine face, and the noise level generated by the shockwaves. The design tool written in MATLAB is working as intended. Two dimensional axisymmetric CFD simulations validation has been done and the design meets the minimum requirement. As for the 3D inlet geometry, with a little modification on diffuser and equipping vent to release the buildup pressure, the inlet has been successfully met the military standard on inlet performance (MIL-E-5007D). This design method also has feature to fit every possible throat cross sectional shapes and has been proven to work as designed.*

Keywords*: Inward-turning, Supersonic, Engine Intakes, Low- noise, Design Method.*

I. Introduction

Supersonic intakes have a major role in supplying air to the engine exploiting shockwaves [14]. Air properties such as pressure, Mach number, and temperature must be met the engine needs by adjusting the shockwave position and strength. The efficiency of the intake must be maintained as high as possible and it is measured from the ratio of total pressure between at the engine face and at the undisturbed surrounding air. The most efficient intake configuration theoretically is the spike inlet which applies the conical supersonic flow. However, the spike intakes produce rather strong shockwave which directed to all direction. Thus, the spike intakes generate loud sonic boom and also higher drag in operation. Although the best efficiency spike intakes could offer, this intake configuration is not widely used.

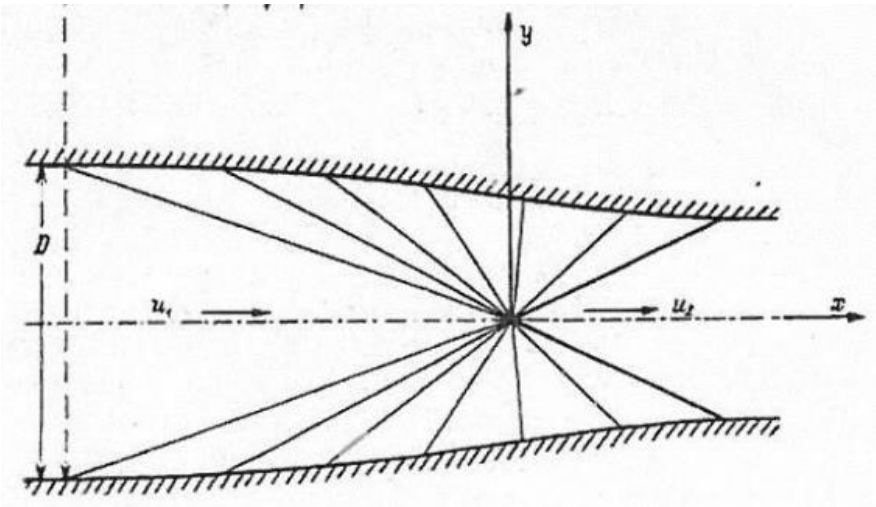

Figure 1. Busemann Intake is the first Inward-turning principle ever proposed [5].

A better intake configuration has to be invented considering lower noise and higher efficiency for commercial supersonic aircraft.

Inward-turning intake then is introduced to weaken the terminal shockwave. This design has several advantages including reducing shockwave drag, noise, and may also eliminate the complex support system for the intake such as adjustable spike position [3]-[6],[11]. One of the well-known inward-turning intake is Busemann intake which theoretically the most efficient supersonic intake. Unlike spike intakes, the capture area of the inward-turning intake is not limited while able to maintain the spike intake's efficiency. However, the inward-turning intakes have limited spillage which can induce problems such as “unstart” [3]. This unstart condition must be avoided because this can cause engine burn out due to low air mass flow entering the inlet.

II. Theoretical basis

In supersonic flows, the air properties changes are very extreme such as shockwaves. In the supersonic regime, the energy equation in Navier-Stokes equation cannot be neglected. The flow is no longer incompressible and the kinetic energy can be dissipated into heat. Thus, a sudden property changes can happen and it's called shockwave. The properties of shockwaves have been long known and their behavior when interacting with solid moving objects has been formulated. There are three main shockwaves, *Normal Shockwave, Oblique Shockwave, and Expansion Fan* [1].

A. Normal Shockwave

When the shockwave appears perpendicular to the flow direction, it is called normal shock. This type of shockwave is irreversible process. Normal shockwave usually occurs when the flow is turned by large deflection in supersonic condition and the shock created cannot remain attached to the wall. The normal shockwave’s behavior can be described as equations below.

$$M_2 = \sqrt{\frac{(\gamma-1){M_1}^2+2}{2\gamma {M_1}^2-(\gamma-1)}} \quad (1)$$

B. Oblique Shockwaves

Oblique shockwaves are similar to the normal shockwave unless they are not perpendicular to the flow direction. They work just like normal shockwaves but the flow is projected to direction that perpendicular to the oblique shockwave. Oblique shockwave occurs when the flow is compressed or contracted. The flow deflection angle can be determined with an equation called $\theta - \beta - M$ relationship. Where θ is the flow deflection angle and β corresponds the shock angle.

$$tan\theta = 2cot\left[\beta\left(\frac{{M_1}^2 sin^2(\beta)-1}{M^2(\gamma+cos(2\beta))}\right)\right] \quad (2)$$

The property equation of oblique shockwave is similar, unless the flow direction must be projected to perpendicular to the shockwave first.

$$M_2 = \sqrt{\frac{(\gamma-1)(M_1 sin\beta)^2+2}{2\gamma(M_1 sin\beta)^2-(\gamma-1)}} \quad (3)$$

C. Expansion Fan

Expansion fan or widely known as Prandtl-Meyer Expansion fan is an expansion process when the supersonic flow turns around the sharp convex corner. This happens because expansion fans consist of infinite number of Mach waves [1]. The weakest point of an oblique shockwave or in other words that the flow speed is close to the speed of sound is called Mach wave. There are three main properties that characterize the expansion fan

1. The downstream Mach number is larger than the upstream or increasing the flow Mach number.
2. The Expansion Fan is actually the anti-thesis of oblique shockwave thus the density, pressure and temperature decrease through expansion fan.
3. Since it has infinitely number of Mach wave, the process is continuous inside the expansion fan between the forward and rearward Mach line. Angle of each mach line can be expressed where $\mu_1 = arcsin(1/M_1)$and $\mu_2 = arcsin(1/M_2)$
4. The flow's streamlines through the expansion fan are smooth curved lines.
5. The expansion fan is an isentropic process because of continous process of Mach wave. Therefore, downstream properties can be calculated using isentropic relation.

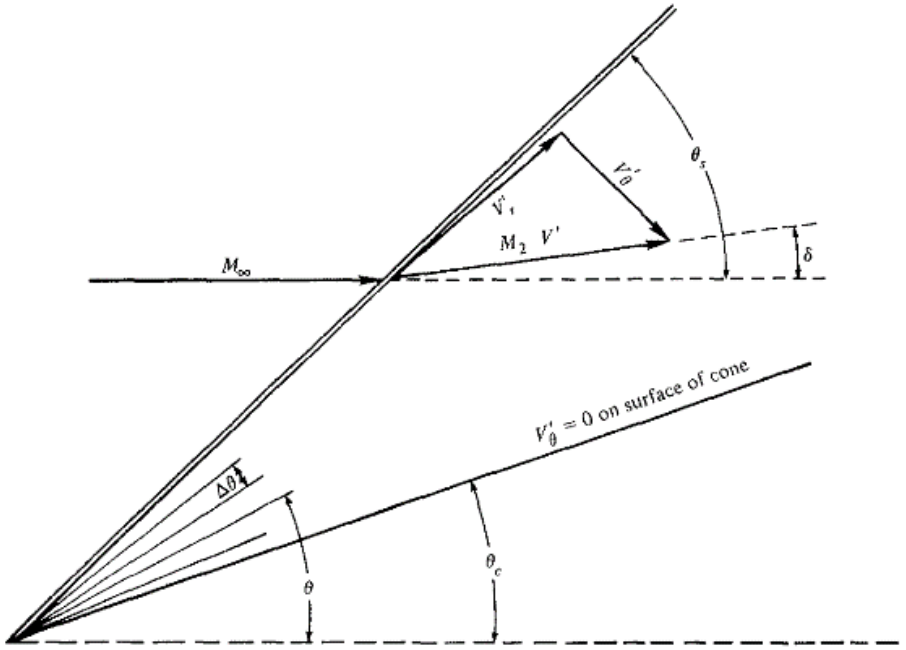

Figure 2. Geometry for the numerical solution of Taylor-Maccoll equation

In practice, downstream Mach number is often needed to find the downstream properties. The Prandtl-Meyer function (often symbolized as υ) is a function to find the downstream Mach number in calorically perfect gas assumptions.

$$\upsilon(M) = \sqrt{\frac{\gamma+1}{\gamma-1}}tan^{-1}\left(\sqrt{\frac{\gamma+1}{\gamma-1}(M^2-1)}\right) - tan^{-1}\sqrt{M^2-1} \quad (4)$$

$$\theta_2 = \upsilon(M_2) - \upsilon(M_1) \quad (5)$$

In three-dimensional space, the supersonic flow is not as restricted as the two-dimensional space. Therefore, Conical supersonic flow has its own calculation which works in three-dimensional space. Since conical shape can be simplified into two dimensional axisymmetric, assumed the calculation is done in spherical coordinates, this calculation only needs to observe two directions namely radial and axial direction.

The supersonic flow over cone bodies or conical flow is expressed by Taylor-Maccoll equation respecting the conservation of momentum and based on Euler equation.

$$\frac{\gamma-1}{2}\left[{V_{max}}^2 - {V_r}^2 - \left(\frac{dV_r}{d\theta}\right)^2\right]\left[2V_r + \frac{dV_r}{d\theta}cot\theta + \frac{d^2V_r}{d\theta^2}\right] - \frac{dV_r}{d\theta}\left[V_r\frac{dV_r}{d\theta} + \frac{dV_r}{d\theta}\left(\frac{d^2V_r}{d\theta^2}\right)\right] = 0 \quad (6)$$

where

$$V_\theta = \frac{dV_r}{d\theta} \tag{7}$$

$$\frac{V}{V_{max}} \equiv V' = \left[\frac{2}{(\gamma-1)M^2} + 1\right]^{-0.5} \tag{8}$$

In designing the inward-turning Busemann intake, the supersonic flow streamline must be determined first. Later, this streamline can be replaced as intake wall. In order to find the

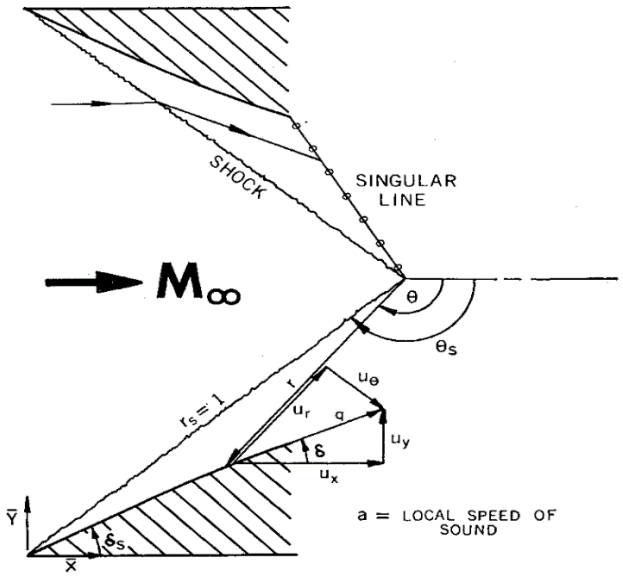

Figure 3. Notation for Internal Conical Flow A (ICFA)[6].

streamline, Busemann parent flowfield equation, Taylor-Maccoll equation discussed in previous subsection, is used. As opposed to the conical flow, the flow inside Busemann intake is turned inward to the center line axis. The calculation process is also reversed where the calculation must be started at the downstream area of the intake [5]. Therefore, it needs boundary condition such as the exit Mach number, the freestream Mach number, and the terminal shockwave angle. Since the calculation process is done in non-dimensional, the design result is resizable and can be fit to the engine specification.

Even though it has the best efficiency compared to other intake design, disadvantages using this kind of intake has been discovered and has been the main problem to solve in the last decade. Busemann intake needs very long structure to achieve its highest efficiency

through isentropic compression. Long intakes can also cause friction loss from the wall and increase structural weight. Busemann intake is also sensitive to the angle of attack which may now work for a slight angle of attack. Moreover, due to very precise geometry, it is not "self-starting" as opposed to the convential ramp intake that can be easily started.Some modification for Busemann intakes have been discovered recently to reduce these disadvantages.

One of many solutions to solve the truncated area problem, at the leading edge, an Internal Conical Flow A (ICFA) principle can be applied. It was first discovered by Sannu Molder as one of four solutions to the Taylor-Maccoll equation. the ICFA principle is similar to the flow over cone body but reversed. the flow is inward turned, satisfying for the Busemann intake needs.

Unlike the Busemann intake, which the flow inside follows the wall, ICFA flow is not directly follow the wall rather slowly turned the direction after oblique shockwave until parallel to the wall and the singularity point is reached which pretty similar to the flow behaviour over cone body [6]. ICFA can be the solution for truncation of Busemann intake. Rather than using truncation angle as the design parameter, first deflection angle (denoted by δ_s) is better. The ICFA then is merged to the truncated Busemann intake at the singularity line.

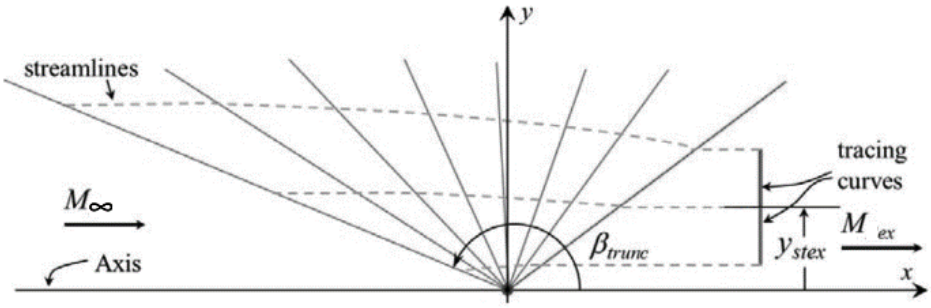

Figure 4. Integration of streamline from the tracing curve.

At the merging point, the flow properties such as Mach number and flow direction must be fit to each other. Expansion fan would appear since the flow direction between ICFA and truncated Busemann intake is different. Thus, this merging point must be calculated in iterative process and can be useful to determine the suitable terminal shock angle.

Calculation until merging procedure is still in quasi one-dimensional view or simply a two-dimensional design. However, this calculation can be converted into three dimensional by replacing the streamline with intake's wall. The three-dimensional streamline can be generated from the axisymmetric parent flowfield calculated before. Thus, a tracing shape is needed to shape the overall intake [3,][4],[16].

By placing the tracing curve inside the parent flowfield, its role is to be the initial seed for generating streamline. By definition, no flow crosses streamline. Therefore, the network streamlines can be replaced by a solid surface defining the intake's wall [9]. The axial projection of the leading edge onto a plane perpendicular to the axis-of-symmetry defines the shape of the capture cross-section of the intake. The area of the capture cross-section is the theoretical capture area of the inlet.

III. Numerical Implementation and tool development

In general, this inlet is divided into two main parts; ICFA section and Inward Turning Busemann section. These two sections are calculated separately while the design iteration process is in sync with each other following the merging procedure. Flowchart shown is the

main calculation process on how this tool designs and generate the supersonic inlet in both 2D and 3D.

A. ICFA Design Calculation

Internal Conical Flow A (ICFA) is a type of supersonic inlet which derived from the Taylor-Maccol equation with constant deflection angle along the wall. Therefore, based on these condition, a singularity could be found in Taylor-Maccoll equation which become the end of ICFA section. Beyond this singularity point, either separation would occur or a shockwave might appear.

The deflection angle or the lip angle is determined first. As the lip angle increase, the oblique shockwave it produces will get stronger and vice versa. Stronger oblique shockwave creates lower Mach number at the downstream side, therefore the required inlet length is decreased. Even though the length is shorter, the total pressure recovery is also decreased. It needs a certain balance of lip deflection angle because it determines the rest of the inlet design.

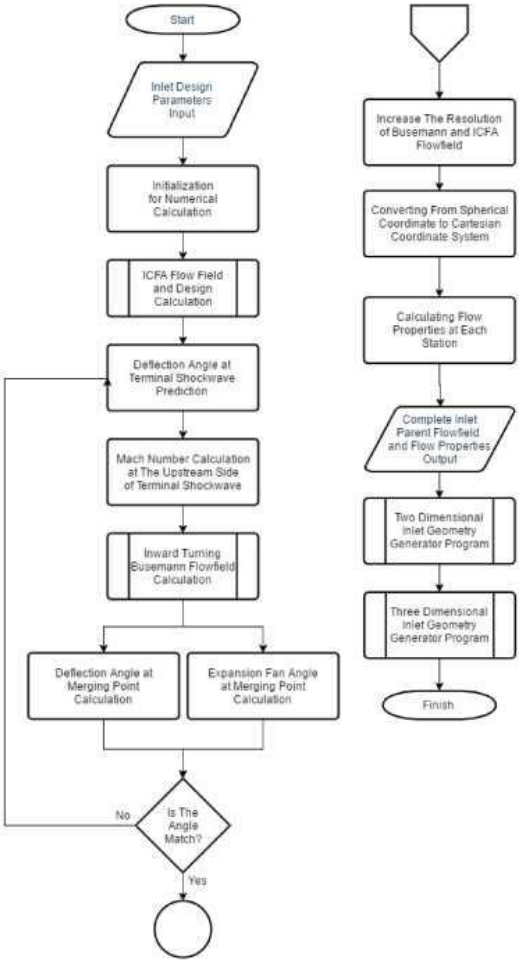

Figure 5. Work flow diagram showing the calculation process in designing theInward Turning Busemann Supersonic Inlet

B. Busemann Inlet Design Calculation

In this inlet section, an isentropic compression process occurs. The flow in this section is turned inward respecting the Taylor-Maccoll equation and at the same time decreasing flow's Mach number [5]. In contrast to ICFA section where the wall is constant at certain angle, the Inward Turning section (or Busemann Inlet section) wall is generated from flow's streamline that respects the Busemann Parent Flowfield generated from the Taylor-Maccoll equation. This flowfield is the important key in producing the Inward Turning Busemann Inlet.

The Busemann Flowfield is calculated from downstream to the upstream the opposite of the ICFA. Therefore, the downstream air properties is needed for the boundary condition for solving the flowfield equation. In Taylor-Maccoll equation, the angle (δ) that represents location in polar coordinates is the driving variable or the flowfield scope. In ICFA flow calculation, singularity is present at certain angle and it becomes the end of ICFA section. This angle then is used as the upper limit of the Busemann Flowfield. While the terminal shock angle, which is predicted first, is used as the lower limit.

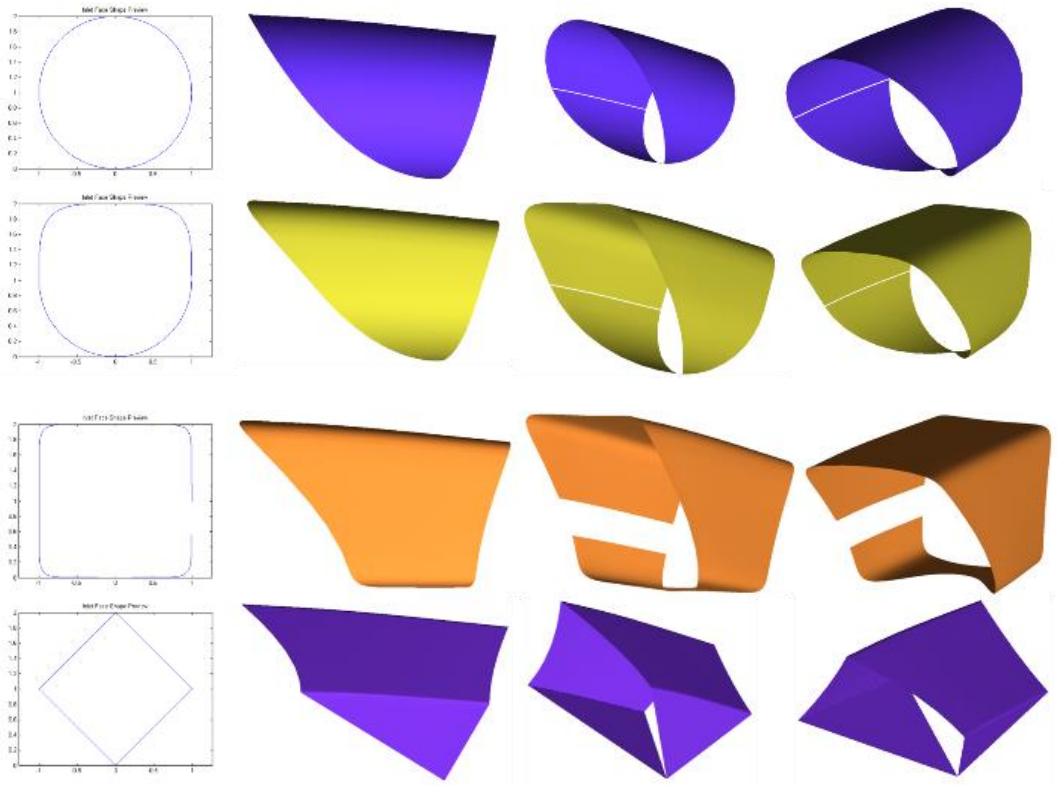

Figure 6. The 3D geometry output from the MATLAB codes. The 0.9 exit Mach number design is used as example. Throat cross-sectional shape from the top: circle, flat-top, square, diamond

C. Merging Procedure

The merging procedure follows after the Busemann section calculation. This procedure ensures the flow is matched between the end of ICFA section and at the beginning of the Busemann section thus it flows continuously without interruption. Since the flow angle between these section is different, a turning point between these sections must be placed by either generate oblique shockwave or expansion fan. However, in this case, the lip deflection

angle is steeper than the flow direction at the leading part of Busemann section thus an expansion fan is expected to occur at the merging point.

Up to this point, two flow angle difference between these two sections can be calculated which the angle difference produced from ICFA and Busemann flowfield calculations and from the expansion fan equation. The flow angle difference from the expansion fan can be acquired from known Mach number at both ICFA section exit and Busemann section entrance. These flow angle difference must be match to satisfy the flowfield criteria and expansion fan phenomena. If they don't match, the calculation must be repeated again with different guessed terminal shock angle knowing that the ICFA section exit condition always constant until both flow direction difference match. Thus, the Busemann section design must be refitted until correct terminal shock angle is found.

IV. Design Tools Output

This design tool produces the 3D geometry which the method is already discussed. The 3D inlet is defined by streamline tracing that follows the Busemann Parent Flowfield and pre-defined tracing curve. Different tracing curves will produce a completely different inlet shape. For demonstration, four different tracing curve such as circle, circle with flat side at the top, diamond shape, and square with rounded corner. Each 3D inlet geometry from those tracing curves will be represented. However, only two tracing curves that will be used for 3D CFD simulation which are the circle shape and the circle with flat side at the top. This demonstration shows how flexible the design tool can be which can be used for better integration with the fuselage or aircraft's wings.

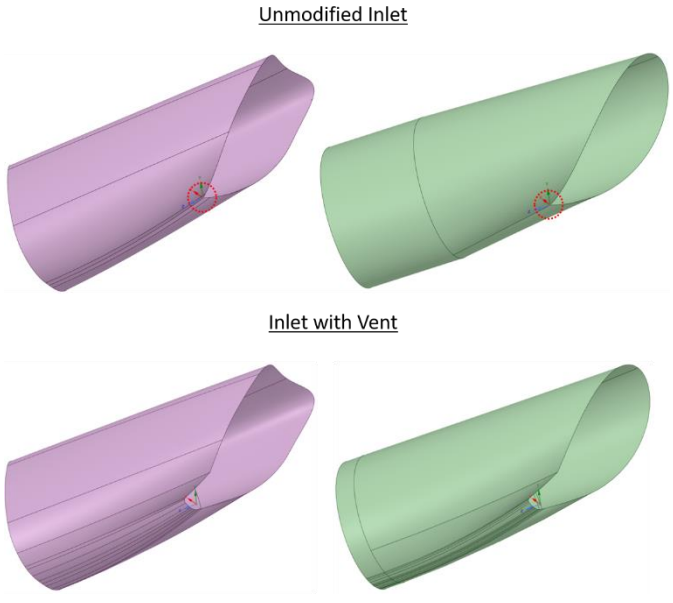

Figure 7. The comparison between the unmodified inlets and inlets after vent is added. Red circles shows where the inlet's focal point is.

Table 1. Atmosphere condition at 14000 m from sea level with 15^0 C temperature offset

Air Properties	Value
Temperature	231.65 K
Pressure	14100 Pa
Density	0.2121 kg/m^3
Speed of Sound	305.113 m/s
Dynamic Viscosity	0.0000151601 Pa.s

Since this inlet is designed without using any bleed system thus making it difficult to start, thus a vent is needed. The purpose of this vent was to allow increased flow spillage during starting and sub-critical operation of the inlet. The main cause this inlet is hard to start is because the flow is focused in a single point which is at the focal point that blocks the flow and therefore spillage is needed to get back to critical operation where the inlet can work at the upmost efficiency. The vent region is modified by specifying a new downstream cowl lip location along with azimuthal angles to define the extent of the modification. The cowl was translated aft by an axial distance equal to 55 mm to the downstream. The upstream half angle was set to 21^0 and was used to specify the circumferential extent of the modification on the original cowl lip.

V. 3D simulation validation

The validation of this design is done using Computational Fluid Dynamic (CFD) approach. Some simulation is done to represent the inlet design performance at different working condition. The inlet simulation is done with freestream velocity at Mach 1.7 and at altitude of 14 km. The air properties in this condition are specified in Table 1. In this research, the mass flow is the variable for the simulation as it represents the inlet working condition. These simulations also ensure that the inlet will fit the minimum requirement of the engine. In this case, the GE F414 turbofan engine is used as reference. The main reason is this engine is going to be used by the future supersonic aircrafts.

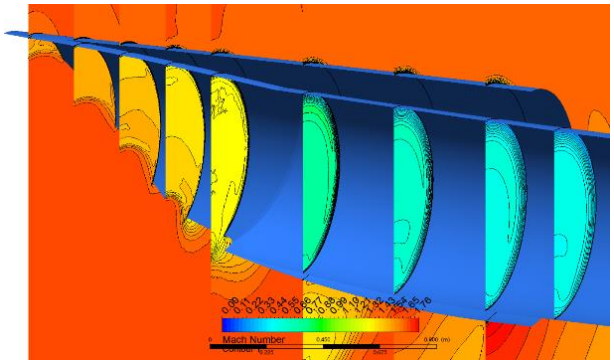

Figure 8. Mach contour in every section inside the modified circle throat inlet case showing the conical shockwave from the leading edge.

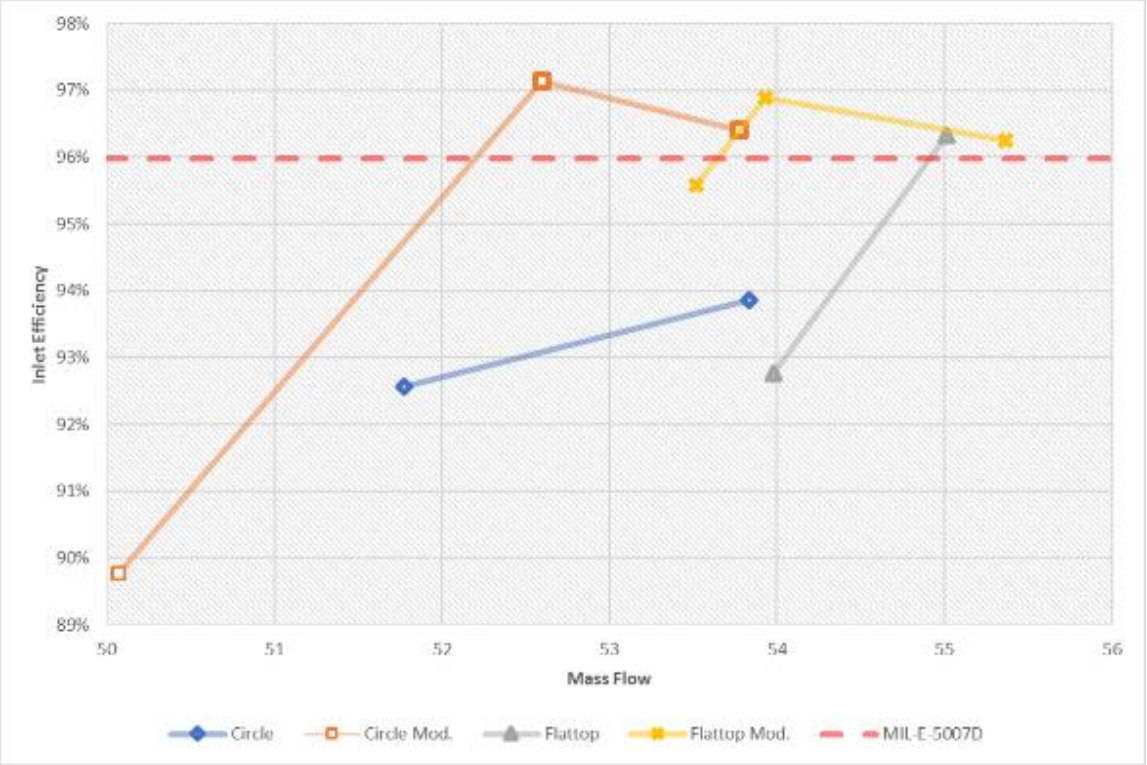

Figure 9. Each inlet performance compared to MIL-E-5007D inlet efficiency standard. The minimum uncorrected mass flow required is 48 kg/s.

By design, there would be two shockwaves in the shape of cone generated by the inlet. The first conical shockwave appears at the inlet's lip or inlet's leading edge that spans up to the inlet's focal point or the venting area. The conical shockwave formed from the leading edge to the focal point. This proves that the 3D inlet design is working as designed and the design methodology is proven and can be applied in 3D inlet. The terminal shockwave in the other hand, it is difficult to see whether it is a conical or planar shockwave since by design, the cone angle is so large and it almost resemble normal shockwave. This would affect the inlet performance, since the isentropic compression is disturbed by the terminal shockwave, stronger terminal shock would appear which reduce the total pressure recovery.

In comparison with the circle shaped throat design, the inlet performance of the flattop design is slightly worse. The only problem arise here is the distortion shape imprints the throat shape. A separation is found in supercritical condition but it is still small compared to the whole engine face area. This also affect inlet's total pressure recovery which at critical condition. The maximum total pressure can be achieved by the inlet is only 96.9% compared to 97.1% for circular design. But these number still meet the MIL-E-5007D standard. Overall, these flattop design work as intended can be used for real world application.

The minimum mass flow required that needs to be supplied to the engine while the engine working at full thrust is 77.1 kg/s. This mass flow is measured at sea level condition. This is the reference of the mass flow required. However, this requirement changes that depend on the atmospheric condition due to the conservation of mass. Therefore, the corrected mass flow is needed. Usually, at higher altitude, engine needs less mass flow to work [14]. Here the minimum mass flow required at the altitude of 14,000 m is 48 kg/s which if mass flow

correction formula is added, the corrected mass flow is exactly 77.1 kg/s. All inlet designs are able to supply enough airflow to F414 engine.

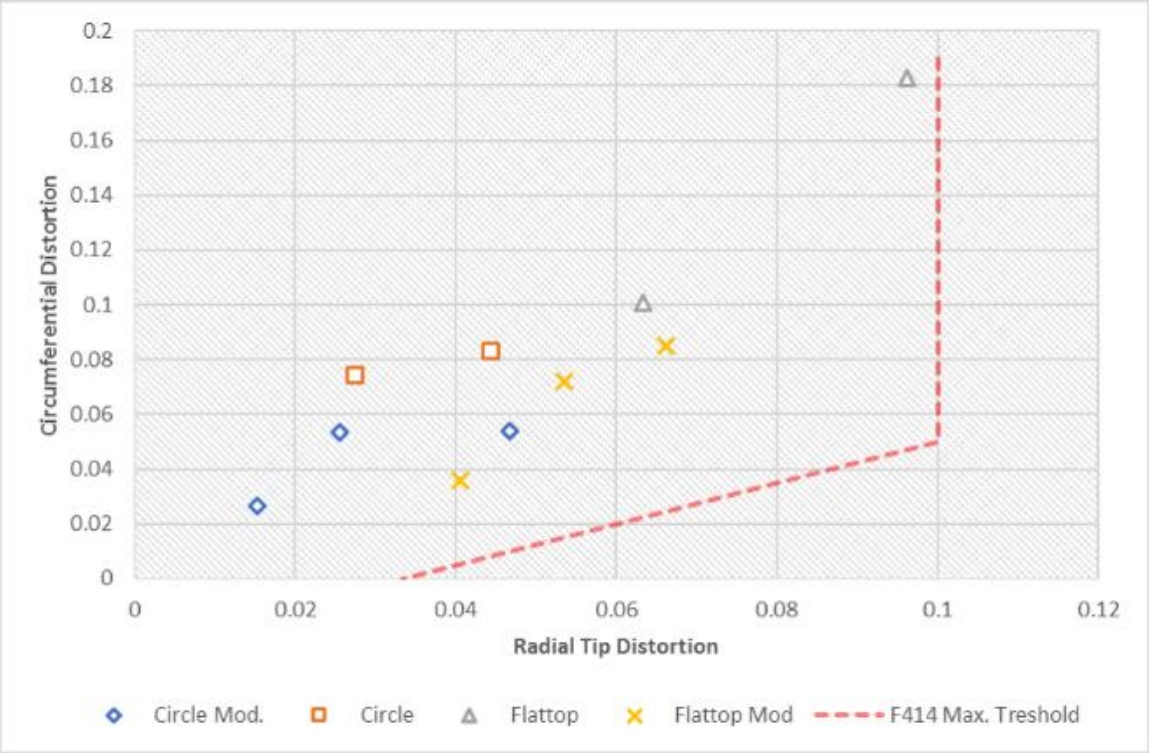

Figure 10. Distortion of each inlet design compared to F414 maximum distortion treshold.

The radial and circumferential distortion intensity are represented as a scatter graph to illustrate the inlet's distortion level compared to maximum distortion level allowable by the F414 engine. All inlets are met the distortion level criteria. The circle throat design has lower distortion level compared to the flattop design. This is due to the absence of shape transition in circular throat design. The unmodified inlets have higher distortion level than the modified one. Then it can be concluded that the vent has a role to reduce the distortion level in inward-turning inlet design.

VI. Conclusion

The inlet design methodology for supersonic inward-turning inlet has successfully been developed. The design method has been written into a code to automatically generate the inlet geometry and its theoretical performance. Then, the inlet generated from this code is simulated to validate the design method and the tools written in MATLAB. Overall, the design tools and the design method are validated and proven that this design tool can produce an inlet geometry that works as intended.

The ICFA flowfield was used to incorporate the inward-turning cowl leading edge for low drag and sonic boom. This was merged with a Busemann conical compression, terminating in a strong oblique wave. This design methodology allows inlet designer to freely shape the inlet since one of this inlet's design parameter is throat shape. Therefore, this design methodology is perfect for inlets which blends with diffuser although this claim might need to be proven. But, theoretically this design method could produce every possible inlet's shape. From the code validation, we also know that the design parameter of Mach 0.9 exit Mach number is consistent with MATLAB code calculation. Thus, Mach 0.9 exit Mach number design is chosen for 3D inlet's reference design.

The inward turning design performs as expected. All inlet design with venting modification can perform better than MIL-E-5007D standards at critical condition which can achieve efficiency as high as 97.2%. This efficiency can be cranked up even further if active boundary layer control system is equipped. However, the unmodified inlets do not perform any better and failed to satisfy the standards. Overall, the inlet with circle throat is better by a small margin than the flat top throat design. Inlet distortion level of all inlet designs are still acceptable for F414 engine use. The circle throat design has lower distortion level than the flattop throat design. It is recommended to use the circle throat design if possible.

References

[1] *Anderson, John D.* Modern Compressible Flow: With Historical Perspective. *Boston: McGraw-Hill, 2003.*

[2] *Ascher, Uri M., and Linda R. Petzold.* Computer Methods for Ordinary Differential Equations and Differential-Algebraic Equations*. Philadelphia: SIAM, 1998.*

[3] Otto, Samuel E., Charles J. Trefny, and John W. Slater. *Inward-Turning Streamline-Traced Inlet Design Method for Low-Boom, Low-Drag Applications.* Cleveland: NASA Glenn Research Center, 2015.

[4] *Slater, John W.* Methodology for the Design of Streamline-Traced External-Compression Supersonic Inlets*. American Institute of Aeronautics and Astronautics, 2014.*

[5] Mlder, S. and Szpiro, E.J. *Busemann Inlet for Hypersonic Speeds.* AIAA Journal of Spacecraft and Rockets, Vol. 3, No.*8*, pp. 1303-1304, August 1966.

[6] Mlder, S. *Internal, Axisymmetric, Conical Flow*. AIAA Journal, Vol. 5, No. 7, Jul. 1967, pp. 1252-1255.

[7] Zhao, Zhi, Wenyang Song. *Effect of Truncation on the Performance of Busemann Inlet*. Canada: CCSE Modern Applied Science Journal, 2009.

[8] O'Brien, Timothy F. and Jesse R. Colville. *Analytical Computation of Leading Edge Truncation Effects on Inviscid Busemann Inlet Performance.* Reno: AIAA Aerospace Sciences Meeting and Exhibit, 2007.

[9] Xiao, Yabin, Lianjie Yue, Peng Gong, and Xinyu Chang. *Investigation on a Truncated Streamline-Traced Hypersonic Busemann Inlet.* Dayton: AIAA International Space Planes and Hypersonic Systems and Technologies Conference, 2008.

[10] Ramasubramanian, Vijay, and Mark Lewis. *Performance of Various Truncation Strategies Employed on Hypersonic Busemann Inlets*. AIAA/DLR/DGLR International Space Planes and Hypersonic Systems and Technologies Conference, 2009.

[11] You, Yancheng, Chengxiang Zhu, Junliang Guo. *Dual Waverider Concept for the Integration of Hypersonic Inward-Turning Inlet and Airframe Forebody.* AIAA/DLR/DGLR International Space Planes and Hypersonic Systems and Technologies Conference, 2009.

[12] Courant, Richard, Friedrichs, K.O. *Supersonic Flow and Shock Waves.* New York: Springer-Verlag, 1976.

[13] *Hutomo, Muhammad Adnan.* Desain Konseptual Mixed-Compression Intake pada Kecepatan High Supersonic*. Institut Teknologi Bandung, 2015.*
[14] Mattingly, Jack D. *Aircraft Engine Design.* Virginia: American Institute of Aeronautics and Astronautics, 2002.
[15] Guide for the Verification and Validation of Computational Fluid Dynamics Simulations. *Renton: American Institute of Aeronautics and Astronautics, 1998.*
[16] Slater, John W. *Design and Analysis Tool for External-Compression Supersonic Inlets*. Cleveland: American Institute of Aeronautics and Astronautics, 2012.
[17] *Bloch, Gregory S.* An Assessment of Inlet Total-Pressure Distortion Requirements for the Compressor Research Facility*. Ohio: Aero Propulsion and Power Directorate, 1992.*
[18] Farmer, Clinton J. *Inlet Distortion, Vorticity, and Stall in an Axial-flow Compressor.* Springfield: Naval Postgraduate School Thesis, 1972.

Development of Optimization Methodology for Short Range Air-to-Air Missile (#718)

Romie Oktovianus Bura[1,a], Yudki Utama[1,b], Muhammad Farraz [1,c]
[1] Flight Physics Research Group, Faculty of Mechanical and Aerospace Engineering, Institut Teknologi Bandung (ITB), Ganesha 10, Bandung 40132, Indonesia
[a]romiebura@ae.itb.ac.id, [b]ignatius.yudki.u@s.itb.ac.id, [c]muhammad.farraz93@gmail.com

Abstract. *This paper illustrates the development and the use of conceptual sizing tools integrated with optimization tools. The conceptual sizing tool is based on empirical and simple analytical calculation that simple and robust enough for wide range of inputs. The genetic algorithm optimization method then used to explore the global optimum for given variables. System response analysis is conducted to gain insight about the sensitivity of objective function because of design variables.*

Keywords: *Conceptual Design, Missile, Optimization, System Response Analysis, Evolutionary Algorithm.*

I. Introduction

MISSILE technology is an important part of achieving independent ability in developing weapon system and domestic defense industry. This is also important for Indonesia, which has participated in the development of fighter aircraft together with South Korea. Hence, air-to-air missile (as seen in Figure 1) development is a necessary parallel effort to arm the fighter. The missile development is a long process, starting from conceptual design to production and manufacturing. One of the most important phases in the design process is the conceptual phase of design, in which the initial shape of the rocket to be made is determined.

One of the methods already developed in conceptual rocket design is the design method by Fleeman [1]. In order to generate better design, an optimization method is applied on Fleeman method, starting from the missile aerodynamics, propulsion, trajectory, and finally the structure.

II. Methodology

The method used in this research is numerical method that is using equation of empiric equation and work flow on Fleeman method [1], by adding optimization method. A code for analysis and optimization is developed the conceptual design process starts from the definition of mission requirement and then selects the design baseline for short range air to air missile. Python programming language [3] is used in the code because the open source nature and its simplicity. The conceptual design is initiated in the aerodynamics, propulsion and structure parts by utilizing the optimization method. The addition of optimization method to this Fleeman method will result in faster processing time and better design than by using Fleeman method alone. The optimization method applied is Genetic Algorithm. Genetic Algorithm works so that optimization get the global optimum.

In this initial work, the tools developed is limited to short range air-to-air missile with focus on the aerodynamics, propulsion, trajectory, and structure conceptual design.

A. Conceptual Design and Sizing Methods

Fleeman method developed in this work is based on Tactical Missile Design (TMD) spreadsheet [2]. Tactical Missile Design (TMD) spreadsheet is a conceptual sizing tool for the design of tactical missile that includes analyses for many disciplines. The spreadsheet disciplines are aerodynamics, propulsion, trajectory, structure, warhead, radar, and dynamics. The spreadsheet calculation can be divided by two major calculation. The first calculations are an intercoupled calculation built from aerodynamics, propulsion, and trajectory calculations as shown in Figure 1. Second vehicle calculations include structure, warhead, radar, and dynamics. However, because of the scope in this work mentioned before, the second calculation just include structure calculation. The primary calculation is not intrinsically connected with the second calculations. Outputs from the second calculation is not become inputs for primary calculation, but vice versa.

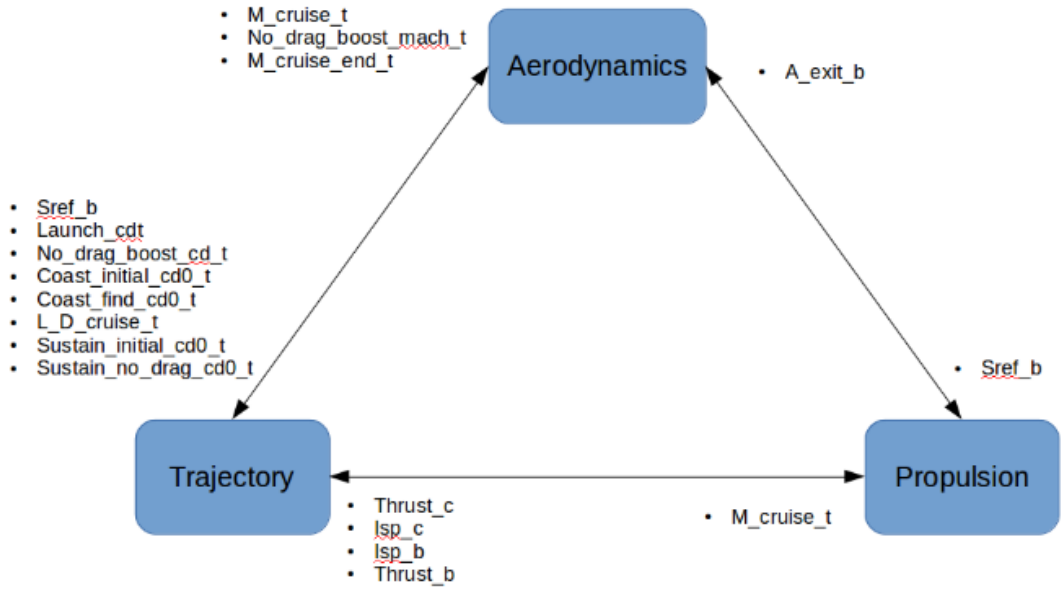

Figure 1. Intercoupled primary range calculation.

1) *Primary Range/Flyout Calculation Coupling*

Aerodynamics

The aerodynamics discipline calculation is based on Sparrow Medium-Range Air-to-Air Missile (MRAAM).

Propulsion

For propulsion calculation, according to the limitation mentioned before, the developed code operates with just one type of engine that is solid propellant. Solid propellant based propulsion is generally used for short range air-to-air missile.

Trajectory

Trajectory calculation done with assumption that the missile flies a constant flight path angle. By assuming a constant flight angle, trajectory calculation can be built with simple one degree of freedom model.

2) *Secondary Vehicle Calculation*

Structure

As mentioned before, there is no feedback from the structure calculation to primary range calculation. From available material properties, expected loads on missile, and the maximum Mach number input, structure module produces structure sensitive estimation such as required motor dimensions and weight and the skin temperature of the missile.

3) *Convergence criteria*

One advantage to translate the TMD spreadsheet into a Python code is that some

iterative process that could be tedious to be done in spreadsheet can be done easily. In this code, the iteration process is done whenever the iteration has reach the maximum iteration or the residual root mean square (rms) value from initial and calculated values of booster exit area, cruise Mach number, end Mach number from no drag equation, and end cruise Mach number is below rms criteria. Figure 2. shows all residual rms mentioned before from an example case. In this case, the rms criteria default is 1e-5. As shown, the iteration stops at 4th when residual rms reach rms criteria.

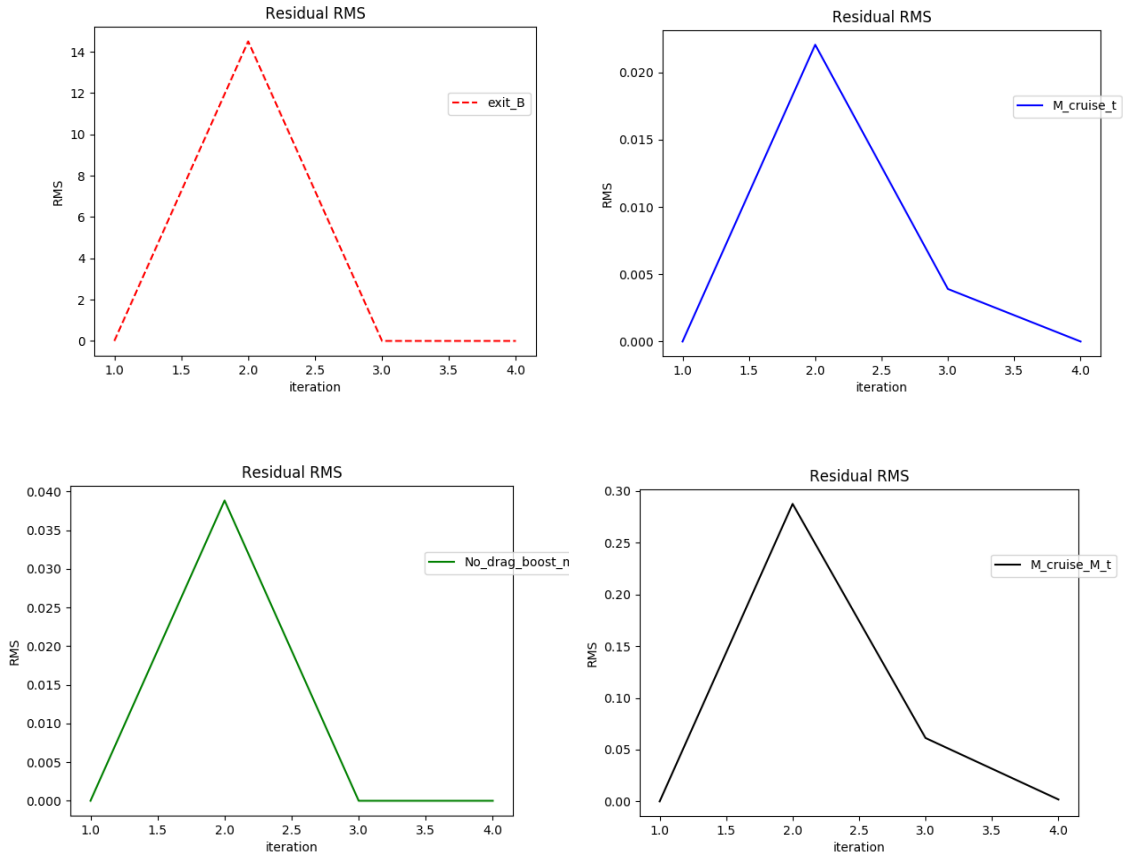

Figure 2. Residual rms iteration history.

B. Optimization Methods

The optimization problem in this work refer to previous work by Frits as follows:

1. *objective min flight time (Total_time_t))*
2. *constraints:*
   1. *turn radius < 4000 feet = 1219.2 m*
   2. *flight range >= 10 nmi = 18520 m (Total_range_t)*
   3. *missile weight = 500 lbm = 226,796kg (W_launch_t))*
3. *variables:*
   1. *launch weight (W_launch_t)*
   2. *diameter (a2)*
   3. *nose length (LN)*
   4. *wing area (SW)*
   5. *expansion ratio (e_b,e_c)*
   6. *boost chamber pressure (Pc_b)*
   7. *sustain chamber pressure (Pc_c))*
4. *Optimization methods (GA)*

III. Results

A system response analysis was conducted to study how the objective function response with variation of design variables. Results of system response analysis is shown in Figure 3.

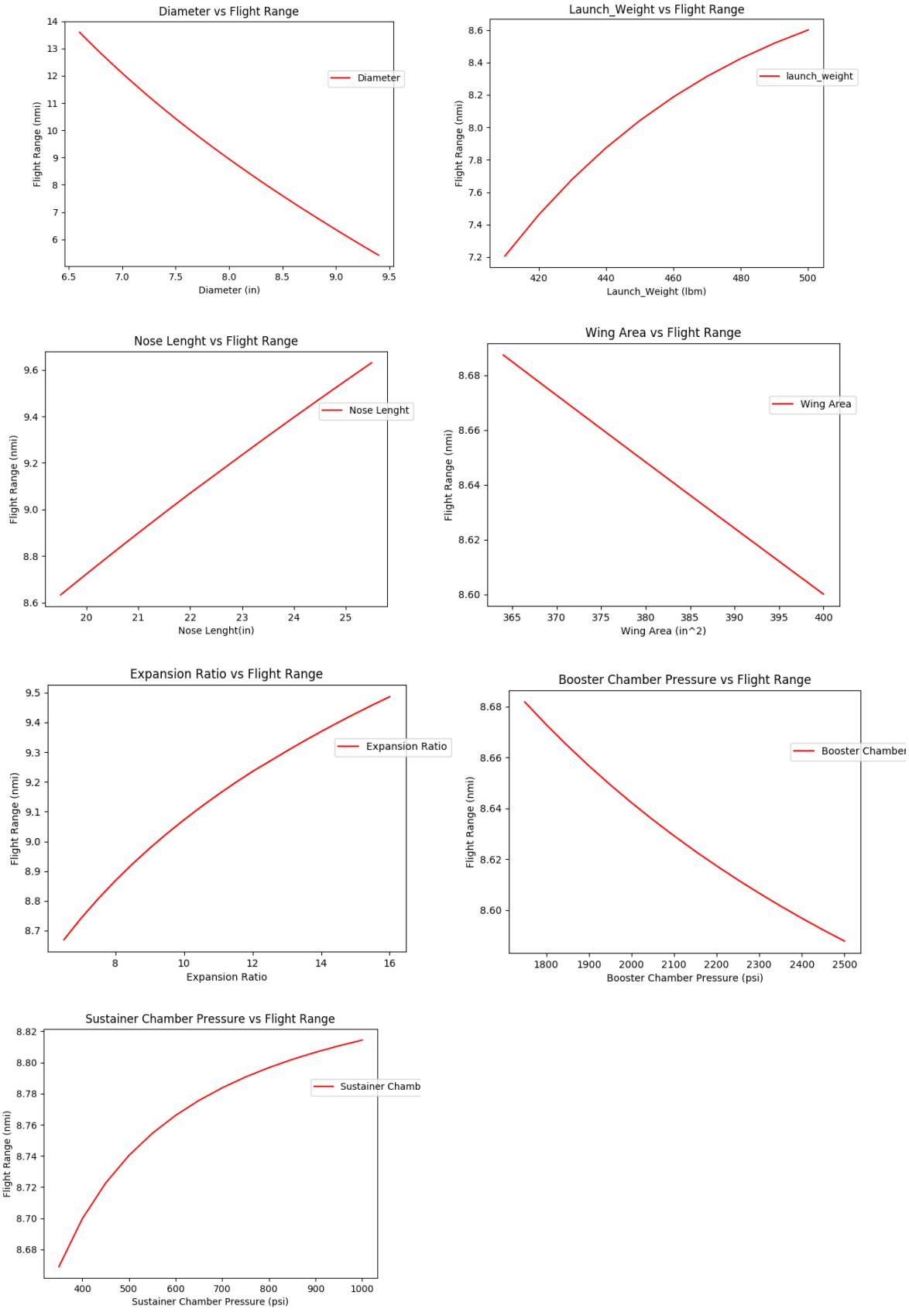

Figure 3. System response analysis results

IV. Conclusion

In this work, a Python code for primary range/flyout calculation was made. Genetic algorithm optimization was implemented in the code. Due to lack of missile databases for validation this work just conducted program verification with TMD Spreadsheet. Future works includes technology readiness consideration, dynamics and other modules integrating, new database generation, and development of all discipline prediction methods. To be able to implement technology readiness consideration, development of intercoupled primary and secondary calculation is mandatory, for example, calculation of the optimum aerodynamics, propulsion, and trajectory characteristic based on available material technology. Finally, this work will explore more on the optimization methods.

Acknowledgment

This work was supported in part by the National Innovation System Research Incentive (INSINAS) Grant, Ministry of Research, Technology, and Higher Education of Indonesia

References

[1] Fleeman, Eugene L. Tactical missile design. American Institute of Aeronautics and Astronautics, 2006.
[2] Frits, Andrew P., Eugene L. Fleeman, and Dimitri N. Mavris. "Use of a Conceptual Sizing Tool for Conceptual Design of Tactical Missiles (U)." .(2002).
[3] Van Rossum, Guido, and Fred L. Drake. Python 3: Reference Manual. SohoBooks, 2009.

Estimation of Bearing Degradation Trend Using Least Square Support Vector Machine and Exponential Regression (#721)

Didik Djoko Susilo[1,a], Achmad Widodo[1], Toni Prahasto[1,b] , Muhammad Nizam[2,c]
[1]Department of Mechanical Engineering, Universitas Diponegoro, Semarang, Indonesia
[2]Department of Electrikal Engineering, Universitas Sebelas Maret, Surakarta, Indonesia
[a]djoksus@uns.ac.id, [b]toni.prahasto@gmail.com, [c]nizam_kh@ieee.org

Abstract—*Bearings are frequently found in rotating machinery as the load-bearing members. They play as the critical component in the machine. Their failure can interrupt the production and causing unscheduled downtime. So the bearing monitoring become very important in the bearing maintenance policy. Monitoring involves measurement of bearing signals using certain sensors. Vibration sensor is the most used sensor to monitor the bearing condition. Any damage to a bearing will cause a vibration signal to degrade from its normal state. By tracing this degradation trend, one can obtain the bearing condition and predict its future state. This work is aimed to estimate bearing degradation trend of a bearing using least square support vector machine (LS-SVM) and compare the result using conventional exponential regression. The estimation was performed on the bearing signal obtained from bearing run to failure experiment. The degradation trend was constructed from a time series of degradation indicators extracted from raw vibration signal. The degradation indicator used in this paper are two statistical feature in time domain. They are root mean square and kurtosis. The estimation performance was measured using root mean square error and mean absolute error. The results showe that LS-SVM function estimation method work better than conventional exponential regression to estimate the bearing degradation trend.*

Keywords—*Bearing, degradation trend, estimation, lssvm, exponential regression.*

I. Introduction

Bearing is a mechanical element that commonly be found in rotating machines. They are not only supports the load but also permits relative motion between two parts, such as shaft and the housing. They are the critical component to the machine function and often the cause of failure.

The presence of faults in bearings results in severe vibrations of rotating machinery. Unexpected bearing failures can interrupt the production, cause unscheduled downtime and economic losses to the customer. Thus for the last decades, bearing condition based maintenance (CBM) has been the subject of extensive research. CBM is the use of machinery run-time data to determine the machinery or their components condition and hence their current fault condition which can be used to schedul the required repair and maintenance prior to breakdown [1]. A significant objective of CBM is to predict the machine health and the remaining useful life (RUL) instead of their service time, which leads to anticipate usage of the machine, reduction in downtime and enhanced operational safety.

The researches on bearing condition monitoring generally can be divided into two categories, they are fault diagnosis and prognosis. In the fault diagnosis, researchers have been developing methodologies to detect the bearing fault, isolate which component is faulty, and decide on the potential impact to the machinery. The researches have been covered traditional method like usage of demodulation or enveloping based method [2],[3],and[4], until the usage of artificial intelligent as artificial nueral network, and support vector machine [5], [6], [7], and [8].

The second category is the bearing prognosis. Researhes in this area attempt to predict accurately the remaining useful life (RUL) of a faulty bearing. Some researches in the bearing prognosis are summarized in [9].

In the practice, the life of a bearing can be divided into two stages. The first stage is refered to as the normal stage where no significant deviation from the normal operation. The second stage is called the failure delay period, since a defect may be initiated, and progessivelly develope into an actual failure. With the help of conditioning monitoring, hidden defects already present in the bearing may be detected. And for maintenance planning purpose, the prediction of the innitiation of the second stage and the residual life thereafter is important. [10].

Assesment of bearing condition can be done by estimation the bearing degradation trend. The degradation trend is represented by a series of statistical features that are obtained from vibration signal. These features are nonlinear and complex. So it is need function estimation to the bearing degradation trend for the remaining useful life prediction. Several researches in this area can be mentiones as [11], [12], and [13].

Least square support vector machine (LS-SVM) is one of the machine learning technique. It is a least squares modification to the Support Vector Machine (SVM). The major advantage of LS-SVM is that it is computationally very cheap while it still possesses some important properties of the SVM. Application of the LSSVM can be used for non linear classification, fuction estimation, and density estimation. One of the potential application of LSSVM is for time series degradation [14], [15], [16], and [17]

This paper is attempt to estimate the bearing degradation trend using LSSVM function estimation on time series of bearing signal extracted feature to monitor the bearing condition predict its future state.

II. Least Square Support Vector Machine

Support vector machine (SVM) is a machine learning method that is widely used for data analyzing and pattern recognizing including classification and regression. The algorithma was invented by Vapnik [18]. The LS-SVM is reformulations to standard SVMs which lead to solving linear Karush Kun Tucker (KKT) system. LS-SVM are closely related to regularization network and Gaussian processes but additionally emphasize and exploit primal-dual interprestation. An LS-SVM formulation employs the quality constraints and sum-squared error (SSE) cost funtion, instead of quadratic program in traditional SVM. In this section, it will be described a brief theory about LS-SVM method for non linear function estimation [19] and [20]

Consider first a model in the primal weight space in the following form:

$$y(x) = w^T \varphi(x) + b \qquad (1)$$

Where $x \in \Re^n, y \in \Re, \varphi(.): \Re^n \to \Re^{nh}$ is the mapping into the high dimensional space and potentional infinite feature space.

Giving a training set $\{x_k, y_k\}_{k=1}^N$, we can formulate then the following optimization problem in the primal weight space:

$$\min J_p(w,\varepsilon) = \frac{1}{2} w^T w + \gamma \frac{1}{2} \sum_{k=1}^{N} \varepsilon_k^2$$

$$\text{Such that } y_i = w^T \varphi(x_i) + b + \varepsilon_i, \quad i = 1,...,N \qquad (2)$$

Where the fitting error is denoted by ε_i. The hyper-parameter γ controls the trade-off between the smoothness of the function and the accuracy of the fitting. This optimization problem leads to a solution,

$$\hat{f}(x) = \sum_{i=1}^{N} \alpha_i K(x, x_i) + b \qquad (3)$$

Where α_i are the coefficiens and $K(x, x_i) = \varphi(x)\varphi(x_i)$ is the kernel. A common choice for the kernel is the Gaussian RBF,

$$K(x, x_i) = \exp - \frac{\|x - x_i\|^2}{2\sigma^2} \qquad (4)$$

The main benefit of the LS-SVM technique is that it transforms the traditional quadratic problem to a simultaneous linear system problem, thus ensuring simplicity in computations, fast convergence and high precision.

III. Methodology

A. Bearing Data Collection

The bearing data used in the paper was obtained from the experiment generated by NSF I/UCR Center on Intelligent Maintenance Systems (http://www.imscenter.net/). The description of the data is as follow: Four bearings were installed on one shaft. The rotation speed was kept constantly at 2000 RPM. 6000lb radial load is placed onto the shaft and bearing by a spring mechanism. All bearings are forced lubricated. On each bearing two PCB 353B33 High Sensitivity Quartz ICP Accelerometer were installed for a total of 8 accelerometers (one vertical Y and one horizontal X on each). The signal was sampling using frequency of 20 kHz. The Figure 1 below shows the test rig and illustrates sensor placement.

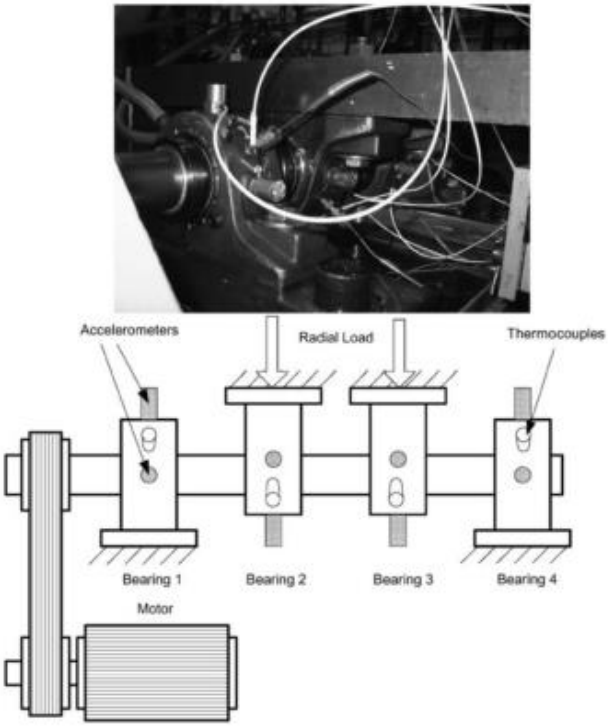

Figure 1. Bearing test rig and sensor placement ilustration.

B. Feature Extraction and time Series Construction

Feature extraction to find sensitive feature to the bearing incipient fault is important. Refer to [6] and [23], two statistical features in the time domain used in this paper. They were extracted from the raw vibration signal obtained from run to failure experiment. These features are root mean square and kurtosis.

The rms and kurtosis were taken from successive vibration measurements. Total measurement amounted to 2156. Then, these features were constructed to form a bearing state time series. The fuction estimation was applied to these time series.

C. LS-SVM Training

The LS-SVM training process was done to get the model for function estimation. The hyperparameters λ and σ^2 would be obtained from this process. The optimization using simplex method with cost function of leaveoneout and kernel function of radial basis function (RBF)

D. Fuction Estimation of Bearing Degradation Trend

The bearing degradation trend was estimated using LS-SVM method and double exponential regression. These methods were applied on the time series of features that contain normal state and faulty condition of bearing.

E. Performance Evaluation

The estimation performance was evaluated using two parameter, i.e. : Mean Absolute Error (MAE), and Root Mean Square Error (RMSE). The MAE give the measure absolute deviation of estimated values from the measured data. It shows the magnitude of overall error occured due to predicting. For a good estimation, the obtained MAE shoud be small as small as possible.

Meanwhile the RMSE measure the quare root deviation of the estimated values. The RMSE emphasizes the fact that the total estimation error is in fact affected by large individual error. This error gives an overal idea of the error occured during estimation.
The MAE and RMSE are formulated as follows:

$$MAE = \frac{1}{n}\sum_{i=1}^{n}\left|y_i - \bar{y}_i\right| \quad (6)$$

$$RMSE = \sqrt{\frac{1}{n}\sum_{i=1}^{n}\left[x(i) - \bar{x}(i)\right]^2} \quad (5)$$

Where y_i and x_i are the measured data, and $\bar{y}_i$ and $\bar{x}_i$ are the estimation.

IV. Result and Discussion

Usually the bearing life cycle will follow the normal condition and faulty condition. Before undergo faulty condition usually there is a transition from normal to faulty condition. The vibration signal acquired at those three condititions in the bearing run to failure testing are shown in the Figure 2 until Figure 4.
From those signals, it can be seen that there is change in the signal amplitudes, and finally the vibration amplitudes change drastically at the faulty condition.

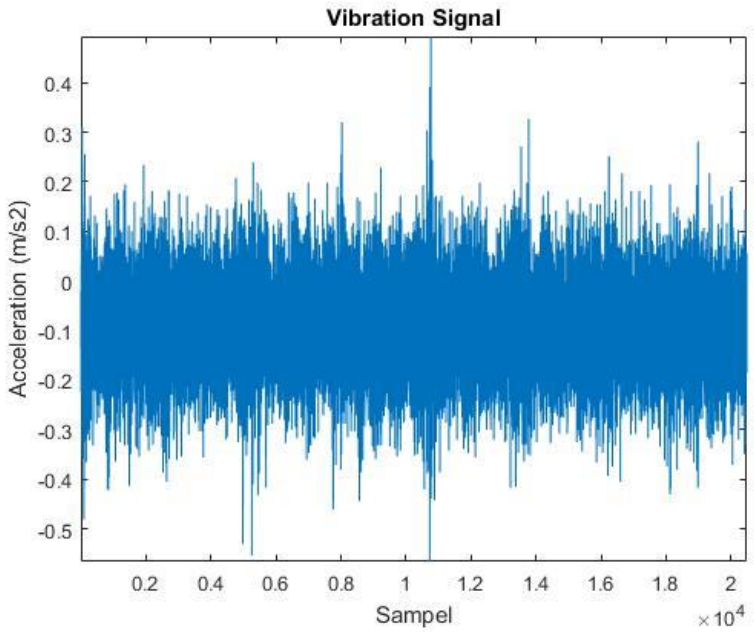

Figure 2. Bearing vibration signal at normal condition

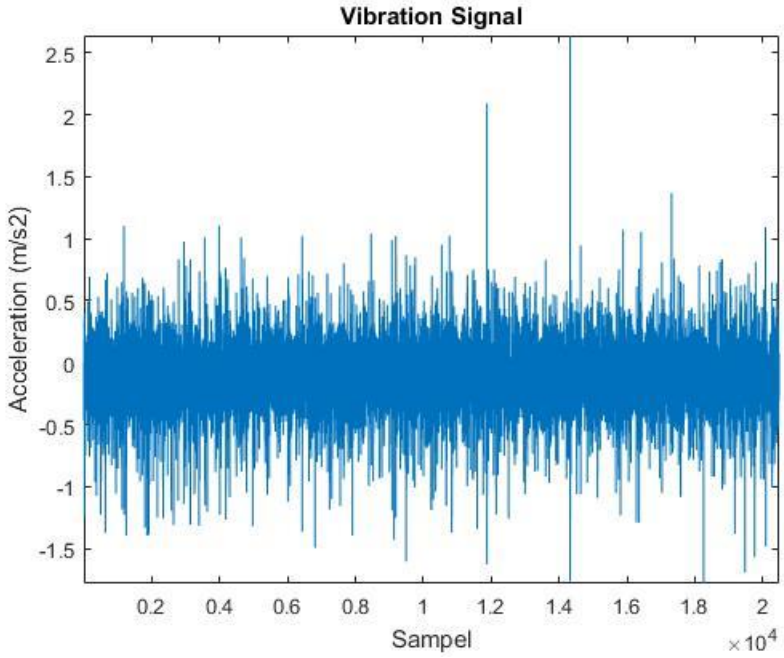

Figure 3. Bearing vibration signal at transition from normal to faulty condition

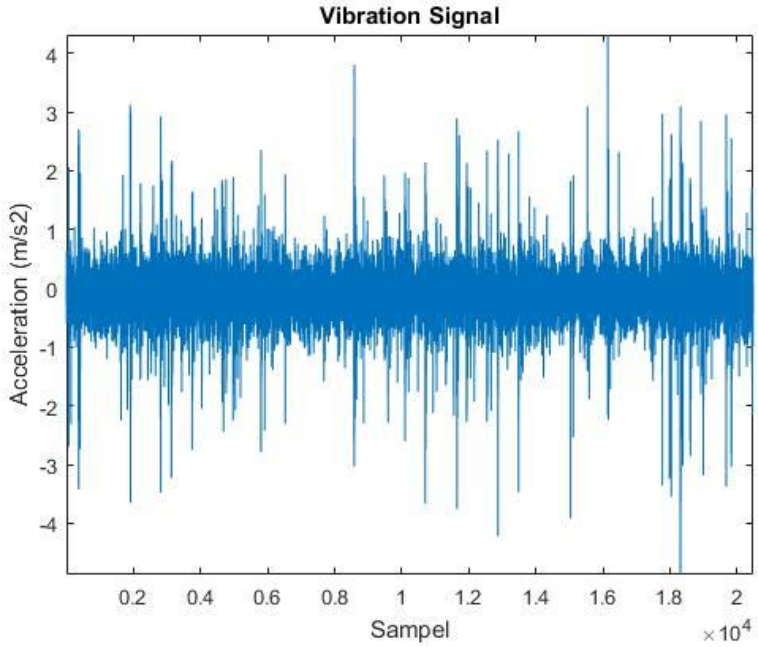

Figure 4. Bearing vibration signal at faulty condition.

To make observation of the change of bearing condition more clear, it is needed to construct a bearing degradation trend. So, it will need features extracted from bearing signal that can reflect the bearing condition. In this paper, two features are selected. They are rms and kurtosis feature. These features were extracted from series measurements of vibration signal from totally 2156 measurements. The results are shown in the Figure 5 and Figure 6.

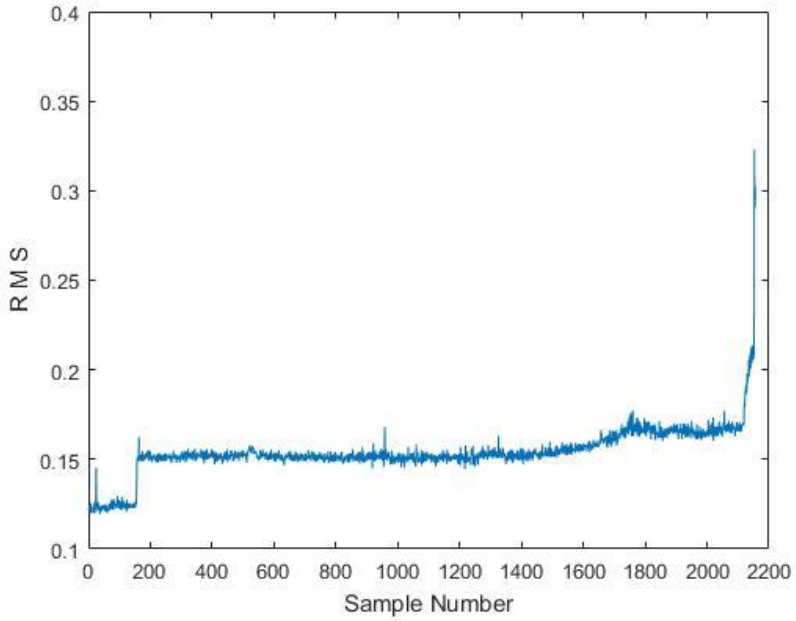

Figure 5. RMS feature

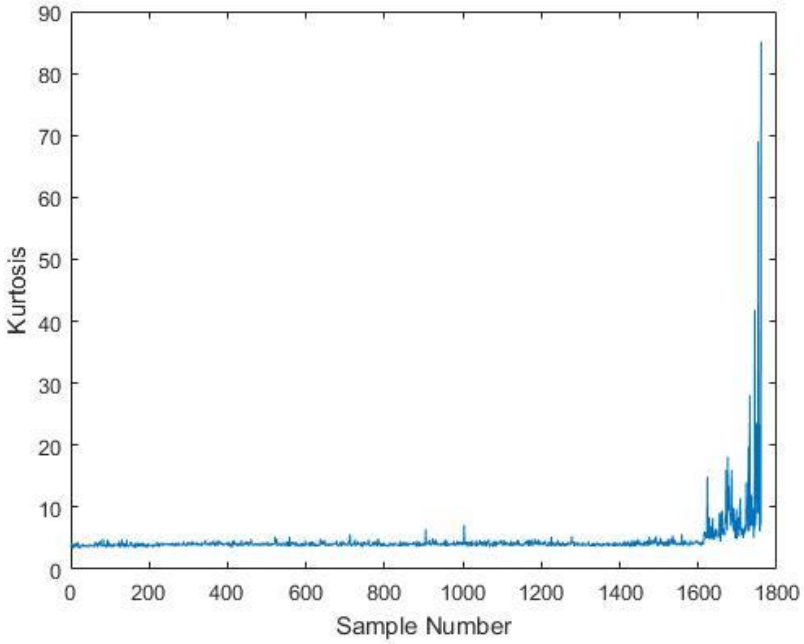

Figure 6. Kurtosis feature

Now, it can be seen clearly the degradation process of the bearing. If we adopt the failure threshold of bearing when the kurtosis value is 40 as mention in the reference [5], we can state that at the sample number 1 until 1600, the bearing was running normally, sample number 1601 until 1743 were the transition between normal to faulty condition, and then the bearing was fail at the sample number of 1744 when the kurtosis value exceed 40.

In the maintenance perspective, we have to avoid bearing catastrophic failure, because it will bring significant impact to the system. So, tracking the bearing condition should be done by generating an approximation function that can estimate the bearing degradation trend. For this purpose, the degradation data is taken 1000 series sample numbers from normal condition until the the bearing experince failure. So that the time series still represent normal,

transition, and faulty condition. Two methods applied in this function estimation. They are LS-SVM method and double exponential regression. The results are presented in the Fig 7 until Figure 10.

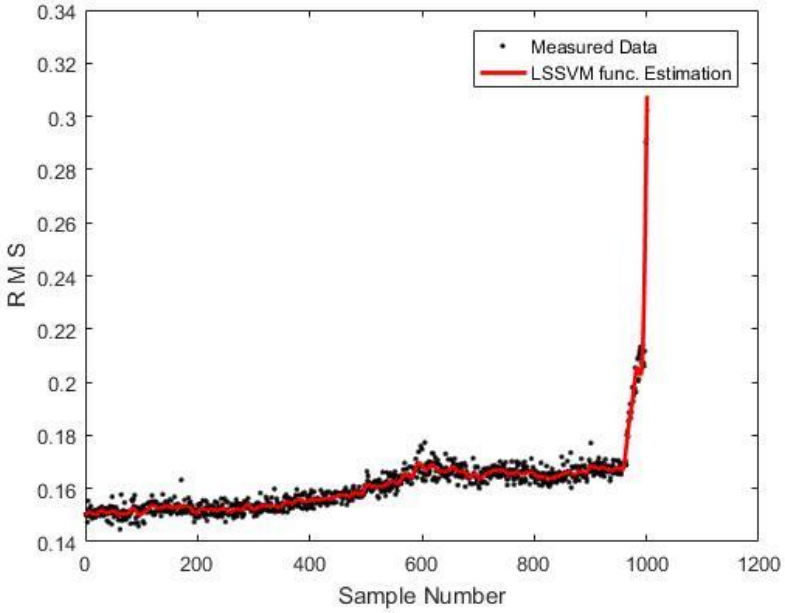

Figure 7. Bearing degradation trend estimation using LS-SVM for rms feature.

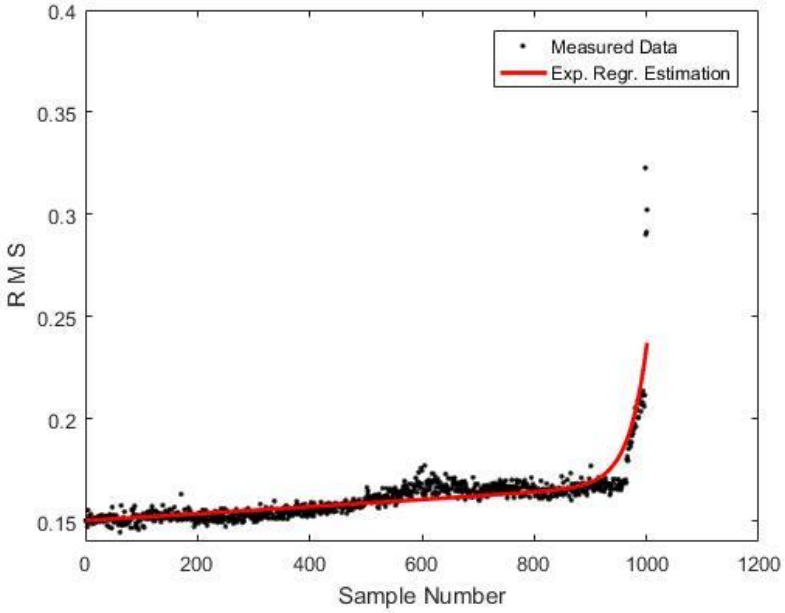

Figure 8. Bearing degradation trend estimation using double exponential regression for rms feature.

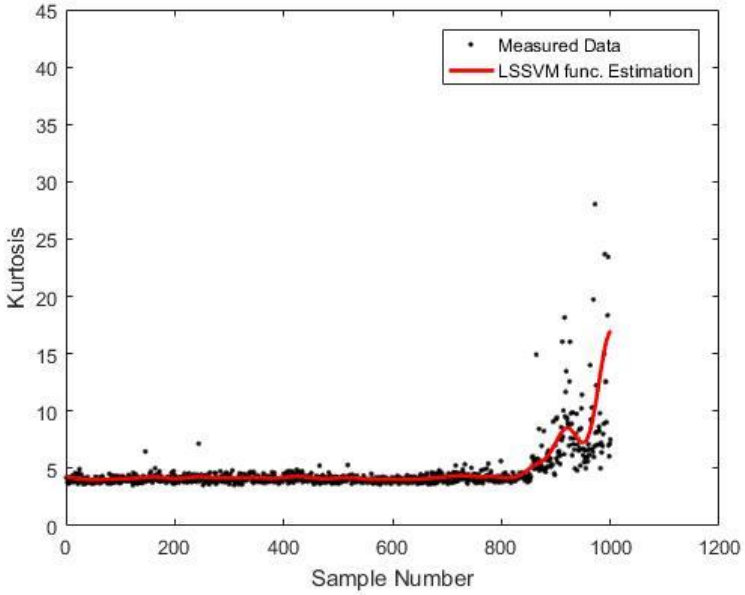

Figure 9. Bearing degradation trend estimation using LS-SVM for kurtosis feature.

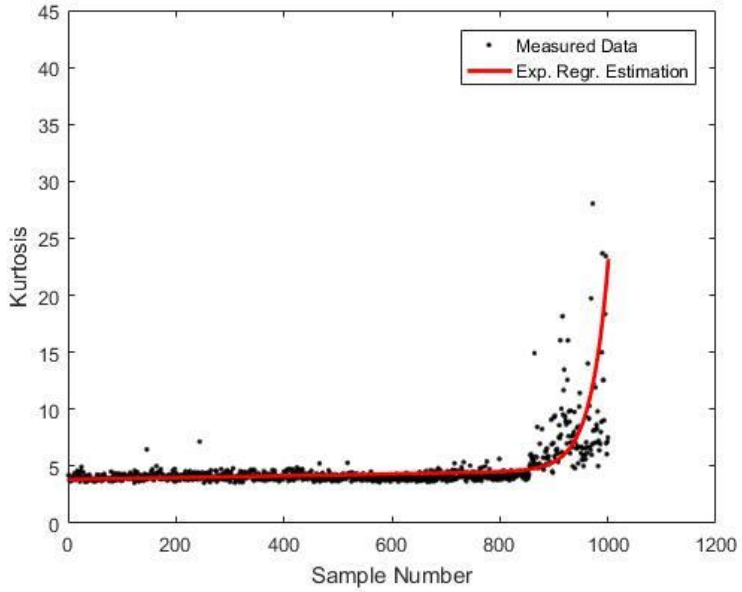

Figure 10. Bearing degradation trend estimation using double exponential regression for kurtosis feature.

The performance of those function estimation is summarized in the TABLE 1 below.

TABLE 1.Performance of function estimation.

Estimation Performance Criteria	Feature	LS-SVM	Double Exponential Regression
MAE	RMS	0.0018	0.0035
	Kurtosis	0.7254	0.8328
RSME	RMS	9.6500e-18	9.2253e-04
	Kurtosis	0.0425e-15	0,0561

The TABLE 1 shows that the overall performance the estimation are very good. All of the errof are quite small. The LS-SVM method yield high accuracy in predicting the bearing degradation trend. It is outperform than double exponential regression method in all features for both MAE and RSME criteria. This make the LS-SVM method be a better candidate to be applied in remaining useful life prediction of bearing.

V. Conclussion

Bearing degradatin trend estimation has been done in this paper using the LS-SVM method and Double Exponential Regression Function. The estimation was applied to the series of rms and kurtosis feature extracted from the bearing vibration signal.

The estimation performance of both methods are very good. However, the LS-SVM performance in estimation is much better than the exponential regression. This degradation trend estimation method can further be used for bearing future state prediction or RUL prediction that will be conducted in the future work.

Acknowledgement

The authors gratefully acknowledge the fully financial support from Sebelas Maret University through PNPB Doctor Dissertation Grant to this study.

References

[1] G. Vachtsevanos, F.L. Lewis, M. Roemer., A. Hess., B., Wu, *Intelligent Fault Diagnosis and Prognosis for Engineering Systems*, John Wiley and Son, New Jersey, 2006, pp. 13-14

[2] P. McFadden, J. Smith, "Vibration Monitoring of Rolling Element Bearings by The High Frequency Resonance Technique – a Review", *Tribology International*, Vol. 17, pp.3-10, 1984.

[3] N. Tandon, A. Choudry, *"A Review on Vibration and Acoustic Measurement Methods for the Detection Defect in Rolling Element Bearing"*, Tribology International, Vol. 33, pp. 469-480, 1999.

[4] R. Randall, J. Antony, "*Rolling Element Bearing Diagnostics – A Tutorial*", Mechanical System and Signal Processing, Vol. 25, pp. 485 – 520, 2011.

[5] A. Widodo, B.S. Yang, "Machine Health Prognostics using Survival Probability and Support Vector Machine", *Expert Systems with Application*, Vol. 38, pp. 8430-8437, 2011.

[6] D.D. Susilo, A. Widodo, T. Prahasto, M. Nizam, "Fault Diagnosis of Roller Bearing Using Parameter Evaluation Technique and Multi-Class Support Vector Machine, AIP Conference Proceeding, Vol. 1788, pp. 030081-1-030081-12, 2016

[7] S.D. Wu, P H. Wu, C.W. Wu, J.J. Ding, C.C. Wang, Bearing Fault diagnosis Based on Multiscale Permutaion Entrophy and Support Vector Machine, Entropy, Vol. 14. Pp. 1343-1356, 2012.

[8] D.H. Pandya, S.H. Upadhyay, S.P. Harsha, "ANN Based Fault Diagnosis of Rolling Element Bearing Using Time-Frequency Domain Feature", International Journal on Engineering, Science, and Technology (IJEST), Vol. 4, pp. 2878-2886, 2012.

[9] N.S. Jammu, P. K., Kankar, "A Review on prognosis of Rolling Element Bearing, *International Journal of Engineering Science and Technology (IJEST)*, Vol. 3(10), pp. 7497-7503, 2011.
[10] A. Widodo, *Application of Intelligent System for Machine Faultd Diagnosis and Prognosis*, Badan Penerbit Universitas Diponegoro, Semarang, 2009, pp. 309-310
[11] R. L. C., Keong, D. Mba., "Bearing Time-to-11]Failure Estimation using Spectral Analysis Features', *Structural Health Monitoring*, Vol. 13 (2), pp. 219-230, 2014.
[12] P. B. Kosasih, W. Caesarendra, K. Tieu, A. Widodo, C.A.S. Moodie, "Degradation Trend Estimation and Prognosis of Large Low Speed Slewing Bearing Lifetime", *Applied Mechanics and Materials*, Vol. 493, pp. 343-348, 2014.
[13] B. Zhang, L. Zhang, J. Xu, P.Wang, Performance Degradation Assesment of Rolling Element Bearings Based on an Index Combining SVD and Information Exergy, *Entrophy*, Vol. 16, pp. 5400-5415, 2014.
[14] T. Karna., F. Rossi., A. Lendasse, " LS-SVM Functional Network for Time Series Prediction", ESAN 2006 *Proceeding – European Symposium on Artificial Neural Networks*, Bruges, 26-26, April, 2006.
[15] P. Samui, "Application of Least Square Support Vector Machine (LSSVM) for Determination of Evaporation Losses in Reservoir", Engineering, Vol. 3, pp. 431-434, 2011.
[16] U. Thissen, R. Van Brakel, A.P. de Weijer, W.J. Melsen, L.M.C. Buyden, "Using Support Vector Machine for Time Series Prediction, *Chemometrics and Intelligent Laboratory Systems*., Vol 69, pp. 35049, 2013.
[17] S.M. Pandhiani, A.B. Shabri, "Time Series Forecasting Using Wavelet-Least Squares Support Vector Machines ND Wavelet Regression Models for Monthly Stream Flow Data, *Open Journal of Statistics*, Vol.3, pp. 183-194, 2013.
[18] V.N. Vapnik, *Statistical Learning Theory*, John Wiley and Son, Canada, 1998
[19] J.A.K. Suykens, J. Vandewalle, "Least Squares Support Vector Machine Classifiers', *Neurol Processing Letter*, Vol. 9, pp. 293-300, 1999.
[20] J.A.K. Suykens, T. Van Gestel, J. De Brabanter, B. De Moor, J. Vandewalle, *Least Squares Support Vector Machines*, World Scientific Press, Singapore, 2002
[21] H. Huang, H. Ouyang, H. Gao, L. Guo, D. Li, J. Wen, " A Feature Extraction Method for Vibration Signal of Bearing Incipient Degradation", Measuring Science Review, Vol 16 (3), pp. 149-159, 2016.
[22] L. Cheng, Y. Huang, "Performance Degradation Assesment and Fault Diagnosis of Bearing Based on EMD and PCA_SOM, Vibroengineering Procedia, Vol. 2, pp. 12-16, 2013.
[23] K. De Brabanter, P. Karsmaker, F. Ojeda, C. Alzate, J. De Brabanter, K. Pelckmans, B. De Moor, J. Vandewalle, J.A.K. Suykens, LS-*SVMlab Toolbox User's Guide version 1.7*, ESAT-SISTA Technical Report 10-146, Katholieke Universiteit Leuven, 2010.

Micro Gas Turbine Engine Auto-Start System (#726)

Firman Hartono[1,a], Gunta Akhiri[2], Adidharma Soelaiman[3]
[1]Aerospace Engineering Study Program, Faculty of Mechanical and Aerospace Engineering Institute of Technology Bandung, Jl. Ganesha 10 Bandung, Jawa Barat
[2]PT Aering, Jl. Pasirluyu Barat no. 34, Bandung, Jawa Barat
[3]PT Techno Multi Utama, Jl. Pesantrean 76, Cimahi, Jawa Barat
[a] firman7738@gmail.com

Abstract. *An experimental micro gas turbine engine has been developing. The engine consists of a turbocharger based gas generator (compressor – turbine pair), a combustion chamber, a power turbine system and engine accessories. Two types of fuel are used to operate the engine. They are gas fuel (LPG) for engine ignition, mixed gas and liquid fuel (kerosene) for engine acceleration up to idle condition, and liquid fuel for engine operation above idle. Starting the engine is one of the most difficult task. Highly skilled and experienced operators are required to start the engine properly without explosion, flame out, over heat or other incidents during starting process. Hence an automatic start system has been developed to assist the operator for easy and safe operation especially during engine starting. The automatic start system controls the starting process from zero speed to idle condition. The operation phases are initiation, select mode, manual operation, pre-ignition (purging), ignition (dry cranking and light off), acceleration, fuel transition, engine idle, engine operation and normal shutdown.*

Keywords: *micro turbine, gas turbine engine, automatic start*

I. Introduction

The gas turbine engine is a power plant, which produces a great amount of energy for its size and weight [1]. Gas turbines are used in diversified services from jet engines and simple mechanical drives (on land, sea and air) to sophisticated gas lasers and supersonic wind tunnels [2]. The author's development of gas turbine as jet engine (turbojet) can be seen in [3,4,5].

Gas turbine engine can be devided into open cycle and closed cycle. The more common gas turbines are of open cycle type with internal combustion [6]. An open cycle gas turbine can have a single shaft, a twin shaft or a multispool arrangement [7]. A twin shaft, open cycle micro gas turbine engine has been developing. The engine consists of a gas generator and a power turbine system as its main components. For proper operation, the engine is completed by subsystems such as fuel system, oil system, water cooling system, etc.

One of the most technically challenging aspects of gas turbine performance is probably starting the engine. During starting processes, the engine could suffer explosion, over heat and flame out. Hence to avoid incident, accident and engine damage due to improper starting process, an automatic start system embedded in instrumentation system have been developed. The automatic start system must be able to: 1. controls the engine during starting process to ensure safe and proper operation of the engine, 2. stabilize engine speed when operated in idle condition, 3. ensure smooth and safe shut down process.

II. Methodology

Generally, normal operation process of an engine consist of starting, operation and shut down. The starting process consists of five phases, i.e. dry cranking, purging, light off, acceleration to idle and thermal soakage [8]. In dry cranking phase, the engine high pressure shaft is rotated by the starter with no fuel being metered to the combustor. Purging is done to ensure that there is no fuel from previous operation or failed start attempt in the engine gas path or exhaust that may ignite and cause damage. In light off phase, fuel is metered to the combustor and igniters are energized. This causes ignition within the combustor. After light off, the fuel flow is steadily increased with the starter continued assisting. This will accelerate the engine speed to idle condition. After idle condition achieved, the engines are often held at idle to allow the carcass to thermally soak to the new temperature to preserve cyclic life. The typical rotational speed versus time during starting of a free power turbine turboshaft engine is shown in Figure 1.

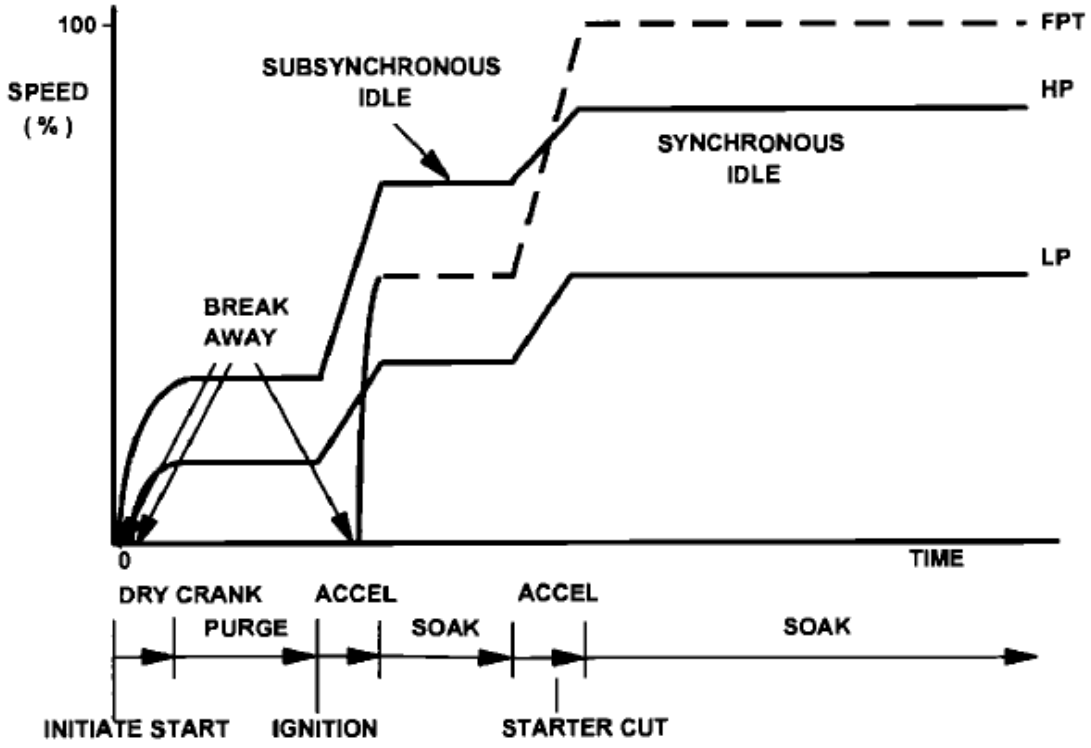

Figure 1. Rotational speed vs time during starting a turboshaft engine [8]

The starting phases of the developed experimental gas turbine engine is slightly different from basic starting process explained above. This is because the experimental engine uses two types of fuel for its operation. They are gas fuel (LPG) during light off and then after successful ignition liquid fuel is injected to replace the gas fuel. Hence in this case, an additional phase, i.e. fuel transition phase, must be defined. In fuel transition phase, gas fuel is slowly reduced until gas valve totally closed while liquid fuel valve is controlled to keep the engine still in its normal operation. After transition phase, the engine operates using liquid fuel. Thus, the detail starting process for the experimental gas turbine engine consists of dry cranking, purging, light off (igniter energized and gas fuel valve opened), liquid fuel metered, acceleration to idle, fuel transition and idle condition.

Among other operating conditions, starting the engine is probably one of the most technically challenging aspects of gas turbine performance. It covers engine operation from when the operator selects a start, through to stabilization at idle. Depends on engine size, the overall time required for starting (to idle) process can be only 10 seconds to more than 1 hour. All the starting phases explained above can be controlled manually. However, during starting process the engine operates in transient condition and an unexperienced operators often failed to start the engine due to several causes. Hence, to prevent danger operations and engine damage during starting process, an electronic controlled automatic start system must be developed. By using an automatic-start system, starting process can be done easily and saver even when operated by an average skilled operator. The automatic-start system will be included in the instrumentation system.

The engine instrumentation system was developed to measure and record important data that affect engine operation and performance and then uses the recorded data as an input to control engine operation. The block diagram of the instrumentation system is shown in Figure 2.

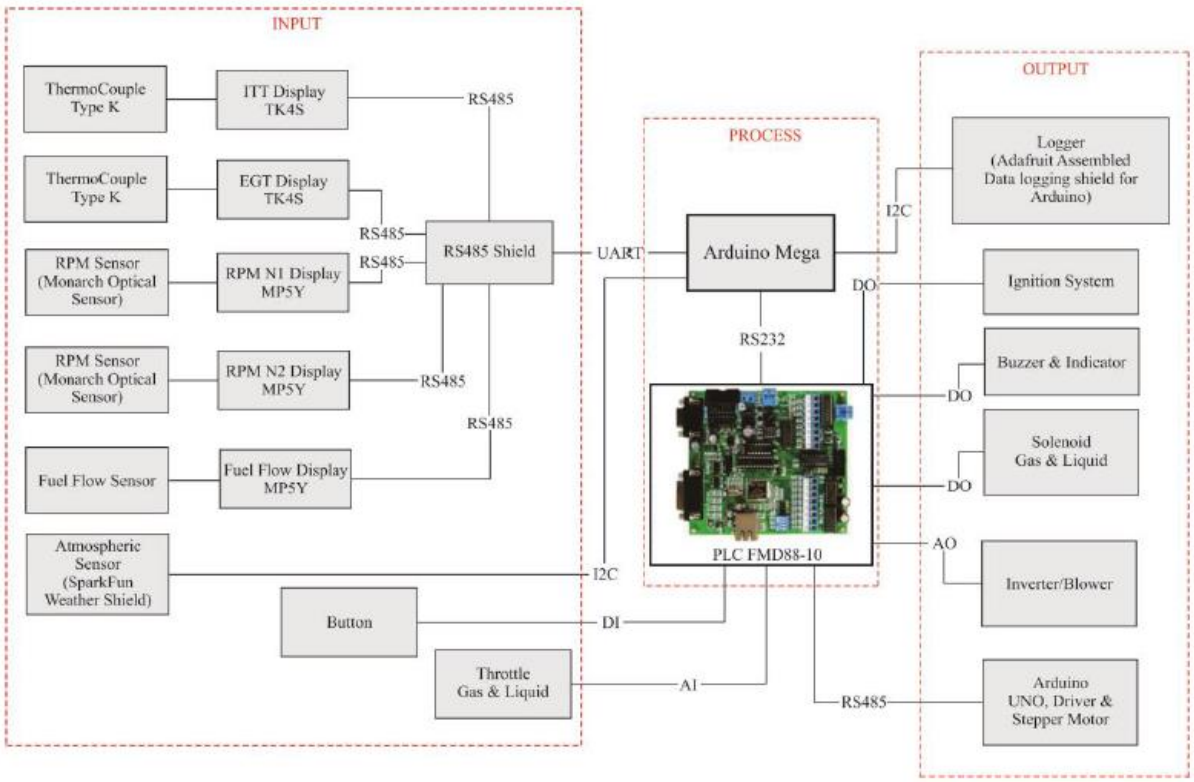

Figure 2. Instrumentation system block diagram

As can be seen from Figure 2, the instrumentation system reads and records: atmosphere data (pressure, temperature and humidity), engine speed (N1 and N2), inter turbine temperature, exhaust gas temperature, fuel flow and operator inputted push button and throttle position. The recorded data are then processed by the main processor. After processed, some of the data are displayed in a monitor while other data are used to control actuators. The instrumentation system also completed by emergency button to be pushed by the operator in case of emergency situation.

The instrumentation system covers all engine operating conditions from start to shut down. Included in the instrumentation system is automatic-start system. Figure 3 shows the instrumentation system operation flowchart

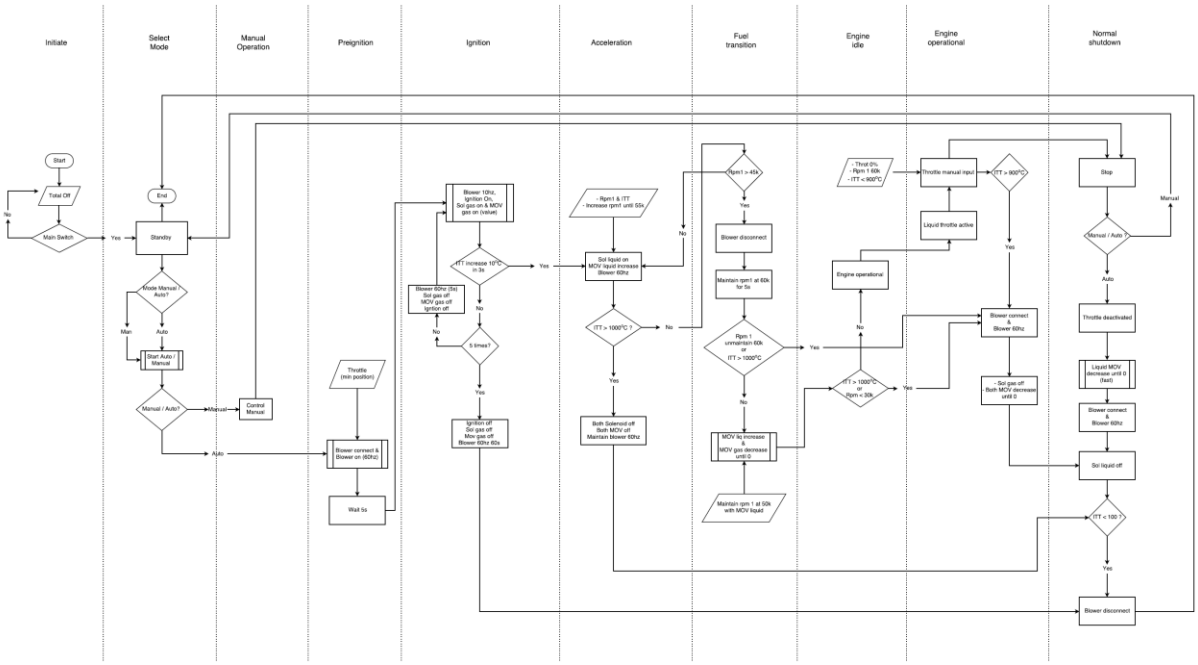

Figure 3. Engine instrumentation system flowchart

Refers to Figure 3, the instrumentation system has ten operation phases with five phases are for starting process. The operation phases are initiation, select mode, manual operation, pre-ignition (purging), ignition (dry cranking and light off), acceleration, fuel transition, engine idle, engine operation and normal shutdown. Below are the detail explanation of the operation phases.

The operation phases starts from initiation. In the initiation phase, the operator could turn the engine on (or off after normal shutdown). The on position will start all system. After initiation phase, the operator could select manual operation or automatic operation. If manual operation is selected, all system must be operated manually from starting to shut down. If automatic operation is selected then the system will start the engine automatically up to idle (the detail starting process will be explained in the following paragraph). After idle condition, the operator can take over the engine and operate it manually to the required power output. Before shutting down, the operator must set the throttle position manually back to idle condition. Automatic normal shut down works after the operator push shut down button. In automatic operation, the engine control system keep the engine speed constant during idle condition.

As explained before, the starting process consists of five phases. The first phase for starting is pre-ignition. In pre-ignition phase, the engine is purged by using air flow from a centrifugal blower. After pre-ignition, the next phase is ignition. In ignition phase, ignitor is energized and gas fuel is injected. If ignition fails, the engine will be purged again to ensure no fuel exist in the combustion chamber and the ignition process will be repeated. If flame exists, the next phase is acceleration. In acceleration phase, the inlet air flow is increased by changing blower speed until reaching maximum speed and the liquid fuel is injected. During acceleration, the engine speed increases. While blower speed at its maximum, liquid fuel

flow steadily increased until idle rpm first achieved. In this first idle rpm, the engine still uses two types of fuel, i.e. gas fuel and liquid fuel. Hence the next phase is fuel transition. In fuel transition phase, first the blower is disconnected from engine intake and turned off and then the gas fuel flow rate is slowly decreased while liquid fuel flow rate should be fine adjusted to avoid engine flame out during transition. After fuel transition, the engine operates at idle speed by using liquid fuel only. This condition is called engine idle phase. In automatic operation, all starting process described above are controlled by instrument automatic-start system. After engine idle phase, the operator can operate the engine manually by changing throttle setting to the required power output.

III. Results and discussion

One of the most important steps before using an automatic-start system is setting the system for correct operation. The engine characteristic is different from one engine to another and according to the experience no computer based simulation method can be directly applied to set the automatic-start system. It seems that the only way to correctly set the automatic-start system is by using experimental data. In our case, the experimental data can only be collected by running the experimental engine in manual operation. Hence, several tests of the experimental engine have been done to collect important operation data. In manual operation mode, successful engine starting are seldom achieved. Hence the data from one or two successful manual start of the engine is then used as the input to preset the automatic-start system.

In order to check the performance of the system, starting processes using automatic start system are repeated several times. During experiments, the engine data terminal records important performance variables such as fuel flow rate, gas generator speed (N1), power turbine speed (N2), ITT and EGT. The results of some automatic-start testing are shown in Figure 4 below. For brevity, only N1 and ITT results will be shown in this paper

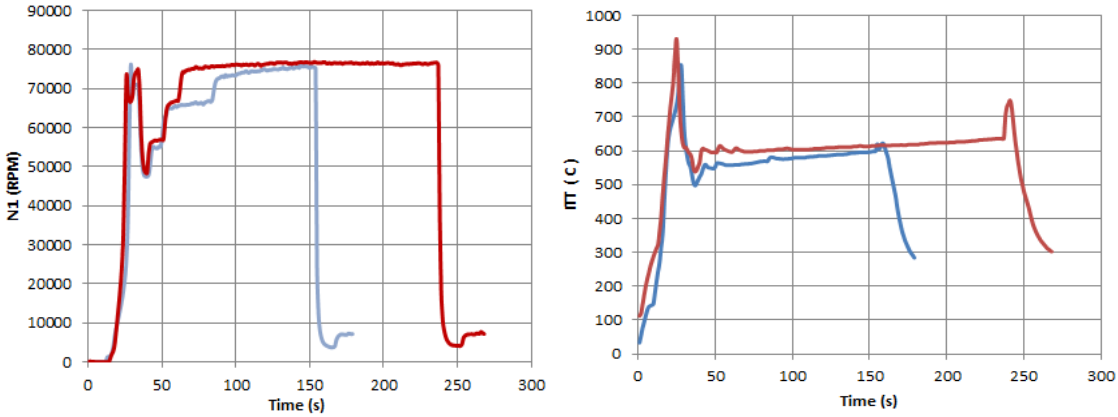

Figure 4. Automatic-start test: N1 vs time (left), ITT vs time (right)

Figure 4 shows N1 rpm vs time and ITT vs time for two measurements data. First of all, the consistency of the automatic start system can be clearly seen by comparing two curves in Figure 4, especially before 50 seconds. From the left hand side of Figure 4, it can be seen

that for time less than 50 seconds, the two N1 data shows similar results qualitatively and (almost) quantitatively. Also, the same results is shown by ITT vs time curves in the right hand side of Figure 4. For time more than 50 seconds, the data are different due to different engine operation. By comparing the red and blue line in Figure 4, it can be seen that the red line is the case when the engine was operated in longer time than the blue line. The experimental results in Figure 4 can also be compared with typical engine starting sequence from references. Figure 5 below shows a typical starting sequence of a turbojet engine from [9].

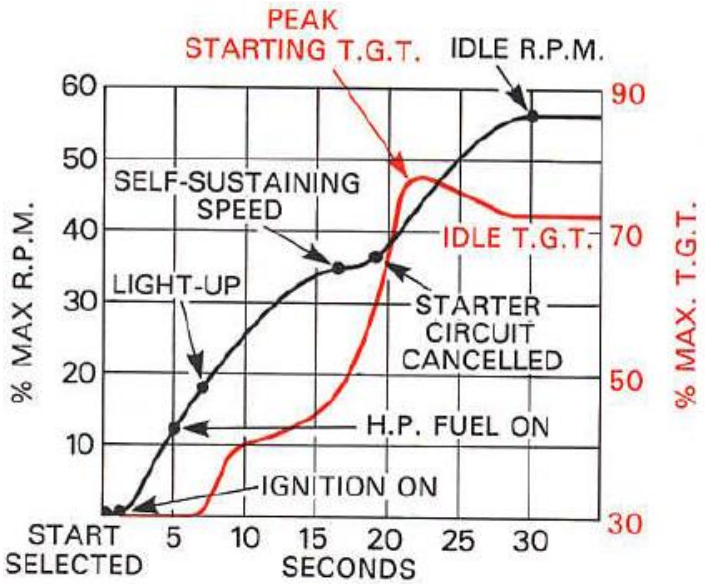

Figure 5. Typical starting sequence of a turbojet [9]

The N1 vs time data from developed automatic start system, Figure 4 left, can be compared to black line in Figure 5. Before further analyzing, please note that the experimental gas turbine engine in the current project uses two type of fuel while the turbojet engine in reference [9] uses only liquid fuel. The use of two type of fuel in our case causes the requirement for fuel transition from fully gas fuel to fully liquid fuel operation. Hence the engine rpm in Figure 4 first increased to more than its idle speed and then decreased until achieving its idle condition. During rapid deceleration from high speed to idle speed, the fuel rapidly change from mixing gas – liquid fuel to fully liquid fuel. The idle condition is defined at time 50 second. If the fuel transition sequence is neglected, by comparing the left hand side of Figure 4 and the black line of Figure 5 qualitatively, it can be seen that the developed automatic start system works properly.

The ITT vs time data from developed automatic start system, Figure 4 right, can be compared to red line in Figure 5. Also notes that there exist a transition phase in the experimental engine. In order to avoid engine flame out during transition, the mixing gas – liquid fuel flow rate is first increased until more than the required fuel flow in idle condition. The high fuel (gas – liquid) flow causes high ITT. After some predetermined point, the gas fuel flow rapidly decreases until gas fuel valve fully closed and only liquid fuel remaining. During gas fuel decrement, the ITT also decreases. In transition phase, the automatic start system controls the fuel flow rate to avoid engine flame out. By comparing the right hand side of Figure 4 and the red line of Figure 5 qualitatively, it can be clearly seen that both curves show similar phenomenon, i.e. the existing of peak starting temperature. However, in our experimental gas turbine, the peak starting temperature is much higher due to the existence

of transition phase. If the transition phase is neglected, then it can be said that the automatic start system works properly.

IV. Conclusion

An automatic-start embedded in an instrumentation system has been developed. It enable to assist a starting process for the experimental micro gas turbine engine. The operation phases of the instrumentation system are initiation, select mode, manual operation, pre-ignition (purging), ignition (dry cranking and light off), acceleration, fuel transition, engine idle, engine operation and normal shutdown. Five of the normal operating phases are starting phase. For correct automatic start operation, some of the control parameters in instrumentation system must be preset by using the control parameters data obtained from engine's manual start operation experiments. The data from successful engine manual start experiment is then used to preset the automatic-start system. In order to check the performance of the automatic start system, engine's automatically starting processes has been conducted and are repeated several times. During experiments, the engine data terminal records important performance variables such as fuel flow rate, gas generator speed (N1), power turbine speed (N2), ITT and EGT. By comparing the experimental results, it can be said that, at least based on two case data, the automatic start system has worked properly and consistently.

Acknowledgment

The authors thank to the Ministry of Research Technology and Higher Education, PT Techno Multi Utama and PT Aering for supporting this research.

References

[1] M.P. Boyce, Gas Turbine Engineering Handbook 4th Edition, Elsevier Inc., 2011

[2] A. Giampaolo, Gas Turbine Hand Book Principles and Practices 5th Edition, Fairmont Press Inc., 2015

[3] F. Hartono, The Design of Small Turbojet Engine for HS UAV, *Proc. of Regional Conference of Mechanical and Aerospace Technology*, 505, Bali, 2010

[4] F. Hartono, The Development of TJE500FH Small Turbojet Engine, *Proc. of International Conference on Fluid and Thermal Energy Conversion* (FTEC), p024, Zhengzhou, China, 2011

[5] F. Hartono, The Development of Turbojet Based on Turbocharger, Paper 1570212628, *11th International Conference on Intelligent Unmanned Systems*, Bali, Indonesia, 2015

[6] J.H. Horlock, Advances Gas Turbine Cycles, Pergamon Press, Oxford, 2003

[7] H.I.H. Saravanamuttoo, G.F.C. Rogers, H. Cohen and P. Straznicky, Gas Turbine Theory, 6th edition, Pearson Education Canada, 2008

[8] P.P. Walsh and P. Fletcher, Gas Turbine Performance 2nd Edition, Blackwell Science Ltd., Oxford, 2004

[9] Rolls Royce plc, The Jet Engine, 5th Edition, 1996

Study On The Influence of Jigging Operating Variables to Increase Monazite Concentration from Tin Ore Processing Plant (#736)

Alfitri Rosita [1], Lucas Donny Setijadji [1], Himawan Tri Bayu Murti Petrus [2,a]
[1]Department of Geological Engineering, Faculty of Engineering, Universitas Gadjah Mada, Indonesia
[2]Chemical Engineering Department, Faculty of Engineering, Universitas Gadjah Mada, Indonesia
Jl. Grafika 2 Yogyakarta, 55281
[a] bayupetrus@ugm.ac.id

Abstract. *In the process of tin mining, Cassiterite is the main mineral that has to be separated. Apart from cassiterite, there are some valuable minerals such as monazite which is a rare earth elements mineral that is wasted as tailings. The experiments conducted in this study aims to determine the effect of the variable length of the stroke, the speed of horizontal water flow and the type and size of ragging in the jigging process in order to obtain optimal results in increasing the percentage of monazite mineral fraction and reduce the losses that occur. Initial condition of the tin processing at KIP 11 dredge PT. Timah (Persero) Tbk, has not reached the company target due to the monazite mineral participated in the tailings. At the time of observation, the arrangement of the tool and the type of ragging that was used was not appropriate in capturing the monazite minerals so that it was disposed of as tailings. The study was conducted on 27 samples. Each sample represents a different set of variables to obtain optimal results for each variable. Variables that are done change is the length of stroke 5, 10, 20 mm. The speed of the horizontal water flow is 0,1; 0,2; 0,5 m/s. Ragging is transformed into Granite because it has a specific gravity between heavy and light minerals. Granite size is 1,5; 2,5; 3,5 inch. The percentage fraction of monazite and cassiterite minerals in each sample is equal to 15%. The optimal condition was obtained in capturing monazite minerals at 20 mm length, 0,2 m/s horizontal flow rate, and 2,5 cm granite ragging. The mineral fraction percentage of monazite and cassiterite at concentrate averaged > 35% with the highest percentage mineral weight fraction reaching> 55%. While the losses on the tailings were minimized with the percentage of monazite mineral fraction was only 0 - 0.17%. Newton's efficiency is 98. Experiments in this study succeeded in increasing the percentage of monazite fraction and reducing losses.*

Keywords*: Jigging, Monazite, Optimization*

I. Introduction

Tin ore processing conducted by PT. Tin (Persero) Tbk is now more concentrated on the grade and recovery of the major minerals contained in the tin ore is cassiterite (SnO_2), while the associated minerals such as monazite (Ce, La, Y, Th) PO_3, as mineral carrier of the rare earth elements wasted in the process of processing that is at the concentration stage. The process of concentration on KIP 11 dredge starts with the sludge (slurry) which is inhaled and then supplied to the rotary filter (Trommel Screen). Undersize rotary filter will be channeled towards the jig to obtain a concentrate grade of 30-40% Sn, while Oversize will be thrown into the tailings. However oversized still contained impurity minerals among them monazite that go wasted because of less optimal performance of jigs so that the necessary

studies and efforts to optimize the performance of Jig that monazite discharged into the tailings can be minimized and recovery monazite in the processing of tin in the KIP 11 dredge Increased.

Regional Geology

Bangka Island is the largest island in the Sunda-Sunda Shelf, and is a Sunda Peneplain, has a 692 m high mountain (Mount Maras) north of Bangka and Padang Mountain 654 m south (Bemmelem, 1949). "The Indonesian Tin Island" (The Indonesian Tin Island), as people call the tin-producing islands of Indonesia, is the southernmost tip of "The Southeast Asia Tin Belt" (Southeast Asia tin line or Southeast Asian tin belt). This tin belt stretches from Central Burma (southern Shan state) to Tennaserim and continues south including West Thailand, Southern Thailand, Western Malaya Peninsula, to Karimun Kundur, Singkep, Bangka, Belitung, Karimata islands and ends at West Kalimantan (Sujitno, 2007).

In Geological Map of North Bangka Sheet scale 1: 250.000, Mangga and Djamal (1994) published by Geological Development Research Center, stratigraphy of North Bangka region from old to young as follows: Pemali (CPp), Diabas Penyabung (PTd), Granit Kelabat (TJkg), Tanjunggenting Formation (Tt), Ranggam Formation (TQr) and Aluvium (QA). Strong and broken structures have many orientations. The general direction is north-south, northeast-southwest, and southeast-northwest. Fractures and stocks are closely related to folding (Katili, 1967). The fault is a fracture up, shear, and a normal fracture. The north-south trending fault pattern is the youngest fracture phase (Mangga and Djamal, 1994). The rising and normal fault has a relatively northwest-southeast direction, as well as a horizontal fault with a relatively north-south direction cuts a relatively older fault (Crow, 2005).

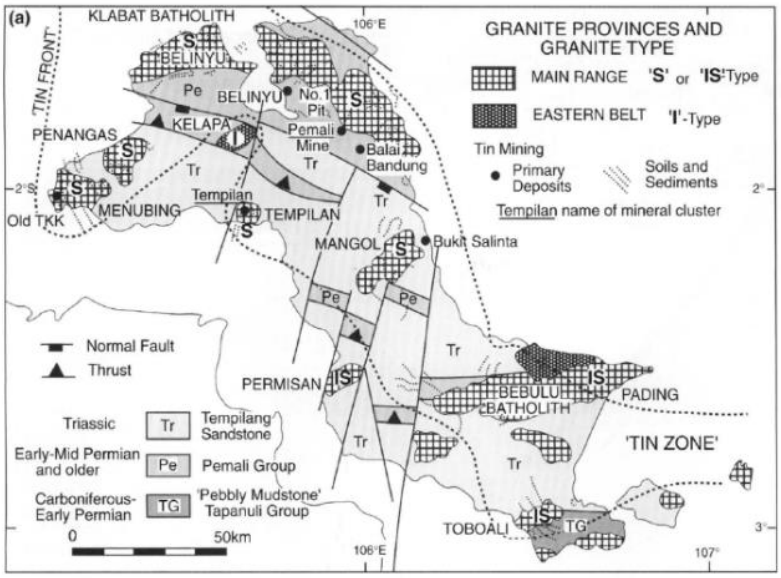

Figure 1. Primary Tin and Placer Location Map in Bangka (Crow and Van Leeuwen, 2005)

Material And Method

This experiment used a material of 27 (twenty seven) samples as a feed where each sample had the same percentage of composition that is 2000 gr of tailing of tin mining (quartz and mineral minerals), 100 gr monazite, and 200 gr of cassiterite. In addition to these samples, samples from KIP 11 suction boats were also taken for trial.

Figure 2. Mixing quartz, monazite and cassiterite samples as feeds

Experiments using Jig are done so that the separation of monazite minerals can be done optimally by changing the variable length of the stroke, horizontal water flow and the type of ragging and its size. While the other variables are fixed variables. Ragging used in this study using granite because granite has a specific gravity between monazite minerals with quartz hence more feasible when compared to ragging that has been used that is hematite. Granite stone to be used as ragging consists of 3 (three) sizes that is 1 "-2"; 2 "-3"; And 3 "-4".

The results of 60 (sixty) sample samples consisted of 27 (twenty seven) concentrate samples and 27 (twenty seven) sampling contents, and 3 (three) samples of concentrate samples and 3 (three) tailings samples which were samples of vessel KIP 11. Then the samples are delivered to the laboratory of PT. Tin (Persero) Tbk to be analyzed using GCA (grand counting analysis) method to know how much monazite and cassiterite content in the sample.

II. Result and Discussion

Design Laboratory Scale Jig

In this study, the study was conducted using a jig instrument with a smaller scale, which aims to optimize the course of research implementation. When the experiment was conducted using a Jig with a smaller scale, the jig was made to represent the jig used by the KIP 11 vessel either rheology or variation from intrinsic system conditions but with smaller scale or size.

Figure 3. JIG Apparatus

Variable Justification in Jig

In this research, this experiment is done by changing some variables on jig that is stroke length, horizontal water flow rate, and type and size of bed. These variables are chosen because the variables are significant in the jigging process and it is quite easy to make changes or changes compared to other variables because it is arranged in such a way as the standard jig and if you want to change the variables need to dismantle the jig and require sufficient cost high.

Particle Model

The material used in the research of each sample has the same weight that is 2000 gr of quartz sand, 100 gr monazite, and 200 gr cassiterite This composition is chosen to facilitate the analysis side to be easily detected whether the monazite mineral losses still occur or not. In addition, if we use a sample with a limited weight and have little concentration concentrates it will be difficult to analyze the sample statistically. These materials are materials that are concentrated from the natural conditions, so that from the size and shape of the particles, these materials present the actual particle conditions.

Laboratory Test Results and Heavy Mineral Fraction Percentage

Through the results of laboratory analysis, we can determine which samples give the best results in our experiments. The best result parameters are the absence of the monazite minerals that are wasted on the tailings or the absence of monazite mineral losses in the tailings.

Table 3. Results of sampling experiment after variable change

No.	Weight of feed (gram) (F)	Percentage (%) of Monasit Fraction in Feed (fM)	Percentage (%) of Sn Fraction in Feed (fK)	Weight of Concentrate (%)		Weight of Tailing (%)		Total Percentage (%) of Heavy Mineral Fraction (Cassiterite + Monazite) In Concentrate	Total Percentage (%) of Heavy Mineral Fraction (Cassiterite + Monazite) In Tailing
				Cassiterite (cK)	Monazite (cM)	Cassiterite	Monazite		
1	2000	5	10	17,0	9,8			29,4	0
2	2000	5	10	9,2	18,5	0,43		55,4	0,029
3	2000	5	10	7,0	17,3	0,13	1,41	52,8	0,107
4	2000	5	10	9,8	6,9			20,7	0
5	2000	5	10	4,6	6,9			20,7	0
6	2000	5	10	11,7	11,3			33,7	0
7	2000	5	10	9,1	18,5			55,6	0
8	2000	5	10	13,7	11,5	0,04	0,24	34,6	0,025
9	2000	5	10	15,7	18,1			54,1	0
10	2000	5	10	13,9	7,3			21,7	0
11	2000	5	10	6,0	7,5			22,3	0
12	2000	5	10	13,2	11,9	0,01		35,7	0,001
13	2000	5	10	8,5	6,7	0,07		20,1	0,014
14	2000	5	10	6,0	6,6			19,9	0
15	2000	5	10	7,8	8,8			26,3	0
16	2000	5	10	11,8	11,6	0,08		34,9	0,007
17	2000	5	10	14,3	9,0	0,24		26,7	0,027
18	2000	5	10	11,4	7,8	0,5		23,2	0,070
19	2000	5	10	17,0	11,8	0,05		35,3	0,004
20	2000	5	10	15,3	6,1	0,15		18,4	0,041
21	2000	5	10	11,3	8,3	0,14		24,9	0,018
22	2000	5	10	8,4	7,7	0,79	0,43	22,9	0,174
23	2000	5	10	9,6	5,6	0,02	0,01	16,7	0,015
24	2000	5	10	12,3	10,6			31,6	0
25	2000	5	10	10,8	11,1	0,05		33,3	0,005
26	2000	5	10	12,3	10,6	0,06		31,6	0,006
27	2000	5	10	11,8	7,0			20,8	0

Table 3 is the result of laboratory test of PT. Tin (Persero) Tbk uses GCA method on 54 (fifty four) samples tested. The experimental results by changing the stroke length variable, the horizontal water flow rate, and the size and type of ragging show an increase in the% mineral fraction> 15% and the losses contained in the tailings are so small that the desired target of the experiment is achieved. From these data, the graph obtained as shown in Figure 4 shows that before the experiment, the monazite and cassiterite minerals fraction is equal to 15%. After an experiment on 27 samples, the monazite and cassiterite fractions at concentrates increased significantly, and the% monazite and cassiterite fractions in the tailings were close to 0%.

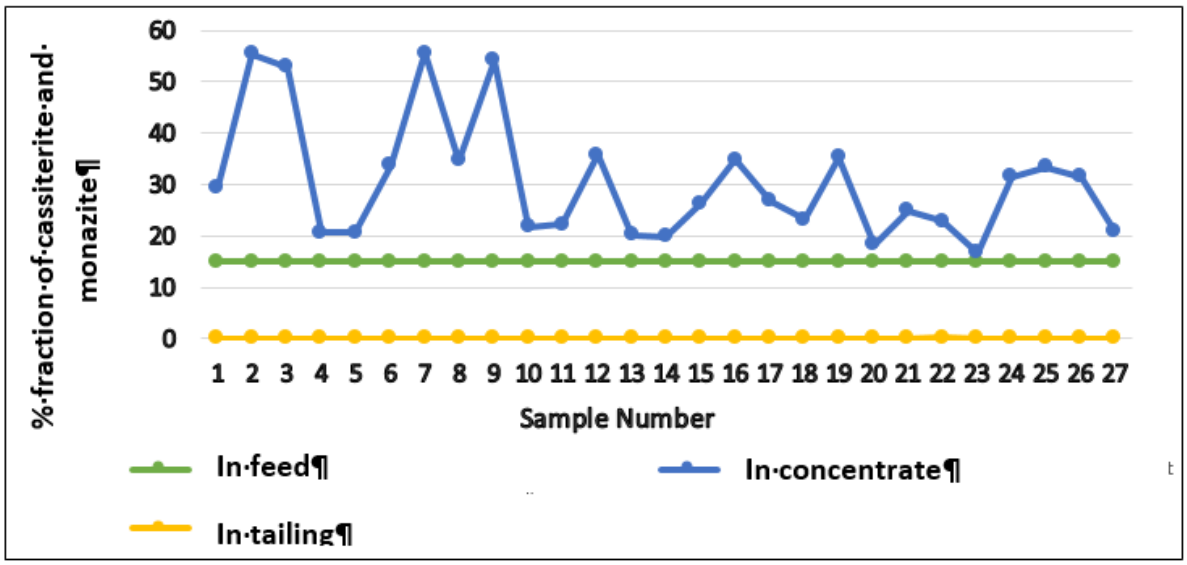

Figure 4. Percentage of monazite and cassiterite mineral fractions in bait, concentrate, and tailings

Newton's Efficiency

Newton's efficiency is a parameter that identifies the effectiveness of a separation process. Newton's efficiency formula is as follows:

$\eta N = Rc-(1-R_{fa})$

Where :

ηN: Newton's efficiency;
Rc: Recovery Monazite and Cassiterite (%);
Rfa: Quartz Recovery (%).

Recovery of monazite, cassiterite, and quartz minerals is further formulated in material balance, based on monazite and cassiterite minerals in predicted feeding, concentrates and tailings, respectively as in the following equation:

$$Rc = \frac{CcWc}{CfWf} = \frac{(Cf-Cfa)Cc}{(Cc-Cfa)Cf}\ x\ 100\%$$

$$Rfa = \frac{Wfa\,(1-Cfa)}{Wf\,(1-Cf)}\ \frac{(Cf-Cc)(1-Cfa)}{(Cfa-Cc)(1-Cf)}\ x\ 100\%$$

Where :

Wf = Weight of feed (kg);
Wc = Monazite and Cassiterite Weights at Concentrate (kg);
Wfa = Quartz Weight at Concentrate (kg);
Cf = Monazite and Cassiterite Concentrations on Feed (%);
Cc = Concentration of Monazite and Cassiterite at Concentrate (%);
Cfa = Monazite Concentration on Tailings (%).

Table 4. Newton Efficiency calculation results

Number of Sample	Weight of Feed (gram)(F)	Weight of Monazite + Cassiterite in Concentrate	Weight of Quartz in Concentrate	Concentration of Monazite and Cassiterite in Feed	Concentration of Monazite and Cassiterite in Concentrate	Monazite Concentration in Tailing	Recovery of Monazite and Cassiterite	Recovery of Quartz	Newton's Efficiency
	Wf (gr)	Wc (gr)	Wfa (gr)	Cf (%)	Cc (%)	Cfa (%)	Rc (%)	Rfa (%)	ηN
1	2000	300	720	15	29,4	0,000	100,00	-3,50	95,50
2	2000	299,14	240,86	15	55,4	0,029	99,86	-5,06	93,80
3	2000	298,33	266,67	15	52,8	0,107	99,49	-4,57	93,91
4	2000	300	1150	15	20,7	0,000	100,00	-1,96	97,04
5	2000	300	1150	15	20,7	0,000	100,00	-1,96	97,04
6	2000	300	590	15	33,7	0,000	100,00	-3,96	95,04
7	2000	300	240	15	55,6	0,000	100,00	-5,21	93,79
8	2000	299,68	565,32	15	34,6	0,025	99,91	-3,95	94,95
9	2000	300	255	15	54,1	0,000	100,00	-5,16	93,84
10	2000	300	1080	15	21,7	0,000	100,00	-2,21	96,79
11	2000	300	1045	15	22,3	0,000	100,00	-2,34	96,66
12	2000	299,98	540,02	15	35,7	0,001	100,00	-4,14	94,86
13	2000	299,86	1190,14	15	20,1	0,014	99,98	-1,80	97,18
14	2000	300	1210	15	19,9	0,000	100,00	-1,75	97,25
15	2000	300	840	15	26,3	0,000	100,00	-3,07	95,93
16	2000	299,84	560,16	15	34,9	0,007	99,97	-4,04	94,93
17	2000	299,52	820,48	15	26,7	0,027	99,92	-3,05	95,87
18	2000	299	991	15	23,2	0,070	99,83	-2,35	96,48
19	2000	299,9	550,1	15	35,3	0,004	99,98	-4,09	94,89
20	2000	299,7	1330,3	15	18,4	0,041	99,95	-1,27	97,69
21	2000	299,72	905,28	15	24,9	0,018	99,95	-2,79	96,17
22	2000	297,99	1002,01	15	22,9	0,174	99,60	-2,05	96,54
23	2000	299,95	1500,05	15	16,7	0,015	99,99	-0,70	98,29
24	2000	300	650	15	31,6	0,000	100,00	-3,75	95,25
25	2000	299,9	600,1	15	33,3	0,005	99,98	-3,91	95,07
26	2000	299,88	650,12	15	31,6	0,006	99,98	-3,73	95,25
27	2000	300	1140	15	20,8	0,000	100,00	-2,00	97,00

Table results of newton efficiency calculations can be seen in Table 4. It can be seen that sample 23 has the highest efficiency newton value of 98,28. And sample 7 has the lowest efficiency newton value of 93.78.

Data Verification Using Samples Obtained From KIP Dredge 11

Research using experiments using the particle method with this smaller tool gives a positive result. To verify, an experiment was conducted using samples taken from a KIP 11 vessel. The consideration of the selection of the vessel location as it appears in the previous chapter of the Belo Sea, Muntok is a rich area of lead minerals and the KIP 11 vessel is a vessel that contributes to the monazite as concentrate on the tin processing.

Tabel 5 : Result of the KIP 11 dredge sampling, Belo Sea, Muntok

Sample Name	Weight Of Sample (gr)	Sn Content (%)	gr Sn /Hours	% Monazite	gr Monazite /hours
Tailing 1 KIP	10.46	-	-	-	-
Tailing 2 KIP	9.94	0.01	0,00099	-	-
Tailing 3 KIP	8.5	0.04	0,0034	-	-

Tabel 6 : Result of the experiment with changing some variables

Samples Name	Weight of Sample (kg)	% Sn	Kg Sn /Hours	% Monazite	Kg Monazite /Hours
Primary Tailing 1. Right	0,298	0,0038	0,204	0,01695	0,908
Primary Tailing 2. Right	0,204	0,00545	0,2	0,01781	0,654
Primary Tailing 1. Left	0,247	0,00273	0,121	0,01218	0,54
Primary Tailing 2. Left	0,204	0,00141	0,052	0,00753	0,276
Total of Primary Tailing Right and Left (A)			**0,576**		**2,379**
Tailing of Right Clean Up	0,119	0,00602	0,077	0,01879	0,241
Tailing of Left Clean Up	0,162	0,00189	0,033	0,00675	0,118
Total of Clean Up Tailing Right and left (B)			**0,11**		**0,359**
Total of Tailing (A+B)			**0,687**		**2,738**

With a fixed particle model, the particle size distribution and density of each mineral have not changed and it becomes an important parameter in determining the separation. Preliminary data in KIP 11 as shown in Table 5 shows that the monazite loss is about 2.7 kg / hr. The condition of mineral tin separation process followed by jigging process in KIP 11 dredge is still using bed hematite as one medium heavy mineral separator with light. It is known that the hematite density ranges from 4.9 to 5.3 whereas the lead minerals are monazite which will be concentrated as concentrate having a specific gravity ranging from 4.6 to 5.7. After the change, the original bed hematite converted into granite with specific gravity between 2.6-2.7 successfully separated the monazite as a concentrate and reduced the wasted monazite in the tailings band. The difference between before and after the experiment can be seen in Table 5 and Table 6 above.

Operational Visibility

When the monazite mineral succeeds in entering the concentrate, then the cassiterite which has a higher specific gravity than the monazite also concentrated into the concentrate so that the recovery will be high but the cassiterite level will decrease. Although the cassiterite level decreases, the quantity and quantity of cassiterite itself is not reduced. There is no significant effect on the concentration of the cassiterite minerals themselves if the monazite minerals are also concentrated as concentrates on the processing of the sand.

With the inclusion of monazite minerals and other minerals that have the same or higher concentrations into the concentrate, the amount of minerals entering the concentrate will be more than before. With the increase in the quantity of concentrate it is possible that the cost of transporting the concentrate to the next processing unit will be slightly higher than before. However, the advantages of tin follow-up minerals taken as concentrates are much higher than the cost of transporting concentrate from the concentration process on board to the next processing unit.

III. Conclusions

Based on the results of the discussion, can be drawn some conclusions is the changing the ragging of hematite into granite is considered successful in capturing the optimal monazite minerals.Setting the jig variable in tin concentration process succeeds in raising the% of monazite and cassiterite fractions on the concentrate and decreasing the amount of monazite and cassiterite mineral losses on the tailings. Using surface response method can be seen that the optimum value of the experiment is at the time of variable length stroke 20 mm, 0.2 m / s horizontal flow rate, granite ragging with 2.5 inch size can reduce the losses of monazite minerals with Newton Efficiency value 97. Using a 15 mm variable stroke, a horizontal water flow rate of 0.3 m / s, and a 2.5-inch ragging size, the Newton Efficiency we get can be> 98.

References

[1]. Chehreh, C. S., 2015, A review of rare earth minerals flotation: monazite and xenotime. *Mining Science and Technology*, 877-883.

[2]. Cierpisz, S., Cyrca, M., & Sobierajski, W. (2016). Control of coal separation in jig using a radiometric meter. *Mineral Engineering Elsevier*, 59-65.

[3]. Crespo, E. F., 2015. Modeling segregation and dispersion in *jigging* beds in terms of the bed porosity distribution, *Mineral Engineering Elsevier*, 38-48.

[4]. Gupta, C., 2003, *Chemical Metallurgy: Principles and Practice, Chapter 2: Mineral Processing.* Weinheim: Wiley-VCH.

[5]. Hafni., 2000, Pengolahan Monasit dari Limbah Penambangan Tin : Pemisahan Logam Tanah Jarang (RE) dari U dan T, *Prosiding Presentasi Ilmiah*, 54-60.

[6]. Katili, J., 1966, Structure and Age of The Indonesian Tin Belt with Special Reference to Bangka, *Tectonophysics*, 403-418.

[7]. Kumari, A., 2015, Process development to recover rare earth metals from monazite mineral : A review, *Minerals Engineering*, 102-115.

[8]. Maninji, L., 2015, *Geology and Deposit Model of Primary Tin Mineralization in Bangka Island Indonesia; Case Study on Pemali Tin Mine,* Yogyakarta: Gadjah Mada University.

[9]. Ng, S, W-P., W-P., Whitehouse, M.J., Roselee, M.H., Teschner, C., Murtadha, S., Oliver,G.J.H., Ghani, A.A., Chang, S-C., 2017, Late Triassic granites from Bangka, Indonesia: A continuation of the Main Range granite province of the South-East Asian Tin Belt. *Journal of Asian Earth Science*, 548-561.

[10]. Sujitno, S., 2007, *Sejarah Penambangan Tin di Indonesia Abad 18 - Abad 20.* Pangkalpinang, Bangka: PT. Tin (Tbk).

[11]. Viduka, S. M., (2013). Discrete Particle Simulation of Solid Separation in A Jigging Device. *International Journal of Mineral Processing*, 108-119.

Voltage Profile Improvement through Load Shedding Action Using Linear Programming-based Optimal Power Flow (#738)

Lukmanul Hakim[1,a], Annisa Zauhar Nafisah[1], Herri Gusmedi, Khairudin[1]
Electrical Engineering Departement, University of Lampung, Bandar Lampung, 35145, Indonesia
[a]plgsekip@eng.unila.ac.id

Abstract**—***This paper proposes a load shedding scheme to improve voltage profile of a power system. A linear programming approach to optimal power flow is utilized to obtain optimum amount of load to shed in order to bring power system to an acceptable operating region. In this work, ±5% voltage variation is considered to be acceptable and hence, an immediate control action should be taken if power system is operated beyond this limit. The proposed method was tested on the IEEE 57-bus test system. Results showed that the proposed approach was able to provide a minimum amount of load shedding action to improve voltage profile of the studied power system.*

Keywords**—***voltage profile improvement, load shedding, linear programming, optimal power flow*

I. Introduction

RECENT increase in power system loads has led such power system to operate near, even violate, its acceptable limits. In a short span of operating time horizon, an emergency action is commonly adopted to bring power system to a secure operating condition. One example of such emergency action is load shedding where a certain amount of load is required to be shed from the system to improve the overall performance of the power system.

In terms of time horizon, load shedding can be used to improve both transient (as an emergency action of a special protection system) and steady state security. As for power system variables, load shedding is usually carried out in the case of under frequency or under voltage occurs. Examples of utilizing load shedding for mitigating under frequency conditions are provided in [1], [2]. For mitigating under voltage problems, load shedding is utilized in [3]-[9]. Congestion management is also a class of problem to solve using load shedding. Such work was reported in [10].

In this work, voltage at all buses must be within the ±5% voltage variations from the nominal voltage. In order to achieve it, a minimum amount of load must be shed from the system if current loading condition results in under voltage situation. Therefore, a linear programming-based optimal power flow method is utilized to find the location where minimum load shedding can be carried out to bring bus voltage to be within the ±5% limits. This work extends our previous works as reported in [11], [12] by utilizing polar representation of the bus complex voltage. In [12], linear programming optimal power flow was applied to reactive power allocation problem while in this work, the method is modified to find optimum load shedding amount for voltage profile improvement. Moreover, to allow easier handling of voltage magnitude constraint, voltage is represented in polar coordinate using vector form which differs from rectangular representation in our previous works.

II. Problem Formulation

Mitigating voltage violation can be approached by actuating controls available in power system to bring it to its secure operating conditions. In this work, load shedding is an available control action. Therefore, final complex load at bus *k* after load shedding is:

$$S_k^{new} = S_k^{spec} - S_k^{shed} \quad (1)$$

The amount of load shedding per iteration may move towards both positive and negative directions. To accommodate this nature, load shedding variable is represented by two additional slack variables for both positive and negative directions during iteration process. Therefore total amount of load shedding at each bus of current iteration is updated by the following equation:

$$S_k^{shed} = S_k^{+} - S_k^{-} \quad (2)$$

Please note that in this work, load power factor remains constant as specified in the input data. In order to maintain power factor at bus *k*, relationship between active power and reactive power load held by the following relationship:

$$\rho_k = \tan\left(\cos^{-1}\left(P_k / \sqrt{P_k^2 + Q_k^2}\right)\right) \quad (3)$$

Due to additional slack variables of load shedding, complex power mismatch equation per iteration in equation (4) can be modified by accommodating equation (2) and results in equation (5):

$$\Delta S = S_{scheduled} - S_{calculated} \quad (4)$$

$$\Delta S - S_{load}^{+} + S_{load}^{-} = S_{gen} - S_{load}^{spec} - S_{calculated} \quad (5)$$

It is of important that the amount of load to be shed must be minimal and this can be achieved by using optimization method. Linear programming, due to its speed and robustness, is the preferable choice and incorporated into optimal power flow solution. Therefore, the linear objective function is minimization of overall load to be shed subject to operational power system constraints including the ±5% variations of nominal voltage at each bus. Equations (6) and (7) show the optimization model of load shedding minimization for voltage profile improvement. In this model, any changes in other variables, apart from the load shedding variables, have no cost associated to them.

Objective function:

$$min. \sum_{k \in K} C_k^{+} \cdot P_k^{+} + C_k^{-} \cdot P_k^{-} \quad (6)$$

Subject to:

$Real\left\{\frac{\partial \Delta S}{\partial V}\right\}$	$Real\left\{\frac{\partial \Delta S}{\partial \theta}\right\}$	-1	1	0	0	0	0	-1	1	0	0
$Imag\left\{\frac{\partial \Delta S}{\partial V}\right\}$	$Imag\left\{\frac{\partial \Delta S}{\partial \theta}\right\}$	0	0	-1	1	-1	1	0	0	-ρ	ρ

$$\cdot \begin{bmatrix} \Delta V_i \\ \Delta \theta_i \\ P_g^+ \\ P_g^- \\ Q_g^+ \\ Q_g^- \\ Q_s^+ \\ Q_s^- \\ P_k^+ \\ P_k^- \\ Q_k^+ \\ Q_k^- \end{bmatrix} = \begin{bmatrix} Real\{\Delta S_i\} \\ Imag\{\Delta S_i\} \end{bmatrix} \quad \square\square\square$$

$i \in \mathbf{N};\ g \in \mathbf{G}; s \in \mathbf{S};\ k \in \mathbf{K}$

For all generators and loads, S = P ± *j*Q
Where :

S	is complex power injection at each bus in power system
ΔS	is mismatch of complex power injection *S*
ΔV	is voltage magnitude update variable at each bus
Δθ	is voltage angle update variable at each bus
P_g^+	is active power generation update variable in positive axis
P_g^-	is active power generation update variable in negative axis
Q_q^+	is reactive power generation update variable in positive axis
Q_q^-	is reactive power generation update variable in negative axis
Q_s^+	is reactive power synchronous condenser update variable in positive axis
Q_s^-	is reactive power synchronous condenser update variable in negative axis
P_k^+	is active power load shedding update variable in positive axis
P_k^-	is active power load shedding update variable in negative axis
Q_k^+	is reactive power load shedding update variable in positive axis
Q_k^-	is reactive power load shedding update variable in negative axis
ρ	is trigonometric tangent of power angle
C_k^+	is cost coefficient of active power load shedding update variable in positive axis
C_k^-	is cost coefficient of active power load shedding update variable in negative axis
N	is a set of all buses in power system
G	is a set of all generator buses in power system
S	is a set of all synchronous condenser buses in power system
K	is a set of all load buses in power system

In this model, all variables of voltages and powers are limited by their respective operational

constraints.

Voltage is updated by the following equations:

$$V = V + \Delta V \quad (8)$$
$$\theta = \theta + \Delta\theta \quad (9)$$

III. Results and Discussions

The proposed method was applied to the IEEE 57-bus test system [13]. Single line diagram of this system as well as system data is available online in the public domain from [13]. By solving the base case, it was observed that this test system suffers from voltage violation of the acceptable ±5% variations. Base case scenario was conducted using standard Newton-Raphson power flow analysis.

As seen in figure 1, bus 31 experiences low voltage profile of below 95% limit in the base case scenario. Total load connected to this bus is 5.8 MW of active power and 2.9 MVAr of reactive power. In order to bring voltage magnitude at this bus to be within the acceptable limits, a certain amount of load must be shed. The same test system was then calculated using the proposed method to obtain how much load must be shed and at which bus. In this case, we assume that cost of performing this control action is similar at any bus, however; accommodating different cost coefficient to different bus for taking into account different contract scheme is trivial in the proposed formulation.

The proposed method suggested that 0.8025 MW and 0.4012 MVAr must be shed from Bus 31 in order to bring its voltage magnitude at 95% of the nominal voltage. Voltage profile of the IEEE 57-bus system after load shedding is shown in figure 2.

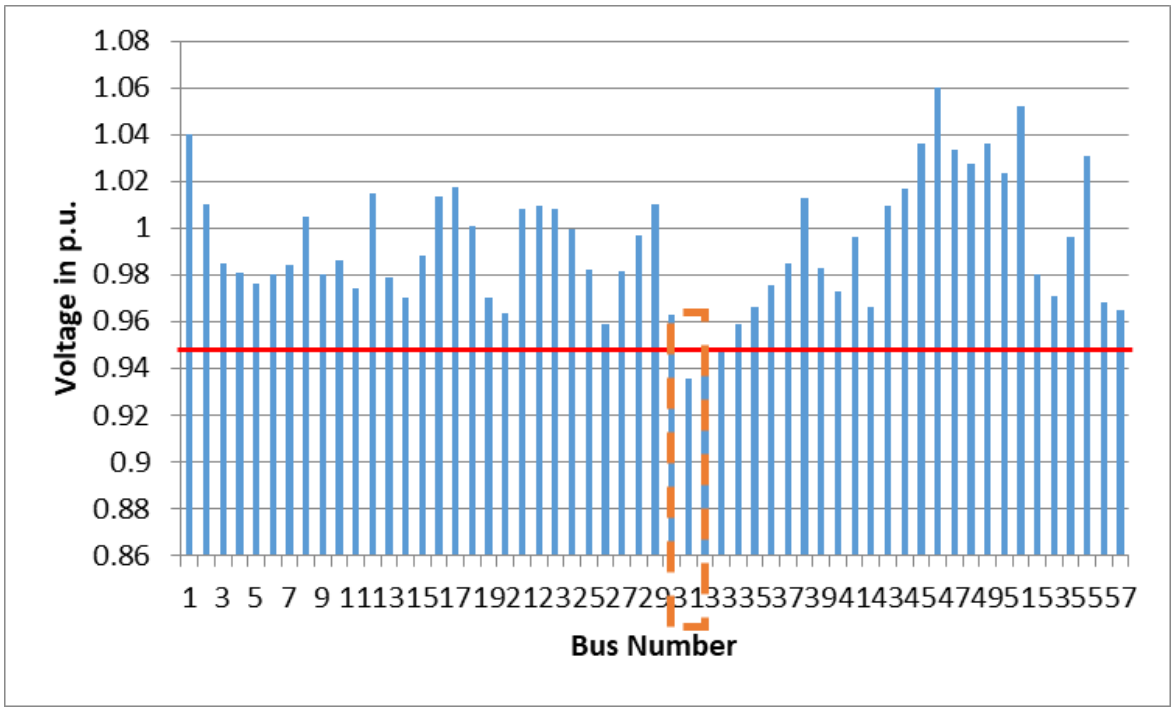

Figure 1. Voltage profile of base case scenario of IEEE 57-bus

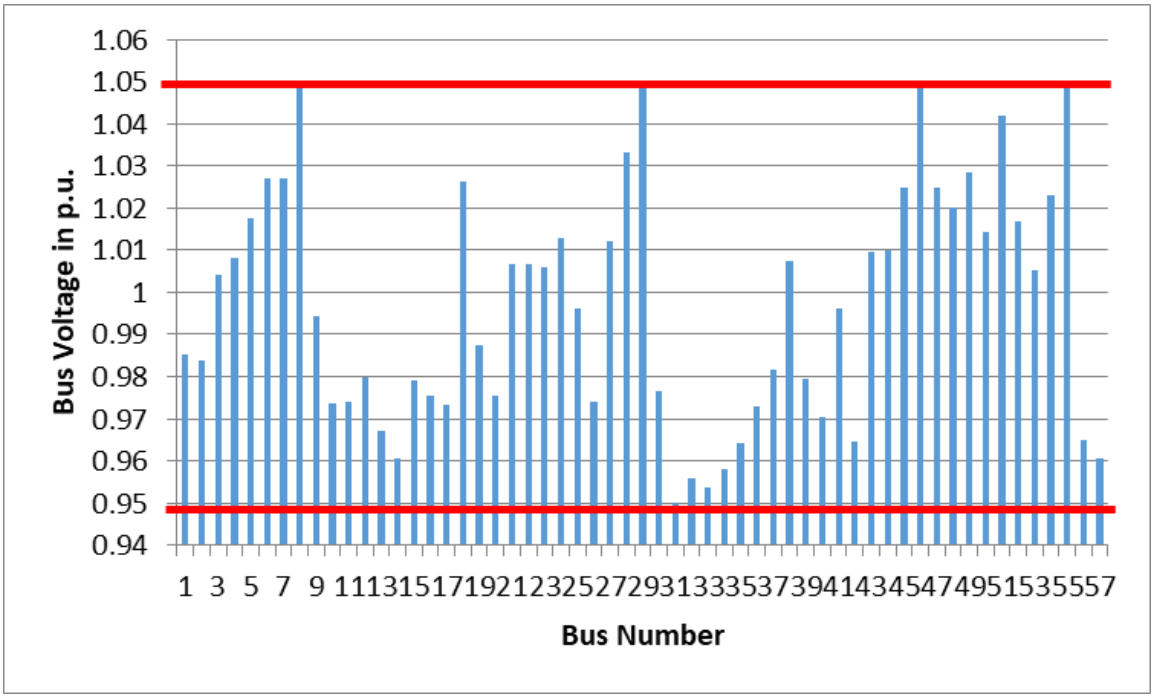

Figure 2. Voltage profile of IEEE 57-bus after load shedding

The next test for the developed method is solving low voltage profile problem in many buses. In this case, the IEEE 57-bus is modified such that it is loaded 1.3 times of the original loading condition. This is achieved by multiplying all initial loads with a scalar value of 1.3. This increase of loading condition results in almost one-third of total buses suffers from voltage magnitude of lower than 95% limit. Voltage profile of this situation is indicated in figure 3.

In order to tackle this poor voltage profile in figure 3, the developed method suggested a total of 11.61 MW load to be shed. Due to very low voltage magnitude at Bus 31, i.e. 84% of the nominal voltage, a large amount of load is required to be shed, i.e. 5.24 MW. Table 1 shows the amount of load shedding required to improve voltage profile of the modified case of the IEEE 57-bus. An improved voltage profile is shown in figure 4.

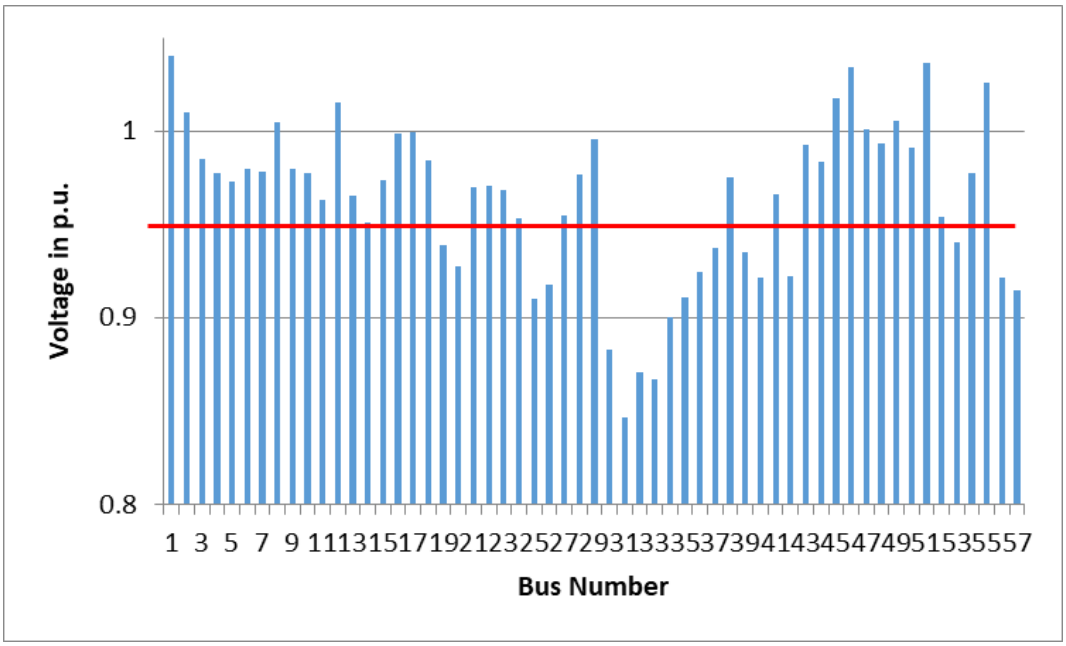

Figure 3. Voltage profile of modified loading scenario of IEEE 57-bus

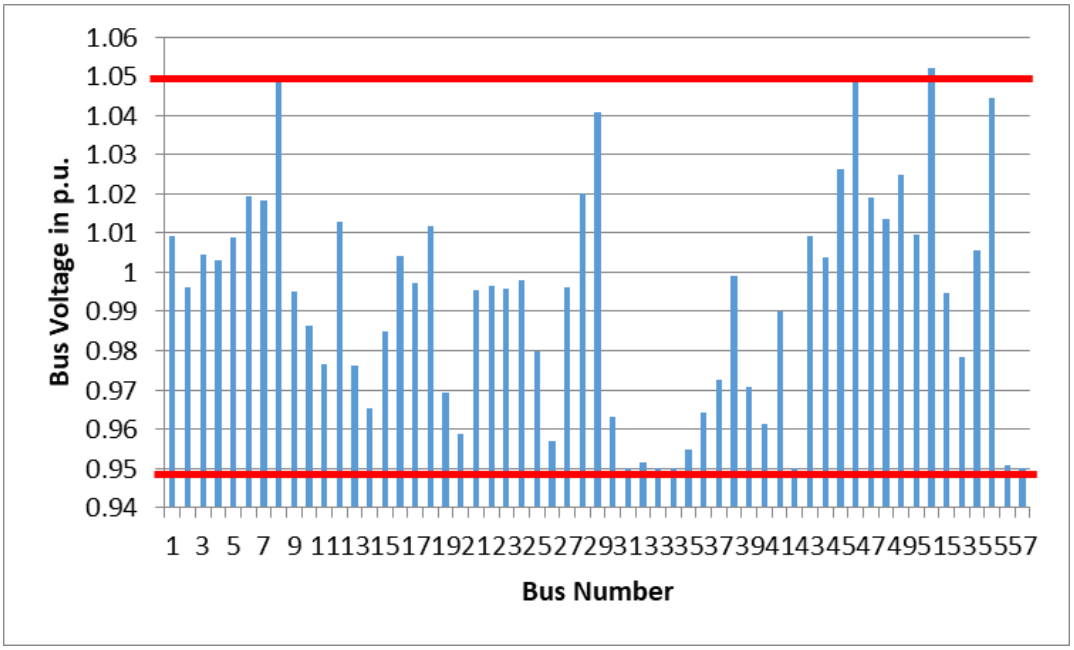

Figure 4. Voltage profile of modified loading scenario of IEEE 57-bus after load shedding

TABLE 1. LOCATION AND AMOUNT OF LOAD SHEDDING REQUIRED

Bus #	Active Power Load Shedding	Reactive Power Load Shedding
31	5.24 MW	2.62 MVAr
33	2.39 MW	1.19 MVAr
42	0.25 MW	0.16 MVAr
57	3.73 MW	1.11 MVAr

IV. Conclusions

System suffers from low voltage magnitude profile or experiences under voltage condition, requires an emergency action to bring such system to an acceptable operating region. In this work, load shedding is proposed as the control action and the amount load to be shed is calculated by means of linear programming-based optimal power flow. Two cases were considered in this work, i.e. single bus and several buses experience under voltage. Results show that the developed approach is able to provide minimum amount of load shedding to bring the voltage to acceptable limits. Future work will include more control variables to the formulation and application of the developed approach to smart grid may be further examined.

References

[1] Das, K., Nitsas, A., Altin, M., Hansen, A.D., Sorensen, P.E., "Improved load shedding scheme considering distributed generation," IEEE Trans. on Power Delivery, vol. 32, no. 1, Feb. 2017, pp. 515-524.

[2] Hirodontis, S., Crossley, P.A., "Load shedding in a distribution network," Proc. of 2009 Int'l Conf. on SUPERGEN, Nanjing, 6-7 April 2009

[3] Pushpendra Singh, Titare, L.S., Arya, L.D., Choube, S.C., "Strategy to Optimize the Load Shedding Amount Based on Static Voltage Stability using SFLA," Proc. of 2016 Biennial Int'l. Conf. on PESTSE, Bangalore, 21-23 Jan. 2016

[4] Echavarren, F.M., Lobato, E., Rouco, L., "A corrective load shedding scheme to mitigate voltage collapse," Int'l Journal of Electrical Power and Energy Systems, vol. 28, no. 1, 2006, pp. 58-64

[5] Perumal, N., Amran, A.C., "Automatic load shedding in power system," Proc. of 2003 Power Engineering Conference, Bangi, 15-16 Dec. 2003.

[6] Wang, Y., Pordanjani, I.R., Li, W., Xu, W., Vaahedi, E., "Strategy to minimize the load shedding amount for voltage collapse prevention," IET Gen. Trans. & Dist., vol. 5, no. 3, March 2011, pp. 307-313.

[7] Aziah, K., Shareef, H., Mohamed, A., "Islanding detection and load shedding scheme for radial distribution systems integrated with dispersed generations," IET Gen. Trans. & Dist., vol. 9, no. 15, Nov. 2015, pp. 2261-2275.

[8] Kaffashan, I., Amraee, T.,"Probabilistic undervoltage load shedding using point estimate method," IET Gen. Trans. & Dist., vol. 9, no. 15, Nov. 2015, pp. 2234-2244.

[9] Dehghan, S., Darafshian-Maram, M., Shayanfar, H.A., Kazemi, A., "Optimal load shedding to enhance voltage stability and voltage profile based on a multi-objective optimization technique," Proc. of 2011 IEEE PowerTech, Trondheim, 19-23 June 2011.

[10] Surender Reddy, S., "Multi-objective based Congestion Management using Generation Rescheduling and Load Shedding," IEEE Trans. on Power Systems, vol. 32, no. 2, May 2016, pp. 852-863.

[11] Hakim, L., Wahidi, M., Handoko, T., Gusmedi, H., Soedjarwanto, N., Milano, F.,"Development of a power flow software for distribution system analysis based on rectangular voltage using python software package," Proc. of 2014 ICITEE, Yogyakarta, 7-8 Oct. 2014.

[12] Hakim, L., Murdika, U., Gusmedi, H., Zaini, S., "A study on reactive power allocation for electrical power distribution system with low voltage profile," ARPN Journal of Engineering and Applied Sciences, vol. 11, no. 7, April 2016, pp. 4767-4771.

[13] Dabbagchi, I., Christie, R., "Power System Test Case Archive: 57 Bus Power Flow Test Case," University of Washington Electrical Engineering, Washington, August 1993 [Online]. Available: https://www2.ee.washington.edu/research/pstca/pf57/pg_tca57bus.htm

The Synthetic Activities of TiO_2 - *Moringa Oleifera* Seed Powder in the Treatment of the Wastewater of the Coal Mining Industry (#741)

Marhaini[1,a], Legiso[1,b], Trilestari[1,c]
[1]Department of Chemical Engineering, Faculty of Engineering, Muhammadiyah University, Palembang, Indonesia
[a]marhainiump@yahoo.co.id, [b]legiso_poniman@yahoo.co.id, [c]trilestari1994

Abstract. *To process the coal wastewater, the combination of chemical based technology of Advanced Oxidation Process (AOP) of a strong oxidizer using TiO_2 photocatalyst and biological treatment of moringa seed powder (Moringa oleifera) is used in the composite form. AOP can be used as an alternative treatment of coal wastewater which is quite economical and environmentally friendly. The XRD results of TiO_2 powder and the synthesis of TiO_2 - is moringa seed powder in the form of tetragonal crystals. The degradation results of the quality of the coal wastewater using TiO_2 powder reached a decrease of (TSS, Fe, Mn, Zn, Hg, Cu, Co, Cr, Al and Ni) by an average of 70% and the increase of pH value of 7 at 200 minute stirring time. The decrease of the wastewater quality using the synthesis of TiO_2- moringa seed powder by using sunlight and without sunlight is detected negative (-) at 200 minute stirring time.*
Keywords: *Advanced Oxidation Process (AOP), moringa oleifera seed, Degradation, TiO_2*

I. Introduction

The release of heavy metals from the wastewater of coal mining industry has become a threat to the ecosystem [1]. One of the damages that occurs in coal mining activities is the decrease in water pH due to the interaction between the atmosphere, water and rocks. The decrease in the pH of water is not only due to the interaction between the atmosphere, water and rocks, but also due to the coal itself which can lead to acid mine drainage, because generally coal has a humidity range of between 2 - 40%, sulfur content of 0.2 - 8% and ash content of 5 - 40% which can have an effect on the value of coal as an energy source that can cause pollution in its use. Acid mine drainage has a high acidity and is often characterized by a lower pH value below 5.[9] In addition, acid mine drainage will erode soil and rocks that causes dissolving of various metals such as iron (Fe), cadmium (Cd), manganese (Mn), zinc (Zn), mercury (Hg), nickel (Ni), cobalt (Co) , Cadmium (Cd), lead (Pb) and arsenic, which are heavy metals known for their non-degradable toxicity and are largely non-biodegradable. Therefore, in addition to having a low pH, acid mine drainage also contains high concentrations of metals that can adversely affect both environmental and human health and their presence above specified limits in the body can cause severe damage to the body's vital organs, such as the kidney, the liver and the brain, the reproductive system and the nerves.[10]

To overcome this problem, coal wastewater treatment needs to be carried out by combining applied technology, namely chemical-based technology of Advanced Oxidation Process (AOP) using strong oxidizer by using photocatalyst of TiO_2 and biology of Moringa oleifera seed powder in composite form. This advanced oxidation process can be used as an economically viable alternative wastewater treatment.[22] Commercially, TiO_2 powder is also easy to obtain and to produce in large quantities.[20] In addition, TiO_2 is a semiconductor that

has a melting point, photoactivity, high thermal and chemical stability, has a non-toxic nature and also one of the best catalysts to be applied in the environment because of its inert biological and chemical properties and the price is relatively cheap.[12] Based on its properties, TiO_2 is the most effective photocatalyst to be used, as one of the semiconductor materials, and has been widely studied mainly in the processing of solar energy sources and the processing of hazardous waste,[15] and it is also used for hospital waste treatment.[7] TiO_2 photocatalyst is highly efficient in reducing heavy metals of Fe, Cr and Pb in wastewater by 96-98% and TiO_2 photocatalyst through the sunlight shows higher result in degrading dye waste compared to commercial TiO_2.[6] According to previous studies Moringa seeds contain bioactive compounds of rhamnosyloxy-benzyl-isothiocyanate, which is able to adopt and neutralize the particles of sludge and metals contained in the suspension waste with dirt particles floating in water and their effect on the content of bacteria Coli, Moringa oleifera seeds can reduce bacteria Coli by about 28%.[14]

II. Research Method

One hundred fifty (150) ml of Moringa seed powder solution is added with 300 gram of sol Tetanium Tetra Isopropoxide (TTIP) which is then stirred with stirrer slowly for 24 hours at room temperature to form a nanoparticle suspension. The suspension is sonicated for 30 minutes. Then, it is evaporated to free water and calcined at a temperature of 500°C for 2 hours. The wastewater of the coal industry of 2 L is added to the photocatalytic synthesis of TiO_2-powder of moringa seed. The activity test is carried out without sunlight and with sunlight for 50 minutes, 100 minutes, 150 minutes, 200 minutes, 250 minutes and is added with 1.0 mL H_2O_2 30% . Then it is put into the reactor, stirred at a speed of 60 rpm. The results of the observation were analyzed using AAS (Atomic Absorption Spectophotometry) to measure the quality of residual wastewater degradation and X-Ray Diffraxion (XRD) for the analysis of the concentration test of the synthesis of TiO_2-Moringa oleifera seed powder.

III. Research Results and Discussion

A. Analysis Results of XRD Synthesis of TiO_2- Moringa oleifera Seed Powder

The XRD results of TiO_2 powder and the synthesis of TiO_2- Moringa oleifera Seed Powder in the anatase phase are shown in Figures 1a and 1b.

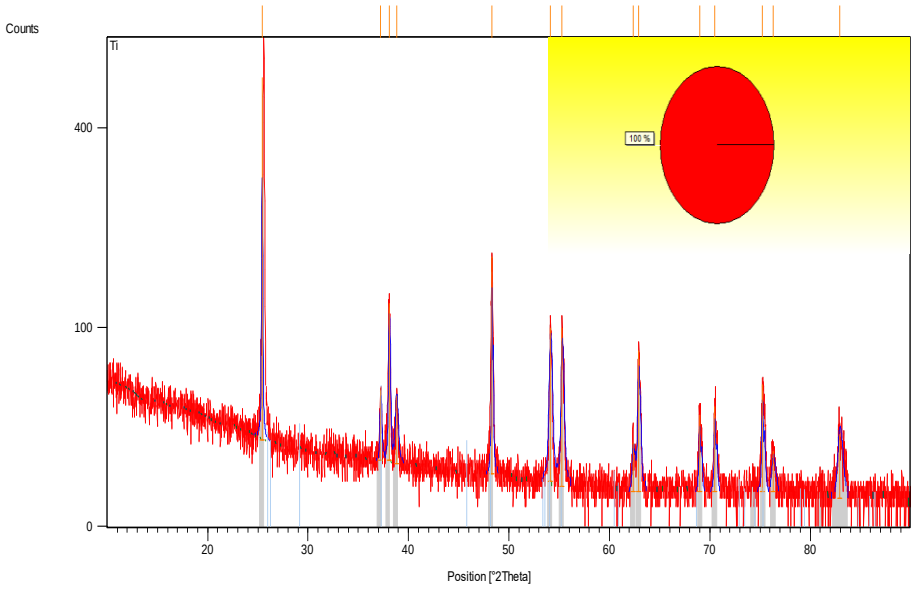

Figure 1a. XRD TiO_2

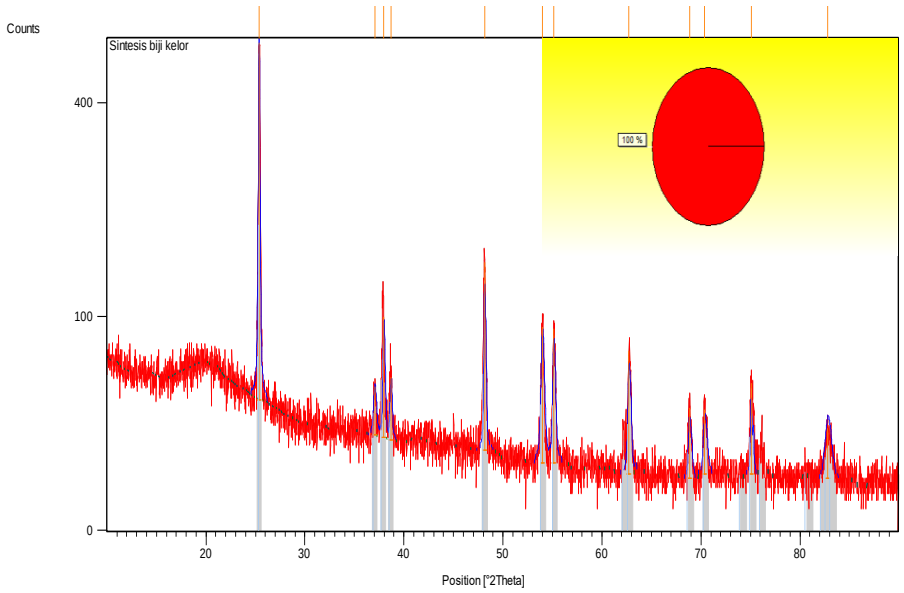

Figure1b. XRD Synthesis TiO_2-Moringga oleifera

The results of the study showed that the powder of TiO_2 and the synthesis of TiO_2-Moringa oleifera seed powder had a tetragonal crystalline form with the space group of 141 / amd and the lattice parameter data as shown in Table 1.

Table 1. Lattice parameters of TiO_2 and Synthesis of TiO_2-Moringa oleifera Seed Powder

Sample	a (Å)	b (Å)	c (Å)	Alpha (°)	Beta (°)	Gamma (°)
TiO_2	3,7760	3,7760	9,4860	90	90	90
Synthesis of TiO_2-Moringa oleifera Seed Powder	3,7760	3,7760	9,4860	90	90	90

B. The Effects of the Quality of Coal Wastewater using TiO_2 Crystals

The ability of TiO_2 as a photocatalyst is to provide H^+ with a large oxidation radical. It can provide a continuous hydroxyl radical in accordance with the source of the light. The nature of TiO_2 as a strong oxidizer makes it capable of oxidizing heavy metal compounds contained in coal wastewater. The results of the measurement of the quality of the coal wastewater using TiO_2 with the stirring variables showing a rise in pH up to 7 in 250 minute stirring time and decreasing the quality of wastewater (TSS, Fe, Mn, Zn, Hg, Cu, Co, Cr, Al and Ni) reaching the average of 70% in stirring time of 200 minutes (Table 2). This is because TiO_2 is a strong oxidant that is chemically and biologically inert, producing OH ions and can oxidize and mineralize almost all chemicals that are environmentally friendly [15,23] and can also damage microbial cells by attacking cell walls, cytoplasmic membranes and intracellular structures.[18]

Table 2. The Effect of the Quality of Coal Wastewater on TiO_2 Crystals

Parameters	Quality of Wastewater	Maximum Concentration*	Unit	Stirring Time (Minutes)				
				50	100	150	200	250
TSS	70	200	mg/L	60	45	27	12	2
pH	2,68	6 - 9	mg/L	3,5	5	6,3	6,8	7
Fe	15	7	mg/L	14,8	11,5	8,2	5,6	1,9
Mn	10	4	mg/L	9,32	7,35	5,29	2,47	0.88
Zn	5	5	mg/L	4,39	3,67	2,56	0.98	<0,01
Hg	0,0045	0,002	mg/L	0.0040	0,003	0,0021	0,001	<0,001
Cu	2,5	2	mg/L	2,5	2,13	2,01	1,99	1,72
Co	0,5	0,4	mg/L	0,49	0,35	0,31	0,29	0,25
Cr	0,7	0,5	mg/L	0,69	0,62	0,62	0,51	0,45
Al	2,4	0,5	mg/L	1,73	1,23	0,89	0,13	<0,001
Ni	0,25	0,2	mg/L	0,24	0,19	0,001	<0,001	<0.001

C. The Effects of Using Synthesis of TiO_2-Moringa oleifera Powder With Sunlight and Without Sunlight on the Quality of Coal Wastewater

The test of the effects of long illumination shows that the longer the time spent in illumination using sunlight, the more heavy metal concentration (TSS) will decrease and the higher the value of pH will be. TiO_2 photocatalyst material has a very strong oxidizing power when activated by sunlight. The results of the study are shown in Table 3.

Table 3. Effects of Using Synthesis of TiO_2-Moringa oleifera Seed Powder Without Sunlight on the Quality of Coal Wastewater

Parameter	Quality of the Wastewater (mg/L)	Stirring time (Minutes)									
		Without Sunlight Illumination					With Sunlight Illumination				
		50	100	150	200	250	50	100	150	200	250
TSS	70	55	35	21	7	(-)	56	23	8	(-)	(-)
pH	2.68	4.2	6.5	7	7.2	7,5	4.5	6.4	7	7.2	7.5
Fe	15	13.46	10.21	6.47	1.21	(-)	11.5	5.24	0.001	(-)	(-)
Mn	10	8.32	6.21	3.15	0.001	(-)	10.24	5.98	0.0097	(-)	(-)
Zn	5	4.12	3.07	1.01	<0.001	(-)	3.13	1.45	0.001	(-)	(-)
Hg	0.0045	0.0021	0.0013	<0.001	<0.001	(-)	0.001	0.0001	<0.0001	(-)	(-)
Cu	2.5	2.01	1.001	<0.001	<0.001	(-)	1.99	0.467	0.005	(-)	(-)
Co	0.5	0.32	0.101	<0.001	<0.001	(-)	0.003	0.0001	<0.0001	(-)	(-)
Cr	0.7	0.69	0.037	0.001	<0.001	(-)	0.001	<0.001	<0.001	(-)	(-)
Al	2.4	2.09	1.27	0.001	<0.001	(-)	1.78	0.0497	0.001	(-)	(-)
Ni	0.25	0.199	0.0009	0.001	<0.001	(-)	0.21	0.007	<0.001	(-)	(-)

The results of the observations with naked eyes showed that the wastewater that was originally yellow looked more clear with the addition of illuminating time, so that the results of the wastewater quality of 200 minutes stirring time showed a negative result, but the results of the analysis without the use of sunlight with 250 minutes stirring time just produced negative water quality. The wastewater treatment conducted through AOP (TiO_2) by sunlight[11-16,4-18] could substantially reduce waste treatment costs and was more favorable from an environmental perspective.[17] The effect of adding 30% H_2O_2 is enlarging the concentration of coal wastewater quality and more ^oOH is produced through reduction reactions. Excessive H_2O_2

can have a negative effect on degrading heavy metals in coal wastewater rather than ^{o}OH which can partially reshape H_2O_2. HO_2^{o} can prevent the transfer of photon energy, this is because HO_2^{o} is a gas molecule that is not dissolved, and occurs only on the surface of the photocatalyst.[25]

IV. Conclusions

The degradation of coal wastewater quality using TiO_2 shows that the quality of wastewater at 200 minutes of stirring time reaching an average of 70%. The synthesis of TiO_2- Moringa oleifera seed powder with and without illumination of sunlight can be applied as a coal wastewater treatment with a stirring time of 200 minutes resulting in a decrease in the quality of coal wastewater which is detected negative.

References

[1]. Achla Kaushal, S.K., Singh.2017.Removal of Heavy Metals by Nanoadsorbents: A review. Journal of Environment and Biotechnology Research, Vol 6,No.1,96 - 104

[2]. Arung, E.T., 2002. Breakthrough, Seed of Moringa oleifera as River Water Purifier, Suara Merdeka, Jakarta

[3]. Byrne, J.A., Fernandez-Ibanez, P.A., Dunlop, P.S., Alrousan, D.; Hamilton, J.W. 2011. Photocatalytic Enhancement for Solar Disinfection of Water: A Review. Int. J. Photoenergy ,doi:10.1155/2011/798051.

[4]. Blanco, J., Malato, S.,Fernández-Ibañez, P., Alarcón, D., Gernjak, W., Maldonado, M. 2009. Review of feasible solar energy applications to water processes. Renew. Sust. Energ, 13, 1437–1445.

[5]. Byrne, J.A., Dunlop, P.S., Hamilton, J.W., Fernandez-Ibanez, P., Polo-Lopez, I.,Sharma, P.K., Vennard, A.S. 2015. A review of Heterogeneous Photocatalysis for Water and Surface Disinfection. Molecules, 20, 5574–5615.

[6]. Chih-Ho Su.,Chi-Cheng Hu.,Yen-Chun Sun.,Yu-Cheng Hsioo. 2016. Highly active and thermo-stable anatase TiO_2 photocatalysts synthesized by a microwave-assisted hydrothermal method, Journal of the Taiwan Institute of Chemical Engineering

[7]. Chong.M.N.,Cho.Y.J.,Poh.P.E.,Jin.B. 2014. Evaluation of Titanium Dioxide Photocatalytic Technology for the Treatment of Reactive Black 5 dye in Synthetic and Real Grey Water Effluents. Journal of Cleaner Production 89.

[8]. Fatta-Kassinos, D., Meric, S. 2011. Nikolaou, A. Pharmaceutical Residues in Environmental Waters and Wastewater: Current State of Knowledge and Future Research. 399, 251–275.

[9]. Gautama, Rudy Sayoga. 2012. Management of Acid Mine Drainage. Technical Guidance, Reclamation and Post-Mining In Minerals and Coal Mining Activities - DIRECTORATE GENERAL OF MINERALS AND COAL, MINISTRY OF ENERGY AND MINERAL RESOURCES.

[10]. Goel,P.K.2006.Water Pullution Causes Effects and Control (Revised 2nd Edition). New Age International pubblishers, New Delhi. India

[11]. Gogate, P.R.; Pandit, A.B. 2004. A Review of Imperative Technologies for Wastewater Treatment I: Oxidation Technologies at Ambient Conditions. Adv. Environ. Res. 8, 501–551.

[12]. Hoffmann, M.R., S.T. Martin., W. Choi, dan Bahnemann.D.W 1995. Environmental Applications of Semiconductor Photocatalysis. Chemical Reviews. 95

[13]. Johnson, D. Barrie; Hallberg, Kevin B; Acid mine drainage remediation options: A review; Science of the Total Environment 338 3– 14, 2005

[14]. Juli N., Suriawilis U., Birsyam I., 1986. *Exploratory Study* of Natural Plant-Based Coagulant Materials and their Effects on Coli Bacterial Content, Ministry of Education and Culture, *Institute* of *Technology*, *Bandung* (ITB)

[15]. Lu.C.H.,Wu.W.H.,Kale.R.B. 2008. Micro Emulsion-Mediated Hydrothermal Synthesis of Photocatalytic TiO_2 Powders.J.Hazard.Mat 154

[16]. Malato, S., Fernández-Ibáñez, P., Maldonado, M.I., Blanco, J., Gernjak, W 2009. Decontamination and Disinfection of Water by Solar Photocatalysis: Recent Overview and Trends. *147*, 1–59.

[17]. Munoz, I., Peral., J.Ayllon, J.A.,Malato, S., Passarinho, P.,Domenech, X. 2006. Life Cycle Assessment of a Coupled Solar Photocatalytic-Biological Process for Wastewater Ttreatment. 40, 3533–3540.

[18]. Oller, I., Malato, S.,Sánchez-Pérez, J. 2011. Combination of Advanced Oxidation Processes and Biological Treatments for Wastewater Decontamination—A review. *409*, 4141–4166.

[19]. Robertson, P.K.,Robertson, J.M.,Bahnemann, D.W.2012. Removal of Microorganisms and Their Chemical Metabolites from Water using Semiconductor Photocatalysis. J. hazard. Mater. 211, 161–171

[20]. Slamet., Syakur R., Danumulyo W., 2003. Treatment of Waste of Heavy Metal Chromium (VI) with TiO_2 Photocatalyst. Makara, Technology, 7 (1): 27-32.

[21]. Sutherland, J.P., Folkard, G.K., Mtawali, M.A. and Grant, M.A., Moringa Oleifera as a Natural Coagulant, 1994, Paper 20th WEDC Conference Affordable Water Supply And Sanitation, Colombo, Sri Lanka

[22]. Wang.C.,Liu.H,Qu.Y., 2013.TiO_2-Based Photocatalytic Process for Purification of Polluted Water: Bridging Fundamentals to Applications. Hindawi Publishing Corporation Journal of Nanomaterials Article ID 319637,14

[23]. Widowati, W., Sastiono, A., Jusuf R, R., 2008. Toxic Effect of Metals; Prevention and Overcoming of Pollution. Yogyakarta:

[24]. Wols, B., Hofman-Caris, C. 2012. Review of Photochemical Reaction Constants of Organicmmicropollutants Required for UV Advanced Oxidation Processes in Water. *46*, 2815–2827.

[25]. Zhang, H., Yang, Z., Zhang, X., Maio, N., 2014, Photocatalytic Effect of Wool Fibers Modified with Soley TiO_2 Nanoparticles and N-doped TiO_2 Nanoparticles by Using Hydrothermal, Elsivier,Vol. 254, 106-114

Simulation Multilevel Inverter Single Phase Type H-Bridge With Resistive-Inductive Load (RL) (#767)

Abdul Haris[1], Aji Penetrap Raga[2,a], EndahKomalasari[3]
[1]Department of Electrical Engineering, Faculty of Engineering, University of Lampung
Jl. Prof. SumantriBrojonegoro 1 Bandar Lampung 35145
[a]aji.penetrap@gmail.com

Abstract *- Inverter is an electronic circuit that serves to convert electric power Direct Current (DC) into the form of electric power Alternating Current (AC). Inverter basically produces harmonic distortion is large enough. Multilevel inverter reduces harmonic distortion inverter to increase the number of inverter level. The method in this study using multilevel inverter single phase with 3 stage, stage 5, and 7 stage H-bridge type. The output voltage of the multilevel inverter is the resultant Vout of each constituent level inverter. Extra levels of a multilevel inverter can reduce the Total Harmonic Distortion (THD) with the value of the RL load. THDv value generated by above 47% and THDi generated over 19%.*

Keywords *: FFT, H-Bridge, Harmonic, Inverter, Multilevel inverter, Total Harmonic Distortion (THD).*

I. Introduction

Energy conversion technology is now growing with power electronics technology. One rapidly growing technology is an inverter that serves as a converter for converting electric power Direct Current (DC) in the form of electric power Alternating Current (AC). Inverters are used in renewable energy sources such as solar cell to convert DC into AC power that can be used in everyday life.

The working principle of the inverter uses electronic switching to generate the output waveform in the form of a sinusoidal wave. As a result of switching on the inverter electronics has resulted in a sinusoidal output waveform distortion harmonics. Harmonics that arise will result in inverter output power suffered losses and also can result in damage to the equipment.

Harmonics generated by the inverter can be reduced by using multilevel inverter type H-bridge. Multilevel inverters generate waveforms in the form of wave ladder or staircase. With each level of multilevel inverter voltage generated will produce output waveform is getting better too. In the multilevel inverter is not required high switching frequency to produce a sinusoidal waveform.

II. Research Methods

In this study, using the method Multilevel Inverter single phase H-bridge type. Large output voltage in the multilevel inverter is the sum of the output voltage of the inverter each level.

$$V_{out} = \sum_{i=1}^{P} V_{aci} \qquad (2.1)$$

multilevel inverter H-bridge type having the simplest construction and arrangement is simple too. But pick a good wave output with the level of a high level. In multilevel inverter is

not required high switching frequency to produce a sinusoidal waveform. In multilevel inverter with separate DC source itself or will produce output voltage corresponding to the level of the inverter stage. Where to an inverter with two DC sources, the output voltage (Vo) will have five levels, namely + 2Vdc voltage, Vdc, 0, -Vdc, and -2Vdc. [3]

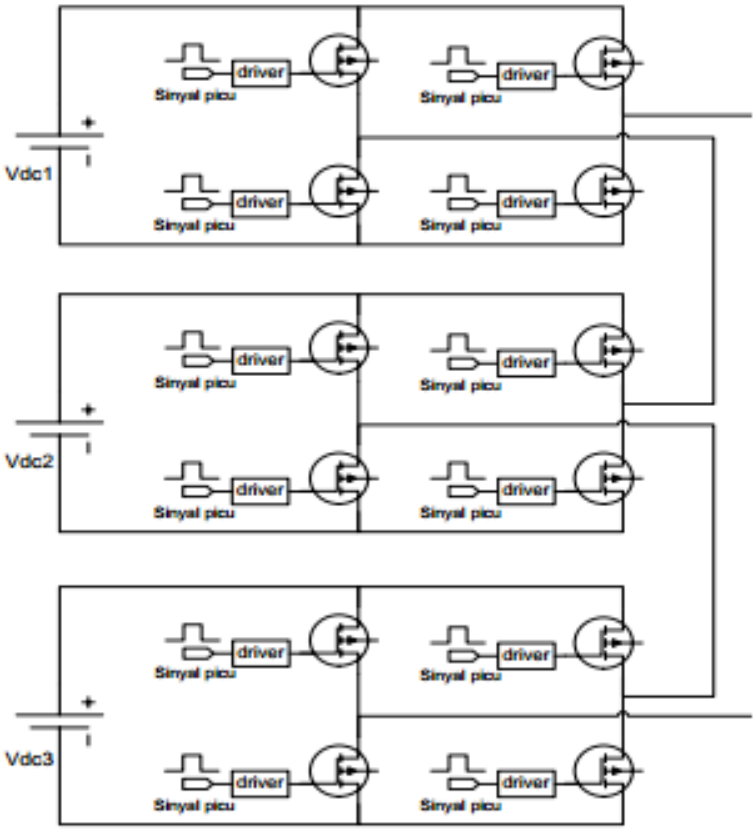

Figure1. *Multilevel inverter* type H-bridge

From the results of the series will be the effect of load RL to the output waveform and harmonic waves and THDv and THDi the huge market for simulation results. In addition to the loading effect, will also show the effect of adding to the level of the multilevel inverter 3 stage, stage 5, and 7 stage against THD is generated. Software used in this study is the MATLAB Simulink R2014a. To view the results THDv and THDi generated in simulation using MATLAB FFT Analysis in software.

III. Circuit Simulation Research

The circuit used in this study is a multilevel inverter 3 stage, stage 5, and 7 stage. Switching components used are mosfet. In the third stage multilevel inverter using mosfet 12, using 20 mosfet stage 5 and 7 stage uses 28 mosfet. With an output voltage generated is approximately 220V. Where each inverter is given two Pulse Generator as input waveform for mosfet gate to generate a signal.

Variations load used with a value of R = 50ohm, 100ohm and 150ohm, while the load L = 100mH and 147mH. An inverter circuit made in the form subsystem to simplify a string that is used in this study. The circuit is used as shown below:

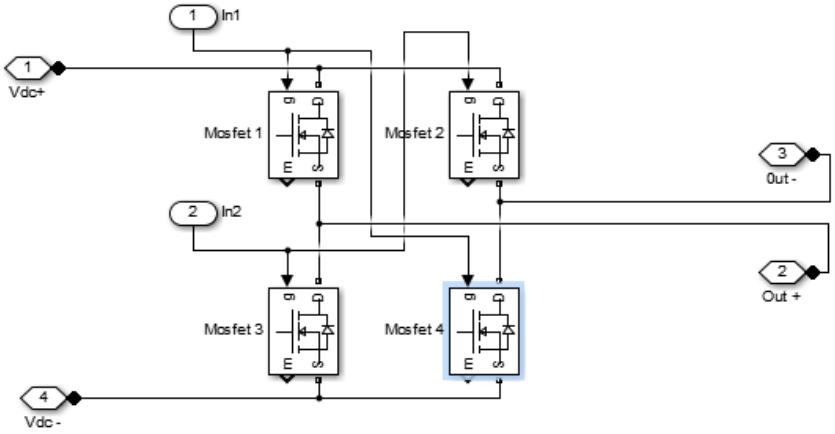

Figure 2 In the inverter circuit Subsystem

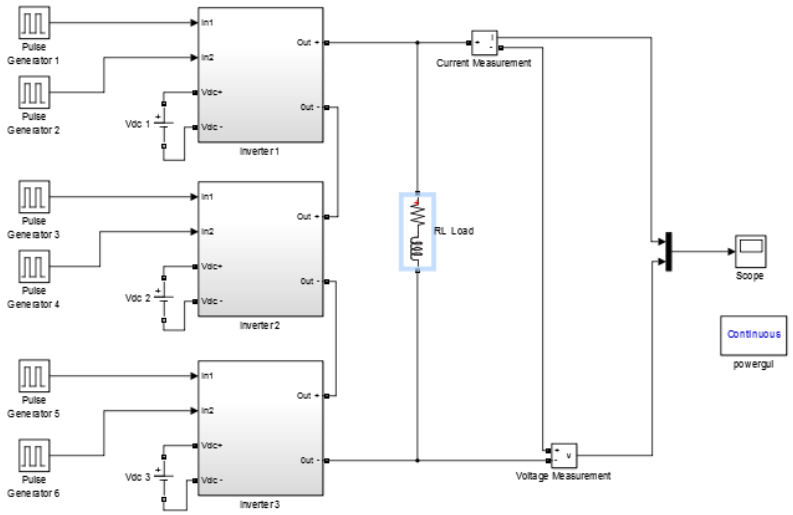

Figure 3. Multilevel Inverter 3 Stage with Load RL

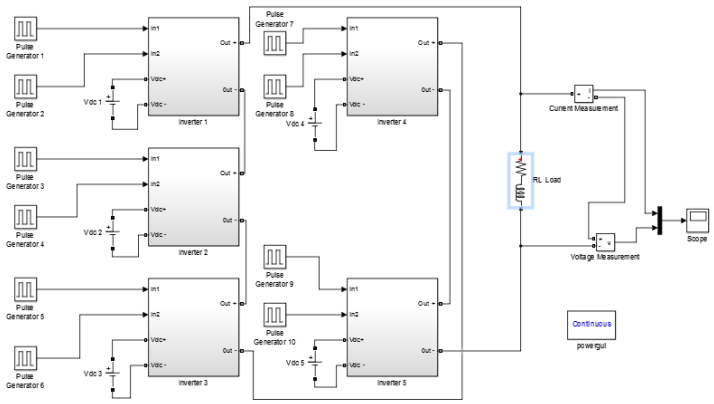

Figure 4 Multilevel Inverter 5 Stage with Load RL

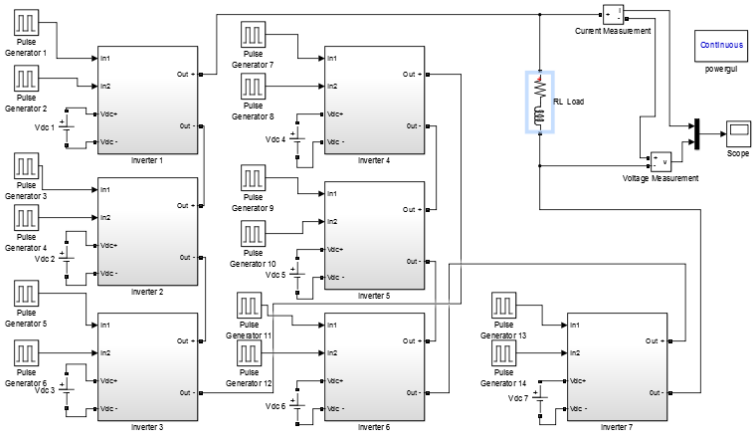

Figure 5 Multilevel Inverter 7 Stage with Load RL

IV. Research Result

Simulations in this study resulted in multilevel inverter voltage at the output of 225V. The following table test results with the resulting waveform:

Table 4.1 Results Data Load Voltage and Current in RL

LOAD		VOLTAGE (V)			FLOW (A)		
L (MH)	**R (Ohm)**	***3 stage***	***5 stage***	***7 stage***	***3 stage***	***5 stage***	***7 stage***
100	**50**	225	225	224	3.93	3.94	3.95
	100	225	225	224	2.2	2.2	2.2
	150	225	225	224	1:49	1:49	1.5
147	**50**	225	225	224	3:43	3:47	3:48
	100	225	225	224	2:12	2:12	2:12
	150	225	225	224	1:47	1:47	1:47

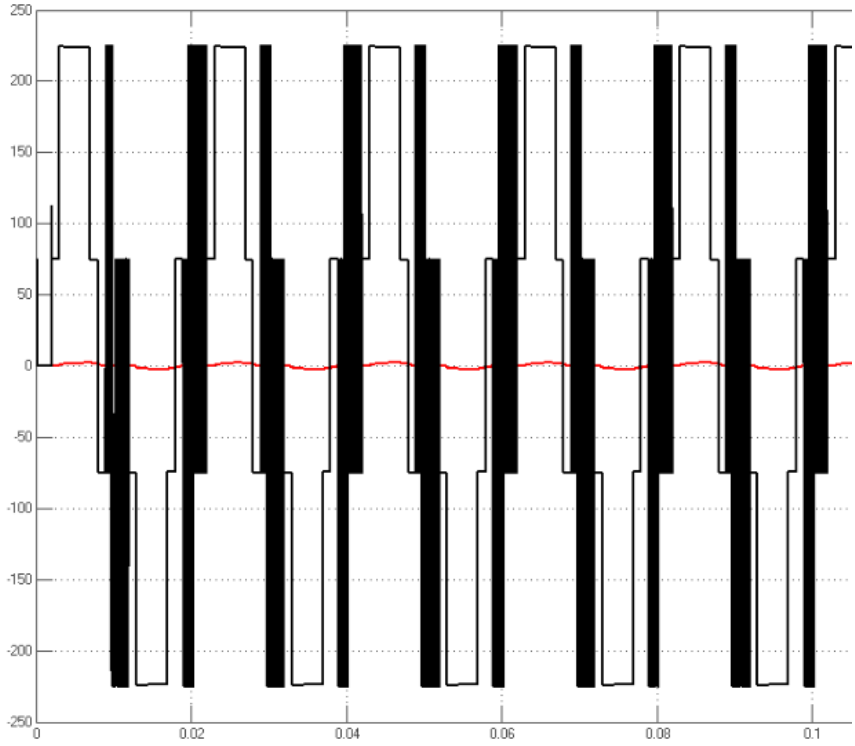

Figure 6 Multilevel wave Inverter 3 Stage Expenses R 100 Ohm and L 100mH

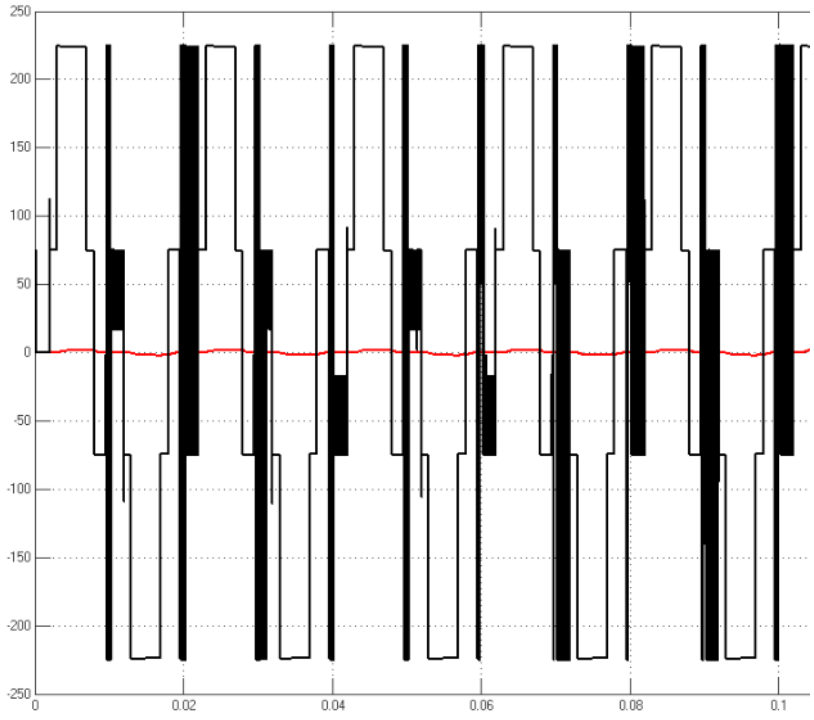

Figure 7 Multilevel wave Inverter 3 Stage Expenses R 100 Ohm and L 147mH

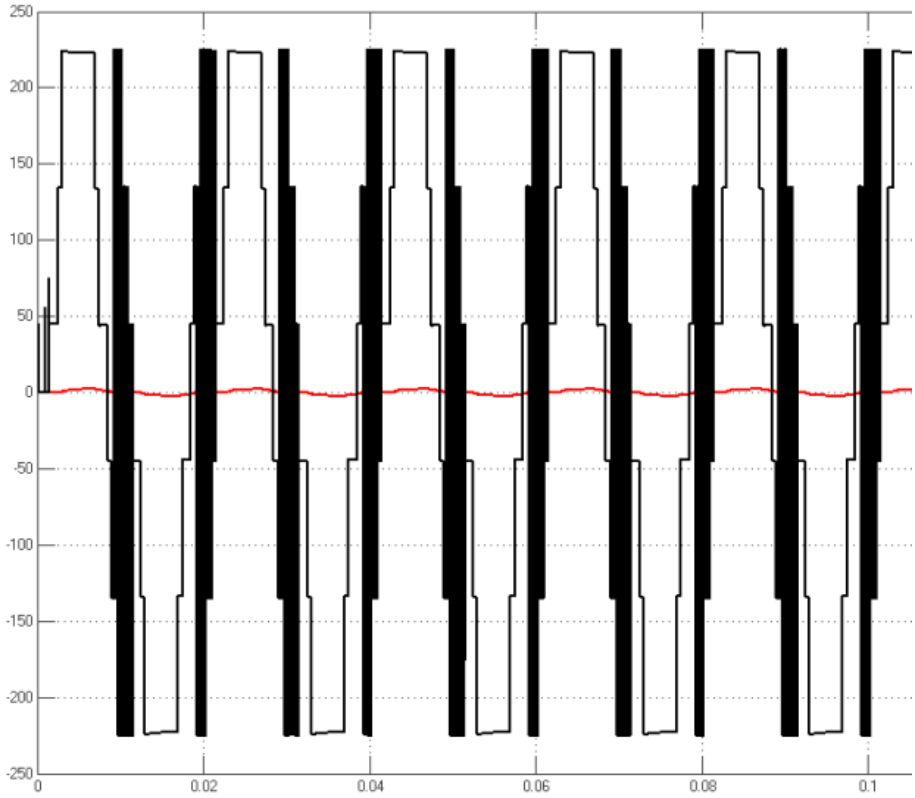

Figure 7 Multilevel wave Inverter 5 Stage R 100 Ohm Load and L 100mH

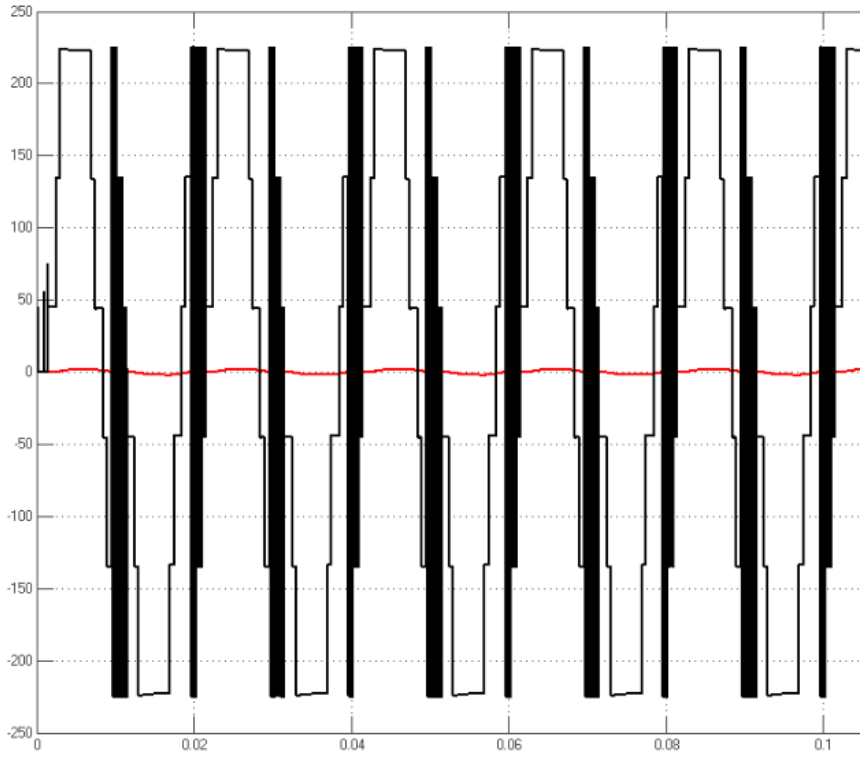

Figure 8 Multilevel wave Inverter 5 Stage R 100 Ohm Load and L 147mH

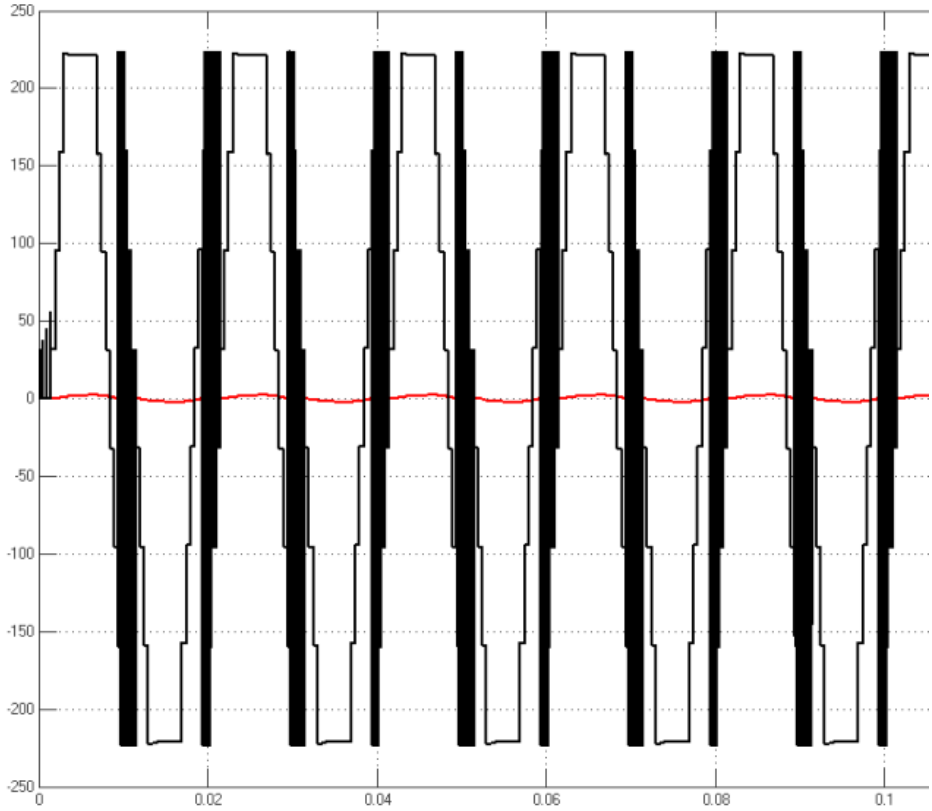

Figure 9 Multilevel wave Inverter 7 Stage Expenses R 100 Ohm and L 100mH

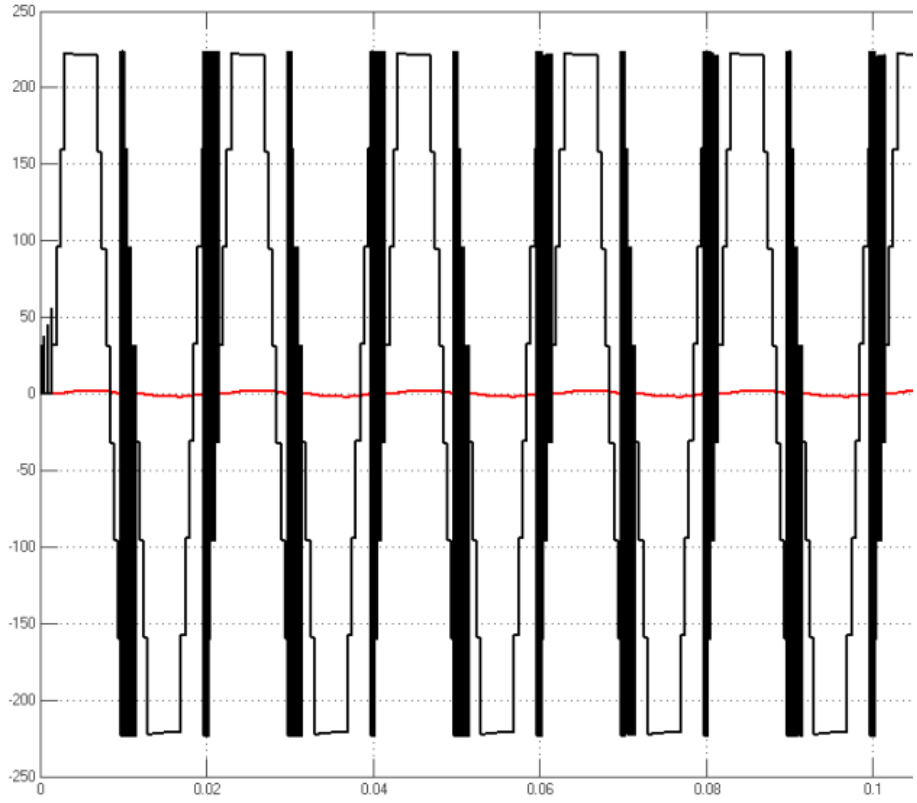

Figure 10 Multilevel wave Inverter 7 Stage Expenses R 100 Ohm and L 147mH

From Table 1 shows the test data voltage and current to the load RL in multilevel inverter circuit. On the addition of inductive load on the string makes the magnitude of the resulting current is more stable on each additional level of the multilevel inverter. This occurs

because the current value proportional to the voltage value but is inversely proportional to the value of the load used (Ohm's law). Voltage waveform generated in the load testing is experiencing a lot of disruption resulting from the effects of adding inductive load. But the current wave produced better and closer to sinusoidal.

This is because the inductive load will save the electric current flowing in the load in the form of a magnetic field, and then returned to the load inducted mounted on a circuit. When the multilevel inverter switching circuit on condition on, then current will flow to the load and inductive load will keep the current flowing into the magnetic field. When conditions multilevel inverter switching circuit pad off condition, then the magnetic field stored in the inductive load will be the source to the circuit to induce a magnetic field that has been stored. Then, when the switching circuit upon the condition on, then re-storing inductive load electric current flowing to the load into a magnetic field to be induced back.

Having obtained the data from the voltage and current waveform, further testing is done to see the effect of inductive load on THDv and THDi in a multilevel inverter circuit. Here are results of test data load RL on multilevel inverter circuit:

Table 2 Data Results THDv and THDi on Load RL

LOAD		THDv (%)			THDi (%)		
L (MH)	**R (Ohm)**	***3 stage***	***5 stage***	***7 stage***	***3 stage***	***5 stage***	***7 stage***
100	**50**	60.1	56.32	50.41	29.72	24.9	21.66
	100	67.09	54.9	45.65	37.47	29.58	25.86
	150	55.42	54.04	46.41	39.57	31.5	27.71
147	**50**	66.12	58.69	52.45	25.22	21.94	19:23
	100	69.41	57.12	47.74	33.65	27.28	23:54
	150	60.50	56.06	47.38	37.5	29.71	25.94

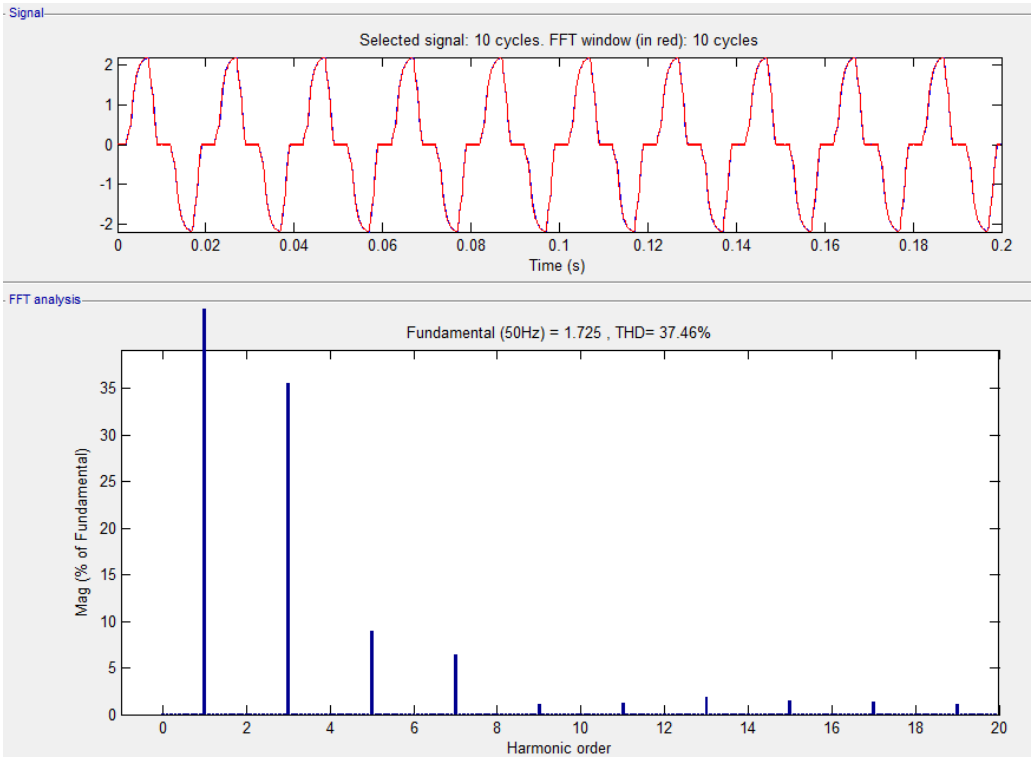

Figure 11THDi Multilevel Inverter 3 Stage Expenses R 100 Ohm and L 100mH

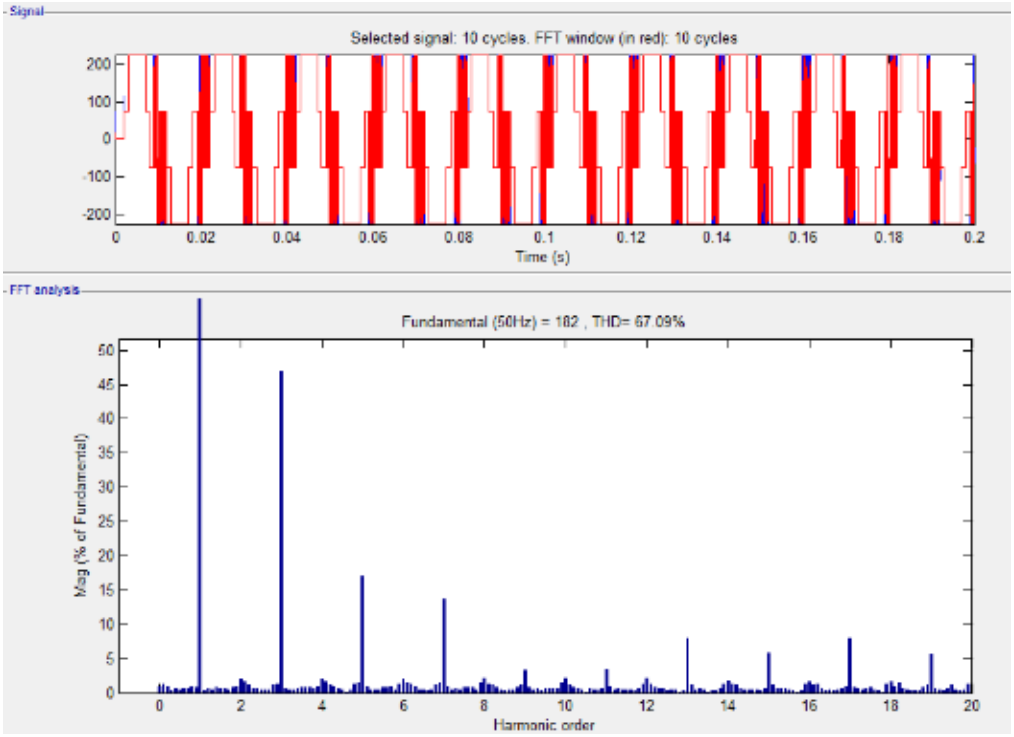

Figure 12THDv Multilevel Inverter 3 Stage Expenses R 100 Ohm and L 100mH

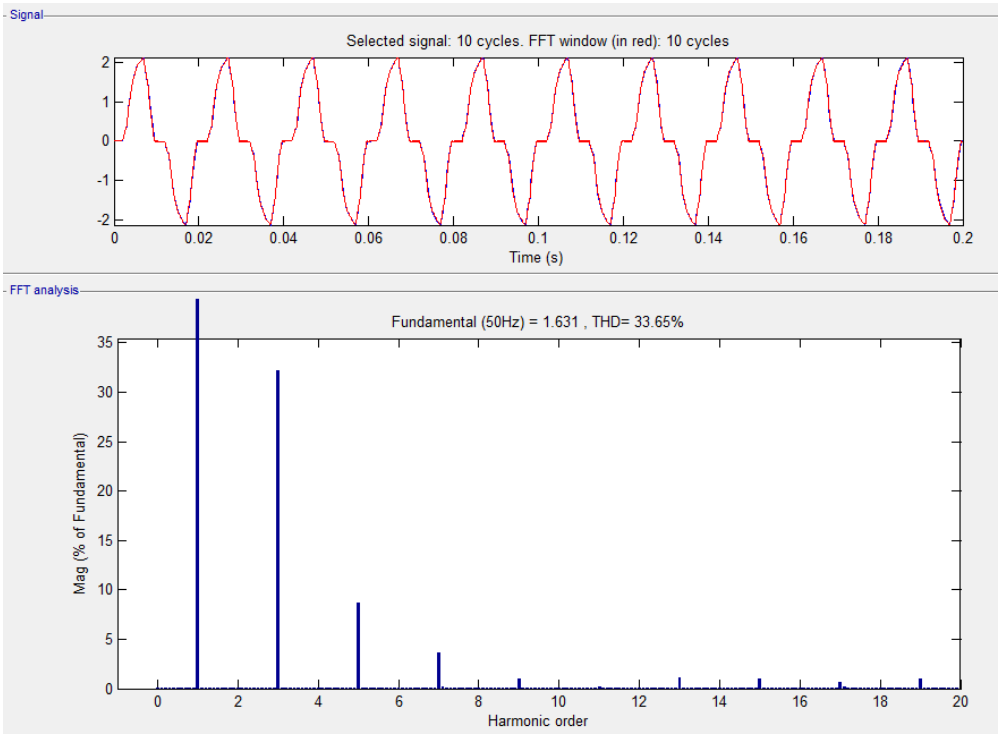

Figure 13THDi Multilevel Inverter 3 Stage Expenses R 100 Ohm and L 147mH

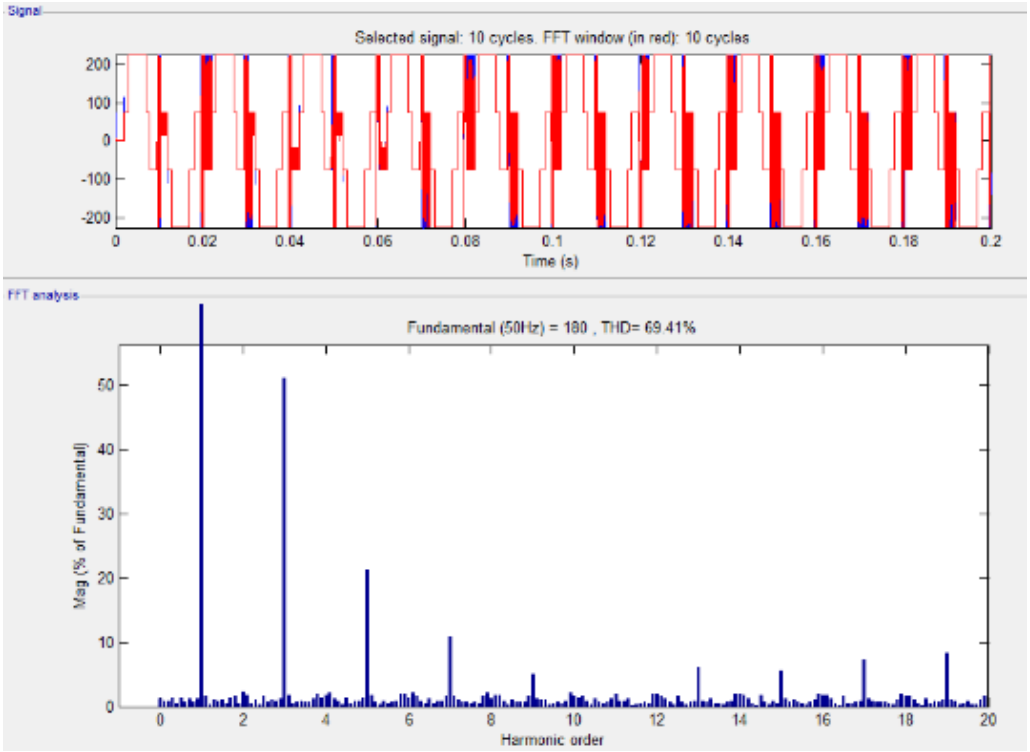

Figure 14THDv Multilevel Inverter 3 Stage Expenses R 100 Ohm and L 147mH

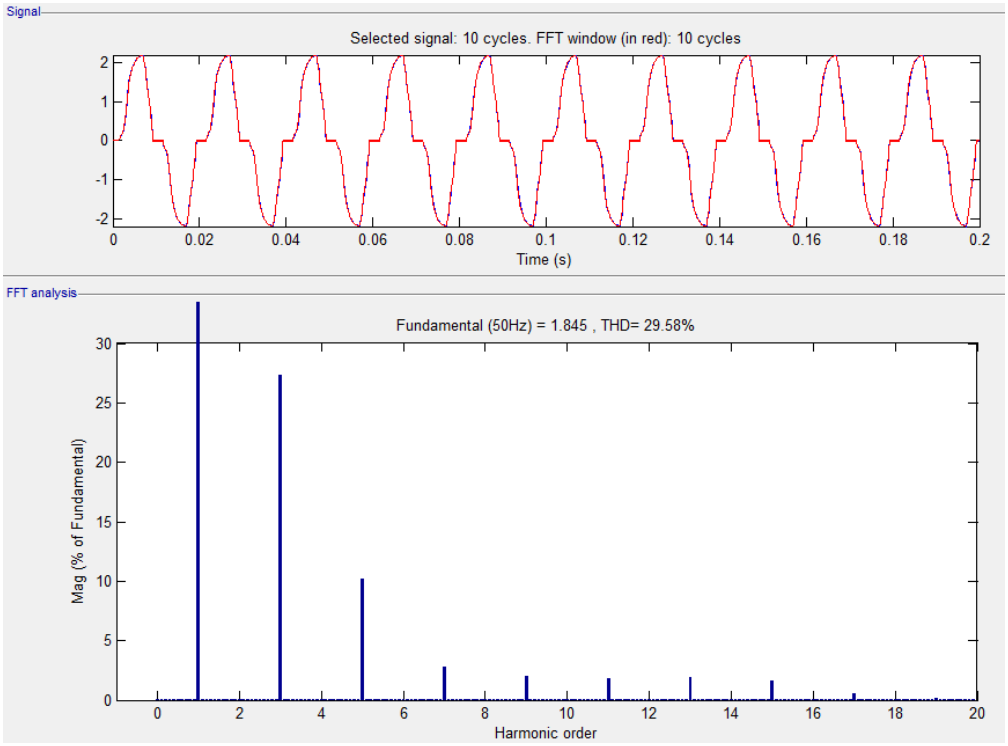

Figure 15THDi Multilevel Inverter 5 Stage R 100 Ohm Load and L 100mH

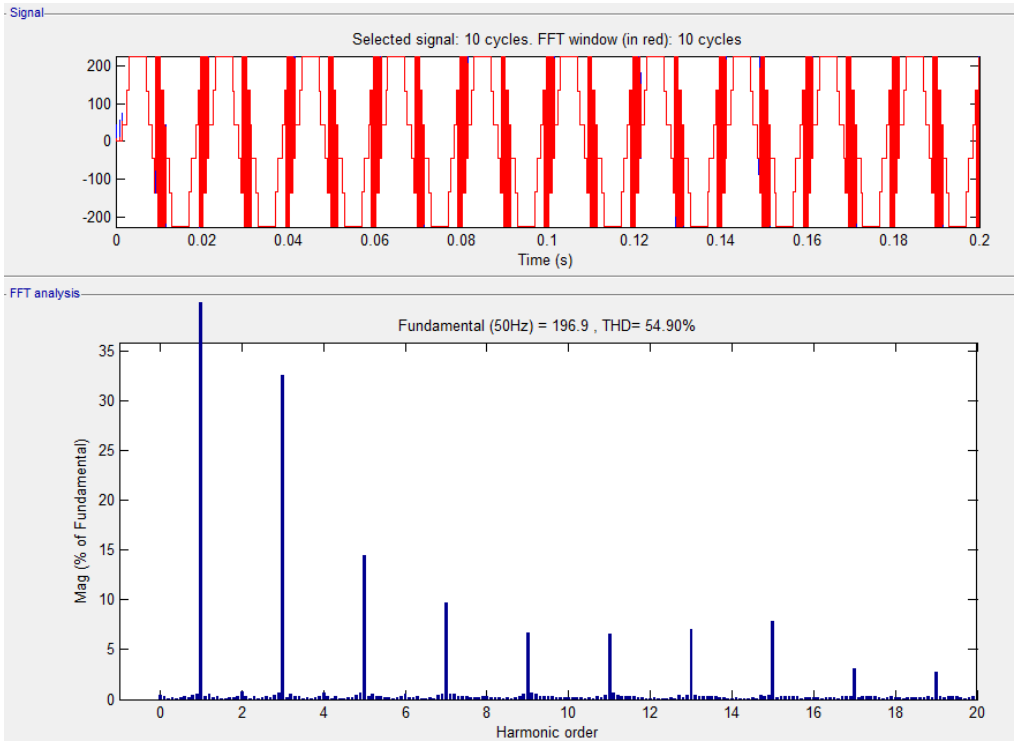

Figure 16THDv Multilevel Inverter 5 Stage R 100 Ohm Load and L 100mH

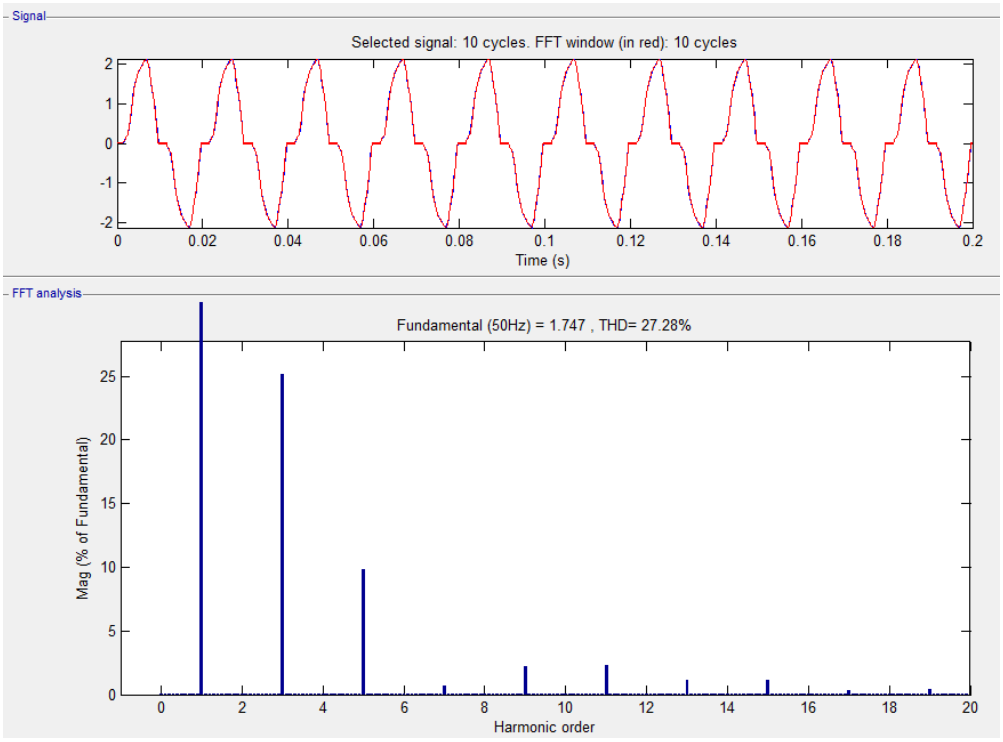

Figure 17 THDi Multilevel Inverter 5 Stage R 100 Ohm Load and L 147mH

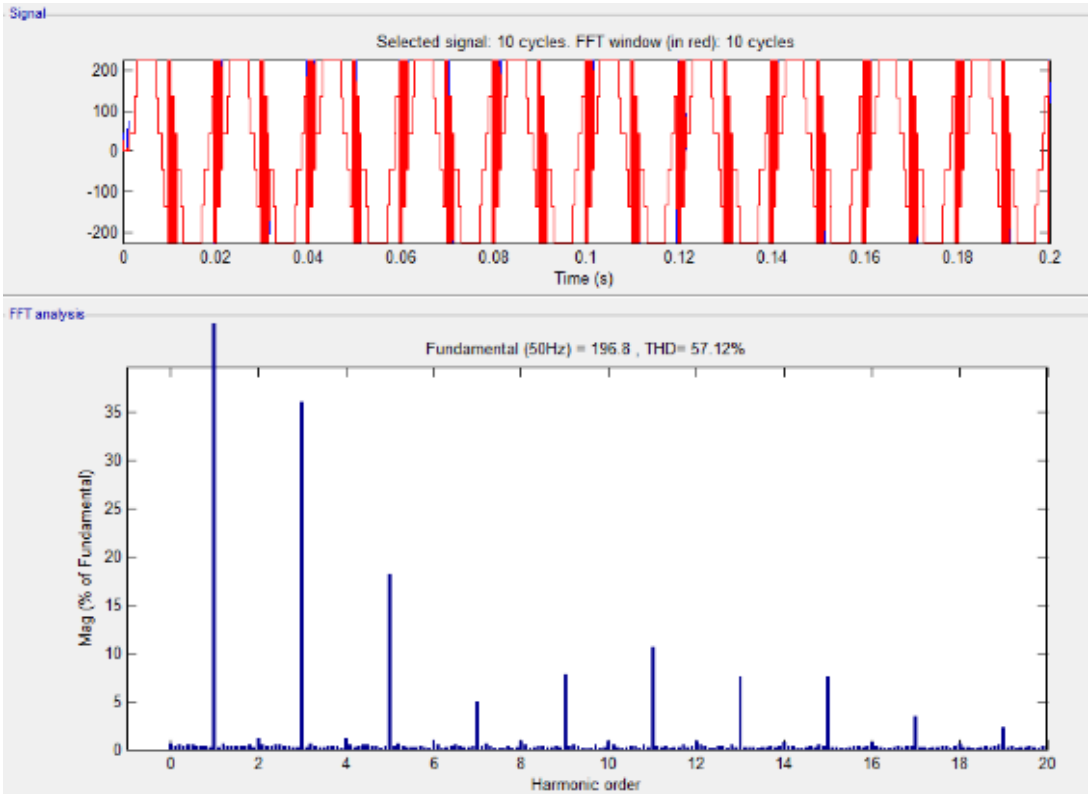

Figure 18 THDv Multilevel Inverter 5 Stage R 100 Ohm Load and L 147mH

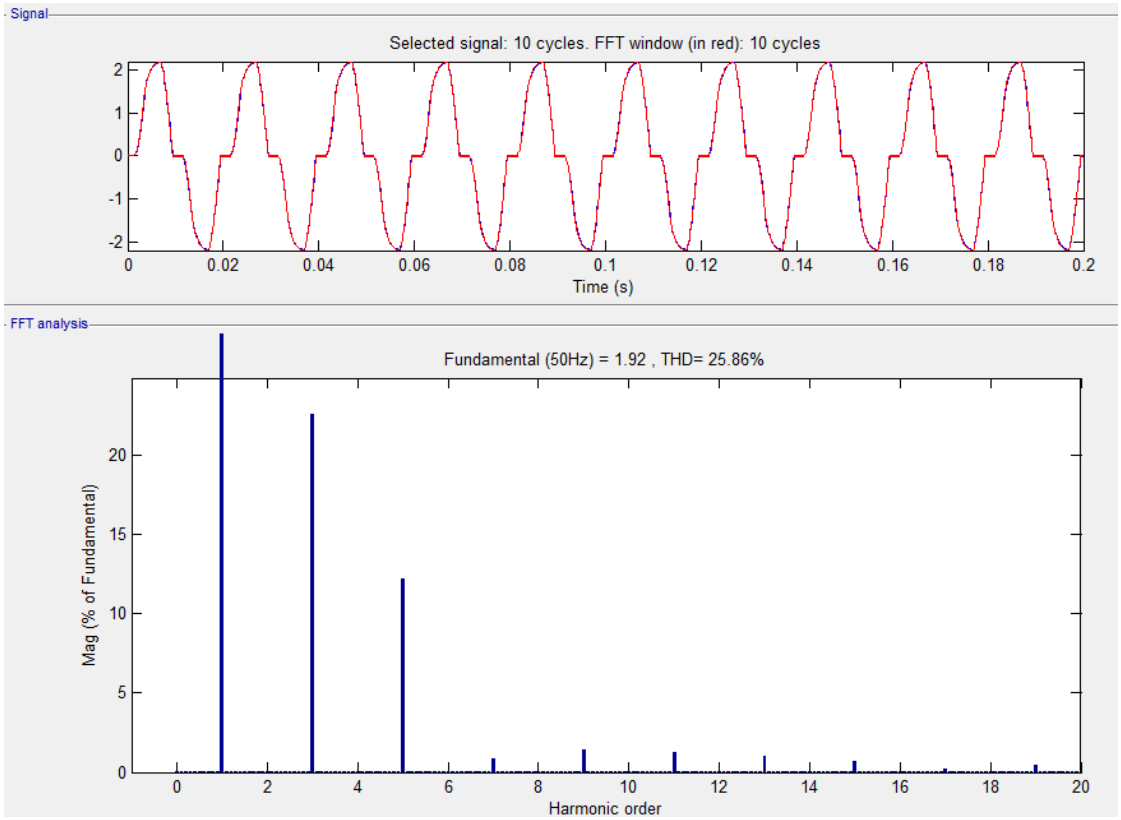

Figure 19 THDi Multilevel Inverter 7 Stage Expenses R 100 Ohm and L 100mH

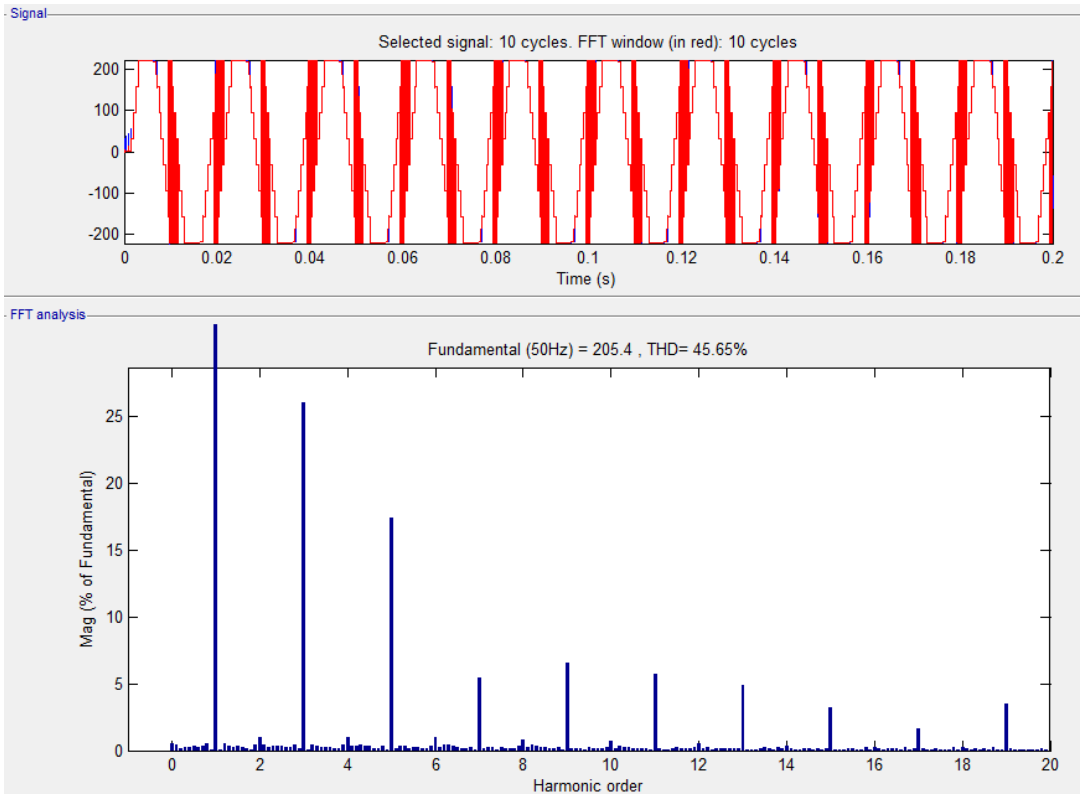

Figure 20 THDv Multilevel Inverter 7 Stage Expenses R 100 Ohm and L 100mH

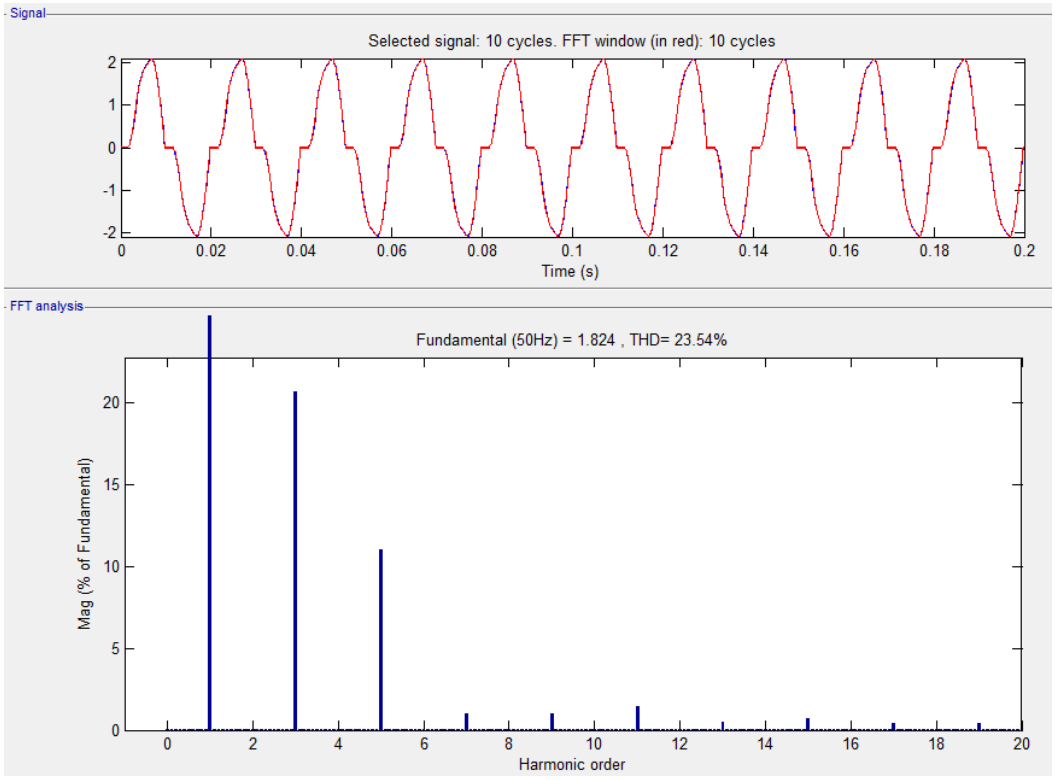

Figure 21 THDi Multilevel Inverter 7 Stage Expenses R 100 Ohm and L 147mH

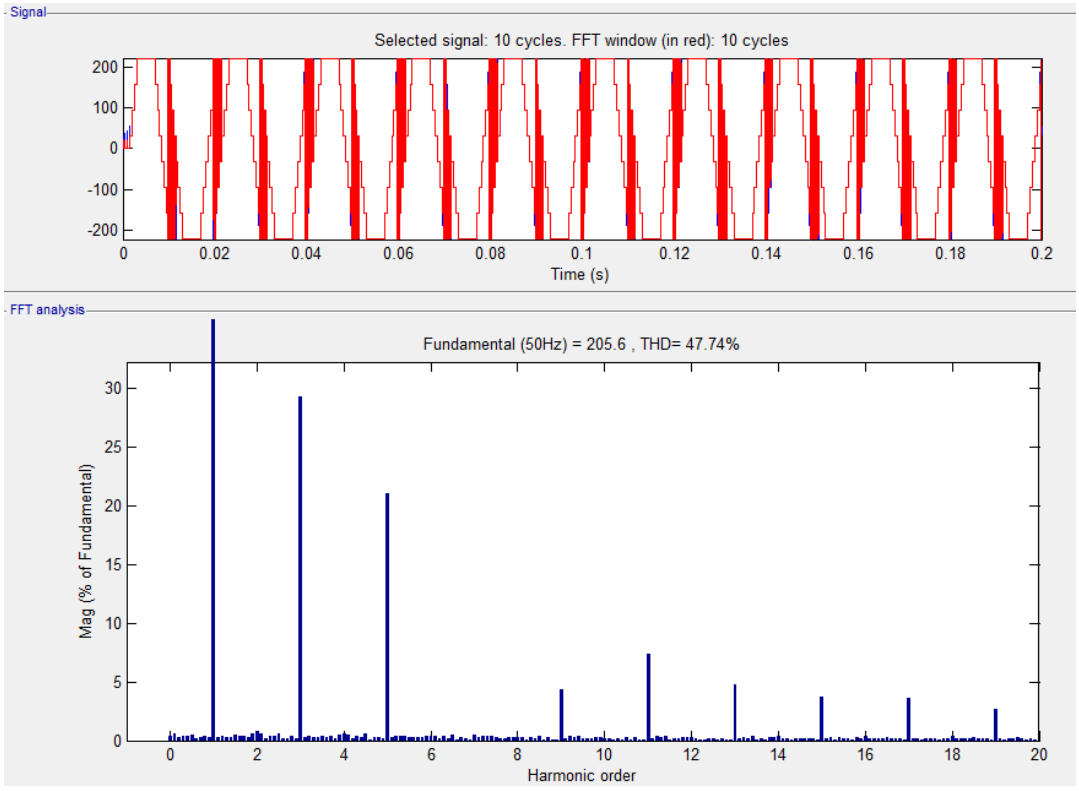

Figure 22 THDv Multilevel Inverter 7 Stage Expenses R 100 Ohm and L 147mH

From Table 2 it can be seen the effects of loading on the load RL of the results generated THD. With the addition of inductive load is seen that the value generated THDv

great with a value above 47%. This is caused because the inductive load can not reduce the ripple voltage at the output waveform of the multilevel inverter. In the third stage, multilevel inverter harmonics generated waves up to 19th harmonic sequence (H19). Similarly, in the multilevel inverter circuit, 5 and multilevel inverter stage 7 stage resulted in a wave harmonics up to the 19th order harmonics (H19).

With the addition of the level of the multilevel inverter 3 stage into 5 stages impaired THDv although the level of harmonics equal to H19, but the percentage of each order of harmonics is smaller. In the multilevel inverter circuit 7 stage THDv the resulting value becomes smaller than the multilevel inverter 5 stages and 3 stages. From the data that has been obtained, it can be seen that with the addition of the level inverter used in the multilevel inverter can degrade and improve THD value generated in the multilevel inverter output.

In addition, inductive load has resulted in THDi resulting smaller than the value THDv. This is because the inductive load characteristics that stores electric current flowing to the load into a magnetic field and improve the value of the current generated by cutting the current ripple.

On the results of FFT Analysis MATLAB Simulink seen that in multilevel inverter stage 3 and stage 5 generates harmonic waves up to 17th harmonic (H17). In multilevel inverter, 7 stages generate harmonic waves up to 15th harmonic (H11). From the results of these THDi can be seen that more and more switching components are used it will result in more harmonic sequences. But more and more switching components are used then the percentage of each order of harmonics is smaller so that the resulting THD will be smaller.

The addition of the value of the resistive load used affects THDv and THDi value generated in this multilevel inverter. However, the addition amount of the rate constant multilevel inverter can reduce THDv and THDi value with the decrease is not too large percentage is around 3% -8%.

V. Conclusion

In this study, the multilevel inverter single phase H-bridge type can reduce the value of Total Harmonic Distortion (THD) at the loading RL. Effect of resistive load (R) in the multilevel inverter output waveform that dampens wave level for R load characteristics that consume electrical energy. Wherein R load change waveform but does not cause a phase shift of current or voltage. The influence of the inductive load (L) on the harmonic wave that is far THDi value at the inverter output wave. But not far THDv value for the load L only cut not with the current wave ripple voltage waveform generated.

Use of the method of the multilevel inverter with single phase inverter type H-bridge may be one way of reducing the value of THD without using filters. However, an arrangement of Duty Cycle and Phase Delay precise as wave input on switching gate (mosfet). With the right settings on the switching component, it will produce sinusoidal wave approaching the storey. So the larger the inverter output waveform close to sinusoidal then the resulting THD value would be diminished.

The setting value Duty Cycle and Time Phase Delay in this study still needs further investigation to obtain better results in the use of the method Multilevel Inverter Phase One's H-Bridge mode.

References

[1]. O. Lopez, R. Teodorescu, F. Freijedo and J. DovalGandoy, "Leakage current evaluation of a singlephasetransformerless PV inverter connected to the grid," APEC 07 - Twenty-Second Annual IEEE Applied Power Electronics Conference and Exposition, Anaheim, CA , USA, 2007, pp. 907-912.

[2]. Tri AptonoYuwono, E, Warsito. A, and Facta. M. 2011. "Multi-Level Inverter Bridge Type Single Phase Level With Microcontroller AT89S51". E-Journal UNDIP. Vol. 13, No. 4; pp.135-140.

[3]. W. Hart, D. 2011. Power Electronic. McGraw-Hill Companies, New York.

[4]. H. Rashid, M. 1993. Power Electronics: Circuits, Devices, and Applications (2nd Edition). Prentice Hall, New York.

[5]. KocalmisBilham. A, Akbal. E. "Modeling and Simulation of Two-Level Space Vector PWM Inverter Using Photovoltaic Cells As DC Source". International Journal of Electronic. Vol. 2, No. 4, pp. 311-317.

[6]. E. Johnson. D, R. Johnson. J, L. John. H. 1989. Electric Circuit Analysis. Prentice Hall, New Jersey.

Simulation and Control of Clean Water Supply on Campus Toilets Using Passive Infrared Receiver Sensor Technology and Flow Liquid Meter (#630)

Fahmi[1,a], Baihaqi Siregar[1], Erna Budhiarti Nababan[1], Ilhamuddin Hasibuan[1], Ulfi Andayani[1], Heru Pranoto[2]

[1]Department of Information Technology, University of Sumatera Utara, Medan, Indonesia

[2]Department of Electrical Engineering, University of Sumatera Utara, Medan, Indonesia

[a]fahmimn@usu.ac.id

Abstract *- The use of tap water on campus toilets is often problematic due to careless user. The water faucet on campus toilets is often left open, and this leads to wasteful and inefficient use of water. For that, we need a solution to save and control water usage on campus toilets with automatic faucet so that water usage can be used only when they are necessary or needed. Control of water usage on campus toilets using fluid mechanics and physics kinematics method by using solenoid valve as a valve to open and close the flow of water and flow liquid meter to calculate the water discharge data through it. While, PIR sensor that serve to detect the presence of humans in the toilets so that the solenoid valve can open and let the water flows. While Arduino UNO as microcontroller and Wi-Fi shield used to deliver the water discharge data to application that had been built. The test results show that the method used is able to work with stable to control water supply on campus toilets.*

Keywords*: flow liquid, fluid mechanics, physics kinematics, solenoid valve, Arduino, Wi-Fi shield, and PIR sensor.*

I. Introduction

Water is the source of life for every living being. Also, water is one of the main needs in our live. The high level of human needs of water is not proportional to the availability of water on earth, because of all the water that is in the earth, 97% is sea water, while the remaining 3% is fresh water and only 1% is available for human use.

The amount of wasteful use of water causes wasteful use of water. Until now the level of water demand is increasing along with the increasing rate of world population growth. So it is not exaggeration if UNESCO predicts by 2020 the world will experience a global water crisis.

Monitoring of water usage in toilets is expected to reduce excessive water use. This monitoring is supported by Passive Infrared Receiver (PIR) sensor. Passive Infrared Receiver is an infrared-based sensor. However, it is not as common as most infrared sensors that consist of an IR LED and a phototransistor. PIR does not emit anything like IR LEDs. As the name implies 'passive', this sensor only responds to the energy of the passive infrared beam held by every object detected by it. Objects that can be detected by these sensors are usually the human body.

This is due to an IR filter that filters the wavelength of passive infrared light. IR Filter in a PIR sensor module is capable of filtering the wavelength of passive infrared light between 8 to

14 micrometers, so the wavelength produced from the human body ranging between 9 to 10 micrometers can be detected by the sensor.

So when someone walks through the sensor, the sensor captures the emission of a passive infrared beam emitted by the human body which has a different temperature from the environment causing the pyroelectric material to react and generate an electric current due to the heat energy carried by the passive infrared beam. Then an amplifier circuit amplifies the current which is then compared by the comparator to produce the output.

Based on previous research this series of automatic water faucet is manufactured using microcontroller and the motion sensor is used to activate the automatic switch circuits which serve as input to the washer pump to control the valve to close or open. This will open automatically when the sensor is blocked. When the sensor is obstructed then the series will be active.

II. Problem Identification

Water is one of the main needs in everyday life. The amount of water used in the bathrooms become one of the main causes of waste water consumption, when someone opens the water faucet in the bathroom, then often forgets to close it. This is one of the main causes of wasteful use of water consumption. Therefore, we need an approach to control the water flow needed so the efficiency of water usage in the bathroom can be achieved.

III. Previous Research

Several studies have been done to conserve water usage in toilets. In 2010, Gabriel conducted research for automatic faucet control in male toilets using PIR sensors. In his research, Gabriel utilized the PIR sensor as its control center and object detection in the form of human body. The PIR sensor will give instructions to the relay to move the solenoid that acts as a valve. The results of analysis showed that the PIR sensor in this tool can detect the object within a maximum distance of 1.5 meters [1].

A second study in 2011, Alfarobi undertook research for the manufacture of an automatic faucet system for water savings in ablution using motion sensors. In his research, he made a system of automatic ablution faucet by placing the sensor at a certain point, so that when someone finishes, the faucet will automatically close [2].

In 2014, Subandi conducted a research for automation on water faucet to save water consumption. He used an ultrasonic sensor to detect the presence of a limb that is directed to the faucet and stop the flow of water if no limb is directed to the sensor. Ultrasonic sensor will convert physical quantities into mechanical quantities. He used an Atmega16 microcontroller as the system controller. Test results indicated that there was a difference in the amount of volume of water released using automatic faucet and ordinary faucet [3].

In 2014, Yano et al. conducted a research to measure water consumption and compare savings from tap water usage using Wireless Sensor Network. This research used RFbee Sensor to collect, send, and receive data. Data retrieved by RFbee sensors will be collected and then sent wirelessly to a computer connected directly to the RFbee sensor [4].

In 2017, Rahmat et al conducted a research showed that computation of science, especially fluid mechanics and kinematics physics is implemented on microcontroller. Arduino chip-based ATmega328P can be used to detect the location of leaks in pipes by using a data rate of water flow and the system is able to work stably to determining the location of the leak with a maximum distance of 2 meters and it can determine the location of the leak closest to the actual location of the leak with an average flow rate of 10 litters per minute [5].

IV. Methodology

This research consists of several steps begins from data collection which is retrieved automatically through the sensor. For more information about the input and output process of the built system can be seen in Figure 1.

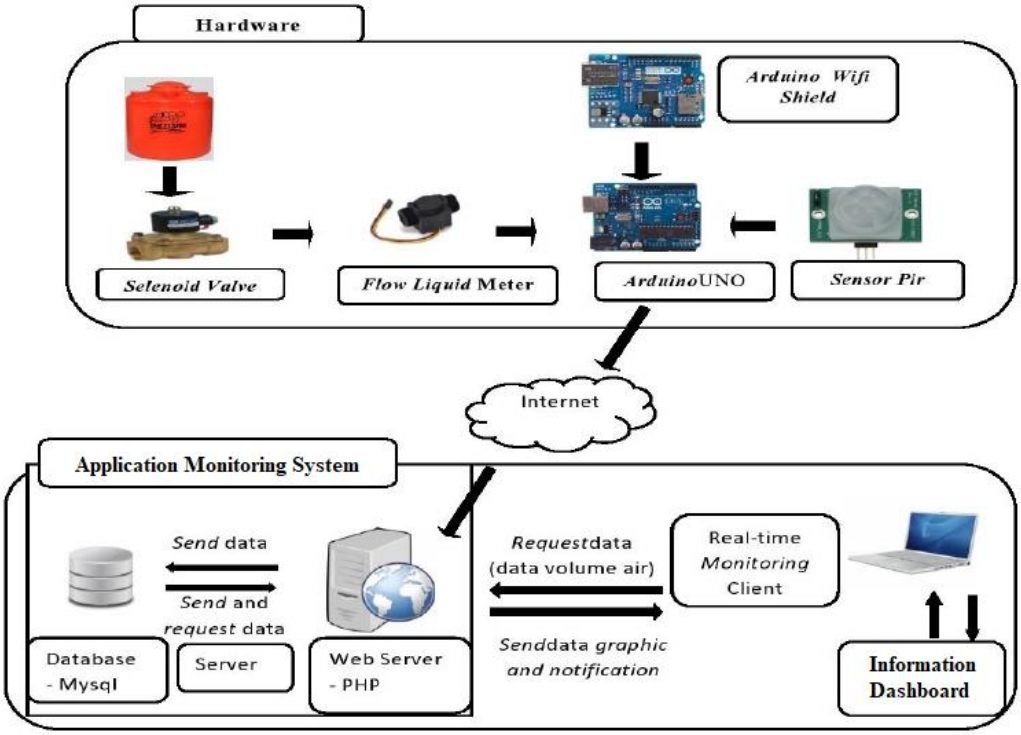

Figure 1. General architecture

A. Hardware and Sensor Monitoring Application System

1) Hardware Sensor

This section shows the process of data retrieval by the sensor to then be sent to Arduino as well as data transmission by Arduino to the monitoring application system assisted by Wi-Fi shield.

This process starts from the water that flows on the pipe and goes through the solenoid valve. Then, it flows through the flow liquid meter sensor that previously installed in the pipe. The sensor will collect data from the water passing through it, and will be sent to the Arduino. Flow liquid meter sensor will transmit data to Arduino via digital pin 2.

Then, Arduino calculates how much water discharge per second that passes through a flow liquid meter sensor. The water discharge per second that had been obtained is first stored in the server where the water discharge data is collected. Server will then directly send the data to the monitoring application system in real time. Collection of data from Arduino to server

using Wi-Fi shield, to connect server with Arduino, Arduino will access the IP address of the server. After it is connected, Arduino will send water discharge data using POST method by accessing web page on server. Wi-Fi shield is mounted with stackable method on Arduino and will connect Arduino with server directly using RJ-45.

2) Application Monitoring System

Monitoring application system that will be built is a web-based application system using PHP.

3) Web Server

Web server used is a standalone web server. This web server will serve as a place of service and data processing between Arduino, database, and client.

Web server will receive the water discharge data sent by the server where the data is collected. This water discharge data will then be stored into the database and ready to be processed and be represented back to the client in the form of graphs. These graphs will be displayed within a certain time interval and will always be updated automatically every second as long as the Arduino sends the water discharge data to the system. The water discharge data will be processed and ready to be represented back to the client either when they access the web server or not.

4) Client

The client will access a web page on the web server to perform monitoring and only the specific client who has permission will be able to access this page. This page will display the amount of water discharge used per day or the amount of water discharge that flows on the flow liquid meter. Water discharge will be displayed in the form of graphs and tables. Water usage graphs will be changed when the water flows through the flow liquid meter and updated automatically in the form of graphs and tables.

B. Data Used

The data used in this research is data which is obtained directly from the sensor. Then the Arduino will receive data from the sensor. The data is number of turns of the mill inside the sensor caused by the flow of water through the liquid meter flow sensor. The number of turns of the mill is further processed using the equation 2.1 so that water discharge data is obtained through the sensor every second. Then Arduino will send the data assisted by Wi-Fi shield into the server that had been provided. The data transmitted is in the form of volume water discharge data that had been used.

C. Hardware Design

1) Design of Solenoid valve Sensor, Relay, PIR Sensor with Arduino

Arduino has several pins that serve as a place of data processing and power. On this system, pins are used for processing data sent from the sensor. The solenoid valve sensor will be connected to the digital pin 6 to receive data from the sensor. To open and close the flow of water, adaptor is used to assist by connecting the relay as a current limiter.

PIR is an infrared-based sensor. However, it is not as common as most infrared sensors that consist of an IR LED and a phototransistor. PIR does not emit anything like IR LEDs. As the name implies 'passive', this sensor only responds to the energy of the passive infrared beam held by every object detected by it. Objects that can be detected by these sensors are usually the human body. PIR sensor detects infrared waves that come from the body heat of

living creatures including humans (Agung, et al., 2013). These waves are emitted as humans move. The PIR sensor will connect to the Arduino via digital pin 8 can be seen in Figure 2.

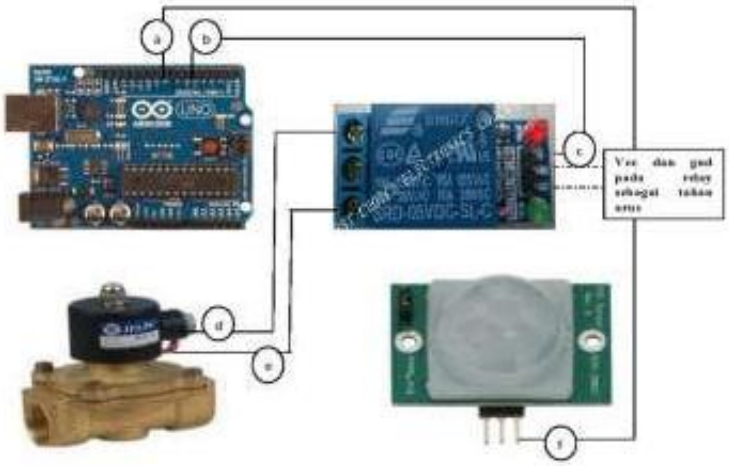

Figure 2. Design of solenoid valve Sensor, PIR sensor with Arduino

2) Design of flow liquid meter with Arduino

Arduino has several pins that serve as a place of data processing and power. On this system, pins are used for processing data sent from the sensor. The flow liquid meter sensor will be connected to the digital pin 2 to receive data from the sensor, GND pin and 5V pin as power for the sensor. To design flow liquid meter with Arduino can be seen in Figure 3.

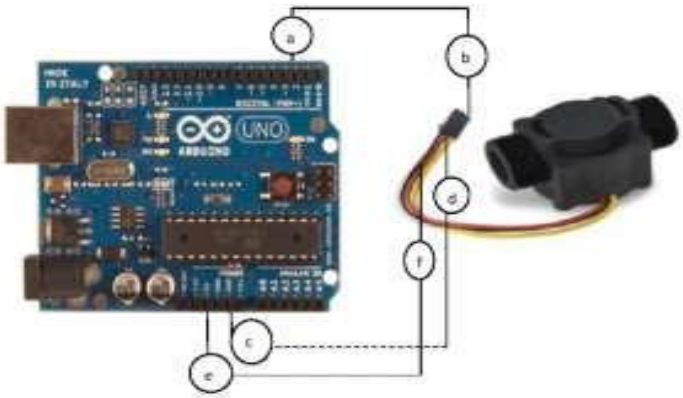

Figure 3. Flow liquid meter design with Arduino

3) Design of Wi-Fi Shield and Arduino

Wi-Fi shield is an additional module used on the Arduino to connect to a server using a Wi-Fi network connection. This module will be mounted with stackable method on the Arduino as shown in Figure 4.

Figure 4. Design of Wi-Fi shield and Arduino

V. Study and Result

System performance test is performed to determine the performance of the system in monitoring whether the system is running well or not.

1) The test performed will display the graph of the amount of water used only when the tool works. The display of the graph will drop because of the interaction of the PIR sensor detects the presence of humans in the room, this will cause the water in the tube to be reduced. Graph can be seen in Figure 5.

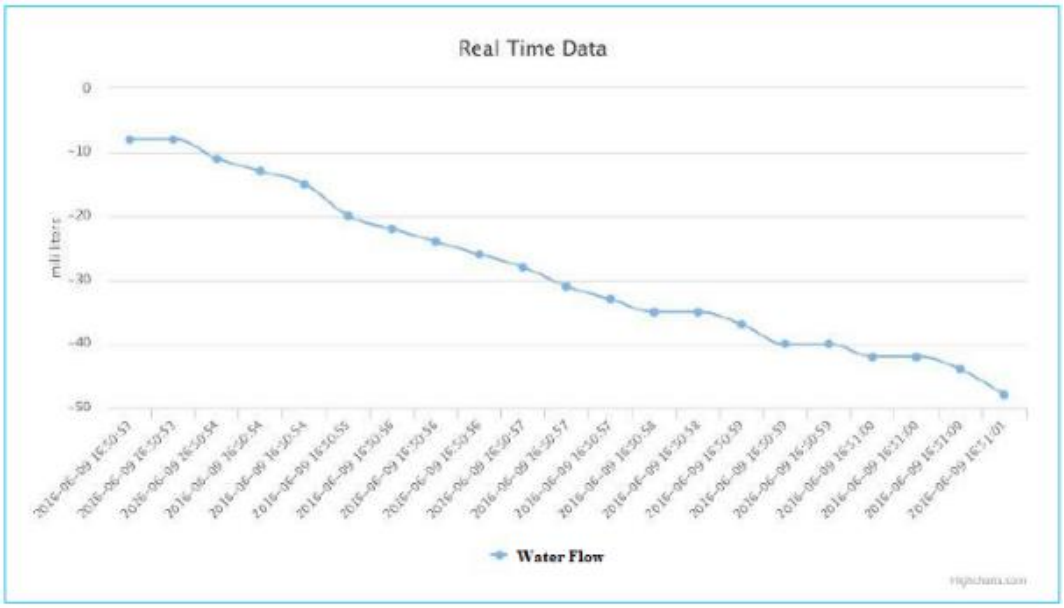

Figure 5. The display of water usage in graph

2) The second phase test will display the test results based on the large number of toilet users. The results of this test will be displayed in tabular form based on testing that have been done. Based on the results of testing the number of toilet users, if there is no toilet users, then the system or tool built will not work. This is due to the PIR sensor does not accept or detect the presence of humans in the toilet. So the water will not flow because the valve on the solenoid valve is not open. When one person enters the toilet, the built-in sensor or system will

work, and that's because the PIR sensor detects the presence of a human in the toilet. Then the valve on the solenoid valve will open so that water can flow when it's needed. What is detected by the PIR sensor is the heat wave generated by the human body. Similarly, when 2, 3, and 4 people enter the toilet, the built system or tool can still work well. From the tests conducted based on the number of toilet users can be concluded that the tool can work well. This study shows that the large number of users will not affect the performance of the sensor or system built. The table can be seen in Table 1.

Table 1. Pir sensor testing based on number of toilet users

No	Number of toilet users	Work	Does Not Work
1	0	-	Does Not Work
2	1	Work	-
3	2	Work	-
4	3	Work	-
5	4	Work	-

3) The next test will display the test results ranging from distance that can still be detected by the sensor. The test results performed will be displayed in tabular form. Based on the tests that have been done, the maximum distance that can be detected by the PIR sensor can only work at a distance of 3 meters, but the PIR sensor test with a distance of 3 meters is not as accurate as a distance of 1 meter or 2 meters. Because the heat wave generated by the human body is too far to reach the PIR sensor. If the toilet user is more than 3 meters away then the PIR sensor will not detect the presence of humans in the toilet and the automatic sensor will not work. Can be seen in Table 2.

Table 2. Pir sensor testing based on distance detectable by sensor

Distance / Meter	Detected	Not Detected
1 m	Detected	-
2 m	Detected	-
3 m	Detected	-
4 m	-	Not Detected

VI. Conclusion

The conclusions can be taken based on Simulation and Control of Clean Water Supply are The built system can reduce the level of human negligence in the use of water on campus toilets. The built system can improve the efficiency of water usage in campus toilets to reduce and anticipate the wasteful use of water. PIR sensor will not operate if blocked by objects or something thick, such as doors and walls of the toilet room.

References

[1] E. G. Sakliressy, "Kendali Keran Otomatis pada Toilet Pria dengan Sensor PIR (Passive Infrared)," *Skripsi Universitas Gunadarma,* 2010.

[2] Alfarobi, "Pembuatan Sistem Kran Otomatis Untuk Penghematan Air pada Tempat Wudhu dengan Sensor Gerak," *Skripsi Universitas Gunadarma,* 2011.

[3] Subandi, "Sistem Aplikasi Kran Otomatis Untuk Penghematan Air Berbasis Mikrokontrol Atmega 16," *Jurnal Teknologi Technoscientia,* vol. 6, no. 2, pp. 203-210, 2014.

[4] V. C. Oliveira and I. H. Yano, "Wireless Sensor Networks For Measuring The Consumption Of Save Water Taps," *American Journal of Applied Science,* vol. 11, no. 6, pp. 899-905, 2014.

[5] R. F. Rahmat, I. S. Satria, B. Siregar and R. Budiarto, "Water Pipeline Monitoring and Leak Detection using Flow," in *International Conference on Electrical Engineering, Computer Science and Informatics (IAES)*, 2017.

Tracking and Modelling of Flexible Wing Flapping Motion (#728)

Taufiq Mulyanto[1,a] , Nguyen Tien Dat
[1]Faculty of Mechanical and Aerospace Engineering, Institut Teknologi Bandung, Indonesia
[a]taufiq.mulyanto@ae.itb.ac.id

Abstract— *In flying animal world, there are different wing flapping motions to produce lift and thrust depending on their species and size, ranging from insects to big birds. The wing upstroke and downstroke movement combined with wing twisting produce the necessary aerodynamic forces.*

Studies generally limits the flapping motion into a simple sinusoidal upstroke and down-stroke motion in one vertical plane. The main aim of this thesis is to enrich the existing model of flapping motion and validate with experiment results. The study shows that flapping motion of a membrane wing is more complex than a permanent sinusoidal and rigid body motion. A flapping motion model has been developed to match the motion.

Keywords— *flapping motion, non-rigid wing, image processing*

I. Introduction

The aerodynamic phenomena around flapping wing are very complex. They varies according to the geometry and size of wing, flapping motion, and surrounding airfield. Whereas, bigger flying animal such as eagle or albatross, the aerodynamic phenomena is closer to those of flying aircraft, for smaller animal like insects, they are mostly unsteady, taking into account clap and fling, wake capture, and leading edge vortex [1]. The long term of the research is the development of a flapping wing UAV capable of hover flying. Typically flapping wing UAV uses a leading edge-membrane wing configuration which has certain flexibility that hasn't taken into account in the flapping wing aerodynamic model [2].

The widely used flapping wing aerodynamic model is DeLaurier model [3,4]. The motion of the wing is the combination between flaps up and down with pitching motion with some assumptions:

a. Upstroke and down stroke motion have equal time duration;
b. Both flapping and pitching movements are taken as sinusoidal functions with certain amount of lag;
c. Local wing pitching angle varies linearly along the wing span;
d. Wing is rigid.
e. Wing flapping axis coincides with body axis.

Flapping, and pitching angle varies as sinusoidal function

$$\beta(t) = \beta_0 \cos(\omega t) \qquad (1)$$

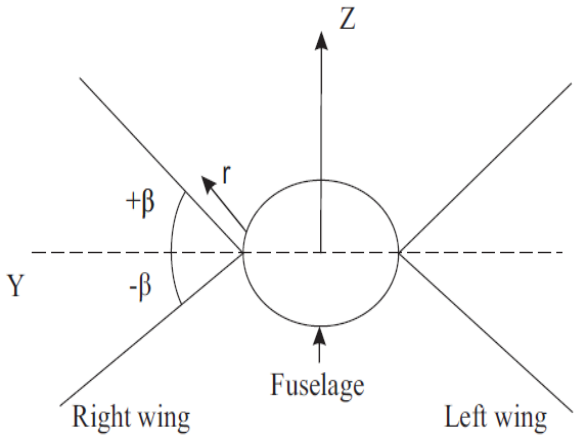

Figure 1. Flapping angle definition.

Where β_0 is the maximum flapping angle in horizontal plane. Fig.1. shows some parameters which *r* represents coordinate along the wing semispan and *B* is the semispan length.

For produce ability reason, almost all of bird sized flapping wing UAV used a membrane attached to oscillating leading edge to produce aerodynamic force. Despite its simplicity, the combined motion creates a combination of flapping and twisting wing motion. Structure used for leading edge is usually a long solid or hollow tube made of metal, plastic or composite. Considering the flexible mature of the leading adge and the membrane, the wing motion would be different from a simple sinusoidal motion.

The work presented introduced a function to model a flexible flapping wing motion based on data collected from experiment.

II. Tracking Flapping Wing Motion

Experimental Setup

To understand the motion of flapping wing, a flyable commercial product named Avitron v2.0 was used. It is a mono flapping wing with no hover flying capability. Avitron ‘s specifications are :

- Weight: 8.5g, length 17 cm, Wingspan: 33cm
- W ing flapping frequency: 18 Hz
- Wing amplitude angle: 550

EPIX camera system was used to capture the motion. It has a maximum quality of 640 x 480 10 bit image @ 211 fps. But it was set to 405 fps, with 480 x 300 pixel resolution. The total number of images captured was 241. With a flapping frequency of 16 Hz, the total number of image taken for one flapping cycle is 26.

Focusing on one side of the wing, six marker were located on wing leading and trailing edge. Each pair located close to the root, mid and tip.

Experimental Results

The markers were tracked and processed to determine their corresponding positions. Markers located spanwise showing flapping angle are presented in Figure 2. It can be seen that wing flapping is not sinusoidal and that the motion varies spanwise.

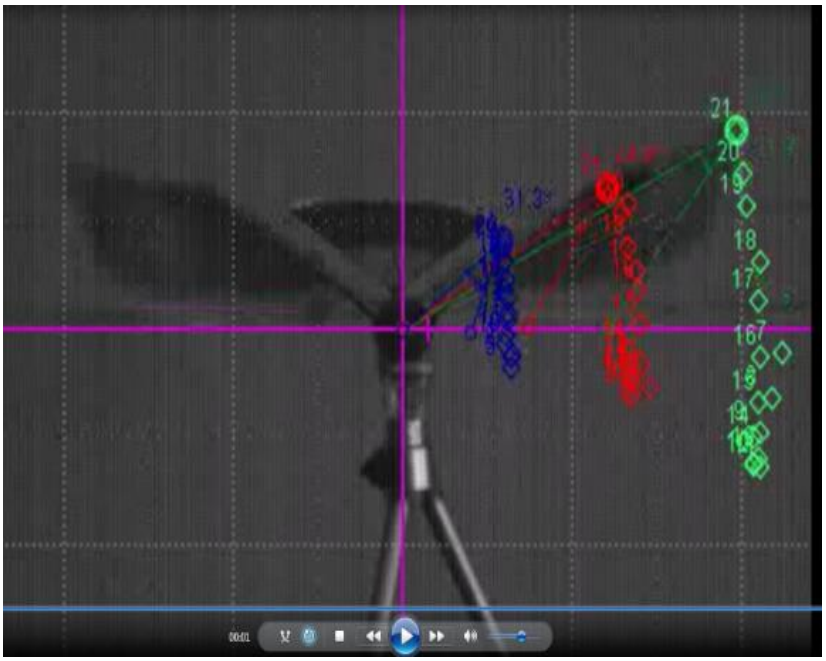

Figure 2. Image captured during motion tracking process.

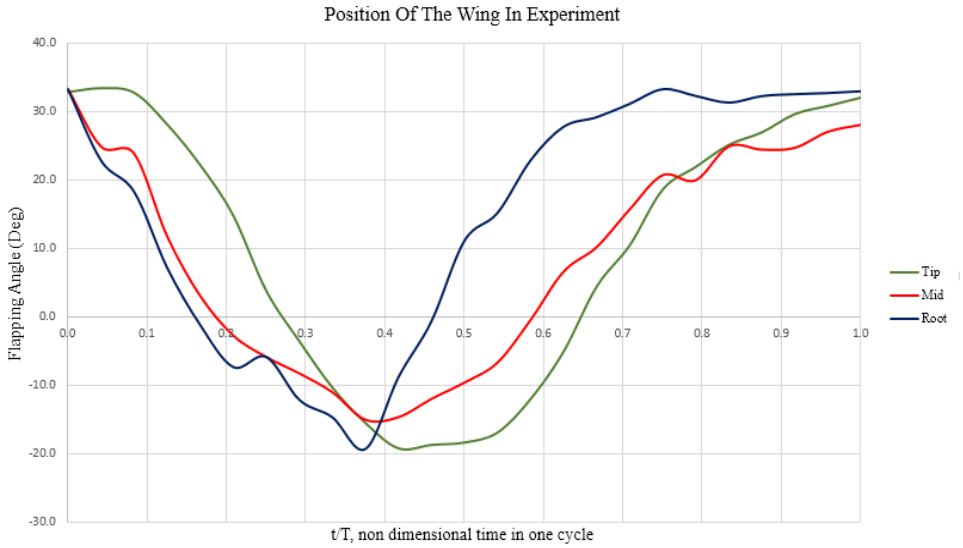

Figure 3. Flapping angle of each marker placed at leading edge.

Figure 3 presents markers leading edge position as it is seen from the front. Figure 4 shows half flapping cycle beginning with a downstroke motion and reached a minimum flapping at around 38% cycle. Figure 4 also shows the second half flapping cycle. It shows clearly that flapping motion is different than sinusoidal motion.

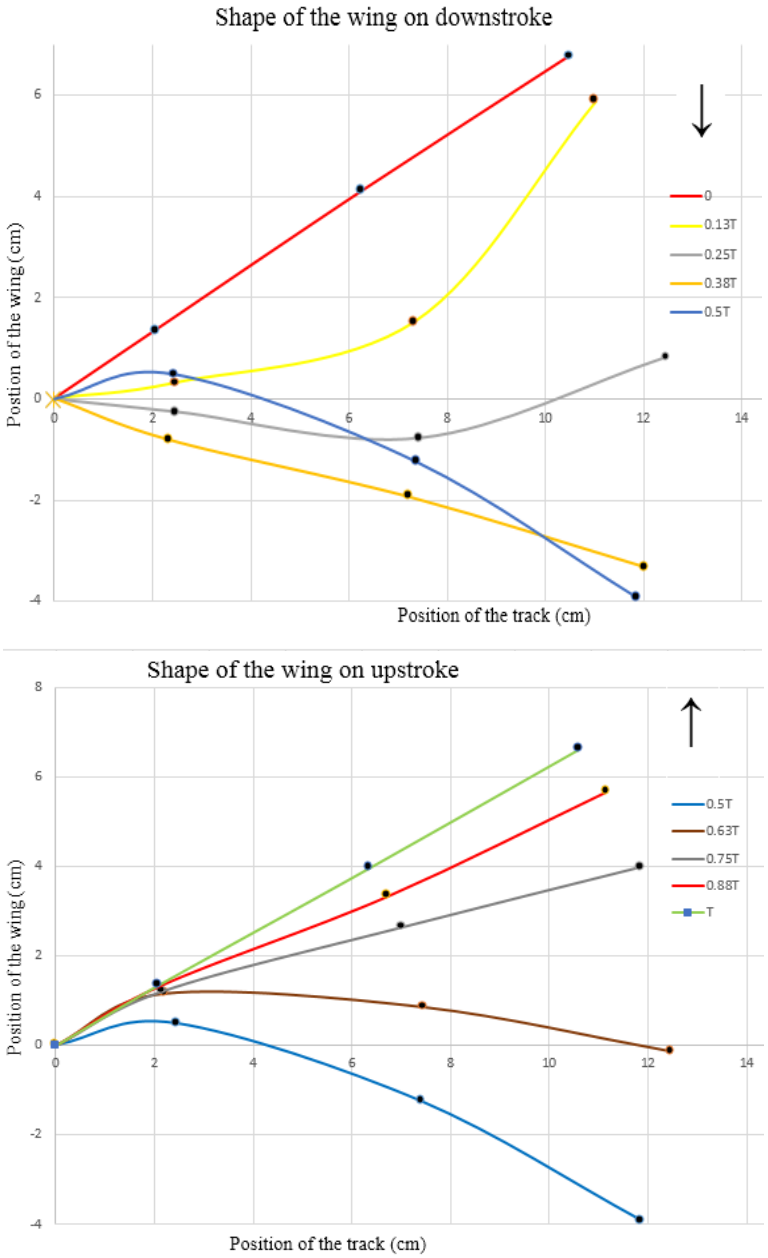

Figure 4. Flapping motion reconstruction of wing leading edge.

Non sinusoidal flapping motion model

The proposed function to model the flapping motion is:

$$\beta = a + \beta_0 \cos((\omega t) - x(\frac{2}{\pi} - \frac{4}{\pi}(\frac{\cos(2wt)}{3} + \frac{\cos(4wt)}{15} + \frac{\cos(6wt)}{35})) \quad (3)$$

Where:

β_0 : is the maximum flapping angle in assumption

a : the mean flapping angle

ω : flapping frequency

x : The frequency modulation parameter as a function of spanwise location.

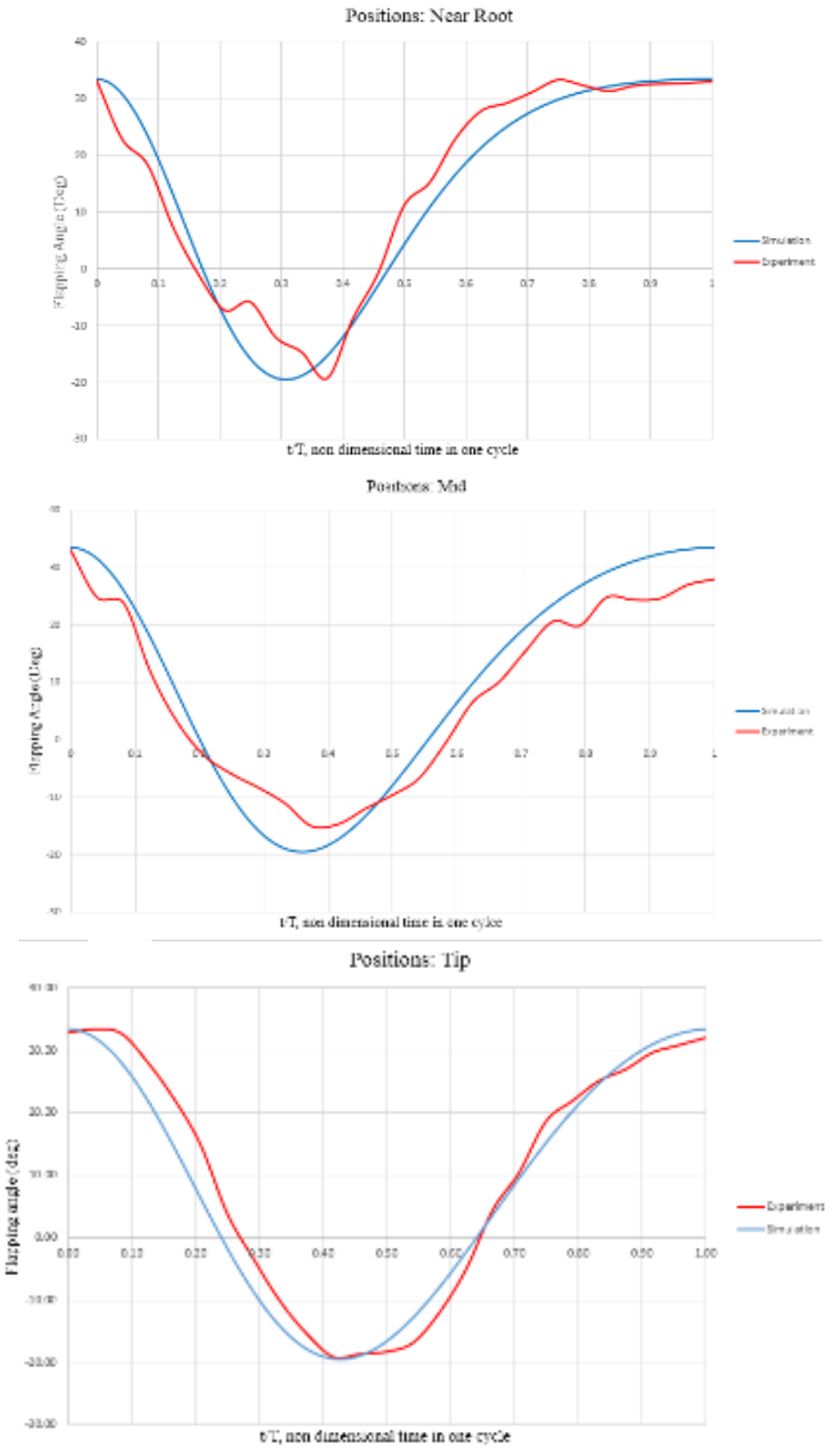

Figure 5. Flapping angle at near root, mid and tip of the wing approximation.

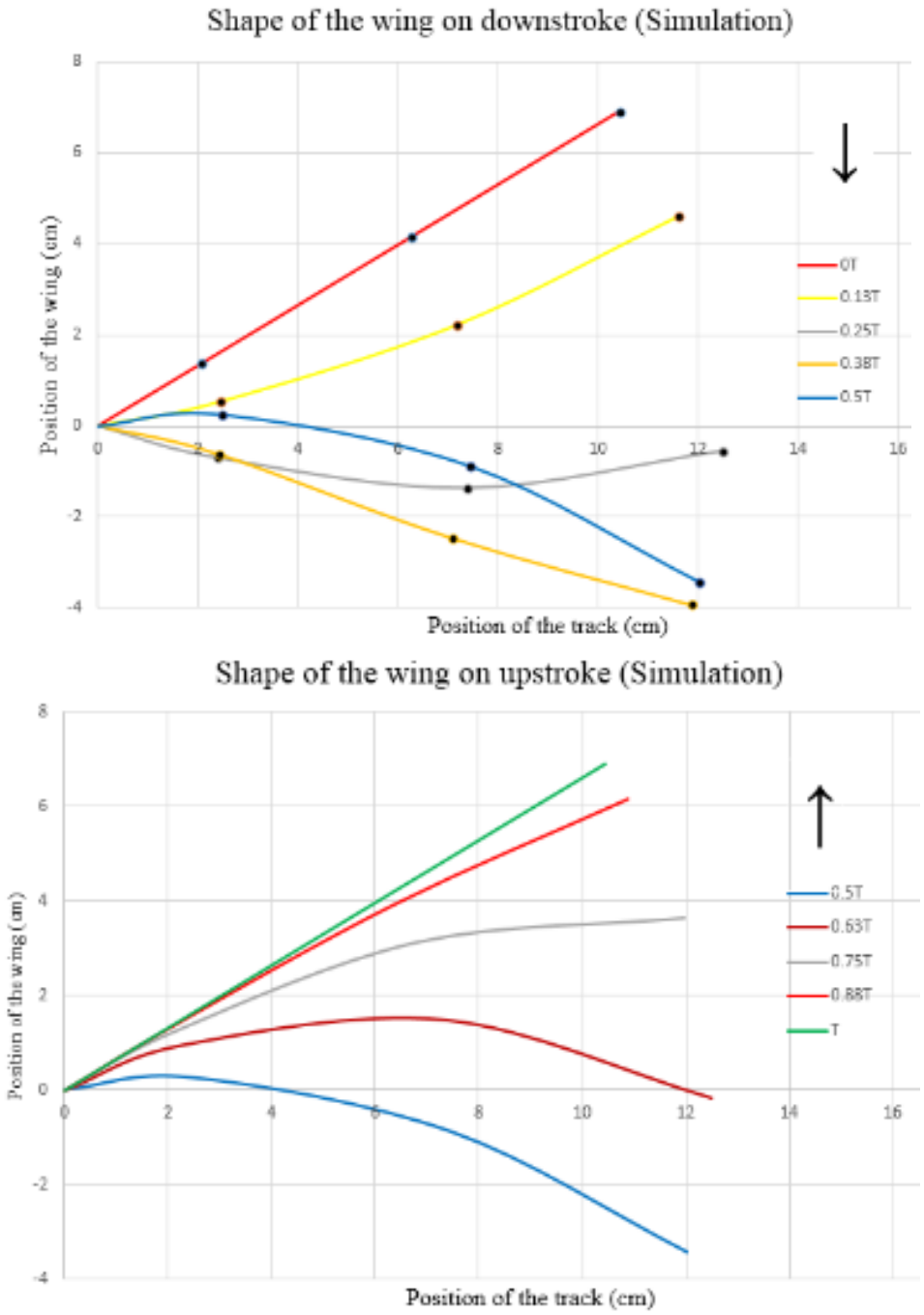

Figure 6. Flapping motion approximation of wing leading edge.

Figure 5 and Fig.6. show the function proposed can model the wing flapping motion well, not only for one section, but also for the whole semispan motion.

III. Conclusion

A function to model a flexible flapping wing motion was determined and showed to have a good conformity with experimental result. The function is able to model a non-sinusoidal motion which itself differs spanwise.

References

[1] D.E. Alexander, *Nature's Flyers. Bird, Insects and the Biomechanics of Flight*, The Johns Hopkins University Press, 2002
[2] T. Mueller (Ed), "Fixed and flapping wing aerodynamics for micro air vehicle applications, progress in Astronautics and Aeronautics". American Institute of Aeronautics and Astronautics, 2001
[3] J.D Delaurier, "An Aerodynamic model for flapping-wing flight", The Aeronautical Journal of The Royal Aeronautical Society, 1993
[4] T.D. Nguyen, S. Sdywaliva, T. Mulyanto, "Modelling of Wing Flapping Motion" Applied Mechanics and Materials, Vol. 842, 2016, pp 132-140

An Assessment Method for Beyond Visual Range Combat Capability of Fighter Aircraft (#724)

Khairul Ummah[1,a], Hisar Manongam Pasaribu, Dhani Anandito
[1] Bandung Institute of Technology,
[a]khairulu@ae.itb.ac.id

Abstract— *Modern air-to-air combat uses the advantage of stealth aircraft, long-range missile, and information network support. This tactic is known as beyond visual range (BVR) combat. Since this tactic is completely different to conventional within visual range (WVR) combat, information about the threat capability of opponent aircraft is necessary. The aims of the study are developing a method to assess threat capability and building a database of aircraft superiority as a basis for the development of BVR combat system. Thirteen important parameters have been identified and clustered into four categories. The assessment uses Analytical Hierarchy Process (AHP) method. The result shows the superiority rank of fighter aircraft based on BVR combat capability.*

Keywords— *beyond visual range, air-to-air combat, fighter aircraft, analytical hierarchy process*

I. Introduction

Modern military aircraft have many different roles including fighter, bomber, command control, attack, antisubmarine, and so on. A fighter aircraft is a military aircraft designed primarily for air-to-air combat against other aircraft. Fighter aircraft has been evolved in many years. The most advanced fighter aircraft today is the fifth generation fighter. The fifth-generation fighters are characterized by being designed from the start to operate in a network-centric combat environment and to feature extremely low multi-spectral signatures using advanced materials and shaping techniques [1].

With the new capability of the modern fighter, a new combat strategy has been developed. With the advance of electronic technology, a line of sight combat is not necessary anymore. The concept of beyond visual range (BVR) combat becomes the main tactics in the future. The BVR is beyond 15 nm combat that relies heavily on powerful radar and a long-range missile. Since this tactic is completely different to conventional within visual range (WVR) combat, an information about the threat capability of opponent aircraft is necessary [2]. In BVR confrontation, a fighter must have superior position against the opponent. For example, higher altitude position can increase the success of long-range missile to hit the enemy.

To assess and evaluate the combat performance of military aircraft, Robert Ball suggests several important parameters; they are including flight performance, weapons and tactics, threat warning, threat suppression, expendables, jamming and deceiving, and signature reduction [3]. Zikidis et al. provide an insight of aircraft stealth technology [1]. Rao describes the importance of microwave and infrared manipulation to increase aircraft survivability [4], and White explains the countermeasure technologies [5]. This paper focuses on how to assess the capability of military aircraft in beyond visual range combat. The aims of the study are

developing a method to assess threat capability and building a database of aircraft superiority as a basis for the development of BVR combat system.

II. Materials And Methods

Military aircraft data from several Southeast Asia nations are collected. About 23 fighter aircraft will be evaluated, including fourth and fifth generation aircraft such as Su-27SKM of Indonesia, F-15SG of Singapore, Su-30MKK of Malaysia, and F-35A of Australia. The data, such as flight performance, armaments, and combat features, are collected from various public information. To evaluate the threat capability, fighter aircraft parameters are clustered into four categories that are agility, flight performance, armament, and defense. The agility criteria are maximum speed, thrust-to-weight ratio, thrust vectoring control, and maximum G. The agility criteria are important in BVR combat because aircraft can avoid missile using a sudden maneuver. The agility usually is a combination between aerodynamics performance and powerful engine. The flight performance criteria are ferry range, combat range, and service ceiling. These criteria are important to gain superior position, because higher altitude will give aircraft an advantage to fire the enemy using a long-range missile. The armament criteria are radar range, short range missile, and medium-long range missile. This condition reflects the ability to strike the opponent, because BVR combat tactics rely on superior radar tracking and a long-range missile. The defense criteria are stealth, countermeasure, and camouflage, which are important because reducing the susceptibility of aircraft to be hit by enemy's missile.

The threat assessment is performed using Analytical Hierarchy Process (AHP) method. The AHP method is a structured technique for organizing and analyzing complex decisions. It uses weighting process to calculate a relative rank of some alternatives. Some of the combat features, such as lower radar signature, thrust vectoring capability, and radar performance cannot be compared quantitatively, hence the AHP uses qualitative judgment as measurement. The AHP method uses a comparison of two aircraft for every evaluation step, and calculates the inconsistency index. When the comparison is performed consistently then the inconsistency index will be lower, and the result becomes more reliable. For example if there are three alternatives, name A, B, and C, and A is higher than B, and B is higher than C, then A must be higher than C. This is an example of a consistent judgment. But, if the judgment says that C is higher than A, then this judgment is inconsistent. The comparing process is performed to all aircraft. After comparing all of the aircraft, the result will show a relative superiority among the aircraft.

III. Results

The result of AHP with the goal of aircraft superiority is shown in Figure 1. The left side shows the relative importance of the criteria. For example, in Figure 1.a the Power criteria (as a representation of agility) are more significant compare to Defense criteria. Using these weighted criteria, the AHP evaluation will show a superiority rank as shown on the right side (Figure 1.b). In this result, the F15SG has the highest score, followed by SU-27SK.

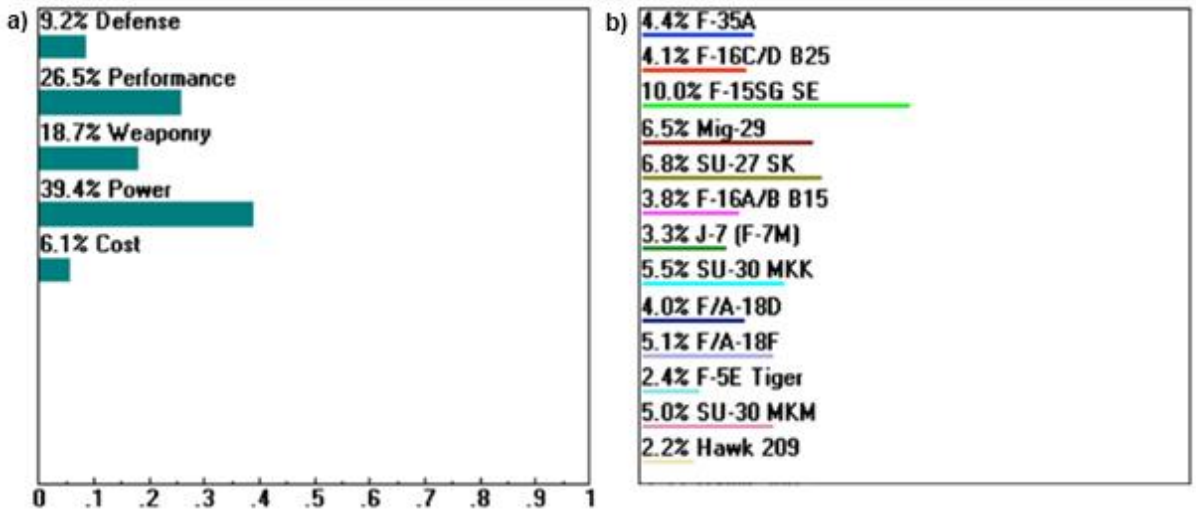

Figure 1 Threat capability of fighter aircraft. When power criteria are more important than other (a), the result of the superiority rank will show the benefit of powerful engine (b).

Figure 1 shown the result when defense criteria are less important than performance and weaponry. The result shows that using power (agility) and performance as the most important criteria, the bigger fighter aircraft will be more superior to the smaller one, since bigger aircraft has more powerful engine to gain superior combat position. But when the defense criteria are adjusted as an important criterion (as shown at Figure 2), the aircraft with stealth feature such as F-35A becomes more superior. In this result, the F-15SG still has the highest score, but the F-35A take over the Su-27SK as the second highest score. This result shows that in BVR combat scenario, the stealth feature can give an advantage for the fighter.

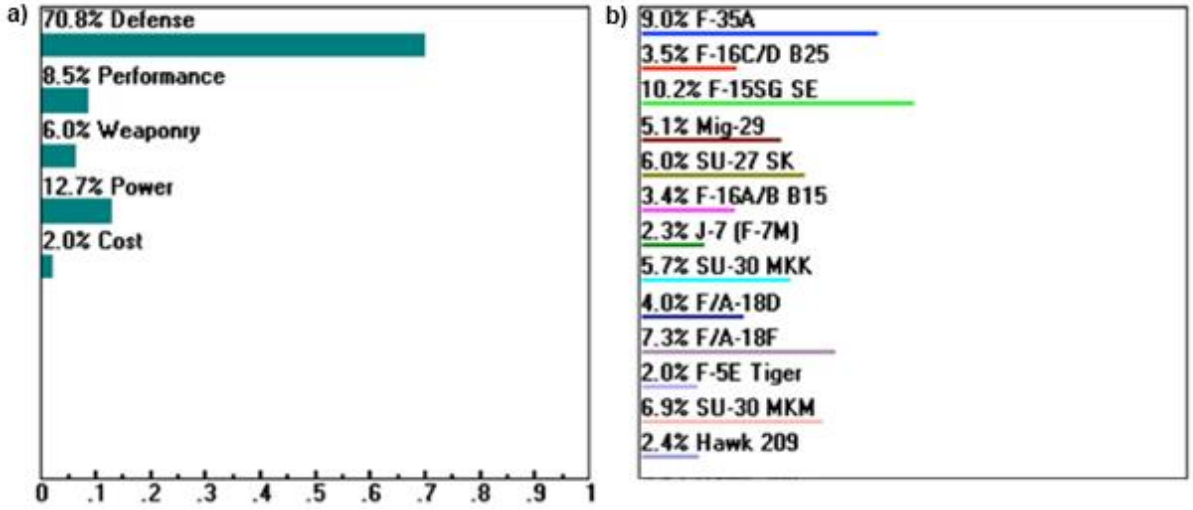

Figure 2 Threat capabilities of fighter aircraft. When the defense criteria are more important than other (a), the result of the superiority rank will show the benefit of stealth feature (b).

This result depends on the availability of data and the judgment from fighter pilots. Since the importance of every criterion will influence the final rank, the result may differ for a different scenario. For example, in BVR combat scenario, the fighter aircraft can gain superiority through powerful engine (Figure 1) or stealth characteristic (Figure 2). Depend on the situation; an aircraft can be more superior to the opponent using good tactics. A powerful engine fighter will

take higher altitude as the main tactics, when the stealth fighter will choose camouflage as his main tactics. It means that if the two aircraft with different superiority involved in BVR air-to-air combat, then the more superior aircraft can strike the enemy in the longer distance, hence increasing the probability to defeat the enemy.

This result is based on BVR combat scenario. In the modern combat tactics, aircraft superiority is not a single determinant factor. The concept of BVR combat requires radar-network support, long-range missile, and advanced firing logic. In the BVR combat system, a superiority database can be combined with fuzzy logic algorithm to build a combat decision support system. This system will help fighter pilot to choose the best tactics based on the current situation.

IV. Conclusion

An assessment method to evaluate BVR combat capability has been formulated. The method uses thirteen parameters clustered into four categories. Using Analytical Hierarchy Process method, several fighter aircraft can be compared. The result shows the relative superiority of fighter aircraft in BVR air-to-air combat scenario. This superiority information can be built into a database which is combined with fuzzy logic algorithm to create BVR combat decision support system.

Acknowledgment

This research is funded by P3MI Research Grant at Bandung Institute of Technology.

References

[1] K. Zikidis, A. Skondras, C. Tokas, “Low Observable Principles, Stealth Aircraft, and Anti-Stealth Technologies,” Journal of Computations & Modelling, vol. 4, no. 1, Scienpress Ltd, 2014, pp. 129-165.

[2] L. Xiao, J. Huang, “Maneuver Strategy in Beyond-Visual-Range Air Combat,” International Conference on Information Communication and Management IPCSIT, vol.16, IACSIT Press, Singapore, 2011.

[3] R. E. Ball, “The Fundamentals of Aircraft Combat Survivability Analysis and Design,” American Institute of Aeronautics and Astronautics, 2003.

[4] J. V. R. Rao, “Introduction to Camouflage and Deception,” DRDO Monographs/ Special Publication Series, Defence Scientific Information & Documentation Centre (DESIDOC), Defence R&D Organisation, Delhi, 1999.

[5] J. R. White, “Aircraft Infrared Principles, Signatures, Threats, and Countermeasures,” Naval Air Warfare Center Weapons Division Point Mugu, California, 2012.

Analysis and Simulation of Leakage Current in On-Grid Transformerless Solar Power System (#771)

Endah Komalasari[1,a], Reinaldy Aulia Kurniawan, Abdul Haris
[1]Department of Electrical Engineering, University of Lampung, Bandar Lampung
Jl. Prof. SumantriBrojonegoro 1 Bandar Lampung 35 145
[a]endah.komalasari@eng.unila.ac.id

Abstract—*The increasing of energy demands us to find other sources to solve this problem of energy scarcity. Solar power plants (PV) are often an alternative because of the many advantages of PV systems. PV is a collection of solar panels capable of converting solar energy into electrical energy. The output of a PV is a direct current, therefore, a mechanism is required that converts it into AC power for daily use. PV with a large power, usually using a transformer while the PV with little power, the transformer is not used. Consequently, there is a leakage current due to the parasitic capacitance of the earth. This paper aims to analyze the amount of leakage current that may occur within the system.*

Keyword *- leakage current, on-grid , PV, simulation, transformerless*

I. Introduction

Electricity has become one of the basic needs of society nowadays. Electricity is almost needed in every aspect of our lives, from households to industry. Electrical energy needs increase every year. This growing need is certainly a problem for our country's electricity provider, because most of the electricity supply comes from non-renewable sources. In other words, the fulfillment of the demands are more difficult.To help solve this problem, we need another renewable power source such as solar energy, water, waves, and so on. To convert solar energy into electrical energy, it takes a device called solar cells or commonly known as solar panels or photovoltaic.

Solar cells can convert solar energy into direct current / DC electricity, but most of the electrical equipment we use requires alternating current (AC) power to operate. Therefore, it needs a mechanism that converts DC power into AC or commonly called the inverter. Solar Power Generation or commonly abbreviated with PV can be a solution that can help reduce the scarcity of energy. PV with large power generally use a transformer to raise the voltage according to the working voltage of the grid. But on a small powered PV, the transformer is not used and the PV is directly connected to the grid to reduce losses and minimize costs. This system still has flaws. Galvanic relationship between the grid and the PV can cause a leakage current due to the parasitic capacitance of the earth. This current increase electromagnetic emissions and harmonics injected into the grid [1].

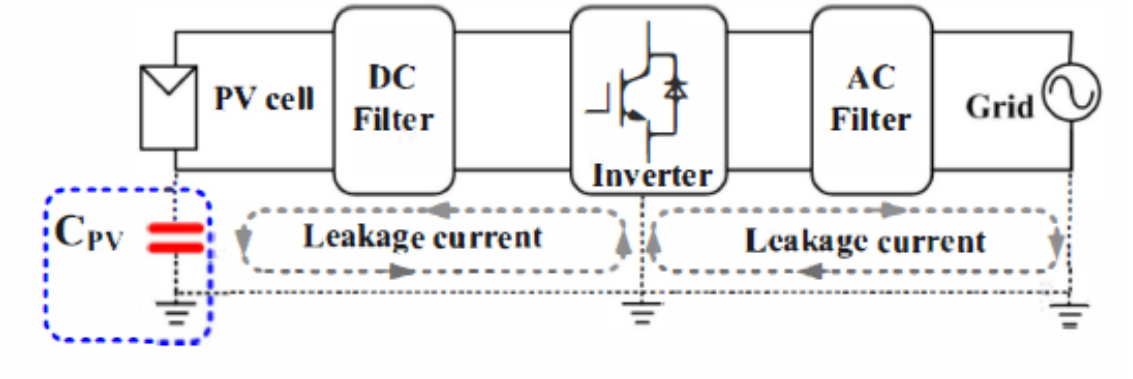

Figure 1 on-grid transformerless solar power system[3]

II. Simulation Model

This research uses MATLAB Simulink as software to perform simulation. This study evaluates the amount of leakage current with the following series:

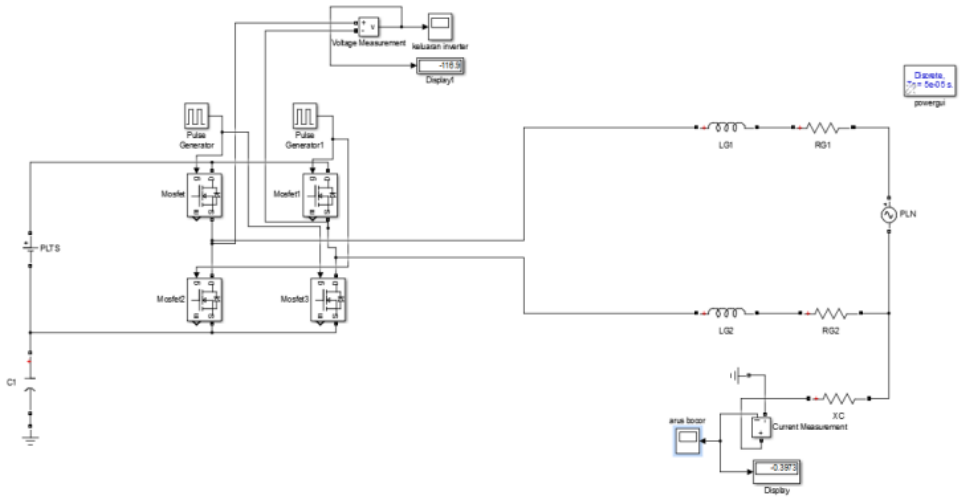

Figure 2 modeling circuit transformerless grid on solar power

The series is created in MATLAB Simulink workspace. The PV component is supplied with a grounded 220V DC voltage source. Then connected with a full-bridge inverter circuit single phase consisting of 4 pieces NPN MOSFET and fueled by two pulse generators. The output of the inverter is connected to the load (fixed load). Load or grid is given by an inductor and a resistor connected to the AC voltage source, as the PLN. The output of the grid is connected to a resistor component as the parasitic capacitive reactance modification which causes a leakage current. The model of Figure 1 was built to study the leakage current . The model includes a capacitor Cp that models the parasitic earth capacitance.

The ground resistor Rp was added for damping the leakage current at the resonant frequency. A value of 100 Ω was used to adjust the amplitude of leakage current of the simulationwaveforms to the experimental results.

III. Mathematical Modeling

a. Analysis of cell-to-frame Parasitic Capacitance

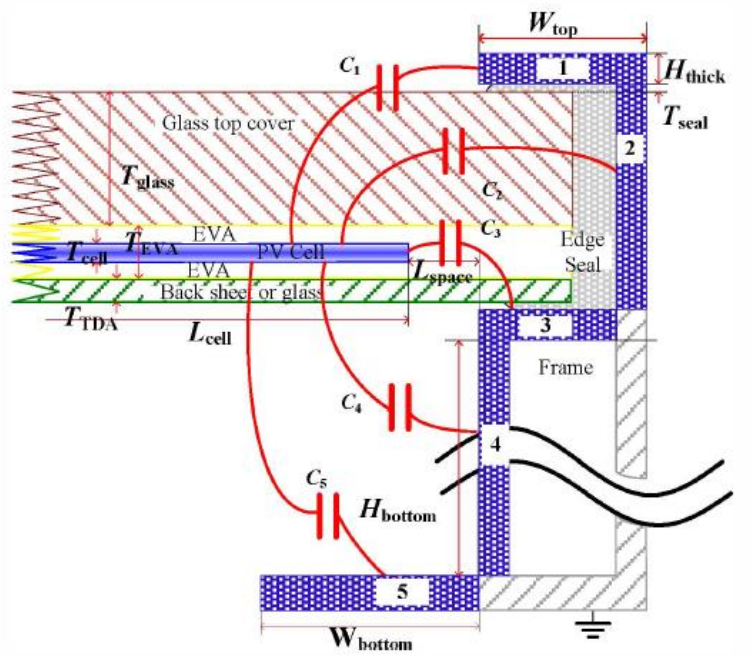

Figure 3 Field line contours are partitioned into five regions withcapacitance components defined as C1- C5[3]

For the computation region separated by Cl-C5, each component can be calculated through a fringe capacitance model, in which two conducting plates are not identical to each other. As shown in Fig. 3, the edge capacitance (perunit length) is composed of four components, generally, C_{top}, C_{side}, C_{bottom} and C_{in} . By using Schwarz-Christoffel mapping[4], these capacitance are derived as:

$$C_{top} = \frac{\varepsilon}{\pi}\ln(1+\frac{L}{a+b})$$

$$C_{in} = \frac{\varepsilon_0 \varepsilon_r L}{a} \quad (1)$$

$$C_{bottom} = \frac{(2-\ln 4)\varepsilon}{\pi} \quad (2)$$

and

$$C_{side} = \frac{\varepsilon}{\pi}\ln[2k\sqrt{k^2-1}+2k-1] \quad (3)$$

where

$$k = 1+\frac{b}{a} \quad (4)$$

$$C_{side1} = \frac{2\varepsilon}{\pi}\ln\left[\frac{a+\eta b+\sqrt{c^2+(\eta b)^2+2a\eta b}}{c+a}\right] \quad (5)$$

$$+\frac{M\varepsilon}{\pi}\ln\frac{\pi}{\sqrt{c^2+a^2}}\exp\left(-\frac{c-a}{c+a}\right)$$

with

$$\eta = \exp\left(\frac{d+c-\sqrt{c^2+b^2+2ab}}{\tau d}\right) \quad (6)$$

There is another way of analysing the parasitic capacitance, using a simpler method. It could be calculated if the amount of leakage current and ground voltage were known. The equation would be:

$$C_p = \frac{1}{2\pi f}\frac{I_{C_p}}{V_{C_p}} \tag{7}$$

b. Equivalent Circuit

The circuit shown in fig 2 can be simplified into simplier circuit shown in fig 3 :

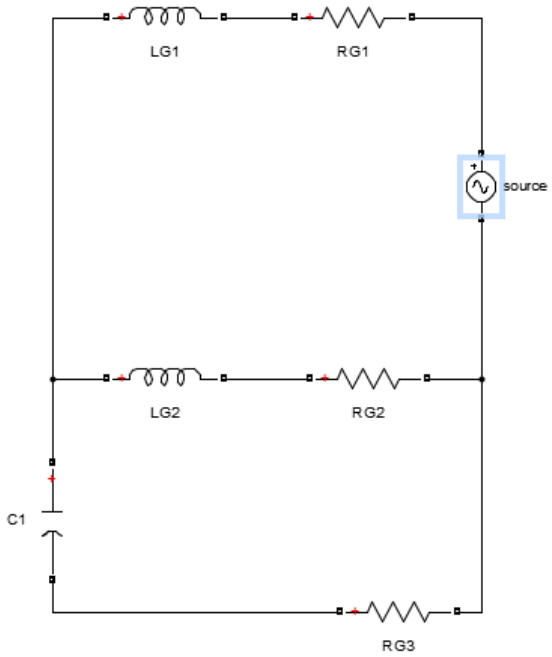

Figure 4 simplified equivalent circuit

Where source is both PLN and PV joined, LG and RG are the grid, and C1 is the paracitic capacitance of the system.The circuit can be analyzed by loop method. From the previous researches, the parameter of the sicrcuit can be found in table I.

TABLE I Components parameter

Parameter	Value
Vac	220V
f	50Hz
Lg	0.04 mH
Rg	0.1Ω
Rground	100 Ω
Cp	13.6 µF

IV. Simulation result

The simulation works in MATLAB Simulink.The PV component is supplied with a grounded 220V DC voltage source. Then connected with a full-bridge inverter circuit single phase consisting of 4 pieces NPN MOSFET and fueled by two pulse generators. The output of the inverter is connected to the load consisted of 0.04 mH inductor and 0.1 Ωresistor. Load or grid is given by an inductor and a resistor connected to the AC voltage source, as the PLN that has 220V peak voltage and 50 Hz of frequency. The output of the grid is connected to 100 Ωresistor component as the ground resistor Rp was added for damping the leakage current at the resonant frequency.The model includes13.6 µF capacitor Cp that models the parasitic earth capacitance.

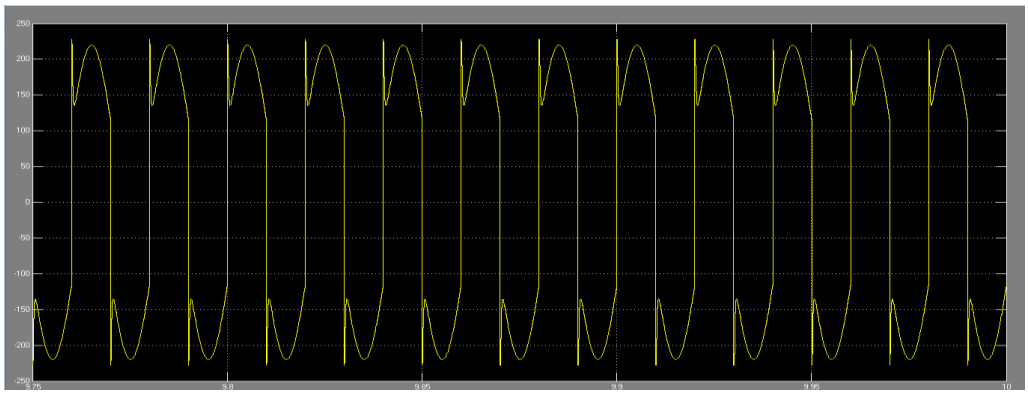

Figure 5 Inverter output after coupled with the grid without transformer

Figure 5 shows the result of inverter output waveform that has been coupled with the grid. The waveform has 33.3% of THD since it has not been connected to any filter. The waveform before connected to the grid would be block-waveform because it was using regular PWM switching technique as it shown in figure 6 below:

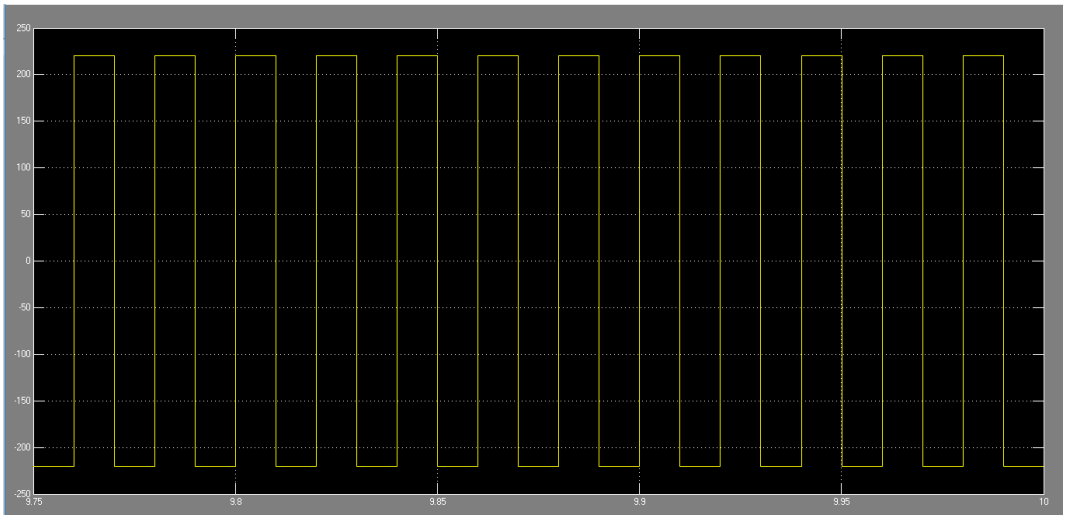

Figure 6 original inverter result

It has 220 V peak. From the simulation concluded that the leakage current is zero when the inverter has not been connected to the grid. After it has been connected, here is the leakage current waveform:

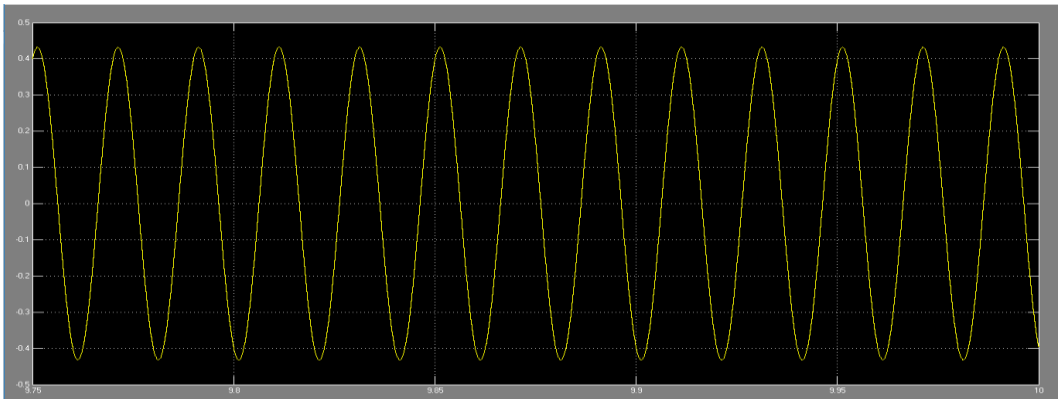

Figure 7 leakage current caused by Cp

As we can see from the diagram, there are some amount of leakage current after the solar power connected to the grid. This was calculated approximately 0,4 A peak.

This leakage current phenomenon of course can be handled by several solution. Without transformer, there is a galvanic connection of the grid and the DC source and thus a leakage current appears. Disadvantages of the appearing leakage current are increased system losses, impairing of electromagnetic compatibility and safety problems [5]. Ground current is limited by standards.In general, the leakage current is superimposed to the linecurrent therefore the harmonic content is increased comparedwith inverters without transformer. In transformerless grid connected systems a resonant circuit is created if the DCgenerator is not grounded. This resonant circuit includes the ground capacitance, the filters, the inverter and the impedance of the connected utility grid. Magnitude of the mentioned capacitance depends on the DC source and on the environmental conditions. For fuel cells this ground capacitances is very small so leakage currents with this kind of sources is not a topic.Nevertheless, in photovoltaic applications the panels ground capacitance goes from nanofarads up to microfarads [6], [7] and here leakage current is an important topic. It is important to know the resonance frequency in order toget a properly working system, because the first measure toreduce the ground currents is to decrease the excitation of theresonant circuit. A problem arises due to the great dependenceof the ground capacitance with environmental conditions, and hence the resonant frequency of the system. The resonance of the system can be controlled by a damping resistor or the choice of the LCL filter[1].

There are other solution in solving this problem. According to previous research, modulation technique was also giving significant result difference. Bipolar modulation is more recommended than unipolar modulation since the leakage current aused by that technique is lower than the other one[1]

Leakage current can also be reduced by using galvanic isolation technique and common-mode voltage (CMV) damping. The galvanic isolation can be achieved via dc-decopling or ac-decoupling, for isolation on the dc- or ac- side of the inverter. Nevertheless, leakage current cannot be simply eliminated by galvanic isolation and modulation techniques, due to the presence of switches junction capacitances amd resonant circuit effects. Hence, CMV damping is used in some topologies to completely eliminate the leakage current[8]

V. Conclusion

In this paper, the leakage current in a single-phase transformer-lessinverter connected to the grid was evaluated. Waveforms of the measured ground voltage and leakage currentwith different modulation strategies and under different outputpower conditions are presented. Without the isolation capabilitiesof the transformer, a resonant circuit arises due to theground capacitance of the PV panels. The study of the leakage current is needed in order to anticipate any unwanted harm from the current.

Based on the simulation results, the ground capacitance of the PV panels was estimated and a simple model that producessimilar results was built. From this, a resonant circuit model should be proposed and an expression to calculate the approximateresonance frequency of the system was derived and in order to be a filter upon noises within the output of inverter wave. Values estimated of ground capacitance change with frequencyso further investigation in this topic is needed in orderto obtain an improved model that provide accurate results.

Acknowledgement

In addition, a deepest grattitude to The Insitution of Research and Civic Serving in University of Lampung (LPPM Unila) that had granted the funding needed in order to finish the research. The funding was originated from the superior research for universities (PUPT).

References

[1] Oscar Lopez, Remus Teodorescu, Francisco Freijedo, “Leakage Current Evaluation of a singlephase transformerless PV inverter connected to the grid”, IEEE, 2007
[2] Asnal Efendi, “Pembangkit Listrik Sel Surya pada Daerah Pedesaan”, Institut Teknologi Padang, vol 1 no 1, Jan 2012
[3] Wenjie Chen, Xiaomei Song, Hao Huang and Xu Yang, “Numerical and Experimental Investigation of parasitic edge capacitance for Photovoltaic Panel”, The International Power Electronics Conference, 2014
[4] L. Wei, 1. Deng, and H.-S P. Wong, "Modeling and performance comparison of 1-0 and 2-D devices including parasitic gate capacitance and screening effect," IEEE Trans. Nanotechnol., vol. 7, no. 6, pp. 720-727, Nov. 2008
[5] J. Myrzik and M. Calais, "String and module integrated inverters forsinglephase grid connected photovoltaic systems -a review," in 2003IEEE Bologna Power Tech Conference Proceedings, vol. 2, Jun. 23-262003.
[6] M. Calais, V. Agelidis, and M. Meinhardt, "Multilevel converters forsinglephase grid connected photovoltaic systems: An overview," SolarEnergy, vol. 66, no. 5, pp. 325-335, August 1999.
[7] M. Meinhardt and P. Mutschler, "Inverters without transformer in gridconnected photovoltaic applications," in Proceedings of 6th EuropeanConference on Power Electronics and Application (EPE 95), vol. 3,Sevilla, Sep. 1995, pp. 3086-3091.
[8] Tan Kheng Suan Freddy, “Comparison and Analysis of Single-Phase Transformerless Grid-Connected PV Inverters”, IEEE Transactions on Power Electronics, vol 29, No 10, October 2014

Anaerobic Wastewater Treatments : Prediction of Retention Time on RT/RW Plant (#635)

Dessy Agustina Sari[1,a], Sukanta[2,b], Azafilmi Hakiim[2,c]

[1]Electrical Engineering Department of Engineering Faculty, Universitas Singaperbangsa Karawang – West Java, Indonesia
[2]Industrial Engineering Department of Engineering Faculty, Universitas Singaperbangsa Karawang – West Java Indonesia
[a]dessy.agustina8@gmail.com, [b]sukanta.tsm@gmail.com, [c]aza252116@gmail.com

Abstract*—Waste water treatment gave major problem in higher of chemical oxygen demand that backgrounded by amount and type of PT RT/RW products. The waste was polymer, mixture of nitrogen, mixture of phosphate, and oil. This factory used active sludge and microorganism (anaerobic condition). Research result showed that pH ranged 4,94 until 8,02. This data gave a decreasing sharply in acidic condition. The thing could be caused acetogenic phase in area pond anaerobic. The phenomenon might be recited because possibility of biologist living this waste did not take place as well and or could give deathly affect to the anaerobic bacteria. Customary pH for the bacteria was 6,8 – 7,4. Temperature data reached 28-33^{o}C so their activities were good. Then, efficiency of anaerobic waste water treatment was 62,95 to 66,06%. The data indicated that the research was not accordance with SOP companies. Inlet concentration of chemical oxygen demand had variation and gave unbalancing affect to digestive bacteria load. Estimation to get valid COD was 11-14 days. The duration was required by the microorganism to digest the matter organic perfectly to be methane and carbon dioxide gas.*

Keywords*—anaerobic process, COD, pH, retention time, temperature*

I. Introduction

NOWADAYS, a to-do industry was being one of any development in Indonesia country, especially Karawang regency – West Java. Customer demands were the reason to build many plants and that thing created much effect as the consequence from industry sphere environment Waste that produced had stained the soil. Quality reduction of clean water was to be dilemma for civil resident in surroundings the area. Bumi Pangkal Perjuangan was loaded chemical industry, manufacture, automotive, and others. More than one thousand factories (local and foreign) were present in here. Their location was nearly Citarum stream current where blackened the industry disposal. Waste water contained many chemical substances such as Fe and Mn dissolve, Cr, Hg, Cu, Pb, and others that to be poison and dangerous so the waste water treatment should be applied. The banishment to river or domain had accomplished standardization which ruled by KEP-51/MENLH/10/1995 [1].

Company RT/RW was one of factory that making specialty chemical matters for water treatment, power generation, cooling system, wood and paper industry, metal factory, then

process and refinery oil plant. The RT/RW liquid waste was managed by itself with four steps assembling that resumed in belong to Figure 1. The composition was polymer, mixture nitrogen, mixture phosphate, and oil. The detail was showed on Table 1 below.

Table I . The Liquid Waste PT RT/RW

Source	Flowrate, m^3/day
Blending wash from plant	2
Container wash and ex drum	3
Laboratory and kitchen wash	1
Total	6

That waste handling had given many troubles for Waste Water Treatment Unit, higher chemical oxygen demand (COD), temperature, total dissolved solid (TDS), biological oxygen demand (BOD), pH, mixed liquor suspended solid (MLSS), etc. Prefix problem was sum and type products. The company determined the anaerobic waste water treatment system. This method could reduce the treatment volume, enhance stability, destruction pathogens, and producing methane [2], [3]. The COD parameter goal could reach efficiency in the amount of 80-90%. Generally, more than 84% was a good point for both the COD and BOD [4]. Much organic material became the processing principle background.

Duration of retention time was needed to explore the range of optimally liquid waste treating. This thing was did because its minus gave an unpleasant odor (most important while produced sulfide acid), the activity required more time to accomplish its job before the sample went to the aerobic proceed, contributed in nitrite level enhancing (be existed the advanced handling before the waste was flowed to disposal channel). Longer retention time made almost all of volatile acid to be methane and carbon dioxide gas. Furthermore, limit of acidity degree (pH) for the waste was 6 – 9. The distance helpful the water animal plant growth. Number of 28-30^{o}C acted as valid temperature for the safe waste. Both of temperature and pH could affect the performance of reactor.

The score of COD process that measured was 14 - 28 times from the standard quality (maximum 300 mg O_2/L). This case study proposed to evaluate the performance of anaerobic waste water treatment (efficiency segment). There was the estimation of retention time to predict the organic substance dissociation perfectly before going into the next step.

II. Waste Water Treatment and Sample Testing

The waste passed four ways to reach a good quality before exiled to the circles. The sampling was on the third step (see Figure 1) and the procedure for the thing was explained on Figure 2 this below.

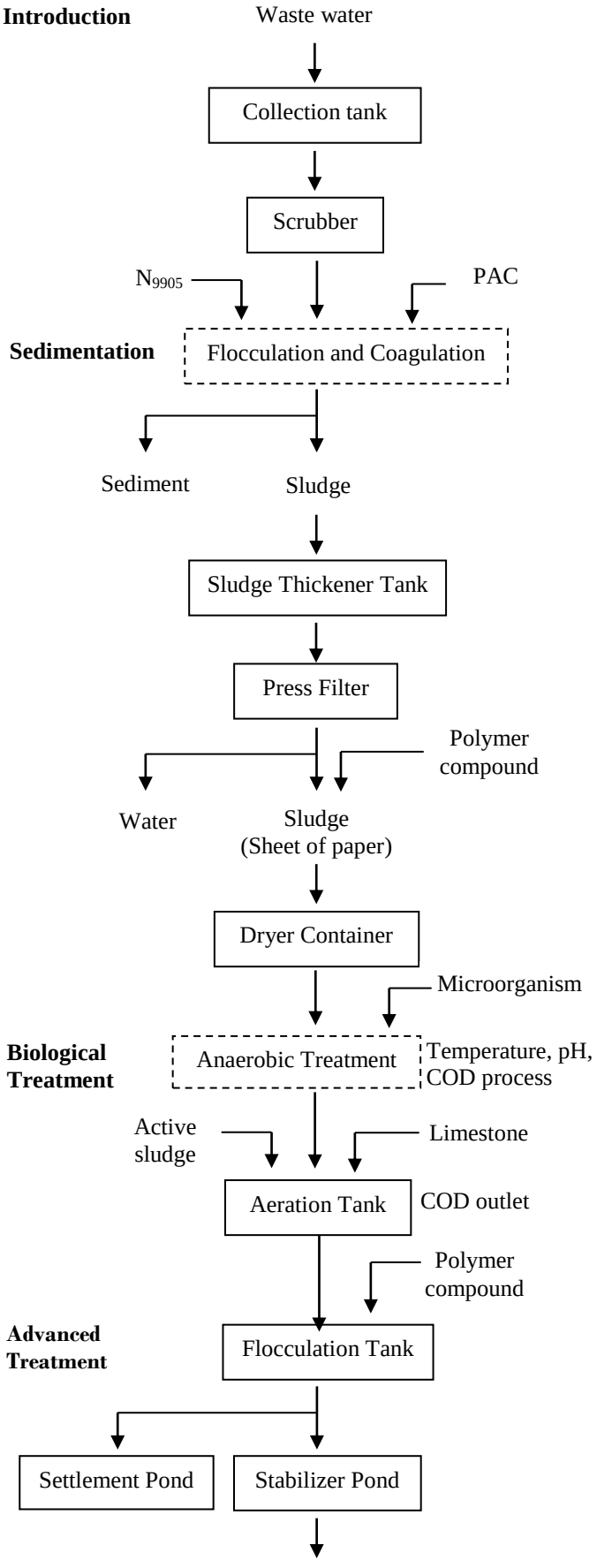
Introduction
Waste water
Collection tank
Scrubber
N_{9905}
PAC
Sedimentation
Flocculation and Coagulation
Sediment
Sludge
Sludge Thickener Tank
Press Filter
Polymer compound
Water
Sludge (Sheet of paper)
Dryer Container
Microorganism
Biological Treatment
Anaerobic Treatment
Temperature, pH, COD process
Active sludge
Limestone
Aeration Tank
COD outlet
Polymer compound
Advanced Treatment
Flocculation Tank
Settlement Pond
Stabilizer Pond

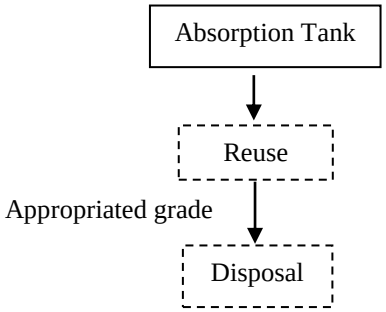

Figure.1. Waste water treatment scheme

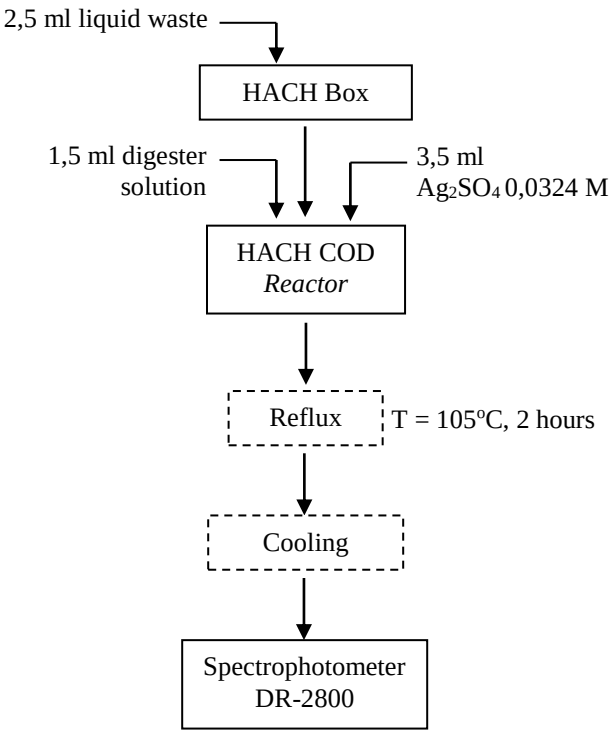

Figure.2. Measuring procedure of chemical oxygen demand

III. Result and Discussion

The liquid waste processing used trial time as along six days to reduce the COD contents. This research made an assumption that the parameter value decreased logarithmically. The experiment data could be seen in Figure 3. The pH and temperature gauging in the discharge anaerobic treatment were given in Table 2.

Table 2. Temperature and Acidity Degree in the Anaerobic Process

Day	Temperature, ^oC	pH
1	28	8,02
2	29	7,50
3	31	5,06
4	30	5,72
5	31	6,71
6	29	6,78

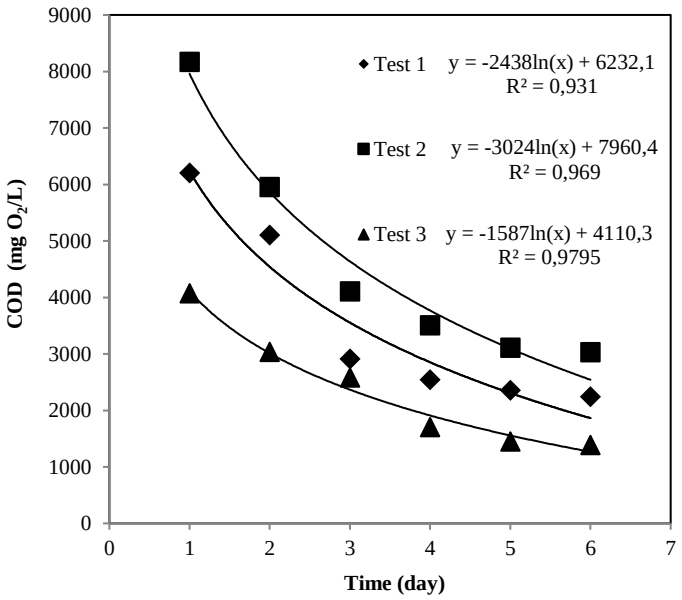

Figure.3. Reduction of waste chemical oxygen demand in six days

The research has been done as three times and Table I was the one of its result. The graph of COD data to time delivered the estimate equation of retention time. The organic matter digestion was well done which requiring 11 until 14 days to complete the process. This effort was aimed to get the reasonable COD quality. The first to third experiments had the different final score of COD process (± 6300, 8200, and 4100 mg O_2/L respectively research) so the same way of treating in anaerobic process also gave a significantly difference on COD outlet data (± 2300, 3200, and 1400 mg O_2/L, consecutively). The COD parameter had efficiency range of 62 – 66% as long six days for trial and error experiments. The result revealed that possibility of organic matter deterioration was overloading. Longer time was needed for methane generation to stabilize [5]. The same statement was in anaerobic digester plant about level of volatile fatty acid [6]. The output also showed that the waste was not compatible to throw away. Thus, reason of low COD removal rate was imbalance in microbial activities, and negative-collapse of the deterioration [7], [8].

Longer retention time could be option through the mathematic calculation. However, company RT/RW could not do the scientific solution because this case had amount of waste and factory product that be various made unpredictable load. This incident would be over tank capacity. More than 10 days of retention time gave a risk. Existing of partial sludge stabilization happened in activated sludge process and caused in low efficiency both from a

processing and economic aspect. Possible chance that took company RT/RW was the microorganism quantity improvement to describe organic matter to be methane and carbon dioxide gas. Other idea was the anaerobic step to be staged, and or parallel process (distribution of processing) to get the COD of 150-300 mg O_2/L. That option would be done if the test result on Advanced Treatment was far away from standardization.

This resulted was also supported by review article that giving suggestion to enhance the efficiency of reactor through maintenance optimal of operating conditions [9]. Using a semi-continuous stirring tank could decrease the retention time with waste activated sludge from 32 to 6,4 days on sludge reduction, soluble chemical oxygen demand, and dehydration capability [10]. pH achievement gave average value of 6,63; 6,20; and 6,54 in each repetition experiment. Then, the waste temperature was 29,67; 30,00; and 29,83 in respectively. Both of testing has been corresponding. Temperature played an important role to support the activity of digestive bacteria on the anaerobic liquid waste treatment. This data indicated that the process that occurring did not disturb their doing in anaerobic tank. However, the lacking would be happen if condition was under 10^{o}C. On food waste research, discharge of temperature mesophilic was 35-57^{o}C. This thing could improve reaction rates, higher gas production and also destruction of pathogen [11].

Significant losing was present at the third measuring where the waste became more acidic. This phenomenon could be caused acetogenic phase that taking place on the anaerobic tank. The microorganism needed environment with pH of 6,8 – 7,4. Less 6 or up 8 point gave an effect that the creature could not work very well. The water pH that not being neutral produced a difficult in biological treatment, and also this thing could kill the bacteria in the water.

IV. Conclusion

The waste water treatment in company RT/RW needed almost 2 weeks for the bacteria to remodel the organic fed in totality before going to the aerobic process. The research also produced pH and temperature that reaching the disposal quality. Processing development was keep built to reduce COD so the retention time was no more six days.

References

[1] M. L. H. Menteri Lingkungan Hidup, *Lampiran : Keputusan Menteri Lingkungan Hidup Nomor : KEP-51/MENLH/10/1995 tentang Baku Mutu Limbah Cair Bagi Kegiatan Industri*. Kementerian Lingkungan Hidup dan Kehutanan Republik Indonesia, 1995.

[2] L. Appels, J. Baeyens, J. Degrève, and R. Dewil, “Principles and Potential of The Anaerobic Digestion of Waste-Activated Sludge,” *Prog. Energy Combust. Sci.*, vol. 34, no. 6, pp. 755–781, Dec. 2008.

[3] A. Mottet, J. P. Steyer, S. Déléris, F. Vedrenne, J. Chauzy, and H. Carrère, “Kinetics of Thermophilic Batch Anaerobic Digestion of Thermal Hydrolysed Waste Activated Sludge,” *Biochem. Eng. J.*, vol. 46, no. 2, pp. 169–175, Oct. 2009.

[4] D. Bolzonella, P. Pavan, P. Battistoni, and F. Cecchi, “Mesophilic Anaerobic Digestion Of Waste Activated Sludge: Influence Of The Solid Retention Time In The Wastewater Treatment Process,” *Process Biochem.*, vol. 40, no. 3–4, pp. 1453–1460, Mar. 2005.

[5] D.-J. Kim and J. Lee, “Ultrasonic Sludge Disintegration for Enhanced Methane Production in Anaerobic Digestion : Effects of Sludge Hydrolysis Efficiency and Hydraulic Retention Time,” *Bioprocess Biosyst. Eng.*, vol. 35, no. 1–2, pp. 289–296, Jan. 2012.

[6] I. H. Franke-Whittle, A. Walter, C. Ebner, and H. Insam, “Investigation Into The Effect Of High Concentrations Of Volatile Fatty Acids In Anaerobic Digestion On Methanogenic Communities,” *Waste Manag.*, vol. 34, no. 11, pp. 2080–2089, Nov. 2014.

[7] N. Krakat, A. Westphal, S. Schmidt, and P. Scherer, “Anaerobic Digestion of Renewable Biomass : Thermophilic Temperature Governs Methanogen Population Dynamics,” *Appl. Environ. Microbiol.*, vol. 76, no. 6, pp. 1842–1850, Mar. 2010.

[8] C. Dennehy *et al.*, “Process Stability And Microbial Community Composition In Pig Manure And Food Waste Anaerobic Co-Digesters Operated At Low HRTs,” *Front. Environ. Sci. Eng.*, vol. 11, no. 3, Jun. 2017.

[9] K. V. Rajeshwari, M. Balakrishnan, A. Kansal, K. Lata, and V. V. N. Kishore, “State of The Art of Anaerobic Digestion Technology for Industrial Wastewater Treatment,” *Renew. Sustain. Energy Rev.*, vol. 4, no. 2, pp. 135–156, 2000.

[10] X. Li, Y. Peng, Y. He, S. Wang, S. Guo, and L. Li, “Anaerobic Stabilization Of Waste Activated Sludge At Different Temperatures And Solid Retention Times: Evaluation By Sludge Reduction, Soluble Chemical Oxygen Demand Release And Dehydration Capability,” *Bioresour. Technol.*, vol. 227, pp. 398–403, Mar. 2017.

[11] J. K. Kim, B. R. Oh, Y. N. Chun, and S. W. Kim, “Effects of Temperature and Hydraulic Retention Time on Anaerobic Digestion of Food Waste,” *J. Biosci. Bioeng.*, vol. 102, no. 4, pp. 328–332, Oct. 2006.

Analysis of Surface Roughness Value when Drilling Magnesium AZ31 using Taghuci Method (#654)

Gusri Akhyar Ibrahim[1,a], Arinal Hamni[1], Sri Maria Puji Lestari[2]

[1]Mechanical Engineering Department of University of Lampung
[2]Mechanical Engineering Department of University of Malahayati
[a]gusri.akhyar@eng.unila.ac.id

Abstract- *Magnesium alloy is one of super alloys material which wide used in manufacturing of automotive, biomedic, sport and electronic components. It was due to very light and resistent to corrosion. Surface roughness value has an important role to estabilish the quality of components. To produce a good surface roughness of machined surface, one of the important thing depends on the friction between the cutting tool and workpiece material when cutting process occurred. The aim of this paper is to analyse the surface roughness values of machined surface when drilling of magnesium alloy AZ31 using design of experiment of Taguchi Method. The experimental trials took place at cutting rotation of 635, 970 and 1420 rpm, feed rate of 0.10, 0.18 and 0.24 mm/rev, diameter tool of 10, 12 and 14 mm. The cutting of magnesium alloy was done by using a convensional drilling machine with TCA - 35 Erlo. Analysis of variance on the data of surface roughness value was done to get which factor is the most significant. The result shows that the feed rate is the most significant factor that contributed on the surface rougness value of machined surface. The minimum surface roughness value was attained at cutting rotation of 970 rpm, feed rate of 0.10 mm/rev and diameter of tool of 14 mm. Therefore, it can be stated that selecting the low feed rate factor produced low surface roughness value. Another hand, using high cutting rotation resulted low surface roughness value.*

Keywords*: drilling, surface roughness, magnesiun AZ31, Taguchi Method*

I. Introduction

Pure magnesium and magnesium alloy have been known as materials that have characteristic such as very light, easy to burned and very easy to react to others materials. Pure magnesium does not has enough strength, therefore magnesium is very good when blended with other elements to get better characteristics. One is the important attribute of magnesium alloy is strong at high weight ratio [1,2]. Pure magnesium produced by casting, forming and machining. One of important produced methods is machining to make a precision component. The aim of machining of magnesium alloy is to achieve surface quality of component.

One of dominant magnesium characteristics is easy to react with other materials (pyrophepric), so that high risks flame/burn. In spite of products from magnesium have a risk as long as machining process, but manufactured process can be controlled [1].

In field of biomedic and health, using material magnesium as replacing bone has some advantages. The advantages are such as mechanical properties similar to bone and good biocompatible with the body. In the body, magnesium alloys degrade naturally for certain

time priode. In the case of bone joint use pin which is manufactured from magnesium alloy, not need second surgery to take away the implant from the body. In addition to using magnesium alloy is more economical compare to others materials, such as titanium and stainless steel [2].

Aplications of magnesium alloys in industrial manufactures purpose to get an unique characteristics. Magnesium alloys applied as coating on surface of ferroes materials and steels to protect them from corrosion. Its application on electronic components due to magnesium alloys has good conductivity. In the industrial aerospace, application of magnesium alloy aims to reduce weight and increase saving energy [2, 3].

Similar to industrial aerospace field, application magnesium alloys in the automotive industries to get very light components, resistant to corrosion and interested performance (good accessories). One of application of magnesium alloys is an engine block, which has light weight, conductive material, resistant when operate at high temperature and high strength [3].

Beside of some good characteristics of magnesium alloys, surface roughness value is an important thing as represent the quality of product. The surface roughness value has a significant role in machining process due to influence on coefficient friction between the cutting tool and workpiece material [4,5].

Some previus researchers were done experiment to reduce surface roughness value by optimizing cutting parameters. Faruk and Bunyamin [6] identified the effect of tool diameter and feed rate on surface roughness value. The results showed that the surface roughness value tend to increased when cutting at low tool diameter. It was caused by high cutting speed generated smooth machined surface. Whereas selecting high feed rate and low cutting speed produced the rought machined surface. The highest surface roughness was as effect of the feed rate dominantly.

Other experimental result stated that the surface roughness value influenced by cutting parameters, mainly by feed rate [7]. Cuting by using high feed rate produced high surface roughness value. Even, the feed rate was a significant factor which influenced the surface roughness value.

Taguchi Method is a design experimental method that widely used in industrial manufacture. This method purposed to optimize on machined parameters. Surface roughness value is an indicator to achieve good machined surface quality and the lowest surface roughness is the main goal in optimizing machined parameter. Therefore, this experiment aims to apply Taguchi Method to determine optimal machining parameters which produces the best surface roughness value. Quantitative analysis is done to get significant effect for eah parameter.

II. Experimental Method

Magnesium alloy used in this experiment is magnesium alloy AZ31 with chemical composition 3% of aluminium and 1% of zinc. Magnesium alloy was drilled by using drilling machine with merk of TCA-35 Erlo. Drilling process was done in dry machining or without using coolant or lubricant. Surface roughness of machined surface was measured by using the surface roughness tester. The cutting tool used twiss drill type with material of high speed steel.

Machining of magnesium alloy was done by drilling maching are at rotation speed (n) of 635 rpm, 970 rpm and 1420 rpm; feed rate (f) of 0.10 mm/rev, 0.18 mm/rev and 0.24 mm/rev;

and diameter of twist drill (d) of 10 mm, 12 mm and 14 mm. Taguchi Method recommended that if consist of three factors and three levels, orthogonal array with L9 used. Detailly, arthogonal array with L9 and its combination as shown in Tabel 1 and Tabel 2.

Table 1. Factors and levels for each machining parameters

Factors	Levels		
	1	2	3
Diameter pahat bor (mm)	10	12	14
Kecepatan putaran (rpm)	635	970	1420
Gerak makan (mm/rev)	0,10	0,18	0,24

Table 2. Design matric for orthogonal array L9

No	Machining parameters		
	Diameter of twiss drill	Rotation speed	Feed rate
1	1	1	1
2	1	2	2
3	1	3	3
4	2	1	2
5	2	2	3
6	2	3	1
7	3	1	3
8	3	2	1
9	3	3	2

Drilling processes were done nine times with different setting parameters. Surface roughness values were recorded after drilling by using surface roughness tester. Data of surface roughness were analyzed quantitatively by using minitab software to get imformation about variance analysis, which parameter contribution significantly, and correlation of graphic for each parameter.

III. Results and Discussions

Table 3 shows the surface roughness values of machined surface that machined by using drilling at dry cutting condition. The surface roughness values are range in 0.99 – 1.53 µm. The lowest surface roughness value is 0.99 µm, which is reached at machining condition with diameter tool of 14 mm, feed rate of 0.10 and rotation speed of 970 rpm. Althought the surface rougness values are fluctuation for every combination of setting parameters, but the range of fluctuation is not more than of 50%.

Table 3. Experimental results data

No	Diameter of tool (mm)	Rotation speed (rpm)	Feed rate (mm/rev)	Surface roughness (µm)
1	10	635	0.1	1.29
2	10	970	0.18	1.52
3	10	1420	0.24	1.34
4	12	635	0.18	1.43
5	12	970	0.24	1.32
6	12	1420	0.1	1.03
7	14	635	0.24	1.38
8	14	970	0.1	0.99
9	14	1420	0.18	1.25

***Analysis of variance (ANOVA)* for S/N ratio**

Analysis of variance (Anova) is used for get imformation about the effect on each parameter on response parameter (surface roughness). Table 4 shows analysis results of the surface roughness by using Minitab 14 software

Tabel 4. *Analysis Of Variance* ***for*** S/N ratio on the surface roughness

	DF	Seq SS	Adj SS	Adj MS	F	P
Diameter of tool (mm)	2	24,573	24,573	12,287	9,65	0,094
Rotation speed (rpm)	2	19,512	19,512	0,9756	7,66	0,115
Feed rate (mm/rev)	2	77,110	77,110	38,555	30,27	0,032
Residual error (%)	2	0,2548	0,2548	0,1274		
Total	8	123,743				

Value of each factor is as shown in columb P (significant value). Feed rate is the most significant factor which contributes on the surface roughness. The significant value of feed rate is 0.32, in which this value is lower than other factors (diameter of tool is 0.094 and rotation speed of 0,115). Theoritically, the feed rate directly contributes on surface roughness of machined surface. If feed rate was increased, so surface roughness value also increases quadratically. As stated by previous researcher that for machining of superalloys material (including magnesium), the feed rate significant influenced on surface roughness value [8]. Selecting bigger feed rate contributed on profile of machined surface in term of feed mark and valley.

Table 5. Response table for signal to noise ratio with characteristic of smaller is better.

Levels	Tool diamter (mm)	Tool speed (rpm)	Feed rate (m/rev)
1	-2,7969	-2,7054	-0,7937
2	-1,9250	-1,9870	-2,8939
3	-1,5495	-1,5790	-2,5837
Delta	1,2474	1,1264	2,1002
Ranking	2	3	1

Table 5 shows response values of S/N ratio surface roughness each factor. It clearly that the feed rate is at rank 1 as factor which significantly contribute on the surface roughness, and followed by diameter of tool and tool speed. However, diameter of cutting tool gave a contribution but it is not signifincant. The contribution of tool diameter is 9,4%. This value is bigger than contribution of rotation speed of cutting tool. Diameter of cutting tool has a direct correlation with cutting speed; because of the cutting speed depend on the diameter of tool.

The delta value of feed rate is 2.1002 as shown in Table 5, in which bigger than others values. The range of minimum value and maximum value of S/N ratio explains the effect of its factor. For factor feed rate, the response value between level 1 and level 2 is 2.1002 (2.8939 – 0.7937). This value is bigger than the response value between level 2 and level 3. It is very possible due to the range value of feed rate between level1 and level 2 also bigger than the range between level 2 and level 3. In the experimental analysis, it's better to set range velues among level is constant.

Figure 1 shows main effect of signal to noise ratio (S/N ratio) for each factor on the surface roughness values. For diameter of the cutting tool at level 3 give more effect compare to others factors.Therefore, it can be stated that diameter of cutting tool with level of 3 produced the lowest surface roughness value (smoother). Such was this case, the tool speed at level 3 also give more contribution on the surface roughness of machine surface [9]. Contradiction with the diameter of tool that feed rate at level 1 gives more contribution on the surface roughness. Specially for the feed rate, it can be concluded that lower feed rate produced lower surface roughness values.

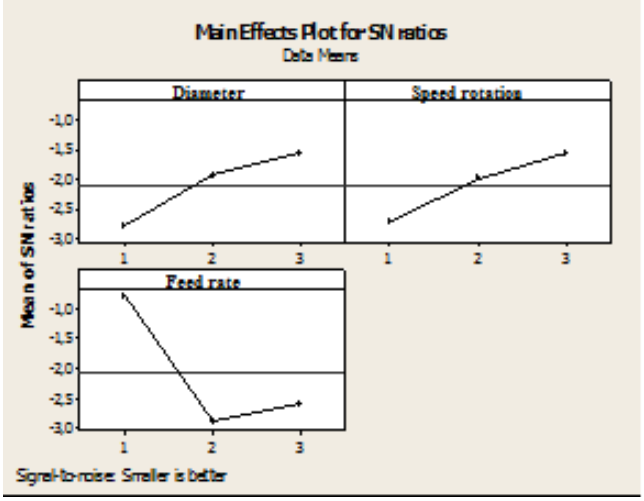

Figure 1. Main effect plot for S/N ratio of surface roughness values

IV. Conclusions

From the analysis it can be concluded that Taghuci Method can be applied to analize the machining parameters when drilling magnesium AZ31, in which tool diameter of 14 mm, rotation speed of 970 rpm and feed rate of 0.10 mm/rev is the best machining condition which produced the lowest surface roughness value. Analisys of Varian on *signal to noise ratios* shows that the feed rate is the significant factor which contribute of 0.032 (3.2%). The graph analysis and ANOVA for show the result that using cutting tool with diameter of 14 mm, speed rotation of 1420 rpm, and feed rate of 0,10 m/rev gave the most significant factor on surface roughness value

Acknowledments

These authors acknowledge the financial support from Directorate General of Higher Education of Ministtry of Research and High Education of Indonesia. The acknowledments also for University of Lampung which facilitated the equipments to finish this experiment.

References

[1] Suhairi, 2010, Pengaruh variabel pemotongan terhadap kualitas permukaan produk dalam meningkatkan produktifitas, Jurnal Jurusan Teknik Mesin Politeknik Negeri Padang.

[2] Badeges, A. 2012, Analisis proses biodegradasi magnesium yang telah melaui proses equal chanel angular pressing ecap dalam cairan fisiologis (Invitro), Universitas Indonesia.

[3] Bruni, C., Forcellese, A., Gabrielli, F., Simoncini, M. 2004, Effect of temperature strain rate and fibre orientation on the plastic flow behaviour and formability of AZ31 magnesium alloy, Department of Mechanics, Università Politecnica delle Marche, Via Brecce Bianche, Ancona 60131. Italy.

[4] Gusri, A.I. 2015, Analisa nilai kekasaran permukaan paduan magnesium AZ31 yang dibubut menggunakan pahat potong berputar, Proceeding Seminar Nasional Tahunan Teknik Mesin XIV (SNTTM XIV.

[5] Gusri, A. I., Suryadiwansa, H., Arinal, H. 2016, Surface roughness values of magnesiaum alloy AZ31 when turning by using rotary cutting tool, Insist, Vol.1, No. 1, pg. 54-59.

[6] Faruk, K. 2016, Effect of the tibn coating on a hss drill when drilling the mg alloy, Yildiz Technical University Istanbul Turki.

[7] Gusri, A. I. 2014, Identifikasi nilai kekasaran permukaan pada pemesinan paduan magnesium, Universitas Lampung

[8] Ibrahim, G.A., Che Haron, C.H., Ghani, J.A. 2010, Taguchi optimization method for surface roughness and material removal rate in turning of Ti-6Al-4V ELI, *International Review of Mechanical Engineering,* Vol. 4, No. 3, pp. 216-221.

[9] Gusri, A.I. 2011, Aplikasi metode Taguchi untuk mengindentifikasi kekasaran permukaan dalam pembubutan paduan titanium, *Jurnal Teknik Mesin Indonesia,* Vol. 6, No. 1, pp. 84-88

Development of Pipe Leak Detection based on Long Wave Infrared Camera for Unmanned Aerial Vehicle Application (#773)

Mona Arif Muda[1,a], Syaiful Alam[1,b], Rizki Alandani[1,c]
[1]Department of Electrical Engineering, Universitas Lampung
[a]mona.batubara@eng.unila.ac.id, [b]syaiful.alam@unila.ac.id, [c]rizki.alandani@students.unila.ac.id

Abstract-- *Oil and gas distribution pipeline require handling in case of leakage. Leaks on the pipeline cause economic losses and have an impact on the environment, so detection must be done in early and rapidly. One method of detecting leakage is through infrared radiation readings. This paper is based on our research to detect the leakage of pipes through infrared image which reading radiation of thermal that emitting from pipe and surrounding area. The detection is processed by a thermal camera with a resolution of 80x60 pixels and a mini computer carried by a multirotor unmanned aerial at varying altitudes. The leakage of the pipe is simulated by flowing water in certain heat into a galvanized pipe that has a leakage point.*

Keywords-- *pipeline leak detection, infrared camera, thermal vision, remote sensing*

I. Introduction

Oil and gas distribution in industries uses pipelines with large construction and long distances. Oil and gas pipelines are spread over underground canals, above ground level, even deep under the sea. Due to its large and very long size, pipeline monitoring every mile for leak detection will be difficult and inefficient. The pipeline in the oil and gas industry is valuable and vulnerable to hazards. Consequently routine monitoring and maintenance are undertaken to reduce both adverse and undesirable incidents and accidents. Zhao and Yang shows that pipeline leakage detection can use infrared radiation reading technology emitted by pipeline leaks [1]. The mapping of infrared energy radiated by the pipe surface makes it possible to recognize leaks even in conditions that are hard to see by the eye.

Leak detection technology is needed in the oil and gas industries today. Therefore further research is required to improve the quality of the heat object measurements through infrared wave radiation. Universitas Lampung in its research center UNILA Robotics and Automation (URO) continues to develop its research in the field of Unmanned Aerial Vehicle (UAV) and its application. This research is part of the achievement of research roadmap in UNILA Robotics and Automation (URO).

II. Literature Review

A. Thermal Radiation

Heat energy can move by three methods which are conduction, convection and radiation. Heat or thermal is the energy produced from the volatility of electrons, atoms, ions, and molecules

in large quantities. If given to the material then some of the energy will be transferred and moved resulting in increased local temperature. The displacement of a solid is heat conduction, in liquid is convection, and no medium is called radiation. Radiation by nature has been introduced by Maxwell as electromagnetic waves, extending from X-rays to microwaves through visible light and infrared.

The thermal radiation seen in the human eye is at the wavelength of 0.4 to 0.8 microns (visible light waves). Every object that emits thermal radiation has a temperature greater than absolute zero (temperature where there is no vibrational motion on the atomic object, temperature -460-deg F). High atomic vibrations exist in objects with hot properties, otherwise cold objects have low vibrations. Positive (proton) and negative (electron) electrical particle reactions create electromagnetic fields and waves that are commensurate with the large emission of thermal radiation. When electromagnetic wave radiation reaches the cold, the electromagnetic field and electric field react to the particles of cold object atoms. In this condition the cold object will absorb the electromagnetic energy of the object hot. Energy is transferred from hot objects to cold objects without physical contact and no medium between them. [2]

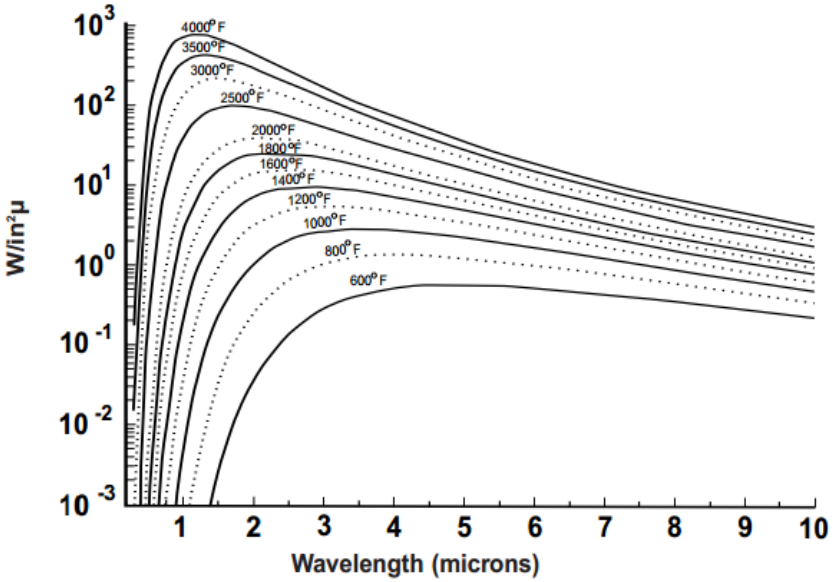

Figure 1. Linear scale graph of Planck curve [3]

Most thermal energy radiation from objects that have heat is in the infrared spectrum, ie from 0.1 to 100 microns (1 microns = 10-6 m). The amount of energy radiated by heat objects and electromagnetic waves is determined by the temperature of the object. The relationship between radiation energy and electromagnetic waves is shown on a graph called "Planck's Curve" -see figure 1 - found by Max Planck. From the graph we can see that the hot object radiates its energy above the wave spectrum. It can also be seen that the higher the heater temperature the peak wave energy will decrease. Peak energy wavelenght and temperature are calculated using Wien transfer law:

$$\text{Peak Energy Wavelength} = \frac{5269 microns°R}{Temp.(°F)+460} \qquad (1)$$

There are physical parameters that must be considered when calculating how much heat energy object [3], they are:

Stefan-Boltzman Equation - is used to calculate the amount of radiant power from the surface of the object (blackbody) at a certain temperature, shown in the formula

$$E = \sigma T4 \qquad (2)$$

E = energy per unit area (W m-2)
σ = cons (5.67 x 10-8 W m-2 K-4)
T = surface temperature (oK)

View Factor - explains the percentage of energy that the object emits about the product. The Stefan-Boltzman equation only counts the radiation from a heat source, but does not calculate the radiant energy that is about the object. There is a geometric relationship between the heater size and the receiving object, and the distance between the two. The closer the heater to the receiving object, the more efficient the heat transfer will be.

Emmisivity - explains how radiation energy is absorbed by the product. Not all the energy that reaches the object is absorbed. Some will be reflected and others will be forwarded.

Total Incident Energy = Absorbed + Reflected + Transmitted

It is the physical property of the product that determines how well the object absorbs the radiative energy that it is exposed to. This physical property determines how well a surface radiates radiation energy. Emissivity is a numerical value with a scale between 0 and 1 that shows how well the object's ability to absorb or radiate radiation energy. Objects that perfectly absorb radiation energy are called blackbody (having emissivity = 1).

B. Infrared Spectrum on Electromagnetic Waves

Electromagnetic waves are waves that do not require transmission medium and are described with velocity, frequency, and wavelength (see figure 2). Based on differences in wavelength and frequency of electromagnetic waves consisting of gamma rays (<0.01 nm), X-rays (0.01-10nm), ultraviolet (10-400 nm), visible light (390-750 nm), infrared (0.75-1 mm), microwave (1 mm - 1 m), and radio waves (1 mm - km) as shown in figure 3. Infrared waves include all electromagnetic radiation that is more than visible light waves, but shorter than microwaves.

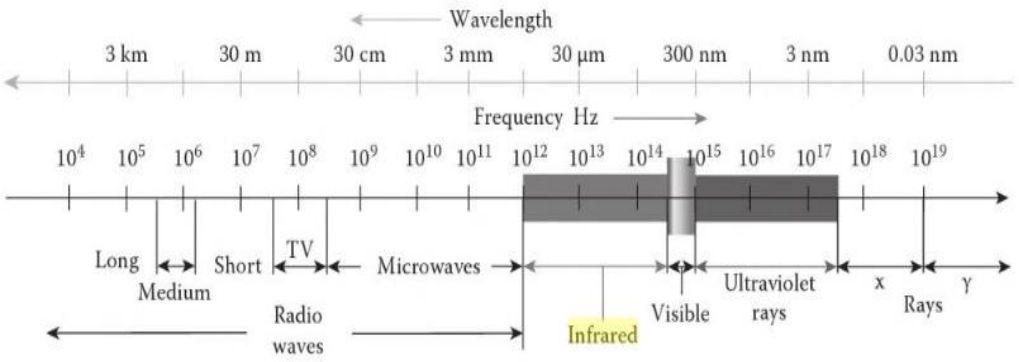

Figure 2. The spectrum of electromagnetic waves [4]

The infrared spectra are divided into several spectra including Near Infrared (NIR), Shortwave Infrared (SWIR), Midwave Infrared (MWIR), and Longwave Infrared (LWIR). NIR wavelengths have a range between 0.7-1.0 um, SWIR waves with wavelength ranges between 1.0-2.5 um, MWIR on wavelength ranges between 3.0-5.0 um, and LWIR wavelengths are in the 8.0-14.0 um range. The width of the infrared wave spectrum can be seen in figure 4.

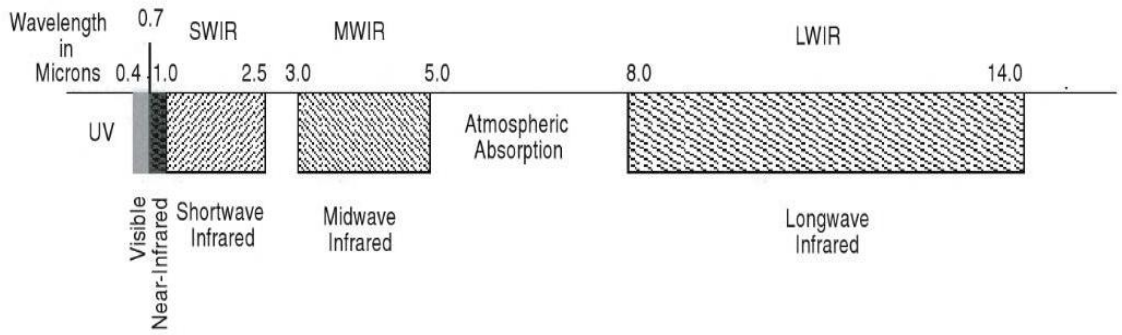

Figure 3. Infrared wave spectrum with its types (NIR, SWIR, MWIR, LWIR) [4]

At a wavelength of 3 μm or higher, the imaged radiation of the objects radiates according to temperature significantly, thereby often referred to as thermal infrared. The thermal infrared spectrum is divided into two main spectrums: MWIR and LWIR. Between these two spectra lie the atmospheric emission with a wavelength of between 5 and 8 μm. On this spectrum, thermal imaging is very difficult to do because it is so fuzzy with thermal air. Spectrum range with wavelength over 14 μm is termed Very Longwave Infrared (VLWIR) with higher application, but in this study only discussed until LWIR spectrum.

The radiation value depends on the temperature and emissivity of the material. For example in the human body with average temperature (37 deg C), through empirical measurement at least emissivity value is 0.91 at MWIR and at least 0.97 in LWIR. Objects with high efficiency reflect light, then less efficiency emits its thermal energy (emissivity) [4]. The maximum emissivity value of 1.0 (usually e = 0.99 or greater) means that objects perfectly absorb and emit radiation, the usual maximum emissivity termed with blackbody, and lower emissivity commonly called graybody. In many cases, object detection with thermal infrared is better using LWIR because LWIR emissions are higher than MWIR. Figure 5 shows the comparison of imaging results on different between visible light and infrared spectra.

Figure 4. Facial images captured simultaneously in (a) visible light spectrum 0.4-0.7 μm with grayscale results, (b) longwave infrared 8.0-14.0 μm with colormap

C. Infrared Detection with LWIR Camera (Lepton FLIR)

The material used for infrared detection is one type of bolometer, which can measure the strength of electromagnetic radiation based on material heat with a temperature-dependent electrical resistance. More specifically, the microbolometer type of material is used as a detector on a non-cooling thermal camera commonly called an uncooled microbolometer. Research has shown that the microbolometer has a near-ideal performance for room temperature infrared sensors and is intended for infrared imaging construction without low-cost cooling [5]. The microbolometer array is placed on the camera for the detection of heat radiation (infrared) on objects with a wavelength of 7.5-14 um.

Most thermal cameras used for remote-sensing are cooled systems. Cooled system is very sensitive and accurate in thermal sensing, this system is also big, expensive, and takes a lot of power. Due to its size and large power consumption, the system cooled thermal cameras are not used in small unmanned aerial vehicles. However, thermal camera microbolometers are not as sensitive and as accurate as cooled systems [6].

Lepton FLIR is one of infrared camera system integrated with LWIR microbolometer sensor array, fixed-focus lens assembly, and signal-processing electronics. FLIR Lepton Camera has embedded digital thermal image processing functions including automatic thermal environment compensation, noise filter, non-uniformity correction, and gain control integrated in one system.

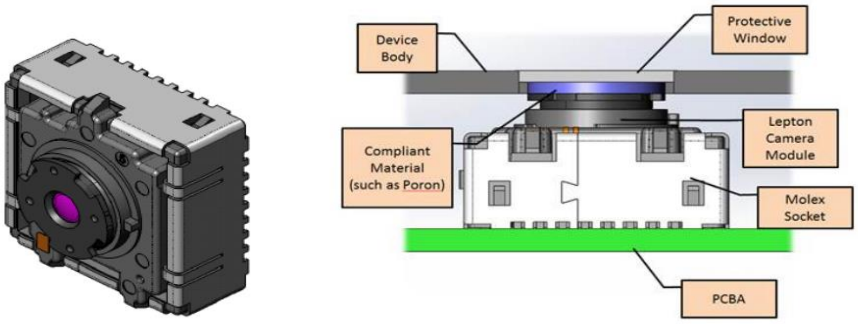

Figure 5. (a) Physical appearance (b) FLIR Lepton camera design structure [7]

Heat detection of objects using Uncooled vanadium-oxide (Vox) microbolometer sensor technology where the temperature will fluctuate according to the incident flux response. Changes in temperature will cause a proportional change in each microbolometer resistance. The Vox microbolometer material on the camera has a high temperature coefficient of resistance (TCR) and low noise, resulting in excellent thermal sensivity and stable uniformity. The thermal detection sensitivity of this camera is less than <50 mK or 0.050 C. [7]

The shape and physical structure of FLIR Lepton camera can be seen in figure 6. With size 8.5 x 11.7 x 5.6 mm (without socket), 10.6 x 11.7 x 5.9 mm (with socket). Based on the specifications, the lens section has a FOV-horizontal 51-deg, and 63.5-deg diagonal with 80 (h) × 60 (v) active pixels used to capture relatively larger images of thermal cameras in general. The imaging results of the lens segment are sent to the Focal Plane Array (FPA) to be

converted and generate a periodic stream. Serial streams from FPA are received by on chip system devices (SoCs) that provide signal processing and output formatting. A simple architectural diagram of the Lepton camera module is shown in figure 7.

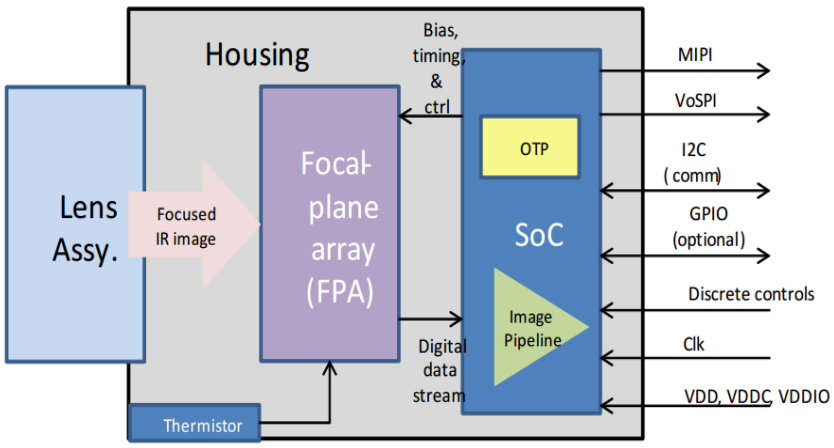

Figure 6. Lepton camera architecture. [7]

Thermal camera is one of the instruments to measure and image the heat of an object through the infrared radiation it emits. The array sensor in the camera will work by mapping the radiation to produce the temperature and thermal distribution information of an object.

D. Unmanned Aerial Vehicle (UAV)

Research on UAVs is increasingly focused on smaller and more reliable embedded hardware, making on-board data processing on UAVs more qualified. Data processing is capable of working even for video processing in real-time and fast algorithms for object detection and tracking [8]. Smaller unmanned aerial vehicles (UAVs) can be efficient devices for low cost thermal imaging [6]. Generally, thermal cameras used in UAVs are cooled systems that have large size, costly, and consume a lot of electrical power. Due to these conditions, thermal cameras with a light, low-cost, low-power uncool system are suitable for small unmanned aerial vehicles. In this study used multirotor type where take off and landing vertically and can maintain a certain altitude and position.

III. Research Methods

Scenario of Pipe Leak Simulation

For leakage simulation scenarios on pipes can be illustrated in Figure 7.

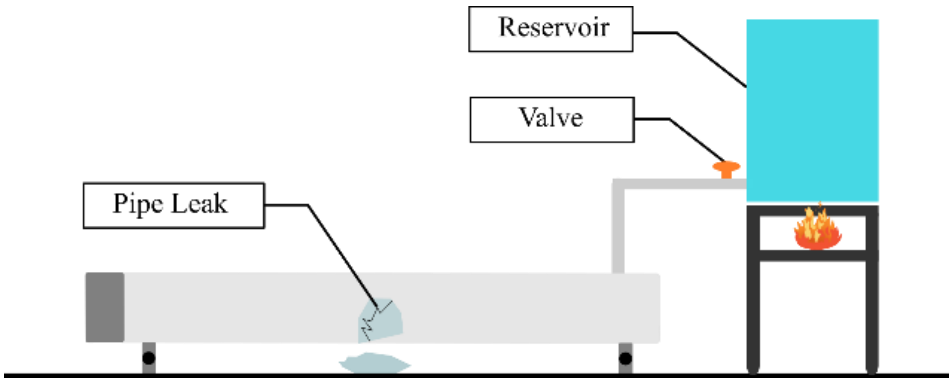

Figure 7. Illustration of leakage simulation scenario in oil and gas pipeline with hot water flow

As a substitute for oil and gas, this research uses water heated to room temperature of oil and gas distribution pipes. The reservoir is heated by fire with water temperature in the reservoir ranging from 130-170 degrees Farenheit (pipe room temperature) to obtain a representative result with conditions in the field. The heated water is supplied through a tube whose output is controlled by a tap into a galvanized pipe that has been manually leaked. Spot leakage pipe is made at the center of the pipe with a 5mm leak diameter. Galvanized pipe is placed at a height of 0.5 meters and a reservoir height of 1 meter above ground level.

Designing Tools and Systems

Table 1. Component Use of Justification

No	Component Name	Justification Usage
1	LWIR (Long Wave Infra-Red) FLIR Lepton Camera	Captures heat radiation from the pipeline and digitally imaging it
2	USB Visible Light Camera	Imaging pipe on the visible light spectrum as a comparison
3	Raspberry Pi 3	The main processing computer for processing and storing digital images
4	Raspbian Linux-based Operating System	Operating system used Linux based to facilitate communication between devices
5	Library OpenCV and IDE C++	Software for digital image processing based on coding with C ++ language
6	Laptop Corei3 2,4 Ghz 4GB RAM	Laptop as user interface to program and see infrared image processing
7	Multirotor	Aircraft carrier unmanned thermal camera

Imaging of the object is taken by using an infrared thermal camera to view the scattered heat visualizations on the surface of the pipe. The thermal camera will image the pipe surface and the existence of a pipe leak point at a certain height. In this research will be seen the heat distribution on the surface of the pipe and its effect on leakage.

Figure 8 below shows the design of a heat detection imaging system on objects captured by thermal cameras.

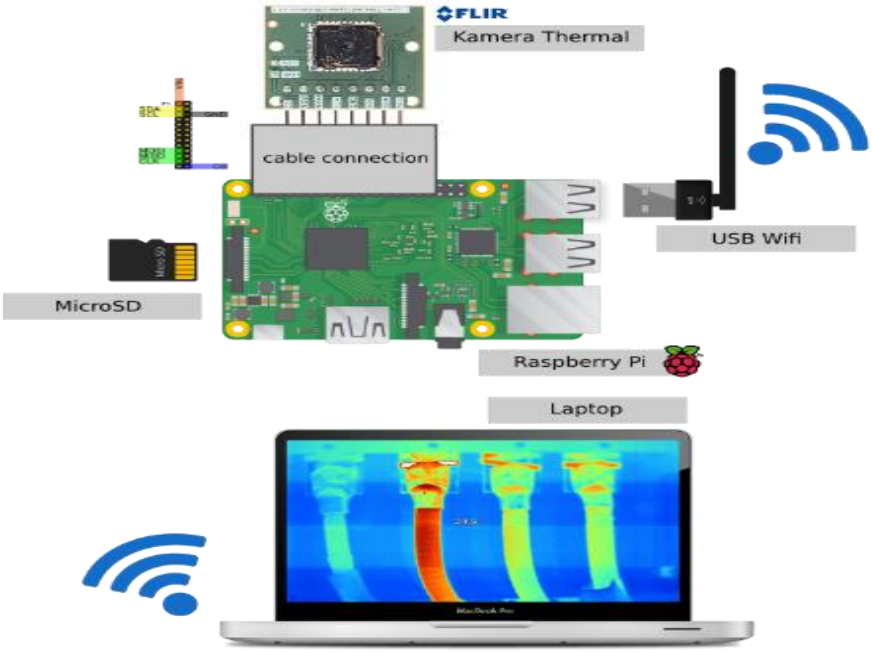

Figure 8. (a) Sketch of the main components of Raspberry Pi, (b) Raspberry Pi internal hardware diagram

Data retrieval

The data is taken by imaging the pipe that has a leak point with the air rides. However, in this research, data collection is not performed in real field, but still pay attention to the character and rule of pipe leak detection so that this research representative with detection in field.

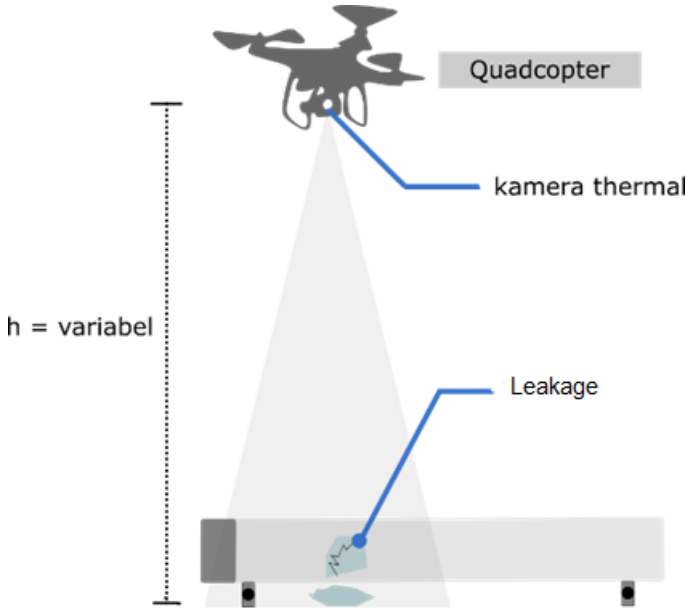

Figure 9. Illustration of pipeline imaging works on unmanned aerial rides

Data retrieval is done by simulating imaging of leak line. The pipe is spread over a certain length, and is imaged through the air at a certain height. The height of the shooting is determined not far from the pipe to maintain the quality and detail of the pipe image. With a certain length and a small camera resolution (80x60 pixels) at a certain height there will be some separate pipe images. Raising the distance of the shoot will indeed produce an image that reveals a wider pipe viewing angle, but will reduce the quality and detail of the pipe image. So it needs to maintain certain heights, to improve detection details.

Pipe imaging is done by flying a multirotor carrying an infrared camera along with a mini-computer. Multirotor flown at a predetermined distance and captures the pipe under conditions multirotor is steady-state. The altitude variable used is at a height of 1-10 meters. Pipe leakage will cause the liquid to come out of the pipe and give effect to the surrounding area. Data retrieval undertaken by fliying multirotor will only imaged the top surface only. Detection properties in this research is to detect the presence or absence of leakage in certain area and not detect the location of point/hole leak.

Prior to the pipe leakage imaging, some temperature data retrieval was conducted for reference. Temperature data that is the temperature of the pipe surface temperature before and after the hot water, the ambient temperature, the temperature of the ground surface, and the temperature of the hot water coming out of the pipe leak hole.

IV. Data Result and Discussion

Initial stage in this research is assembling component at multirotor. As in design, FLIR lepton cameras are connected with raspberry pi as the main processor. Raspberries and cameras mounted on the lower body of multirotor. Both the thermal camera and the visual camera are positioned facing down. The power supply from the battery is connected to UBEC 5V 3A to keep current and voltage stable for raspberry pi. From the software side, the raspberry boot is set to connect automatically to the access point created by the user's computer. Remote connection settings are always enabled to easily connect raspberries with laptops.

After the assembly process, the thermal camera is tested whether it works properly. Thermal camera reading program uses source code in C++ programming language. In addition to camera readings and displays, programs are also added to store images and print the maximum value the camera generates. The value read on the thermal camera represents the heat on the monitored object. Figure 2 shows the varieties of values of camera reading values to reality temperatures that are not so linear in their changes. If the value range is not too large then the graph of change is quite linear.

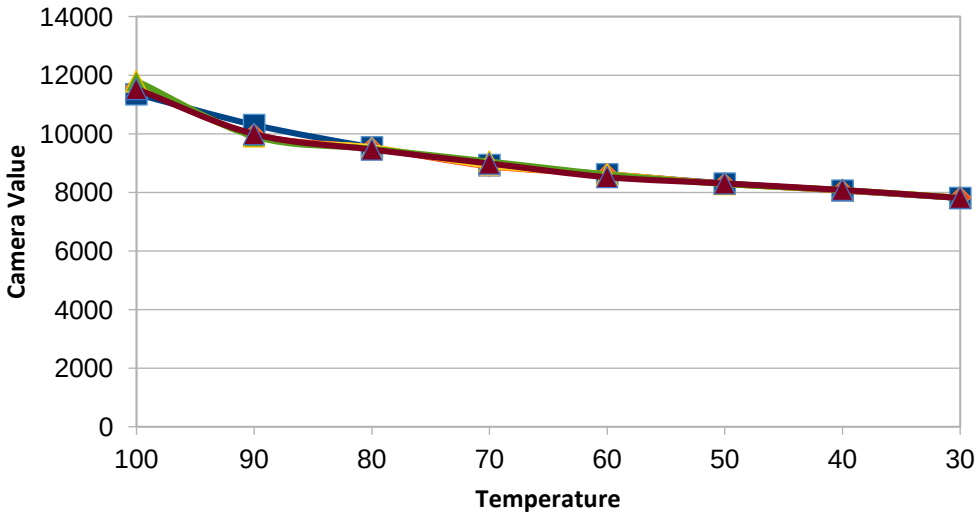

Figure 10. Graph of reality temperature relation with value of lepton camera

Pipe leakage is done by simulating the flow of hot water into the galvanized pipe. The first simulation is the flow of water with a temperature of 76 degrees Celsius. Imagery is divided into two, they are pipe imaging that has leak point and imaging without a leak point. The results of pipe imaging can be seen in the figure 11. There is a difference between the image of the pipe that has leaks with no leakage. The pipe with the leak point has significantly different heat with the other pipe surfaces and there is another heat on the soil affected by the leak. Otherwise image without leakage, the heat on surface has no significant difference and there is no heat emission from the ground around the pipe.

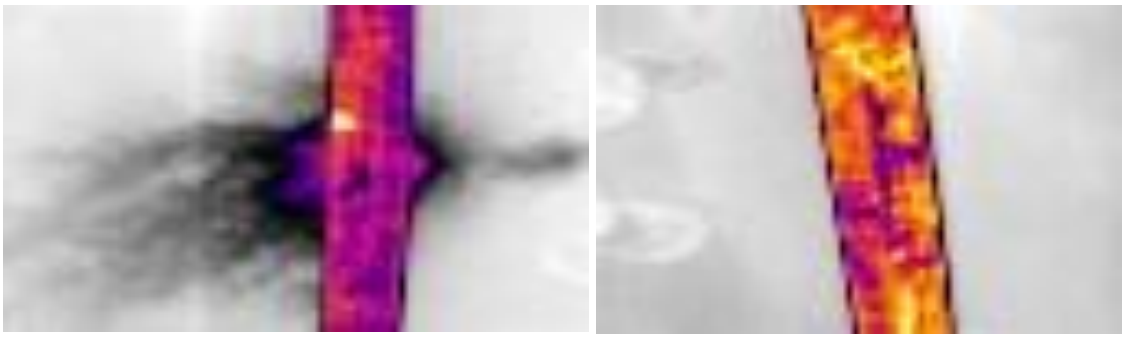

Figure 11. The infrared camera image results in the area (a) the pipe having a leakage point (b) of the pipe without a leak point

Taking images at different altitudes will also produce different detection results. Taking next data done with imaging at a height of 1 to 10 meters. Imaging is executed ten times at 1 meter intervals. The temperature of the water that flowed into the pipe was 58 degrees, the surface temperature of the pipe measured 37 degrees, and the water leak temperature was 39 degrees.

Table 2. Value thermal camera in the leakage image of the pipe with different heights

Lepton Value		Altitude (meter)
Peak Value	Bottom Value	
8140	7407	10
8331	7412	9
8379	7373	8
8315	7424	7
7810	7435	6
7964	7389	5
7970	7428	4
8094	7408	3
8137	7475	2
8335	7461	1

At different altitudes, the value of thermal camera readings against pipeline leaks has vary values. The resulting image is different to the altitude of the image, as shown in the figure 12.

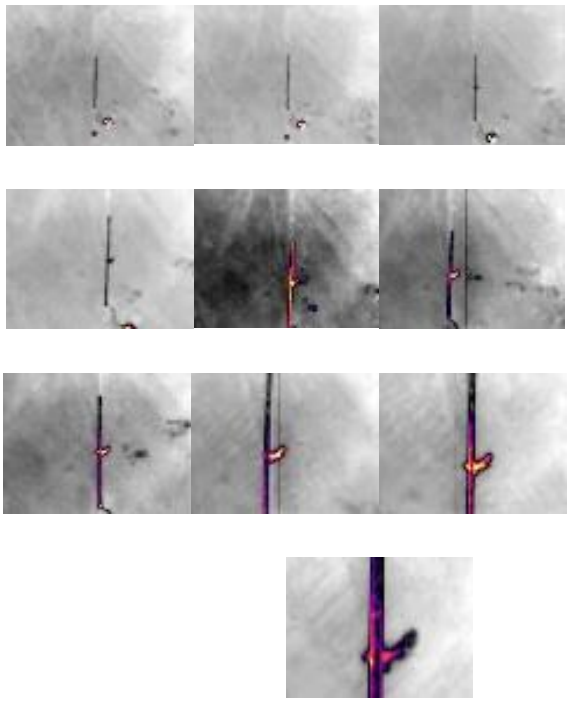

Figure 12. Thermal camera imaging results against pipeline leaks at altitude (a) 10 meters, (b) 9 meters, (c) 8 meters, (d) 7 meters, (e) 6 meters, (f) 5 meters, (g) 4 meters, (h) 3 meters, (i) 2 meters, (j) 1 meter

With a 80x60 pixels spatial resolution camera, the images above 6 meters altitude have poor detection quality where only the visible pipe form but not with its leakage point. At this altitude, what are shown hot is a reservoir that contains hot water. At an altitude of 1 to 6 meters, there is a well-visible leak in the infrared image. There is a dispersion of heat around the pipe indicating there is a leak in the area. The lower the altitude so the leak detection becomes more obvious.

V. Conclusion

Thermal camera can be applied on pipeline leak detection. Using microbolometer Long Wave Infrared (LWIR) placed on a multirotor unmanned aerial vehicle, it is able to detect leakage on pipeline well. But with 80x60 pixel thermal camera, small spatial resolution only detect leakage less than 7 meter.

References

[1] L. Zhao and H. Yang, “Small-target leak detection for a closed vessel via infrared image sequences,” *Infrared Phys. Technol.*, vol. 81, pp. 109–116, Mar. 2017.
[2] X. Maldague, Ed., *Infrared methodology and technology*. Yverdon, Switzerland ; Langhorne, Pa., U.S.A: Gordon and Breach Science Publishers, 1994.
[3] “Radiant Heating With Infrared; A Technical Guide To Understanding And Applying Infrared Heaters.” Watlow Electric Manufacturing Company, 1999.

[4] B. Bhanu and I. Pavlidis, Eds., *Computer vision beyond the visible spectrum*. London: Springer, 2005.
[5] P. W. Kruse, Ed., *Uncooled Infrared Imaging Arrays and Systems Volume 47*. Academic Press, 2011.
[6] A. M. Jensen, M. McKee, and Y. Chen, “Procedures for processing thermal images using low-cost microbolometer cameras for small unmanned aerial systems,” in *2014 IEEE Geoscience and Remote Sensing Symposium*, 2014, pp. 2629–2632.
[7] “FLIR LEPTON Long Wave Infrared (LWIR).” FLIR, 2014.

Section 2
Life and Applied Sciences

Integrated Sci-Tech :
Interdisciplinary Research Approach
Volume 3

Case Study of Converter Performance Evaluation on Sulfuric Acid Production (Department III PT B) (#573)

Azafilmi Hakiim[1,a], Dessy Agustina Sari[2,b], and Vita Efelina[1,c]
[1]Industrial Engineering Department of Engineering Faculty, Universitas Singaperbangsa Karawang – West Java, Indonesia
[2]Electrical Engineering Department of Engineering Faculty, Universitas Singaperbangsa Karawang – West Java, Indonesia
[a]aza252116@gmail.com, [b]dessy.agustina8@gmail.com, [c]vita.efelina@mail.ugm.ac.id

***Abstract*—*Converter was one tool unit that consisting 4 beds in the production process of sulfuric acid. The performance of this converter was supported by the addition of a vanadium pentaoxide (V_2O_5) catalyst. The process that occurring in the converter was double contacts – double absorbers. The purpose of this case was converter performance evaluation that using by SO_2 conversion parameter to SO_3. Primary data was the dry air flow rate that entering the burner, the SO_2 gas content that be into the converter, the catalyst temperature of each converter bed, and the catalyst pressure in each bed converter. Data on the field showed that activity on bed I was 72,96%, and theoretical was 60%. Then, bed II gave 91,22%; 87%; on bed III was 96,85%; 94%; and bed IV was 99,9%; 99,73% as respectively. From these experiments could be concluded that result data was greater than the theoretical. The difference of this conversion indicated that the performance of the converter did not increase.*

Keywords*—*absorber, bed, converter, SO_2 conversion, performance.

I. Introduction

converter is unit used to produce sulfuric acid in PT B production department III which consists of 4 beds. The catalyst used Vanadium Pentaoxide (V_2O_5)[1]. The eprocess used is double contact double adsorber. Converter consists of 4 bed, and three bed is the first level conversion and the fourth bed is a second level conversion. Gas process containing SO_2 wit temperature of 430^{o}C goes to converter bed I. About 60% of SO_2 gas is converted to SO_3 [2] wit the following reaction :

$$SO_2 + 1/2\ O_2 \leftrightarrow SO_3 + Q \quad (1)$$

Reaction (1) is reversible exothermic reaction with her release of 23,49 x 10^3 Kcal/kg.mol. The gas output of bed I using SO_3 gas with temperature 610^{o}C goes into heat exchanger I where the heat is given to going into bed IV, then gas from bed I goes to bed II with temperature 440^{o}C and will happen subequent conversions. The output gas II with temperature 520^{o}C goes into heat excharger II then gas with temperature 430^{o}C goes to bed III, in converted heat excharger gas giving its heat to the gas entering bed IV. The output from bed III containing SO_3 gas with temperature 450^{o}Cgoes into economizer I where it is cooled to 220^{o}C before entering the absorber tower I. After SO_3 gas absorber with H_2SO_4 in the absorber tower, the remaining gas at 80^{o}C through the demister is separated in parallel and then into piping heat excharger I dan II, then become one before going into bed IV. Before gas to entering bed IV is heated in di heat excharger I becomes 420^{o}C. The output gas bed IV with a temperature 440^{o}C goes into economizer II, where the gas is cooled to

190°C before entering the absorber tower II. To prevent the possibility of condensation from the absorber tower output gas I the equipped with tracking mounted on the gas line between the absorber tower I and heat exchareger II [3],[4].
Controlling temperature of each bed and maintaining the desired SO_2 gas concentration in the gas to be generated in the converter is most important operating process. This temperature rise should not exceed 62°C for bed output 1 , its purpose is to avoid catalyst damage and other equipment in the converter. It can be controlled by closing or opening the heat regulator. Hot gas temperature drop inside heat excharger.
The balance of the reaction depends on the temperature, total pressure, and reactant concentration. The equilibrium conctants for this reaction are calculated from the respective gas parallel trace as follow :

$$Kp = \frac{p(SO_3)}{p(SO_2).p(O_2)^{0,5}} \quad (2)$$

The relationship between Kp and temperature according to bodenstein and pohl is as follows:

$$\text{Log Kp} = 5186,5/T + 0,611 \log T - 6,75 \quad (3)$$

The conversion achieved in double contact double absorber process is better than single contact process. In a single contact process the maximum conversion achieved with 4 bed catalysts is 99.5-98% depending on the composition of the incoming gas. While in double contact double sbsorber process can each more than 99,7%.
Converter on PT B using array 3+1. The reactant gases first enter the bed reactor 1, the ouput gas from bed 1goes into bed 2 and so on until bed 3, between the bed is always cooled and before entering bed , the gas from bed 3 is passed by absorber 1 for SO_3 absorption. This is used H_2SO_4 98,5% as an absorbent. It is expected thet SO_3 will be bound by the water contained in sulfuric acid. In this case no pure H_2O is used as an absorbent because the SO_3 dissolving heat in H_2O is higher so that a portion of H_2O is evaporated and carries the H_2SO_4 molecule and creates a haze that is difficult to remove so that the absorption is not perfect. SO_2 gas output from absorber 1 is fed to bed 4 to convert SO_2 to SO_3 leftover. From bed 4gas enters absorber 2 for SO_3 gas absorption. With this process is expected to exchaust gas free gas SO3 gas.
In process of making H_2SO_4 especially in the process thet occurs in the converter unit is indispensable heat exchangers, because the process of SO_2 conversion to SO_3 an extermic reaction. This exothermic reaction will cause the temperature of the output on each bed to be increased so that a heat excharger is required to cool the bed temperature so that it is equal to the operating conditions on the next bed.
Basically the heat excharger used is heat exchanger used is HE and economizer. HE (heat exchanger) is usesd to cool SO_2 and SO_3 outputs of bed 1 and 2, while the economizer is used cool the SO_3 outputs of bed 3 and 4. The type of heat trapper is shell and tube type, where the SO_3 gas will be cooled throught the shell side, while the coolant which is useds through the tube side. HE shell and tube usually use steel pipe containing Fe metal element so it can cause corrosion if react with SO_2 gas and SO_3, although this process happened slowly but will still degrade the performance of the heat exchanger.

II. Procedure Method

A. How to obtain Data

Primary data obtained from central control room of production acid sulfate II Departemenr III PT B, among others:

1) *Dry air flow rate enter burner*
2) *SO2 Gas into converter*
3) *Temperature of catalyst in each bed of converter*
4) *Catalyst pressure in each bed of converter*

B. Data Processing

From the data obtained is done data processing as follows:

1) *Calculating the incoming gas composition on each converter bed based on reaction stoichiometry and mass balance is converted.*

	SO2 + ½ O2 ↔	SO3 (4)
Initial	a b	c
Reaction	ax ½ ax	ax
Balanced	a(1-x) b-½ ax	c + ax

For SO2 converter coming from bed 1 already known percentage of data contained in laboratory, then from the data we can calculate the number of moles of SO2 with the following formula :

	S + O2 →	SO2 (5)
Initial	L F	-
Reaction	L L	L
Balanced	- F-L	L

SO_2 Gas inlet converter = L kmol
O_2 Gas reaction in furnace (burner) = L mol
O_2 Gas left out in furnace = M kmol
= F-L kmol
N2 in which are included in th air burner = N kmol
Then :

$$\% SO_2 \text{ inlet converter} = \frac{nSO_2}{nSO_2 + nO_2 + nN_2}$$

$$= \frac{L}{L + M + N}$$

Calculate the conversion of each bed by trial and error method with the formula used Bodenstein dan Pohl (3) :

Log Kp = 5186,5/T + 0,611 log T – 6,7497 = f(x)
f(x) is prepared based on the respective concentrations of the reactants in equilibrium. The balance state of Kp is structured as follows :

	SO2 + ½ O2 ↔	SO3 (4)
Awal	a b	c
Reaksi	ax ½	ax
Setimbang	a(1-x) b-½ ax	c + ax

SO_2 = a-ax = A
O_2 = b-½ ax = B
SO_3 = c + ax = C
N_2 = d = D
Total = a-ax + b-½ ax + c + ax + d = E
= a + b + c + d -½ ax = E

$$Kp = \frac{\left(\frac{C}{E} xPabs\right)}{\left(\frac{A}{E} xPabs\right)\left(\frac{B}{E} xPabs\right)^{1/2}}$$

$$Kp = \frac{\left(\frac{C}{A}\right)}{\left(\frac{B}{E} xPabs\right)^{1/2}}$$

of the temperature of each bed obtained the value of Kp each bed by the method of trial and error by counting the conversion (x).

2) *Calculate the conversion of each bed by trial and error method :*

Bed I = $\frac{SO_2\ inlet - SO_2\ Outlet\ I}{SO_2\ inlet} x\ 100\% = xI\%$ (2)

Bed II = $\frac{SO_2\ inlet - SO_2\ Outlet\ II}{SO_2\ inlet} x\ 100\% = xII\%$ (3)

Bed III = $\frac{SO_2\ inlet - SO_2\ Outlet\ III}{SO_2\ inlet} x\ 100\% = xIII\%$ (4)

Bed IV = $\frac{SO_2\ inlet - SO_2\ Outlet\ IV}{SO_2\ inlet} x\ 100\% = xIV\%$ (5)

III. Result and Discussion

The conversion calculation from data processing in apliance resulting bed converter temperature parameter in Table 1.

TABLE I The conversion calculation on the converter appliance using the resulting bed convert temperature parameter

Bed	Calculation of converter (%)	Converter teoritis
I	72,96	60
II	91,22	87
III	96, 85	94
IV	99,9	99,73

IV. Conclusion

The conclusion of the formation of SO_3 desaign tool amount to 99,7% of the calculation of actual data obtained conversion of 99,93%. From the data can be seen that the conversion calculation is greater than the theoritical conversion. This conversion difference indicates that the performance of the converter is not suffering.

References

[1] Stauffer Chemical Company, Vanadium Sulphuric acid Catalyst hand Book, 1974.
[2] H. Fiscer, *An* Introduction to Their Industrial Chemistry and Technology, The British Sulphur Coorporation Ltd.
[3] Austin, George T, Shreve's Chemical Process Industries, 5th edition, Mc Graw Hill Publishing, New Delhi. 1996.
[4] Geankoplis, J. C, and Bacon, "Transport and Unit Operations", 2nd edition, The Ohio University, Inc, Tokyo. 1983.

Utilization of Coal Fly Ash as Heterogeneous Catalyst of ZSM-5 Impregnated Cobalt for Methanol Synthesis (#618)

Fusia Mirda Yanti[1] , S.D.Sumbogo Murti[1],Yuni K. Krisnandi[2], Adiarso[1]
[1]Agency for Assessment and Application of Technology, Jl. M.H Thamrin 8, Jakarta Indonesia
[2]Department of Chemistry, Faculty of Mathematics and Natural Science, Universitas Indonesia, Depok 16424, Indonesia

Abstract— *Coal is Indonesia's most abundant and widely distributed fossil fuel, with global proven reserves totaling nearly 32 billion. The major problem in coal-fired power generation is that the plenty of solid waste so-called fly ash (of about 30% of raw coal) is produced. Focus of this work has the synthesis of heterogenous catalyst ZSM-5 using coal fly ash , as the main raw material. First, coal fly ash was subjected to pre-treatment in order to extract silicate (SiO_4^{4-}) and aluminate (AlO_4^{5-}). Then the catalyst of ZSM-5 were synthesized through hydrothermal treatment from coal fly ash and added of rice husk ash as silica's sources using template. Then, it was modified with Cobalt through impregnation method. The as-synthesized catalyst was then characterized using FTIR, XRD, and XRF. The as-synthesized catalyst from fly ash also was compared with commercial ZSM-5. The result of FTIR showed peaks at 1250-950 cm^{-1} ($v_{asymetric}$ T-O), 1100-700 cm^{-1} ($v_{symetric}$ T-O), and at 650-500 cm^{-1} confirming the presence of the five number ring of the pentasil structure. The result of XRD showed the appearance of certain peaks in the position 2 theta between 7-9^o and 22-25^o indicative of catalyst ZSM-5 structure and also 37 ^{0} and 47 ^{0} indicative of Cobalt , but also showed the pattern of low intensity magnetite and hematite. Furthermore, the XRF result showed the concentration of impregnated Cobalt is 1.99 %. The catalytic activity of catalyst Co/ZSM-5 zeolites as heterogeneous catalysts for methanol synthesis were tested and compared with that commercial one. The result showed that catalyst of ZSM-5 impregnated Cobalt from coal fly ash were potential for methanol synthesis and % conversion of methanol of ZSM-5 impregnated Cobalt is 6.28% (30 minute) and 12.43% (60 minute) and commercial ZSM-5 is 8.78 % (30 minute) and 21.36% (60 minute).*

Keywords— *coal fly ash, catalyst, Co/ZSM-5, impregnated, methanol synthesis*

I. Introduction

COAL is still one of the most potential energy resources besides petroleum and gas. Coal can still be an alternative fuel given its abundant reserves. Coal is Indonesia's most abundant and widely distributed fossil fuel, with global proven reserves totaling nearly 32 billion [1]. The coal combustion from power plant was produced solid waste like fly ash and bottom ash and volatile materials such as CO_2, SO_2, NO_2 and H_2O. The amount of coal fly ash, released by power plant has been increasing throughout the world, and disposal of the large amount of coal fly ash has become a serious environmental problem especially in developing country [2]. The production in Indonesia estimated to be about 4000 ton/days.

Coal fly ash contains at least 50 % of alumina and silicate which is composed of

amorphous solid and hollow sphere [3]. Due to these similarities in the composition between coal fly ash and zeolite, coal fly ash has been viewed as potential as main raw material to conversion zeolite [4].

Zeolite, an aluminasilicate mineral is one of the heterogeneous catalysts that has been developed synthesis, modification and characterization by many researchers both in research institutions, universities and the industrial world. This is because zeolites constructed from silicate (SiO_4^{4-}) and aluminate (AlO_4^{5-}) have unique structures and morphologies, such as having uniform pore size (<2nm) that causes it to have a high internal area. In addition, in the zeolite structure there are Si-OH and Al-OH groups which cause the zeolite to have the required acidity properties in its function as a catalyst [5].

One of the most commonly used zeolite types in the industry is ZSM-5, which has many applications such as petroleum and petrochemical catalysts. ZSM-5 has a ratio of silica and alumina between 10-100. However, the ratio of silica and alumina in coal fly ash is too low to synthesis ZSM-5 (mole ratio= 3.59). In order to obtain the appropriate SiO_2/Al_2O_3 mole ratio, the silicate was added to adjust the mole ratio of coal fly ash. One source of silicate from rice husk ash. Rice husk ash contains about 85-96 % of silicate [6]. From economic point of view, the silicate prepared from rice husk ash was used instead of commercial ones because there is abundant supply of rice husk in Indonesia [7].

ZSM-5 has many application as catalyst especially in petroleum and petrochemical such as catalyst to synthesis methanol. Methanol is one bulk chemical being widely used in chemical industry. Methanol is used as solvent, a gasoline, additive, and a chemical feedstock fo production of biodiesel and hundred of other chemical [8]

Beznis et al, 2010 [9] has been investigated about oxidation of methane to methanol and formaldehyde over Co-ZSM-5 molecular sieves. Beznis has been reported that the selectivity and reactivity of methanol products increases with the presence of impregnated cobalt atoms on the surface of ZSM-5. Therefore, in the research was focus to synthesis of heterogenous catalyst ZSM-5 impregnated Cobalt using coal fly ash , as the main raw material, and application to synthesis methanol.

II. Experimental

A. Materials

The materials used were : Coal Fly Ash from Paiton, Indonesia, rice husk from Bogor, Indonesia, sodium hydroxide (NaOH) pellet, Chloride acid (HCl) 1M, Tetrapropylammonium hydroxide, TPAOH 1M (Sigma Aldrich), Poly Diallyl Dimethyl Ammonium Chloride (PDDA 35 %) (Aldrich), Cobalt (II) Nitrate (Co(NO3)2.6H2O) (Sigma Aldrich), methane gas (99.99 % BOC), N_2 gas (99.99 % UHP) and deionized water.

B. Pretreatment

Coal fly ash was dried and sieved using a 200 mesh sieve, and then activated in a furnace at a temperature of 800 ^oC for 2 hours, then refluxed with 1M HCl for 3 hours at 90 ^oC. After this, the mixture were washed with distilled water to pH neutral. Then the product were filtered with filter paper, and then samples were dried in an oven with a temperature of 105 ^oC for 6 hours. Then characterized by AAS and XRD

Rice husk samples was washed, then dried in an oven at 105 ^oC for 1 hour, after this, the sample was crushed and sieved 60 mesh, then burned with a furnace at 700 ^oC for 4 hours, and then characterized by AAS and XRD.

C. Synthesis of ZSM-5

The synthesis of ZSM-5 from coal fly ash following the procedure have been reported previously [7]. Synthesis was prepared with a molar ratio : 12 NaOH: 30 SiO_2: 0.75 Al_2O_3: 6 TPAOH: 1800 H_2O [10]. In this experiments, coal fly ash was mixed with 30 ml of 0.4 M NaOH solution (mixture A) at 100 ^oC. Then rice husk ash was added with 70 ml of 0.4 M NaOH and then stirred at 100 ^oC (mixture B). Furthermore, mixture's B was slowly added to the mixture A, then TPAOH was added to the mixture, and glacial acetic acid was added to adjust pH up to 11. Stirring was continued for 3 hours at a temperature of 100 ˚C. After that, added 1 g of PDDA (10 wt%) to the mixture and stirred again for 15 hours at room temperature. Then the reaction mixture was transferred into the autoclave and heated for 144 hours at a temperature of 150 ˚C in the oven. The reaction product was be cooled, washed with aquademin, filtered, and dried at room temperature for one night. After that, the product was calcined for 8 hours at a temperature of 500 ˚C. The synthesized crystals of mesoporous ZSM-5 was characterized by XRD instruments, FTIR, and BET Analyzer.

D. Impregnation Cobalt to ZSM-5

Cobalt impregnation to zeolite is done by using wet impregnation method. Cobalt metal impregnation was performed by dissolving 0.7272 grams Co $(NO_3)_2.6H_2O$ with aquadest to 10.0 mL. Then, 1.7 mL of a solution which has formed was mixed with 1,000 grams of mesoporous ZSM-5 and stirred for 24 hours at room temperature to form a paste. The formed paste was then dried at 60 ° C for one night and calcined at 500 ° C for 3 hours. The synthesized zeolites were characterized by XRD, FTIR and XRF instruments

E. Catalytic Test : Methanol Synthesis

Catalytic test for methanol synthesis from methane by partial oxidation reaction. The testing procedure has been reported previously [11]. The catalyst used for each reaction is 0.5 g, which has been activated at 500 ^0C. The reaction was performed at 150 ^0C with methane pressure of 0.75 bar and a nitrogen pressure of 2 bar with a variety of reaction time of 30 minutes and 60 minutes then extracted with ethanol, and characterized using Gas Chromatography-FID

III. Result and Discussion

A. Pretreatment of Coal Fly Ash and Rice Ash Husk

Coal fly ash and rice husk were subjected to pre-treatment in order to extract silicate (SiO_4^{4-}) and alumninate (ALO_4^{5-}) and separated from the impurities [7]. Pretreament of coal fly ash consist of purification and activation process. The result of characterization showed by Figure 1 and Figure 2.

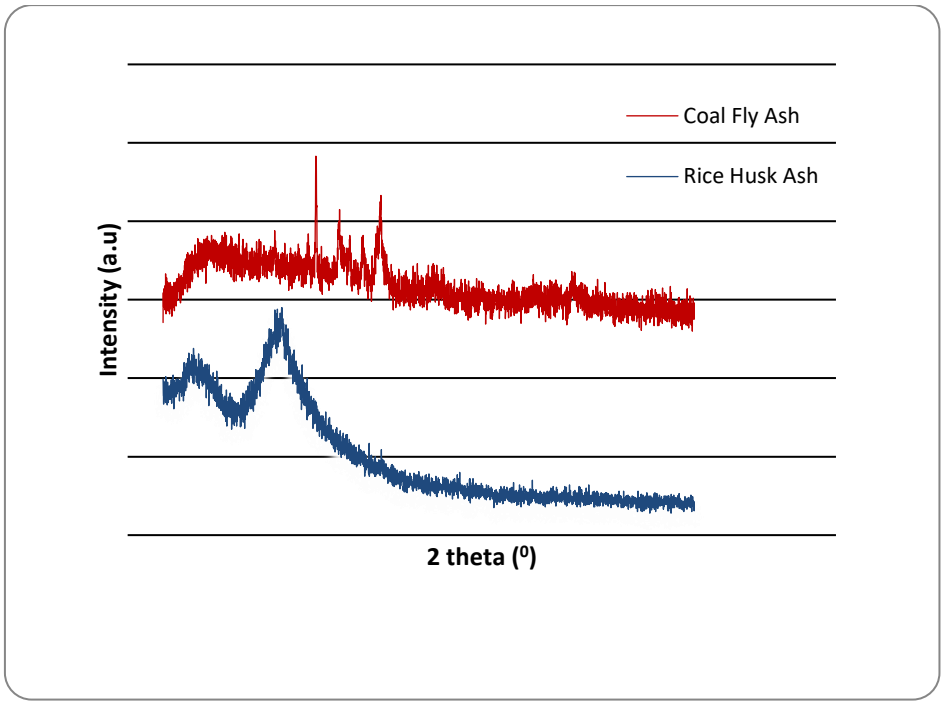

Figure 1. XRD Pattern of Coal Fly Ash and Rice Husk Ash

Figure 1 showed diffraction pattern of coal fly ash and rice husk ash. Figure 1 showed the appearance of certain peak of rice husk ash in the position 21.4 ^{0}, indicative of amorphous silica. This indicates that rice husk ash is reactive, and coal fly ash contained silica quartz peaks with low intensity at position 2 theta 26.5 ^{0}. In addition to silica quartz, in coal fly ash there is also a peak hematite (Fe_2O_3) at position 2 theta 24 ^{0}; 33 ^{0}, 49 ^{0}; 54 ^{0}, 62 ^{0} and Magnetite (Fe_3O_4) at position 2 theta 31 ^{0}; 36 ^{0}; 43 ^{0}; 57 ^{0}; 63 ^{0}.

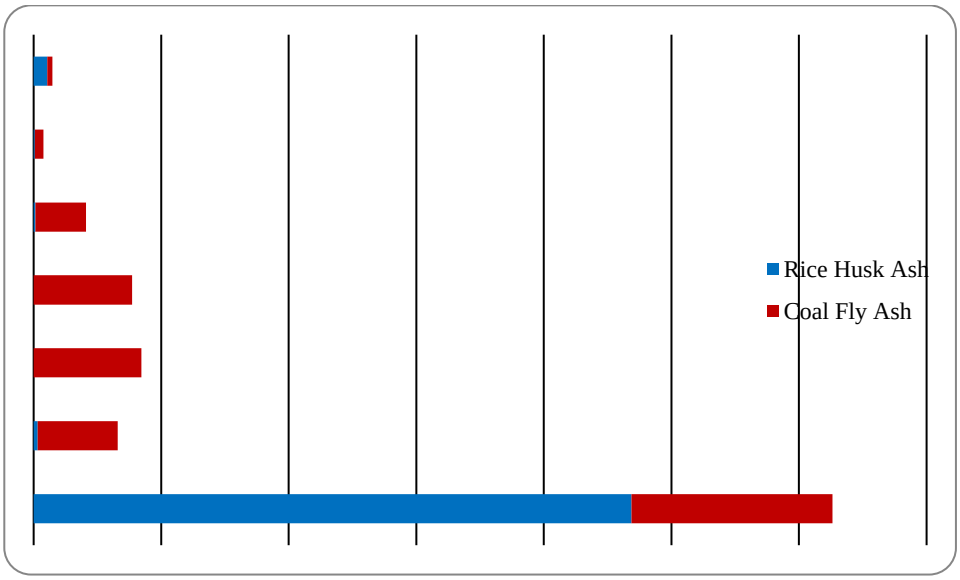

Figure 2. AAS Result of Rice Husk Ash and Coal Fly Ash

Figure 2 showed that rice husk ash contains SiO_2 about 93.37%, and coal fly ash containing Al_2O_3 of 12.57%, so rice husk ash and coal fly ash is potentially used as raw material for ZSM-5 zeolite catalyst synthesis.

B Synthesis of ZSM-5 from Coal Fly Ash

The ZSM-5 zeolite from coal fly ash and rice husk ash were synthesized through hydrothermal alkalin method using NaOH. Synthesis of ZSM-5 was prepared with a molar ratio 12 NaOH: 30 SiO_2: 0.75 Al_2O_3: 6 TPAOH: 1800 H_20 [10]. The aluminate source is obtained from coal fly ash and silicate source comes from rice husk ash. Templates used include Tetrapropylammonium hydroxide TPAOH, (C_3H_7) NOH as steering structures MFI, and Polydiallyldimethylammonium PDDA, ($C_8H_{16}ClN$) n) as structure-directing agent for mesoporous structures.

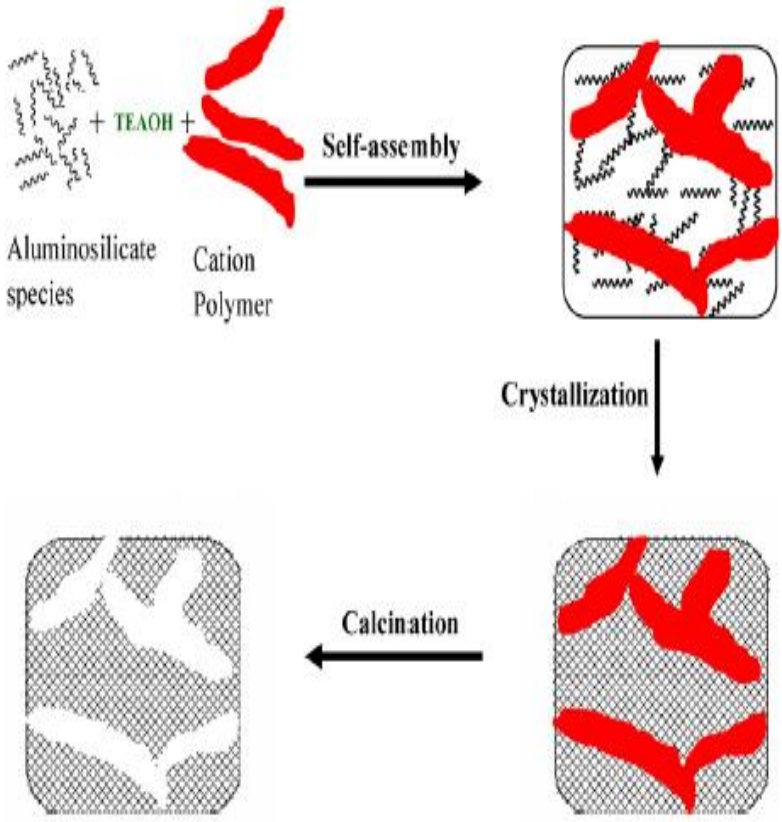

Figure 3. Ilustration of ZSM-5 Zeolite Synthesis [12]

The process of impregnation of cobalt on ZSM-5 refers to the method used by Pieter J. Smeets et al (2008) with modified. Impregnation has been done by using $Co(NO_3)_2$. 6H2O 0.249 M to produce metal loading of 2.5%. The impregnation method was used in this study to optimize the number of cobalt specimens impregnated on the zeolite surface. Beznis has been reported that the selectivity and reactivity of methanol products increases with the presence of impregnated cobalt atoms on the surface of ZSM-5. In the cobalt impregnation process, the cobalt species formed in the zeolite are CoO and Co_3O_4 species. The XRF result showed the concentration of impregnated Cobalt is 1.99 %. The result of ZSM-5 after impregnation was showed by Figure 4, Figure 5 and Table 1

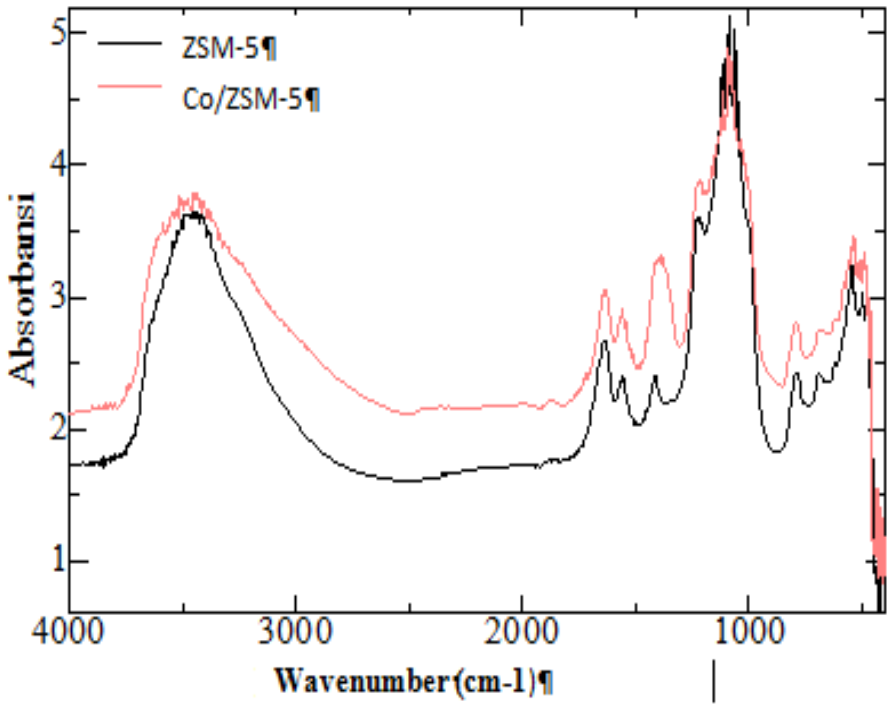

Figure 4. FTIR Spectra of ZSM-5 and Co/ZSM-5

Figure 4 shows the FTIR spectra of ZSM-5 and Co/ZSM-5. The characteristic absorption bands of ZSM-5 were found at around 1250-950 cm^{-1} ($v_{asimetri}$ T-O), 1100-700 cm^{-1} ($v_{simetri}$ T-O), and also were found at round 650- 500 cm^{-1} indicated the presence of double 5- ring in ZSM-5.[12].

Figure 4 also shows the cobalt impregnation process doesn't causes difference typical spectra of the aluminasilicate compound at 1250-950 cm^{-1} (vasimetri TO), 1100-700 cm^{-1} (vsimetri TO), and a peak in the 650-500 cm^{-1} indicating the double ring of the pentacyl framework which is the specific to MFI type zeolite. This means that the process of impregnation of cobalt to ZSM-5 does not changing functional groups in the typical spectra of ZSM-5.

Figure 5 shows the diffraction patterns of ZM-5 zeolite from fly ash and Co/ZSM-5 (impregnated Cobalt to ZSM-5) showed the appearance of certain peaks in the position 2 theta between 7º to 9º and 22º to 25º, indicative of successfully synthesized ZSM-5 structure.

Figure 5 also shows the intensity of the Co/ZSM-5 difractogram was a decrease at position 2 theta between 7 ^{0}-9 ^{0}. This indicates the crystallinity of ZSM-5 decrease after cobalt impregnation. The diffraction pattern at position 2 theta between 37 ^{0} and 47 ^{0} indicate the presence of the Co_3O_4 species [13].

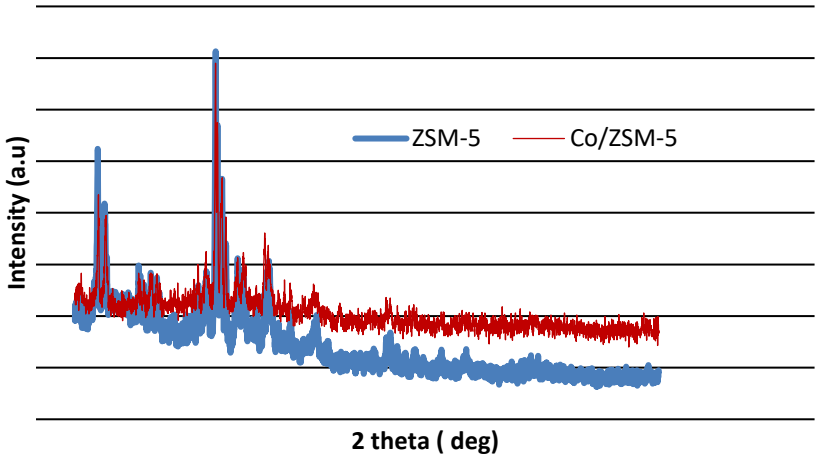

Figure 5. XRD Pattern of ZSM-5 and Co/ZSM-5

Tabel 1. Surface area analyses of ZSM-5 calculated from BET

Sample	S BET (m2/g)	S ext (m2/g)	V tot (cm3/g)	V meso (cm3/g)	V micro (cm3/g)	Average diameter pore (nm)
ZSM-5	43.759	43.759	0.287	0.287	-	26.2618
Co/ZSM-5	30.229	30.229	0.1263	0.1263	-	16.71

The results of surface area analyses of ZSM-5 are summarized in Table 1.

The results of surface area analyses of ZSM-5 and Co/ZSM-5 are summarized in Table 1. It can be seen that the surface area of ZSM-5 from fly ash is still to low, due to ZSM-5 from fly ash still has many impurities especially Fe which could as inhibitor in zeolititation process

Tabel 1 shows that the process of impregnation of cobalt metal causes a decrease in surface area, pore volume and diameter pore. The decrease of surface area, pore volume and pore size indicates that cobalt has entered into the pores of ZSM-5.

C. Catalytic Test : Methanol Synthesis

The catalytic reaction was initiated by activation of ZSM-5 and Co / ZSM-5 catalysts at 550 ° C for 3 hours. This activation has purpose to form cobalt oxide species which constitute the active site of the catalyst Co/ZSM-5. Furthermore, flushing was carried out using nitrogen gas to remove organic impurities, water vapour and excess oxygen in the reactor. The condition of the reaction was adapted from the work reported by Krisnandi et al [11] and Bezniz et.al[9] . The first set of experiments was carried out at 150 ^{o}C with reaction time of 30 min and 60 min, and CH_4 pressure (Pmethane) of 0.75 Bar in 200 cm^3 stainless steel vessel. The gas product formed is extracted with ethanol, and then characterized using Gas Chromatography-FID. The results of this experiment are summarized in Figure 6

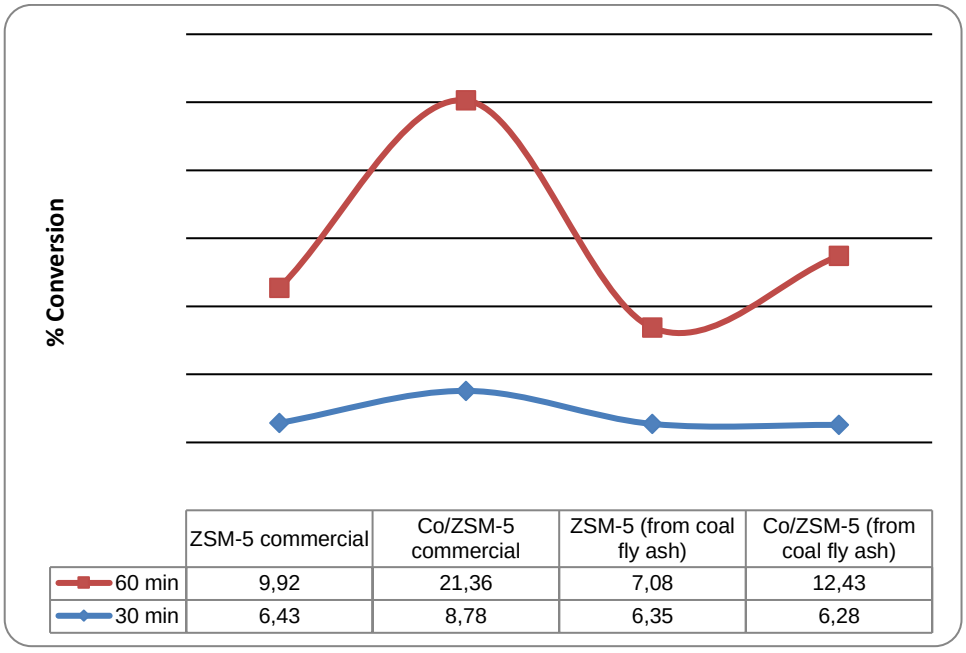

	ZSM-5 commercial	Co/ZSM-5 commercial	ZSM-5 (from coal fly ash)	Co/ZSM-5 (from coal fly ash)
60 min	9,92	21,36	7,08	12,43
30 min	6,43	8,78	6,35	6,28

Figure 6. % methane conversion to methanol from reaction carried out at 150 ^{o}C, t= 30 and 60 min and methane pressure of 0.75 Bar

Fig 6 showed that hence the catalytic activity of ZSM-5 and Co/ZSM-5 from fly ash was still inferior (7.08% and 12.43% conversion of methane) compared to commercial one (9.92% and 21.36%), they were potential to be used as catalyst in the partial oxidation of methane to methanol. The activity of ZSM-5 and Co/ZSM-5 from fly ash inferior compared to the commercial materials caused ZSM-5 from fly ash has lower surface area than ZSM-5 commercial materials. The cobalt-loaded ZSM-5 catalysts gave higher conversion than the ZSM-5 without cobalt-loaded because imprenated Co/ZSM-5, mainly containing cobalt oxidic spesies at the zeolite outer surface, were more selective towards methanol [7,9]

IV. Conclusion

1. ZSM-5 zeolite has been successfully syntesized from coal fly ash.
2. The results of ZSM-5 and Co / ZSM-5 synthesized from coal fly ash are potential to catalyze the partial oxidation reaction of methane to methanol, although the % conversion becomes methanol produced smaller than commercial ZSM-5.
3. The cobalt oxide that is impregnated in the ZSM-5 zeolite serves as an active species that can increase the activity of partial oxidation reaction of methane to methanol.

Acknowledgment

This research was funded by : Hibah PUPT BOPTN No. 0545/UN2.R12/HKP/05.00/2015 and BPPT SK No. No.211a/2014.

References

[1] .*Sci.* [Online]. Available: https://finance.detik.com/infografis/3417754/ri-punya-cadangan-batu-bara-24-miliar-ton-yang-masih-perawan

[2] Yayuan WEI, Qunying WANG, guangwei YING, Zhungyang LUO, and Yoshihiko MINOMIYA. Characteristic and Utilization of Fly Ash from Coal Fired Power Plant in China. CWULAJ Conference in Navshiville. TN-My 5-7.2015

[3] Zacco (2014). *A. review of fly ash inertisation treatments and recycling*. Environmental Chem let 2014:12:153-157

[4] ZhaoXS, Lu GQ, Zhu HY. *Effect of ageing and seeding on the formation of zeolite Y from coal fly ash,* J. Porous Mater.1997:4:245-51

[5] Giraldo, L.F., Lopez, B.L., Perez, L., Urrego ,S.,Sierra,L.,and Mesa, M. 2007. *Mesoporous Silica Application.* Macromolekular Symposia, 258, (1)129-141

[6] Prasad C.S., Maiti K,N., Venugopal R., (2001), "*Effect of rice husk ash in whiteware compositions"*, Ceramic International, 27, 629-635

[7] Mirdayanti F, Sumbogo Murti, Yuni. K. Krisnandi, Adiarso. Partial Oxidation of Methane to Methanol Over Catalyst ZSM-5 from Coal Fly Ash and Rice Husk Ash. MATEC Web of Conference 101.02005.2017

[8] Luigi T. De Luca, Propulsion physics (EDP Sciences, Les Ulis. 2009).

[9] Beznis, Nadzeya V., Bert M. Weckhuysen, Johannes H. Bitter. (2010). *Parsial Oxidation of Methane Over Co-ZSM-5.* Tuning the oxygenate Selectivity by altering the preparation. Catal Lett 136 (2010) 52-56

[10] Kordatos, K. S. Gavela A. Ntiziouni, K.N.Pistiolas, A. Kyritsi, V. Kasselouri, Rigo Paulou. 2008. *Synthesis of Highly Siliceous ZSM-5 Zeolite using Silica From Rice Husk.*Microporous and Mesoporous Material. 189-196

[11] Krisnandi Y, Putra Bimo AP, Bahtiar M, Zahara, Abdullah M, Howe Russell F. 2015. *Parsial Oxidation of Methane to Metanol over Heterogeneous Catalyst Co/ZSM-5*. Procedia Chemistry 14(2015) 508-515

[12] Meng, X., Nawaz, F., and Xiao, F.S.2009. Templating route for synthesizing mesoporous materials. Microporous and Mesoporous Materials, 125, (3) 170-223.

[13] Susianto Nirwan. 2014. Studi Spektroskopi Struktur dan Sifat Zeolit ZSM-5 Mesopori Terimpregnasi Oksida Kobalt. Departemen Kimia FMIPA Universitas Indonesia.

Characterization of Rusip Along with the Amino Acid and Fatty Acid Profile (#639)

Dyah Koesoemawardani[1,a], Sri Hidayati dan Subeki[1]
[1]Department of Agricultural Technology Faculty of Agriculture Lampung University
Jl. Prof. Sumantri Brojonegoro No. 1 Bandar Lampung
Lampung 35145 Indonesia,
[a]dyahthp@gmail.com

Abstract. *This research aims to find out the chemical and microbiological characteristics, the amino acid and fatty acid profile of spontaneous and non-spontaneous Rusip. The results showed that the chemical and microbiological characteristics of spontaneous Rusip and non-spontaneous Rusip by adding mixed cultures respectively were total acid 2.28% and 3.60%; protein content 14.45% and 13.64%; fat content 0.38% and 0.44%, reducing sugar 6.42% and 5.01%; water content 66.52% and 67.27%; salinity 24.94% and 19.49%; pH 5.61 and 5.74; TVN 31.76 mgN/100g and 20.19 mgN/100g; total lactic acid bacteria 9.66 log cfu/g and 12.09 log cfu/g; total mold 7.58 log cfu/g and 5.81 log cfu/g; total microbial 9.84 log cfu/g and 8.42 log cfu/g. Amino acid composition showed that the contents of glutamic acid, aspartic acid, while methionine and lysine on both Rusip mutually significantly different. The dominant fatty acid respectively were docosahexaenoat acid (C22:6n3) and palmitic acid (C16:0).*

Keywords: *amino acids, chemical characteristics, fatty acids, microbiological characteristics, and Rusip.*

I. Introductions

Rusip was a typical food of Bangka, Bangka Belitung province, Indonesia, namely in the form of a fermented food anchovies or other fish (Koesoemawardani 2007[b;] Andriani, 2015). The other materials were 25% salt and 10% of palm sugar, and then cured for 1-2 weeks, usually Rusip consumed as a sauce or mixed in cooking, while Rusip characters were color brown to dark gray, sweet, sour and salty and the flavor typical (Koesoemawardani 2007[a,]b). Koesoemawardani 2007[a] state that Rusip TVN value was still high, so that the necessary repairs Rusip processing. Furthermore, Koesoemawardani et al (2013) make the observation of changes in microbiological and chemical properties of the spontaneous and non-spontaneous Rusip (by adding liquid culture at Rusip processing). The observations showed that there are changes in the microbiological and chemical properties Rusip during fermentation and non-spontaneous Rusip have the microbiological and chemical properties better. Change the chemical nature of biochemistry, microbiology, amino acids, fatty acids, bioactive compounds and sensory also occur in some fermented products are made from fish by differential processing and treatment (Giri et al, 2012; Anggo et al., 2014; Anggo et al., 2015; Khairi et al, 2014; Kim et al, 2014; Skara et al, 2015; Thapa, 2016; Koo et al, 2016). Additionally, Adesokan et al, (2011) stated that the lactic acid bacteria can affect the nutritional quality, acceptability and shelf life Nono fermented milk products from Nigeria. Therefore, this study aims to find out the chemical and microbiological characteristics, the amino acid and fatty acid profile of spontaneous and non-spontaneous Rusip.

II. Materials and Methods

1. Preparation processing Rusip
   Rusip spontaneous made from Anchovy *(Stolephorussp)*, salt 25% (w/w) and palm sugar 10% (w/w), and then mixed evenly. After that, incubated for 2 weeks. Meanwhile, the manufactured of non-spontaneous Rusip by adding mixed cultures (*Streptococcus, Leuconostoc and Lactobacillus*) as much as 2% (w/v) of anchovy weight before incubation. (Koesoemawardani, et al., 2013).
2. Observations chemical and microbiological include: total acid (AOAC, 2005), protein content AOAC (2005), fat content AOAC (2005), the sugar reduction method of Nelson Somogyi (Sudarmaji, et al., 1997), the water content AOAC (2005), salinity (Sudarmadji, et al, 1997), pH (Apriyantono, et al, 1989) and TVN (Apriyantono, et al., 1989), total lactic acid bacteria (Fardiaz, 1989), total microbial (Fardiaz, 1989), total molds (Fardiaz, 1989), amino acid profile (HPLC) and fatty acid profile (GC-MS).
3.

III. Results and Discussion

In this study made spontaneous Rusip and non-spontaneous Rusip with the same incubation period for two weeks. Here are the results of observations of the chemical and microbiological spontaneous Rusip and non-spontaneous Rusip.

Table 1. Characteristics of chemical and microbiological properties of Rusip

Parameter	**Rusip spontan**	**Rusip non spontan**
Total acid	2.28 (%) [a]	3.60 (%) [b]
protein content	14,45 (%) [a]	13,64 (%) [a]
Fat content	0,38(%) [a]	0,44(%) [a]
Sugar reduction	6.42 (%) [a]	5.01 (%) [b]
Moisture content	66,52 (%) [a]	67,27 (%) [a]
Salinity	24,94 (%) [a]	19,49 (%) [b]
pH	5,61 [a]	5,74 [a]
TVN	31.76 mg N/100g [a]	20.19 mg N/100g [b]
Total lactic acid bacteria	9.66 log cfu/g [a]	12.09 log cfu/g [b]
Total mold	9.66 log cfu/g [a]	5.81 log cfu/g [b]
Total microbe	9.84 log cfu/g [a]	8.42 log cfu/g [a]

Protein content of these studies had higher were respectively 13.64% and 14.45% compared Rusip on research Khairi et al (2014) that was equal to 12.81%. In Table 1, shows that there are differences in some characteristics spontaneous Rusip and non-spontaneous Rusip. The difference was much affected due to differences in the total amount of lactic acid bacteria in Rusip. Non-spontaneous Rusip contains more lactic acid bacteria, because there were adding mixed culture (*Streptococcus, Leuconostoc* and *Lactobacillus*) as much as 2% (w/v) of the weight of the fish then the lactic acid bacteria dominated from the start of fermentation (Koesoemawardani et al (2013). This is in line with research Afriani (2010) which stated that the mixed culture of starter generate velocity total production of lactic acid bacteria is much

higher than single culture. Therefore, the difference for some characteristics Rusip, the value of total acid, salinity , TVN, total lactic acid bacteria, total fungi and total microbes.

Non-spontaneous Rusip containing total acid more than Rusip spontaneously, because the amount of lactic acid bacteria are added at the beginning of fermentation makes lactic acid bacteria capable of producing rapid growth rate, so the larger role of lactic acid bacteria produce lactic acid through the process heterof ermentatif and homofermentatif (Koesoemawardani et al, 2015). One of the lactic acid bacteria are added to the process of making rusip *(Leuconostoc sp)* is a group of bacteria heterofermentatif (Lahtinen, et al, 2011). Based on the research results Kurniati (2006) noted that *Leuconostoc sp* always there for 15 days of fermentation. Das (2014) also added starter cultures in fermented food Sindol of fish from the Indian Assam, the result was the addition of starter culture to give change in organoleptic properties, physicochemical and microbiological Sindol.

The best saline of non- spontaneous Rusip research results contain high levels of salt that was lower than spontaneous Rusip (Koesoemawardani et al. 2015). The dominance of lactic acid bacteria at the start of fermentation could suppress the growth of spoilage bacteria and pathogens (Rosma et al., 2009), so as to control the fermentated process from beginning to end, resulting in the use of salt on the processing rusip may be reduced to 20% (Koesoemawardani et al. 2015). The high lactic acid bacteria in non-spontaneous rusip also affect the reduction in TVN value, total fungi and total microbial (Koesoemawardani et al., 2013; Koesoemawardani et al. 2015). The addition of the culture at fermentation products could act as antimicrobial, so that it could improve the sensory, nutritional and shelf live product (Sholeva et al. 1998; Savadago et al, 2004; Adesokan et al, 2009; Adesokan et al, 2011).

Table 2. Amino acids profile of Rusip

Amino acids	**Rusip spontaneous (%)**	**non-spontaneous Rusip (%)**
aspartic acid	1,39 a	1, 41a
glutamic acid	2,07 a	2.06 a
serine	0,56 a	0.56 a
histidine	0.31 a	0.28 a
glycine	0.57 a	0.61 a
threonine	0.55 a	0.51 a
arginine	0.55 a	0.53 a
alanine	0.91 a	0.90 a
tyrosine	0.43 a	0.45 a
methionine	0.33 a	0.07 b
valine	0.66 a	0.66 a
penilalanin	0.54 a	0.53 a
I-leucine	0.57 a	0.59 a
leucine	0.99 a	0.99 a
lysine	0.85 a	1.28 b

Table 2 showed that the amino acid profile of spontaneous Rusip and non-spontaneous Rusip complete enough good essential amino acids and non-essential. Amino acid composition showed that the contents of glutamic acid and aspartic acid were higher than other amino acids, while methionine and lysine on both Rusip mutually significantly different. In the study Khairi et al (2014) showed that glutamic acid, aspartate acid and lysine, amino acids that were dominant in Rusip. Ijong and Ohta (1995) stated that mixed cultures

could increase the amount of amino acids. Meanwhile, Rusip amino acid variations in these studies with research Khairi et al (2014).

Furthermore Khairi et al (2014) stated that Rusip has a value of amino acid composition and value of digestibility of protein is higher than Budu, while Je et al (2005) stated that the content of free amino acids were fermented oyster (Crassostreagigas) sauce fluctuated during fermentation, but mostly increased during fermentation. Amino acids profile of Rusip were also similar to other fermented fish products such as fish sauce (Jiang et al, 2007; Dincer et al, 2010); fermented shrimp (Hajeb and Jinap, 2012). anchovy paste (Anggo et al. 2015); budu and Rusip (Khairi et al. 2014). Some of these studies stated that amino acids were prominent in the fermented fish product was glutamic acid. The difference in the number of each amino acid was caused by the difference in the free amino acid balance produced by autolysis and microbial activity (Jiang et al,2007). Amino acids were contributing significantly to a sense of Yu-lu (Lopetcharat et al. 2001; Jiang et al,2007). For example: glutamic acid provides meaty aroma type (Jianget al, 2007); glycine, alanine, serine and threonine give a sweet taste, while valine, phenylalanine and histidine give a bitter taste (Liu, 1989).

Table 3. The fatty acid profile of Rusip

fatty acid	**Rusip spontaneous (%)**	**non-spontaneous Rusip (%)**
Caprylic acid, C8: 0	0.05a	0.05 a
Capric acid, C10: 0	0.03a	0.04 a
Lauric acid, C12: 0	0.34a	0.30 a
Tridecanoic acid, C13: 0	0.11 a	0.11 a
Myristic acid, C14: 0	3.21 a	2.87 a
Pentadecanoic acid, C15: 0	0.61 a	0.56 a
Palmitic acid, C16: 0	10.95 a	9.62 a
Palmitoleic acids, C16: 1	3.26 a	2.89 a
Heptadekanoic acid C17: 1	0.82 a	0.71 a
Cis-10-heptadecanoic acid, C17: 1	0.16 a	0.15 a
Stearic acid, C18: 0	4.12 a	3.52 a
Elaidic acid, C18: 2n6c	0.08 a	0.06 a
Oleic acid, C18: 1n9c	4.66 a	4.15 a
Linoleic acid, C18: 2n6c	0.67 a	0.61 a
arakidic acid, C20: 0	0.31 a	0.26 a
g-linolenic acid, C18: 3n6	0.15 a	0.13 a
Cis-11-eicosenoic acid, C20: 1	0.08 a	0.07 a
Linolenic acid, C18: 3n3	0.40 a	0.25 a
Heneicosanoatic acid, C21: 0	0.09 a	0.08 a
Cis-11,14-eicosedienoic acid, C20: 2	0.10 a	0.10 a
Behenic acid, C22: 0	0.43 a	0.37 a
Cis-8,11,14-eicosetrienoic acid, C20: 3n6	0.13 a	0.13 a
Erucic acid, C22: 1N9	0.02 a	0.03 a
Cis-11,14,17-eicosetrienoic acid, C20: 3n3	0.04 a	0.05 a
Arachidonic acid, C20: 4n6	4.53 a	4.01 a
Tricosanoic acid, C23: 0	0.08 a	0.12 a
Lignoceric acid, C24: 0	0.79 a	0.74 a

Cis-5,8,11,14,17-eicosapentaenoic, C20: 5n3	4.05 a	3.37 a
Nervonic acid, C24: 1	0.23 a	0.19 a
Cis-4,7,10,13,16,19-docosahexaenoic acid, C22: 6n3	16.62 a	14.77b

Table 3, show that predominant composition fatty acids in Rusip respectively were docosahexaenoat (C22:6n3) and palmitic acid (C16:0),whereas other fatty acids that have high amounts respectively were oleic acid (C18: 1n9c); arachidonic acid (C20: 4n6); stearic acid (C18: 0); cis-5,8,11,14,17-eicosapentaenoic acid (C20: 5n3); palmitoleic acid (C16: 1) and myristic acid (C14: 0). Composition fatty acid of spontaneous Rusip and non-spontaneous Rusip were mostly not significant, only Cis-4,7,10,13,16,19-docosahexaenoic acid (C22:6n3) was different. Docosahexaenoat acid (C22:6n3) spontaneous Rusip have a higher value than the non-spontaneous Rusip. Dincer et al (2010) stated that docosahexaenoat acid content (C22) which leads to high fish sause favorable for human counsumption.

Meanwhile, Sutrisno and Apriyantono (2005) mentioned that the content docosahexaenoic acid (C22) in bekasem anchovy lower than content the docosahexaenoic acid (C22) in anchovy fresh, while the content docosahexaenoic acid (C22) in bekasem anchovy with the addition of pure cultures higher than bekasem anchovy spontaneously. However, there were some fatty acids decreased after the non-spontaneous fermented (with the addition of a pure culture). This happens because of the salt content of anchovy bekasem non-spontaneous used lower salt concentration. Rusip non spontaneous in this study also had a lower salt content than Rusip spontaneous because with the addition of a liquid culture at Rusip can reduce the use of salt from 25% to 20% and produce a better Rusip character (Koesoemawardani et al, 2015).

MUFA and PUFA were essential fatty acids that are needed by the body, usually obtained from food, eg fish (Rauf, 2015). Meanwhile, Mohammed, (2015) states that free radicals attack important macromolecules leading to cell damage and homeostatic disruption. Targets of free radicals include all kinds of molecules in the body. Among them, lipids, nucleic acids, and proteins are the major targets. Antioxidant substances can prevent this damage by inhibiting the production of the main catalysts of lipid peroxidation. Maillard reaction products (MRPs) which could be formed during the fermentation was responsible for the increase in antioxidant activity (Noguchiand and Niki,1999). Anggo et al (2015) stated that the fermented shrimp paste with the addition of salt by 25%, during the fermentation showed antioxidant activity, while the fatty acid composition has not changed during the fermentation of 36 days. In line with that, Rusip in this research also a fish fermented products, so allegedly also showed antioxidant activity obtained from the fatty acid content.

IV. Conclusions

Characteristics of spontaneous Rusip and non-spontaneous Rusip different were the total acid, reducing sugar, salt content, TVN, total lactic acid bacteria, total fungi and total microbes. The differences were due to the influence of the amount of lactic acid bacteria in non-spontaneous Rusip higher. Amino acid composition showed that the contents of glutamic acid and aspartic acid were higher than other amino acids, while methionine and lysine on both Rusip mutually significantly different. The essential fatty acid found was docosahexaenoat acid (C22:6n3) which was higher than other fatty acids on both Rusip,

whereas other fatty acids that have high amounts, respectively were palmitic acid (C16:0); oleic acid (C18: 1n9c); arachidonic acid (C20: 4n6); stearic acid (C18: 0); cis-5,8,11,14,17-eicosapentaenoic acid (C20: 5n3); palmitoleic acid (C16: 1) and myristic acid (C14: 0).

References

[1]. Adesokan, I.A., Ekanola, Y.A., Fakorede, S.S., Oladejo, O.O. and Odutola, O.L. 2009. Infuence of lactic starters on sensory properties and shelf life of wara-a Nigerian (unripened) soft cheese. J. Applied Biosci., 13:714-719.

[2]. Adesokan, I.A., Odetoyinbo, B.B., . Ekanola, Y.A, Avanrenren, R.E. and Fakorede, S. 2011. Production of Nigerian Nono using lactic starter cultures. Pakistan Journal of Nutrition 10 (3): 203-207.

[3]. Afriani. 2010. Effect of lactate acid bacteria starter use *Lactobacillus plantarum* and *Lactobacillus fermentum* to total lactic acid bacteria, acid concentration and pH value of cow milk dadih. Jurnal Ilmiah Ilmu-Ilmu Peternakan. 8(6):279-285.

[4]. Andriani, S. 2015. Rusip, the typical extreme sauce of Bangka. http://lifestyle.okezone.com /read/2015/09/09/298/1211430/rusip-sambal-ekstrem-khas-bangka.

[5]. Anggo, A.D., Ma'ruf, W.F., Swastawati, F., and Rianingsih, 2014. The quality of organoleptic and chemically in rebon shrimp paste to different of salt concentration and duration fermentation. JPHPI. Vol. 17 (1):53-59.

[6]. Anggo, A.D., Ma'ruf, W.F., Swastawati, F., and Rianingsih, L. 2015. Changes of amino and fatty acids in anchovy (*Stolephorus* sp) fermented fish paste with different fermentation periods. Procedia Environmental Sciences 23:58 – 63.

[7]. Apriyantono, A., Fardiaz, D., Puspitasari, N.L., Sedarnawati and Budiyanto, S. 1989. Food Analysis Laboratory instructions. Inter-University Center for Food and Nutrition. Institut Pertanian Bogor. Bogor. Pp 229

[8]. Association of Official Analytical Chemist. 2005. Official Methods of Analysis of The Association of Official Analytical Chemist. Arlington. Virginia (USA): Association of Official Analytical Chemists Inc.

[9]. Das, M. K. 2014. Starter culture development of sindol-a fermented fish product of Assam. International Journal of Agricultural Science and Research. Vol. 4 (2):107-114.

[10]. Dincer, T., Cakli, S., Kilinc, B and Tolasa, S. 2010. Amino acid and fatty acid composition of fish sauce. Journal of Animal and Veterinary Advance. Vol. 9 (2): 311-315.

[11]. Fardiaz, S. 1992. Food Processing Advanced Microbiology. Inter-University Center for Food and Nutrition. Institut Pertanian Bogor. Bogor. Pp 283.

[12]. Giri, A., Nasu, M., and Ohshima, T. 2012. Bioactive properties of Japanese fermented fish paste, fish miso, using koji inoculated with *Aspergillus oryzae.* International Journal of Nutrition and Food Sciences. Vol. 1(1):13-22.

[13]. Hajeb, P and Jinap, S. 2012. Fermented Shrimp Products as Source of Umami in Southeast Asia. J Nutr Food Sci S10:006. doi:10.4172/2155- 9600.S10-006:1-5.

[14]. Ijong, F.G., and Ohta, Y. 1995. Characteristics of bakasang fermented with lactic acid bacteria-mixed culture. Journal of the Faculty of Applied Biological Science. Vol. 34 (3):1-10.

[15]. Je, J-Y., Park, P-J., Jung, W-K., and Kim, S-K. 2005. Amino acid changes in fermented oyster (*Crassostrea gigas*) sauce with different fermentation periods. Food Chemistry. Vol.91 (1):15-18.

[16]. Jiang, J-J., Zeng, Q-X., Zhu, Z-W., Zhang, L-Y. 2007. Chemical and sensory changes associated Yu-lu fermentation process – a traditional Chinese fish sauce. Food Chemistry. Vol. 104 (4):1629-1634.

[17]. Khairi, I.N., Huda, N., Abdullah, W. N. W., and Al-Karkhi, A. F. M. 2014. Protein Quality of Fish Fermented Product: Budu and Rusip. Asia Pacific Journal of Sustainable Agriculture Food and Energy. Vol. 2 (2): 17-22.

[18]. Kim, Y-B, Choi, Y-S., Ku, S-K., Jang, D-J., Hasnah, and Moon, K. B. 2014. Comparison of quality characteristics between belacan from Brunei Darussalam and Korean shrimp paste. Journal of Ethnic Foods. Vol. 1:19-23.

[19]. Koesoemawardani, D, Rizal, S., and Tauhid, M. 2013. Microbiological and chemical changes of Rusip during fermentation. Agritech Vol. 33(3):265-272.

[20]. Koesoemawardani, D., Yuliana, N., and Sari, M. 2015. Chemical properties and microbiology rusip during fermentation with different concentration of salt. Proceedings of the national seminar and exhibition of food products in 2015 the Association of Indonesian food technologists (PATPI) Semarang 2015: "Innovation for Strengthening the role of industrial technology Toward Fulfillment acceleration of national food". Semarang 20-21 October 2015. Pp:593-604.

[21]. Koesoemawardani, D[a]. 2007. Karakteristik rusip dari pulau Bangka. Prosiding Seminar Hasil Penelitian dan Pengabdian Kepada Masyarakat . Universitas Lampung. 6-7 September 2007.

[22]. Koesoemawardani, D[b]. 2007. Analisis sensori Rusip dari Sungai Liat-Bangka. Jurnal Teknologi dan Industri Hasil Pertanian. Vol. 12 (2). Hal 36-39.

[23]. Koo, O. K, Lee, S. J., Chung, K. R., Jang, D. J., Yang, H. J., and Kwon, D. Y. 2016. Korean traditional fermented fish products: jeotgal. Journal of Ethnic . Vol. 3:107-116.

[24]. Kurniati, Y. (2006). Isolation and identification of lactic acid bacteria from Rusip . Eassy. Fakulty of Agriculture. Lampung University. Bandar Lampung.

[25]. Lahtinen, S., Ouwehand, A. C., Salminen, S., Wright, A. V. 2011. Lactic Acid Bacteria : Microbiological and Functional Aspects. Fourth Edition. CRC Press. Pp: 798.

[26]. Liu, Pei-zhi (1989). The umami of Yu-lu. Food Science (Chinese), 4, 37–40.

[27]. Lopetcharat, K., Choi, Y. J., Park, J. W. and Daeschel, M.A.. 2001. Fish Sauce Products and Manufacturing: A Review. Food Reviews International. 17: 65–68.

[28]. Mizutani, T., Kimizuka, A., Ruddle, K., Ishige, N. 1992. Chemical components of fermented fish products. Journal of Food Composition and Analysis. Vol. 5 (2):152-159.

[29]. Mohammed, M. T., Kadhim, S. M., Jassimand and Abbas, S. I. 2015. Free radicals and human health. International Journal of Innovation Sciences and Research. Vol.4 (6):218-223.

[30]. Noguchi, N., and Niki, E. *Chemistry of active oxygen species and antioxidants*. In A. M. Papas (Ed.), Antioxidant status, diet, nutrition and health. pp 3–20. Florida: CRC Press. 1999.

[31]. Rauf, R. 2015. Kimia Pangan. Andi Offset. Yogyakarta. Pp 255

[32]. Rosma, A., Afiza, T.S., Wan Nadiah, W.A., Liong, M.T. and Gulam, R.R.A. 2009. Short communication microbiological, histamine and 3-MCPD contents of

Malaysian unprocessed 'budu'. International Food Research Journal 16: 589-594.

[33]. Savadogo, A., Ouattara, C. A. T., Bassole, I. H. N., and Traore, A. S. 2004. Antimicrobial activities of lactic acid bacteria strains isolated from Burkina Faso fermented milk. Pakistan Journal of Nutrition. Vol. 3 (3):174-179.

[34]. Sholeva, Z., Stefanova, S. and Chipeva, V. 1998. Screening of antimicrobial activities among *Bulgarian lactobacilli* strains. Journal of culture collections. Vol. 2:15-20.

[35]. Skåra, T., Axelsson, L., Stefânsson, G., Ekstrand, B., and Hagen, H. 2015. Fermented and ripened fish products in the northern European Countries. Journal of Ethnic Foods. Vol. 2:18-24.

[36]. Soetrisno, U.S.S., and Apriyantono, R.R.S. 2005. Nutrient quality and the safety bekasam as fermented small fish by addition of selected lactic acid bacteria or spontaneous fermentation. Jurnal Penelitain Gizi & Makanan. Vol. 28 (1):38-42.

[37]. Sudarmadji, S., Haryono, B. and Suhardi. 1997. Analysis Procedures for Foodstuff and Agriculture. Third Ed. Liberty. Yogyakarta. Pp 160.

[38]. Thapa, N. 2016. Ethnic fermented and preserved fish products of India and Nepal. Journal of Ethnic Foods. Vol. 3:69-77.

Alginate Addition on Geblek (#640)

Fibra Nurainy[1,a], Dyah Koesoemawardani[1], Novita Herdiana[1], Ivana Regin Saragih[1]
[1]Department of Agricultural Technology Faculty of Agriculture Lampung University
Jl. Prof.Sumantri Brojonegoro No. 1 Bandar Lampung
Lampung 35145 Indonesia,
[a] fibranurainy@gmail.com

Abstract- *The objective of this research was to obtain the appropriate alginate addition to the best physical, chemical, and sensory characteristics of Geblek. The experiment was arranged in a non-factorial Random Complete Block Design (RCBD) in four replications. The treatment given on each replication was the alginate addition that consisted of six different levels, they were 0% (A0), 1% (A1), 2% (A2), 3% (A3), 4% (A4), dan 5% (A5) (w/w). The data were evaluated by using The Smallest Real Difference Test (SRD) of 5%. The results showed that the appropriate concentration of alginate addition was 1% with the following criteria texture was not tough; preferred by panelists based on texture, colour, and taste attributes; has a hardness value of 0.475 mm/g/dt; water content of 39.864%;oil absorption of 5.567%, fat contentof 3.905% protein of 5.849%, ash of 2.039%, and carbohydrate of 40.776%.*

Keywords*: Alginate, Geblek, and quality of Geblek*

I. Introduction

Cassava was one of agricultural commodities in Indonesia which has a important role in fulfilling the national food needs because of its abundant availability. Fresh cassava tuber has a very low economic value at the big harvest time. Therefore, it requires effort to increase the added value of cassava tuber . One of cassava tuber diversification process was geblek.

Geblek was one kind of traditional food from Kulonprogo, Yogyakarta. Raw materials of geblek were wet starch, cassava dregs, coconut slices or grated coconut and spices (Koesoemawardani, et al., 2016). The colour of geblek was cloudy white, printed in small ball or can be formed in another custom, when it was bitten likes a sluggish cracker, its taste was savory and most tasty was consumed a few minute after fried in while warm (Sije, 2013; Koesoemawardani, et al., 2016). One of the problem of geblek was its texture become hard in cold condition. Therefore, the innovation to improve its texture was dobe by using a binder material that can synergize with cassava tuber , especially in making geblek.

Ji-Sheng et al. (2011) states that alginate has groups of hydroxyl and numerous carboxyl, which determine the physicochemical and biological characteristics of alginates, even affecting their reactive functional groups. Thus, alginate was very flexible to be used in many potential applications of foodstuffs (Abd El-baki, 1982; Sim, 2011; Santana et al., 2013; Khoury et al., 2014; Fransiska et al., 2014; Rockower, et al, 1983 ; Ahmed et al., 1983) and non-foodstuffs (Davies et al., 1994; Mandal, 2006; Liew, et al., 2006). Therefore, this research uses alginate to improve the texture of geblek. The purpose of this research was to

obtain appropriate addition amount of alginate in the making of geblek, in order to produce the best physical, chemical, and sensory characteristics of geblek.

II. Materials and Methods

The materials for making geblek were cassava tubers , sodium alginate, water, garlic, salt, coconut pulp, and grated coconut, while the other materials are materials for analyst. The tools were geblek processing tools, glass and instrument tools for analysis.

III. Research Methods

This research was arranged in nonfactorial within Randomized Complete Block Design (RCBD) consisting of 6 levels of alginate addition, ie 0%, 1%, 2%, 3%, 4%, and 5% (w / w). Results were expressed by means of values. Comparison of means performed by ANOVA and followed by LSD ($p< 0,05$)(Steel and Torrie, 1995). Fried geblek were evaluated on physical, chemistry, and sensory properties. Evaluation on sensory characteristic covers attributes of texture (hedonic and scoring methods), colour, flavor, and taste with hedonic methods (Meilgaard et al.,2006)). Evaluation of physical and chemical properties on geblek product were test of product hardness (Sumarmono, 2012), colour with Digital Image (Eko, 2012), water content (AOAC, 1984), and Oil Holding Capacity (AOAC, 1995). The best product from physical and sensory properties test result then will be tested on protein (AOAC, 2007) and carbohydrate content (by difference).

IV. Results and discussion

A. Texture (Scoring test) and Hardness Level

The result of analysis of texture by scoring test and hardness level showed that the addition of alginate concentration has significant effect on geblek texture. This is in line with Santana et al (2013) study which stated that the addition of alginate has an effect on hardness, springiness, and cooking yield on soy sauce fish; Abd El-Baki et al (1982) states that alginate can increase water holding capacity (WHC), increased considerably the cooking yield of sausage and plasticity on fresh buffalo sausage. Sim et al (2011) states that sodium alginate can improve the texture of the wheat dough and the Chinese steamed bread to be softer for a long time during storage. The score of texture value of geblek product with the addition of alginate concentration of 0-5% is 2,65-4,02 which means hard,rather hard, and no hard texture (Table 1).

Based on the LSD test (Table 1) it is known that the value of geblek texture score with the addition of alginate concentration of 1% is significantly different with the texture value of geblek in the addition of alginate concentration of 0%, 2%, 3%, 4%, and 5%, while geblek texture with alginate concentration addition of 3%, 4%, and 5% were not significantly different. The highest score of geblek texture score was in addition of alginate concentration of 1% with a score of 4.02 (no hard), whereas the lowest score of texture scoring at Alginate concentrationaddition of 3%, 4%, and 5% with score 2.65-2,86 (rather hard)

Table 1. Scoring test score on geblek texture with addition of alginate at various concentrations

Treatment	Middle Score
A1 (Alginates addition of 1%)	4,02[a]
A0 (Alginates addition of 0%)	3,55[b]
A2 (Alginates addition of 2%)	3,38[b]
A3 (Alginates addition of 3%)	2,86[c]
A4 (Alginates addition of 4%)	2,73[c]
A5 (Alginates addition of 5%)	2,65[c]
BNT0,05 = 0,416	

Note: Different numbers mean each treatment is significantly different in test on Least Significance Different (LSD) of 5% level

Tablel 2. Hardness level of geblek with addition of alginate at various concentrations

Treatment	Middle Score
A1 (Alginates addition of 1%)	0,48[a]
A0 (Alginates addition of 0%)	0,46[b]
A2 (Alginates addition of 2%)	0,46[b]
A3 (Alginates addition of 3%)	0,44[c]
A4 (Alginates addition of 4%)	0,44[c]
A5 (Alginates addition of 5%)	0,43[d]
BNT0,05 = 0,008	

Note : Different numbers mean each treatment is significantly different in test on Least Significance Different (LSD) of 5% level

Based on LSD test (Table 2) it is known that the value of geblek texture score with the addition of alginate concentration of 1% is significantly different with the value of geblek texture in the addition of alginate concentration of 0%, 2%, 3%, 4%, and 5%. The highest hardness value was obtained at geblek with the addition of alginate concentration of 1% i.e. 0.48 mm / g / dt, while the lowest hardness was obtained at geblek with 5% alginate concentration treatment i.e. 0.43 mm / g / dt . In the frying process found expansion which determined by the water content of the material. According to Muliawan's (1991) research, this expansion is the result of a large number of explosions of chained water that evaporate rapidly during the frying process and simultaneously form air cavities that are spread evenly throughout the product structure. If the starch gelatinization process runs perfectly then will find more empty cavity and leave little space between the cavities. When product become cool, the empty cavity will shrink and make the texture geblek without the addition of alginate become hard.

The hardness level of geblek is influenced by the amount of water trapped by alginate in forming gel. Natrium alginate can bind water very strongly because it contains a large number of carboxylic anions (COO-) trapped in the three-dimensional structure (Marseno 1988, Ji-Sheng et al., 2011). If given alginate concentration is too high, geblek texture

produced will get harder. This is directly proportional to research on the parameter of water content value, i.e. geblek with large addition of alginate concentration has low moisture value, if it's fried the amount of evaporated water will be less, thus the water content of the product will decrease. Low water content geblek has a high hardness level, and vice versa (Koesoemawardani et al., 2012). The influence of alginate addition to water content also found in Prawira research (2008), i.e. the alginate addition with high concentration, can produce low water content in kamaboko. Based on hedonic test on geblek, it was found that geblek with alginate addition of 1% yielded the most preferred texture with score 4.14 (very favorable).

B. Colour

The analysisof variance result showed that the addition of alginate concentration had significant effect on panelist's hedonic score on geblek colour (Prawira, 2008; Syafarini, 2009; Santana et al. 2013) . Colour score of hedonic test of geblek product with the addition of alginate concentration of 0 -5 % is 2.25-4.29 which means the resulting texture is rather un-favorable, neutral, and very favorable.

Table 3. Hedonic score on the colour of geblek with the addition of alginate at various concentrations

Treatment	Median
A0 (Alginate addition of 0%)	4,29a
A1 (Alginate addition of 1%)	4,03ab
A2 (Alginate addition of 2%)	3,75b
A3 (Alginate addition of 3%)	3,30c
A4 (Alginate addition of 4%)	2,68d
A5 (Alginate addition of 5%)	2,25e
BNT0,05 = 0,318	

Note: Different numbers mean each treatment is significantly different in the Least Significance Different Test (LSD) of 5%

Table 3 shown that the hedonic value of geblek color with the addition of alginate concentration of 0% is not significantly different with the value of geblek color in the addition of alginate concentration of 1%, but significantly different with the color of geblek in the addition of alginate concentration of 2%, 3%, 4 %, And 5%. The highest hedonic value on colour is obtained in geblek with the addition of alginate, 1%, and 2% concentration with a score of 3.75-4.29 (favorable). Geblek with the addition of alginate at high concentration, making the geblek colour darker than Geblek with alginate addition at low concentrations. The addition of alginate in geblek of 0%, 1%, and 2% has a white to slightly brownish white appearances, while the addition of alginate 3%, 4% and 5% has a slightly brownish up to brownish appearance. Therefore geblek with the addition of alginate at high concentrations was less favorable to the panelists than geblek with the addition of alginate at low concentrations.

The result of the hedonic test on geblek colour is directly proportional to this research on color parameters analyzed by using digital image. Samples of geblek that categorized in the white threshold value is geblek with alginate addition treatment of 0%, while geblek with the

addition of alginate of 1% to 5% not categorized in the white threshold value. Produced geblek with the addition of alginate 1% to 5% has a white brownish, slightly brownish up to brownish appearance. The effect of alginate addition to geblek color in line with Prawira research (2008), that is more alginate concentration added resulting in more lesswhite level in kamaboko, and it guessed related to the water holding capacity possessed by alginate. Kamaboko with high water binding capability has a lower brightness levelcompare to low one. Kamaboko with high water binding yield produced lower free water content in the product, causing the product becomes less bright, whereas kamaboko with low water binding capability produced high free water content causing the product becomes more brighter.

C. Colour Using Digital Image Test

The process of capturing light by cones cell of human eye basically divided into three main groups, namely red (red), green (Green), and blue (Blue). Then they converted into HSI colour modeling (Hue, Saturation, Intensity) to simplify the process of color clarification. Based on the results of color analysis using digital images of MATLAB applications obtained data as follows.

Table 4. HSI values in geblek colour with addition of alginate at various concentrations

Treatment	H	S	I
A0 (Alginate addition of 0%)	0,2038	0,2205	0,1658
A1 (Alginate addition of 1%)	0,1539	0,2852	0,1521
A2 (Alginate addition of 2%)	0,1527	0,2848	0,1520
A3 (Alginate addition of 3%)	0,1491	0,2822	0,1568
A4 (Alginate addition of 4%)	0,1487	0,2641	0,1535
A5 (Alginate addition of 5%)	0,1485	0,2621	0,1512

Hue (H) is an attribute or property of light used to distinguish colours and determine redness, greenness, and so on. The weakness and strength of this hue are described in saturation. Saturation (S) is a component used to describe the strength and fade of a colour received by the eye. Intensity (I) is an attribute that expresses the representation of the number, much of a light reflected or transmitted by an object (Kiswanto, 2012). According to Sije (2013), Geblek has a cloudy white physical appearance. An object can be said to be white if it has a threshold value of Hue between 0.2 to 0.7; Saturation value is between 0.01 to 0.3; And the Intensity value is between 0.1 and 1. Based on the MATLAB results, the samples which categorized in the white threshold value are geblek with 0% alginate addition treatment, while the geblek with the addition of alginate of 1% to 5% are not in the white threshold value. Produced Geblek with the addition of alginate 1% to 5% has appearance of a slightly brownish white, slightly brownish up to brownish.

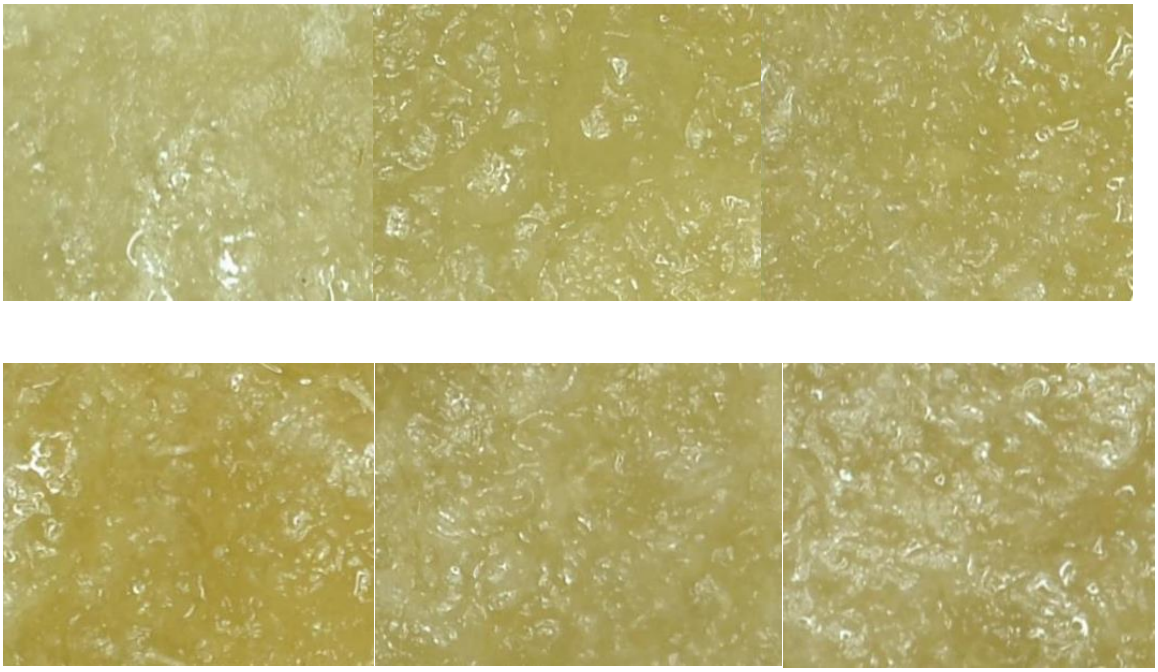

Figure 1. Geblek colour with addition of alginate at various concentrations

D. Flavors

The results of analysis of variance showed that the addition of alginate concentration significantly affected the panelist's preference on the geblek taste. This is in line with Wanstedt et al's (1981) study; Ahmed et al. (1983). The score of hedonic on flavor of geblek products with the addition of alginate concentration of 0-5% was 2.35-4.12 (slightly favorable to very favorable).

Table 5. Hedonic score on the taste of geblek with the addition of alginate at various concentrations

Treatment	Mean
A1 (Alginate addition of 0%)	4,12a
A0 (Alginate addition of 1%)	3,93a
A2 (Alginate addition of 2%)	3,68b
A3 (Alginate addition of 3%)	3,06c
A4 (Alginate addition of 4%)	2,74d
A5 (Alginate addition of 5%)	2,35e
BNT0,05 = 0,229	

Note : Different numbers mean each treatment is significantly different in the Least Significance Different Test (LSD) of 5%

Table 5 shows the hedonic value of geblek flavor with the addition of alginate concentration of 1% is not significantly different with the hedonic value of geblek at the addition of alginate concentration of 0%, but significantly different with the flavor of geblek in the addition of alginate concentration of 2%, 3%, 4 %, And 5%. The highest hedonic value of

taste was obtained at geblek with the addition of alginate concentration of 1% and 0% with score 3,93-4,12 (favorable), whereas the hedonic value on the lowest flavor was the addition of 5% alginate concentration with score 2,35 (un-favorable). Addition of alginate with higher concentration causes geblek has a bitter taste compared with the addition of alginate with lower concentrations. This results in products with high alginate concentration not favored by the panelists.

E. Water content

The analysis of variance result showed that the addition of alginate concentration significantly affected the water content of geblek product. The value of water content of geblek products with the addition of alginate concentration of 0 - 5% is 41,532-31,554%.

Table 6. Value of geblek water content with the addition of alginate at various concentrations

Treatment	Mean
A1 (Alginate addition of 0%)	42,53[a]
A0 (Alginate addition of 1%)	39,86[b]
A2 (Alginate addition of 2%)	37,91[c]
A3 (Alginate addition of 3%)	35,86[d]
A4 (Alginate addition of 4%)	34,55[d]
A5 (Alginate addition of 5%)	31,55[e]
BNT0,05 = 1,922	

Note: Different numbers mean each treatment is significantly different in the Least Significance Different Test (LSD) of 5%

Table 6 shows that the water content of geblek with the addition of alginate concentration of 0% is significantly different with the water content of geblek on the addition of alginate concentration of 1%, 2%, 3%, 4%, and 5%. The highest water content value was obtained in geblek with the addition of 0% alginate concentration that is 42.53%, while the lowest geblek hardness value was at the addition of 5% alginate concentration that is 31.55%. The ability of alginate in water binding was very high, more alginateconcentrationgiven to geblek, then it shows the tendency of more lower water content produced, and vice versa, less alginate concentration given to geblek, more higher the water content (Prawira, 2008; Mastuti, 2008; Koesoemawardani, et al 2012). Sodium alginate can bind water very strongly because it contains large amounts of carboxylic anion (COO -) .The water binding able to form gel because the large amount of water trapped in the three-dimensional structure). When dissolved in water, sodium alginate will form a mesh-like grid that can bind strongly many water molecules and hold water-soluble well (Marseno, 1988; Ji-Sheng et al., 2011). The increased concentration of Na-alginate allows more chemical reaction of gel formation. Gel formation causes free water in tendon to be used for forming complex bonds of gel matrix consisting of water-protein-polysaccharides, so less free water in the meat system (Prawira, 2008).

F. Oil Absorption Strength

Oil absorption strength is the amount of oil absorbed in the product during the frying process. Oil absorption is obtained from the reduction of fat content value after fried with water content value before frying. Analysis of Variance result (Table 43) showed that the addition of alginate concentration had significant effect on the absorption of oil of geblek products. The absorption capacity of geblek oil with the addition of alginate concentration of 0-5% was 5,58-15,62%.

Table 7. Absorption value of geblek oil with the addition of alginate at various concentrations

Treatment	Mean
A0 (Alginate addition of 0%)	15,62[a]
A1 (Alginate addition of 1%)	10,41[b]
A2 (Alginate addition of 2%)	9,83[c]
A3 (Alginate addition of 3%)	9,23[d]
A4 (Alginate addition of 4%)	7,19[e]
A5 (Alginate addition of 5%)	5,58[f]
BNT0,05 = 0,098	

Note: Different numbers mean each treatment is significantly different in the Least Significance Different Test (LSD) of 5%

Table 7 shows that the absorption of oil in geblek among all treatments of alginate concentration addition is different. The highest oil absorption is obtained in geblek with the addition of 0% alginate concentration, while the lowest oil absorption is obtained in geblek with the addition of alginate concentration of 5% . If more alginate concentration is given, then the less absorption of oil in geblek happens.

According to Dalimunthe's (2014) study, the strength reduction of oil absorption is due to decreased water content and fat content, so in the frying process will create less water-filled cavities, then the water will out and fill by oil. This is in line with the value of moisture content in this study, ie higher moisture content results in higher product oil absorption, whereas low moisture content results in low oil product absorption. High temperatures cause more dehydration on the surface of the material so that there is more empty space filled with oil (Ketaren, 1986). The fried foods have the same structure,they are outer zone surface, crust and core. The absorbed oil used for soften food crust, match with the amount of water that evaporates during frying.

G. Best Treatment

The best product selection is based on the results of geblek products testing with organoleptic, physical, and chemical parameters.Geblek with the addition of 1% alginate treatment is the best product which has a texture that is no hard criteria; favored by panelists based on texture, color, and taste attributes; Has a hardness value of 0.475 mm / g / dt; water content of 39,864%; and oil absorption of 5,567%.

V. Conclusion

Based on the results of research that has been done, it can be concluded that the appropriate concentration of alginate addition to the best physical, chemical, and organoleptic characteristics of geblek, is geblek with the addition of alginate of 1% which has a texture that is not hard; Favored by panelists based on texture, color, and taste attributes; Has a hardness value of 0.475 mm/g / dt; Water content of 39,864%; Oil absorption of 5,567%, fat content of 3,905%, protein of 5,849%, ash content of 2,039%, and carbohydrate level of 40,776%.

References

[1]. Abd El-Baki, M.M., Askar, A., El-Dashiouty, M.S., El-Ebzary, M.M. 1982. Characteristics of sausage as prepared with alginate and alginate casings. Molecular Nutrition & Food Research 26 : 295–303.

[2]. AOAC. 1995. Official Methods of Analysis. Association of Official Analytical Chemists. Washington DC.

[3]. AOAC. 2007. Official Methods of Analysis. Association of Official Analytical Chemists. Washington DC.

[4]. Dalimunthe, H., Novelina dan Aisman. 2012. Karakteristik Fisik, Kimia, dan Organoleptik Donat Kentang *Ready to Cook* Setelah Proses Pembekuan. Universitas Andalas. Padang.

[5]. Davies, N.M., Farr , S.J. , Kellaway, I W, Taylor, G., Thomas, M. 1994. A comparison of the gastric retention of alginate containingtablet formulations with and without the inclusion of excipient calcium ions.International Journal of Pharmaceutics 105 : 97–101.

[6]. El Khoury, D., Goff, H.D., Berengut,S., Kubant, R and G.H., Anderson. 2014.Effect of sodium alginate addition to chocolate milk on glycemia, insulin, appetite and food intake in healthy adult men. European Journal of Clinical Nutrition 68: 613–618.

[7]. Fransiska, D., Permatasari, A.I., Haryati,S., Munandar, A., Subaryono, Darmawan, M dan R.Wahyu. 2014. Penambahan Kalsium Karbonat pada Pembuatan Tepung Puding Instan Berbahan Alginat. JPB Perikanan Vol. 9 : 69-81.

[8]. Graha, R.T. 1989. The effect of calcium carbonate and sodium alginate on the color and bind strength of restructured beef steaks.Meat sci.25:163-175.

[9]. Ketaren, 1986.Minyak dan Lemak Pangan. Universitas Indonesia Press, Jakarta.

[10]. Koesoemawardani, D., S. Hidayati dan Susanti. 2012. Rusip Kering dengan Teknik Restrukturisasi.Prosiding Seminar Hasil Penelitian dan Pengabdian kepada Masyarakat. Lembaga Penelitian Universitas Lampung. Bandar Lampung. Hal 19-33.

[11]. Koesoemawardani, D., Fakih dan A. Suryani. 2016. Geblek Ikan Sebagai Camian Sehat. Prosiding Hasil : Seminar Hasil Nasional Pengabdian Kepada Masyarakat. Universitas Lampung. Bandar Lampung.

[12]. Liew, C.V., Chan, L.W., Ching, A.L., SiaHeng, P.W. 2006. Evaluation of sodium alginate as drug release modifier in matrix tablets.International Journal of Pharmaceutics 309: 25–37.

[13]. Mandal, S, ,Puniya,A.K., Singh, K. 2006. Effect of alginate concentrations on survival of microencapsulated Lactobacillus casei NCDC-298. International Dairy Journal 16:1190–1195.

[14]. Marseno, D.W. 1988. Hand Out Mata Kuliah Kimia dan Teknologi Karbohidrat. Program Studi Ilmu dan Teknologi Pangan PascaSarjana. Universitas Gadjah Mada. Yogyakarta.

[15]. Mastuti, R. 2008. Formulasi Konsentrasi Bahan Pengikat Produk Daging Kambing Tetelan Restrukturisasi Mentah. Jurnal Ilmu dan Teknologi Hasil Ternak Vol. 3, No. 1 Hlm 15-23.

[16]. Meilgaard, M.C., Civille, G.V., Carr, B.T.2006. Sensory Evaluation Technique 4th Edition.CRC Press. New York.

[17]. Prawira, A. 2008.Pengaruh Penambahan Tepung Alginat (Na-Alginat)Terhadap Mutu Kamaboko Berbahan Dasar Surimi Ikan Gabus (Channa Striata). Skripsi.Program Studi Teknologi Hasil Perikanan Fakultas Perikanan Dan Ilmu Kelautan Institut Pertanian Bogor. Bogor.

[18]. Rockower, R.K., Deng, J. C., OTWELL, W.S., CORNELL , J.A. 1983 .Effect of Soy Flour, Soy Protein Concentrate and Sodium Alginate on the Textural Attributes of Minced Fish Patties .Jurnal of food science 48 : 1048–1052.

[19]. Santana, P., Huda, N., Yang, T.A. 2013. The Addition of Hydrocolloids (Carboxymethylcellulose, Alginate and Konjac) to Improve the Physicochemical Properties and Sensory Characteristics of Fish Sausage Formulated with Surimi Powder . Turkish Journal of Fisheries and Aquatic Sciences 13: 561-569

[20]. Sim, S.Y., NoorAziah, A.A. , Cheng, L.H. 2011. Characteristics of wheat dough and Chinese steamed bread added with sodium alginates or konjacglucomannan. Food Hydrocolloids 25: 951-957.

[21]. Soemarmono, J. 2012. Pengukuran Keempukan Daging dengan Pnetrometer. Laboratorium Teknologi Ternak. Fakultas Peternakan Universitas Soedirman. Purwekerto.2 hlm.

[22]. Steel, R.G.D dan J.H. Torrie. 1995. Prinsip dan Prosedur Statistika Suatu Pendekatan Biometrik. PT. Gramedia Pustaka Utama. Jakarta.

[23]. Syafarini, I.2009. Karakteristik Produk Tepung Es Krim dengan Penambahan Hidrokoloid Karaginan dan Alginat. Skripsi. Institut Pertanian Bogor.

[24]. Wanstedt, K.G., Seiderman, S.C., Donnely L.S., Quenzer. N.M.1981. Sensory Attributes of Precooked, Calcium Alginate-Coated Pork Patties. Journal of Food Protection 44 : 732-735.

[25]. Yang, J., Xie, Y.J., He, W. 2011. Research progress on chemical modification of alginate: A review. Carbohydrate Polymers. 84 : 33–39.

Effect of the Reactant Concentrations on Manganese Oxide Structures and Their Catalytic Performance for Methylene Blue Degradation (#677)

Amir Awaluddin[1,a], Siti Saidah Siregar, Rizki Rilda Aulia, Nismala Dewi, Indah Puspita Sari, Deasi R. Doloksaribu

[1]Department of Chemistry, University of Riau, Pekanbaru, Riau, 28293, Indonesia

[a] amirawaluddin01@gmail.com

Abstract**—***Various Mn oxide structures have been successfully synthesized by sol-gel method. The influences of different KMnO4/glucose molar ratios of prepared Mn oxides has been investigated by XRD, SEM, and N2 adsorption/desorption measurements. The MnO and δ-MnO2 can be obtained at too and moderately concentrated reactant concentration, respectively, whereas α-MnO2 was prepared at diluted reactant concentration. The catalytic activities of the as-synthesized Mn oxides were evaluated by carrying out the degradation study of methylene blue. The MnO is highly effective in heterogeneous activation of hydrogen peroxide to generate hydroxyl radicals for methylene blue degradation with the activity order of MnO>α-MnO2>δ-MnO2, with the conditions of 50 mg/L MB, 25 mg catalyst, and 15 mL H2O2 at room temperature in 120 min. The experimental data were analyzed using the zero, first, second-order kinetics and Chu kinetic model. The degradation kinetics of methylene blue by the manganese oxide catalysts follow the Chu kinetic model.*

Keywords**—***Manganese oxide, sol-gel, methylene blue, kinetic model*

I. Introduction

Manganese oxides have attracted great deal of attention due to their unique crystal structures and physicochemical properties. Manganese oxides are known to display several crystallographic forms such as tunnel and layered structure [1]-[2]. The basic unit of manganese oxide is octahedral MnO_6, which could combine with different connectivity to form various arrangements such as tunnel and layered materials. These manganese oxides have been used in a wide application such as supercapacitors[3]-[4], lithium batteries [5] and as a catalyst in oxidation of ethanol [6], CO [7],formaldehyde [8], benzene and toluene [9].

The various tunnel manganese oxides are reported and referred to as manganese oxide octahedral molecular sieve (OMS). Based on the size of the tunnel, several polymorphs of manganese oxides are produced such as pyrolusite (1x1 tunnel structure), cryptomelane (2x2 tunnel structure) and todorokite (3x3 tunnel structure)[10]. The cations such as alkali metals and water molecules residue in the manganese oxide pores, which serve to maintain the stability and neutrality of manganese oxides. Birnessite, on the other hand, is well-known as octahedral layered manganese oxides with cations alkali metal and water molecules located in the interlayer spacing of this material.

One of the extensive research for the application of manganese oxides is in the area of organic dye degradation. Organic dye pollutions have become major environmental problem due to their rapid grow of dye industry. Direct releasing the dye residues to environment could pose severe problems to ecosystem because they are toxic, mutagenic and carcinogenic for

aquatic life as well as humans. Therefore, removal of dye residues from water effluents is extremely important because water pollution with dye even as low as 1 mg/L leads to water that is unsuitable for human consumption [11].

Recently, there has been a growing interest in development of advanced oxidation process based on Fenton reaction to remove dye residues from wastewater[12]. Several heterogeneous catalysts have been tested for the Fenton-like reaction for generation of OH radical, which serves as strong oxidation agent for the degradation of the organic dye[13]-[14]. The catalyst with multiple oxidation states should have an excellent catalytic performance. Due to the various oxidation states of Mn element, manganese oxides can be used as an effective catalysts because of their structural, physical, and chemical properties[15].

Manganese oxide was reported to show a good ability to decompose methylene blue above 90% in the presence of H_2O_2. It has been reported that the active radicals such as HO•, O_2•$^-$, HO_2• are generated in MnO_2/H_2O_2 system which using hydrothermal and reflux method to synthesized manganese oxide[16]-[18]. Manganese oxide that prepared by sol-gel method also showed a good catalytic activity for methylene blue degradation more than 90% in less than 30 min using H_2O_2 as an oxidant [19]- [21].

Different methods of manganese oxide synthesis can produce different types of polymorphs. The structural properties, such as polymorphs, morphology, particle size, and crystallinity that related to preparation method, type of precursor, and operation condition have an influence in catalytic activity of methylene blue degradation as reported by Ye *et al.*; Kim *et al.*; and Cao *et al.*[9],[15],[22]. In this research, we report the synthesis of three types of manganese oxides with different structure; layered structure of birnessite (δ-MnO_2), tunnel structure of cryptomelane (α-MnO_2) and Manganosite (MnO) by sol-gel method and their catalytic activities are evaluated for removal of methylene blue dye.

II. Experimental Section

A. Synthesis of Catalysts

Manganese oxides having different crystal structures were prepared by sol-gel method via redox reaction between $KMnO_4$ and glucose.

1) δ-MnO_2, birnessite

A 5.976 g (0.033mol) sample of solid glucose was added to a stirred solution containing 15.8 g (0.1 mol) of $KMnO_4$ dissolved in 400 mL of water. The gel was allowed to settle in 90 minutes and dried at 110 °C overnight and calcinated at 450 °C for 2 h. The product was pulverized, washed three times with 10 ml of 0.1 M HCl and distilled deionized water and then dried at 110 °C.

2) α-MnO_2, cryptomelane

A 4.752 g (0.0264 mol) sample of solid glucose was added to a stirred solution containing 12.64 g (0.08 mol) of KMnO4 dissolved in 800 mL of water The gel was allowed to settle and after 90 minutes was isolated by filtration and washed four times with 400 mL of water. A xerogel formed after drying at 110 °C overnight. Calcination of the xerogel at 450 °C for 2 h. The product was pulverized, washed three times with 10 ml of 0.1 M HCl and distilled deionized water and then dried at 110 °C.

3) MnO, manganosite

A 47.52 g (0.2625 mol) sample of solid glucose was added to a stirred solution containing 27.65 g (0.175 mol) of KMnO4 dissolved in 500 mL of water. The gel was allowed to settle and

after 60 minutes was isolated by filtration and washed four times with 250 mL of water. A xerogel formed after drying at 110 °C overnight. Calcination of the xerogel at 700 °C for 2 h. The product was pulverized, washed three times with 10 mL of 0.1 M HCl and distilled deionized water and then dried at 110 °C.

B. Characterization

The catalysts were characterized by X-ray powder Diffraction (XRD) using a XRD-700 MaximaX X-ray diffractometer with Cu Kα radiation (λ = 1.54060 A˚) at a tube voltage of 40 kV and a tube current of 30 mA. The morphology of the samples was obtained by Scanning Electron Microscopy (SEM) model EVO-50 (ZEIZZ). The Brunauer−Emmett−Teller (BET) surface area was measured at 77.3 K by nitrogen adsorption-desorption using a Quantachrome Gas Sorption Analyzer (GSA) after the sample was degassed in a vacuum at 300 ^{o}C for 3 h.

C. Methylene Blue Degradation

The catalytic reaction was carried out in a 250 mL glass beaker at room temperature, which contained 25 mL of MB dye solution (50 mg/L), 60 mL of distilled water, and 25 mg of catalysts. Before H_2O_2 addition, the suspension was vigorously stirred magnetically for 30 min for achieving adsorption/desorption equilibrium. After adding 15 mL of 30 wt% H_2O_2 solution, the mixture was allowed to react with continuous stirring. For a given time interval, 2,5 mL of mixture solution was pipetted into a volumetric flask, quickly diluted with distilled water to 25 ml and then cooled in ice bath. The diluted solution was immediately centrifuged in order to remove the catalyst particles. The centrifuge dye solution was put into a quartz cell and the absorbance was measured with Shimadzu UV mini 1240 UV–vis spectrophotometer. A linear calibration curve for the dye concentrations was obtained by monitoring the peak intensity at λ_{max}= 664 nm for a series of standard solutions according to the Beers law.This procedure were done using different Mn oxides (MnO, α-MnO_2, δ-MnO_2) and in triplicate. To maintain the same total volume as in the case of reaction solution, we added 75 mL of aquades in condition without addition of H_2O_2 (total volume 100 mL).

III. Results and Discussion

Table 1 Effects of reactant concentration on sol-gel reactions between kmno$_4$ and glucose

[$KMnO_4$] (M)	[Glucose] (M)	Molar ratio [$KMnO_4$: Glucose]	Condition	Calcined product
0.25	0.083	3:1	calcined product (450 °C, 2 h)	*K-Birnessite*
0.10	0.033	3:1	calcined product (450 °C, 2 h)	*Cryptomelane*
0.35	0.525	2:3	calcined product (700 °C, 2 h)	*Manganosite*
0.25	0.375	2:3	calcined product (700 °C, 2 h)	*Hollandite* + *Hausmanite*
0.10	0.150	2:3	calcined product (700 °C, 2 h)	*Hausmanite* + *Hollandite* + *Romanchite*
0.05	0.075	2:3	calcined product (700 °C, 2 h)	*Hausmanite* + *Hollandite* + *Romanchite*

The effect of various molar ratios of $KMnO_4$: glucose and calcination conditions on the crystal structures of manganese oxides is listed in the Table 1. The increased concentration of $KMnO_4$ leads to different crystal types of manganese oxides even with the same ratio of $KMnO_4$: glucose. The similar observation is also reported by Ching *et al*. [23] using the same $KMnO_4$ as oxidant, but different reductant (fumaric acid as reductant instead of glucose). For the molar ratio of $KMnO_4$: glucose is equal to 2:3, too dilute $KMnO_4$ concentration (0.05M) produces the mixture of hausmanite, cryptomelane, and romanchite with intense peak at$2\theta = 32.985°$ due to hausmanite, whereas the reflection peaks attributed to hausmanite and cryptomelane are weak. The more pure cryptomelane is formed at higher concentration of $KMnO_4$ (0.25 M) without the presence of romanchite phase. Further increase of $KMnO_4$ concentration (0.35 M) produces manganosite MnO. This latter observation has never been reported by previous studies.When the molar ratio of $KMnO_4$:glucose is adjusted to 3:1, the 0.25M $KMnO_4$ produces birnesite-type manganese oxide octahedral layer, while 0.1M $KMnO_4$ generates the cryptomelane-type manganese oxide octahedral molecular sieve. The different crystal phases (birnessite or cryptomelane) produced are correlated with the potassium content of manganese oxide gels. The similar results are also observed by Ching *et al.*[23] in which the high concentration of $KMnO_4$ generates octahedral layered birnessite, while lower concentration of $KMnO_4$ produces cryptomelane-type manganese oxide octahedral molecular sieve. Their hypothesis is supported by conducting various reaction conditions and workup procedures.This results are consistent with the fact that cryptomelane has far lower potassium content than birnessite [24].

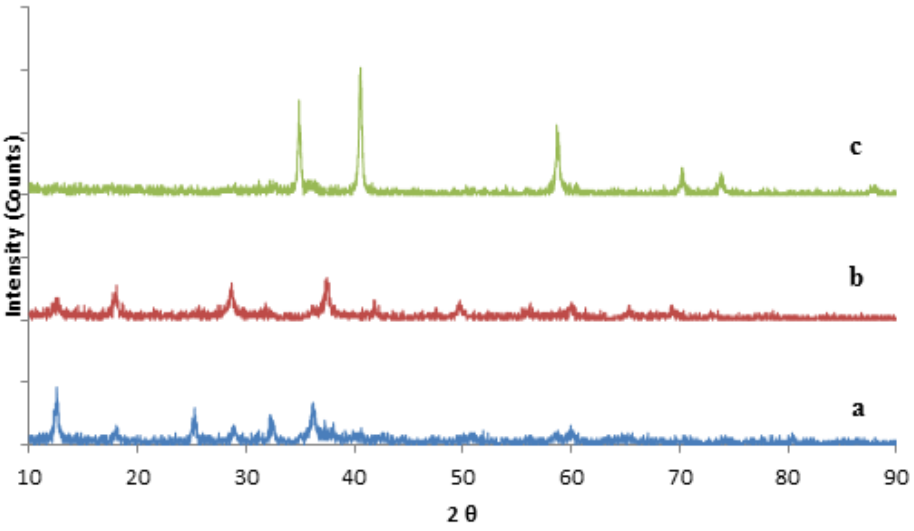

Figure 1. XRD patterns of (a) δ-MnO_2, (b) α-MnO_2, and (c) MnO obtained from the $KMnO_4$/glucose by sol-gel method

XRD was used to identify phases and crystallinity of the as-synthesized manganese oxide samples (Figure 1.). The XRD pattern obtained for as-synthesized manganese oxide compares well with MnO (JCPDS Card, No 07-0230) andshows a lattice spacing of 0.26 nm, corresponding to the (111) plane of MnO. X-ray patterns of δ-MnO_2 and α-MnO_2 confirm to the formation of the birnessite phase (JCPDS Card, No 80-1098) and cryptomelane phase (JCPDS Card, No 06-0547) respectively. Lattice spacing of 0.70 nm corresponds to the (001) plane of δ-MnO_2.

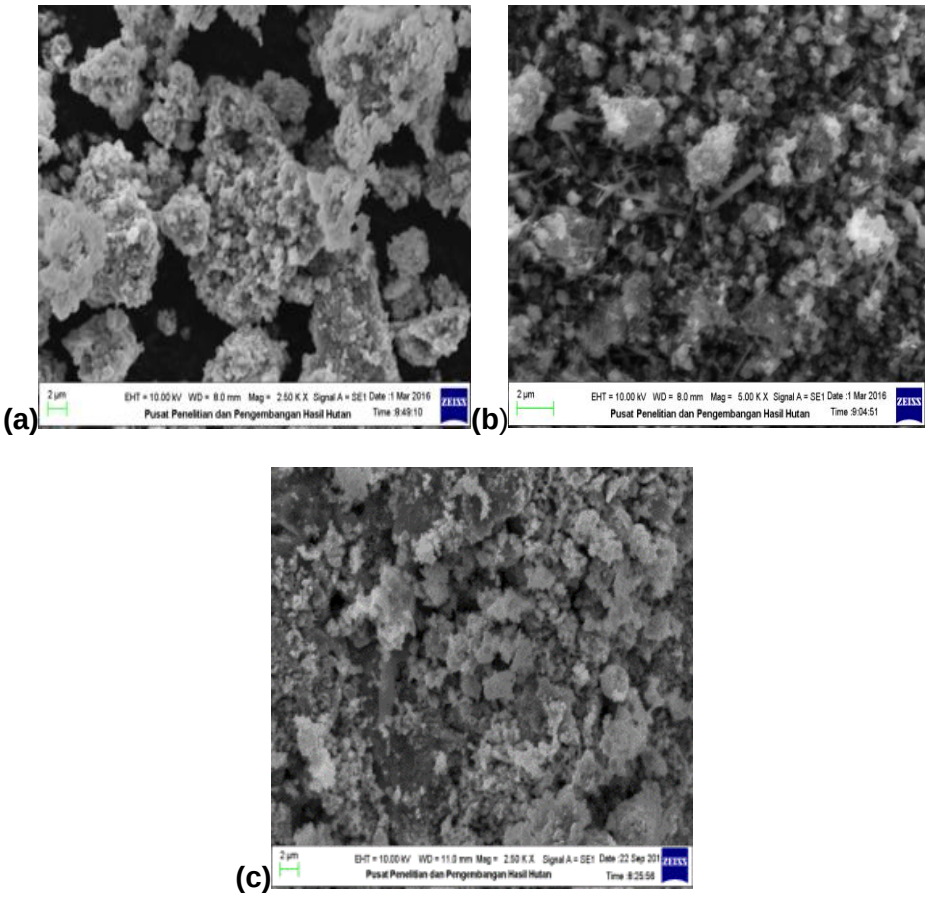

Figure 2. SEM images of (a) δ-MnO_2, (b) α-MnO_2, (c) MnO prepared by sol-gel method from the $KMnO_4$/glucose precursor.

Figure 2.shows that as-synthesized Mn oxides (δ-MnO_2, α-MnO_2, and MnO) obtained from different ratios of KMnO4/glucose have similar morphology. The SEM data reveal that Mn oxides consist of aggregates of particles. Brunauer−Emmett−Teller (BET) measurements were used to determine surface areas of the samples. The surface areas of the three catalysts, δ-MnO_2 ,α-MnO_2, and MnO are 8.892; 66.66; and 11.223 m^2/g, respectively (Table 2).

Table 2 surface areas of catalysts used in this study

Catalyst	Surface area (m^2/g)
δ-MnO_2	8.892
α-MnO_2	66.66
MnO	11.223

Experiments were performed to compare the dye degradation activity of different manganese oxide catalysts with and without H_2O_2. The results are presented in Figure . 3. In the absence of H_2O_2, the catalysts show the activity in less than 21% over 120 minute time of reaction. Among all of these catalysts, MnO showed the best catalytic effect followed by δ-MnO_2whereas α-MnO_2showed hardly any activity without H_2O_2. When H_2O_2 was present, MnO showed the highest activity, totally removed the dye from the solution 90% and δ-MnO_2catalysts are a little less active. MB concentration over a period of 120 min for δ-MnO_2,α-MnO_2,MnO were 72.43%; 35.92%; and 9.61% respectively.

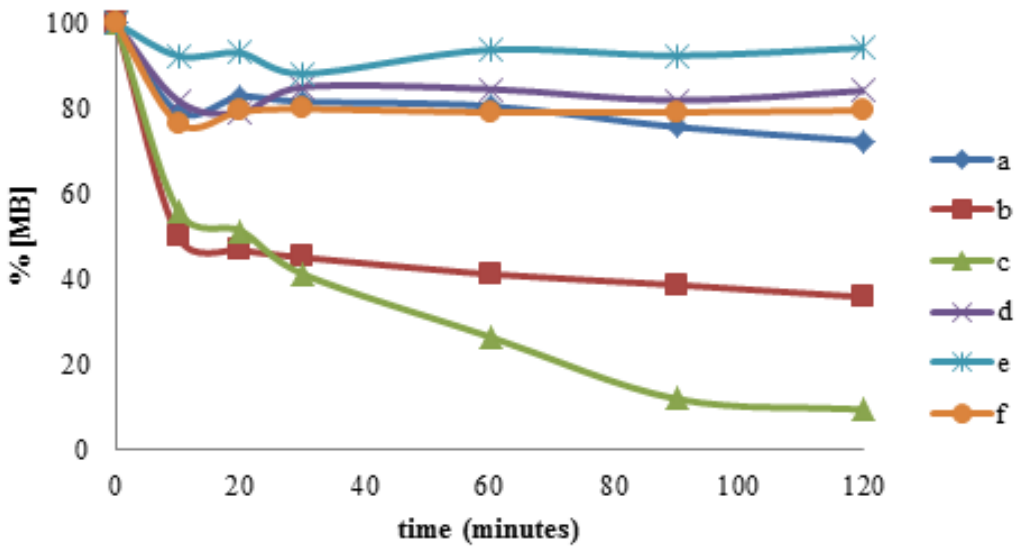

Figure 3.Degradation of MB with and without H_2O_2using different Mn oxides: (a) δ-MnO_2+ H_2O_2 (b) α-MnO_2+ H_2O_2 (c) MnO + H_2O_2 (d) δ-MnO_2 without H_2O_2 (e) α-MnO_2 without H_2O_2 (f) MnO without H_2O_2.

Catalytic behavior of Mn oxides materials shows variations in their dye degradation activities and the differences are probably due to variations in surface area. Surface areas of all of the materials range from ~8 to 66 m^2/g. In this study, the surface area of the catalyst follows the order of α-MnO_2 >MnO> δ-MnO_2, whereas the degree of decomposition in the presence of catalyst alone follows the order of MnO>δ-MnO_2> α-MnO_2 and the catalyst with H_2O_2 follows the order of MnO>δ-MnO_2> α-MnO_2. MnO with a smaller surface area than the other Mn oxide has shown better MB degradation in both cases. A higher surface area is not consistent with the higher activity of all of the catalysts used.

TABLE 3
The parameters of kinetic models and correlation coefficients (R^2) for the degradation of methylene blue

Catalyst	Zero-order kinetic model		First-order kinetic model		Second-order kinetic model		Chu kinetic model		
	k_0	R^2	k_1 (min^{-1})	R^2	k_2 (L mg^{-1} min^{-1})	R^2	a	p (min)	R^2
δ-MnO_2	0.0111	0.7595	0.0010	0.7646	0.0001	0.7691	3.4741	49.276	0.9572
α-MnO_2	0.0160	0.9649	0.0028	0.9793	0.0005	0.9894	1.5229	7.6814	0.9984
MnO	0.0592	0.9481	0.0173	0.9799	0.0063	0.9541	0.9496	19.743	0.9893

In the present study, zero, first, and second-order reaction kinetics were used to study the degradation kinetics of MB. The individual expression was presented as below:

Zero order reaction kinetics:

$$\frac{d[MB]}{dt} = k_0 \qquad \text{(a)}$$

First-order reaction kinetics:

$$\frac{d[MB]}{dt} = -k_1[MB] \qquad \text{(IV.}$$

Second-order reaction kinetics:

$$\frac{d[MB]}{dt} = -k_2[MB]^2 \qquad \text{(V.}$$

Where [MB] is the concentration of MB, k_0, k_1, and k_2 represent the apparent kinetic rate constants of zero, first, and second-order reaction kinetics, respectively, t is the reaction time.

By integrating the equation, (1), (2), and (3) equation (4), (5), and (6) could be obtained:

$$[MB]_t = [MB]_0 - k_0 t \qquad \text{(b)}$$

$$[MB]_t = [MB]_0 - e^{-k_1 t} \qquad \text{(c)}$$

$$\frac{1}{[MB]_t} = \frac{1}{[MB]_0} + k_2 t \qquad \text{(d)}$$

Where $[MB]_t$ is the concentration of MB at reaction time t (minute).

Regression analysis based on the zero-, first-, and second-order reaction kinetics for the degradation of MB in heterogeneous catalytic process was conducted and the result are presented in Table 3. Comparing the correlation coefficient (R^2), it can be seen that R^2 based on the second-order reaction kinetics was obviously much better than that based on the zero-order and the first order reaction kinetics. The results indicated that the degradation kinetics of MB by Mn oxides catalysts along with H_2O_2 followed the second-order kinetics (k_2) with respect to dye concentration.

Chu *et al*. [25] have derived a mathematical model to stimulate the reaction kinetics that shown in Eq. (7). This kinetic model is known as Chu kinetics model. Behnajady *et al*. also developed this mathematical model [26] and known as BMG kinetics model but with different notation (Eq. 8.)

$$\frac{C_t}{[C]_0} = 1 - \frac{t}{p + at} \qquad \text{(e)}$$

$$\frac{C_t}{[C]_0} = 1 - \frac{t}{m + bt} \qquad \text{(f)}$$

The linear forms of the Chu kinetics model (7) are given in Eq. (9).

$$\frac{t}{1 - \frac{C_t}{C_0}} = p + at \qquad \text{(g)}$$

By plotting Eq. (9), $t/[1-(C_t/C_0)]$ *vs* t , a straight line with an intercept of p and a slop of a was obtained. If the experimental data of degradation have the regression results with very high R^2 , the Chu kinetics model is followed. The constants of p and a can be determined by taking derivation of Eq. (7) to give:

$$\frac{d(C_t/C_0)}{d_t} = \frac{-p}{(p+at)^2} \qquad \text{(h)}$$

The physical meanings of the constants (p and a) were therefore inspected by examining two extreme cases. When t is very short or approaching zero, Eq. (11) can be written as follows:

$$\frac{d(C_t / C_0)}{d_t} = -\frac{1}{p} \qquad \text{(i)}$$

Its physical meaning is the initial of degradation rate in the process. Therefore the higher 1/*p* value indicates the faster initial degradation rate of the dye. When t is long and approaching infinity, the 1/*p* value indicates the theoretical maximum oxidation capacity of Fenton-Like process at the end of the reaction:

$$\frac{C_{t\to\infty}}{C_0} = 1 - \frac{1}{a} \qquad \text{(j)}$$

C_t = concentration at ttime (minute)
C_o = initial concentration (minute)
1/*p* = the reaction kinetics constants
1/*a* = the oxidation capacities constants

Based on the linearity coefficient (R^2) values seen in Table 3., the degradation of methylene blue using the three types of manganese oxides (δ-MnO_2, α-MnO_2, (c) MnO) as catalysts also confirm to follow the kinetics model proposed by *Chu et al.*[25]. Chu *et al.*revealed that in the process of degradation there are two stages of the reaction that occurred. The first stage takes place very quickly then followed by the next stage which runs very slowly [25]. This two-stage degradation process can not be modeled by a first or a second order reaction kinetics.Therefore, Chu *et al.*proposed a mathematical model to describe the reaction kinetics known as the Chu kinetics model. Chu *et al.* reported that the first stage is rapid process confirmed by a large number of radical production. The next stage is very slow showing that almost all hydrogen peroxide was reacted to form radicals [25].The same results are also shown in this study, in the first 10 minutes there was a sharp decrease in the concentration of methylene blue and in 30 minute until 120 minute there was only a slight decrease in the concentration of methylene blue. Rapid concentration decline in early minutes of degradation is also affected by a very short (nanosecond) 'lifetime' of hydroxyl radicals. Hydroxyl radicals can only react when formed so that rapid degradation occurs in the early minutes [27].

The Chu kinetics model is obtained from the degradation results using Fenton reagent which is a homogeneous catalyst. However, the Chu kinetics model can also be used in this study because the values of R^2 for the three manganese oxide catalyst are very good (between 0.9572-0.9984), which is better than R^2 obtained from the second reaction order (between 0.7691-0.9894). Similar results were also reported by Haji *et al.*[28] who studied FeY-zeolite/H_2O_2 (CWPO) to remove azo Reactive yellow P2RN/181 dyes. The R^2 value of the second order is between 0.847-0.960 and shows better results if modeled with kinetic model with R^2 between 0.979-0.999. The manganese oxide used in this study and Fe-Y-Zeolite by Haji *et al.*[28] is a heterogeneous catalyst. Thus, this Chu kinetic model can be applied for degradation with homogeneous and heterogeneous catalysts which show the similarity of the degradation mechanisms of these two systems.

VI. Conclusion

Manganese oxide prepared by sol-gel method via redox reaction between $KMnO_4$ and glucose with different molar ratio and concentrationshowed different structures. X-Ray Diffraction data showed that the structure ofMnO and δ-MnO_2 can be obtained at too and moderately concentrated reactant concentration ($KMnO_4$ and glucose), respectively, whereas

α-MnO_2 at diluted reactant concentration. The MnO structure prepared by a sol-gel technique has never been reported previously as a catalyst in methylene blue degradation and it revealed highly effective in heterogeneous activation of hydrogen for methylene blue degradation compared to the other two catalysts (α-MnO_2 and δ-MnO_2). The Chu kinetic model provided the best correlation of the used experimental data compared to the pseudo-first and second-order kinetic model.

References

[1] C. K. Remucal, & M. Ginder-vogel, "A critical review of the reactivity of manganese oxides with organic contaminants",*Environ. Sci. Process. Impacts,*vol. 16,pp. 1247–1266, 2014.

[2] A. Awaluddin, Prasetya, T. A. Amri, "Synthesize, characterization and aplication mangane oxide mesoporous', in *Proc. Seminar UKM-UNRI ke-4,* 2010.

[3] S. Zhao, T. Liu, D. Hou, W. Zeng, B. Mao, S. Hussain, X. Peng, & M.S. Javed,"Controlled synthesis of hierarchical birnessite-type MnO_2 nanoflowers for supercapacitor applications",*Appl. Surf. Sci.*, vol. 356,pp. 259–265, 2015.

[4] B. Yin, S. Zhang, Y. Ziao, Y. Liu, F. Qu, & X. Wu,"Facile synthesis of ultralong MnO_2 nanowires as high performance supercapacitor electrodes and photocatalysts with enhanced photocatalytic activities",*Cryst.Eng.Comm*,.vol. 16, pp. 9999-10005, 2014.

[5] X. Liu, C. Chen,Y. Zhao, B. Jia, "A review on the synthesis of manganese oxide nanomaterials and their applications on lithium-ion batteries",*J. Nanomater.,*vol. 2013,pp. 1–7, 2013.

[6]. C. Almquist, M. Krekeler, &L. Jiang, "An investigation on the structure and catalytic activity of cryptomelane-type manganese oxide materials prepared by different synthesis routes",*Chemical Engineering Journal,*vol. 252,pp. 249–262, 2014.

[7] W. Y. Hernandez, M. A, Centeno, S. Ivanova, P. Eloy, E. M. Gaigneaux, & J. A. Odriozola,"Cu-modified cryptomelane oxide as active catalyst for CO oxidation reactions",*Appl. Catal. B. Environ.,*vol. 123–124,pp. 27–35, 2012.

[8] J. Wang, P. Zhang, J. Li, C. Jiang, R. Yunus, & J. Kim, "Room-temperature oxidation of formaldehyde by layered manganese oxide: Effect of water",*Environ. Sci. Technol.*, vol. 49,pp. 12372–12379, 2015.

[9] Q. Ye, H. Lu, J. Zhao, S. Cheng, T. Kang, D. Wang, & H. Dai,"A comparative investigation on catalytic oxidation of CO, benzene, and toluene over birnessites derived from different routes",*Appl. Surf. Sci.*, vol. 317,pp, 892–901, 2014.

[10] Z. H. Liu, &K. Ooi, "Preparation and alkali-metal ion extraction/insertion reactions with nanofibrous manganese oxidehaving 2 x 4 tunnel structure",*Chem. Mater.*, vol. 15,pp. 3696–3703, 2003.

[11] L. Al-Amri, M. Al Subhi, &R. Namdeti, "Comparison studies for the removal of methylene blue from aqueous solution using tea and coffee powder",*Int. J. ChemTech Res.*, vol. 6,pp. 619–627, 2014.

[12] A. D. Bokare&W. Choi, "Review of iron-free Fenton-like systems for activating H_2O_2 in advanced oxidation processes",*J. Hazard. Mater.*, vol. 275,pp. 121–135, 2014.

[13] M. Zhu, D. Meng, C. Wang, , J. Di, &G. Diao, "Degradation of methylene blue with H_2O_2 over a cupric oxide nanosheet catalyst",*Chinese J. Catal.*, vol. 34,pp. 2125–2129, 2013.

[14] L. G. Covinich, D. I. Bengoechea, R. J. Fenoglio, &M. C. Area, "Advanced oxidation processes for wastewater treatment in the pulp and paper industry : A Review",Am. J. Environ. Eng., vol. 4,pp. 56–70, 2014.

[15] E. J. Kim, D. Oh, C. S.Lee, J. Gong, J. Kim, Y. S Chang, "Manganese oxide nanorods as a robust Fenton-like catalyst at neutral pH: Crystal phase-dependent behavior",*Catal.*

Today, vol. 282,pp. 71–76, 2016.

[16] Z. Ma, X. Wei, S. Xing&J. Li, "Hydrothermal synthesis and characterization of surface-modified δ-MnO_2 with high Fenton-like catalytic activity", *Catal. Commun. J.*, vol. 67,pp. 68–71, 2015.

[17] G. Cheng, L. Yu, T. Lin, R. Yang, M. Sun, B. Lan, L. Yang, & F. Deng,"A facile one-pot hydrothermal synthesis of β-MnO_2 nanopincers and their catalytic degradation of methylene blue", *J. Solid State Chem.*, vol. 217,pp. 57–63, 2014.

[18] H. J, Cui, H. Z. Huang, M. L. Fu, B. L. Yuan,&W. Pearl, "Facile synthesis and catalytic properties of single crystalline β-MnO_2 nanorods",*Catal. Commun.*, vol. 12,pp. 1339–1343, 2011.

[19] A. Awaluddin, M. Agustina, R. R. Aulia, & Muhdarina. "Precursor effects on the morphology and crystallinity of manganese oxides and their catalytic application for methylene blue degradation". in *International Conference on Chemistry, Chemical Process and Engineering (IC3PE)*,Yogyakarta, 2017.

[20] R. Kannan, A. Jegan, A. Ramasubbu, K. Karunakaran, &S. Vasanthkumar, "Synthesis and catalytic stuides of layered and oms type nano manganese oxide material",*Dig. J. Nanomater. Biostructures*, vol. 6,pp. 755–760, 2011.

[21] L. Zhang, Y. Nie, C. Hu, &X. Hu, "Decolorization of methylene blue in layered manganese oxide suspension with H_2O_2. *J. Hazard. Mater.*, vol. 190,pp. 780–785, 2011.

[22] G. Cao, L. Su, X. Zhang, &H. Li, "Hydrothermal synthesis and catalytic properties of α- and β-MnO_2 nanorods",*Mater. Res. Bull.,*vo. 45,pp. 425–428, 2010.

[23] S. Ching,J. L. Roark, N. Duan, &S. L. Suib, "Sol-gel route to the tunneled manganese oxide cryptomelane". *Chem. Mater.*, vol. 4756,pp. 750–754, 1997.

[24] P. Strobel, J. Vicat, &D. T. Qui, "Thermal and physical properties of hollandite-type $K_{1.3}Mn_8O_{16}$ and $(K,H_3O)_xMn_8O_{16}$,vo. 55, pp. 67–73, 1984.

[25] W. Chu, C. Y. Kwan, K. H. Chan, &C. Chong, "An unconventional approach to studying the reaction kinetics of the Fenton's oxidation of 2 ,4-dichlorophenoxyacetic acid",*Chemosph.,* vol. 57,pp. 1165–1171, 2004.

[26] M. A. Behnajady, N. Modirshahla, &F. Ghanbary, "A kinetic model for the decolorization of C. I. Acid Yellow 23 by Fenton process",*J. Hazard. Mater.*, vol. 148,pp. 98–102, 2007.

[27] C. Galindo, P. Jacques, &A. Kalt, "Photochemical and photocatalytic degradation of an indigoid dye : a case study of acid blue 74 (AB74)",*J. Photochem. Photobiol. A Chem.,*vol. 141,pp. 47–56, 2001.

[28]S. Haji, M. Khalaf, M. Shukrallah, J. Abdullah, &S. Ahmed, "A kinetic comparative study of azo dye decolorization by catalytic wet peroxide oxidation using Fe–Y zeolite/H_2O_2 and photooxidation using UV/H_2O_2",*Reac.Kinet.Mech.Cat.*, vol. 114,pp. 795–815, 2014.

Ripeness Classification of On Tree-Oil Palm Fresh Fruit Bunches Using Laser Based Imaging (#730)

Minarni Shiddiq[1,a], Zulkarnain[1,b], Alvika Juliardi Pratama[1,c]

[1]Department of Physics, Universitas Riau, Pekanbaru, Riau 28293 Indonesia
[a]minarni@ unri.ac.id, [b]zulkarnain22@ gmail.com, [c]alvikayuliardi1108@ gmail.com

***Abstract*—**Ripeness classification of oil palm Fresh Fruit Bunches before harvesting is very crucial factor for obtaining good quality FFBs. A laser based system operated by two diode lasers of 405 nm and 650 nm wavelengths, was used to analyze the relationship of gray values and their firmness levels. The samples are on tree-oil palm FFBs of 3 meter height. Three fruits from 3 parts of each FFB were illuminated by the laser beam and their images were recorded by the camera. The FFBs were then harvested. The fruits were detached for firmness measurement. ROI of 50 x 50 pixels was used to obtain gray value of each image. The 650 nm laser shows higher linear correlation ranges from R^2 = 0.52-0.87. Higher correlations are also obtained for fruits on middle parts. There is inconsistency of results using the 405 nm laser. This method is potential for classifying FFB ripeness stages.

Keywords—Laser based imaging, On tree, Oil palm fresh fruit bunches, Ripeness, Firmness

I. Introduction

Indonesia is one of the largest exporter countries for crude palm oils (CPO). However Indonesian oil palm industries face many problems such as low CPO qualities and plant diseases. Ripeness stages of oil palm fresh fruit bunches (FFBs) are the key factors to obtain good quality FFB and then good quality CPO. Good quality FFBs are ripe FFB which have maximum total product content (oil) [1]. Such FFBs depend strongly on harvesting, sorting, and grading processes which are mostly carried out traditionally and manually. There are a lot of efforts have been done to develop cost effective, reliable, and fast method of harvesting decision to obtain good quality oil palm fresh fruit bunch (FFB) before sending to oil palm mills.

Sorting and grading methods for oil palm FFBs have been developed more intensively compared to harvesting methods. Electronic, automatic, computerized, nondestructive methods are preferable due to their effectiveness. Traditional ripeness classification is based on color change and number of fruits loosed from the bunch. Ripeness of oil palm FFBs are usually classified into three main stages i.e. unripe, ripe, and overripe. Manual grading of FFBs at mill site is mostly done collectively. The traditional method needs experience graders. Computer vision is one of the nondestructive methods that have been used for sorting and grading machine of oil palm FFBs which uses a color camera and a computer accompanied by image processing software [2]. Many image processing techniques for computer vision are based on color model to classify the FFB ripeness stages i.e. using red,

green, blue (RGB) digital number [3], HSI (hue, saturation, and intensity) color model [4]. Other techniques were using MRI and bulk NMR [5], using four-band sensor system [6]. Destructive methods were also used to classify oil palm FFB ripeness based on physical, mechanical, and chemical properties of oil palm fruit i.e. fruit firmness and oil content [7] and flavonoid and anthocyanin content [8].

Ripeness detection and classification techniques for on- tree oil palm FFBs before harvesting are less explored compared to sorting and grading methods for postharvest FFBs. Standard procedures for harvesting FFBs on tree have been established and used by oil palm farmers or industry which are based on color change and number of fruit loosed from bunches. The traditional methods always need experience harvesters and have some flaws. Electronic, cost- effective and automatic system for ripeness detection are needed, especially for higher tree which only small parts of a FFB can be seen. Some efforts have been done to differentiate oil palm FFB ripeness stages, using three lamps with different wavelength range and a color camera based on RGB intensity [9] and using laser based computer vision with different laser wavelength [10]. Both experiments still used FFBs that have been harvested. Computer vision method using color based image processing algorithm has some drawbacks for on-tree (attached) fruits especially for remote or high trees and sunlight environment. This study is a preliminary study aimed to develop a laser induced fluorescence imaging (LIFI) system for ripeness detection of oil palm FFBs. This technique has worked for plant leaves and single type of fruits not bunched and complex fruits such oil palm FFBs [11] – [13].

The system built in this study is intended to be low cost, automatic, miniature, and easy to operate, for ripeness stage recognition of on tree oil palm FFBs, to make right decision for harvester before harvesting oil palm FFBs. Two diode lasers with 405 nm and 650 nm in wavelength are used to assess internal properties of oil palm fruits such as chlorophyll, antocyanin, and oil content. The system employ A USB- Board CMOS-monochrome camera with a camera lens and a color filter. Nowadays, small size- board CMOS or CCD cameras are available commercially which can be integrated to microcontrollers such as arduino and raspberry hence miniaturization is possible.

This system is situated in an acrylic box and mounted on a tripod for easy height and angle adjustments, then was brought to an oil palm plantation. Samples are on tree oil palm FFBs which are potential to be harvested by the plantation harvesters. Each of three fruits from three parts of a potential harvested FFB was illuminated by a focused laser beam consecutively for one second while its image was recorded by the camera. Then the FFBs were harvested and brought to laboratory for fruit firmness test. The recorded images were processed using the open source image processing software, ImageJ to extract mean gray values [14]. These gray values will represent the fluorescence intensities. Correlation between the intensities and fruit firmness levels were analyzed. Ratios of the fluorescence intensities for 405 nm and 650 nm were used to classify the ripeness stages of oil palm FFBs. There is a very significant correlation between fluorescence intensities and fruit firmness, especially for 650 nm laser. However the classification method and image processing algorithm need to be improved.

II. Literature Review

A. Optical Methods

Classification methods using interaction of light and fruit are being studied for fruit quality. The computer vision methods are able to assess the external properties of fruits such as shape, size, and color. Classification of fruit ripeness based on internal properties needs different approach. Light impinges on fruit surface can be reflected, absorbed, scattered, or transmitted which depend on internal properties of the fruits and light wavelength used. Internal properties of fruits are represented by textures and tastes, biochemical contents. Biochemical contents such as pigment, sugar, starch, water, and proteins are sensitive to light wavelengths [15]. The optical method used to assess the internal properties is known as spectroscopy. Nowadays, types of spectroscopy can be differentiated based on sensor or detector used. If charge coupled devices (CCD) and complementary metal oxide semiconductor (CMOS) detector are used, the systems are called imaging. Different wavelengths of electromagnetic waves have been used for this method, VIS, NIR, MID –IR, and UV. The imaging system can be divided further which depends on light interaction involved such as reflectance or fluorescence imaging, wavelength such as IR and VIS imaging, and number of filters used, hyperspectral or multispectral imaging. To build a relationship between physical and chemical properties of fruits and attributes chosen for qualities of agriculture products using electromagnetic waves need 3 important factors i.e. effective sensors, sophisticated mathematical models, and computer algorithm [16].

Applications of spectral imaging methods in agricultures have become widespread interests for researchers for some reasons. The intensive development of computer technology and software makes the applications more possible. The spectral imaging method combines digital imaging technique and spectroscopy hence more quality attributes can be defined based on physical and biochemical properties of fruits and vegetables and images. The availability of light sources such as LEDs and diode lasers with different wavelengths contributes to low cost applications. Many imaging techniques have been used for fruits [11] – [13]. [17]. Light based imaging techniques have also been used for oil palm fruits [18]–[19].

B. Remote Detection

The applications of optical methods have also been investigated for harvesting systems. These applications have become part of precision agriculture development. Precision agriculture uses recent technologies in computers and sensors, and interdisciplinary fields to solve many problems in traditional agricultures which facing growing world population and in needs of new food production technologies. Field of precision agriculture is aimed to reduce labor and operational cost by automation and real time measurements [20]. Precision Agriculture involves robotic harvesters, sensors for real time measurements of soil nutrients, local weather, early detections of plant diseases, yield estimations, and field management. These technologies are possible due to fast development on wireless communications and data mining.

Remote detection for on tree- fruits has become research interests because of its relation to robotic harvesters. Locating and identifying fruits are two important examples of tasks for harvesting fruits. Robotic harvesters are intended to harvest delicate fruits where tree shaker

machines are avoided. Methods such as computer vision, hyperspectral and fluorescence imaging, NIR spectroscopy, and LIDAR (light ranging) have been explored for harvesting technologies. Laser based imaging system provides more advantages compared to those using other light sources because of its long range, higher intensity, and good quality light beam. The systems with pulsed or modulated laser beam are better used to reduce surrounding light or sunlight effect. Laser based computer vision has been applied for fruit recognition which combine computer vision and laser range-finder to recognize fruits from shade on tree leaves [21]. A multispectral imaging system with Time of Flight (TOF) camera was also developed for harvesting robots which used white light and some color filters [22],

Fluorescence is one of processes that happen when light interacts with matter. Information about internal characteristics of the matter can be attained from the intensity and wavelength of the fluorescence image or signal. Laser and light emitting diode (LED) are often used as excitation light source to induce fluorescence processes. Diode lasers and monochromatic LEDs available commercially in optical power and wavelength which are compact, small, cost effective hence can be integrated for portable devises. Methods of using fluorescence processes induced by laser or LED light are called laser–induced fluorescence (LIF). If chlorophyll of plant leaves or fruits is induced, the methods are called laser–induced chlorophyll fluorescence (LCIF). While if the detector used is CCD or CMOS, the methods are called LIFI. The LIFI method is potential to assess fruit conditions [23]. LED is often used for short distance detection because of its beam characteristics, short range, divergence, and low optical intensities. Laser light has distinct characteristics over other light sources which are low divergence, high intensities, coherence, however it has imminent dangers for human eyes and skin. Commercial fluorometers and other distance fluorescence detection devices that have been developed are still in short range detection (less than 5 m) [24], [13]. Spectral imaging system for fluorescence process is needed for remote detection.

III. Material and Methodology

A. Materials

Samples of this study were on tree-oil palm fresh fruit bunches from Tenera variety which consist of two clones which grown in most Indonesian oils palm plantations, We called Tenera A (Topaz clone) and Tenera B (Marihat clone). Both have distinctions in bunch size, fruit size, and fruit density, number of fruits in a bunch. Tenera A FFBs have smaller bunch and lower fruit density than Tenera B. The on tree-oil palm FFBs were the potential FFBs to be harvested at an oil palm Laboratory plantation of Faculty of Agricultures, Universitas Riau, on the harvest day. The classification of ripeness stages of the FFBs after harvested were done traditionally based on color change and number of fruits loosed by an experience harvester. The ripeness stages of potential harvested FFBs (called fraction) on a tree can consist of F0 and F1 (unripe), F2 and F3 (ripe), and F4 (over ripe), each stage can have 2 or 3 replicates which depend on the harvest days. The heights of oil palm fresh fruit bunches observed were 3.0–3.2 m measured by a laser meter from ground to the middle part of bunches. Due to some circumstances in the plantations, FFB samples for Tenera A were taken twice at two different days, a month a part, while for Tenera B, were taken once. The laser beams from the LIFI system were aimed to three fruits consecutively for three parts of a FFB bunch (top, middle, and bottom) located between two fronds.

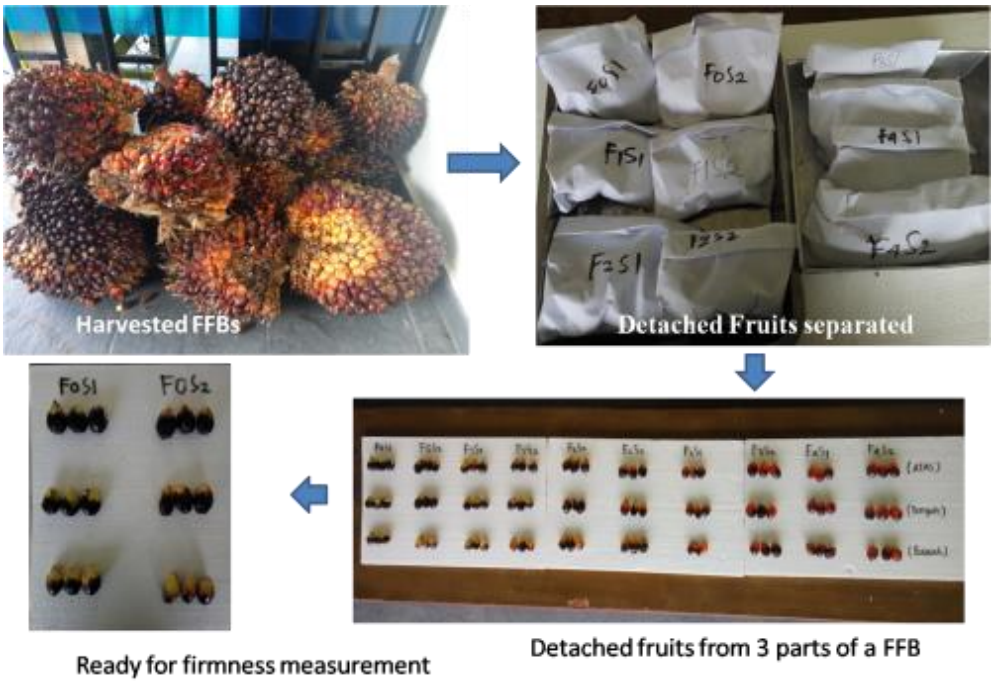

Figure.1. Harvested oil palm FFBs ready for firmness measurement.

After illuminated by laser beam, and images recorded, the FFB samples were harvested the next day by the plantation harvesters, brought to Lab, cleaned from dirt, weighted. Nine fruits from three parts of a bunch which were illuminated, were detached, collected, and labeled according of their ripeness stages as shown on Figure 1. Mass of each fruit was measured, followed by measuring their firmness levels by a manual penetrometer (Agricultuesolution). The penetrometer tip used was 8 mm tip intended for soft fruits (0.5 – 12 kg/cm^2) in kg force/cm^2 unit. Firmness level for each part of a bunch is represented by the average firmness levels of three fruits. The firmness level of a detached oil palm fruit is the average of firmness values of the fruit's two sides. Oil contents of oil palm fruits were also measured using Soxhlet method for comparison.

B. Methods

This study was aimed to use a laser based- fluorescence imaging method to investigate the relations between the fluorescence intensities of oil palm FFB to firmness levels of the FFB fruits which represents the ripeness levels of the FFB. Simple linear regression was used to classify FFB ripeness.

The fluorescence imaging system consists of two diode lasers with 405 and 650 nm of wavelength, respectively, a USB-board monochrome CMOS camera, two color filters. Both lasers and camera were positions in a triangulation scheme to the FBB. The system was enclosed in an acrylic box which can be mounted easily on a tripod. The system and tripod then was brought to the plantations, positioned in front of a 3 m - potential oil palm tree as shown in Figure 2. For each possible oil palm tree, the system and tripod was positioned about 2.5 meter in front of the tree, 1 meter from the ground. All candidate trees were chosen at about 3 m (2.5 m –3.5 m) of height. All the measurements were conducted using a digital laser level meter.

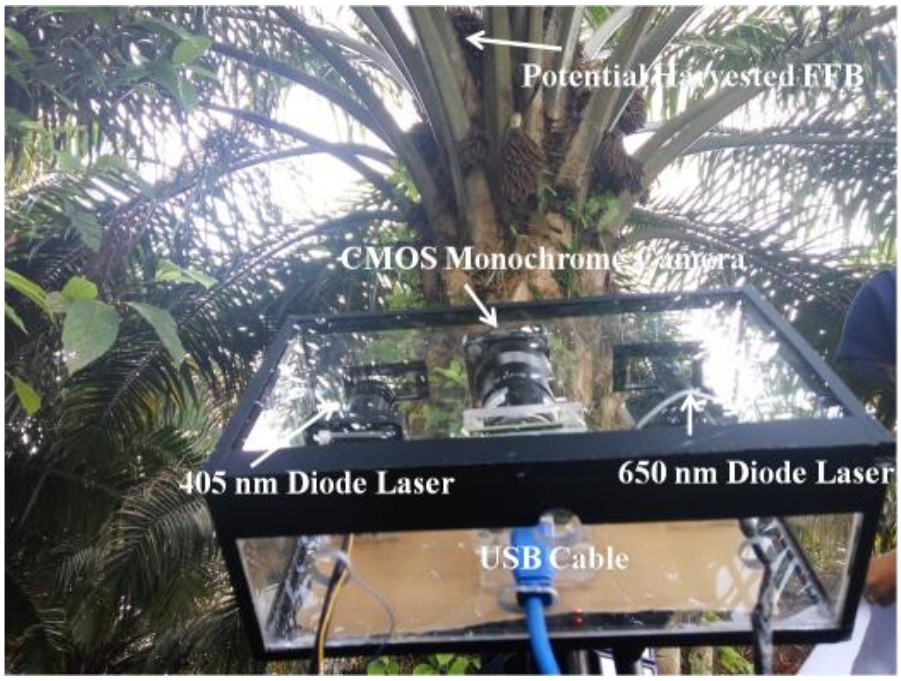

Figure 2. LIFI System on tripod 2 m from a 3 m oil palm tree.

The key components of the system are the camera, color filters, and diode lasers. The camera used was a small board CMOS camera (e-consystem camera) which has USB 3.0 data connection to a PC and accompanied by image software. The camera has board size of 40 mm × 44 mm, maximum 1280 × 720 resolution at 60 fps, and an external trigger input. Smaller camera size allows cost effective and smaller system, and can be integrated to a microcontroller for stand-alone, automatic operation. The sensor in this camera has 1/3 “form factor and global shutter. The camera also has a CS-mount lens holder where different focal length lenses can be chosen for certain purpose, here 75mm, F/2.5 MP Machine Vision Lens, 2/3" Format was used. Two exchangeable color filters with different bandwidth were applied in front of the camera. Both filters (Thorlabs) are two band- color filters, magenta (395 nm–440 nm, 645 nm–750 nm) for 650 nm laser and blue (390 nm–480 nm, 540 nm –750 nm) for 405 nm diode lasers. The filters were used to assess pigment and other chemical contents of the oil palm fruits especially chlorophyll, anthocyanin, oil, water contents [8], [13]–[14]. Both lasers used are Roithner diode lasers, violet diode laser with maximum optical power of 20 mW, red diode laser with power of 24 mW, both have TTL modulation capability.

Ripeness detection of oil palm FFB started after the LIFI system had been set up and the candidate oil palm trees were marked. Due to inflexibility of this system to electric sources, the measurements were held for oil palm trees close to electric sources hence the attached FFBS height varieties were limited hence we chose only 3 m height of FFB. Surrounding sunlight intensities were recorded every time an image was recorded. First, the 405 nm laser beam without an expander beam was aimed to one of fruits at the middle part of a harvested potential FFB (parts seen between two fronds), an image of a FFB part illuminated by a laser beam was recorded using the CMOS camera, saved in JPEG format. For each image taken, image of the spot without laser beam was also recorded. The procedure was repeated for other fruits in the middle part and further for fruits in other parts of a FFB. After all parts of potential FFBs were illuminated by 405 nm laser beam, the procedures were then repeated for 650 nm laser beam. These measurements were held in one day period. Traditional

classification of the FFBs was completed after harvesting them on the next day morning. Fruit firmness measurements then were continued after FFB harvesting.

C. Image Processing

After all the images of fluorescence imaging were recorded and saved, average gray values were calculated using the open source image processing software, ImageJ 1.47v [22]. The method used was using the same ROI of 50 pixel × 50 pixel for each image. Due to changes of sunlight intensity during measurement, Gray values were taken from reduced images (images with laser spot and without laser spot). The gray values represent the fluorescence intensities [13] of laser induced fluorescence imaging applied to oil palm FFBs. The relationships of the fluorescence intensities and fruit firmness for each part of an oil palm FFBs and performance using diode laser with different wavelength were analyzed. Classifications of ripeness stage using the 650 nm laser based on linear regression methods was used.

IV. Result and Discussion

This study is aimed to investigate the possibility of using a laser induced fluorescence imaging to classify the ripeness of oil palm fresh fruit bunches on tree before harvesting. Laser used were diode lasers with two different wavelengths. The images of fruits of FFBs illuminated by laser beam were recorded by a monochrome CMOS camera. After harvesting the ripeness of FFBs is classified first traditionally based on color change and number of fruits loosed on bunches. Then the ripeness stages are presented by fruit firmness level of oil palm fruits which measured by a penetrometer. The results are presented in graphs and figures.

Figure 3 shows some images taken by the LIFI system. The 650 nm laser beam illuminated a fruit in each part of a bunch, respectively. The images were recorded in JPEG format and processed using ImageJ software to extract gray values which represents the fluorescence intensities.

Figure 3. Images of fruit illuminated by 650 nm laser spot for three parts of an on-tree oil palm FFB

Figure 4 and 5 show the relationship between the fruit firmness and ripeness stages (fractions) which are categorized traditionally right after harvesting. The figures demonstrate that the fruit firmness decreases as the ripeness stages increases. There is a slightly difference of firmness between Tenera A and Tenera B FFBs where Tenera A fruits are harder and the decrease is sharper. There is also a slightly difference in firmness for each

part of a bunch, especially for unripe FFB (F0 and F1 fractions). The firmness values are the same for all parts for ripe (F3) and over ripe (F4) FFB. The fruit firmness is measured for fruits facing sunlight (fertile fruits), not the fruits which located between fronds (infertile fruits).

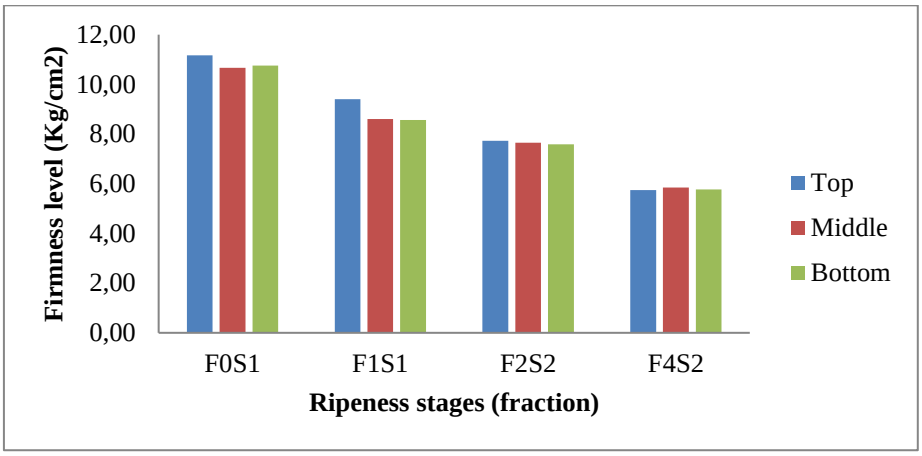

Figure 4. Relationship of fruit firmness values of each part of oil palm FBBs to ripeness stages (fractions) using based on color-traditional method (Tenera A).

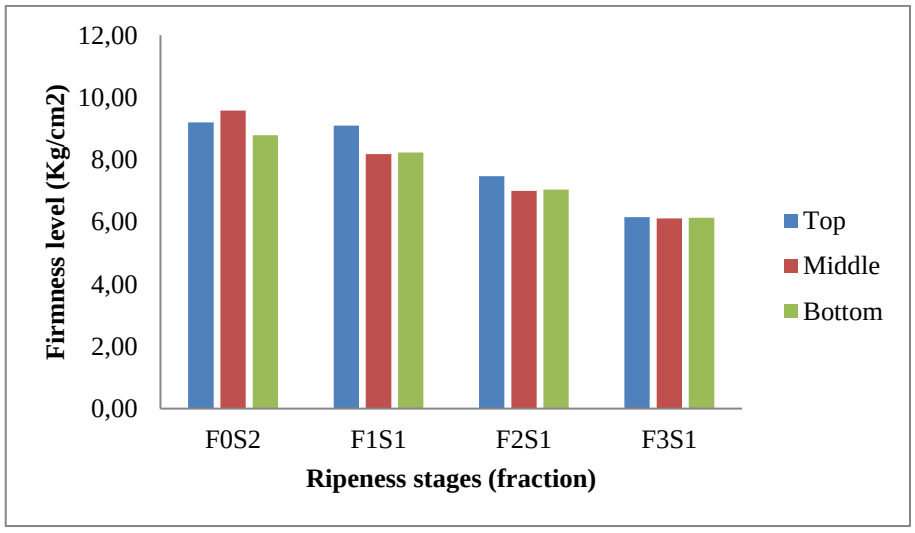

Figure 5. Relationship of fruit firmness values of each part of oil palm FBBs to ripeness stages (fractions) using based on color-traditional method (Tenera B).

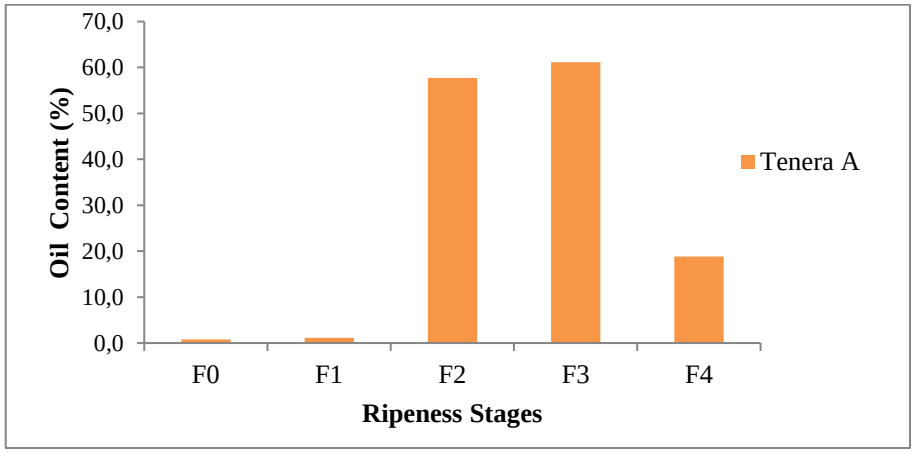

Figure 6. Oil content measured by Soxhlet methods for Tenera A

Figure 6 is the graph of oil content from oil palm fresh fruits measured by Soxhlet methods for Tenera A. It shows that the maximum oil content is for F3 fraction (ripe2), followed by F2 (ripe1). The oil content of F4 fraction FFBs decreases. The fruits for oil content measurement was taken from three parts (front) FFB. The graph also shows that unripe fractions have very low oil contents due to small size fruits which less fruit extract can be obtained.

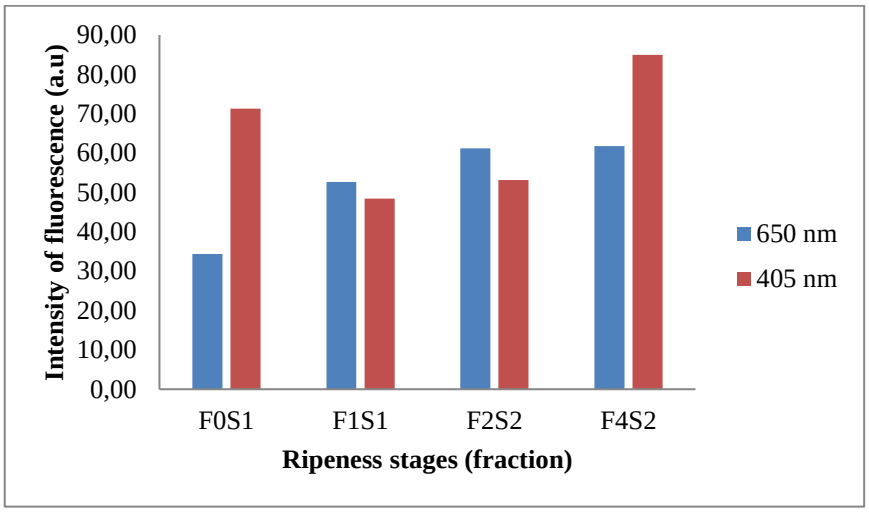

Figure 7. Fluorescence Intensities vs. fruit firmness values of Tenera A FFB using the 650 nm diode laser (Middle part), for 1st harvest day.

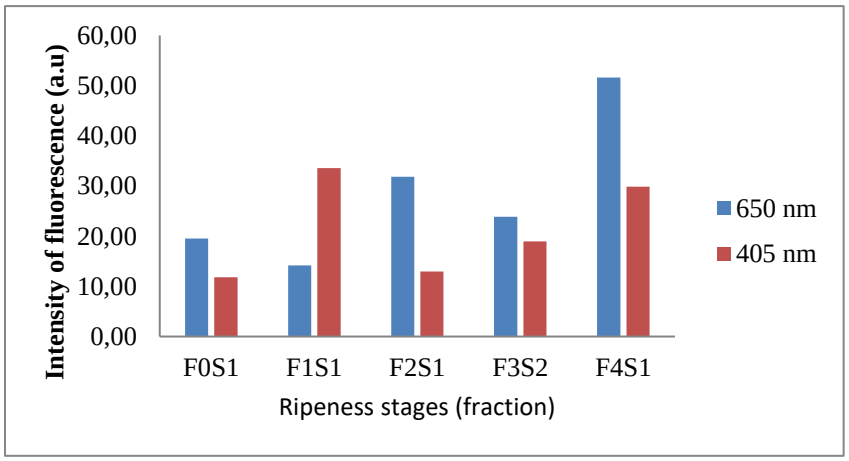

Figure 8. Fluorescence Intensities vs. fruit firmness values of Tenera A FFB using the 650 nm diode laser (Middle part), for 2nd harvest day.

Figure 7 and 8 are the graphs of fluorescence intensities versus the traditionally categorized ripeness of oil palm fruits detached after harvested, for 3 m tree height at different inducing laser beam. Laser with 650 nm shows more consistency that fluorescence intensity higher as the ripeness increases. This could relate to decreasing in chlorophyll and anthocyanin content, also increasing in oil content. Further investigation required. The other reason could be the quantum efficiency of the CMOS camera higher in red and NIR region.

Figure 9 an 10 show high correlation that the fluorescence intensity decreases as the firmness increases which related to increases in ripeness level. This correlation is higher for Tenera A.

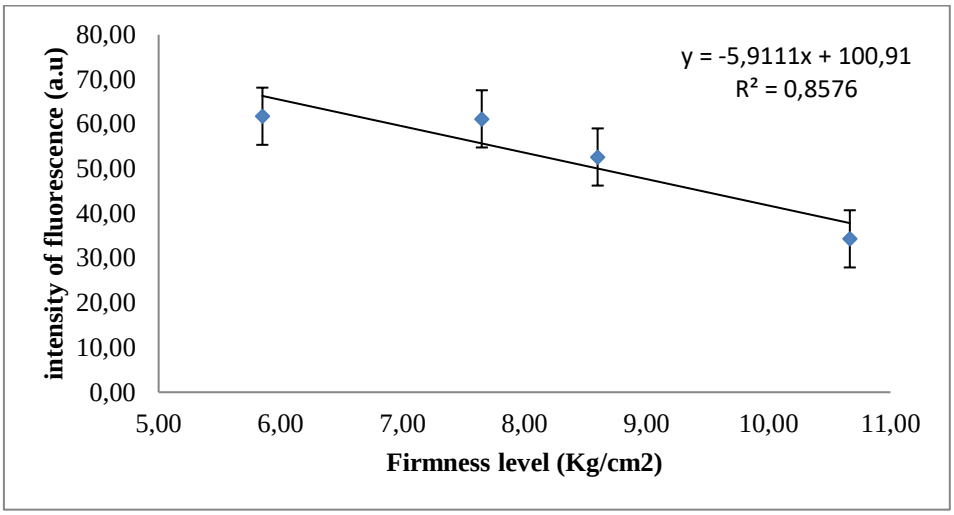

Figure 9. Fluorescence Intensities vs. fruit firmness values of Tenera A FFB using the 650 nm diode laser (Middle part), for 1st harvest.

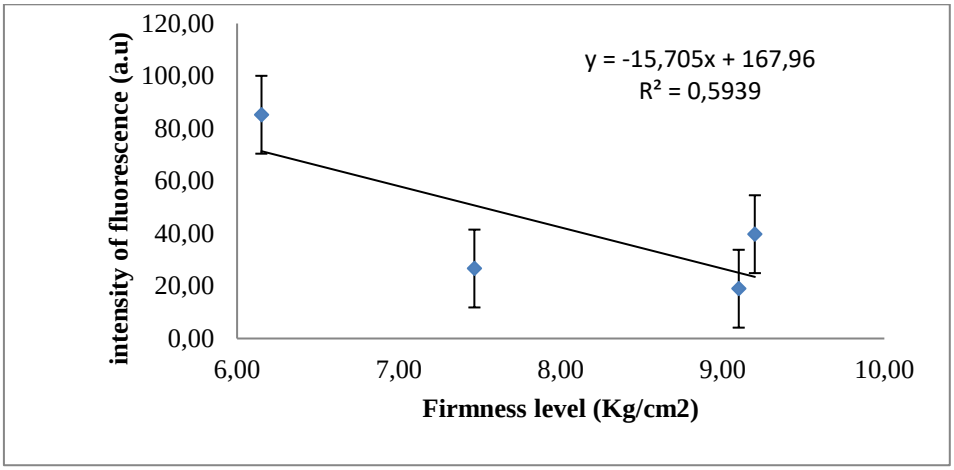

Figure 10. Fluorescence Intensities vs. fruit firmness values of Tenera B FFB using the 650 nm diode laser (Middle part) for 1st harvest

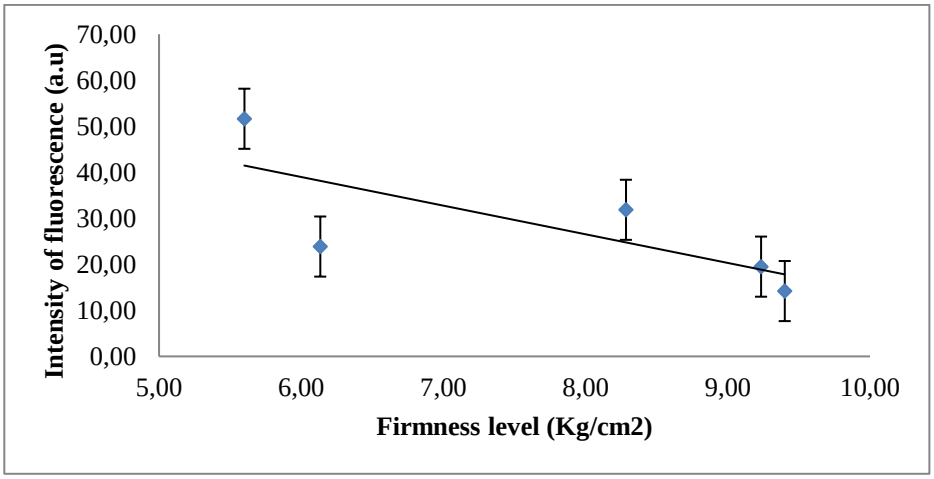

Figure 11 Fluorescence Intensities vs. fruit firmness values of Tenera A FFB using the 405 nm diode laser (bottom part) for 2nd harvest

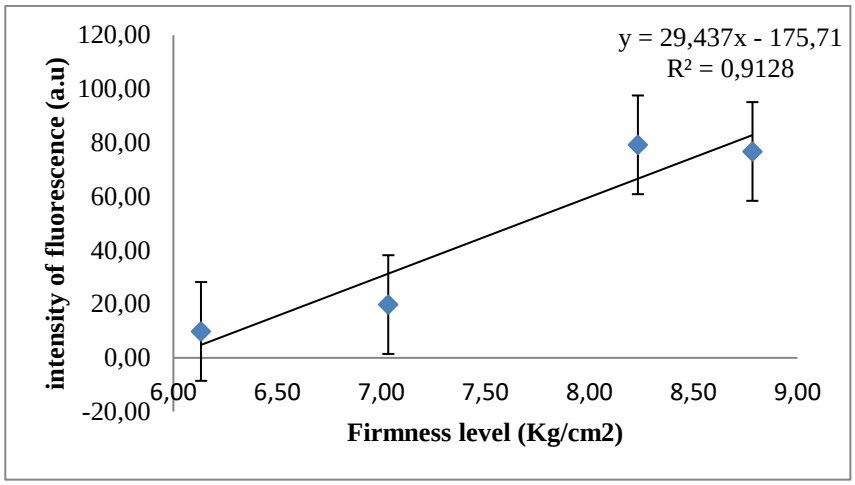

Figure 12 Fluorescence Intensities vs. fruit firmness values of Tenera B FFB using the 405 nm diode laser (bottom part) for 1nd harvest

Figure 11 and 12 are the graphs of fluorescence intensities versus fruit firmness for 405 nm of oil palm fruits detached after harvested, for 3 m tree height, different clones. Tenera B shows increases of intensities as firmness increases which relates to decreasing on chlorophyll content [13]. Reference [13] used acnic light (UV). The reason for Tenera A showing different trend could be due to smaller fruit size where chlorophyll content is small.

Figure 13 shows the relationship between ratio of intensities measured by 405 nm laser and 650 nm for middle part of a bunch. There is a relation between them, it show good correlation.

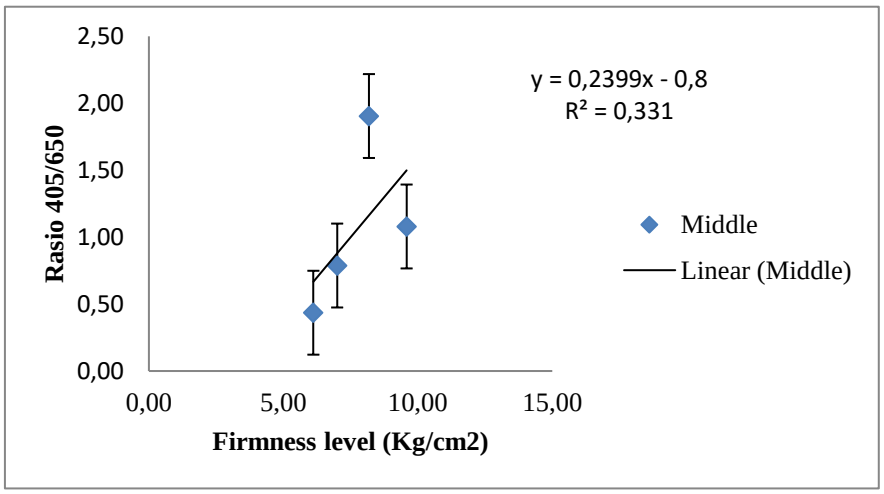

Figure 13. Ratio of fluorecence intensity measured using 405 nm laser and 650 nm laser for Tenera A, middle part.

V. Conclusions and Future Works

This study has successfully showed the possibility of using LIFI system for assessing oil palm FFBs on tree, hence is potential to be used in a portable, cost effective instrument for harvesting decision. There is obvious truth that the fruit firmness of oil palm fruits decreases as the ripeness stage increases, however a slightly difference is showed between the clones. This fact can be used to differentiate between clones for sorting and grading machine vision.

Diode laser beam of 650 nm wavelength give higher correlation between fluorescence intensities to fruit ripeness levels of oil palm FFBs which could be related to higher oil and water content, the fruits becomes softer as ripen. Diode laser of 405 nm could show higher correlation of fluorescence intensities to pigment contents, chlorophyll and anthocyanin if both pigment concentrations were measured.

This study will be continued for some research purposes. More on tree FFBs needed to obtain higher correlations between fluorescence intensities and firmness levels, and more rigorous image processing methods are needed. Effects of height varieties will be investigated since the portable instrument is intended for higher trees. The future work will be to obtain a low cost, portable, automatic, arduino or rasberry based device which can be used in field for oil palm farmer or harvesters.

Acknoledgments

This research was supported by Universitas Riau and funded by DRPM under the Ministry of Research, Technology, and Higher Education (Research GRANT 478 (2017). The authors would like to thank Faculty of Agriculture, Universitas Riau for providing the FFB samples.

References

[1] M. H. Razali, , A. Somad, M. A. Halim, S. Roslan, “A Review on Crop Plant Production and Ripeness Forecasting, ” International Journal of Agriculture and Crop Sciences, vol. 4, pp. 54-63, 2012

[2] J. A Kodagali and S. Balaji, “Computer Vision and Image Analysis based Techniques for Automatic Characterization of Fruits – a Review,” International Journal of Computer Applications (0975 – 8887), vol. 50, July 2012

[3] M. S. M. Alfatni, A.R.M. Shariff, H.Z.M. Shafri, O.M.B. Saaed, O.M. Eshanta, “ Oil palm fruit bunch grading system using red, green and blue digital number,” J. Appl. Sci. vol. 8, pp. 1444–1452, 2008

[4] M.K. Shabdin, A.R.M. Shariff, M. N. A. Johari, N. K. Saat, Z. Abbas, “A study on the oil palm fresh fruit bunch (FFB) ripeness detection by using Hue, Saturation and Intensity (HSI) approach,” IOP Conf. Series: Earth and Environmental Science, vol.37 (2016) 012039

[5] S.M. Shaarani, A. Cárdenas-Blanco, M.G. Amin, N.G. Soon, L.D. Hall, “Monitoring development and ripeness of oil palm fruit (Elaeis guneensis) by MRI and bulk NMR,” International Journal of Agriculture and Biology, vol. 12, pp. 101-105, 2010.

[6] O. M. B. Saeed, S. Sankaran, A.R.M. Shariff, H.Z.M. Shafri, R. Ehsani, M.S. Alfatni, M.H.M. Hazir, “Classification of oil palm fresh fruit bunches based on their maturity using portable four-band sensor system,” Computers and Electronics in Agriculture, vol. 82, pp. 55-60, 2012.

[7] A. Keshvadi, J.B. Endan, H. Harun, D. Ahmad, and F. Saleena, “The Relationship Between Palm Oil Index Development and Mechanical Properties in the Ripening Process of Tenera Variety Fresh Fruit Bunches,” Res. J. Appl. Sci. Eng. Technol., vol. 3, pp. 218-226, Jan. 2011

[8] M.H.M. Hazir, A.R.M. Shariff, M.D. Amiruddin, “Determination of oil palm fresh fruit bunch ripeness-Based on flavonoids and anthocyanin content,” Journal Industrial Crops and Products. vol. 36, pp. 466-475, 2012

[9] D. Cherie, S. Herodian, U. Ahmad, T. Mandang, M. Makky, “Optical Characteristics of Oil Palm Fresh Fruits Bunch (FFB) Under Three Spectrum Regions Influence for Harvest Decision,” International Journal on Advanced Science Engineering Information Technology, vol. 5, pp. 255-263 , 2015

[10] M. Shiddiq, Fitmawati, R. Anjasmara, N. Sari, and Hefniati,” Ripeness detection simulation of oil palm fruit bunches using laser-based imaging System ,” The 6th International Conference on Theoretical and Applied Physics (The 6th ICTAP) AIP Conf. Proc., vol.1801, pp. 050003-1–050003-7, 2017

[11] H.K. Noh, R. Lu,”Hyperspectral laser-induced fluorescence imaging for assessing apple fruit quality,” Postharvest Biology and technology, vol.43, pp.193-201, 2007

[12] L. Bodria, M. Fiala, R. Guidetti, R. Oberti, “Optical Techniques to Estimate The Ripeness of Red-Pigmented Fruits,” Journal American Society of Agricultural Engineers, vol. 47, pp. 815-820, ..2004.

[13] S. Lenk, L. Chaerle, E. E. Pfündel, G. Langsdorf, D. Hagenbeek, H. K. Lichtenthaler, D. Van Der Straeten, and C. Buschmann,” Multispectral fluorescence and reflectance imaging at the leaf level and its possible applications,” Journal of Experimental Botany, vol. 58, pp. 807–814, 2007

[14] A.C.L. Lino, J. Sanches, and I.M.D. Fabbro, “Image processing techniques for lemons and tomatoes classification,” Bragantia, Campinas. vol. 67, pp.785-789,2008

[15] J.A. Abbot, “Quality measurement of fruits and vegetables,” Postharvest Biology and Technology Journal, vol. 15, pp. 207-225, 1998.

[16] M. Ruiz Altisent, L. Ruiz-Garcia, G. P.Moreda, R. Lu, N. Hernandez-Sanchez, E.C. Correa, B. Diezma, B. Nicola, J. Garca-Ramos, “Sensors for product characterization and quality of specialty crops—A review,” Computers and Electronics in Agriculture, 2010.

[17] G. A. L.Valenzuela, “Assessment of External and Internal Quality of Blueberries Using Images”. Ph.D thesis, Office Of Research And Graduate Studies, Pontificia Universidad Catolica de Chile Escuela de Ingenieria. Santiago, Chile, 2013.

[18] O. M. Bensaeed, A.M. Shariff, A. B. Mahmud, H. Shafri, M. Alfatni, “ Oil palm fruit grading using a hyperspectral device and machine learning algoritm,” in IOP Conf. Series: Earth and Environment Science, vol.20, 2014, 012017.

[19] M.S.M Kassim, W. I.W. Ismail, L.H. Teik, “Oil Palm Fruit Classifications by using Near Infrared Images,” Research Journal of Applied Sciences, Engineering and Technology, vol, 7, pp. 2200-2207, 2014.

[20] A. Zujevs, V. Osadcuks, P. Ahrendt, “Trends in Robotic Sensor Technologies for Fruit Harvesting: 2010-2015”, Procedia Computer Science vol. 77, pp. 227 – 233, 2015

[21] A. Jiménez, R. Ceres, J. A Pons, “ Vision system based on a laser range-finder applied to robotic fruit harvesting,” Mach. Vis. Appl., vol.11, pp. 321–329, 2000.

[22] R. Fernández, C. Salinas, H. Montes, and J. Sarria, “Multisensory System for Fruit Harvesting Robots,” Sensors, vol. 14, pp. 23885-23904, 2014.

[23] H. Abbasi., M. Nazeri, A. Balooch, S. A. Mireei, “LIF Spectroscopy of Fruits: Study of Excitation Wavelength Independence,” The third Iranian Conference on Engineering Electromagnetic (ICEEM 2014), Dec. 3-4, 2014

[24] R. Van Beers, L. L. Gutiérrez, A. Schenk, B. Nicolaï, E. Kayacan, W Saeys, “ Optical measurement techniques for the ripeness determination of Braeburn apples, “Proceedings International Conference of Agricultural Engineering, 06-10.07.2014.

[25] G. A. Leiva-Valenzuela GA, R. Lu, and J.M. Aguilera,"Prediction of firmness and soluble solids content of blueberries using hyperspectral reflectance imaging. Journal of Food Engineering," vol. 115, pp.91-98, 2013

Using GNU Octave and Modification of Prim's Algorithm to Solve the Multi Periods Degree Constrained Minimum Spanning Tree (#734)

Wamiliana[1,a], Warsono[1], Mas Dafri Maulana[1]

[1] Department of Mathematics, Universitas Lampung, Bandar Lampung, Indonesia
[a]wamiliana.1963@fmipa.unila.ac.id

Abstract. *The Minimum Spanning Tree (MST) is a wellknown problem and used as the backbone problem in many network design problem. Given a graph G(V,E), where V is the set of vertices and E is the set of edges connecting vertices in V, and for every edge e_{ij} there is an associated weight c_{ij} ≥0, The Multi Period Degree Constrained Minimum Spanning Tree (MPDCMST) is a problem of finding an MST while also considering the degree constrained on every vertex, and satisfying vertices installation on every period. We developed two algorithms for solving this problem (MPDCMST_early and MPDSMST_later) and used GNU OCTAVE for coding and visualization. We implement those algorithms using 300 generated random problems. Moreover, we compare our algorithms using those that already in the literature and show that our proposed algorithms are competitive.*

Keywords: *multi periods, degree constrained, Prims' algorithms, GNU OCTAVE*

I. Introduction

Most in network design problems, The Minimum Spanning Tree (MST) is usually used as the backbone. If we add degree restriction on its vertices (can represent cities, stations, etc) of the graph (represents the network), the problem becomes the Degree Constrained Minimum Spanning Tree (DCMST) problem. Moreover, if we restrict and devide the stages or periods of the network's instalation, the problem emerges as The Multi Period Degree Constrained Minimum Spanning Tree (MPDCMST) problem. The later constraint occurs usually because of the fund limitation for installing (connecting) the network. This problem arises when we want to design a network which requires that every vertex (node) restricts the number of connections/interfaces whilst also must to consider a set of vertices that have to be connected/ installed in a certain period due to the fund restriction, weather, etc.

In this paper we organize the discussion as follows: In Section 2 we give the history of the problem; In Section 3 we discuss how to apply the algorithms developed using GNU Octave and implement them; in Section 4 we discuss the results, followed by conclusion.

II. The Constrained Minimum Spanning Tree Problem

Because of its specific structure and used in many network design problems, the Minimum spanning tree problem have been studied extensively and a variety of fast algorithms have been developed. An efficient and fast minimum spanning tree algorithm that requires computational time nearly linear in the number of edges had been developed [1]. The MST problem is one of the classical problems where the objective is to construct a minimum cost/weight network. This problem usually arises in many network design applications that must satisfy other graph parameters such as: degree, distance, diameter, connectivity, flow, etc. For instance, in a transportation network a distance restriction on the flow commodities could represent the maximum distance allowed for delivery.

The Degree Constrained Minimum Spanning Tree (DCMST) problem is a Minimum Spanning Tree with degree restriction on every vertex. This problem arises on designing

network where the degree restriction represents the number of allowable links on that vertex, i.e. the handling capacity of each of the vertices imposes a restriction on the number of edges (or wires/roads) that can be connected to a vertex. For example, the application of The DCMST is in designing the road system, where the set of roads must connect a collection of suburbs/towns, but there is a restriction that no more than certain number of roads (example: four roads) are allowed to meet at an intersection.

There are lots of investigations regarding the DCMST problem. Because of its NP-Completeness [2], heuristic methods have been dominated such as: greedy algorithm based on Prim's and Kruskal's algorithm [3], Genetic Algorithm [4], Iterative Refinement [5], Simulated Annealing [6], Modified Penalty [7], and Tabu Search [8-10].

In real situation, to connect all components in a network need certain time and process in order to be completed. The time of completion can vary depends on the need and priority of the network itself. The Multi Period Degree Constrained Minimum Spanning Tree (MPDCMST) problem was introduced and the proposed method to solved it by using branch exchange and Lagrangean relaxation [11] with asumption 10 years planning horizon. WADR1 and WADR2 algorithms developed by doing some modifications in Kruskal's algorithm [12], WADR3 and WADR4 are the algorithms developed as varians of WADR1 and WADR2 [13-14]. Motivated by the connectivity property on the process of finding MST by Prim's algorithm, the WADR5 was developed [14]. WADR3 and WADR4 are similar algorithms developed by modifying WADR1 and WADR2. The information and illustration why the solutions of WADR3 and WADR4 are different are given in [15].

III. GNU Octave, MPDCMST and Implementation

GNU Octave is a free software that runs on GNU/Linux, macOS, BSD, and windows. This software originally was intended as acompanion to a chemical reactor design course, but the one who first developed it is John W. Eaton [17]. Since this is free software, the users are encouraged to modified and developed this software and free to distribute it.

The different of using GNU Octave and other language programming (such as Java) is in GNU Octave more rigid, we have to follow certain rules (such as we have to convert to matrix form or others), not as Java where we are more flexible to developed the program. For example, the data used for implementation represent the edges of complete graph for certain vertex order. For vertex order 10, the number of edges is 45, which is got from the formula n(E) = $\frac{n(n-1)}{2}$, n =10. Before putting in GNU Octave, we have to modify this equation to be $2n(E)) = n^2 - n$. This is quadratic equation and to find n is $n = \frac{1+\sqrt{1+8n(E)}}{2}$. Thus, to read the data, the source code for reading the data (vertex order) is as following (let n(E) = Un) :

```
function vertex = check_vertex(matrix)
  bykisi=length(matrix);%bykisi=Un
  c=2*bykisi;
  n=(1+sqrt(1+(4*c)))/2;
  vertex=n;
end
```

WWM1 AND WWM2 ALGORITHMS

We develop two algorithms to solve the MPDCMST based on Prim's Algorithms and modified it to satisfy the constrained given and implement them using the same data used in [12 -14], the HVT_i, number of periods, and $MAXVT_i$ is the same as [15]. The reason of using Prim's algorithm because Prim's algorithm maintain the connectivity during the process of finding the MST. Both WWM1 and WWM2 use vertex 1 as central vertex.

WWM1 Algorithm

WWM1 algorithms starts by setting vertex 1 as root and then check the nearest vertices in HVT_i to be connected/installed in the network (T), and continue connecting those vertices in HVT_i as long is not violate the degree restriction. If there degree violation occurs,

do edge exchange while also maintaning the connectivity of vertices in HVT_i . Next, check the $MAXVT_i$. Connect the edges whose smallest edge weight to T as long as the connection not violate the degree constrained. If the number of vertices connected on that period already the same as $MAXVT_i$, then continue to the next period, and continue the process as the previous period until all vertices are connected/installed. The following figures illustrate the process in every period:

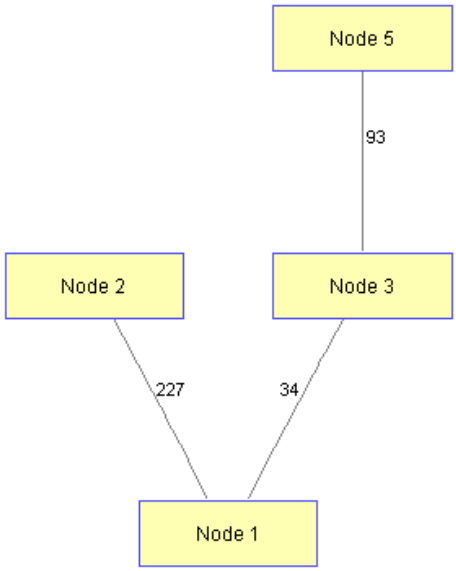

Figure-1. The first period of WWM1 algorithm

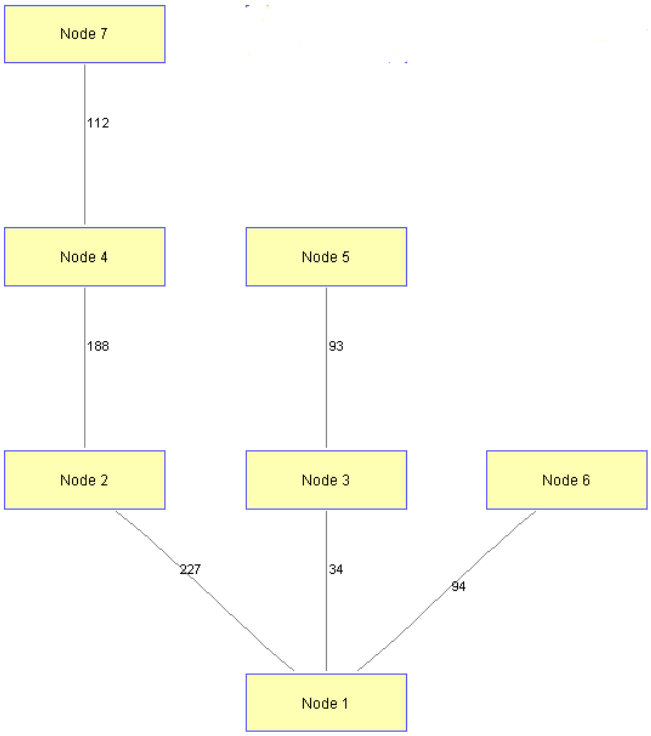

Figure-2. The second period of WWM1 algorithm

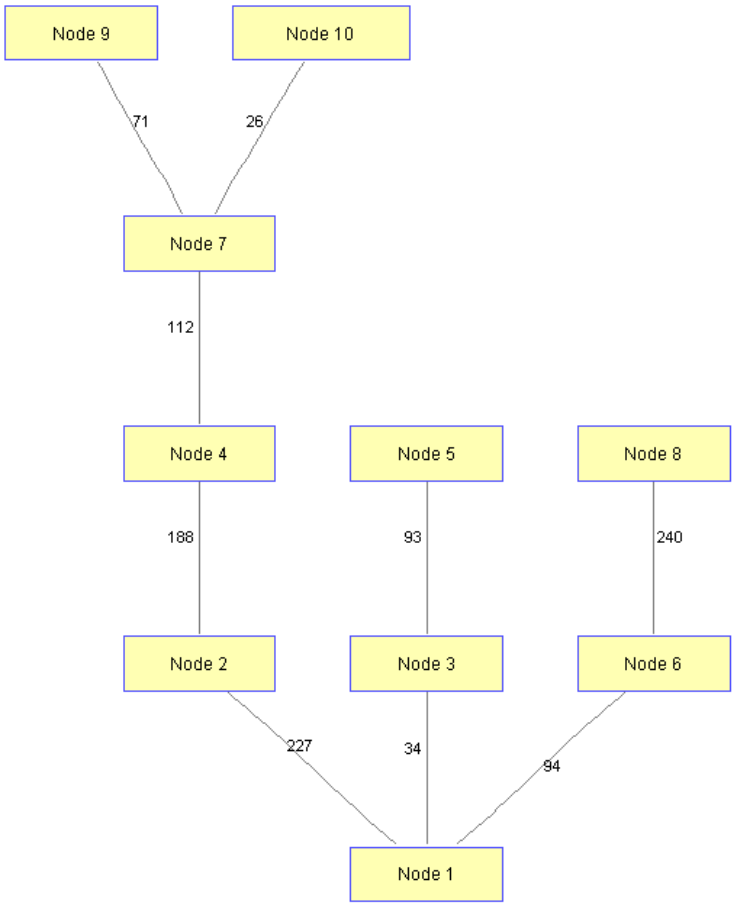

Figure-3. The third period of WWM1 algorithm

WWM2 Algorithm

The WWM2 algorithm is similar with WWM1 algorith, except in the WWM2 the process of connecting the vertices in HVT_i is more flexible. Those vertices in HVT_i can be installed in the beginning of the period or at the end, as long as the installation/connection process still at that period. The following figures show the process of installation in every period of WWM2 algorithm.

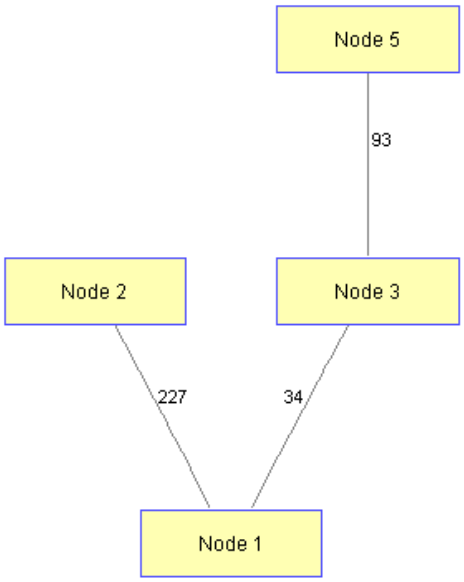

Figure-4. The first period of WWM2 algorithm

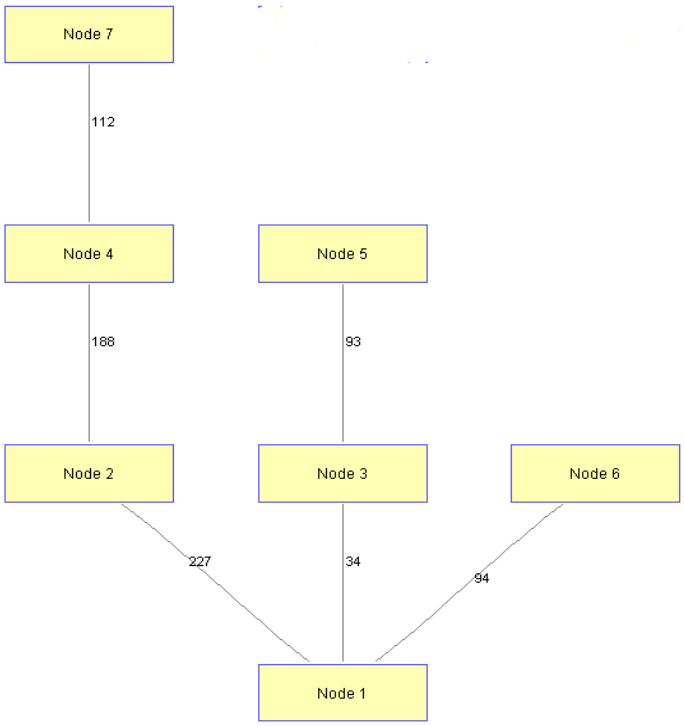

Figure-5. The second period of WWM2 algorithm

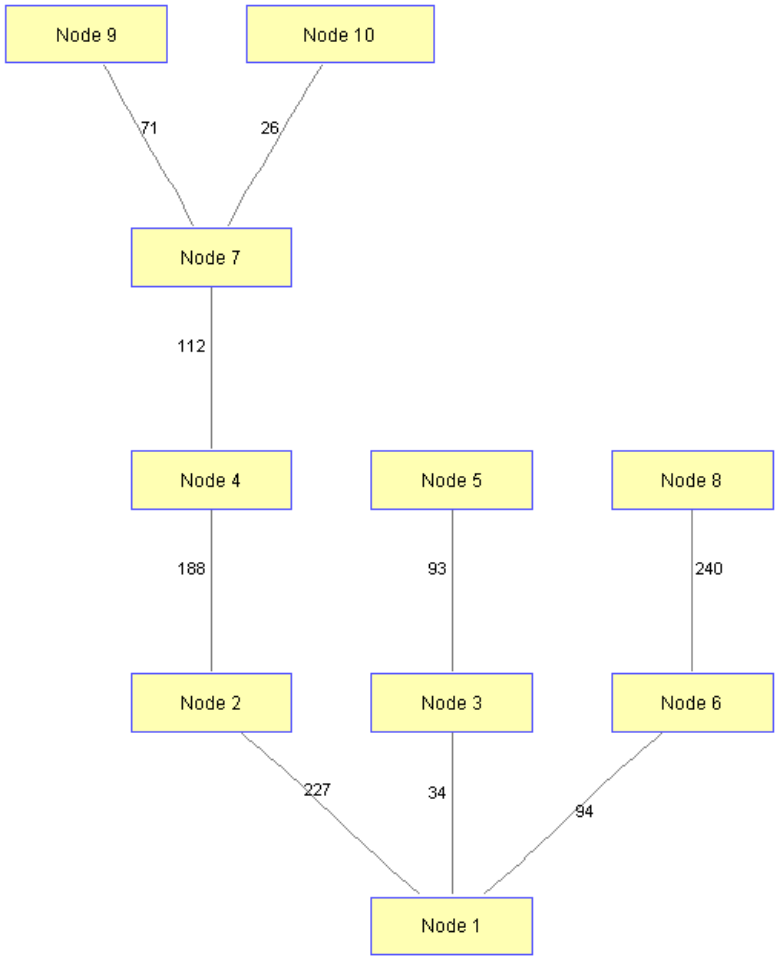

Figure-6. The third period of WWM2 algorithm

IV. Results and Discussions

We compare WW1 and WW2 algorithms agains WADR5 algorithm because those three algorithms are developed based on the same algorithms which is Prim's algorithms. Moreover, we use the same data for implementation, same set of HVT_i, , $MAXVT_i$ and the number of periods. The data used for implementation is the random problems generated using uniformly distribution with weight range from 1 – 1000 (integer). For every vertex order there are 30 problems generated and the vertex order used are 10 to 100 with increment 0f 10. Therefore there are total 300 problems implemented. The solution taken is the average solution from 30 problems for every vertex order. The following table show the result:

Table-1. The comparative solutions of the methods

Vertex order	The average solution				
	MST	DCMST	WADR5	WWM1	WWM2
10	1129,43	1178,8	1341,933	1498,6	1286,6
20	1196,1	1299	1557,63	1804,97	1428,57
30	1177,43	1319,53	1755,4	2039,97	1490,03
40	1151,23	1286,3	1719,27	2117,1	1440,03
50	1223,43	1356,47	1844,1	2427,27	1566,6
60	1175,57	1320,73	1851,2	2389,87	1573,57
70	1242,1	1410,03	1963,83	2558,5	1612,27
80	1236,83	1410,23	1942,4	2579,4	1675,2
90	1248	1404,93	1941,3	2618,43	1613,23
100	1234,1	1370,8	1992,4	2564,07	1567,53

V. Conclusions

From the result and discussion we can see that among the three algorithms, WWM2 performs the best. The flexibility in the process of connecting/installing the vertices but not violate the rules gives better solution than if the vertices must be connected in a certain order.

Acknowledgment

This research work was supported by Research Grant No: 582/ UN26.21/KU/2017. The authors would also like to acknowledge the contributions and financial support from the Directorate General of Higher Education, The Ministry of Research, Technology and Higher Education, The Republic of Indonesia.

References

[1] Gabow H.N and R.E. Tarjan, "Efficient algorithms for a family of matroid intersection problems", *Journal of Algorithms*, vol 5, pp.80-131, 1984.

[2] Garey, M.R.,and Johnson, D.S., *Computers and Intractibility, A Guide to the Theory of NP-Completeness.* Freemann, San Francisco; 1979.

[3] Narula,S.C., and Cesar A.Ho, "Degree-Constrained Minimum Spanning Tree", *Computer and Operation Research*. Vol. 7; pp. 239-249, 1980.

[4] Krishnamoorthy,M.,A.T. Ernst and Yazid M Sharaila, "Comparison of Algorithms for the Degree Constrained Minimum Spanning Tree", *Journal of Heuristics*, Vol. 7(6): pp. 587-611, 2001.

[5] Deo N. and Nishit Kumar, *Computation of Constrained Spanning Trees: A Unified Approach. Network Optimization* (Lecture Notes in Economics and Mathematical Systems, Editor : Panos M. Pardalos, et al. ,Springer-Verlag, Berlin, Germany, pp. 194 – 220., 1997.

[6] Zhou, G. and Mitsuo Gen,"A Note on Genetics Algorithms for Degree- Constrained Spanning Tree Problems", *Networks*, Vol. 30: p.91 – 95, 1997.

[7] Wamiliana, " Solving the Degree Constrained Minimum Spanning Tree Using Tabu and Penalty Method", *Jurnal Teknik Industri*: p.1-9, 2004.

[8] Caccetta L. and Wamiliana, Heuristics Algorithms for the Degree Constrained Minimum Spanning Tree Problems, Proceeding of the International Congress on Modelling and Simulation (MODSIM),Canberra, Editors: F. Ghassemi et.al; p. 2161-2166, 2001.

[9] Wamiliana and Caccetta, Tabu search Based Heuristics for the Degree Constrained Minimum Spanning Tree Problem, Proceeding of South East Asia Mathematical Society, p. 133-140, 2003.

[10] Wamiliana and L. Caccetta, The Modified CW1 Algorithm for The Degree Restricted Minimum Spanning Tree Problem, Proceeding of International Conference on Engineering and Technology Development, Bandarlampung 20-21 June. 2012; p. 36-39.

[11] Kawatra R. "A multi period degree constrained Minimum Spanning Tree Problem", *European Journal of Operational Research*, Vol **143**, pp. 53 – 63 , 2002.

[12] Wamiliana, Dwi Sakethi, and Restu Yuniarti, Computational Aspect of WADR1 and WADR2 Algorithms for The Multi Period Degree Constrained Minimum Spanning Tree Problem, Proceeding SNMAP, Bandar lampung 8 – 9 December 2010. p. 208 – 214.

[13] Wamiliana, Amanto, and Mustofa Usman, Comparative Analysis for The Multi Period Degree Constrained Minimum Spanning Tree Problem, Proceeding The International Conference on Engineering and Technology Development (ICETD), pp. 39 – 43, 2013.

[14] Wamiliana, Faiz A.M. Elfaki, Mustofa Usman, and M. Azram, "Some Greedy Based Algorithms for Multi Periods Degree Constrained Minimum Spanning Tree Problem", *ARPN Journal of Engineering and Applied Sciences,* 2015; Vol. 10 (21): pp.10147 – 10152, 2015.

[15] Wamiliana, Mustofa Usman, Dwi Sakethi, Restu Yuniarti, and Ahmad Cucus, "The Hybrid of Depth First Search Technique and Kruskal's Algorithm for Solving The Multiperiod Degree Constrained Minimum Spanning Tree Problem", The 4th International Conference on Interactive Digital Media (ICIDM). IEEE Explore, Dec 2015.

[16] "GNU Octave", 2017.[Online].Available: https://www.gnu.org/software/octave [Accessed : 05-May-2017].

Section 3
Medical Sciences and Biomedical Engineering

Integrated Sci-Tech :
Interdisciplinary Research Approach
Volume 3

Deceptive is Effective Negotiation Strategies to Customers for using Condoms Consistently (#709)

Putu Sukma Megaputri[1,a], Putu Kusuma Dewi Dian Prima[1,b], Cindy Meilinda Sari[1,c], I Dewa Ayu Rismayanti[2,d]
[1]Midwifery Program, STIKes Buleleng;
[2]Nursing Department, STIKes Buleleng;
[a]megaputri_sukma@yahoo.com, [b]dian_pkd@yahoo.com, [c]cindymeilinda@gmail.com, [d]rismajegeg@gmail.com

Abstract. *Consistent using of condoms by their customers is very low. One of the problems is the lack of negotiations carried out by sex workers to its customers. This study aims to determine the most effective negotiation strategies used so that customers consistently use condoms. The study was survey cross sectional of sex workers directly with a sample of 100 people, selected by cluster random sampling in Denpasar. The collection of data by interviews using a questionnaire about the characteristics and modification CISQ developed by Noar. A total of 63% of customers consistently using condoms in the past week. Effective negotiation strategies used so that customers consistently using condoms is a deceptive (AOR: 2.5 95% CI: 1.06 to 5.62). While other variables associated with consistent of using condom are the availability of condoms (AOR: 13.7 95% CI: 4.45 to 42.2) and age (AOR: 10.6 95% CI: 2.4 to 47.3). Deceptive is the most effective strategy to increase consistent condom use.*
Keyword: *Negotiations Condoms, Female Sex Workers, Consistency of Condom Use*

I. Introduction

The incidence of HIV/AIDS by 2015 in some countries fell by 35% in terms of 2000, but this does not seem in Indonesia. Global Report in 2014 also showed 1.2 million people have died from AIDS appears to have declined 42% from 2005 resulting from the use of anti-retro viral (ARV). A total of 15.8 million people living with HIV / AIDS (PLHIV) has been accessed ARVs in 2015, an increase of 2014 were only 13.6 million [1]. Board of the United Nations (UN) has declared that the HIV/AIDS will be addressed in 2030, as stated in the *Sustainable Development Goals* (SDGs) as one of the *goals* by reducing the incidence of HIV/AIDS and increasing the use of antiretroviral drugs for people living with HIV.

HIV/AIDS epidemic in Asia are still mostly concentrated in populations at risk, and the majority of transmission through heterosexual [2]. Estimates of direct female sex workers live in Indonesia was 124.996, while the estimated indirect female sex workers as many as 104.860 and estimates of people living with HIV are 591.823 [3]. Almost the entire territory of Indonesia with a concentrated epidemic pattern, except the eastern part of Indonesia, especially in Papua with the pattern of the epidemic generalization. Concentrated epidemics also appear in Bali with an estimated 3.378 direct sex workers, 3.464 indirect sex workers and the estimated people living with HIV 26.000 [3]. Cases of HIV / AIDS in Bali, Denpasar with the highest percentage of HIV cases as much as 40.14% and the majority of cases are

found in sex workers. One of the triggers for the increased incidence of HIV / AIDS is a lack of awareness of condom use during sex to its customers.

Condom use or condom use consistenly by customers of several studies indicate still very low only 35% [4], 65% in Denpasar [5]. One of the problem condom use is still low because many sex workers do not negotiation condom use to its customers. Research on the negotiation of condoms by sex workers is still very low. Measurement negotiation is only measured by a few questions without looking in depth the strategies practiced by sex workers. As one of the studies on methods for measuring condom negotiation was originally used in the United States with nine questions and only six questions were validated [6]. The method was adapted in Cambodia to measure condom negotiation conducted by sex workers to its customers [7]. This research thus be interesting to do with adapting the measurement strategy condom negotiation in Bali.

II. Methods

This study is a survey research with approach, *cross sectional* with a target population of direct sex workers and affordable population is direct sex workers in the city of Denpasar in 2016. Total sample of 100 people chosen at *random cluster* sampling. Data collection was conducted through interviews where sex workers work, assisted by six enumerators and the use of questionnaires which have been tested previously. Questions about condom negotiation adoption of CISQ [6]. In this study of nine components CISQ only use six components in accordance with the test results of questionnaires namely: *withholding* sex, *direct request, seduction conseptualizing relationship, risk information* and *deception.* Measurement of negotiations was assessed using three questions on each component, then the measurement was assessed by comparing the *cutoff* results of total respondents of each component. The data were analyzed using univariate, bivariate with *chi square* and multivariate with logistic regression analysis using software.

III. Results

The average age of sex workers was 38 years old, with the average length of working as a sex worker is 25 months (± 2 years) and the average length of work in the last location of the interview was 38 months (± 3 years). Most of the sex workers with higher education 87%, with a good perception of 70%. Most in the location provided condoms as much as 76%. Negotiation strategies that most people do are direct request and risk information (76%). A proportion of consistent condom use during the last week by the customer as much as 63%.

Table 1. Frequency Distribution

Variable	f (%)
Age (mean ± SD)	38 ± 39.1
Length in the work (Mean ± SD)	25 ± 36.1
Lengtu of work in the site (months) (mean ± SD)	38 ± 39.1
Education	
Higher	87 (87%)
Low	13 (13%)
Perceived Susceptibility	
Good	70 (70%)
Intermediate	30 (30%)
Availability of condoms	
Always	74 (74%)
Rarely	26 (26%)
Negotiations	
Witholding sex	70 (71%)
Direct request	76 (76%)
Seduction	55 (55%)
Conceptualizing relationship	53 (53%)
Risk information	76 (76%)
Deception	57 (57%)
Condom Use	
Consistent	63 (63%)
No	27 (27%)

Table 2. Analysis of Bivariat

Variables	Used Condom Consistenly		p Value
	Use (%)	Not (%)	
Age			
Younger(≤38 years)	95.2	73.0	0.001
Tua (> 38 years)	4.8	27.0	
Education			
Higher	55.6	45.9	0.3
Low	44.4	54.1	
Knowledge of			
Good	90.5	81.1	0.18
Internediate	9.5	18.9	
Perceived susceptibility			
Good	76.2	59.5	0.07
Intermediate	23.8	40.5	
Condom availability			
Always	90.5	45.9	<0.0001
Rarely	9.5	54.1	
Negotiations			
Yes	69.8	37.8	0.002
No	30.2	62.2	

The result of table 2 above the limit of p value can be incorporated into the multivariate analysis was 0.2. Then that variable can be entered into the multivariate analysis were age, knowledge, perceived susceptibility, availability of condoms and condom negotiation.

Table 3. Bivariate Analysis Negotiation Strategies

Variable	Consistent condom used		P Value
	Wear (%)	No (%)	
Witholding Sex			
Do	76.2	62.2	0.14
None	23.8	37.8	
Direct Request			
Do	82.5	64.9	0,046
None	17.5	35.1	
Seduction			
Do	55.6	54.1	0.85
None	44.4	45.9	
Conceptualizing Relationship			
Do	55.6	48.6	0.5
None	44.4	51.4	
Risk Information			
Do	79.4	70,3	0.3
None	20.6	29.7	
Deception			
Do	65.1	43.2	0.03
None	34.9	56.8	

Table 3 above explain the analysis bivarat six valid strategy for negotiating condom. By looking at p value limits, the strategy can be entered into the multivariate analysis was withholding sex, direct request and deception.

Table 4. Multivariate Analysis

Variable	OR	P Value	95% CI	
			Lower	Upper
Strategy negotiation				
Witholding sex	1.4	0.5	0.54	3.61
Direct request	2.1	0.12	0.82	5.68
Deception	2.5	0.035	1 06	5.62
Availability of condoms	13.7	<0.0001	4.45	42.2
Age ≤ 38 years	10.6	0.002	2.4	47.3
Knowledge of STDs	2.2	0.28	0.5	9.1
Perceived susceptibility	1.4	0.5	0.44	4.72

Multivariate analysis using logistic regression with the results of the most effective strategies to increase consistent condom use. Strategies to deceptive customers 2.5 times increase in the customers use condoms consistently. Other variables associated with consistent condom use are age and the availability of condoms.

IV. Discussion

The condoms use consistently is generally measured by assessing the use of condoms by consistent within one week, the proportion obtained was 63%. This is consistent with research in Semarang on the consistency of condom use. Only 56.3% consistent use of condoms [8]. Consistent results were also mentioned in the report Behavioral Biology Integrated Surveying (IBBS) in 2011 that the consistent use of condoms only 14% [4].

The most effective strategy to increase consistent condom use is to deceptive the customers (AOR: 2.5 95% CI: 1.06 to 5.62). That sex workers are pursuing a strategy of negotiation with the customer lying to 2.5 times increase customers to use condoms during sexual intercourse. Deceptive strategy is a effective strategy and valid as the solicitation of sex workers to the partner/customers to use condoms [6]. *Deception* was reportedly used by 35% of men and women in affecting couples to use condoms. The strategy is made by lying to customers so that customers use condoms consistently [9]. Measurement of negotiation strategies through this deceptive is an adaptation of the questionnaire CISQ way to tell the customer that the use of condoms to prevent pregnancy even though in fact to prevent STDs. Another strategy to explain to the customer that all customers use in the fact not all customers to use condoms [6].

Beside the condom negotiation strategies, other related variables were age ≤ 35 years of sex workers (young). Age is one of the internal factors that influence a behavior. Direct sex workers when younger age appears significantly associated with condom use and 4.8 times higher than the old sex workers (OR: 4.8; 95% CI 3.1 to 7.5) [10]. Research in Vietnam also getting the younger of sex workers consistent in the use of condoms to customers [11]. Woman sex workers is less open to change in terms of behavior, so behavior condom use is not consistent settling and unchanged [12].

Availability of condoms in the location is also a variable that relates to the consistency of condom. Research in the Philippines also show the same thing about the availability of condoms with condom use [13]. The same results were consistent and were also found in the study in Indonesia [14], India [15], Republic of Congo [16], Ghana [10] that the availability of condoms in locations associated with the consistent of using condoms. Other research results in Indonesia also showed the same results that the availability of condoms have a significant relationship with the practice of the use of condoms [17].

V. Conclusions

Condom negotiation strategies are most effective for improving the consistency of condom use on customers is to deceive customers. Variables associated with consistent condom use is the age of sex workers who are young and availability of condoms at the location.

References

[1]. UNAIDS. Global AIDS Response Progress Reporting 2015 2015.

[2]. Ruxrungtham K, Brown T, Phanuphak P. HIV / AIDS in Asia. Lancet. 2004; 364: 69.

[3]. Ministry of Health. 2012 Size Estimation of Key Affected Populations (KAPS). 2012.

[4]. The Ministry of Health DG P2PL. IBBS 2011 (Integrated Biological and Behavioral Surveillance). 2011.

[5]. Wirawan D. et al. Trends in HIV Prevalence, Condom Use and Associated Factors among Female Sex Workers in Denpasar, Bali, Indonesia. Prev Med Public Heal Arch. 2014; II.

[6]. Noar BC, Morokoff PJ, Harlow LL. Condom Negotiation in Heterosexually Active Men and Women: Development and Validation of a Condom Influence Strategy Questionnaire. Health Psychol. 2002; 17 No. 6: 711-35.

[7]. Bui TC, Markaham CM, Tran LT., Beasley RP, Ross MW. Negotiation and Condom Use Among Female Sex Workers in Phnom Penh, Cambodia. AIDS Behav. 2013; 17: 612-22.

[8]. Irwan B. Consistency of Condom Use by Women Sex Workers / Consumers. J Kesehat mobi. 2012; II.

[9]. Debro S., Campbell S., L. Peplau Influencing a Partner to Use Condom: a College Student Perspective. Woman Physicology Q. 1994; 165-82.

[10]. A Oppong Adu et al. Social Behavioral Determinants of Condom Use Among Female Commercial Sex Workers in Ghana. AIDS Educ Prev. 2007; 160.

[11]. Tran T. et al. Condom Use and Its Correlates Among Female Sex Workers in Hanoi, Vietnam. Behavio AIDS. 2006; 10 No 2.

[12]. Atif M et al. Prevalence of Condom Use and Associated Factor s Among Female Sex Workers In Karachi, Pakistan. Int J Cur Res. 2015; 7 No. 2.

[13]. Urada LA, Morisky DE, Pimentel-Simbulan N, Silverman JG, Strathdee SA. Negotiations Condom among Female Sex Workers in the Philippines: Environmental Influence. PLoS One. 2012; 7 (3).

[14]. Basuki E et al. Reason For Not Using Condoms Among Female Sex Workers in Indonesia. AIDS Educ Prev. 2002; 14, No. 2: 102-16.

[15]. Dandona R et al. High Risk of HIV in Non-Brothel Based Female Sex Workers in India. BMC Public Health. 2005; 5: 87.

[16]. Kayembe, PK, Mapatano, MA, Busangu, AF, Nyandwe, JK, Musema, GM, Kibungu JP. Determinant of Consistent Condom Use Among Female Sex Workers in the Democratic Republic of Congo: Implication for Sexually Transmitted Infection Intervention. 2008; 84 No 3: 202-6.

[17]. Hadi TS. Factors Affecting the Practice Negotiating condom to prevent STIs and HIV / AIDS at the WPS in Resocialization Argorejo Semarang. Diponegoro University; 2004.

Determinants Low Birth Weight in Hospital General Kertha Usada Buleleng Regency Bali (*A Study Done at One of the Private Hospitals in Buleleng Regency)* (#711)

Putu Dian Prima Kusuma Dewi[1,a], Putu Sukma Megaputri[1], Cindy Meilinda Sari[1], Ns. I Dewa Ayu Rismayanti[2]

[1]Obstetrics Departement STIKesBuleleng, Jl Raya Air Sanih Km 11, Singaraja 81171, Indonesia

[2] Nursing Departement STIKesBuleleng, Jl Raya Air Sanih Km 11, Singaraja 81171, Indonesia

[a]dian_pkd@yahoo.co.id

Abstract. *The incidence of low birth weight is an indicator to measure the degree of public health given the wide range of adverse impact on the lives of babies. Study of low birth weight in the private health care facilities are still rarely done. Research conducted at the RSU KerthaUsada, Regency of Buleleng, Bali which aims to look at the determinants of the incidence of low birth weight and gestation characteristics demographic characteristics. The method used is the analytic data from longitudinal cohort of mothers in labor. The analysis that is used to look at the determinants of the incidence of low birth weight i.e. logistic regression. The results showed a determinant that has a direct relationship i.e gestation low birth weight incidence (OR 33.69; p 0.01), is illness history mother (OR 19.85; p 0.01), amniotic rupture early and abnormalities of the location of the placenta (placenta previa) (OR + 3.43; p 0.01), pregnancy (gemeliOr 47.43; p 0.01) and old rawat (OR 4.67; p 0.01). Patients who do not have health coverage being factors protective of the incidence of low birth weight (OR 0.56; p 0.04). Counseling of pregnant and prahamil needed to pregnant women and their husbands, families and pregnancy screening with ultrasounds to detect pregnancy gemeli.*

Keywords: low birth weight, kertha usada, determinants, logistic regretion

I. Introduction

The chance of survival and the vulnerability of children to disease in the future very determined also by the weight or size at birth children born weighing less than 2.5 kilograms, that is low birth weight (LBW), risk higher child mortality at an early age (1).

The high Infant mortality rate (AKI) in Indonesia, largely due to asphyxia, low birth weight and infection. According to Riskesdas 2013 LBW in Indonesia year 2013 amounting to 10.2 (2).

Riskesdas 2013 showed the highest incidence of low birth weight in women (11.2%) than male (9.2%), but the percentage of birth weight ≥ 4000 grams in males (5.6%) was higher than for women (3.9%) (3) babies born with low weight has the function of organ systems that have not been regularly so that it can have difficulties to adapt to the environment.

The incidence of low birth weight is one of the indicators for measuring the degree of public health, given the wide range of harm against the life of the baby. Women with IMT < 18.5 (skinny categories) have a high risk for giving birth to babies with low birth

weight (LBW) (4). The size of the Anthropometry as seen from size 23.5 cm LILAC < also affects the incidence of low birth weight (5). Mother's education are high 33% as factors protective of incident low birth weight (6).

Low birth weight can be classified into two, the first pure prematuritas is a baby born with a gestational age (UK) < 37 weeks and weight infants in accordance with gestation or preterm neonates referred to according to the time of her pregnancy, her baby is small gestastional age (SGA) that is the weight of the baby is born is incompatible with pregnancy. Small gestastional age (SGA) itself consists of three types namely symmetrical, asymmetrical, and dismaturitas (7).

Some of the factors investigated have a relationship and risk factors of low birth weight among them, namely the sex of the baby, pregnant, gemeli, gestational age, parity, and the nutritional status of mothers (5, 6, 8 – 21). The smaller the gestation time of delivery then the risk of low birth weight incidence also increases (14, 15.22). However, such research shows things are inconsistent and largely done at Government health facilities. Whereas the number of LBW in the private service of Genesis is also quite high and need to get attention.

One of the private hospitals in Buleleng Regency is a General Hospital Kertha Usada that experience progression each year in health care including the services the PONEK characterized by the presence of spaces, as well as NICU documentation is neatly stored from year to year. The number of births during the month of January-December 2015 as much as 5.8718 births with low birth weight.

II. Research Methods

This study is a longitudinal research analytic secondary data analysis by conducting a retrospective cohort study on the mother in the maternity Department in General Hospital Kertha Usada Singaraja period January-December 2015. Kertha Usada is one of the largest private hospital in the Regency of Buleleng. The research was conducted in the basement of VK, NICU medical record room and RSU KerthaUsada. Data collected using forms of data collection in the form of hard copy was made into the shape of soft copy (in the form of microsoft excel to facilitate analysis.

III. Results

Based on table 1 above shows demographic characteristics on the incidence of LBW 98.6% of mothers who have a college education with the status of having health coverage as much as 53.5%. Further views of the characteristics of gestation that the incidence of LBW 81.7% born in sectiocaesarea (SC), 15.5% in pregnancy gemeli, 15.5% with a history of KPD and placenta previa, 22.9% in gestational age < 37 weeks, 14.1% with parity > 4 children, 5.6 % occur in mothers who have a medical history, 59.2% with long rawat ≤ 3 days and 53.5% occur in the female gender. Analysis of the results of this research is done in stages include analysis of univariate analysis, percentage distribution by bivariat with test chi square and with multivariate logistic regression

Table 1. Variable incidence of LBW in the General Hospital Kertha Usada Buleleng Bali

Demographic Characteristics and Gestational	*LBW* (N = 71)n (%)
1	2
Demographic Characteristics	
Education	
Higher	70 (98.6)
Education	
low education	1 (1.4)
Status Health Insurance	
Having	38 (53.5)
Not having	33 (46.5)
Length Stay	
≤ 3 Days	42 (59.2)
>3 Days	29 (40.8)
Characteristics of gestation	
process Birth	
Normal	13 (18.3)
SectioCesarea (SC)	58 (81.7)
Pregnancy Gemeli	
Single	38 (70.5
Gemeli	11 (15.5)
other conditions	22 (31)
History of Premature rupture of membrane and Placenta Previa	
N	38 (53.5)
Premature rupture of membrane and Placenta Previa	11 (15.5)
Other conditions	22 (31)
Gestational	
≥37 Week	54 (77.1)
<37 Week	16 (22.9)
Parity	
<4 Persons	61 (82.9)
≥ 4 Persons	10 (14.1)
The issue of comorbid	
No	38 (53.5)
there are	3 3 (46.5)
Disease History Mother	
No	67 (94.4)
There were	4 (5.6)
Sex	
Female	33 (46.5)
Male	38 (53.5)

Table 2. Bivariate and Multivariate Analysis of Characteristics Gestational As Genesis Risk Factors LBW General Hospital Kertha Usada Buleleng Bali.

Characteristics	**aOR [95% CI (p)]**
1	**2**
Demographic Characteristics	
Health Insurance Status	
Have	1.00(ref)
Do not have a	0.53[0.29-0.98(0:04 *)]
Characteristics ofGestational	
Gemeli Pregnancy	
Single	1:00 (ref)
Gemeli	47.43[10:27 -218.98 (0:01 *)]
other conditions	0.84 [0.38 – 1.84 9 (0.67)]
History premature rupture of membrane and Placenta Previa	
No	1.00 (ref)
premature rupture of membrane and Placenta Previa	1.26-6.68 [2.90(0,012*)]
other conditions	0.85[0.39-1.84(0.67)]
Gestation	
≥ 37 Week	1, 00 (ref)
<37 Sunday	9.22-123.33[33.69(0.01 *)]
Length Of Hospitalization	
≤ 3	
Days>3 Days	2.46-8.88[4.67(0.01 *)]
Disease History Capital	
No	1.00 (ref)
there were	19.85 [4.13-95.39 (0.01 *)]

*****p-value <0.25 to backward models; p-value <0.05 for multivariate. Table 2 shows the results of bivariate and multivariate analysis gestational characteristics that are detrimental LBW. Based on multivariate analysis, show the characteristics of gestation which is determinant is LBW gemeli pregnancy (aOR 47.43; CI 10.27-218.98; p 0.01), history of premature rupture of membranes (PROM) and abnormal placenta or placenta previa (aOR 3:43; CI 1:25 -9.44; p 0.01), gestational age <37 weeks (aOR 33.69 9.22-123.22 CI; p 0.01), length of more than 3 days (aOR 2,46-8.88 CI 4.67; p 0, 01), a mother who has a history of disease (aOR 19.85 CI 4.13-95.39; p 0.01), While the demographic characteristics, namely ownership of health coverage is protective of the incidence of LOW BIRTH WEIGHT (aOR-0,29 0.98 CI 0.53; p 0.04).

IV. Discussion

The incidence of low birth weight on KerthaUsada Hospital in 2015 as many as 71 infants (9.89%) while that did not experience as much as 647 LBW infants (90.11%). LBW be a condition that deserves a good supervision and control, given the risks of morbidity and mortality is higher. Characteristics and conditions of pregnant women to be a function of control over LBW. During pregnancy, the mother had to do prenatal care at health facilities in

order to fetal growth and development can be monitored and the baby was born safe and sound [14].History of maternal health during pregnancy is also a determinant of the risk of LBW. But the deciding factor is not only the occurrence of low birth weight during pregnancy but also before pregnancy, and therefore the nutritional status of pregnant women should be in good condition. When pregnancy is no nutritional intake should be adequate to prevent impaired fetal growth [5]. The results of this study indicate preterm labor in gestational age of less than 37 weeks increased the risk of LBW by 33.69 times compared to labor at term (≥ 37 weeks). One trigger of preterm delivery is poor maternal nutritional conditions and diseases suffered by mothers [7].

Pregnancy gemeli also have strong relationships at 56.04 times more at risk than singletons. Results of other studies indicate that the incidence of LBW increased on condition gemeli upto 22.8 times higher than in singleton pregnancies [23].

Fetal weight in twin pregnancies lighter than single-fetus pregnancies at the same gestational age. Weight gain is equal to the fetus twins singleton pregnancies at 30 weeks, then gaining weight becomes smaller, due to excessive strain causes placental blood circulation abate. The weight of the fetus in twin pregnancies an average of 1000 grams lighter than the single-fetus pregnancies. Newborn weight in twin pregnancies is generally less than 2500 grams hamper fetal growth during pregnancy [7].

Other gestation characteristics that increase the risk of LBW is labor with premature rupture of membranes (PROM) and aberration of the placenta with a risk of 2.9 times (CI 1.26 to 6.68 p = 0.01). KPD occur due to the reduced strength of the membrane as a result of infection from the cervix and vagina so that it triggers labor conditions. The shorter the gestational age of the fetus is growing more and more rudimentary, both the reproductive organs and the respiratory organs [22]. Placenta abnormalities tend to reduce the intake of nutrients obtained fetus in the womb because the nutrients are received may not be perfectly acceptable to the fetus. Placenta previa has a direct relationship with the incidence of low birth weight [14, 6].

Pregnant women who have a history of poor health had 19.85 times higher risk of experiencing LBW. It is also found in some studies that a higher risk of low birth weight in pregnant women with hypertension, antepartum bleeding, anemia, asthma, and abortion [13,15,16].

Protective factors against LBW occurred in health insurance status, where mothers have health insurance at a lower risk (OR 0.56) to experience LBW or equal to 46% incidence of low birth weight was higher in mothers or families who have health insurance.

Government program that is health coverage for the poor (Assurance) that provide greater access against expected health care can improve the health of mothers and babies with a prime target pregnant women and children. Some research suggests that health coverage is very influential with the utilization of health care services. [25].goverment health insurance program evaluations show that the policy related government health coverage for the poor citizens of the impact is relatively small for the health of the baby is due mainly to the effects of crowding-out who owned such as care services, access to services health, health care utilization, quality health services, discrimination of extra health services, administrative procedures are long and complex [26].

goverment health insurancecan not be separated from social and economic factors that influence the incidence of low birth weight. Mehrad, 2010 states that the risk of low birth weight in lower socioeconomic 1.68 times greater than in the higher socioeconomic.

Similarly, the results of research conducted by Yasmeen S and Azim S in Bangladesh in 2009 that the economy is associated with low birth weight [27].

It can be associated with the condition of Indonesia society which still assume that health coverage is only used by the middle class down. However this has yet to be explained with certainty without knowing the average income earned. Then from further research related to economic conditions need to be traced in relation to the incidence of low birth weight.

Circumstances affecting the mother during pregnancy also have an effect on birth weight of the fetus. 1994 Shieve structural equation model to show that maternal history of medical risk showed independent influence on weight lahir. Kramer in journal determinant of low birth weight to mention that long hospitalization during pregnancy affects the occurrence of low birth weight [28].

There are several factors that affect the length of the mother during pregnancy with LBW is the risk of nutrition in pregnancy in treatment when diagnosed medical illness or treatment that interferes with the absorption of vitamins and minerals. Adequate nutrition is essential for normal development and growth of healthy fetal development. The study of low birth weight and prematurity, as well as neural tube defects and congenital abnormalities other non-genetic, have shown that nutritional status is very important since around the time of conception and during pregnancy [29].

Along with the need for extra calories, pregnant women need to eat a variety of foods, with a focus on vitamin and mineral intake. Women who received nutritional supplements or adequate nutrition through diet give birth to babies who are heavier and have a level lower congenital abnormalities. One study showed that women who received intensive nutrition counseling to every prenatal visit delivered a baby weighing 100 grams more than the group of women who received only one class short of nutrients in nutritional mereka.Risiko early prenatal care can be identified early and dealt with effectively [30].

V. Conclusion

Characteristics of gestation who have a direct relationship and boost the risk of LBW that gestational age, maternal medical history, pregnancy gemeli, premature rupture of membranes and aberration placenta (placenta previa). Instead patients who do not have health insurance becomes a protective factor against LBW.

References

[1] Agency, National Population Planning. Indonesia Demographic and Health Survey. , 2013;

[2] The Ministry of Health RI. Principles of Indonesian Riskesdas 2013. 2013;

[3] MoH RI. Basic Health Research. , 2013;

[4] MOH. Basic Health Research (RISKESDAS) IN 2010.

[5] Reza C. Determinants Infants with low birth weight. 2013; 96-106.

[6] Sonia Silvestrina, ClécioHomrich da Silva b VNH, André AS Goldani d, Patrícia P. Silveira b MZG. Maternal education level and low birth weight a metaanalysis. 2013.

[7] Cooper F & B. Myles Textbook editions 14. Midwives Jakarta: EGC; 2011.

[8] 8.Astuti P, Purwaningsih. Mother Maternity Parity Relationship With Low Birth Weight Babies Genesis Health Center Mergangsan In Yogyakarta Year 2010. 2012;

[9] Heavy B, Low L, Alya D. Factors Associated With Hospital Women & Children in Banda Aceh in 2013 Asked By: 2014;

[10] DewieSulistyorini SS. Analysis of factors affecting urban healthcenters LBW in Banjarnegara district. 2012; 1-6.

[11] DewieSulistyorini SSP. Analysis of Factors Affecting Rural LBW In Banjarnegara district Puskesmas Year 2014. 2015; 1 (01): 23-9.

[12] Antenatal Care Ernawati F. Relationship With birth weight babies in Indonesia (Advanced Data Analysis Riskesdas 2010). 2011; 34 (1): 23-31.

[13] Risk Factors Trihardiani I. Genesis low birth weight in Puskesmas East and North SingkawangSingkawang. 2011; 1-55.

[14] Rosha BC, Princess IS, Amaliah N. Children Aged 0-59 Months In East Nusa Tenggara, Kalimantan Determinant Analysis Of Low Birth Weight (LBW) Children of 0-23 Months in Nusa Tenggara Timur, Central Kalimantan and Papua. 2002;

[15] Septarini D. Relationship Age, parity, history of pregnancy, Practice About Antenatal Care (Anc), Nutritional Status and Workload With Genesis Low Birth Weight Infants (Study on Mother Peasants in PuskesmasCepiring Kendal 2002). 2003;

[16] Sondari F. Relationship Factors Genesis Baerat Mother With low birth (LBW) at Hospital Dr. Hasan Sadikin January-February 2006. 2006; (February): 0-1.

[17] Bukowski R, Smith GCS, Malone FD, Robert H, Nyberg DA, Comstock CH, et al. infant birth weight: prospective cohort study. 2007; (March): 3-7.

[18] Mcdonald SD, Han Z, Mulla S. Overweight and obesity in mothers and risk of preterm birth analyzes. 2009; 1-20.

[19] Oladeinde HB, OB Oladeinde, Omoregie R, Onifade AA. Prevalence and determinants of low birth weight: the situation in a traditional birth home in Benin City, Nigeria. 2015; 15 (4): 1123-9.

[20] Demelash H, Motbainor A, Nigatu D, Gashaw K, Melese A. Risk factors for low birth weight in Bale zone hospitals, South-East Ethiopia: a case - control study. BMC Pregnancy and Childbirth; 2015; 1-10.

[21] Feresu SA, Harlow SD, Woelk GB. Risk Factors for Low Birthweight in Zimbabwean Women: A Secondary Data Analysis. 2015; 1-17.

[22] Characteristics WINDARI F. Relations Pregnant Women With Low Birth Weight Genesis (LBW) in hospitals PenembahanSenopatiBantul, Yogyakarta Year 2014, 2015;

[23] S. Masitoh double Pregnant significant cause low birth weight infants. 2014; 129-34.

[24] BobakLJ. Maternity Nursing Textbook Issue 4. 4th ed. Renata Komalasari, editor. Jakarta: EGC; 2005.

[25] Johnson JA SC. Comparative healthsystems: Global perspectives for the 21st century. Jones & Bartlett, Sudbury. 2010;

[26] G F. An evaluation of the National Health Insurance Program in Ghana. Glob Dev Network (GDN) DisseminationWorkshop. 2009;

[27] Yasmeen S. EAE. Status of Low Birth Weight at a Tertiary Level Hospital in Bangladesh for a Selected Period. South East Asia J Public Heal. 2011;

[28] Kramer MS. Determinants of low birth weight: methodological assessment and meta-analysis. 1987; 65 (5): 663-737.

[29] MehrdadMirzarahimi, SadeghHazrati, Peymaneh Ahmadi RA. Prevalence and risk factors for low birth weight in Ardabil. 2010; 3.

[30] Golestan, M., US Karbasi and RF. Prevalence and risk factors for low birth weight in Yazd, Iran. Singapore Med J. 2011;

Survival people living with HIV-AIDS with adherence and no adherence treatment in Kramat Jati VCT Clinic, East Jakarta, DKI Jakarta, Indonesia Year 2014-2015.

Cicilia Windiyaningsih[1,a], Trisanti[1]
[1]University of Respati Indonesia, Jl. Bambu Apus I no 3,Cipayung, Jakarta Timur 13890
[a]sisilwindi@gmail.com

Abstract. *Data from Director General of CDC, Ministry of Health Republic of Indonesia 2014 has been reported 15.534 new cases of HIV and 1.700 new cases of AIDS.The highest HIV cases at Jakarta 38.464 cases. The antiretroviral theraphy has been used to decrease HIV replication for whole life time, ARV treatment was needed monitoring for successful treatment. Purpose research was to know survival people living with HIV-AIDS in Kramat Jati VCT Clinic, East Jakarta year 2014 to 2015. Method research was quantitative design restrospective cohort, samples 186 patients, data collection from medical records. The analysis by descriptive and multivariate cox regression . The result of research has showed that variable related with survivival people living with HIV-AIDS were the educational background, adherence, treatment, clinical stadium, additional disease, and number of CD4. The result of educational background HR= 0,651, R^2 1,8 %, 95%CI 0,451-0,940, p value 0,022, the median was 503 days, clinical stadium HR= 1,338, R^2 1,5 %, 95%CI 0,926-1,932, p value 0,121, the median was 470 days, Adherence HR= 1,388, R^2 10,7%, 95%CI 0,993-1,938 p value 0,055, the median was 398 days, the number of CD4 ≥200 cels/mm^3 HR 0,609, R^2 19,3% ,95%CI 0,424-0,876,p value 0,008, the median was 470 days, the treatment HR 1,313,R^2 16,6% ,95%CI 0,901-1,912 p value 0,156, the median was 498 days. The conclusion was dominant factor was determinant adherence of treatment. The people living with HIV-AIDS who has the adherence with no combination tratment has a better survived than the people who has no adherence.*

Keywords *: adherence , CD4, education, treatment, stadium, survived*

I. Introduction

HIV / AIDS (human immunodeficiency virus / acquired immune deficiency syndrome) disease is a worldwide health problem, and is a top-ranking cause of death disease with a high mortality rate and a high incidence of disease (morbidity) and requires diagnosis and therapy which is long enough. (Mandal,dkk. 2008) The highest number of HIV cases in Indonesia is in DKI Jakarta (38,464 cases), followed by East Java (24,104 cases), Papua (20,147 cases), West Java (17,075 cases) and Central Java (12,267 cases).

From the data in the spread of HIV / AIDS in West Jakarta was quite worrying. Recorded, since January to September 2014 the number of HIV sufferers in West Jakarta reached 309. While AIDS sufferers as much as 736 people. The number has increased in the same period compared to the year 2013, the 128 peoples of HIV /AIDS as 139. Until September 2015 ago, in North Jakarta found 316 cases of HIV / AIDS. While in 2014 found HIV / AIDS sufferers as much as 645 cases and in 2013 the number of people living with HIV / AIDS in North Jakarta as many as 846 cases. Since the last two years, HIV / AIDS sufferers in South

Jakarta recorded 88 people, that is 46 positive people have HIV and 42 people infected with AIDS.

Besides having the widest area, the densest population, East Jakarta also has the highest number of HIV / AIDS patients compared to other urban areas in Jakarta. HIV / AIDS sufferers in East Jakarta until August 2014 were dominated by male likes alias homos who reached 139 cases. Then followed by housewives 100 cases, female sex workers 51 cases, 15 transvestites and 5 sex worker cases. In Kecamatan Kramat Jati Number of HIV infections reported 2014 as many as 139 cases, up compared to the year 2013 as many as 27 cases, and the Case Aquiared Immuno Devisiency Syndrome (AIDS) in 2014 increased by 3 patients and died 3 peoples, compared to the year 2013 as much as 1 case.

East Jakarta area has 10 subdistricts and 65 sub-districts with 10 sub-district health centers and village health centers 65. Puskesmas Kecamatan Kramat Jati consists of 7 puskesmas kelurahan. In the first year of ARV treatment (10 months) was 0.797 (79.7%). HIV / AIDS not only affects the physical wellbeing of an individual but also the overall quality of life of those who are infected. In this context HIV / AIDS disease is seen as a burden of stress that can affect the quality of life with various dimensions. At first, clients feel uncomfortable, shy, anxious, and other problems. If the ability of adaptation is not sufficient, do not close the possibility of patients when desperate, depressed, and fell in bad health conditions. This will decrease the life of the patient (MOH RI in Khoiruddin, 2010). **AIM:** To prove the role of treatment against the survival of people with HIV-AIDS.

II. Research Methods

Quantitative research, with a retrospective cohort design. The population in this study were all people with HIV / AIDS (ODHA) and were on treatment from January 2014 to December 2015. The population in this study was 200 people. The sample in this study were people with HIV / AIDS (ODHA) from January to December 2015 who visited the Health Center of Kramat Jati, East Jakarta. The data used in this study is secondary data viewed through patient status, and research data is univariat, bivariate and multivariate analyzed. (Tuan Hanni, 2013)

III. Research Result

1. Univariate Analysis

Table .1 Respondent Distribution Based on Life Resilience in People with HIV / AIDS (PLWHA), In HC Kramat Jati East Jakarta, Year 2014--2015

Survivival	Frequency	%	Long Life		Median days
			Longest	Shortest	
Event (death)	10	5.4	2556 days (7years)	34 days	422
Sensor (life)	176	94.6	4747 days (13years	22 days	
Sum	186	100			

Based on Table 1 above shows that the survival of people living with HIV in PKC Kramat Jati East Jakarta is the most is the life (sensor) 94.6%, dies (event) 5.4%. The observation period is 2 years or 720 days, the median survival of the subjects with the longest life time (sensor) 4747 days, the shortest 22 days, while at 2556 days, the shortest is 34 days, with median of 442 days.

Tabel 2 Relationship Beetwen Treatment at People living with HIV-AIDS in HC/VCT. Kramat Jati ,East Jakarta Year 2014-2015

Variable	n Total	Event	sensor	Median (Days)	CI95%	p Value
1.Treatment						
Combination	110	10	100	498	342.5-653.5	0.140
No combination	76	0	76	382	322.2-441.8	
2. Age						
<25 year	**37**	1	36	398	310.9-488.0	0.052
≥25 year	**149**	9	140	470	367.8-572.7	
3.Education						
Lower	**42**	**1**	**41**	**349**	**306.3-391.6**	**0.019**
higher	**144**	**9**	**135**	**503**	**362.5-643.5**	
Job						
Working	**159**	**7**	**152**	**408**	**315.3-500.0**	**0.587**
No Working	**27**	**3**	**24**	**491**	**259.9-722.1**	
Married Status						
Not married	**124**	**6**	**118**	**413**	**328.7-497.2**	**0.870**
Married	**62**	**4**	**58**	**477**	**329.7-624.2**	
Gender						
Male	**140**	**7**	**133**	**413**	**341.5-484.5**	**0.747**
Female	**46**	**3**	**43**	**515**	**293.4-736.6**	
Infectious Opportunity						
Positive	**107**	**10**	**97**	**470**	**355.5-584.5**	**0.506**
Negative	**79**	**0**	**79**	**398**	**289.7-506.3**	
Clinical Stage						
3 &4 stage	**123**	**8**	**115**	**470**	**304.8-635.2**	**0.090**
1&2 stage	**63**	**2**	**61**	**398**	**339.1-456.9**	
Adherence						
Adherence	**57**	**7**	**50**	**681**	**393.9-968.1**	**0.022**
No Adherence	**129**	**3**	**126**	**398**	**315.2-480.8**	
CD4						
<200sel/mm^3	**70**	**9**	**61**	**356**	**236.9-475.1**	**0.057**
≥200 sel/mm^3	**116**	**1**	**116**	**470**	**291.6-648.4**	

Tabel 3. Final Model of Research

No	Variabel	*p value*	RR	95 % CI	R2 %	R2 %	Median Days
1.	Treatment	0,156	1,313	0,901-1,912	16,6	37,6	442
2.	Education	0,022	0,651	0,451-0,940	1,8		
3.	Clinical Stages	0,121	1,338	0,926-1,932	1,5		
4.	Adherence	0,055	1,388	0,993-1,938	10,7		
5.	CD4	0,008	0.609	0,424-0,876	19,3		

IV. Discussion

1. TYPE OF TREATMENT

In this study, treatment was not a combination if PLWHA was given only ARV therapy Line 1, whereas combination therapy if PLWHA was given first-line antiretroviral therapy, substitution, and drug of opportunistic infection. The results of this study show the most use of combination treatment 59.1%, while the treatment was not a combination of 40.9%, most people living with HIV (event) 5.4% get combination treatment because PLWHA who died (event) mostly get drug opportunistic infections and there were also the substitution. The longest and longest life survival of PLWHA (censor) in the combination of 4747 days, shortest 22 days, event deadness of it was longest survival 2556 days, shortest 34 days, with median 498 days.

Bivariate life table and Kaplan Meier analysis showed that survival of PLWHA in VCT Kramat Jati, East Jakarta was the most survival (sensor) in patients using combination treatment 90,9%. The result of statistic with Rank Log test get p value = 0,140 by using ά = 0,05, meaning there was a significant correlation between combination and no combination treatment to PLWHA survival. This study was same with the results of a study conducted by Simbolon (2014), that were not replacing the ARV regimen significantly affected survival in HIV / AIDS (HR = 1.56; 95% CI: 0.921-2,770) patients.The result of multivariate analysis showed that treatment variable with p value = 0,156 means there was a significant correlation between combination treatment and not combination with survival. Value of RR = 0,1,313 means that PLWHA who get combination treatment at risk 1 times more than treatment was not Combination against survival. Value R2 16.6%, meaning treatment contributes 16.6% affect the survival of people living with HIV. So that required the management of toxicity in accordance with existing guidelines (National Guidelines, Ministry of RI 2011 ;WH0.2006); Putri. Aghnia J dan Eryati Darwin, E. 2012.). From the results of the study found that people living with HIV (not survive) who get the combination treatment. So this research is in accordance with existing theory.

The conclusion that there was similarity between the results of this study, theories, and the results of research others (Hiesgen J.et all. 2016; Albuquerque MH, et all.2017;Liu ZQ,et

all.2017; Nancy Dian, A. 2010; Nanang, M, Y. 2011; Nurul.Wandasari, S. 2015; Oktavianus. 2014; Sileshi, B. et. Al. 2013; Sri, U. 2015; Tadesse, K., Haile, F., & Hiruy, N. 2014) that combination treatment (more 1st ARVs, substitutes, and IO medications) are dead (event), this was consistent with the existing theory that the more treatment was given the more side effects are caused, affecting the organs of the body, Such as kidney failure, toxic to the liver, thus affecting the length of his life.

2. Education Level.

The results of this study show the most distribution in high-educated PLHA (SMA / PT) 77.4%, while the low educated (SD / SMP) 22.6%. Survival The longest and longest life-longest living (sensor) of 4747 days, the shortest 22 days, has the longest survival event of 2556 days, the shortest 105 days, with a median of 503 days. The longest and longest life-long survival (Censored) ODHA (sensor) 4747 days, the shortest 22 days, the longest survival event of 2556 days, shortest 105 days, with median 503 days. In bivariate analysis analyzes life table and Kaplan meier seen survival of PLWHA in PKC Kramat Jati Jak-Team that still alive (sensor) mostly in people with high educated people 97,6%. The result of statistic with Log Rank test got p value = 0,019 by using α = 0,05, meaning there is significant relation between high education level and low level of education to survival. In line with the results of Simbolon (2014), we found a significant relationship between low and high education with P value 0.92. This suggests that education has an effect on the survival of HIV / AIDS patients.

Educational variable in multivariate analysis, with RR = 0,651 mean that higher education 0,6 times risk than low education to survival of PLWHA. Educational variables contribute 1.8% affect the survival of people living with HIV. A person's education level affects the stressor so as to determine the ability of coping mechanism (Nursalam, 2009 Bozzette, S. A., & Shapiro, M. F. 2005). The higher a person's education the easier they will receive information, and ultimately the knowledge they have will be more and more. This was the basis for changes in health behavior change, including health service search behavior and environmental health behavior.

The conclusion of this study was in line with the results of other research, that the level of education affect the survival of people living with HIV. The results also show that people with HIV who are highly educated in their survival are also older in accordance with existing theories.High education also corelated with income and longer of survival. (Bozzette, S. A., & Shapiro, M. F. 2005; Nancy Dian, A. 2010; Nanang, M, Y. 2011; Nurul.Wandasari, S. 2015; Oktavianus. 2014; Putri. Aghnia J dan Eryati Darwin, E. 2012; Tadesse, K., Haile, F., & Hiruy, N. 2014)

3. Clinical stages of disease.

The results showed that the highest distribution of ODHA with stage 3, and 4 (66,1%), stage 1 and 2 33,9%. The longest and longest life survival of PLWHA (sensors) in the 3rd and 4th stages was 3646 days, the shortest is 22 days, the longest survival event is 2556 days, the shortest was 34 days, with median 470 days.The result of bivariate analysis shows the life table and Kaplan meier analysis The survival of people living with HIV in PKC Kramat Jati Jak -The team that is still alive (censor) is the highest in PLWHA which is stage 3 and 4 93,5%. The result of statistic with Rank Log test obtained p value = 0,090 using α = 0,05,

meaning there is significant relation between stage 1 with stage 2, 3 and 4 on survival. PLWHA who died in stage 1 and 2 were only 2 patients. Researchers classify stage 3, and 4 because based on the theory in chapter II stage 3 is considered a stadium that is at grave risk to the survival of people living with HIVIn line with Anggraini's (2010) study, the patients who started therapy at stage III and IV had a greater risk of death up to 4.5 times than those who started therapy at stage I and II.

Clinical stages illustrate the phase of HIV travel in reducing the body's immune capabilities. The higher the clinical stage, indicating the severity of a disease (Liu ZQ,et all.2017; Nancy Dian, A. 2010; Nanang, M, Y. 2011; Nurul.Wandasari, S. 2015; Oktavianus. 2014; Putri. Aghnia J dan Eryati Darwin, E. 2012; Sileshi, B. et. Al. (2013). HIV infection in stage II and early stage III increases the incidence of wasting syndrome in 46% of cases characterized by weight loss of more than 10% with prolonged general weaknesses. This situation potentially pushes into a life-threatening immunocompromise status.The conclusion there was an influence between clinical stage of disease on survival of people living with HIV, similar with existing theories, and the results of other studies, because clinical stages of HIV / AIDS earlier in diagnosis will affect their survival, and CD4 counts should also be ≥ 200 Cell / mm ^{3}, so have a chance to live longer.

4. Adherence in Treatment.

The results showed that most PLWHA obedient in the treatment of 69.4%, not obedient 30.6%, meaning as many as 129 PLWHA obedient in treatment. The longest and longest life survival of PLWHA (censors) in the treatment of 4747 days, the shortest 22 days, the longest survival event (event) 480 days, the shortest 34 days, with median 681 days. Result of bivariate life table analysis and Kaplan meier seen survival of PLWHA in PKC Kramat Jati Jak-Team that still alive (censor) mostly on PLWHA who obedient in treatment 97,7%. The result of statistic with Rank Log test obtained p 0,022 by using ά = 0,05, meaning there is significant correlation between obedient with disobedient in treatment to survival. In line with Simbolon's (2014) study, the cumulative probability of survival in a group of HIV / AIDS patients without ARV adherence was 71.23%. The cumulative probability of survival in HIV / AIDS patients whose ARV adherence was 85.36. Adherence or adherence to therapy was a condition in which patients adhere to treatment on a self-awareness basis, not just because they obey the doctor's orders. The failure of antiretroviral therapy was often the result of non-adherence of patients taking antiretrovirals. Many factors affecting medication adherence include health care facilities, patient characteristics, antiretroviral therapy, coexistent characteristics, and patient relationship with health personnel.

The simpler the combination of antiretroviral drugs the higher the rate of medication adherence. Health workers have an obligation to establish good relationships and help patients to achieve good compliance conditions.Conclusion The results of this study have a correlation between adherence in treatment to survival, in line with existing theories that the fewer alloys of drugs given the higher adherence in taking medication, in line with the research of others, because PLWHA obedient in taking medicine and obedient visit To VCT clinics as well as being able to consult can also affect CD4 cell counts, thus motivating and surviving longer. (Albuquerque,et all.2017.Emma Rosamond Nony Weaver.et all.Sept 17,2014; Nancy Dian, A. 2010; Nanang, M, Y. 2011: Nurul.Wandasari, S. 2015; Oktavianus. 2014. Putri. Aghnia J dan Eryati Darwin, E. 2012; Sileshi, B. et. Al. 2013; Sri, U. 2015; Tadesse, K., Haile, F., & Hiruy, N. 2014).

5. Number of CD4

The results of this study showed the most distributions in people with CD4 cell count> 200 cells / mm3 62.4%, while CD 4 <200 cells / mm3 37.6%.Longest and longest life survival of PLWHA (sensor) at CD4 count ≥ 200 cells / mm3 4747 days, shortest 28 days,, event death duration of the longest and shortest of 105 days, media 470days. analisis life table and Kaplan meier sensor at CD4 ≥ 200 sel/mm3 99,1 %. Log Rank p value 0,057 ,alfa 0,05 ,significant number of CD4 ≥ 200 sel/mm 3 long life compare wth CD4 ≤ 200 sel/mm 3.
The result of multivariate analysis obtained p value 0,010, meaning there is significant relation between CD4 cell count ≥ 200 cell / mm^3 with CD4 ≤ 200 cell / mm^3 to survival. RR 0,010, Meaning that PLWHA with CD4 ≤ 200 cell / mm^3 0,6 times risk than with CD4 ≥ 200 cell / mm^3 to survival. The CD4 count variable contributed 19.3% to the survival rate. In line with Indarwati Research.2008, that HIV-positive people with CD4 cell count <50 cells / mm^3 had a 2.1 times greater risk of death compared to those with CD4 counts of 50-199 cells / mm3.
To start antiretroviral therapy, it is necessary to check the CD4 count to determine if the patient is eligible for antiretroviral therapy. According to Yasin (2011), lower CD4 cell counts, below ≤50 cells / mm^3 are more prone to death than patients with higher baseline CD4 cell counts, so survival of patients with an initial CD4 cell count <50 cells / mm^3 will also increase Reduced.
The conclusions of this study are similar to those of others, that CD4 counts have an effect on survival and the theory also suggests that lower CD4 cell counts, up to below 200 cells / mm^3 die faster than patients with more preliminary CD4 cell counts high. (Albuquerque MF,et all.2017; Liu ZQ.2017;Nancy Dian, A. 2010; Nanang, M, Y. 2011. Nurul.Wandasari, S. 2015; Oktavianus. 2014; Putri. Aghnia J dan Eryati Darwin, E. 2012; Sileshi, B. et. Al. 2013; Sri, U. 2015; Tadesse, K., Haile, F., & Hiruy, N. 2014).

V. Conclusion

Resilience of people living with HIV / AIDS (PLWHA), life (censor) 94.6%, who died 5.4%, with the longest life time of 4747 days (13 years.) The longest mortality at 5.4% was 2556 Day (7 years), shortest 34 days Median survival 442 days. Combination treatment 59.1%, still living 90.1%, longest life 13 years, shortest life 22 days, median 498, CI95% 342,5-653,5; 17% (R2). Adherence with PLWHA survival p 0,055. Adherence treatment still lives 97.7%, died 2.3%. Longest life longest 13 years, shortest 22 days, median life 681 days, CI95% 393,9-968.1 days. Contribution of 11% medication adherence (R2). The CD4 influence on the survival of PLWHA p 0.008. CD4 ≥200 cells / mm3 62.4% longest survival 13 years shortest 28 days median 470 days, 95% CI 291.6-648.4 days; Contributed CD4≥200 cells / mm3 19% (R2). There was an effect of education with PLWHA survival, p value 0.022. High education 77.4%, longest life 13 years (4747 days), shortest 22 days, median 503 days, CI95% 362,5-643,5 days. And contribution 2%. Coufounding factor of clinical stages on survival of PLWHA p value 0.121. Clinical stage 3, 4 as many as 66.1% longest survival 3646 days (10 years), shortest 22 days, median 470, CI95% 304.8-635.2 days). Contribution of clinical stages 2%. The dominant factor of PLHIV survival that was Adherence of Treatment.

Reference

[1]. Albuquerque MF, Alves DN, Bresani Salvi CC,Batista JD, Miranda-Filho DB, Melo HR,Maruza M, Montarroyos UR.January 9.2017.*Predictprs of Immunodeficiency-Realated Death in a Cohort of Low Income People Living With HIV: a competing risk survival analysis*.https://www.ncbi,nlm.nih.gov/pubmed/28065185. August 18,2017.10.32.WIB.

[2]. Bozzette, S. A., & Shapiro, M. F. 2005. *"The Effect of Socioeconomic Status on the Survival of People Receiving Care for HIV Infection in the United States"* (Journal of health care for the poor and underserved). 16 (4), 655-76.

[3]. Depkes-RI. 2008. *AsuhanPersalinan Normal*. JNPK-KR. Jakarta

[4]. Dinkes.2014. Data HIV/AIDS. Jakarta Timur

[5]. Emma Rosamond Nony Weaver , Masdalina Pane , Toni Wandra, Cicilia Windiyaningsih, Herlina, Gina Samaan.September 17, 2014. *Factors that Influence Adherence to Antiretroviral Treatment in an Urban Population, Jakarta, Indonesia*. https://doi.org/10.1371/journal.pone.0107543.August 12.10 . 2017.

[6]. Hiesgen J,Schutte C,Olorunju S,Retief J.2016July10. *Cryptococcal Meningitis in a Tertiary Hospital in Pretoria, Mortality and Risk Factors-A Retrospective Cohort Study.*https://www.ncbi.nlm.nih.gov/pubmed/27255493. August10.2017.10.35 WIB.

[7]. Info DATIN, Dalam Analisis dan Situasi HIV/AIDS, Kemenkes RI, 2014

[8]. KementerianKesehatan RI. 2014. *Pedoman Nasional Tata Laksana Klinis Infeksi HIV dan Terapi Antiretroviral pada Orang Dewasa.* Jakarta: Kemenkes

[9]. KementerianKesehatan RI. 2014. *Pedoman Nasional Tata Laksana Klinis Infeksi HIV dan Terapi Antiretroviral pada Orang Dewasa.* Jakarta: Kemenkes

[10]. Liu ZQ,Zhou N,Bai JY,Guo Y,Yu MH.2017 March 10.*Analysis of Surivival and Influencing Factors of HIV/AIDS Patients in Tianjin,2004-2014. https://www.ncbi.nlm.nih.gov/pubmed/28329942.August18.2017.11.30.WIB.*

[11]. Marlina.2014. *pengaruh Koinfeksi Tuberkulosis Terhadap Kesintasan Tiga Tahun Pasien HIV/AIDS yang mendapat terapi Antiretroviral di Rumah Sakit Infeksi.* Tesis.Fakultas Kesehatan Masyarakat Program Magister Epidemologi Kekhususan Epidemologi Terapan Depok.

[12]. Mandal,dkk. 2008. *Penyakit Infeksi*. Jakarta: Erlangga Medical Series

[13]. Nancy Dian, A. 2010. *Ketahanan Hidup Satu Tahun Pasien HIV/AIDS dengan Pengobatan Regimen ARV Lini Pertama Berdasarkan Jumlah CD4 Sebelum Pengobatan ARV* di RSPI Prof. DR. Sulianti Saroso Tahun 2005-2010.Tesis.UniversitasIndonesia : Jakarta

[14]. Nanang, M, Y. 2011. *Analisis Respon Terapi Antiretroviral padaPasien HIV/AIDS.*Fakultas Farmasi Universitas GadjahMada Sekip Utara : Yogyakarta.

[15]. Nasronudin. 2007. *HIV dan AIDS*. Surabaya :Airlangga University Press

[16]. Notoatmodjo, S. .2012. MetodologiPenelitianKesehatan. Jakarta :Rineka Cipta . 2010. *IlmuPerilaku Kesehatan.* Jakarta:RinekaCipta.

[17]. Nurul.Wandasari, S. 2015. *Analisis Ketahanan Hidup 9 Tahun Pasien HIV/AIDS yang Mendapat Terapi Antiretroviral (ARV) Berdasarkan Cara Penularan di RS Kanker Dharmais.* Tesis.Jakarta :Universitas Indonesia

[18]. Oktavianus. 2014. *PrediktorKematian ODHA Pada Tahun Pertama Pengobatan Antiretroviral di RSUD Labuang Bajudan Puskesmas Jumpandang Baru Tahun 2007-2014*. Fakultas Kesehatan Masyarakat Universitas Hasanuddin

[19]. Putri. Aghnia J dan Eryati Darwin, E. 2012. *Pola Infeksi Oportunistik Yang Menyebabkan Kematian Pada Penyandang AIDS Di RS Dr. M. Djamil Padang Tahun* 2010-2012. Jurnal Andalas

[20]. Sastroasmoro S. 2011. *Dasar-dasar metodologi penelitian klinis* Ed. 4. Jakarta: Segung Seto

[21]. Saryono. 2009. *Metodologi Penelitian Kesehatan Penuntun Praktis Bagi Pemula.*SJogjakarta : Mitra Cendikia Press.

[22]. Sileshi, B. et. Al. (2013). *Predictor of mortality among TB-HIV Co-infected patient being treated for tuberculosis in Northwest Ethiopia: a retrospective cohort study*. BMC Infectious Diasease 2013, 13:297

[23]. Sri, U. 2015. *Prediktor Kematian Pasien HIV/AIDS dengan Terapi Antiretroviral (ARV) di Rumah Sakit Umum Daerah Bandung Bali Periode Tahun20062014.*Tesis.UniversitasUdayana : Denpasar.

[24]. Tadesse, K., Haile, F., & Hiruy, N. 2014. "*Predictors of Mortality Among Patients Enrolled on Antiretroviral Therapy in Aksum Hospital, Northern Ethiopia: a Retrospective Cohort Study"* (PloS one). 9(1),e87392.

[25]. Tuan Hanni, 2013. *Model Regresi Cox Proposional Hazard Pada Data Ketahanan Hidup*. FSM Undip. Semarang

[26]. WH0.(2006).*Pedoman Nasional Terapi Antiretroviral* .From https://www.google.co.id/search?q=WHO+2006+tentang+pemberian+ARV&oq=WHO+2006

The Experience Of The Husband Who Accompanied The Wife With Cervical Cancer Who Are Undergoing Treatment (#671)

I Gusti Ngurah Putu Andy Prasetia[1,a], Ni Wayan Trisnadewi[2], Ika Setya Purwanti[3]
[1]STIKes Wira Medika Bali
[a]andyprasetia68@gmail.com

Abstract. *Cervical cancer was a cancer that is highly feared by women because it does not caused symptomps at the beginning of this development. The purposed of this research is to know the description of the experience of the husband who accompanied the wife with cervical cancer who are undergoing treatment. The typed of the study is qualitative research with descriptive phenomenology design. The number of participants in this study is four participants, with purposive sampling technique. Analysis data technique used is with engineering analyisis colaizzi. Result : The results of this research identifies five themes, that knowledge of disease of cervical cancer, psychological response, the source of motivation to cervical cancer patients, treatment efforts and the hope of healing. The husband who accompanied the wife with cervical cancer felt sad when she saw the condition of his wife at this time and keep trying for healing his wife. The researcher suggested to health care personnel so that paying attention to the psychological state of the patient's cervical cancer in addition to paying attention to its physical state.*
Keywords *: the experience of the husband, wife, cervical cancer*

I. Preliminary

Cervical cancer is a cancer that is feared by women, because cervical cancer does not cause symptoms in the early stages of cancer development. Based on the phenomenon that researchers have found for a cervical cancer patients need the support of his family. Such support can increase the motivation itself to recover. Family support is also a very important factor for someone who is facing a problem to improve his mental and spirited life.

One cervical cancer patient reveals "I really need the support of the family that makes me more comfortable". The patient also said "I am grateful for the full support of my family to get well soon". This suggests that support from the family can improve the psychological state that is being felt by cervical cancer patients.

The person closest to cervical cancer patients is the patient's husband. Based on a preliminary study that researchers conducted on February 23, 2107, the patient's husband felt sad when he saw the condition of his wife, As one of the patient's husband said "I must be sad to see the condition of my wife at this time". But there is also one of the patient's husband who said "I feel mediocre when I see the circumstances of my wife". Although there are differences of opinion from the patient's husband, but all give the same hope that hope that his wife quickly heal and get the best treatment in order to perform their daily activities. In addition, the patient's husband said not so know with cervical cancer. This makes husbands feel sad when they know the situation and make them want to quickly check the situation experienced by his wife.

Data in Indonesia cervical cancer is the most common cancer in women causing death, an estimated 40,000 new cases of cervical cancer each year, each day found 41 new cases and 20 deaths at once (Widiantara, 2016). Based on the data Riset Kesehatan Dasar (Riskesdas)

In 2013 the prevalence of tumors or cancer in Indonesia is about 1.4 per 1000 population or 330,000 people. Cervical cancer is a cancer with the highest prevalence in Indonesia in 2013, namely cervical cancer as much as 0.8% or about 98,692 people (Depkes, 2014). Cervical cancer ranks first cancer in women in Bali with a prevalence of 0.7% or about 1438 people. The incidence of cervical cancer in Bali is 43 / 100,000 people (0.89%) (Dinas Kesehatan Provinsi Bali, 2013).

One of the research conducted by Rahayu in 2011 about the phenomenological study of husband experience with wife who had cervical cancer in Jakarta area, States that couples who have wives diagnosed with cervical cancer cause psychological reactions in couples and require adaptation before accepting the conditions that occur in the wife. Changes in life are also experienced by couples including physical, psychosocial and sexual life changes in their marriages (Rahayu, 2011).

From the experience experienced by cervical cancer patients themselves ie research from Negari in 2015. The study, conducted by Negari, on the experience of cervical cancer patients undergoing chemotherapy, states that patients with cervical cancer experience various effects in chemotherapy such as hair loss, abdominal pain and fatique, support from the family is also needed by patients to face the problems it faces (Negari, 2015).

The general purpose of this study is to know the description of the experience of the husband who accompanied the wife with cervical cancer who are undergoing treatment.

II. Materials and Methods

In this research using qualitative research method with descriptive phenomenology approach. Qualitative research is a study that generally explains and provides an understanding of various human behaviors and experiences (individuals) in various forms (Rachmawati, 2014). Descriptive phenomenology requires the researcher to process the bracketing (to confine the assumptions and knowledge about the phenomenon that occurs) to be able to give a complete picture of what kind and how the participants experience the situation and phenomena experienced in the reality of social life based on the point of view of the participants (Rachmawati, 2014).

This research was conducted at Ruang Poly Kebidanan RSUP Sanglah Denpasar. The time of this study was conducted on 1 April to 31 May 2017. The selection of participants is done by purposive sampling that is selected with certain considerations and objectives.

The selection of participants in this study was selected with consideration of inclusion criteria of the husband who accompanied the wife with cervical cancer who are undergoing outpatient treatment in Poly Kebidanan RSUP Sanglah Denpasar. The husband who accompanied the wife with cervical cancer who underwent chemotherapy. The husband who accompanies the wife with cervical cancer is willing to become a participant.

In this study the main instrument is the researchers themselves. Which serves to establish the focus of research, selecting informants as data sources, collecting data, assessing data quality, analyzing data, interpreting data and making conclusions on findings. Analysis of data used in this study using analysis according to Colaizzi where there are seven stages of data analysis process with phenomenology method that Each transcript should be read and re-read to get a general sense of the whole content. For each transcript, significant statements relating to the phenomena under study should be extracted. Meaning must be formulated from this significant statement. The formulated meaning should be sorted into categories, groups and themes. The researcher's findings should be integrated into the full description of the phenomenon under study. The structure of the phenomenon must be explained. Finally the

validation of the findings should be sought from the study participants to compare the descriptive results of the researcher with their experience (Shosha, 2012).

III. Results and Discussion

Participants involved in this research is the husband who accompanied the wife with cervical cancer who are undergoing treatment as many as 4 people with varying age that is 58, 55, 42, 72 years. All participants had a wife who was diagnosed with cervical cancer who was undergoing treatment at the Police Room Kebidanan Sanglah Denpasar Hospital.
Researchers conducted interviews to participants and continued by analyzing the results of interviews with the Colaizzi method, about the experience of the husband who accompanied the wife with cervical cancer who are undergoing treatment.
Based on the results of interviews with participants, in get 5 themes of knowledge about cervical cancer disease where sub theme on this theme is the signs and symptoms of cervical cancer. The second theme is the psychological response where the sub themes in this theme are sad. The third theme is the source of motivation to cervical cancer patients, the theme is sub theme of emotional support from the husband and emotional support from the family. The fourth theme is the treatment effort, the theme is obtained sub theme is following doctor's instructions. The fifth theme is the hope of healing, obtained sub theme of spiritual hope. The 5 themes are:

Knowledge of cervical cancer
Signs and symptoms of cervical cancer
"If cervical cancer is first whitish, after whiteness ... After using KB is whitish, there are little spots like blood"
(P2,L4-7)
"At first my wife complained his stomach ache, keep coming whitish lot and smell, continue 10 days bleeding"
(P3,L4-7)
The first theme obtained in this study is the knowledge of the husband about cervical cancer is needed to be able to make decisions about what action will be done if his wife experienced signs and symptoms of cervical cancer that generally occur. In this research, the sub theme is the husband's patient explain the signs and symptoms of cervical cancer. Signs and symptoms that usually appear in patients with cervical cancer, among others, as follows: When the woman has an advanced stage will experience pain in the thigh or one of the thighs experience swelling, appetite becomes greatly reduced, unstable weight, difficult to urinate, and experience spontaneous bleeding. The results of this study are in line with research conducted by Rahayu, 2011. According Rahayu before the husband learned that his wife suffered from cervical cancer have found some signs and symptoms that appear related to cervical cancer, such as: bleeding outside sexual and also whiteness (Rahayu, 2011). According to the opinion of the researcher in this study obtained that the husband's knowledge about the signs and symptoms complained of by his wife caused different perceptions on each participant. In participants who have a good knowledge of signs and symptoms are complained will make a better reaction to check his wife to the nearest medical services otherwise if the husband's knowledge of the signs and symptoms complained of by his wife less will cause slow efforts to check his wife to the health care Thus resulting when it is known the results of the examination is known his wife is already in an advanced stage.

Psychological response

Sad

"Sad too that I feel seeing my wife's circumstances"

(P1,L275-276)

"My feeling is obviously sad to see the state of my wife at this time"

(P4,L32-34)

The second theme is the result of psychological response. Psychological response is the reaction of human behavior related to the environment, where here the environment in question is the relationship with the wife. On this theme sub theme obtained sadly expressed by the husband of cervical cancer patients. The sadness that arises in people who have the same problems can cause different reactions because the sadness is individual or personal. Sorrow is a natural thing experienced by someone who experiences an unpleasant event or event (Trisnantari, 2015). In addition, this study is also similar to research conducted by Wardani, 2014. According to Wardani the sadness experienced is influenced by several factors that is, because the disease suffered relapse again and never healed, felt the inconvenience of the family, separation with husband and child due to death (Wardani, 2014). According to the opinion of researchers in this study expressed the sad feeling experienced by the husband who was accompanying his wife with cervical cancer undergoing treatment that arises because the husbands do not bear to see the condition of his current wife.

Sources of motivation to cervical cancer patients

Emotional support from husband

"It's a problem so we must continue to support by giving spirit and we always damping"

(P1,L361-363)

“Keep providing support for the spirit of life, motivation, keep accompanying "

(P3,L76-78)

The third theme obtained results motivation sources to patients with cervical cancer. In this study obtained sub themes of emotional support from the husband and emotional support from the family. Participants in this study mentioned the motivation given by himself to the wife who suffered from cervical cancer in the form of emotional support. Motivation is a desire that is in an individual individual who encourages to perform actions, actions, behavior or behavior. Motivation is also interpreted as a stimulus of desire and the force of the will which causes a person to act or behave (Kusumantari, 2015). Research by Erfina, 2010 is similar to the research that researchers do is get the results of participants get support from people around like husband, child, family, neighbors and colleagues. Support obtained is in the form of emotional support (Erfina, 2010). In the opinion of the researcher the emotional support provided by the husband to the wife is very important because the husband is the person closest to the wife so that moral support or spirit given to his wife can grow his wife's spirit to heal.

Emotional support from family

"Yes all support, encourage and children also help what is told by mama, so all family very support mama in treatment"

(P1,L452-455)

"All participate in providing motivation, from children and also all of you participate in encouraging my wife"

(P4,L51-54)

In addition to this study participants also said his wife received emotional support from family and also the people closest. Support is in the form of encouragement and also motivation

provided by the family so as to grow the spirit of his wife in undergoing treatment performed. The family is the smallest unit of society that consists of the head of the family and some who are gathered and live somewhere under a roof in a state of interdependence. Family support is the attitude, action, and acceptance of the family to someone who is ill, in the form of information support, assessment support, instrumental support and emotional support (Murdiana, 2016). The results of this study are in line with research conducted by Sumetriani, 2015. According Sumetriani cervical cancer patients get good emotional support from their families, whether it's a big family of husband and extended family of the patient itself, so the growing spirit to heal (Sumetriani, 2015). In the opinion of the researchers in this study, the support of the family or the closest people is needed by the patient's husband and especially to the wife who suffered from cervical cancer that is useful to foster his spirit to undergo treatment and get healing.

Treatment efforts

Follow the doctor's advice

"The effort trying to find a drug, undergoing a doctor's order because what the doctor's order would be the best, whatever the doctor ordered for treatment undertaken, chemo yes chemo, finished chemo want what this ray yaa rays live"

(P3,L142-148)

"Efforts continue to seek to medicines continue to pray also ... the important thing pokonya my wife quickly recovered live whatever the doctor orders I do not know anything"

(P4,L91-92,L95-97)

The fourth theme is the treatment effort, in this theme obtained sub theme is following doctor's advice. The participant's statement in this study describes the efforts made by the husband accompanying the wife to undergo treatment. His current efforts are to follow the advice given by doctors in undergoing treatment. Health efforts are an effort to realize optimal health status for society, health efforts are carried out with maintenance approach, health promotion (promotif), prevention of disease (preventive), curative disease (curative), and health restoration (rehabilitative) (Hanafiah, 2008). The results of this study are in line with research conducted by Rahayu, 2011. According Rahayu participants prefer treatment with doctors, such as surgery, chemotherapy and radiotherapy or irradiation (Rahayu, 2011). According to the opinion of the researcher in this research explains that the effort done by husband is to follow all the instructions of doctor for treatment which is lived by his wife, the instruction in the form of drug delivery, surgery action and also chemotherapy.

Hope for healing

Spiritual hope

"Hope we will soon recover by trying as hard as possible that we can just, I try as much as possible for healing"

(P1,L565-568)

“Pingin my wife healed, quickly healed can be the best treatment, just what is instructed by my doctor to live "

(P3,L151-154)

The final theme is the hope of healing. Hope is a desire to achieve certain goals and coupled with the motivation. In this research, the sub theme is spiritual hope. Participants in this study expressed the wish they wanted to the wife who was undergoing treatment. Hope is a spiritual hope that his wife will recover quickly. Hope is known to help the individual in finding the meaning of the illness that is when individuals with cancer feel uncomfortable with symptoms of the disease he felt, the increased inability and fear of facing death. Hope can help the

individual to cope with discomfort, live life with illness and live life with power. Expectations relate to spiritual problems, if there are spiritual obstacles causing individuals to have low expectations and cause despair (Negari, 2015). The results of this study are also in line with research conducted by Sumetriani, 2015. According Sumetriani cervical cancer patients expect recovery after undergoing chemotherapy in order to reunite with his family at home. According to the opinion of researchers in this study explained that the husband expects his wife to recover quickly and get the best treatment. Hope is also supported by the husband's efforts to always accompany his wife to undergo treatment.

IV. Conclusions and Recommendations

Conclusion

The results of this study found 5 themes of knowledge about cervical cancer disease where sub theme on this theme is the signs and symptoms of cervical cancer. The second theme is the psychological response where the sub themes in this theme are sad. The third theme is the source of motivation to cervical cancer patients, the theme is sub theme of emotional support from the husband and emotional support from the family. The fourth theme is the treatment effort, the theme is obtained sub theme that is following the doctor's advice. The fifth theme is the hope of healing, obtained sub theme of spiritual hope.

Recommendations

Based on the results of research that has been done is expected to increase nursing care to patients and also expected health workers can provide emotional support and also information to increase hope and spirit of cervical cancer patients who are undergoing treatment.

The phenomenon of the experience of a husband accompanying a wife with cervical cancer who is undergoing treatment provides knowledge and also a different understanding of the experience he experienced. It is encouraging to develop nursing care in patients with cervical cancer who are undergoing treatment.

In this study researchers have difficulty in developing questions when conducting interviews with participants, so for further research is expected to develop this research with a wider coverage and use better interview techniques to get more accurate and interesting results.

References

[1]. Depkes. (2014). Hilangkan Mitos Tentang Kanker. http:/www.depkes.go.id/article/print/201407070001/hilangkan-mitos-tentang-kanker.html. Diakses 9 Februari 2017.

[2]. Dinas Kesehatan Provinsi Bali. 2013. Data Surveilans Terpadu Penyakit Tidak Menular. Denpasar: Dinkes Provinsi Bali

[3]. Erfina. (2010). Pengalaman Perempuan Setelah Menjalani Terapi Kanker Serviks. Jurnal Keperawatan Indonesia, Volume 13, No. 3.

[4]. Hanafiah, J. (2008). Etika Kedokteran & Hukum Kesehatan. Jakarta: EGC.

[5]. Kusumantari, P. N. (2015). Hubungan Tingkat Pengetahuan tentang Vaksinasi Kanker Serviks dengan Motivasi Remaja dalam Melaksanakan Vaksinasi Kanker Serviks. Skripsi. Program Studi Ilmu Keperawatan STIKes Wira Medika PPNI Bali.

[6]. Murdiana, I. K. (2016). Hubungan Antara Dukungan Keluarga Dengan Kepatuhan Diet Pada Pasien Gagal Ginjal Kronik Uang Menjalani Hemodialisa. Skripsi. STIKes Wira Medika PPNI Bali.
[7]. Negari, N. K. (2015). Pengalaman Pasien Kanker Serviks yang Menjalani Kemoterapi. Skripsi. Program Studi Ilmu Keperawatan STIKes Wira Medika PPNI Bali.
[8]. Rachmawati, Y. A. (2014). Metodologi Penelitian Kualitatif dalam Riset Keperawatan. Jakarta: Rajawali Pers.
[9]. Rahayu, T. (2011). Studi Fenomenologi Pengalaman Suami dengan Istri yang Mengalami Kanker Serviks di Wilayah Jakarta. Tesis. Depok: Fakultas Ilmu Keperawatan Program Magister Ilmu Keperawatan Universitas Indonesia Depok.
[10]. Shosha, G. A. (2012). Employment of Colaizzi's Strategy in Descriptive Phenomenology : A Reflection of a Researcher. European Scientific Journal, vol. 8, No. 27.
[11]. Sumetriani, N. L. (2015). Pengalaman Pasien Kanker Serviks yang Menjalani Kemoterapi di Ruang Angsoka II RSUP Sanglah Denpasar. Skripsi. STIKes Wira Medika PPNI Bali.
[12]. Trisnantari, P. (2015). Pengalaman Istri Infertil yang Mengalami kegagalan Mengikuti Program Bayi Tabung. Skripsi. STIKes Wira Medika PPNI Bali.
[13]. Wardani, E. K. (2014). Respon Fisik dan Psikologis Wanita dengan Kanker Serviks yang Telah Mendapat Kemoterapi di RSUD Dr. Moewardi Surakarta. Skripsi. Fakultas Ilmu Kesehatan Universitas Muhammadiyah Surakarta.
[14]. Widiantara, I. K. (2016). Hubungan Dukungan Keluarga terhadap Motivasi pada Pasien Kanker Serviks yang Menjalani Kemoterapi di Ruang Angsoka II RSUP Sanglah, Skripsi. Program Studi Ilmu Keperawatan STIKes Wira Medika PPNI Bali.

Section 4
Agricultural Engineering and Food Science

Integrated Sci-Tech :
Interdisciplinary Research Approach
Volume 3

Isolation and Characterization of Formacell Lignins from Oil Empty Fruits Bunches (#594)

Sri Hidayati[1,a], A. Sapta Zuidar[1], Wisnu Satyajaya[1], Murhadi[1], Dian Retnowati[1]
[1]Departement of Agriculture Technology, Lampung University
Prof. Soemantri Brojonegoro Street, No. 1 Bandar Lampung, Lampung 35145
[a]hidayati_thp@unila.ac.id

Abstract. *Lignin is a largest component in black liquor, it is about 46% of solids total and can be isolated by precipitation using acid and base method. The purpose of this study are to get the best NaOH concentration to produce lignin with yield, solids total content, metoxyle lignins content, weights equivalent of lignin in the black liquor by pulping formacell process from oil empty fruits bunches. This study was done with isolation lignin process in black liquor used by NaOH concentration were 5%, 10%, 15%, 20%, 25%, and 30% from volume black liquor and then precipitationed for 10 hours. The result of this research showed the isolation of lignin with NaOH concentration 30% get the pH 5,42%, yield of lignin are 5,67%, solids black liquor total are 65,11%, levels of metoxyle lignin 14,61%, and equivalent weights of lignin are 1787,23. The result of FT-IR identifications of isolates lignin in NaOH concentration 25 and 30% showed a pattern infiltration spektro IR that almost a part that have the same infiltration at the wave numbers that shows lignin have one of the rings lignin is guaiasil, it is building blocks of non wood lignin.*

Keywords: *lignin, black liquor, lignin isolation, NaOH concentration*.

I. Introduction

Black liquor is dark liquid from byproduct of the process that transforms wood into pulp, which is then dried to make paper. Black liquor contains lignin, which is the material in trees that binds wood fibers together and makes them rigid, and which must be removed from wood fibers to create paper. Black liquor is a problem in the pulp and paper industry because it is highly polluting the environment (Rodriguez-Mirasol *et.al*., 1996; Zhang and Chuang, 2001), and the rejection of this effluent in nature without any treatment is responsible for serious damage to the environment and constitutes a threat for human health (Lara *et al*., 2003). The black liquor consists of almost all the inorganic chemicals used in pulping and organics in the form of dissolved wood constituents (Louhelainen *et al*., 2002). Lignin in the black liquor, is a mixture of polyphenolic compounds with complex chemical structure that resists to conventional biological treatment processes due to their non-biodegradable nature (Helmy *et al*., 2003; Zaied and Bellakhal, 2008). The presence of dark colored lignin cause s limiting ligh trasmission in aquatic plants (Panchapakesan, 1991). Lignin in black liquor also contains aliphatic acids, acids, resins and polysaccharides increase the burden of oxygen demand in water (Mahesh *et al*., 2006). Component of black liquor is lignin which is about 46% of its total

solid (Sjostrom, 1995), therefore isolation and separation of lignin is more likely. Black liquor can be a source of lignin feedstock (Abdelwahab and Nassar, 2011; Alonso *et al*., 2004; Khan *et al*. 2004b .; Mankar *et al*., 2012 Sarkar and Adhikari, 2001; Tejado *et al*., 2007; Zhang *et al*., 2013c). Lignin structure and physico chemical properties depends on isolation method and raw material source (Glasser *et al*., 1983; Glasser and Kelley, 1987; Bykov, 2008; Sahoo *et al*., 2011). Black liquor can be isolated alkaline method or acid method to obtain pure lignin. The research trend is an attempt to harness lignin into more useful chemicals (Angles *et al*., 2003). Commercial use of lignin maybe used carbon fiber, adhesive, polyurethane, polyester, bioplastic, and bio oil for petroleum mixtures of fossils (Bonini *et al.,* 2005; Kleinert and Barth, 2008; Xu *et al*., 2006; Alonso *et al*. , 2004; Tejado *et al*., 2007). The presence of phenolic ring inside lignin can be utilized for phenolic formaldehyde resins (Abdelwahab and Nassar, 2011; Alonso *et al*., 2004; Cheng *et al*., 2013; Khan *et al*., 2004b; Mankar *et al.,* 2012). Beside lignin can be used as a filler and reinforcing phases for polymer blends (Cazacu *et al*., 2004; Gosselink *et al*., 2004c; Hatakeyama *et al*., 2005; Kadla *et al*., 2002; Lora and Glasser, 2002; Reza Barzegari *et al* , 2012; Schorr *et al*., 2014). The advantage of lignin is to have a high number hidroxyl group can be used for the production of polyol and either through direct utilization or after chemical modification for the production of certain polymers such as polyurethane (Cateto *et al*., 2008; Huang and Zhang, 2002; Mahmood *et al*., 2013).

In the world it is attempting to utilize black liquor as a source of lignin feedstock (Min *et al*., 2013). Some lignin isolation methods include: 1). Klason Method; 2). The Björkman method is also called "Milled Wood Lignin / MWL"; 3). CEL Method, Cellulolythic Enzyme Lignin or "lignin of cellulolytic enzymes"; 4). Technical Lignin Isolation Method, namely the lignin isolation method of residual pulp liquor (Guerra *et al*., 2006). The process of lignin isolation from black liquor can use acids such as H_2SO_4, phosphoric acid (H_3PO_4), or HCl (Li, 2011; Vishtal and Kraslawski, 2011). While the basic method can use bases such as NaOH and KOH (Setyawardhani, 2014). In this step about 75% of the lignin is precipitated as the sodium salt. Finally, lignin is separated through a screening process (Vishtal and Kraslawski, 2011). Lignin hydrolysis contains solid lignin residues and large amounts of unhydrolyzed cellulose (Vishtal and Kraslawski, 2011).

The characterization of softwoods and hardwoods black liquor from the pulping of non-wood fibers such as reed canary grass, sugarcane baggasse, wheat straw have been investigated lately (Lora & Escudero, 2000; Baudel *et al*., 2005; Feng *et al*., 2001). However, none works had been done on the black liquor from black liquor formacell EOFB pulping process. Formacell is one of the organosolved pulping methods that use acetic acid and formic acid as cooking solution (Poppius *et al*., 1991; Jiménez *et al*., 1998; Lam *et al*., 2001; Kham *et al*., 2005a,b; Hidayati *et al*, 2017). The pressure and temperature can be lower when formic

acid is used in pulping compared to those used in alcohol or acetic acid pulping. The advantage of organic acid lignin is an optimal feedstock for many value-added products, due to its lower molecular weight and higher reactivity (Kubo *et al*., 1998; Cetin and Ozmen, 2002) and organic acid pulping is the retention of silica on the pulp fiber that facilitates the efficient recovery of cooking chemicals (Seisto and Poppius, 1997).

Sun *et al*. (1999) and Ibrahim and Chuah (2004) reported that only concentrated on lignin isolation from oil palm black liquor and minor on characterization of lignin. Kraft Black liquor from EOFB resulted optimum lignin precipitation was obtained at pH 2 and comparably result could be obtained at pH 4.5 followed by 1 hour heating (Nie, 2008) by addition of anthraquinone (AQ) in the pulping process showed an improved carbohydrates stabilization and better delignification. Cheng *et al* (2007) have use NaOH extraction in order to obtain lignin for use production of polyurethane. The aim of this research is to know the effect of NaOH concentration in isolation process and lignin characterization on the formacell black liquor from empty palm oil bunches. The use of NaOH in the isolation process can be used to precipitate lignin from black liquor.

II. Materials and Methods

A. Raw material

The materials used in this research are black liquor from EOFB formacell pulping, NaCl, NaOH, HCl, water, aquades, ethanol, KBr, filter paper, phenolpthalin indicator, aluminum foil, and clip. The tools used in this research are acid cabinet, acid stove, aluminum cup, digital scales, porcelain cup, oven, desiccator, beaker glass, erlenmeyer, pH meter, dropper drop, volume pipette, stirrer, measuring cup, Funnel, centrifuge, stirrer, titration device and FT-IR (Fourier Transform Infra-Red Spectroscopy) spectrophotometer and SEM (Scanning Electron Microscopy)

B. Research methods

This research begins with the process of purifying liquid waste from pulp filtration (black liquor) by using lignin isolation method which refers to isolation method developed by Lubis (2007) as shown in Figure 1. A total of 100 ml of filtered black liquor (filtrate) Precipitated lignin by stirring and adding by NaOH with concentrations of 5%, 10%, 15%, 20%, 25%, and 30% (percent v / v) of black liquor volume which then homogenized using a stirrer. Stirring process is done slowly then measured pH of each treatment, then subsequently settled for 10 hours for perfect deposition. The lignin deposit is separated from black liquor using centrifuge (2500 rpm, 20 min). The observations were: pH value, total solids content in black leachate EOFB, lignin yield, lignin methoxyl content, lignin equivalent weight, and lignin analysis with FT-IR

spectrophotometer and Scanning electron microscopy (SEM) has been most useful technique for quantification of lignin structural details.

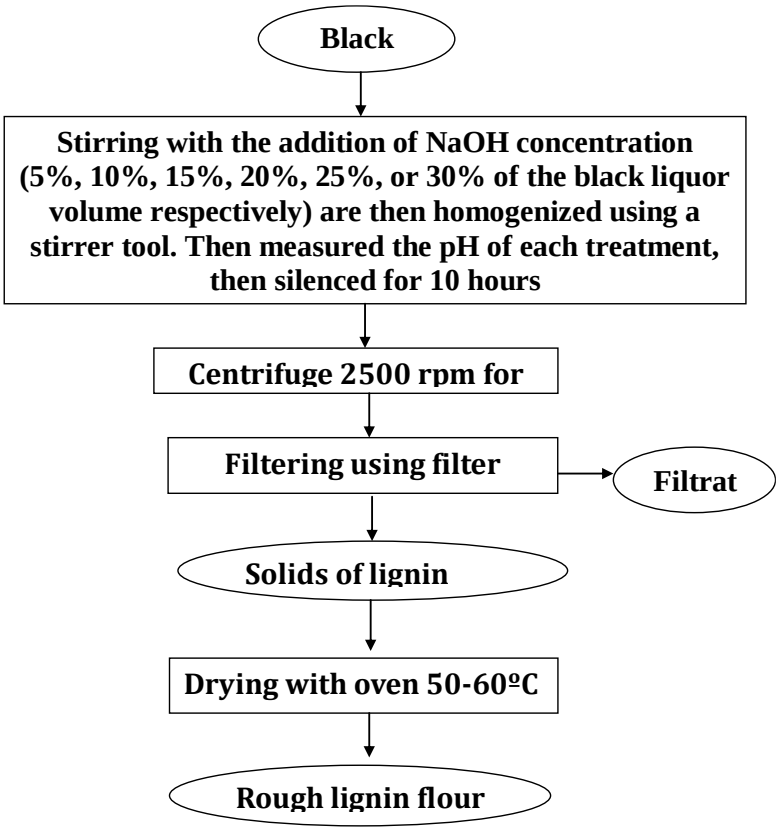

Figure 1. The modified lignin isolation diagram (Source: Lubis (2007)

III. Results and Discussion

Yield of Lignin

The yield was also found to increase for black liquor with a higher total dry solid (TDS) content (Zhu and Theliander, 2015). The average value of lignin isolate content from various concentrations ranged from 1.48% - 5.67% (Figure 2). The result of variance analysis showed that the NaOH concentration teatment had highly significant effect on yield of lignin.

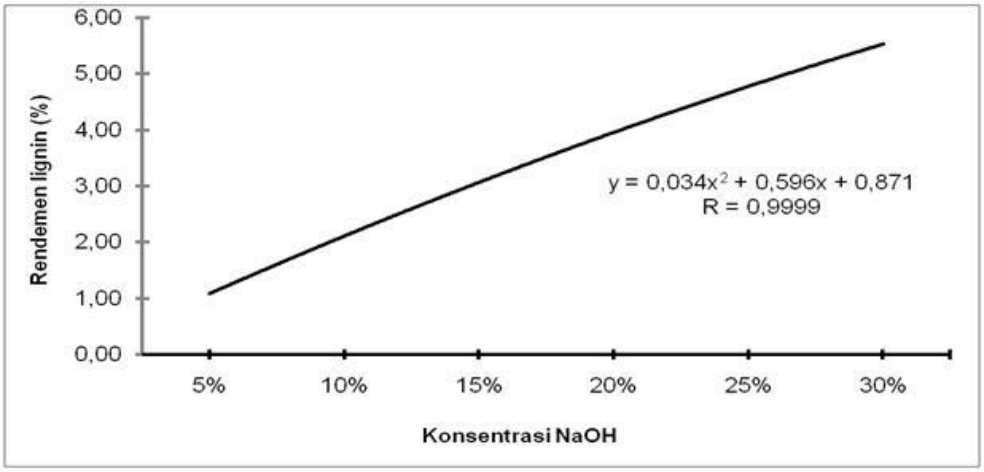

Figure 2. Effect of NaOH concentration on lignin yield

The coagulation of lignin from black liquor occur because the protonation of ionized phenolic group on the lignin molecul. The protonation of phenolic group reduces the electristatic repulsive forces between lignin molecules (Sundin, 2000, Vainio *et al*, 2004) which then become less hydrophylic, leading to precipitation. The highest yield of lignin isolate was found at 30% NaOH concentration with an average of 5.67%. The yield of precipitated activated lignin was influenced by NaOH concentration (Vasileva, *et al*, 2007). According to Heradewi (2007), the yield of isolate lignin due to the influence of addition factor of NaOH concentration give effect to yield yield of lignin isolate. Theliander (2010); Zhu *et al*, (2013) according on how yield/equilibrium in the precipitation step of lignoboost process is influenced by diferrent proces condition, i.e, the pH, temperatur and ion strength of black liquor). In this study showed that the yield of lignin isolate tended to increase according to the addition of NaOH concentration as lignin sedimentation solution. The increase of lignin isolate content in the deposition process using NaOH with concentration of 5%, 10%, 15%, 20%, 25%, and 30%, due to the more basic precipitation process where the higher the NaOH concentration the higher the level of base, It is suspected that there is an increasing condensation reaction in the lignin-making units such as para-koumaril alcohol, coniferyl alcohol, and sinapyl alcohol, which will initially undergo repolymerization and form larger molecules of lignin polymer. In the opinion of Lin (1992), the higher the concentration, the higher the lignin deposits produced. It is suspected that because of the higher concentration of added NaOH, the OHO ions are consumed by acetyl groups of wood shale during cooking, so the OH^{-} ion not only dissolves lignin but dissolves other non-lignin components (Heradewi, 2007). In this study, the highest lignin precipitate was obtained at an average pH of 5.42 with a 30% NaOH concentration. Increasing the concentration of NaOH results in an increase in pH value due to the addition of base or high alkalinity of the substance increases many OH-ions in water. The greater the pH

value of a substance the stronger the degree of base The strength of base can be determined from the scale of basicity which is also expressed by pH value (Setyawardhani, 2014).

Lignin Methoxyl Levels

Methoxyl lignin content in this study has an average value ranges between 14.61 - 20.77% (Figure 3). The result of variance analysis showed that the NaOH concentration treatment had very significant effect on lignin methoxyl content.

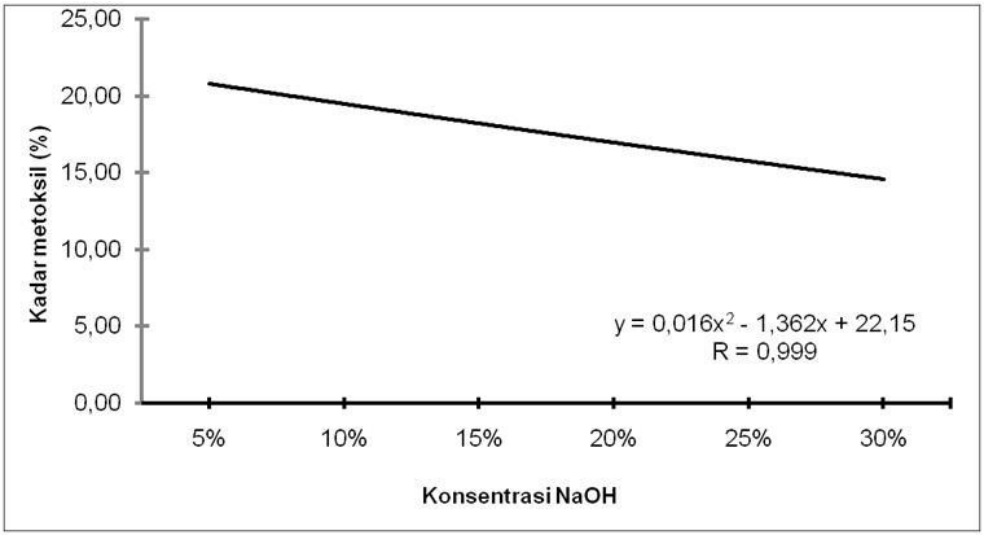

Figure 3. Effect of NaOH concentration on methoxyl lignin levels

The highest levels of methoxyl lignin are present in the addition of 5% NaOH concentration with an average of 20.77%. While the lowest methoxyl lignin levels were found in the addition of 30% NaOH concentration with an average of 14.61%. In general, high methoxyl levels will inhibit lignin reactivity during resin use. Lignin contains phenolic hydroxyl groups which are mostly bonded with adjacent propane phenyl units, allowing the occurrence of lignin bonds with formaldehyde similar to those of a reaction between phenol and formaldehyde (Syahmani, 2000). However, in its use as a raw material of lignosulfonate (surfactant), lignin with high methoxyl content is more advantageous because the more -OCH 3 groups contained in lignin, the lignin is increasingly dissolved in water. Such properties are indispensable to lignosulfonate feedstocks.

Meanwhile, low methoxyl levels are suspected because some of the methoxyl groups are degraded and turned into other compounds due to the overuse of acid or base. In alkaline process, phenolic hydroxyl groups are generated by hydrolysis of β-O-4 bond (Zhao and Ouyang, 2012). According to Kirk and Othmer (1952), low metoxyl levels are caused by changes in methoxyl groups to methyl mercaptan, methyl sulfide, and dimethyl disulfide.

According to Fengel and Wegener (1995), this low metoxyl value is probably caused by the influence of harsh chemicals during isolation, causing the lignin structure to undergo many changes. According to Damat (1989), low lignin methoxyl levels can be utilized in their use as an adhesive, lignin with a lower methoxyl content is more advantageous than high methoxyl levels, since lignin with low methoxyl content is easier to form gel.

Lignin's Equivalent Weight

The average value of the lignin equivalent weight ranges from 1327.64 - 1787.23 (Figure 4). The result of variance analysis showed that the NaOH concentration treatment had very significant effect on the weight of lignin equivalent.

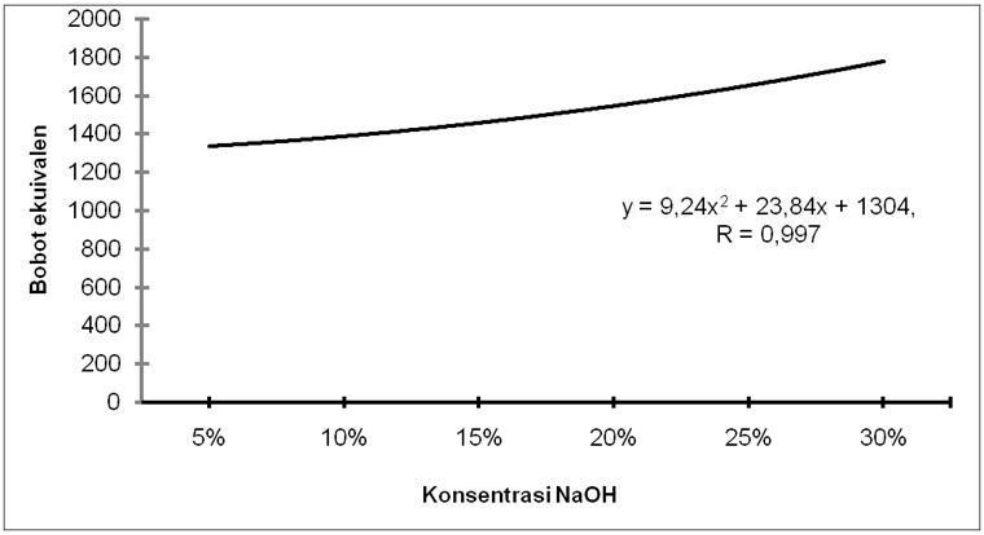

Figure 4. Effect of NaOH concentration on lignin equivalent weight level

At 30% NaOH concentration yields the highest weight of lignin equivalent weight with an average of 1787.23. Meanwhile, the lowest equivalent weight was generated in isolation condition using 5% NaOH concentration with an average of 1327.64. The higher the NaOH concentration as the settling solution, causing the higher lignin equivalent weight. The higher the equivalent weight of a lignin indicates that in lignin insulation, the polymerization proceeds perfectly. In addition, according to Achmadi (1990), the more basic concentrations used at the time of isolation cause lignin to tend to condensate. The condensed lignin composing units form larger molecules so that the weight of the lignin equivalent is increased. The high equivalent weight of EOFB lignin isolates is caused by the lignin structure of EOFB fibers more complex than the lignin structure extracted from the wood. This is due to the complex arrangement of siringil and guaiasil propane units with para-koumaril propane units in EOFB

fibers. The standard molecular weight is unknown but is a multiple of 840, the molecular weight of the lignin-making unit (Casey, 1952). Zhu (2013) states the results show that the precipitation yield of lignin increases with decreasing pH and temperature and/or with increasing ion strength of kraft black liquor used. The concentration of carbohydrates in lignin decreases with decreasing pH or with increasing temperature, and that an increasing amount of lower molecular weight lignin is precipitated at a higher precipitation yield. This principle is similar to the lignin isolation process using NaOH . According to Santoso (2003), the distribution of molecular weight of lignin varies greatly. Lignin is a very complex organic compound, composed of a number of highly variable constituent components, it is difficult to obtain definite molecular weights. According to Connors *et al*. (1978) by means of chromatographic separation obtained data of lignin molecule weights range of 370-44300. While the results of research Santoso (2003) states the molecular weight of lignin isolates from black liquor ranged from 304-4010. Based on the equivalent weight obtained in this study, it meets the criteria based on according to Connors *et al*. (1978) and Santoso (2003).

Lignin Analysis with FT-IR Spectrophotometer

The following is the result of lignin analysis using FT-IR spectrophotometer, using the best sample that is the addition of 25% NaOH concentration is presented in Figure 5 and the addition of 30% NaOH concentration is presented in Figure 6. FTIR was performed to analyze the differentes in the functional groups of the different lignin samples obtained (Namane *et al*, 2016). The FTIR spectrum of commercial kraft lignin (Indulin AT) was utilized as reference.

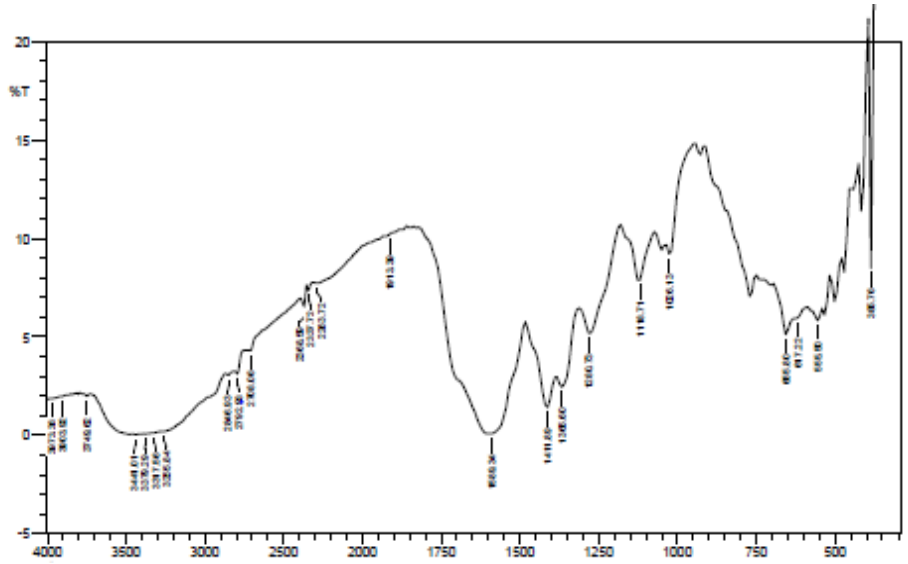

Figure 5. Results of identification with FT-IR spectrophotometer on lignin isolates from EOFB formacell black liquor results in the addition of NaOH concentration of 25%

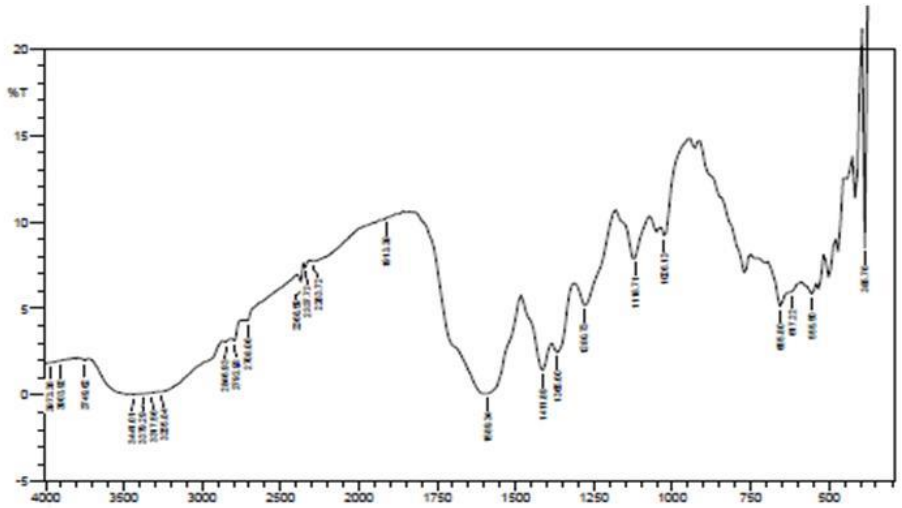

Figure 6. Results of identification with FT-IR spectrophotometer on lignin isolates from EOFB formacell black liquor results in addition of 30% NaOH concentration

Table 1. Fourier transform infrared of two lignin samples

No	Lignin isolate NaOH 25%	Lignin isolate NaOH 30%	Indulin-AT	Band Posistion (cm-1)*)	Assigment
1	3441.01		3411.36	3450-3400	OH stretch
2	2846.93		2936.36	2940-2820	OH strain on the methyl and methylene groups
3	-		-	1715-1710	The C = O range is unconjugated with an aromatic ring
4	-		1668.18	1675-1660	The C = O range is unconjugated with an aromatic ring
5	-		1602.27	1605-1600	Vibration of aromatic rings
	1589.35	1573.91		1595	Aromatic sceletal vibration, C=O stetching (conjugated)
6	-		1511.36	1515-1505	Vibration of aromatic rings
7	-		1465.91	1470-1460	C-H deformation (asymmetry
8	-		1427.27	1430-1425	Vibration of aromatic rings

9	1365.60		1365.91	1370-1365	In-plane deformation vibration of phenolic OH
10	-		-	1330-1325	Vibration of siringyl ring
11	1273	1273.03	1270.45	1270-1275	Vibration of guaiacyl rings
12	-		1031.82	1085-1030	Deformation of C-H and C-O
	1026.13	1026.13		1030	C-O of syringyl and guaiacyl ring, C-H bond in guaiacyl ring

*) Source: Hergert (1971) and Zhu (2013).

The best isolation conditions were lignin isolates with 25% and 30% NaOH concentrations. The lignin isolates were compared with the standard lignin used ie lignin indulin-AT. The purpose of the functional group analysis is to know the functional groups present in lignin from the isolated and standard lignin products used. The two bands at 2900 cm-1 and 2800 cm-1 correspond to methyl (−CH3) and methylene (−CH2) groups. The phenolic OH groups in lignin (band at 1365 cm-1), are produced during chemical process when β-O-4 linkages are cleaved and generate non-etherified hydroxyls. Low intensity of this band in NaOH 30% spectrum shows that small portion of phenolic OH group is generated (due to less β-O-4 linkage cleavage). The intensity of absorption bands at 1268 cm-1 (C-O stretching of guaiacyl ring) spectra is stronger than other lignins because guaiacyl is dominant lignin unit in EOFB. The absorption band range 1030-1025 cm-1 is assigned to deformation vibration of C−H bonds in the guaiacyl ring and also assigned to C-O bonds in both syringyl and guaiacyl (Zhu,. 2013). Bands at 1330-1325 cm-1 were attributed to syringil with C-O stretching. Bands at 1217 cm-1 for OPEFB can be attribute to phenolic OH and ether in syringil and guaiacyl (Lubis *et al,* 2012). The bands observed at 1030-620 cm-1 were attributed to hemicelluloses and silicates contribution (Garcia *et al*, 2009).

Lignin is a complex polymer synthesized mainly from three hydroxycinnamyl alcohols differing in their degree of methoxylation: *p*-coumaryl, coniferyl, and sinapyl alcohols (Higuchi, 1997; Boerjan *et al*., 2003; Ralph *et al*., 2004a). Each of these monolignols gives rise to a different type of lignin unit called *p*-hydroxyphenyl (H), guaiacyl (G), and syringyl (S) units, respectively, when incorporated into the polymer. Lignin is a polymer of phenolic hydroxyl groups, hydroxyl benzylic and carbonyl groups. The lignin polymer contains characteristic methoxyl groups, hydroxyl phenol groups, and some end-aldehyde groups in the side chain (Sjostrom, 1995). The presence of absorption bands at wave numbers with a strong intensity

of about 1.270-1330 cm-1 in lignin isolates resulting from black liquor of this organosolve delignification process with a 30% NaOH concentration suggests the presence of one of the lignin ligands, ie guaiasil which are the units Lignin constituents in non-wood lignin.

Assessment of the structure of OPFEB formacell lignin

The Scaniing Electrom Miscoscope (SEM) studies revealed the details on structural and marfologies of lignin. Lignin was analyzed by using SEM that is lignin with treatment of NaOH concentration that is 5% and 30% (Figure 7).

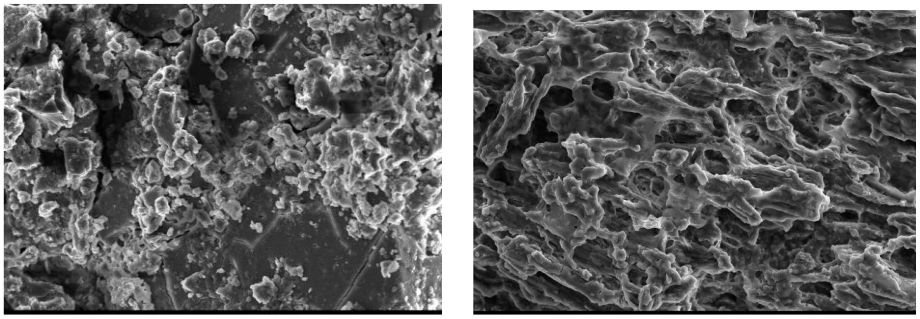

(a) (b)

Figure 7. SEM migrographs of lignin samples (a) isolation by 5% NaOH, (b) isolation by 30% NaOH

The result of SEM analysis showed that lignin isolation treatment using 30% NaOH concentration had a more compact form of agglomeration compared with isolation using 5% NaOH. At the high pH of typical kraft black liquof, the repulsive forces between the ionized hydrophilic groups (mainly phenolic hydroxyl and carboxylate groups) stabilize the colloidal lignin and keep it in solution, thereby preventing lignin agglomeration and precipitation (Herman, 1984). The results of Namane *et al* (2016) showed that the lignin isolation process from liquor derived from formacell produces a constant granular structure.

IV. Conclusion

Based on the research that has been done can be concluded that The best lignin isolates were on lignin deposition with 30% NaOH concentration by total solids content in EOFB black liquor, lignin of yield, lignin methoxyl content, lignin equivalent weight, The average lignin yield is 5.67%, the total solid black liquor with an average of 65.11%, the lignin methoxyl content with an average of 14.61% and the weight of the lignin equivalent with an average of 1787.23.. The result of FT-IR identification from lignin isolate at 30% NaOH concentration shows IR

spectral absorption pattern which almost most have the same absorption pattern at wave number region. Isolates of lignin at a 30% NaOH concentration showed that lignin has one lignin ring ie guaiasil which is lignin composing units in non-wood lignin.

V. Acknowledgment

This research work was supported by Fundamental Research Grant 2017, No. 071/SP2LH/LT/DRPM/IV/2017. The authors would also like to acknowledge the contributions and financial support from Ministry of Research, Technology, and Higher Education of the Republic of Indonesia.

References

[1] Achmadi, S.S. (1990). Wood Chemistry. Department of Education and Culture. Directorate General of Higher Education. Inter-University Center. Life Sciences. Bogor Agricultural Institute. Bogor.

[2] Abdelwahab, N., Nassar, M., (2011). Preparation, optimisation and characterisation of lignin phenol formaldehyde resin as wood adhesive. Pigment & Resin Technology 40, 169-174.

[3] Alonso, M.V., Oliet, M., P rez, .M., Rodr guez, F., Echeverr a, J. (2004). Determination of curing kinetic parameters of lignin–phenol–formaldehyde resol resins by several dynamic differential scanning calorimetry methods. Thermochimica Acta 419, 161-167.

[4] Anglès, M.N., Reguant, J., Garcia-Valls, R., Salvadó, J. (2003). Characteristics of lignin obtained from steam-exploded softwood with soda/anthraquinone pulping. Wood Science and Technology 37, 309-320.

[5] Bonini, C., M. Auria., L. Emmanuel., R. Ferri., R. Pucciarello, and A.R. Sabia. (2005). Polyutrethanes and Polyester from Lignin. Journal Applied Polymer Science, 98 (3): 1451-1456.

[6] Boerjan W, Ralph J, Baucher M. (2003) Lignin biosynthesis. Annu Rev Jornal of Plant Biology, 54: 519–546

[7] Bykov, I. (2008). Characterization of Natural and Technical Lignins using FTIR Spectroscopy. PhD thesis, Lulea University of Technology.

[8] Casey, P. (1980): Pulp and Paper Chemistry and Chemical Technology. Third Edition, Vol 1. Wiley Interscience Publication.

[9] Casey, P.J. (1952). Pulp and Paper, Chemistry and Chemical Technology Vol. 1: Pulping and Paper Making. The Wiley Intersince Publisher, Inc., New York.

[10] Cazacu, G., Pascu, M.C., Profire, L., Kowarski, A.I., Mihaes, M., Vasile, C. (2004). Lignin role in a complex polyolefin blend. Industrial Crops and Products, 20, 261-273.

[11] Cheng, S. (2011). Bio-Based Phenolic Resins And Adhesives Derived From Forestry Residues/Wastes And Lignin. Disertation. Faculty of Natural Resources Management Lakehead University Thunder Bay, Ontario, Canada

[12] Cateto, C.A., Barreiro, M.F., Rodrigues, A.E., Brochier-Solan, M.C., Thielemans, W., Belgacem, M.N. (2008). . Lignins as macromonomers for polyurethane synthesis: A comparative study on hydroxyl group determination. Journal of Applied Polymer Science 109, 3008-3017.
[13] Cheng, S., Yuan, Z., Leitch, M., Anderson, M., Xu, C. (2013). Highly efficient de-polymerization of organosolv lignin using a catalytic hydrothermal process and production of phenolic resins/adhesives with the depolymerized lignin as a substitute for phenol at a high substitution ratio. Industrial Crops and Products 44, 315-322.
[14] Connors, W.J, L.F. Lorenz and T.K. Kirk. (1978). Chromatographic Separation of Lignin Models by Molecular Weight using Sepandhex LH-20. Holzforschung 31.
[15] Damat. (1989). Isolation of Lignin from Cooking Solution by Pulp Factory Using H2SO4 and HCl. (Essay). Department of Agricultural Industrial Technology, Faculty of Agricultural Technology, Bogor Agricultural University.Bogor. 3 p.
[16] Fengel. and G. Wegener. (1984). "Wood: Chemistry, Ultrastructure, Reactions" de Gruyter, Berlin, Pp. 1-729. X111, 613 S. ISBN 3-11-008481-3.
[17] Garcia, A. A. Toledano, L. Serrano, I. Egues, M. Gonzalez, F. Marin, and J. Labidi. (2009). "Characterization of lignin obatain by selective precipitation", *Separation and Purification Technology*, vol. 68, pp. 193-198.
[18] Gosselink, R.J.A., Abächerli, A., Semke, H., Malherbe, R., Käuper, P., Nadif, A., van Dam, J.E.G. (2004). Analytical protocols for characterisation of sulphur-free lignin. Ind. Crop. Prod. 19, 271–281.
[19] Hatakeyama, H., Nakayachi, A., Hatakeyama, T. (2005). Thermal and mechanical properties of polyurethane-based geocomposites derived from lignin and molasses. Composites Part A: Applied Science and Manufacturing 36, 698-704.
[20] Huang, J., Zhang, L. (2002). Effects of NCO/OH molar ratio on structure and properties of graft-interpenetrating polymer networks from polyurethane and nitrolignin. Polymer 43, 2287-2294.
[21] Heradewi. (2007). Lignin Isolation from Black Leafy Process of Organosolv Bunching of Cluster Fibers Empty Palm Oil (EOFB). (Essay). Bogor Agricultural Institute. Bogor. 109 p.
[22] Hergert, H. L. (1971). Infrared Spectra. Willey Interscience, New York. 267-297.
[23] Hermans, M. A. (1984). High intensity black liquor oxidation, PhD. Thesis, Law rence University,
[24] Hidayati, S. Zuidar, A.S and Satjaya, W. 2017. Effect Of Acetic Acid: Formic Acid Ratio On Characteristics Of Pulp From Oil Palm Empty Fruit Bunches (OPEFB). ARPN Journal of Engineering and Applied Sciences, 12(12): 3802-3807
[25] Higuchi T. (1997) Biochemistry and Molecular Biology of Wood. Springer-Verlag, London
[26] Jimenez, L., F. Maestre, J.L. Ferrer, and I. Pérez. (1998). Delignification of wheat straw by use of low-molecularweight organic acids. Holzforschung 52 (2):191–196.
[27] Kadla, J.F., Kubo, S., Venditti, R.A., Gilbert, R.D. (2002). Novel hollow core fibers prepared from lignin polypropylene blends. Journal of Applied Polymer Science 85, 1353-1355.
[28] Kadla, J. F., Kubo, S., Venditti, R. A., and Gilbert, R. D. (2002). Novel hollow core fibers prepared from lignin polypropylene blends. J. Appl. Polym. Sci. 85, 1353–1355. doi:10.1002/app.10640
[29] Khan, M.A., Ashraf, S.M., Malhotra, V.P. (2004a). Development and characterization of a wood adhesive using bagasse lignin. International Journal of Adhesion and Adhesives 24, 485-493.

[30] Khan, M.A., Ashraf, S.M., Malhotra, V.P. (2004b). Eucalyptus bark lignin substituted phenol formaldehyde adhesives: A study on optimization of reaction parameters and characterization. Journal of Applied Polymer Science 92, 3514-3523.
[31] Kirk R.E. And D.F. Othmer. (1952). Encyclopedia of Chemical Technology. Vol.3. The Interscience Encyclopedia, Inc., New York. Pp.327-338
[32] Kleinert, M. and T. Barth. (2008). Towards in Lignicellulosic Biorefinery: Direct One Step Conversion of Lignin to Hydrogen-Enriched Biofuel. Energy Fuels. Vol. 22 (2): 1371-1379.
[33] Lam, H.Q., Bigot, Y.L., Delmas, M., and Avigon, G. (2001). Formic acid pulping of rice straw. Ind. Crops Prod., 14(1): 65-71.
[34] Li, J. (2011). Isolation of lignin from wood, BSc thesis, Faculty of Technology. SAIMAA University of applied science, USA.
[35] Lora, J.H., Glasser, W.G., 2002. Recent industrial applications of lignin: A sustainable alternative to nonrenewable materials. J. Polym. Environ. 10, 39-48.
[36] Lin, S.Y. and W.D. Carlton. (1992). Methods in Lignin Chemistry. Berlin Heidelberg: Springer-Verlag. 69: 627-642.
[37] Lora J. H., Glasser W.G. (2002). Recent industrial applications of lignin: A sustainable alternative to non renewable materials. J.Polym. Environ. 10(1-2), 39-48.
[38] Louhelainen, J., Alen, R., Zielinsk i, J., and Sagfors, P. E. (2002). "Effects of oxidative and non -oxidative thermal treatments on the viscosity and chemical composition of softwood kraft black liquor," Journal of Pulp and Paper Science 28(9), 285 -291
[39] Lubis, A.A. (2007). Lignin Isolation from Black Linde (Black Liquor) Pulp Cooking Process Soda and Pulp Sulphate (Kraft). (Essay). Bogor Agricultural Institute. Bogor. 81 p.
[40] Lubis, M.A.R, A.R Dewi , L Risantoa, LH Zaini, E Hermiatia. (2012). Isolation and Characterization of Lignin from Alkaline Pretreatment Black Liquor of Oil Palm Empty Fruit Bunch and Sugarcane Bagasse. *Mechatronics, Electrical Power, and Vehicular Technology XX . XX-XX* 2. 1-5 p.
[41] Mankar, S., Chaudhari, A., Soni, I., (2012). Lignin in phenol-formaldehyde adhesives International Journal of Knowledge Engineering 3, 116-118.
[42] Mahmood, N., Yuan, Z., Schmidt, J., Xu, C. (2013). Production of polyols via direct hydrolysis of kraft lignin: Effect of process parameters. Bioresource Technology 139, 13-20.
[43] Namane,M; García-Mateos F.J., Sithole, B; Ramjugernath, D; Rodríguez-Mirasol, J And Cordero, T. Characteristics of Lignin Precipitated with Organic Acids as A Source for Valorisation of Carbon Products. Cellulose Chemistry and Technology. Vol. 50 (3-4: 355-360
[44] Poppius –Levlin, K., Mustonen, R., Huovila, T., and Sundquist, J. (1991). Milox pulping with acetic –acid . paperi ja Puu-Paper Timber., 73(2): 154-158.
[45] Ralph SA, Ralph J, Landucci L. (2004) NMR Database of Lignin and Cell-Wall Model Compounds. U.S. Forest Products Laboratory, Madison, WI: http://ars.usda.gov/Services/docs.htm?docid=10491 (July 3, 2006)
[46] Santoso, A. (2003). Synthesis and Establishment of Lignin Resolsinol Formaldehyde Resins for Adhesives Lamina Wood. Dissertation. Post Graduate Program, Bogor Agricultural University, Bogor.
[47] Schorr, D., P. N. Diouf, and T. Stevanovic. (2014). “Evaluation of industrial lignins for biocomposites production”, *Industrial Crops and Products*, vol. 52, pp. 65-73.

[48] Setyawardhani, D. A. (2014). Practical Guidelines for Quantitative Chemistry Analysis. Surakarta.
[49] Sahoo, S., Seydibeyoğlu, M.Ö., Mohanty, A.K., Misra, M., (2011). Characterization of industrial lignins for their utilization in future value added applications. Biomass and Bioenergy 35, 4230-4237.
[50] Sarkar, S., Adhikari, B. (2001). Jute felt composite from lignin modified phenolic resin. Polymer Composites 22, 518-527.
[51] Schorr, D., Diouf, P.N., Stevanovic, T. (2014) . Evaluation of industrial lignins for biocomposites production. Industrial Crops and Products 52, 65-73.
[52] Sun, R.R., Tomkinson, J.J., Lloyd Jones, G.G. (2000). Fractional characterization of ash-AQ lignin by successive extraction with organic solvents from oil palm EFB fibre. Polymer Degradation and Stability 68, 111-119.
[53] Sjostrom, E. (1981). Wood Chemistry, Fundamentals and Applications, Academic Press, New York, 223 p.
[54] Syahmani. (2000). Isolation, Sulfonation and Lignin Acetylation of Oil Palm Bunches and Studies Its effect on Urea Dissolution Process. (Thesis). Faculty of Mathematics and Science, Bandung Institute of Technology. Bandung.
[55] Sundin, J. (2000). *Precipitation of kraft lignin under alkaline conditions.* Ph.D thesis, Royal Institute of Technology, Stockholm, Sweden.
[56] Tejado, A., Pena, C., Labidi, J., Echeverria J.M. And I. Mondragon. (2007). Physico-chemical characterization of lignins from different sources for use in phenol-formaldehyde resin synthesis. Bioresource Technol. 98: 1655-1663
[57] Theliander, H. (2010). The LignoBoost process: Solubility of lignin. International Chemical Recovery Conference 29th March - 1st April 2010 Williamsburg, VA, USA. 33-42.
[58] Vainio, U., Maximova, N., Hortling, B., Laine, J., Stenius, P., Simola, L. K., Gravitis, J. & Serimaa, R. (2004). Morphology of Dry Lignins and Size and Shape of Dissolved Kraft Lignin Particles by X-ray Scattering. *Langmuir,* 20**,** 9736-9744.
[59] Vasileva, T, S. Nenkova, K. Stanulov. (2007). Obtaining of Phenolic Compounds through Alkaline Depolymer-ization of Technical Hydrolysis Lignin, Cellulose Chem. Technol., 41, 7-8:379-384.
[60] Vishtal, A. And Kraslawski, A. (2011). Challenges in industrial applications of technical lignins. BioRes. 6, 3547–3568.
[61] Xu, F., Sun, J.-X., Sun, R., Fowler, P., Baird, M.S. (2006). Comparative study of organosolv lignins from wheat straw. Ind. Crops Prod. 23, 180–193.
[62] Zhang, A.P., Liu C.F., Sun R.C and Xie, J. (2013). Extraction, purification and characterization of lignin fractions from sugarcane bagasse. Bioresources. 8 (2): 1604-1641.
[63] ZHU, W. (2013). Equilibrium of Lignin Precipitation The Effects of pH, Temperature, Ion Strength and Wood Origins. THESIS. Forest Products and Chemical Engineering Department of Chemical and Biological Engineering Chalmers University Of Technology Gothenburg, Sweden.

Characteristics of Retrograded Purple Sweet Potato Flour and Its Physiological Function on Healthy Mice (#626)

Siti Nurdjanah[1,a], Neti Yuliana[1], Nurul Yudaningsih[1], Sihol Marito Br Limbong[1]
[1]Department of Agricultural Product Technology, Faculty of Agriculture, University of Lampung, Bandar Lampung, Indonesia 35145
[a]siti.nurdjanah@fp.unila.ac.id

Abstract. *Modified purple sweet potato flour is very potential to be developed as a main diet for people with obesity and diabetes mellitus. Preparation of modified flour was done by retrogradation processed through partial gelatinization and followed by storing of the flour at 5°C for 24 hours so that the flour contains high level of resistant starch. The aims of this research were to modified starch of purple sweet potato flour through retrogradation, and then investigate the effect of using purple sweet potato flour with a high content of resistant starch as the main diet or rations on blood sugar level, body and faeces weight healthy mice. The experiment consisted of two treatments: the provision of ration standard on healthy mice, provision of ration with the addition of resistant starch rich-purple sweet potato flour on healthy mice. The parameters observed were the blood sugar levels, body weight, and faeces. The results showed that rationing of resistant starch rich-purple sweet potato were able to normalize blood sugar levels, maintained the body weight, and increased the feces weight of healthy mice.*

Keywords*: mice, purple sweet potato flour, resistant starch*

I. Introduction

Local variety of purple sweet potato contains appreciable amount of phenolic anthocyanin (Nurdjanah et al., 2017) which is very potential to be used as sources of food coloring and bioactive compound that benefit to health; however it has not been exploited optimally. Purple sweet potato may be processed in to flour to prolong its shelf life and to widen its uses. The predominant content of the flour is starch. The in vitro digestibility of the starch has been reported to be high which lead to high glycemic index (GI) (Yu et al., 2015). This high GI might not be favorable not only to people who suffer from diabetes, and obesity but also healthy people (Bjork and ASP, 1994). Therefore it is important to modify the starch properties primarily its resistibility for digestion as well as to preserve the bioactive compound in order to utilize it as novel food ingredients. The aim of this study were to investigate the effect of retrogradation on digestibility and physicochemical properties of the purple sweet potato flour, and to investigate its physiological function on healthy mice.

II. Materials and Methods

Materials

A-amylase activity of 30U/mg and glucoamylase activity of 70 U/mg were purchased from Sigma (St. Louis, MO, USA), other reagents were purchased from commercial sources. Local variety purple sweet potatoes (PSP), harvested 120 days after planting, were obtained from Seedling Farm, Agriculture Training Center Lampung**.**

Preparation of retrograded purple sweet potato flour (PSPF)

Freshly harvested PSP were washed under running tap water and grated using a food chopper. The grated PSP was heated in a an electric oven equipped with a single rotary drum to at 90 °C for 30 min, cooled at room temperature, then stored at 5 °C for 48 h. The cold-stored shredded PSP were dried in an oven (Memmert) at 60 °C for 8 hrs to achieve moisture content of 10%, then ground using a hammer mill (FCT Z500, Ramesia) and sieved to pass 80 mesh siever, stored in a sealed plastic bag until further analysis.

Determination of resistant starch (RS) content

The content of RS in the flour was determined according to Association of Official Analytical Chemists (AOAC) methods 2002.02 (AOAC, 2002). The starch in the samples were digested by actions of α-amylase and glucosidase for 16 h at 37°C. The reaction was stopped by adding ethanol 96% and then centrifuged to recover the RS. The RS was dissolved in KOH (2 M) and neutralized with acetate buffer, hydrolyzed with glucosidase, and the resulted glucose, which is a measure of RS was quantified using phenol-sulphuric acid method (Dubois et al., 1956).

Total Anthocyanin

Total content of anthocyanin was quantified using the colorimetric pH-differential method described by Lee et al. (2005) using two buffer systems: potassium chloride buffer, pH 1.0 (0.025 mol/L) (125 mL of 0.2 mol/L KCl and 375 of 0.2 mol/L HCl) and sodium acetate buffer, pH 4.5 (0.4 mol/L) (400 mL of 1 mol/L sodium acetate, 240 mL of 1 mol/L HCl and 360 mL of water) with minor modification . One mL of extracted PSP flour was diluted in 4 mL of each buffer to achieve the absorbance readings at 520 nm or at 700 nm between 0.2 and 0.8. The diluted samples were allowed to stand for 15 min at the dark room before the absorbance was read at 520 and 700 nm using a GENESYS UV-Visible spectrophotometer, with distilled water used as the blank.

Anthocyanin pigment concentration is expressed as cyaniidin-3-glucoside equivalents as follows:

$$\text{Anthocyanin pigment (cyanidin-3-glucoside equivalentsmg/L)} = \frac{A \times MW \times DF \times 1000)}{\epsilon \times l}$$

Where:

A is the absorbance of the sample calculated as: $(A_{520} - A_{700})_{\text{pH 1.0}} - (A_{520} - A_{700})_{\text{pH 4.5}}$

MW is the molecular weight for cyanidin - 3- glucoside (449.2g/mol).

DF = is the dilution factor

ϵ is the molar absorbance of cyanidin-3-glucoside (26900L/(cm x mol)

l is cell path length (1 cm), and
1000 is the conversion factor from g to mg

Scanning Electron Microscope (SEM)Analysis

Retrograded PSPF granule micrographs were acquired using FEI SEM type Inspect S50, EDAX AMETEK. Sample powder was placed in a double-sided carbon taped holder, then coated with Au-Pd using sputter coater (Emitech SC7620). The micrographs were obtained with an accelerating voltage of 10.00 kV.

Animal experiments

Six-week old male mice were purchased from the Veterinary Laboratory Center of Lampung. All animal experiments were conducted in accordance with the guideline for animal welfare . Mice were maintained in cages (10 mice in each cage) in an environmentally controlled room at 25±2°C and 70±5% relative humidity with 12 h light/dark for one week, fed with local commercial diet (bought from a local Pet shop) for acclimation. After acclimating, the mice were randomly divided into two groups as follows: the normal control died and the diet containing retrograded PSPF-treated. Mice in each group were given diet as shown in Table 1. The blood glucose levels were measured from tail vein blood by the Glucose meter, the body weight of the mice were taken for measurement each week for 4 weeks, whereas the faeces were collected for 24 , at day 12, 13 and 14.

Table 1. Composition of the diet

	Diet	
Composition	Control	Diet containing retrograded PSPF
Casein	0. 9	0.19
Cellulose	0.05	0.05
Corn Starch	0.49	-
RS rich PSPF	-	0.49
Corn Oil	0.18	0.18
Sucrose	0.05	0.05
Mineral Mix	0.035	0.035
Vitamin Mix	0.01	0.01

Source: Report of the American Institute of Nutrition Adhoc Committee on Standards for Nutritional Studies (1977) with minor modification

Statistic Analysis

Results were presented as the mean ± standard deviation.

III. Results and discussion

The chemical composition of retrograded PSPF are shown in Table 2,

Table 2. The chemical composition of retrograded PSP Flour

Composition	Content*
Moisture (%)	7.20 ± 0.15
Ash (%)	2.20 ±0.32
Protein (%)	2.72 ±0.22
Fat (%)	0.82 ± 0.12
Carbohydrate (%)	87.06 ± 0.45
Resistant starch (%)	31.89 ± 0.23
Anthocyanin (mg/100 gram)	78.00 ± 0.40

*Values are means of 3 replications ± std

SEM results

Scanning electron micrographs of native , gelatinized and retrograded PSPF showed structural differences. Native flour contains starch granule which are round, spherical and surrounded by cell wall material (Figure 1a). While in gelatinized PSPF the granular characteristic partly changed (Fig 1b) and become bigger and less structured (Figure 1c), and retrograded PSPF became more compact. The change in granular structure may lead to the changes in starch functional properties and physiology function when starch is used for food non food and pharmaceutical purposes.

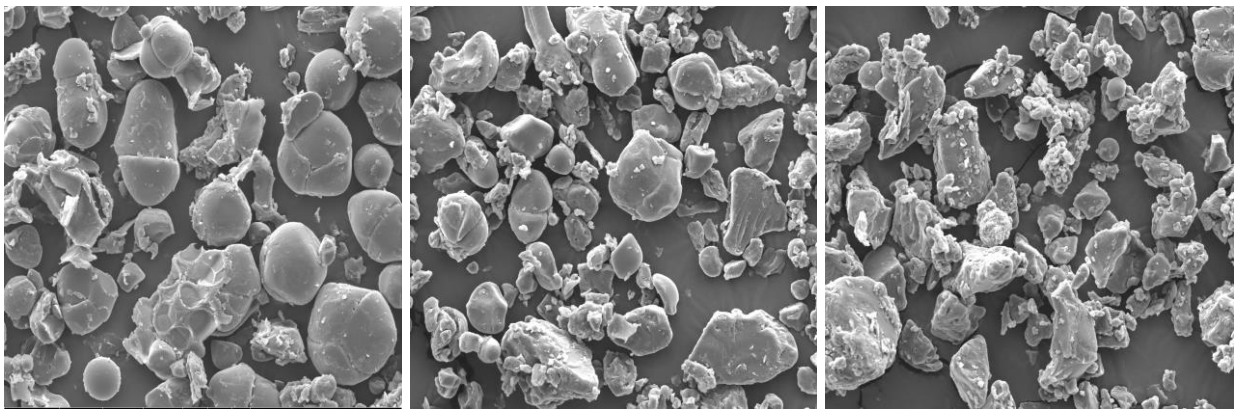

a. Original PSP F b. Gelatinized PSPF c. Retrograded PSPF

Figure 1. SEM appearance of PSPF granule

Blood glucose levels and body weight after acclimation

The functional retrograded PSPF was examined to find its effect on the blood glucose levels of the mice. The retrograded PSPF contained resistant starch 31.8%, whereas the corn starch contained in the standard diet was not detected. During the first three weeks, non-fasting glucose levels in PSPF containing diet were slightly higher compared to those in

the standard diet. However, in week 4 and 5, the blood glucose levels in PSPF group were almost 50% lower than those in standard group (Figure. This indicates that retrograded PSPF containing diet may prevent the rise in blood glucose of healthy mice , probably by the mechanism of suppressing insulin resistant development.

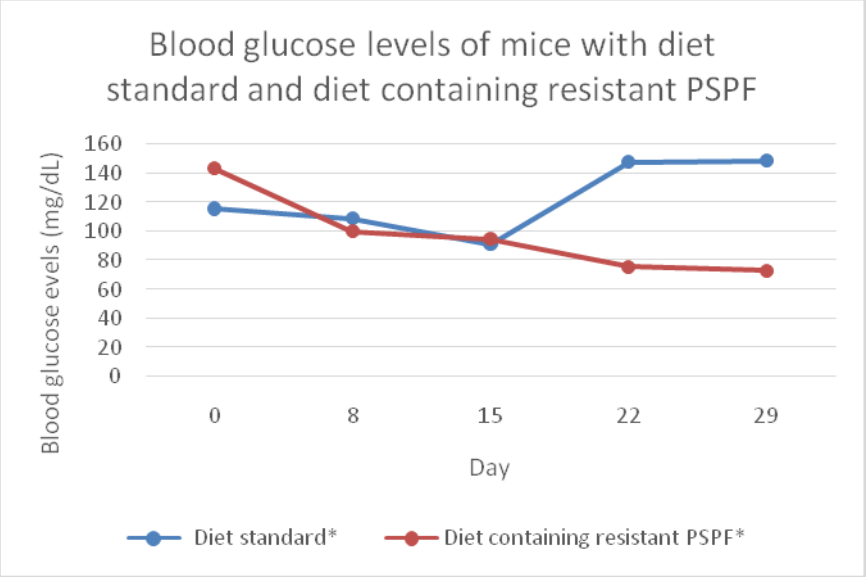

Figure 2. Blood glucose levels of mice fed with diet standard and diet containing retrograded PSPF

Body weight

During the experiment it was observed that the body weight of mice in the two groups decreased from 38.8 g (initially) to 18.3 g at day 29 in the standard group, and from 34.2g to 21.8 g in PSPF group (Figure 3); However the decrease was lower in the PSPF group. This suggest that resistant starch contained in the retrograded PSPF may help stabilize lipid absorbtion in the body.

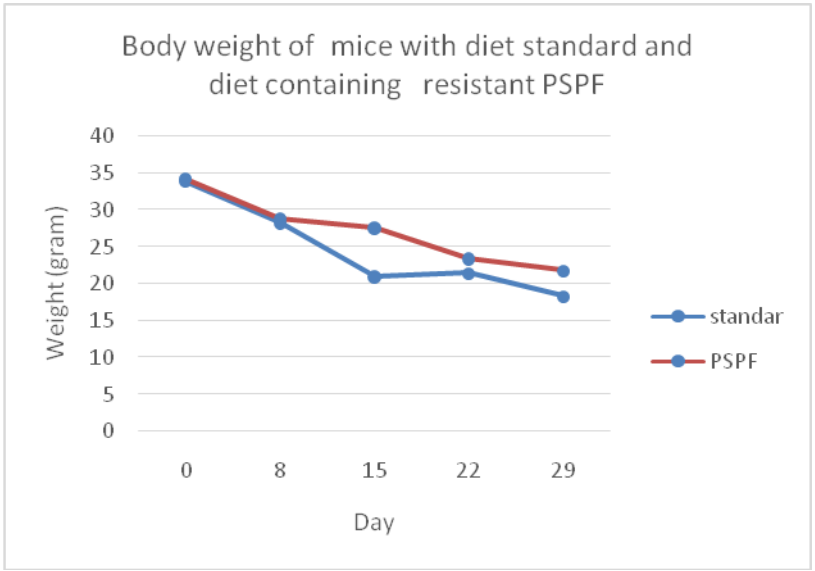

Figure 3. Body weight of mice of mice fed with diet standard and diet containing PSPF

Faeces weight and texture

The results showed that the faeces in standar group was 0,247413 g/ day , whereas those in PSPF group was 0,311393 g/day (Figure 4). This indicates that the inclusion of retrograded PSPF into the diet had increased the faeces as much as 25,86 % . In addition the faeces of the mice in two groups appeared difference. Mice faeces in standard group was soggy , whereas those in PSPF group was more homogen in shape and firmer texture. (Figure 5), this was due to higher fiber content in PSPF compared to those in standard diet.

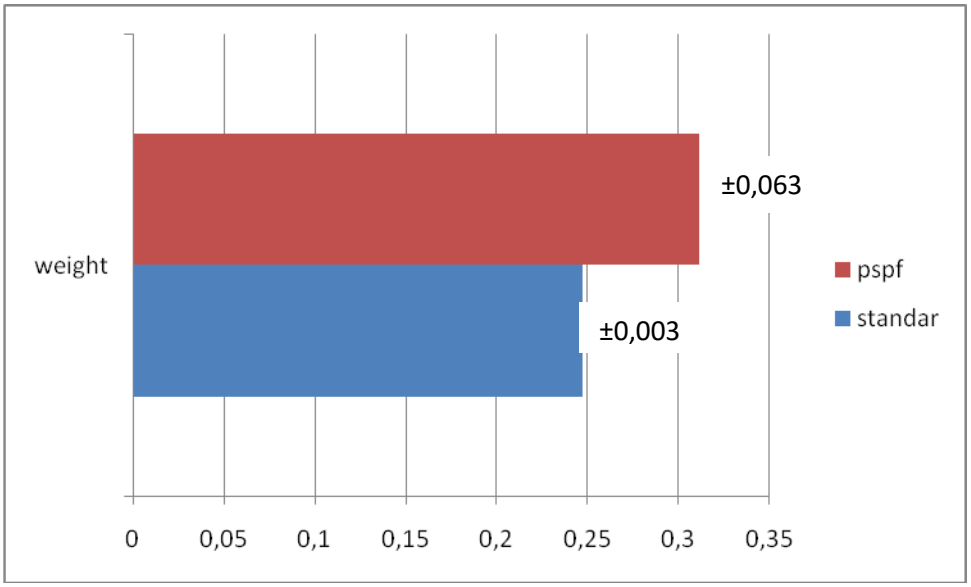

Figure 4. The weight of the mice faeces in diet standard group and diet containing retrograded PSPF.

(a) standard (b) PSPF

Figure 5. Appearance of mice faeces

IV. Conclusions

Inclusion of retrograded purple sweet potato flour into the diet has the beneficial effects in maintaining blood glucose level, body weight, blood , increase faeces weight. It can be expected that retrograded purple sweet potato flour can be use as novel food ingredients with functional properties.

Acknowledgements

The authors would like to thank to The Ministry of Research , Technology and Higher Education of The Republic of Indonesia for funding this project.

References

[1]. Association of Official Analytical Chemists (AOAC). 2002. Official methods of the association official analytical chemists.

[2]. Bjorck, I., and Asp, N.G., 1994. Controlling the nutritional properties of starch in foodsA challenge to the food industry. Trends Food Sci. technol. 5:213-218

[3]. Dubois, M., Gilles, K.S., Hamilton, J.K., Rebers, P.A., and Smith, F. 1966. Colorimetric method for determination of sugars and related substances. Analytical Chem. 28(3):30-356.

[4]. Yu, S-X., Mu, T-H., Zhang, M., and Zhao, Z-K. 2015. Effects of retrogradion and further acetylation on the digestibilityod physicochemical properties of purple sweet potato flour and starch. Starch/*Stärke* 67:892-902.

[5]. Lee, J., R.W. Durst and R.E. Wrolstad. 2005. Determination of total monomeric anthocyanin pigment content of fruit juices, beverages, natural colorants, and wines by the pH differential method: Collaborative Study. J. of AOAC Int. 88(5): 1269-1278.

[6]. Nurdjanah, S., Yuliana, N., Astuti, S., Hernanto, J., and Zukryandry, Z. 2017. Physico chemical, antioxidant and pasting properties of ,re-heated purple sweet potato flour. Journal of Food and Nutrition Sciences. 5(4):140-146. doi:10.11648j.jfns.

Characteristics of Lactic Sweet Corn Milk Drink: Effect of Complementation with Soy Milk (#642)

Neti Yuliana[1], **Marniza**[1], **Hermin Triasih**[1]
[1]Department of Agricultural Product Technology, Faculty of Agricuture, University of Lampung
Sumantri Brojonegoro no 1 Bandar Lampung, Indonesia

[a]neti.yuliana@fp.unila.ac.id

Abstract- *The purpose of this study was to determine the best soy milk complementation ratio on the characteristics of sweet corn lactic milk drink, fermented with Lactobacillus casei FNCC 0090 for 72 hours, which met criteria of lactic drink and essential amino acids fulfillment. The soybean complementation formula consisted of five levels in such an away to obtain the ratio of sweet corn milk : soybeans milk as followed 1: 3; 1: 2 (F2); 1: 1 (F3); 2: 1 and 3: 1. The best treatment was obtained from soybean milk complementation of 1 part and corn milk of 3 parts. This best drink had reducing sugar content of 39.05 mg /100ml; total lactic acid bacteria of 8.43 logs cfu/ml; total acid of 1.31%; pH value of 4.11; with the color, taste, aroma and overall acceptance score closed to 5 (like slightly). In addition, based on the score of amino acids, this lactic sweet corn-soy milk drink was able to over come the deficiency of three essential amino acids (methionine, cysteine and lysine).*

Keywords*: sweet corn lactate milk, soy milk supplementation*

I. Introduction

weet corn, also called sugar corn, is a variety of maize with high sugar content. Sugars observed in sweet corn are glucose, fructose, maltose, and sucrose1,2 with sucrose as the dominant component in the amount of 15.90-40.5 %2 depending on variety. Apart of sugars, sweet corn is a source of complex carbohydrate, proteins, and vitamins, especially vitamin A 400 IU per 100 grams3. Corn protein has relatively good essential amino acid composition, except for tryptophane and lysine4,5, contains bioactive such as α-zein, which is a component of corn protein endosperm 6. Sweet corn is also a source of carotenoids: lutein and zeaxanthin2. In terms of having very delicate kernel skin and kernels, sweet corn meets the requirements of the fruit and vegetable processing industry because of easy to separate from the cobs 1. Sweet corn, therefore has the advantage of composition as raw material of corn milk drink , a potentially protein-rich drink which can be used as a substitute milk for lactose intolerant and favored by panelists 7,8,9 as well as for probiotic drink10

Development of corn milk into probiotics drink through lactic acid bacteria fermentation would imply to corn milk not only as a source of protein but also as a functional food. Lactic acid bacteria (LAB) play a major role in determining the positive health effects of fermented milk and related products. They can improve lactose digestion, play a role in preventing and treating diarrhea and act on the immune system, helping the body to resist and fight infection11. Production of functional milk product of corn probiotic is possible because corn contains good carbon source for fermentation of lactic acid bacteria. Sweet corn contains 58-6.98 % fructose, 1.52-5.13% glucose and 15.70-40.05% sucrose1,2.

To produce high nutritious corn milk drinks with balanced amino acids, complementing with a high protein source of lysine is required. Corn protein is considered deficient in the essential amino acids of lysine4.5. Soy bean is good in lysine but deficient in methionine and cysteine 3. Thus, complementation with soybean offers nutritional advantages in producing high nutritious protein drinks with balanced amino acids 12, 7,13. Nevertheless, some studies also reported that the ratio of soy milk and corn milk affects the characteristics of final blending product14, 15, therefore, fermented drink making from corn-soy milk would also be challenging to be investigated. The objective of this study was to determine the best soy milk complementation ratio on the characteristics (physical, chemical, microbiology, and acceptability) of sweet corn lactic milk drink, fermented with Lactobacillus casei FNCC 0090 for 72 hours, which met criteria of lactic drink and essential amino acids fulfillment. The sweet corn –soy mixed probiotic milk drink with Lactobacillus casei FNCC 0090 as a culture may result in different product characteristics. The culture of Lactobacillus casei FNCC 0090 has been proven to be probiotic and widely applied to milk drinks 16,17, 18.

II. Material and Method

A. Materials

The main raw materials of sweet corn and soybeans, and additional raw material of skim milk (Calci scim) were obtained from local supermarkets in Bandar Lampung. Lactobacillus casei FNCC 0900 culture was obtained from Interagency Center of Food and Nutrition University, UGM, Yogyakarta. Materials for fermentation medium were MRS (De Mann Ragosa Sharp) Broth and MRS Agar.

B. Preparation of Starter

A one ose of the stock culture of Lactobacillus casei FNCC 0900 was transferred into the test tube containing sterile broth medium (10 ml), and subsequently incubated for 48 hours at 37°C. This broth culture (4%) was then inoculated into 100 ml solution containing 10% sterilized skimmed milk and was incubated at 37°C for 48 hours. The ready-working starter was prepared by transferred 4% of this starter into 100 mL of broth containing 10% (w/v) skim milk and 3% (w/v) glucose, and was incubated for 24 h at 37 ° C to obtain 107cfu/ml culture.

C. Sweet Corn Milk Preparartion.

Sweet corn kernels were blanched for 15 minutes then was blended (40 seconds) with a ratio of 10: 1(water: sweet corn). This slurry was then filtered using a filter cloth to obtain sweet corn milk. At the same time, soy milk production was made in the same way as corn milk making. The corn milk and soy milk were then mixed according to the formulation of (w/w) 3: 1 (F1), 2: 1 (F2), 1: 1 (F3), 1: 2 (F4) and 1: 3 (F5).

D. Fermentation of Sweet Corn-Soy Milk

Sweet corn-soy milk was put into a bottle and then a skim milk as much as 10% (v/v) was added. The mixture was stirred uniformly, pasteurized using a Sharp microwave for 15 minutes at medium speed and was then cooled to 37°C. The sweet corn-soy milk was then inoculated with a ready to use of culture starter with a concentration of 3% (v/v) and incubated at 37 °C for 48 hours. Evaluation of product was performed on reducing sugar 19,, total lactic acid bacteria 20, total acid and pH 21, organoleptic test 22. The quantitative amino acids analysis was only performed for the best sensory product.

E. Statistical Anaysis

This study was performed in a complete randomized block design, one factor of complementation formulation with five replications. Complementation formulation between sweet corn and soybeans milk consisted of five ratio levels: 1: 3 (F1), 1: 2 (F2), 1: 1 (F3), 2: 1 (F4) and 3: 1 (F5). ANOVA was used to know the effect of treatments, and when there were significant differences, the data were then analyzed by using the smallest real difference (LSD) test at 5% level of signification.

III. Results and Discussion

A. Physico-Chemical Characteristic, Lactic Acid Bacteria (LAB) of Sweet Corn-SoyMilk

The characteristics of sweet corn-soy milk at the beginning of fermentation are presented in Table 1. The reducing sugar of all treatments showed sufficient quantities for the initiation of lactic acid fermentation, ranging from 37.47-39.05 mg / 100mL or close to 4%

Table 1. Characteristics of sweet corn-soy milk at the beginning of fermantation

Treatments	Reducing sugar (mg/100 mL)	TA (%)	pH	Total LAB (log cfu/mL)
F5 (3:1)	39.05	0.25	6.84	7.76
F4 (2:1)	38.87	0.23	6.84	7.76
F3 (1:1)	38.66	0.22	6.85	7.76
F2 (1:2)	38.21	0.22	6.85	7.76
F1 (1:3)	37.47	0.23	6.85	7.76

Table 2. Characteristic of sweet corn-soy milk after 72 hours fermentation.

Rasio of sweet con milk: soy milk	Reducing sugar (mg/100 ml)	TA (%)	pH	Total LAB (log cfu/mL)
F5 (3:1)	38.41	1.31	4.11	8.43
F4 (2:1)	38.29	1.19	4.13	8.40
F3 (1:1)	38.11	1.13	4.15	8.38
F2 (1:2)	37.80	1.06	4.16	8.37
F1 (1:3)	37.20	1.01	4.18	8.28

Table 3. Changes of the physicochemical properties of sweet corn -soy milk

Ratio of Sweet corn milk: soy milk (v/v)	Reduction of reducing sugar (mg/100 mL)	Increases of TA (%)	Deacrease of pH	Increases of Total LAB (log cfu/mL)
F5 (3:1)	0,65a	1,05a	2,73a	0,67a
F4 (2:1)	0,58ab	0,96ab	2,71ab	0,64a
F3 (1:1)	0,55ab	0,91ac	2,71ac	0,62a
F2 (1:2)	0,41b	0,85bc	2,69bc	0,61a
F1 (1:3)	0,27c	0,78c	2,68c	0,52b

The numbers followed by the same letter in a single column mean no significant difference at the level of 5% with LSD test.

The total acid of all treatments was low, so the pH was close to neutral (6.84-6.85). Total LAB of the initial fermentation was 7.76 log CFU/mL. After 72 hour fermentation, the characteristic of sweet corn-soy milk was changed as presented in Table 2. In general, the characteristics (pH, total acid, and total LAB count) of fermented sweet corn-soy milk produced in this study were not significantly different compared to lactic beverages of similar research15,14, 23. In addition, based on SNI (Standar Nasional Indonesia) no 7552, in year of 2009, fermented milk drinks have at least 1x106 CFU/ml of lactic acid bacteria. This implies that these sweet corn-soy lactic milk products have already met the characteristics of lactic fermented drink.

The ratio of corn and soybean milk significantly affected the change of reducing sugar, pH, TA and total LAB of sweet corn-soy milk. The pattern of the characteristic change showed that higher complementation of soy milk caused lower reducing sugars, total LAB, and TA, and finally increased the pH of the corn-soy milk. This was possibly attributed to the different availability of nutritional components among F2, F1 with F3, F4, and F5. Irmler et al. (2008)24reported that Lactobacillus casei possesses the enzyme that able to degrade cysteine and methionine. Corn is a good in methionine, while soybean is low in methionine. Thus, the higher the soybean complementation in the formula, the lower the methionine content in milk, thus the lower the methionine availability. Therefore, in the ratio with higher soybean content (F1), the change in the amount of LAB and residual reducing sugar content became low; likewise, the total acid change was also low. The consequence of this was the final pH of the F1 treatment was higher than others ratio

B. Sensory Characteristics of Lactic Sweetcorn-Soy Milk

Sensory of lactic sweet corn-soy milk drink is presented in table 4. There was a significant effect of soy milk complementation on the sensory characteristics of lactic sweet corn-soy milk. Higher complementation of soy milk caused decreases of likeness score on the color, aroma, taste and overall acceptance. More addition of soy milk caused to decrease the yellowish white color (F5, F4, and F3) to white color (F2 and F1). A total of 75% of panelists describes the color of sweet corn milk of yellowish white. This color was attributed to presence of zeaxanthin and lutein which are the main pigments in corn2..

In addition to color, flavor and aroma were also an important factor that determined the preferences of this milk drink. Panelists tended to prefer the F5 (3: 1) and F4 (2: 1) in which

the corn milk was dominant component. This formulation had higher total acid and total LAB, thus the aroma and flavor formed were also better than those in F1 (1: 3) and F2 (1: 2). For the overall acceptance, panelists judged the F5 (3: 1) samples as the most preferred sample, and all ratio of lactic sweet corn-soy milk has met the criteria of lactate drinks in general. It is, therefore, all samples of lactic sweet corn-soy milk had already met the standard of flavor and aroma of fermented milk drink based on SNI 7552: 2009. A total of 73% of panelists judged the taste and aroma of lactic sweet corn-soy milk were sweet acids. Most of the panelists describe this product had typical lactic drinks (90% panelist), although 10% of the panelists noted there was soy smell. Nevertheless, during fermentation, the aroma of soy has been reduced as the effect of organic acids that improved flavor

C. Amino Acid Level on Best Sensroy of Lactic Sweet Corn-Soy Milk

From the sensory aspect, the F5 (3: 1) was the best acceptance with a higher score on the color, taste, aroma and overall acceptance. Therefore, the F5 formulation was chosen to be further analyzed on amino acid content, and the results are presented in Table 5. There was an increase of lysine, methionine and cystine score of amino acid in lactic corn-soy fermented milk.. This indicated that blending of soy milk as raw material for fermented corn-soy milk was able over come to the deficiency of amino acid in both corn milk and soy milk. Corn has a deficiency of lysine 5,3, 4, mean while soybean lack of methionine and cysteine3

Table 4. Sensory of lactic sweet corn-soy milk drink

	Ratio of corn milk: soy milk formulation				
Sensory	F1 (1:3)	F2 (1:2)	F3 (1:1)	F4 (2:1)	F5 (3:1)
Color	4.74c	4.56b	5.01a	4.92a	4.91a
Taste	4.23bc	4.16c	4.36b	4.70a	4.57a
Aroma	4.11b	4.18b	4.33a	4.33a	4.28a
Over all acceptance	4.56bc	4.50c	4.60b	4.62b	4.73a

The numbers followed by the same letter in a single row mean no significant difference at the level of 5% with LSD test. Score of taste, aroma and overall of acceptance is 7 for very like, 4 medium and 1 for do not like.

Table 5. Chemical score of lactic sweet corn-soy milk, treatment of F5 (3: 1)

Amino acid	Lactic sweet corn-soy milk (mg/g protein)	Score of amino acid in lactic sweet corn-soy milk	FAO/WHO* Suggested amino acid (mg/g protein)	Score of amino acid in corn**
Essential Amino Acid				
Arginine (Arg)	25.47	na	Na	Na
Histidine (His)	19.66	na	Na	Na
Isoleucine (Ile)	23.25	- 41.88	40	-20
Leucine (Leu)	78.29	11.85	70	51.43
Lysine (Lys)	78.29	**42.35**	55	-52.73
Methionine (Met)	15.21	na	35***	12.6
Phenylalanine (Phe)	19.66	na	60****	30.7
Threonine (Thr)	29.06	- 27.35	40	10
Tyrosine (Tys)	27,69	na	Na	Na
Valine (Val)	44.79	- 10.42	50	-10
Thriptophan	Na	na	10	-30
Non Essential Amino Acid				
Alanine (Ala)	21.03	na	Na	Na
Aspartic acid (Asp)	50.43	na	Na	Na
Cystine (Cys)	11.62	na	Na	Na
Glutamic acid (Glu)	121.37	na	Na	Na
Glycine (Gly)	12.31	na	Na	Na
Proline (Pro)	65,13	na	Na	Na
Serine (Ser)	30,60	na	Na	Na
Methionine +cystine	26.83	**23.34**	35	-11.43
Phenylalanine + tyrosine	47.35	-21.08	60	-7.0

*. Harper (1981)[25]
**. Calculation based on amino acid of Healthy Departement RI (1995) Database
***. The value of methionine + cystine.
****. The value of phenylalanine +tyrosine

IV. Conclusion

Based on the physical, chemical, microbiological and acceptability characteristics, the lactic sweet corn-soy milk drink fermented with Lactobacillus casei FNCC 0090 met the criteria of lactic drinks. Among the treatments, complementation of 1 part soy milk and corn milk of 3 parts was the best treatment. This had characteristic as follows: reducing sugar content 39.05 mg/100ml; Total LAB 8.43 log CFU/ ml; total acid 1.31%; pH 4.11. The color, taste, and overall acceptance score were between 5 (like slightly), while aroma score was 4 (neither like nor dislkike). Blending of sweet corn-soy milk in the ratio of 3: 1, has been able to overcome a deficiency of lysine, methionine, and cysteine.

References

[1]. M. Szymanek. 2012. Processing of sweet corn. In Eissa, H.A (edt). Agricultural and biological sciences. Trends in vital food and control engineering. Pp 85-98. Intech. ISBN 978-953-51-0449-0, 302 p. DOI 10.5772/2354.

[2]. K.L. Curran, A.R. Festa, S. D. Goddard, G. G. Harrigan and M.L. Taylor. "Kernel Compositions of glyphosate-tolerant and corn rootworm- Protected MON 88017 Sweet Corn and Insect-Protected MON 89034 Sweet Corn Are Equivalent to That of Conventional Sweet Corn (*Zea mays*)". 2015. Journal of Agricultural and Food Chemistry Vol 63: 3046−3052DOI: 10.1021/jf505687s

[3]. Departement of Health RI. 1995. Daftar Komposisi Zat Gizi Pangan Indonesia. P69.

[4]. OECD, 2002. Consensus document on compositional considarations for new varieties of maize *(Zea Mays*): Key food and feed nutrients, Anti nutrients, Secondary plant metabolites. Series on the Safety of Novel Foods and Feed no6, 20 August 2002. Environment Directorate. Organisation for Economic Co-operation and Development (EOCD), Paris. 42 pg

[5]. FAO. 1992. Maize in human nutrition. FAO Food and Nutrition Series, No. 25. ISBN 92-5-103013-8

[6]. S. Zilic, M. Milasinovic, D. Terzic, M. Barac and D. Ignjatovic-Micic. 2011. Grain characteristics and composition of maize specialty hybrids. Spanish Journal of Agricultural Research 9(1): 230-241

[7]. O. Omueti , K and K. Ajomale. 2005. Chemical and sensory attributes of soy–corn milk types African Journal of Biotechnology. Vol.4(6): 847- 851.

[8]. C. Y. Trisnawati, L Srianta, Y. Marsono, Y. 2013. Effect of corn varieties on the characteristics of soycorn milk. International Food Research Journal 20(3): 1187-1190

[9]. M.A.A. Gasmalla, H.A.Tessema, A. Salaheldin, Kamal-Alahmad, H.A.M. Hassanin and W. Aboshora. 2017. Health benefits of milk and functional dairy products . MOJ Food Processing & Technology Volume 4(4) : 1-4 .

[10]. Fadro, R. Efendi and F. Restuhadi. 2015. The Influence of skim milk addition on Production of corn (*Zea mays* L.) Milk probiotic drink using *Lactobacillus acidophilus*. Sagu, Vol. 14 (2) : 28-36

[11]. Wedajo, B. 2015. Lactic Acid Bacteria: Benefits, Selection criteria and probiotic potential in Fermented Food. J Prob Health 3: 129. doi: 10.4172/2329-8901.1000129

[12]. O. Omueti, EB Oguntona, O. Jaiyeola, O.A. Ashaye. 2000. Nutritional evaluation of home-level prepared soycorn milk: a protein beverage. Nutr and Food Sci 30: 128–132.

[13]. A.L Kolapo, and G.R Oladimeji. 2008. Production and quality evaluation of soy corn milk. J Appl Biosci 1(2): 40-45.

[14]. A.D. Lestiyani, T.I.P.Suseno,. and I. Srianta. 2014. Characteristics of soy corn yogurt. Journal of Food & Nutritional Disorders (3): 1-4. http://dx.doi.org/10.4172/2324-9323.1000134

[15]. O.M. Makanjuola, 2012. Production and quality evaluation of soy-corn yoghurt. Advance Journal of Food Science and Technology 4(3): 130-134.

[16]. TIP Suseno, S. Surjoseputro, K. Anita. 2000. Minuman probiotik nira siwalayan:Kajian lama penyimpanan terhadap daya anti mikroba *Lactobacillus casei* pada beberapa bakteri patogen. Jurnal Teknologi Pangan dan Gizi Volume 1 (1): 1-13

[17]. W.P. Rahayu , F. Kusnandar, WE Prayitno 2011. Stability of viable counts of lactic acid bacteria during storage of goat milk soft cheese. Microbiology Indonesia Vol 5(4): 149-153. DOI: 10.5454/mi.5.4.1

[18]. P.A Retnowati, J. Kusnadi. 2014. Pembuatan minuman probiotik sari buah kurma (*Phoenix dactylifera*) dengan isolat *Lactobacillus casei* dan *Lactobacillus plantarum*. Jurnal Pangan dan Agroindustri. Vol 2(2) :70-81.

[19]. S. Sudarmaji, B. Haryono, Suhardi. 1997. Analisis bahan makanan dan hasil pertanian. Edisi ke 2. Pusat Antar Universitas Ilmu Pangan dan Gizi UGM. Yogyakarta

[20]. W.F. Harrigan. 1998. Laboratory methods in food microbiology. Academic Press

[21]. AOAC. Official Methods of Analysis. *The Associate of Analitical Chemist* (AOAC) Inc. New York. 2000.

[22]. H.T.Lawless. 2013. Laboratory exercises for sensory evaluation. XIV, 151p. Spinger

[23]. W.Trikoomdun and B. Leenanon. 2016. Production of corn milk yogurt supplemented with probiotics. International Food Research Journal 23(4): 1733-1738

[24]. S. Irmler, S. Raboud, B. Beisert, D. Rauhut and H.Berthoud. 2008. Cloning and characterization of two *Lactobacillus casei* genes encoding a cystathionine lyase. Applied and Environmental Microbiology Vol. 74(1): 99–106

[25]. A. Harper. 1981. Amino Acid Scoring Patterns. Joint FAO/WHO/UNU Expert consultation on energy and protein requirements. Rome. ItalI

Design and Simulation of Air to Air Missile Homing System (#692)

Rahmat Alfi Duhri [1,a], Rianto Adhy Sasongko [1,b], Yayom Dwi Laksmana [1,c]

[1] Aerospace Department Faculty of Mechanical and Aerospace Engineering, Institut Teknologi Bandung (ITB),

Ganesha 10, Bandung 40132, Indonesia

[a] alfiduhri@gmail.com, [b] sasongko@ae.itb.ac.id, [c] yayomdwi41@gmail.com

Abstract.*This paper will talk about AIM 120 AMRAAM missile guidance for pursuing a moving target. The missile guidance system itself consists of missile dynamics, control system, seeker, and guidance methods. For general purpose, the missile dynamics approach will use non-linear equation of motions. The control surface that will be discussed follow the rule BTT (Bank-to-Turn) and control system that will be used is PID control system that widely used for control design. Lastly, the guidance method that will be studied here is proportional navigation and constant bearing course approach. The simulation will be conducted using MATLAB Simulink. The Simulink model consist of target dynamics, and guidance system. From the result of simulation, it will be shown that the missile can pursue its target quite well. Hence, the simulation system can be used well for preliminary design purpose.*

Keywords: *Homing System, Control System, Proportional Navigation, Missile Dynamics, Seeker, Bank-to-Turn, Constant Bearing Course..*

1. Introduction

The security systems of a country nowadays can be represented by the advanced technologies used for defending against intruders. One of those technologies is missile homing system of missile technology. With this technology, the intended target can be shot without any errors caused by human. There are a lot of limitations that can make this human factors become major effects of missing target such as anxiety, nervous, panic, low sight, etc. Hence, it is important to make the missile can pursue its target by itself.

The homing system basically use the concept of tracking and processing the trace of target and take it as commands to the missile for doing certain maneuver. In other words, missile's sensor will receive and interpret the locations and direction of target. After that, the computer or microprocessor that already had those directions will use the locations information as the reference for giving command to the missile through the control surfaces of the missile. The missile will follow this command, following certain path, and eventually it can hit the target. The exact algorithm of this homing system can be seen in the Figure 1.

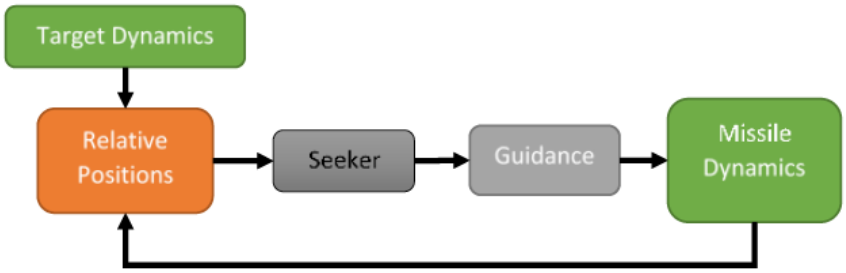

Figure 1. Algorithm of Missile Guidance System.

The guidance can be achieved by a lot of methods and approaches, but in this paper, the methods that will be used is proportional navigation method, that will be explained in the other part of this paper. As for approach, in this paper, it means the routine that must be followed by the missile in order to pursue the target until it hits the target. In this paper, constant bearing approach will be used. This approach basically take advantage of parallelism of two objects. When two objects make a certain parallelism, as both of them move, they will meet at a certain point. For illustration, Figure 2. below can explain how constant bearing course work.

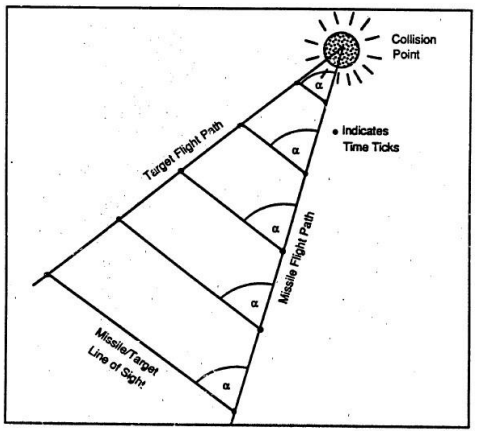

Figure 2. Constant Bearing Course Scheme [3].

The model that is used in this paper is missile AIM 120 AMRAAM (Advanced Medium Range Air-to-Air Missile), as shown in Figure 3. The name suggest that the missile operate from flying aircraft to shot the flying object.

Figure 3. AIM 120 AMRAAM [7].

The overview of the work in the paper have been written in this chapter. In the chapter II, the paper will talk about homing system, its components, and what is the important part of homing system. The next paragraph will explain the equations of motion for both missile and target, and control system that will be used in supporting guidance of missile. In the IV paragraph, the simulation and the result will be shown and discussed. Finally, the last one is Conclusion of this paper.

2. Homing System

Homing system can be divided into three components, those are seeker system, navigation system, and autopilot system or guidance law. Homing system also need other parameters that correspond with aircraft dynamics, they are called Engagement geometries.

A. Proportional Navigation

Proportional Navigation is commonly used method for designing missile guidance. The basic idea of this method is the acceleration command generated in the missile is proportional to the line of sight (LOS) rate. It can be shown in Figure 3.

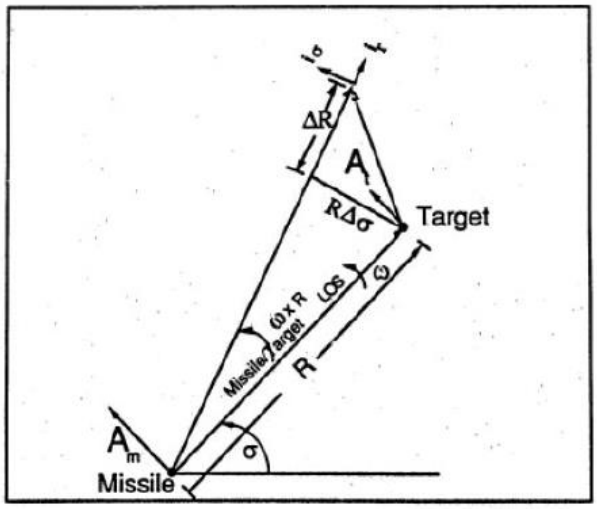

Figure 4. Proportional Navigation System Scheme [3].

The basic idea of this navigation is to maintain missile LOS rate become zero and the missile will have constant bearing course with the target until it hit the target. It can be achieved by giving acceleration command to the missile. The equation of Proportional Navigation can be written as [3]:

$$\dot{\gamma}=N\dot{\sigma} \quad (1)$$

where, $\dot{\gamma}$ is rate of change of missile heading, N is navigation ratio, $\dot{\sigma}$ is line of sight rate.

Navigation Ratio represents the gain that will be processed as command to the missile. The more the value, the missile will be more aggressive with smaller LOS rate. In the other hand, the less the value, the missile will less responsive toward the change of LOS.

B. Seeker System

Seeker is the components of homing for censoring the location of the target. The seeker can detect and follow the movements of the target by sensing the unique characteristics of the target, such as radiation or reflection of energy by the target.

In the guidance system seeker will sense the target with certain error. This can be caused by the movement of seeker head sometimes is slower than the movement of target. Considering that condition, the seeker equation will become the state space as below [3]:

$$\dot{x}sh=Axsh+Bush \quad (2)$$

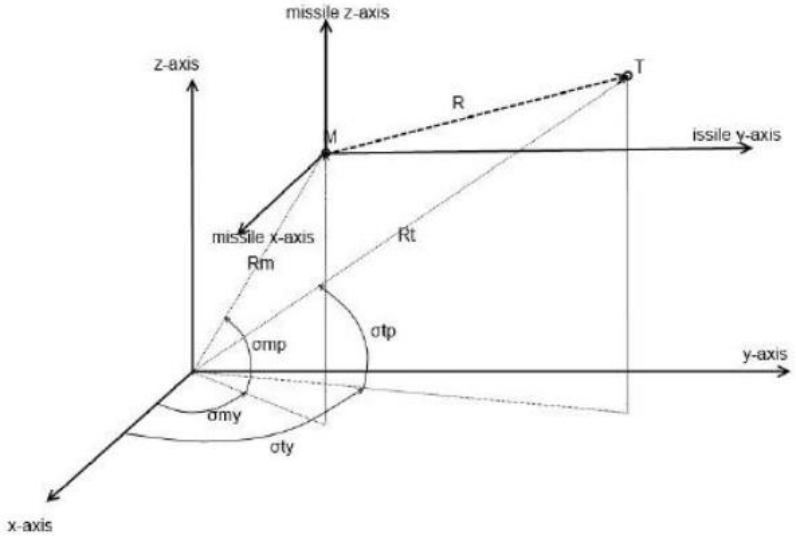

Figure 5. Seeker Sensing Illustration [4].

where [3],

$$x_{sh} = [\beta_{pitch} \quad \dot{\beta}_{pitch} \quad \beta_{yaw} \quad \dot{\beta}_{yaw}]^T, u_{sh} = \begin{bmatrix} \sigma_{pitch} \\ \sigma_{yaw} \end{bmatrix}$$

$$A = \begin{bmatrix} 0 & 1 & 0 & 0 \\ -k_1 & -k_2 & 0 & 0 \\ 0 & 0 & 0 & 1 \\ 0 & 0 & -k_1 & -k_2 \end{bmatrix} \quad B = \begin{bmatrix} 0 & 0 \\ k_1 & 0 \\ 0 & 0 \\ 0 & k_1 \end{bmatrix}$$

with, $\beta pitch$ is seeker output LOS in pitch direction, βyaw is seeker output LOS in yaw direction, $\sigma pitch$ is seeker input LOS in pitch direction, σyaw is seeker input LOS in yaw direction, $k1$ is seeker ratio = 100, $k2$ is seeker ratio= 20.

In the equations of seeker that have been mentioned before, seeker ratio determine the accuracy of seeker and every seeker have this value. For more convenience we will choose the value as stated above.

C. Guidance Law

In part A of Chapter II, the equation of proportional navigation have been stated clearly. In order to implement it into the guidance system, the guidance law must be derived. The guidance law within the missile system determines the best trajectory for the missile based on missile position, target position, missile capability, and desired objectives [3]. The following equation is the guidance law in term of state space [3].

$$x_{gui} = Ax_{gui} + Bu_{gui} \tag{3}$$

Where,

$$u_{gui} = \begin{bmatrix} \dot{\beta}_{pitch} \\ \dot{\beta}_{yaw} \end{bmatrix}, \quad x_{gui} = \begin{bmatrix} \gamma_{m_{pitch}} \\ \gamma_{m_{yaw}} \end{bmatrix}$$

$$A = \begin{bmatrix} -k & 0 \\ 0 & -k \end{bmatrix}, \quad B = \begin{bmatrix} N & 0 \\ 0 & N \end{bmatrix}$$

After that, the heading of the missile, will be applied in the equation below [3].

$$V_{mpitch} = V_m \cos(\gamma_{myaw} - \sigma_{yaw}) \tag{4}$$

$$V_{myaw} = V_m \cos(\gamma_{mpitch}) \tag{5}$$

$$A_{mpitch} = V_{mpitch} \cos(\dot{\gamma}_{mpitch}) \tag{6}$$

$$A_{myaw} = V_{myaw} \cos(\dot{\gamma}_{myaw}) \tag{7}$$

D. Engagement Geometry

In part A of Chapter II, the equation of proportional navigation have been stated clearly. In order to implement it into the guidance system, the guidance law must be derived. The guidance law within the missile system determines the best trajectory for the missile based on missile position, target position, missile capability, and desired objectives [3]. The following equation is the guidance law in term of state space [3].

1) Line of Sight (LOS): Line of sight is the angle between the missile and the target, see Figure 5.

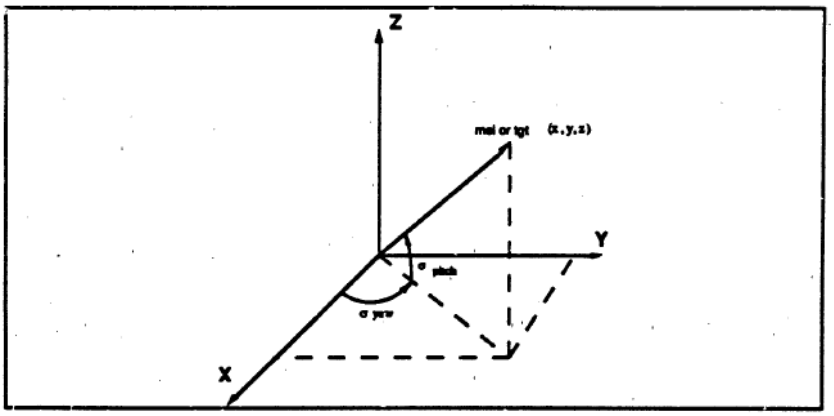

Figure 6. Line of Sight Illustration [3].

The equation of the LOS can be written below [3].

$$\sigma_{pitch} = \tan^{-1}\left[\frac{z_t - z_m}{\sqrt{(x_t - x_m)^2 + (y_t - y_m)^2}}\right] \quad (8)$$

$$\sigma_{yaw} = \tan^{-1}\left[\frac{z_t - z_m}{x_t - x_m}\right] \quad (9)$$

2) Flight Path Angels: Flight path angle represent the attitude of the missile and the target along their trajectory, see Figure 6.

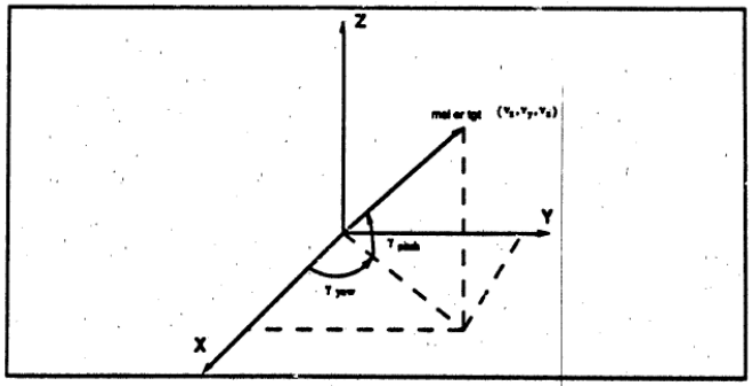

Figure 7. Flight Path Angels Illutration [3].

The equation of flight path angels can be written below [3].

$$\gamma_{pitch} = \tan^{-1}\left[\frac{V_{t_z} - V_{m_z}}{\sqrt{(V_{t_x} - V_{m_x})^2 + (V_{t_y} - V_{m_y})^2}}\right] \quad (10)$$

$$\gamma_{yaw} = \tan^{-1}\left[\frac{V_{t_z} - V_{m_z}}{V_{t_x} - V_{m_x}}\right] \quad (11)$$

3) Velocity and Acceleration: Velocity and Acceleration is important factors here because both of them determine the trajectory and the movement of missile and target. In this section, the one that will be focused is missile acceleration and

velocity because in the guidance system, the acceleration and velocity of missile have direct cause to the movement change [3].

$$V_m = \sqrt{V_{m_x} + V_{m_y} + V_{m_z}} \quad (12)$$

$$A_m = \sqrt{A_{m_x} + A_{m_y} + A_{m_z}} \quad (13)$$

In the yaw direction, the acceleration equation can be represented below [3].

$$\ddot{x}_{m_{pitch}} = -\left(A_{m_{pitch}} \sin \sigma_{pitch}\right) \cos \sigma_{pitch} \quad (14)$$

$$\ddot{y}_{m_{pitch}} = -\left(A_{m_{pitch}} \sin \sigma_{pitch}\right) \cos \sigma_{yaw} \quad (15)$$

$$\ddot{z}_{m_{pitch}} = -\left(A_{m_{pitch}} \sin \sigma_{pitch}\right) \quad (16)$$

In the yaw direction, the acceleration equation can be represented below [3].

$$\ddot{x}_{m_{yaw}} = -A_{m_{yaw}} \sin \sigma_{yaw} \quad (17)$$

$$\ddot{y}_{m_{yaw}} = -A_{m_{yaw}} \cos \sigma_{yaw} \quad (18)$$

Both acceleration will become the basis for deriving tracking controller of missile. The total acceleration that the missile will have can be shown below [3].

$$\ddot{x}_m = \ddot{x}_{m_{pitch}} + \ddot{x}_{m_{yaw}} \quad (19)$$

$$\ddot{y}_m = \ddot{y}_{m_{pitch}} + \ddot{y}_{m_{yaw}} \quad (20)$$

$$\ddot{z}_m = \ddot{z}_{m_{pitch}} \quad (21)$$

3. Dynamic Equations and Control System

A. Missile Dynamics Equations

Missile Dynamic equations that will be used here is nonlinear dynamic equations of motion. The equation of motion consist of translational equations (equation (22)), rotasional equations (equation 23), and kinematic equations of motion. The non-linear equation is chosen because it can generalize the system in any flight conditions.

$$\vec{F}_A + \vec{W}_b + \vec{F}_P = m\left(\frac{\partial \vec{v}}{\partial t} + \vec{\omega} \times \vec{V}\right) \quad (22)$$

$$\vec{\mathrm{M}}_{\mathrm{A}} + \vec{\mathrm{M}}_{\mathrm{P}} = \left(\mathbf{I}\frac{\partial \vec{\omega}}{\partial \mathrm{t}} + \vec{\omega} \times (\mathbf{I} \cdot \vec{\omega})\right) \quad (23)$$

For modelling dynamic equations of motion, there are aerodynamics forces and moments. They are calculated using Missile DATCOM [1]. Instead of using experimental data, Missile DATCOM used because it is easy to use, and have good approximation result.

B. Target Dynamic Equations

The target dynamic equation of motions just consist of translational equations. For this paper, this is enough because the main purpose of this paper is not studying the performance of guidance, but for studying how the guidance system work for non-linear missile system. Lastly, the equation of motions for target can be shown below [3].

$$\dot{x_t} = Ax_t + Bu_t \quad (24)$$

Where,

$$x_t = [x_t \quad \dot{x}_t \quad y_t \quad \dot{y}_t \quad z_t \quad \dot{z}_t]^T, \quad u_t = [\ddot{x}_t \quad \ddot{y}_t \quad \ddot{z}_t]^T$$

$$A = \begin{bmatrix} 0 & 1 & 0 & 0 & 0 & 0 \\ 0 & 0 & 0 & 0 & 0 & 0 \\ 0 & 0 & 0 & 1 & 0 & 0 \\ 0 & 0 & 0 & 0 & 0 & 0 \\ 0 & 0 & 0 & 0 & 0 & 1 \\ 0 & 0 & 0 & 0 & 0 & 0 \end{bmatrix}, \quad B = \begin{bmatrix} 0 & 0 & 0 \\ 1 & 0 & 0 \\ 0 & 0 & 0 \\ 0 & 1 & 0 \\ 0 & 0 & 0 \\ 0 & 0 & 1 \end{bmatrix}$$

In the state space above, the input of the equations is the acceleration of the state. That state can be used for moving object both with acceleration and without acceleration.

C. Control System

1) Tracking Controller: Tracking controller is close Koo feedback system with the purpose to derive the system to track the input that can be shown by the exact tendency of certain output to follow the input. There are a lot of methods to implement tracking controller into the system. One of them is using PID Controller that will be used in this paper.
2) Bank-to-turn is the type of control surface in missile which can only the missile to roll and pitch. It is because the missile just only have a pair of symmetric control surface which can generate pitching momen and a pair of asymmetric control surface that can make the missile able to roll. For tracking controller in homing system, the pitch error can be calculated using az. As for banking angle (φ) error, it can be calculated using the equation below [2].

$$\varphi = \tan{-1}\ ay/az \qquad (25)$$

where, ay and az are both components of missile acceleration.

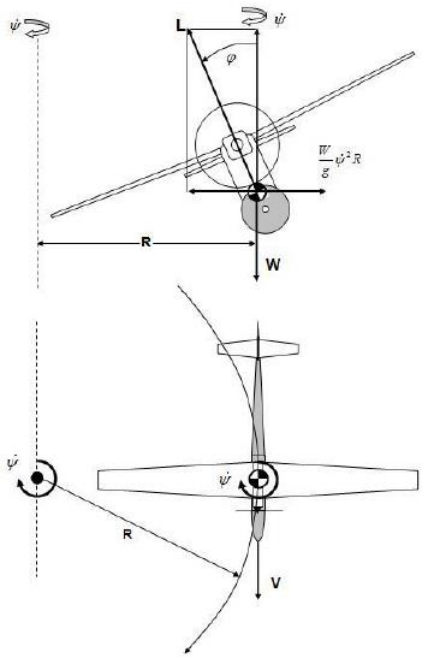

Figure 8. Bank-to-Turn Manuever.

3) PID Controller: PID stands for Proportional Integral Derivative. As the name of its abbreviation, PID itself consists of Proportional gain, Integral gain, and Derivative gain. Proportional gain have a function to amplify the control but does not change the dynamics of control. Integral gain can improve and at the same time also can nullify steady state response. The last one, Derivative gain can improve transient response by improving the error rate that will happen.

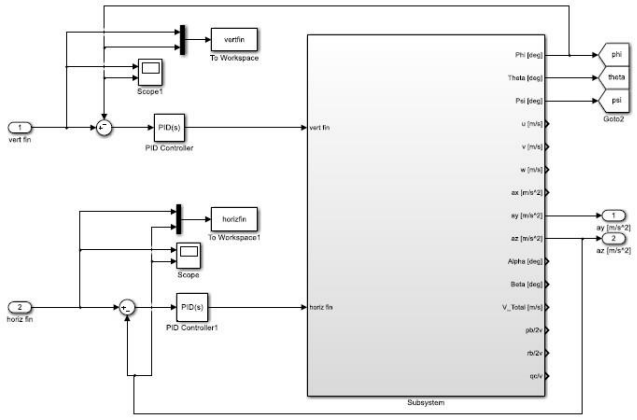

Figure 9. PID Controller for Bank-to-Turn.

4. Simulation and Result

The simulation of missile guidance was conducted in MATLAB Simulink. The result of several case can be seen in this chapter.

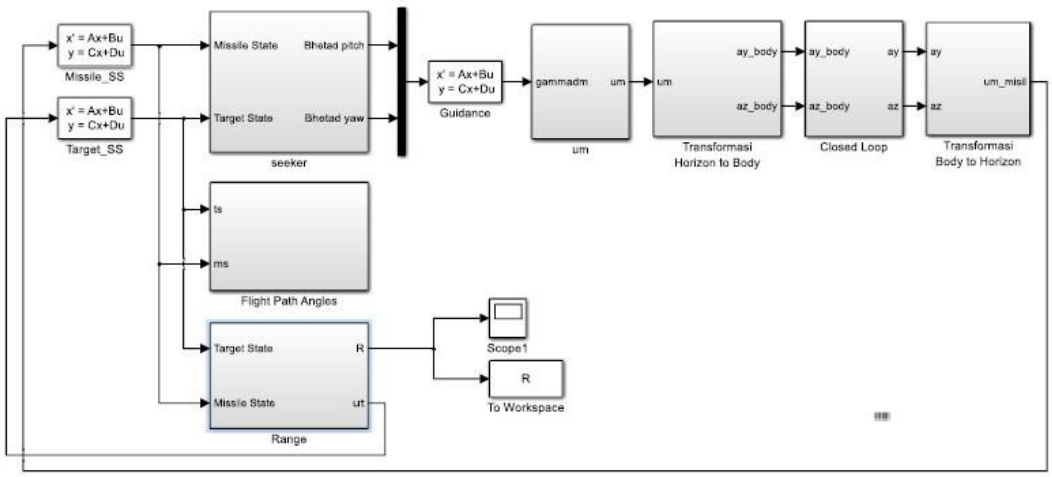

Figure 10. System Guidance Simulation Model.

The model above is used for simulation of missile guidance in pursuing the target. For example, below is the initial condition of a case.

Table 1. Initial Condition Misil dan Target

	Missile	Target
X (m)	0	10000
Y (m)	0	0
Z (m)	4572	4572
Vx (m/s)	1020	0
Vy (m/s)	0	100
Vz (m/s)	0	100
Ax (m/s^2)	0	100
Ay (m/s^2)	0	0
Az (m/s^2)	0	0

The result of the simulation can be shown below.

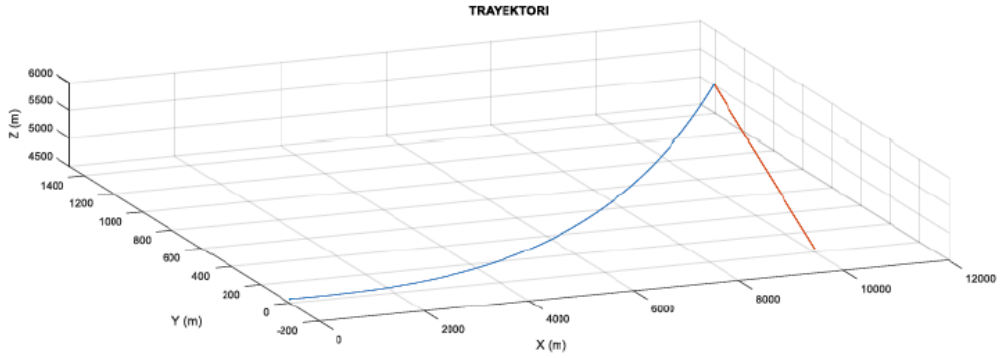

Figure 10. Trajectory of Missile (Blue) and Target (Red).

The above figure show the trajectory of missile and target from initial position until the missile hit the target. From the trajectory, we know that the missile finally can meet the target at one point. Below is the range between the missile and the target that can prove that statement.

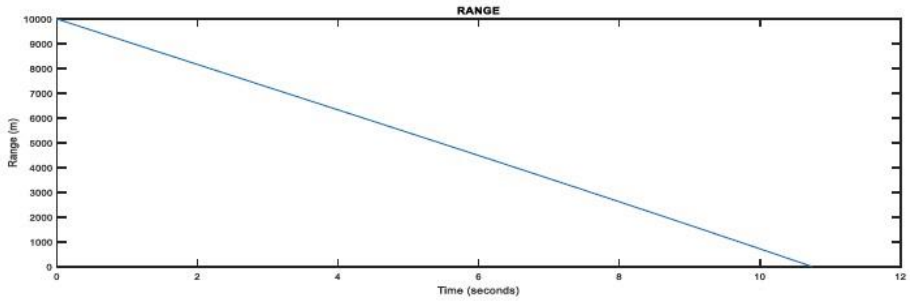

Figure 12. Range between Missile and Target

As for Line of Sight of the missile, the missile continuously undergoes change of Line of Sight with small changing. Ideally, there will be no change in Line of Sight. We know that there are limitations in seeker, guidance system, numeric modelling, etc. can influence the result of simulation. Thus, this is what happen. There will be small change that does not affect the performance of guidance.

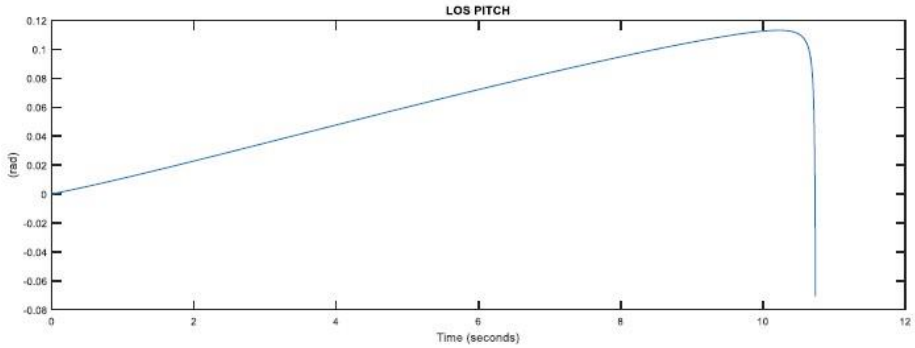

Figure 13. LOS in Pitch Direction between Missile and Target

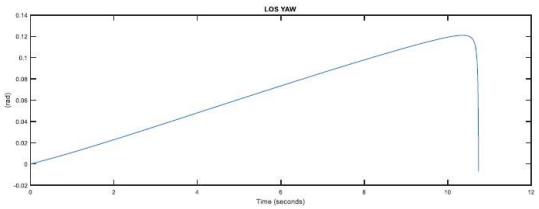

Figure 14. LOS in Yaw Direction between Missile and Target

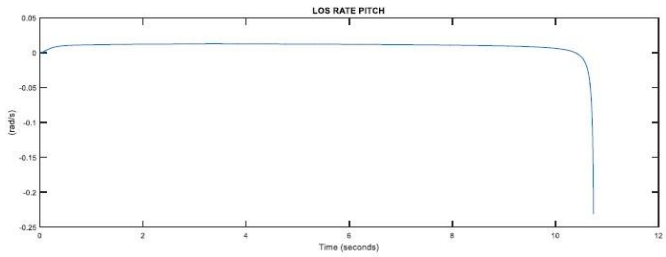

Figure 15. LOS rate in Pitch Direction between Missile and Target

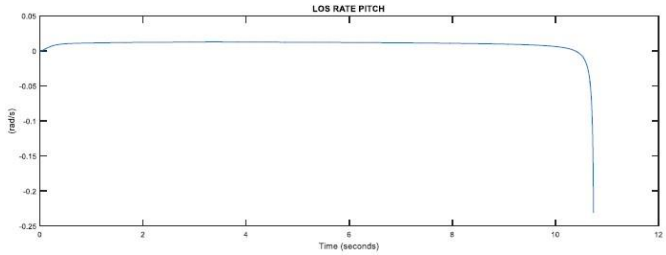

Figure 16. LOS rate in Yaw Direction between Missile and Target

We already discussed about tracking controller, how control system can make the system follow the input exactly. It is very important for the missile to follow the direction of input exactly same so the guidance would not miss too much. From the simulation, we know that our system is powerful enough to follow the input as shown in Figure 15 and Figure 16.

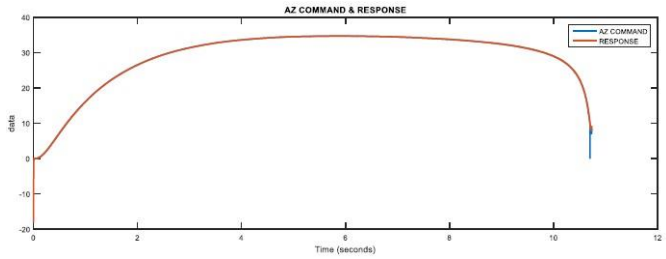

Figure 17. AZ Command (Blue) and Response (Red)

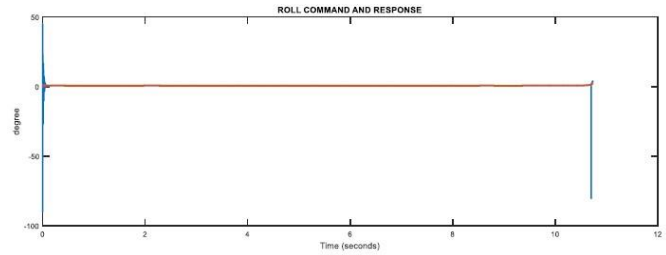

Figure 18. Roll Angel Command (Blue) and Response (Red)

5. Conclusion

Tracking controller system has good approximation. This can be shown from the result that az and roll command is inline with response. Design of guidance system using proportional navigation method can be implemented or used for preliminary design purpose. It is because miss distance of the simulation is less than 10 meter. Proportional navigation method for AIM 120 AMRAAM has powerful performance. It can be shown from the loss rate of the missile along the trajectory is zero along the way to the target.

References

[1] Blake, William. 2011. Missile Datcom User's Manual, United States : U.S. Army Aviation & Missile Research, Development and Engineering Center.
[2] B. Friedland, D. E. Williams. 1989. Design of Autopilot for Bank-to-Turn Missile. United States: Kearfott Guidance and Navigation Corporation.
[3] Francis C, Lukenhill. 1990. A Target/Missile Engagement Scenario using Classical Proportional Navigation, United States: Naval Postgraduate School.

[4] Laksmana, Yayom D. 2016. Perancangan dan Simulasi Sistem Panduan, Sistem Kendali, serta Dinamika Terbang AIM 120 AMRAAM. Indonesia: Bandung Institute of Technology.
[5] Mulder J.A. et al. Flight Dynamics Lecture Notes. Belanda: TUDelft.
[6] Schmidt, David. Modern Flight Dynamics. 2012. New York: McGraw-Hill.
[7] http://militaryedge.org/armaments/aim-120-amraam/ (Accessed in August, 14th 2017, 7:34 PM.

The Development of Agropolitan Lingsar to Support Economy & Tourism in the West Lombok Regency (#733)

Gunawan Prayitno[1,a], Rizki K. Anjani[1], Shely Luthpiana[1], Shinta Kamalia[1]
[1]University of Brawijaya, Department Urban and Regional Planning, Jl. MT Haryono 167, Malang, Indonesia
[a]gunawan_p@ub.ac.id

Abstract. *The development of agropolitan in the agriculture sector needed to improve farmer's welfare. The Lingsar Agropolitan area is one of the areas of agro tourism potential in West Nusatenggara Regency with the various potential of agricultural commodities and good agricultural land management system. Agrotourism is a series of tourism activities utilizing agriculture potential as a tourist attraction, in the form of agricultural areas, the uniqueness and diversity of agricultural production activities and agricultural technology and culture of farmers. This study aims to identify the potential and problems of Lingsar agropolitan area, to support the agro tourism and economy of West Lombok Regency. Analytical methods used include agribusiness subsystem analysis, circle system analysis, land capability and suitability analysis and force field analysis (FFA). The result of this research shows that "ragamadu" commodities could support agro tourism in Lingsar district.*

Keywords*: agro tourism, force field analysis and ragamadu.*

I. Introduction

The concept of agropolitan develop by Friedman in 1975 [1]. He stated that the agropolitan model has room for rural development and is built on the idea of accelerated development that is oriented to human needs with more equitable economic benefits. The agropolitan concept is an approach to planning development from below that promises real economic empowerment for the rural poor [2]. To empower economic of the poor in rural area, in the concept of agropolitan we should identified the potential commodities to support agricultural development in rural area.

The development of potential commodities could support agro tourism development. Agro tourism is a series of tourism activities utilizing agriculture potential as a tourist attraction, in the form of agricultural areas natural landscape and the uniqueness and diversity of agricultural production activities and agricultural technology and culture of farmers. The agro tourism activity aims to broaden knowledge insight, recreational experience and business relationship in agriculture that includes food crops, horticulture, plantation, fishery and livestock [3]. The Lingsar District, West Lombok Regency, is one of the subdistricts in West Lombok with agropolitan diversity activities that have agrotourism potential, from upstream, on the farm to downstream. This sector includes food crops, plantations, forestry, and livestock. Food crops include rice, corn, crops besides rice, vegetables and fruits. As a rice center, rice production in West Lombok Regency becomes an indicator of the success of agricultural programs.

In the Regional Mid Term Development Plan (RPJMD) West Nusatenggara Province (NTB) 2013-2018 [4], one of the goal is to improve the welfare of the community, accelerate poverty reduction and develop regional excellence. Indicators of successful implementation of the program and policy are one of them depends on the condition of food security and nutrition in all region. The indicators of food security are closely related to the agricultural sector. So the development of agricultural sector could improve the economic welfare of the farmer's.

The food crops subsector and the plantation sub-sector in West Lombok Regency also contributed significantly to the West Lombok Regency economy. Coconut and Cashew is a superior product of plantation. With good management of plantation, products in West Lombok are expected to compete with other regions.

Livestock cannot be separated from agriculture, so in line with the agricultural production, West Lombok Regency also develops livestock products as well. Some of the main products of the farm are cows, buffalo, goats, sheep, horses, chickens and pigs. Although it has not been able to contribute significantly to West Lombok's economy, the potential of this livestock sector needs to be explored and developed. West Lombok district has agricultural potentials that are still not utilized to the fullest. The agricultural potentials of West Lombok district if produced, processed and marketed with good planning is believed to improve the economy of the farmers and the district of West Lombok.

The aims of this study are to identify the potential and problem related to the development of agropolitan lingsar, and identified the potential products of agriculture that will develop. While the Scope of Research Area is located in District Lingsar West Lombok Regency.

II. Method

A. Data Collection and Processing Stages

Sampling technique or data collecting used in this study is in the form of interviews with selected key person associated with agriculture, plantation, animal husbandry and agroindustry. Interviews are conducted on the topic of subsystems and their potentials and problems. Also, researchers collect secondary data as needed.

B. Stage Analysis and Data Interpretation

These stages analyze and interpret data from the collected and processed. This will be used as an input for the region to apply the agropolitan commodity rating to be developed. A comprehensive analysis will be presented related to the selection of superior priorities supported by quantitative and qualitative data. Analytical methods used include land suitability and capability analysis, subsystem analysis, linkage system analysis, FFA analysis. These analysis results in the management strategy of Lingsar agropolitan area.

1. Analysis of Land Capability and Suitability
   An analysis of the capability and suitability of the land is used to determine the suitability of land use for existing soil types. This suitability is correlated with the variable weighting analysis. Grouping of soil is into units of ability, sub class, and evaluation based class.

2. Subsystem Analysis
   According to Rustiadi and Dardak (2007), agropolitan subsystem analysis includes upstream agribusiness analysis, farming subsystem analysis, downstream agropolitan analysis, agro-output subsystem analysis and marketing subsystem, and subsystem analysis of support services.
3. Linkage Analysis System
   Linkage system analysis is an analysis used to analyze the macro and comprehensive relationship of a tourist object as a system. The things that will be examined is the relationship between sectors, integrity, and relationships among superior commodities in an area.
4. Force Field Analysis
   Force Field Analysis is a simple tool to analyze the factors found in complex problems. This analysis is divided into two factors that can affect the problem regarding factors or pressures that support the status quo (holding strength) and the pressures that support the change in the desired direction (mover). (Lewin K, 1951)

III. Result and Discussion

A. West Lombok District Land Use

Tabel 1 shows land use in West Lombok Regency, detailing courtyard, building and garden, moor/field, farm land, meadow, community forest and plantation.

Table 1. Land Use Type Of West Lombok Regency

Districts	Court Yard Building & Garden	Moor/Field	Farm land	Meadow	Community Forest	State Forest	Plantation
1. Sekotong	14 720	4 317	4 071	577	3 689	468	632
2. Lembar	886	1 270	546	-	-	761	978
3. Gerung	2 348	4	6	-	323	142	369
4. Labuapi	872	230	-	-	15	20	15
5. Kediri	449	126	-	-	-	156	-
6. Kuripan	689	-	-	-	208	6	-
7. Narmada	2 073	2 272	368	-	61	3956	-
8. Lingsar	856	3 320	-	-	-	4003	-
9. Gunungsari	4 052	3 668	116	-	-	115	268
10. Batu Layar	639	1 799	-	-	652	110	-
Amount */Total*	**27 579**	**17 006**	**5 107**	**577**	**4 948**	**9777**	**2262**

Source: Agriculture, Plantation & Forestry Agency, West Lombok District in West Lombok Regency Data, 2016

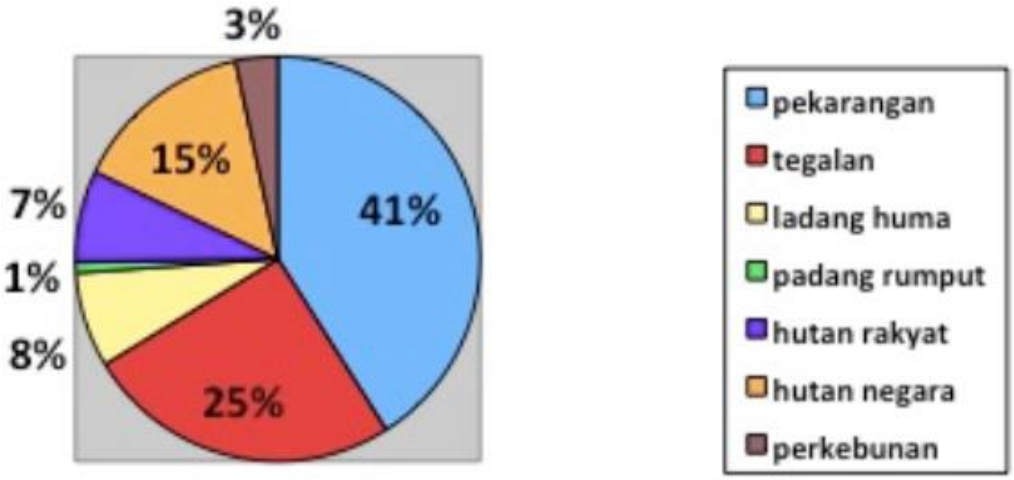

Figure 1. Land Use Diagram in West Lombok Regency.

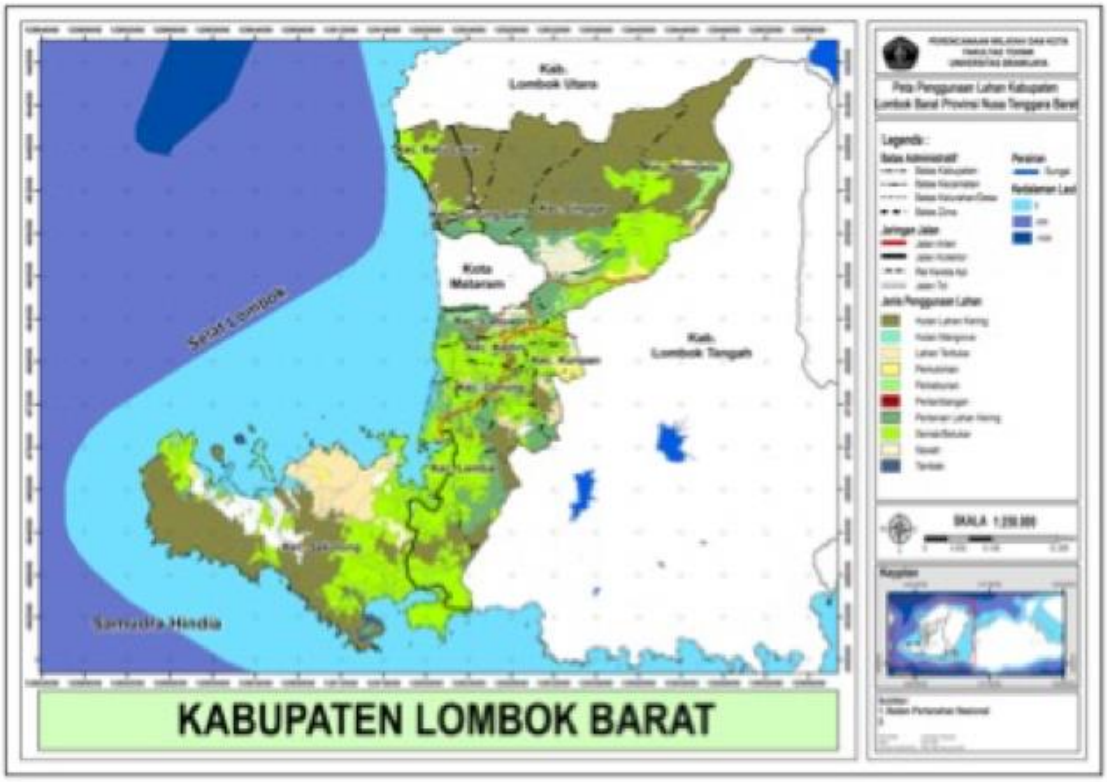

Figure 2. Land Use Diagram in West Lombok Regency.

B. Analysis of Land capability and suitability

Results from the analysis of the land ability and suitability, the Lingsar sub-district is located in the cultivation area and is in accordance to be used as in the agropolitan management. From the land ability and suitability analysis in the agropolitan area, the concept of agrotourism development can be done in Lingsar sub-district.

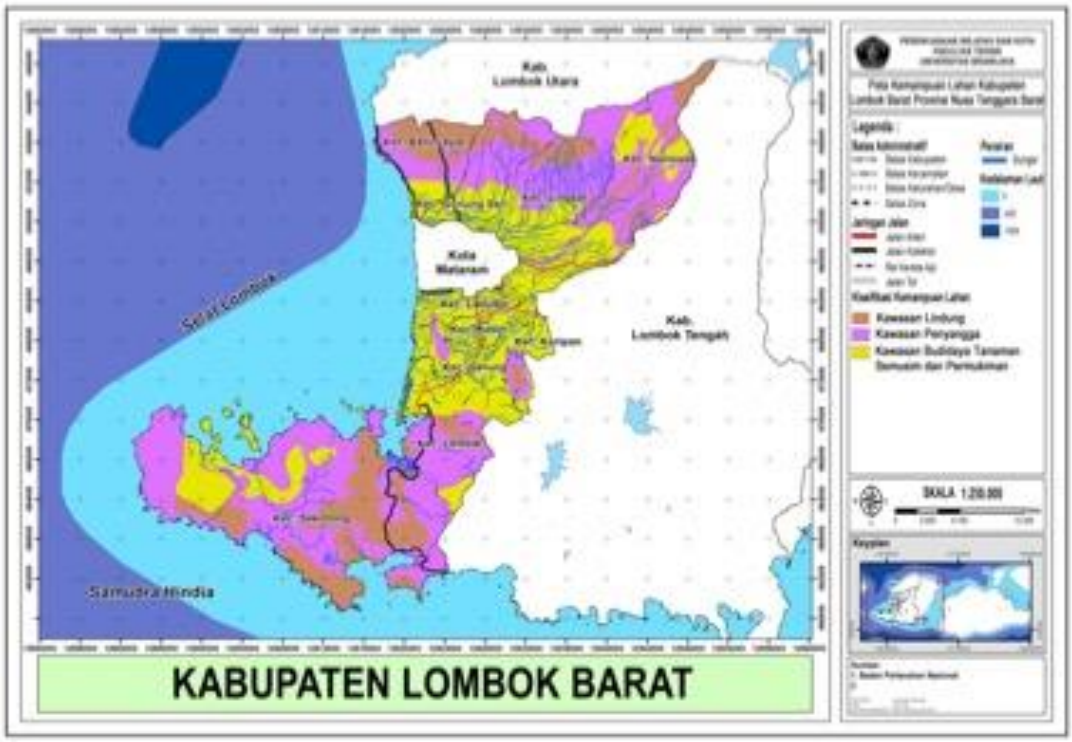

Figure 3. Land Suitability in West Lombok Regency.

C. Subsystem Analysis

Ragamadu is one of the commodities in West Lombok Regency with further development potential. Ragamadu is a combination of Rambutan-Palm Sugar-Mangosteen-Durian which the community intends to develop.

1. Analysis of Upstream Sub System
   Analysis of the upstream subsystem of Ragamadu commodities consists of raw materials and seeds, machinery and equipment, agricultural technology, and human resources. Ragamadu is a land located in the district Gunungsari, Lingsar and Narmada. Commodity developers do not incur expenses for nurseries at the start of the business. Since it grows naturally, palm trees do not require fertilizer or pesticides for treatment.

Figure 4. Commodities Ragamadu in Lingsar Subdistrict (Source: Survey Results, 2017.)

2. Analysis of Farm Subsystem
   Ragamadu plants (rambutan, palm sugar, mangosteen, durian) grown in the garden do not have a special care for production. Plant owners allow the plants to grow without interference and special care.

3. Analysis of downstream subsystems
   Analysis of Ragamadu Downstream Subsystems consists of labor and technical production. In the management of Ragamadu are made into palm sugar and dodol.

Figure 5. Ragamadu Processing Result in Lingsar Subdistrict (Source: Survey Results, 2017.)

4. Analysis of Marketing Subsystem
   The Ragamadu processing products in this agro industry are developed into several ready-to-sell products such as sugar, briquette sugar, ant sugar, sugar sherbet, and liquid sugar. As for mangosteen, rambutan and durian, they are processed into dodol. Marketing is done at local market of NTB province level. Some palm sugar has been exported to japan in small quantities.

5. Analysis of support services subsystem
   The Ragamadu Supporting sub-system analysis discusses the things that help the process from upstream to marketing in the form of counselling and cooperation forms. Bukit Tuan agroindustry business receives assistance in the form of counselling and training. Also it also has a partnership with the brownie cake business for providing raw materials of sugar.

D. Analysis of Inter sector Linkage System

Based on the linkage system between commodity diagram in Figure 5, there is a correlation or relationship between commodities; the relationship between Ragamadu commodities is associated with cattle for using a type of organic fertilizer from cattle dung. The relationship between agriculture and livestock sector is cattle waste used by farmers are made into

manure. The use of manure is beneficial for farmers and cattle ranchers in West Lombok Regency.

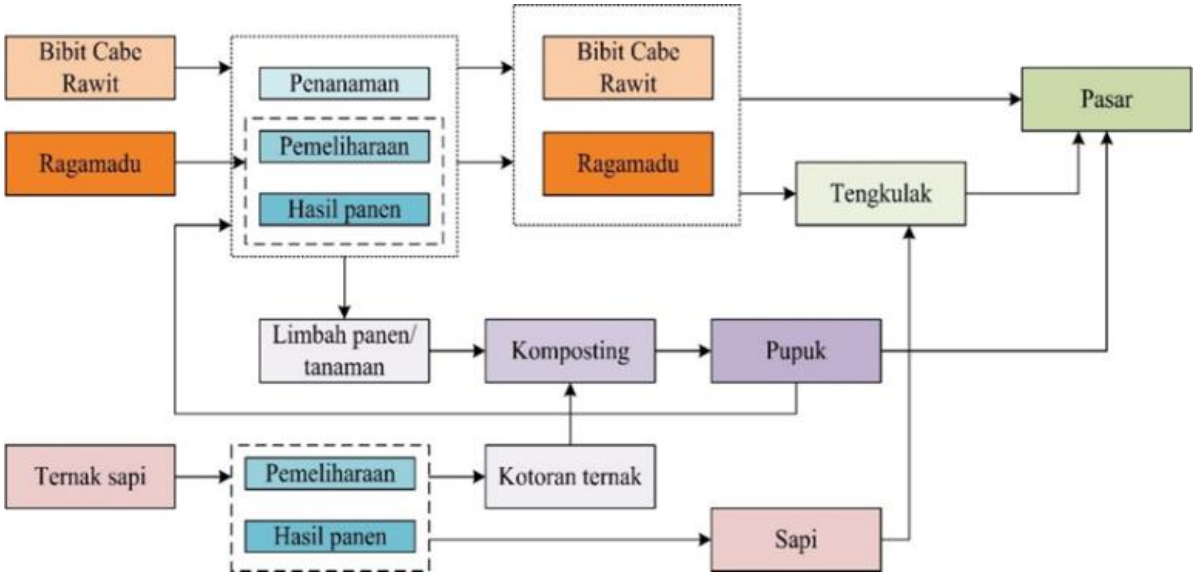

Figure 6. Inter Commodity Linkage System (Source: Survey Results, 2017.)

E. Subsystem Analysis

Force field analysis (FFA) is an analytical tool used in planning changes by identifying the factors supporting and constraining the goals. The supporting factors of force field analysis result are as follows:

Table 2. Table Force Field Analysis

No	Supporting factors	Constraining factor
1	HR, agriculture is relatively large	Narrow land area and limited access to capital resources
2	The agricultural sector has a high multiplier effect	Low quality of human resources
3	Available agricultural areas and potential land that has not been utilized optimally	Limited supporting facilities and infrastructure
4	A great diversity of biological resources that have not been utilized and developed maximally	Low level of productivity
5	The high level of public awareness of the importance of nutritional value of food	Production and quality of agricultural products
6	Demand for agricultural products is increasing	The unfavourable pattern of business partnerships
7	-	The existing agricultural institutions have not functioned optimally.

Based on Table 2. The Force field analysis concludes that there is less supporting factors than constraining factors. It is, therefore, necessary to formulate a strategy in the form of referral processing of commodities results in Lingsar agropolitan area based on the supporting and constraining factors.

F. Management Strategy

Management strategies based on the referral of Lingsar agropolitan area management based on FFA analysis to support the economy and tourism are as follows:

1. Develop the processing industry of ragamadu commodity based on educational tourism
2. Ragamadu processing is fully supported by the government to provide the help needed by farmers.
3. Training for innovations of diverse crops.
4. Training for innovations of diverse crops.
5. Application of minimum selling price so that farmers remain profitable
6. Promotion and marketing of the crop as well as ragamadu processed products

IV. Conclusion

Based on the analysis, the constraining factors in the Agropolitan management to agrotourism is the quality of human resources, unsupporting facilities and infrastructure, suboptimal institution, and unsufficient marketing of results. The strategy used as the direction of agropolitan Lingsar area management are:

- Making lingsar sub-district become the center of agropolitan activity in downstream subsystem and marketing activities
- Lingsar Subdistrict is directed into education-based tourism in the agroindustrial sector as branding of west Lombok district in terms of tourism and improving the local economy.

References

[1] Friedman, John & Douglass, Mike (1975). Agropolitan Development: Towards a New Strategy for Regional Planning in Asia. School of Architecture and Urban Planning, University of California Los Angeles.
[2] Buang, A., Habibah, A., Hamzah, J., & Ratnawati, Y. S. (2011). The agropolitan way of re-empowering the rural poor. World Applied Sciences Journal, 13(13 SPECIAL ISSUE), 1-6.
[3] Sastrayuda, Gumelar S (2010), Model Agro Development in Yogyakarta Gunung Kidul, UMY Technical Journal, volume 14, No. 3, p. 4.
[4] Regional Mid Term Development Plan (RPJMD) West Nusatenggara 2013-2018
[5] Peraturan Menteri Lingkungan Hidup No. 17 tahun 2009 tentang Pedoman Penentuan Daya Dukung Lingkungan Hidup Dalam Penataan Ruang Wilayah.
[6] Lewin, K. 1951. Field Theory in Social Science. Harper and Row, New York.
[7] Rustiadi, E dan Dardak (2007), Agropolitan: Strategi Pengembangan Pusat Pertumbuhan Pusat Pertumbuhan pada Kawasan Perdesaan. Crestpent Press, Bogor.

Feeding Behaviour of Sumatran Rhinoceros (*Dicerohinus sumatrensis*) in Sumatran Rhino Sanctuary Way Kambas National Park (#762)

Athaya Talitha S. Awaliah[1,a], Bainah Sari Dewi[1,b], Gunardi Djoko Winarno[1,c], Sugeng P. Harianto[1,d], Norio Tokita[2,e]

[1]Forestry Departement of Agriculture Faculty University of Lampung
[2]Nippon Veterinary and Life Science University in Tokyo Japan
[a]athayatalithaa@gmail.com, [b]bainahsariwicaksono12@gmail.com, [c]gundowino@gmail.com, [d]sugeng.prayitno@fp.unila.ac.id, [e]tokitan@nvlu.ac.jp

Abstract— *Sumatran Rhinoceros (Dicerorhinus sumatrensis) is nocturnal wildlife with complex behaviour. Sumatran Rhinoceros feeding time usually occurs at midnight before morning and in the morning as well. The feeding behavior of Sumatran Rhinoceros will be different in natural habitat and sanctuary. The information about Sumatran Rhinoceros behaviour can support the conservation effort that undertaken. This research aims to analyze the feeding behavior of Sumatran Rhinoceros in Sumatran Rhino Sanctuary. This research was conducted on July 2017 at Sumatran Rhino Sanctuary Way Kambas National Park and the object was one female Sumatran rhinoceros named "Ratu". The Focal Animal Sampling was used to observe Sumatran Rhinoceros feeding behavior. The results showed that the dynamics of feeding activity with the highest percentage occurs in the morning (07.00-10.00 WIB) that is equal to 70% and the proportion of feeding time in a day is 35% of total daily time. The percentage was comparison of total drop-in feeding activity time at amount 1792 minute and total drop-in feeding activity time at amount 419 minute with Ratu's total daily activity started from 07.00 WIB until 18.00 WIB, in amount of 6359 minute. Drop-in feeding was given twice a day. The drop-in feeding behavior of the Sumatran Rhinoceros is made as natural as possible by minimizing handfeeding like spesificallty put the feed inside the cage and let the rhino eat independently to maintain its natural behavior. Naturally the Sumatran Rhinceros feeding behavior begins by walking to the feed source and sniffing the feed then the Sumatran Rhinoceros will push the trees with their heads or bodies then stepped on with their feet until it fell down, and then they pulling roots, twisting the branches, or breaking branches with mouth.*

Keywords— *Behaviour, Sumatran Rhinoceros, Feeding, Sumatran Rhino Sanctuary, Way Kambas National Park.*

I. Introduction

SUMATRAN Rhinoceros was the only rhino species that had two horns and also known as the smallest rhino in the world[1]. This species was critically endangered with the lowest number of population among the other rhino[2]. Its population in natural habitat was estimated approximately 200-300 individual spread in South East Asia[3]. Reliable population estimates for Sumatran rhinoceros have always been difficult to obtain[4]. This uncertain number of Sumatran Rhinoceros population needs to get more concern[5]. The declining of population was caused by lose of habitat because the land forest over function, encroachment, illegal logging and poaching[6].

The Sumatran rhinoceros is a good example to illustrate the challenges in the conservation of a highly endangered species[7]. Sumatran Rhinoceros was in category critically endangered species[8] and include as Appendice 1 species[9]. Yayasan Badak Indonesia (YABI) was a partner of Forestry Department in order to conserve rhino in Indonesia. YABI had one program named Sumatran Rhino Sanctuary (SRS) that located in Way Kambas National Park[10]. SRS is a rhino sanctuary which managed with semi in-situ program[11] and its made as natural as possible with a little human intervention but still in a intensive supervision. This breeding centre for Sumatran Rhinoceros was established in 1998 as a last-ditch attempt to save the population from extinction [12]. Sanctuary rhinoceroses in Indonesia also browse freely in 10-hectare enclosures and select additional browse items on their own[13].

The knowledge about Sumatran Rhinoceros feeding behaviour was an information about its natural behaviour and how to apply it for supporting the conservation effort that will conducted. The success of Sumatran Rhinoceros protection and conservation was determined by manager's capability that has adequate education about Sumatran Rhinoceros behaviour in order to know what the obstacle in its management[14]. Fewer research about Sumatran Rhinoceros feeding behaviour whether drop-in or in natural habitat made this research necessary. This research aims to analyze how Sumatran Rhinoceros drop-in and natural feeding behaviour in SRS.

II. Procedure

A. Time and Location

This research was conducted in July 2017 at Sumatran Rhino Sumatran Way Kambas National Park, Lampung Province, Indonesia. The only site of which we are aware suitable for such a large rainforest enclosure would be Way Kambas National Park[15]. SRS has a lowland rainforest ecosystem type. The topography was at altitude of 0-50 m above sea level with a wet tropical climate. Geographically located between 4º59'- 5º05' LS and 105º42'- 105º48' BT[16].

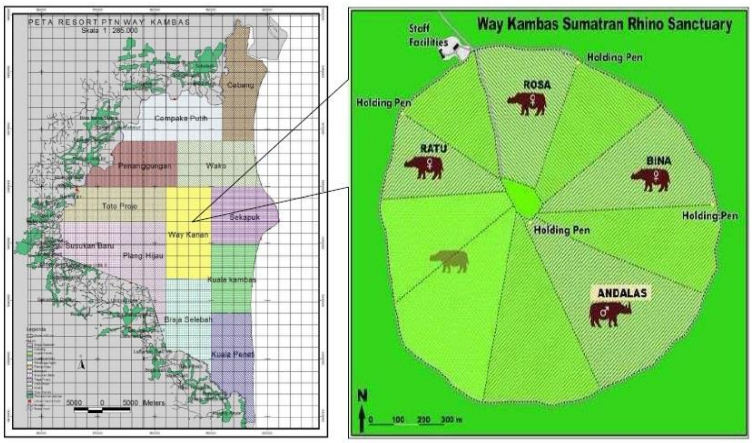

Figure 1. Research Location at Sumatran Rhino Sanctuary, Way Kambas National Park with Scale 1:285.000 [17]

B. Tools and Object

The tools that used in this research were camera, binocular, watch, stationary, laptop and tallysheets, while the object was one female Sumatran Rhino in SRS named “Ratu”.

C. Methods

Data about Sumatran Rhino feeding behaviour was obtained by using Focal Animal Sampling method[18][19]. The collected data were primary and secondary data. Primary data was the Sumatran Rhino feeding behaviour and secondary data were books, journals and other literature which could more amplify the results.

D. Data Analyzing

This research was used the quantitative descriptive techniques. The activity dynamics and time proportion of feeding behaviour was obtained by Focal Animal Sampling equation[18][19] then analyzed quantitatively. The feeding behaviour was analyzed descriptively.

$$\text{Activity Analysis} = \frac{Number\ of\ Activity}{\Sigma\ Total\ Activity} \text{ x } 100\ \%$$

$$\text{Time Anaysis} = \frac{Time\ for\ each\ Activity\ (minute)}{\Sigma\ Total\ Time\ (minute)} \text{ x } 100\ \%$$

III. Results and Discussion

The object was “Ratu” and she was choosen because she can easily adjust stranger presence and she was in parenting period therefore it is not too dangerous to observe. Feeding behaviour is include chewing, swallowing, or inserting any material into the mouth[20][21]. The observation was perfomed for 105 hours observation within 14 days (± 7 hours/ day) and it was separated into two sections which is drop-in feeding behaviour when the rhino inside the cage and natural feeding behaviour when the rhino was released into the forest. Sumatran Rhinoceros behaviour was very complex both in activity dynamics and time proportion. This could be affected by the surrounding enviromental conditions. Ratu’s daily behaviour has different frequency. The activity dynamics was used to know the pattern of activity changes to get the highest frequency of activity in certain hours to represent the trend of Sumatran Rhino activity in general the it is presented in graphic form (Fig 2) as follows.

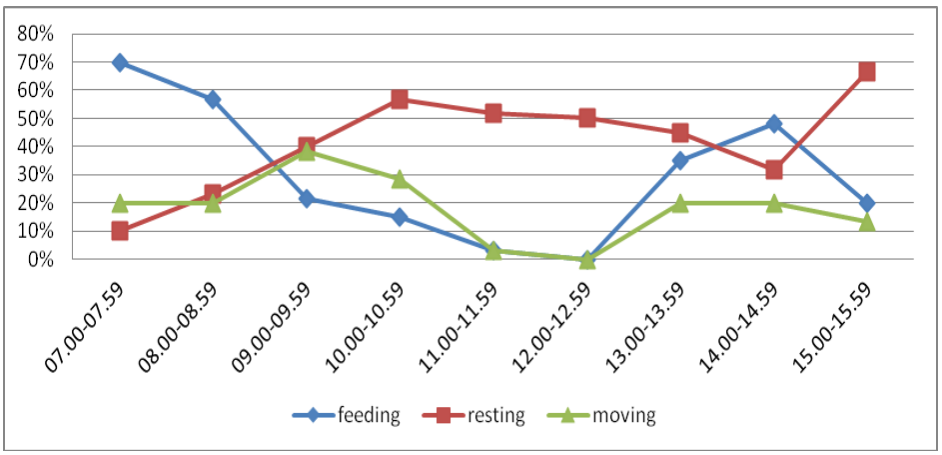

Figure 2. Ratu’s activity dynamics per hours.

Based on Figure 1 it could be seen that the activity with the highest percentage in the morning (07.00-10.00 am) was feeding that is 70% at 07.00-07.59 AM and the lowest percentage was moving which is 10% at 07.00-07.59 AM. This happens because it was the time for rhino to get drop-in feed therefore the most dominant behaviour was feeding. Based on other research Sumatran Rhinoceros feeding behaviour in the cage mostly occurs between 07.00-09.00 AM with the average percentage of feeding time 57,5% [22]. During the day (10.00 AM - 14.00 PM), the behaviour with the highest percentage in the day was resting that is 56,7% at 10.00-10.59 AM and the lowest percentage was moving and feeding at the same amount of 0% at 12.00 AM -12.59 PM. This happens because Sumatran Rhinoceros likes to wallowing during the day to stabilize their body temprature. Usually when the weather is hot, rhino will find the nearest wallow from the cage. During the day, rhino spend more time for wallowing than looking for an extra food in order to keep their body temprature in right. Other research states that at the certain times among 11.00 AM - 13.00 PM Sumatran Rhinoceros had going for wallowing[22]. Activity with the highest percentage in the afternoon (14.00-16.00 PM) was resting that is 66,7% at 15.00-15.59 PM and the lowest percentage was moving in amount 13,3% at 15.00-15.59 PM. This happens because in the afternoon the rhino was given additional drop-in feed around their wallow area, therefore when they were full then they will immediately return to the wallow.

The proportion time of daily activity was the time allocation for each activity based on the total daily time. This data was compared to its total daily time started from 07.00 AM until 16.00 PM. The results were presented in graphical form as follows (Figure 3)

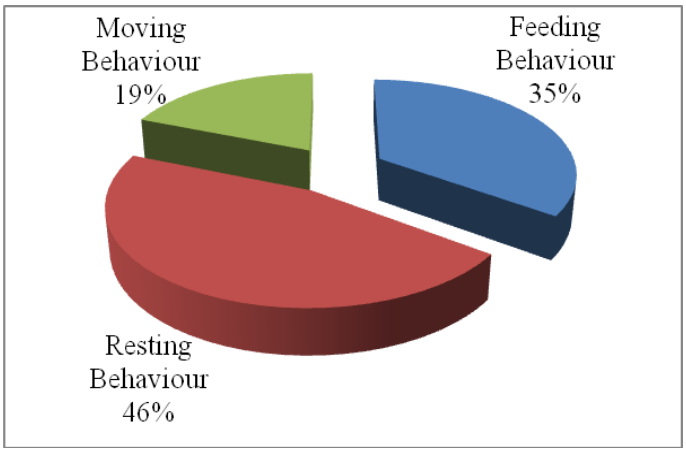

Figure 3. Ratu's time proportion per day

Base on the Fig 3 it could be seen that Ratu spent 35% of her total daily time for feeding behaviour. This number was obtained from the comparison of total drop-in feeding time in amount 1792 minutes summed up total natural feeding time in amount 419 minutes with Ratu's total daily time started from 07.00 AM -16.00 PM in amount 6359 minutes. Rhino spent 49% of their daily time for feeding[23]. This thing was significantly different with this result because the result calculation was obtained based on observation time started at 07.00 AM -16.00 PM while the statement calculation was based on one day observation time. Basically Sumatran Rhinoceros was a nocturnal animal, therefore its feeding behaviour more active at night[24].

Drop-in feeding was made as natural as possible in order to minimize the handfeeding by putting the feed inside the cage and let the rhino eat independently (Fig 4). However, in certain conditions handfeeding can be done, for example when the rhino lacks of appetite

the keeper will separates the preffered feed thus the rhino can eat more voraciously.

Figure 4. Ratu and Delilah had drop-in feeding inside the cage.

Before being fed, the rhino will walk near the feed and the stand still while snorting the feed or sometimes rubbing their head or body to the cage. When feeding, the rhino will bite the part of the branch that has lot of leaves and then the rhino will chewing the feed while standing or sometimes with closed eyes. The average of chewing time in a single input was ±31 seconds with the amount of feed chews as much as ±35 times per input. When the rhino full they will walk around the cage and stand still at the center of the cage it difficult to be fed again. Because this species is an obligate browser that requires a large percentage of its diet to consist of fresh, diverse browse species [25], it is challenging to maintain in zoos and is less likely to receive a higher plane of nutrition than its wild counterparts browsing in their native forests of Sumatra [26]. If the feed in the enclosure is incompatible with its natural diet, this might affected the animal behaviour[27]. The drop-in feeding was also given in the afternoon, but the feeding was not done inside the cage but it was given in the forest (Fig 5) The afternoon drop-in feeding place usually close to the wallow area.

Figure 5. Ratu and Delilah had afternoon drop-in feeding.

Natural feeding behaviour occurs when the rhino was released to the forest at 10.00 AM, but if the feed necessity were already fulfilled from drop-in feeding, ussualy the rhino will go straight to the wallow area. Natural feeding behaviour begins by walking to the feed source then the rhino will sniffing and snorting the feed source. The rhino will push the trunk of the tree with their body or head (Fig 6) then stepped on it with their legs until it completely fell down. Sumatran Rhinoceros was feeding by push the side of the tree with their chest to lie down the tree then stepped the tree until it fell between their legs[22]. Rhino got their feed by destroying, biting, and bending the tree with their horn, teeth, and legs[28].

Figure 6. Ratu pushing the tree with her head.

The rhino also like to eats by stuck out their mouth to reached the hanging roots and then pulling them off (Fig 7). Some literature describe that some plants are being eaten by rhinos by pulled off, especially for the lower plants like lianas and roots[29][30].

Figure 7. Ratu trying to reach the roots with her mouth.

Sumatran Rhinoceros also likes saplings and eat them by twisting and biting them to pick up the leaves (Fig 8). The saplings was placed behind the anterior horn then rhino will twisted the saplings which is a typical rhino feeding behaviour[1].

Sumatran Rhinoceros feeding by taken the leaves from its stem, especially in the shoot part [16]. In one meal, Sumatran Rhinoceros will have as much as eight times picking up leaves before moving to another place.

Figure 8. Ratu's pushing the tree with her head.

IV. Conclusion

Based on the research, the feeding activity dynamics with the highest percentage occurs in the morning (07.00-10.00 AM) was 70%. Time proportion of Ratu's feeding behaviour in a day was 35 % of her total daily time. The feeding methods of Sumatran Rhinoceros were by pushing the tree by their head or body and then stepped it with their legs until fell down, pulling off the roots, twisting the branch, and breaking the branch with their mouth.

References

[1] A.R. Maharani, Sumianto, N. Alim, Apriawan, M. Yunus, A. Mashuri, Sunarwanto, A. Subagyo, dan E. L. Rustiati, "Kajian keberadaan badak sumatera (*Dicerorhinus sumatrensis*) di Taman Nasional Way Kambas berdasarkan jebakan kamera", In *Prosiding Seminar Nasional Sains & Teknologi V Lembaga Penelitian Universitas Lampung,* Bandar Lampung, 19-20 November 2013, pp.1-5 .

[2] Z. Z. Zahari, Y. Rosnina, H. Wahid, K. C. Yap, and M. R. Jainudeen,. "Reproductive behaviour of captive sumatran rhinoceros (*Dicerorhinus sumatrensis*)", *Animal Reproduction Science Journal,* Vol. 85, pp. 327-335, 2005.

[3] H. Nicholls, "Sex and the single rhinoceros", *Nature Journal,* Vol.485, pp. 566-569, May. 2012.

[4] R. G. Havmoller, J. Payne, W. Ramono, S. Ellis, K.Yoganand, B. Long, E, Dinerstein, A. C. Williams, R. H. Putra, J. Gawi, K. Talukdar, and N. Burgess, "Will current conservation responses save the critically endangered sumatran rhinoceros *Dicerorhinus sumatrensis*? ", *Oryx Journal*, pp. 1-5, August. 2015.

[5] F. Nardelli, “The last chance for the sumatran rhinoceros?”. *Pachyderm Journal,* no. 55, pp. 43-53. September. 2014.
[6] H. R. Sadjudin, M. Syamsudin, dan W. S. Ramono, “Status kritis dua jenis badak di Indonesia”, *Al-Kauniyah Jurnal Biologi* ,Vol. 6 (1), pp. 73-83, April. 2013.
[7] P. Kretzschmar, S. Kamer-Schadt, L. Ambu, J. Bender, T. Bohm, M. Ernsing, F. Goritz, R. Hermes, J. Payne, J. Schaffer, S. T. Thayaparan, Z. Z. Zainal, T. B. Hildebrandt, and H. Hofer, ,“The catastrophic decline of sumatran rhino (*Dicerorhinus sumatrensis harrisoni*) in Sabah: historic exploitation reduced female reproductive performance and population viability”, *Global Ecology and Conservation Journal* Vol. 6, pp. 257-275, April. 2016.
[8] International Union for Conservation of Nature and Natural Resource. (2017, May). *IUCN red list of threatened species*. Available: http://www.iucnredlist.org
[9] Convention on International Trade in Endangered Species of Wild Fauna and Flora. (2017, May). *Appendices I, II, and III*. Available: http://www.cites.org
[10] Yayasan Badak Indonesia. (2017, May). *About us*. Available http://www.badak.or.id/tentang-kami
[11] W. Pusparini, P. R. Slevert, T. K. Fuller, T. O Randhir, and N. Andayani, “Rhinos in the parks: an island-wide survey of the last wild population of sumatran rhinoceros*”, PLoS ONE Journal,* Vol. 10 (9), pp. 1-16. September. 2015.
[12] A. W. A. Zafir, J. Payne, A. Mohamed, C. F. Law, D. S. K. Sharma, R. A. Amirtharaj, C. Williams, S. Nathan, W. S. Ramono, and G. R. Clements, “Now or never : what will it take to save the sumatran rhinoceros *Dicerorhinus sumatrensis* from extinction?” *Oryx Journal,* Vol.45 (2), pp. 225 – 233. 2011.
[13] D. Candra, R. W. Radcliffe, M. Khan, I. H. Tsu, and D. E. Paglia, “Browse diversity and iron loading in captive sumatran rhinoceroses (*Dicerorhinus sumatrensis*): a comparison of sanctuary and zoological populations”, *Journal of Zoo and Wildlife Medicine* ,Vol. 43 (3), pp. 66-73. 2012.
[14] I. Paripurnawan, dan B.S. Dewi, “*Studi perilaku berkubang badak sumatera (Dicerorhinus sumatrensis Fischer, 1814) di Suaka Rhino sumatera Taman Nasional Way Kambas”,* Unpublished.
[15] A. H. Ahmad, J. Payne, and Z. Z. Zainudin, “Preventing the extinction of the sumatran rhinoceros”, *Journal of Indonesian Natural History,* Vol.1 (2), pp.11-22. 2013
[16] N. R. Jati, “*Alternatif rencana pengembangan ekowisata di Suaka Rhino Sumatera (SRS) Taman Nasional Way Kambas”*, Unpublished.
[17] Suaka Rhino Sumatera. *Dokumentasi Peta Lokasi dan Sketsa Kandang*. Lampung.
[18] J. Altman, “*Observational study of behavior : sampling methods”*. Universitas of Chicago, Chicago, 1973, pp. 227-267.
[19] D. Suherli, S. P Harianto,dan Y. Widodo, “ Kajian perilaku dan pakan *drop-in* monyet hitam sulawesi (*Macaca nigra*) di Taman Agro Wisata Bumi Kedaton”, *Jurnal Slyva Lestari*,Vol. 4(2), pp. 1-8, April. 2016.
[20] J. A. A. Pambudi, “ *Studi perilaku dan ekologi kukang jawa (Nycticebus javanicus Geoffroy, 1812) di kawasan hutan bodogol*. Tesis. Universitas Indonesia”, Unpublished.
[21] I. Firdilasari, S. P Harianto, dan Y. Widodo, “ Kajian perilaku dan analisis kandungan gizi pakan d*rop in* beruang madu (*Helarctos malayanus*) di Taman Agro Satwa dan Wisata Bumi Kedaton”, *Jurnal Sylva Lestari,* Vol. 4 (1), pp. 97-106, Januari. 2016.
[22] A. Kurniawanto, “ *Studi perilaku badak sumatera (Dicerorhinus sumatrensis Fischer, 1814) di Suaka Rhino Sumatera Taman Nasional Way Kambas Lampung”*, Unpublished.

[23] M. Hutchins, and M. D. Kreger, “Rhinoceros behaviour: implications for captive management and conservation”, *International Zoo Yearbook Journal,* Vol. 40, pp. 150-173, July. 2006.
[24] H. Arief, “*Analisis habitat badak sumatera (Dicerorhinus sumatrensis Fischer 1814) studi kasus: Taman Nasional Way Kambas”,* Ph.D. dissertation, Institut Pertanian Bogor, Bogor, 2005.
[25] E. S. Dierenfeld, R. E. C. Wildman, and S. Romo, “Feed intake, diet utilization, and composition of browses consumed by the sumatran rhino (*Dicerorhinus sumatrensis*) in a North American Zoo”, *Zoo Biology Journal,* Vol. 19, pp. 169-180, May. 2000.
[26] T. L. Roth, P. R. Reinhart, J. S. Romo, D. Candra, A. Suhaery, and M. Stoops, “Sexual Maturation in the Sumatran Rhinoceros (*Dicerorhinus sumatrensis*)”, *Zoo Biology Journal*, Vol. 32, pp. 549-555. 2013.
[27] A. Tiyawati, S. P. Harianto, dan Y. Widodo, “Kajian perilaku dan analisis kandungan gizi pakan drop-in siamang (*Hylobates syndactylus*) di Taman Agro Satwa dan Wisata Bumi Kedaton”, *Jurnal Sylva Lestari,* Vol. 4 (1), pp. 107-114, January. 2016.
[28] A. E. Saputra, “*Anatomi otot daerah panggul dan paha badak sumatera (Dicerorhinus sumatrensis)”*, Unpublished.
[29] M. Borner, “*A field study of the sumatran rhinoceros (Dicerorhinus sumatrensis), ecology and behaviour conservation situation in Sumatera*”, Basel University, Zurich, 1979.
[30] J. B. Hernowo, R. Lisiawati, S. Ulum, T. Titus, P. Adithya, dan A. Salambessy, “*Kajian Terhadap Habitat dan Pakan Badak Sumatera (Dicerorhinus sumatrensis Fischer, 1814) di Suaka Rhino Sumatera di Taman Nasional Way Kambas*”, Unpublished.

Yield Analysis and Phytochemical Screening Leaf Extract of Sansevieria Sp (#611)

Whika Febria Dewatisari[1], Leni Rumiyanti[2] dan Ismi Rakhmawati[3]
[1]Biology Departement of Universitas Terbuka
[2]Physics Departement of Math and Scince Faculty University of Lampung
[3]Math and Scince Departement of Teacher Training and Education Faculty University of Lampung

Abstract—.*This study aimed to determine the results of yield analysis on Sansevieria trifasciata and Sansevieria cylindrica leaf extract. In addition, this study also aimed to determine the qualitative presence of a bioactive group compounds that potentially as antioxidants (phytochemical screening) on the leaves extract Sansevieria trifasciata and Sansevieria cylindrica.The method used in this research was a stratified extraction method with three types of solvent, ie non-polar solvent in the form of N Hexan; A semi-polar solvent of Aceton; And a polar solvent of Ethanol. Further, identification of six types of phytochemical compounds, namely triterpenoid and steroid, saponin, phenol, flavonoid, quinone, and alkaloid groups was conducted.The result of yield analysis showed that Sansevieria trifasciata's yield more than Sansevieria cylindrica's yield. Sansevieria trifasciata's obtained 7,89% yield while Sanseviera cylindrica has 6,79% yield The greater the yield produced, the more efficiently treated applied by not excluding other traits.The result of phytochemical compound analysis obtained three phytochemical compounds contained in Sansevieria trifasciata, namely triterpenoid group compounds and steroids and flavonoids. Meanwhile, the results of analysis of phytochemical compounds contained in Sansevieria cylindrica also obtained three phytochemical compounds, namely triterpenoid compounds and steroidal groups and alkaloids.*

Keywords—Yield analysis , phytochemical compound, Sansevieria sp

I. Introduction

Tongue-in-law plant or Snake plant (Sansevieria sp) is often used as an indoor and outdoor ornamental plant. In addition to its function as an ornamental plant, it can also be reproduced as a traditional medicine for influenza, cough, and inflammation of the respiratory tract. Yield is an important value in production. Yield is the ratio of dry weight and wet weight of a raw material of a product (Yuniarifin, Bintoro, and Suwarastuti, 2006). The extract yieldwas calculated based on the ratio of the final weight (weight of the extract produced) with the initial weight (cell biomass weight used) multiplied 100% (Sani *et al*, 2014). The value of yield is also related to the amount of bioactive compound contained in *Sansevieria sp*. Bioactive compounds are compounds contained in the body of animals and also plants. These compounds have various benefits for human life, such as aresource of antioxidants, antibacterial, anti-inflammatory, and anticancer. Prabowo *et al*. (2014) suggests that studies of bioactive compounds have been conducted for human health purposes, ranging from

supplements to drugs to humans. Stars, Sinurat, and Purwadaria (2007) stated that these bioactive compounds have function as antibacterial, anticancer, anti-inflammatory and antioxidant.

Phytochemical screening is an early stage to identify the content of a compound in simplicia or plant to be tested. Phytochemicals or plant chemicals study the diverse of organic compounds that are formed and stockpiled by plants, it is about the chemical structure, the biosynthesis, the subsequent implications, and Its biological physiology. Chemical compounds as a result of secondary metabolites have been widely used as dyes, toxins, food scents, medicines and as traditional medicines thus research on the use of growing - nutritious plants chemistry as traditional medicine is indispensable. Chemical compounds that are secondary metabolic products in plants are very diverse and can be classified into several classes of natural compounds, namely saponins, steroids, tannins, flavonoids and alkaloids (Putranti et al, 2013)

In Indonesia, studies of phytochemical yield and screening of Sansevieria trifasciata and Sansevieria cylindrica extracts are limited. Based on these conditions, it is necessary to conduct research to analyze the rendemen and determine the qualitative presence of bioactive group compounds potentially as an antioxidant in Sansevieria trifasciata and Sansevieria cylindrica.

II. Methodology research

This research was conducted at Laboratory of Mathematics and Science Faculty, University of Lampung, Bandar Lampung. The study was conducted for 5 months, from March 2016 to August 2016. Methods of data collection consist of:

A. Identification and Preparation of S. trifasciata and S. cylindrica

The preparation of S. trifasciata and S. cylindrica begins with washing, drying and grinding processes. Before it was dried, the sample were weighed to know the wet biomass, then the sample were dried in a protected from direct sunlight place. This were aimed to avoid damage to bioactive compounds material. The dried S. trifasciata were smoothed with a blender, then filtered to obtain uniform grains, inserted in a plastic bag and labeled then weighed with analytical scales and stored in dry conditions for subsequent extraction.

B. Extraction Process

The extraction of active ingredients was carried out were modified with reference to the research of Juniarti et al. (2009) and Santoso et al. (2012). The extraction method used in this research was the extraction plate technique. Harborne (1987) states that extraction plate technique were conducted by soaking the sample with different solvents sequentially, first with a non-polar solvent (n-hexane) then with a semipolar solvent (ethyl acetate) then with a polar solvent (ethanol). Simplicia S. trifasciata Prain and S. Cylindrica were weighed as much as 250 grams and fed into the erlenmeyer, then added the solvent until the final volume reached 1000 ml at a ratio of 1: 4 (w / v). The extraction procedure was carried outby immersing the sample with n-hexane, ethyl acetate and ethanol respectively. The maseration results are then filtered with Whatman 42 filter paper to produce filtrate and residue. Soaking were conducted 3 times until the filtrate close to clear. The obtained filtrate was then concentrated with a vacuum rotary evaporator at 40ºC until a crude extract was obtained in the paste form . The soaking extract was calculated using the formula:

Yield percentage = Total weight of the extract in the form of paste (g) x 100% The amount of dry weight (g)

C. Phytochemical Analysis

Phytochemical analysis is a qualitative analysis conducted to determine the bioactive components contained in each solvent of S. trifasciata and S. cylindrica extracts. Phytochemical analyzes performed included alkaloids, triterpenoids and steroid tests, saponins, phenols, flavonoids and quinones. The analytical method used is based on Harborne (1987).

- Alkaloids: Alkaloid test is done by dissolving in a few drops of 2 N sulfuric acid then tested with 2 alkaloid reagents ie dragendorff reagent and meyer reagent. Positive test results obtained when the formation of red deposits to orange with reagent dragendorff and yellowish white sediment with meyer reagent.

Triterpenoids and steroids: Several samples were dissolved in 2 ml of chloroform in a dry reaction tube and then added 10 drops of anhydrous acetate and 3 drops of concentrated sulfuric acid. The positive reaction is shown by the formation of a red solution for the first time then turns into blue and green

- Saponin (foam test): Saponin can be detected by foam test in hot water. A stable foam will continue to be visible for 5 minutes and foam exist on the addition of 1 drop of HCl 2 N indicates the presence of saponins.

- Phenol: A number of samples were extracted with 20 ml of 70% ethanol. The resulting solution was taken as 1 ml then added 2 drops of 5% FeCl3 solution. Positive reaction is indicated by green or blue green.

Flavonoids: A number of samples were added by 0.1 mg magnesium powder and 0.4 ml of amyl alcohol (37% hydrochloric acid mixture and 95% ethanol with the same volume) and 4 ml of alcohol and then the mixtureof ethanol and alcohol was shaken. Positive reactions are indicated by the apperance of red, yellow or orange on the amyl alcohol layer.

- Quinones: Sample NaOH 1 N added then observed the color change. A positive reaction is

III. Result and discussion

Yield Analysis of Sanseviera sp

The first process before Sansevieria sp yield analysis is extraction process. Sansevieria sp, both Sansevieria cylindrica and Sansevieria trifasciata are extracted by using a extraction method with three types of solvents, ie non-polar solvents of N Hexan; A semi-polar solvent of Aceton; And a polar solvent of Ethanol. Three types of solvent are used to obtain phytochemical compounds from within the cell wall of Sansevieria sp. Although used same solvent , volume used to extract Sansevieria sp is different. The volume of N Hexan, Aceton, and Ethanol used to extract Sansevieria cylindrica is 250 ml. While the volume of N Hexan, Aceton, and Ethanol used to extract Sansevieria trifasciata is 150 ml.

Other similarities between Sanseviera cylindrica and Sanseviera trifasciata is drying's temperature , 6o degrees celcius, and 40 degree c for evaporating. The difference is drying duration, Sanseviera cylindrica was dried for 24 hours and Sanseviera trifasciata dried for 48 hours.Sanseviera sp extraction process shown by Figure 1 below.

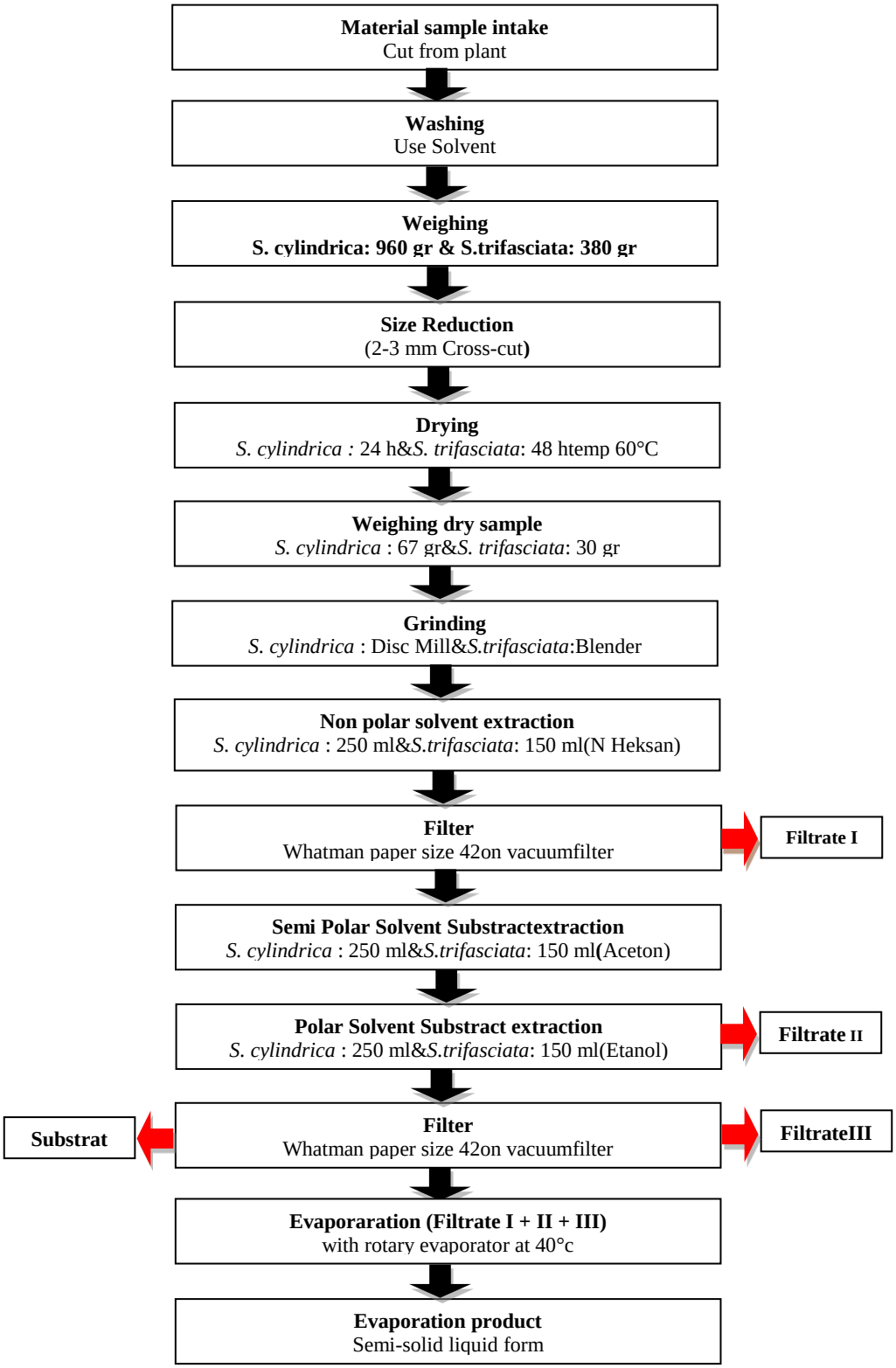

Figure 1 *Sansevieria sp* Extraction ProcessFlow Chart

Yield analysis could be executed after extraction process. Sanseviera cylindrica yield could be calculated with equation below :

$$\mathrm{Pr} = \frac{67}{960} x\ 100\% = 6{,}79\%,$$

While Sanseviera trifasciata yield calculation is

$$\mathrm{Pr} = \frac{30}{380} x\ 100\% = 7{,}89\%.$$

Based on the calculation above can be said that the yield of Sansevieria trifasciata more than Sansevieria cylindrica yield. Evidently, the yield of Sansevieria trifasciata was 7.89% and Sansevieria cylindrica was 6.79%. The larger the resulting yield, the more efficiently the treatments are applied by not ruling out other traits.

Based on the results of yield it can be assumed that the bioactive components contained in Sansevieria trifasciata more than Sansevieria cylindrica. In line with Nurhayati, Aryanti, and Nurjanah (2009) that the high value of yield in line the number of bioactive components contained in it. To prove this assumption, phytochemical screening was performed.

Sansevieria sp. Phytochemical compound screening .

To known the appearance of bioactive compound which is potential as antioxidants in Sanseviera sp extract, six phytochemical compounds was identified. Those phytochemical compounds are triterpenoid and steroids, saponin, phenol, flavonoid, quinone, and alkaloid (Figure 2)

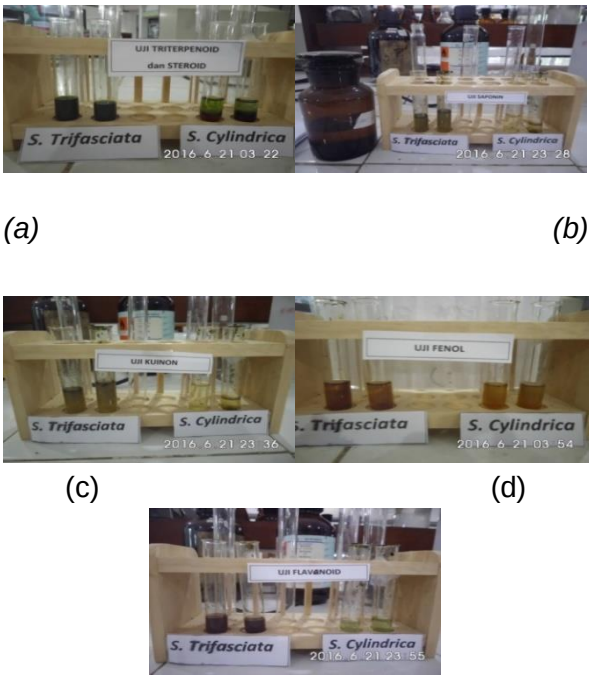

(a) *(b)*

(c) (d)

(e)

Figure 2. Phytochemical Screening

Phytochemical Screening was conducted qualitative base on compound solubility characteristic. Analysis result shown Sanseviera trifasciata content three triterpenoid, steroidal, and flavonoid group. Meanwhile, the results of the analysis of phytochemical compounds contained in Sansevieria cylindrica also obtained three phytochemical compounds, the compounds of triterpenoid and steroidal groups and alkaloids.

Phytochemical compounds assay , the results of color stain semi-solid fluid screening are presented in Table 4.1. In assay of triterpenoid and steroid group compounds, semi-solid Sansevieria sp when extracted with anhydrous acetate and concentrated sulfuric acid produce a reddish color at the bottom of the test tube. This means both Sansevieria cylindrica and Sanseviera trifasciata are positive contained triterpenoid and steroids group. The results of this study are in line with Rahimah (2015) and Philip, Kaleena, and Kumar (2011).

Triterpenoid compounds help the body in the process of organic synthesis and recovery of body cells, whereas steroid compounds exhibit antibacterial, antifungal, antitumor, neurotoxic and anti-inflammatory activity beneficial to the pharmaceutical industry (Robinson, 1995). Meanwhile, according to Fessenden (1982) triterpenoid and steroid compounds for plants play a role in the metabolism and formation of male and female gametes. Both of these compounds are bioactive compounds that have antibacterial and antioxidant activity through the isolation and identification of its activity. Riyanto et al. (2013) states that triterpenoid compounds found in plants serve as protectors for resisting insects and microbial attacks. Bangham and Horne (2006) suggest steroids can interact with impermeable cell phospholipid membranes against lipophilic compounds that cause membrane integrity to decrease, morphology of cell membranes change, and eventually lead to fragile cell membranes and lysis.

In Saponin group compounds assay, the two samples showed no foam when the semi-solid liquid of Sansevieria sp extract had been dripped with HCl. This means both Sansevieria cylindrica and Sansevieria trifasciata negatively contain saponin group compounds.

In phenol group compounds assay, when the semi-solid liquid extract of Sansevieria sp driped with FeCl3 drops, it turns out that the color of the two samples remain brownish yellow not green or blue green. This means both *Sansevieria cylindrica* and *Sansevieria trifasciata* negatively containing phenol group compounds

The flavonoid compound assay in the sample test tube Sansevieria trifasciata formed a reddish orange color when mixed with hydrochloric acid, ethanol, and alcohol. Meanwhile, in the sample *Sansevieria cylindrica* remain clear light green. This means that *Sansevieria trifasciata* positively has *flavanoid* compounds,while *Sansevieria cylindrica* n egatively contains *flavanoid* group compounds. The results of this study are in line with Lombogia, Budiarso, and Bodhi (2016).

Flavonoid compounds have properties as antioxidants that can protect the pancreatic cells damage from free radicals and can lower blood sugar levels by stimulating pancreatic beta cells to produce more insulin (Arjadi and Susatyo, 2010). Meanwhile, according to Bhat et al (2009) flavonoid compounds for plants act as pigments and attractants for insects that assist pollination, while flavonoid compounds are beneficial to humans as antioxidants. Kar et al. (2006) states that flavonoid compounds are non-polar compounds which found in many plant stems.

In quinone group compounds testing, the two test tubes did not change color to yellow when the NaOH was dripped. This meansboth Sansevieria cylindrica and Sansevieria trifasciata negatively contain quinone group compounds.In the alkaloid group compound test, in the Sansevieria cylindrica sample tube contained white precipitate when depressed Mayer reagent. Meanwhile, in the Sansevieria trifasciata sample there was no sediment. This means that Sansevieria cylindrica positively contains an alkaloid compound,

while Sansevieria trifasciata negatively contains alkaloid group compounds. The results of this study are in line with Philip, Kaleena, Valivittan and Kumar (2011).

According to Harbone (1987), alkaloid compounds in Sansevieria cylindrica serves as a regulator of growing or insects attractant. Raharjo (2013) states that alkaloids are not found in all plant species. Alkaloids are mostly found in high-grade Angiospermae plants especially in dicotyledonous plants. Meanwhile, according to Suhartono, Fujiati and Aflanie (2002), the presence of antioxidant alkaloid alkaloid compounds is expected to reduce free radicals' cancer trigger because thesecompounds can donate one or more electrons to overcome free radical.

Tabel 5.1*Sansevieria sp phytochemical screening result*

Phytochemical Screening	**Sample**		**Description**
	Sansevieria trifasciata	*Sansevieria cylindrica*	
Triterpenoidand Steroid	+	+	There was a reddish color at the bottom of the test tube in both samples
Saponin	-	-	Both samples showed no foam
Phenol	-	-	Green and blueish green was not formed (color remain yellow brown)
Flavonoid	+	-	In the *Sansevieria trifasciata* sample reaction tube formed a reddish orange color while in the sample *Sansevieria cylindrica* remain clear green light
Quinone	-	-	The two test tubes was not show yellow color change when dripped with NaOh

IV. Conclusion

Based on the results and discussion, it can be concluded that:

1. Yield analysis result; *Sansevieria trifasciata*yieldhas more than *Sansevieria cylindrica*

2. *Sansevieria cylindrica* and *Sansevieria trifasciata* positively contain triterpenoid and steroid group compounds as but negativelycontain saponins, phenols, quinones group compounds
3. *Sansevieria trifasciata* positively contains flavanoid compounds, while *Sansevieria cylindrica* negatively contains flavanoid group compounds
4. The results of phytochemical compound analysis obtained three phytochemical compounds contained in *Sansevieria trifasciata* are of triterpenoid and steroid and flavonoid groups compound. While *Sansevieria cylindrica* contained the triterpenoid and steroids and alkaloids compound

References

[1]. Arjadi, F. dan P. Susatyo.2010. *RegenerasiSelPulai Langerhans PadaTikusPutih (Rattusnorvegicus) Diabetes Yang DiberiDagingRebusanMahkota Dewa (PhaleriamacrocarpBoerl).*FakultasKedokteranUniversitasJendralSoedirman. Banyumas.

[2]. Bangham AD, Horne RW. 2006. Action of Saponins on Biological Cell Membranes. *Journal Nature.*196:952-953.

[3]. Bhat, S. V., B. A. Nagasampagi and S. Meenakshi. 2009. *Natural Products :Chemistry and Application*. Narosa Publishing House. New Delhi.India.

[4]. Bintang, I.A.K, Sinurat A.P, dan Purwadaria T. 2007. Penambahan Ampas Mengkudu sebagai Senyawa Bioaktif terhadap Performans Ayam Broiler. *JITV.*12(1):1-5.

[5]. Fessenden. 1982. *Kimia Organik*. Erlangga. Jakarta.

[6]. Harbourne, J.B., 2002, Metode Fitokimia : Penuntun Cara ModernMenganalisis Tumbuhan, Diterjemahkan Oleh K. Padmawinata Dan I.Soediro. ITB. Bandung.

[7]. Juniarti, D. Osmeli dan Yuhernita. 2009. Kandungan Senyawa Kimia, UjiToksisitas (Brine Shrimp Lethality Test) dan Antioksidan (1,1-diphenyl-2-pikrilhydrazyl) dari Ekstrak Daun Saga (Abrus precatorius l.).*Makara Sains*, 13(1):50-54.

[8]. Kar P, Laight D, Shaw K. M, Cummings M. H. 2006. Flavonoid Rich Grapeseed Extracts: A New Approach in High Cardiovascular Risk Patients. *International Journal Clin Practice.* 60(11):1484-1492.

[9]. Lombogia, Budiarso, dan Bodhi. 2016. UjiDayaHambatEkstrakDaunLidahMertua (*Sansevieriaetrifasciata folium*) TerhadapPertumbuhanBakteri*Escherichia coli*dan*Streptococcus sp*).*Jurnal e-Biomedik*. 4(1):24-29.

[10]. Nurhayati, T, D. Aryanti, danNurjanah. 2009. KajianAwalPotensiEkstrakSponsSebagaiAntioksidan. *JurnalKelautanNasional*. 2(2):43-51.

[11]. Prabowo, A.Y, T. Estiasih, I. Purwatiningrum. 2014. Umbi Gembili (*Dioscorea esculenta* L.) sebagai Bahan Pangan Mengandung Senyawa Bioaktif. *Jurnal Pangan dan Agroindustri.* 2(3):129-135.

[12]. Philip, Kaeena, Valivittan, dan Kumar, G. 2011. Phytochemical Screening And Antimicrobial Activity of *Sansevieriaroxburghiana*Schult And Schult F. *Middle-East Journal of Scientific Research*. 10(4): 512-518.

[13]. Putranti, Ristyana Ika. 2013.Skrining Fitokimia dan AktivitasAntioksidan Ekstrak Rumput Laut Sargassum duplicatum dan Turbinaria ornata dari Jepara. *Tesis.*Universitas Diponegoro. Semarang.

[14]. Raharjo, TJ. 2013. *Kimia Hasil Alam*. Pustaka Pelajar. Jogjakarta.

[15]. Rahimah, R. 2015. *KarakteristikSimplisiadanSkriningFitokimiasertaUji AktivitasAntioksidandanEkstrakEtanolDaunLidahMertua (Sansevieratrifasciata var. laurentii).*Universitas Sumatera Utara. Medan.

[16]. Riyanto, E.I, Widowati I., dan Sabdono, A. 2013. Skrining aktivitas antibakteri pada ekstrak Sargasum polycystum terhadap bakteri *Vibrio harveyi* dan Micrococcus luteus di Pulau Panjang Jepara. *Journal of Marine Research* 1(1):115- 121.

[17]. Robinson, Trevor. 1995. *KandunganOrganikTumbuhanTinggi*. Edisikeenam.
a. TerjemahanKokasihPadmawinata. FMIPA ITB.Bandung.

[18]. Sani, R.N., Fithri C.N., Ria D.A., dan Jaya M.M. 2014. *Analisis Rendemen dan Skrining Fitokimia* Ekstrak Etanol Mikroalga Laut *Tetraselmis chuii. Jurnal Pangan dan Agroindustri.* 2(2):121-126.

[19]. Santoso, J., N. Aryudhani and S. H. Suseno. 2009. Kandungan Senyawa FenolRumput Laut Hijau Caulerpa racemosa dan Aktivitas Antioksidannya.*Jurnal Kelautan Nasional*, 2 : 109-118.

[20]. Santoso, J., S. Anwariyah, R. O. Rumiantin, A. P. Putri, N. Ukhty and Y. Yoshie-Stark. 2012. Phenol Content, Antioxidant Activity and Fibers profile ofFour Tropical Seagrasses from Indonesia. *Journal of CoastalDevelopment*, 15 (2) : 189-196

[21]. Suhartono, E., Fujiati, dan I. Aflanie. 2002. Oxygen Toxicity By Radiation And Effect Of Glutamic PiruvatTransamine (GPT) Activity Rat Plasma After Vitamin C Treatment. *Prosiding.International Seminar on Environmental Chemistry and Toxycology*.Yogyakarta.

[22]. Tamat, S.R, T. Wikanta, L.S, Maulina. 2007. Aktivitas Antioksidan dan Toksisitas Senyawa Bioaktif dari Ekstrak Rumput Laut Hijau *Ulva reticulata* Forsskal. *Jurnal Ilmu Kefarmasian Indonesia.*5(1):31-36.

[23]. Vijayabakar, P. and V. Shiyamala. 2011. Antibacterial Activities of Brown MarineAlgae (Sargassum wightii and Turbinaria ornata) from The Gulf ofMannar Biosphere Reserve.*Advances in Biological Research*, 5 (2) :99-102.

[24]. ----------. 2012. Antioxidant Properties of SeaweedPolyphenol from Turbinaria ornata (Turner) J. Agard, 1848. *AsianPasific Journal of Tropical Biomedicine* : 90-98.

[25]. Yuniarifin, H, Bintoro VP, Suwarastuti A. 2006. Pengaruh Berbagai Konsentrasi Asam Fosfat pada Proses Perendaman Tulang Sapi terhadap Rendemen, Kadar Abu dan Viskositas Gelatin. *Journal Indon Trop Anim Agric.* 31(1) : 55-61.

Published by :

Research Institute and Community Services, University of Lampung
Jl. Soemantri Brojonegoro No. 1 Gedong Meneng
Kedaton, Bandar Lampung - 35145
Indonesia
http://www.unila.ac.id

ISBN 978-602-70050-4-4

For more information, click
http://ic-star.unila.ac.id

Organised by:

Supported by: